163

BULLETIN OF THE MINERAL RESEARCH AND EXPLORATION

2020

Phone : +90 (312) 201 10 00
Fax : +90 (312) 287 91 88
Adress : MTA 06530 - Ankara - TURKEY
www.mta.gov.tr

BULLETIN OF THE MINERAL RESEARCH AND EXPLORATION

Foreign Edition | 2020 | 163 | ISSN : 0026-4563 E-ISSN : 2651-3048

CONTENTS

Research Articles

First Turolian findings in the Neogene sequence of Denizli Basin (SW Anatolia) and its regional palaeobiogeographic significance ..... Adil DOĞAN, Serdar MAYDA and M. Cihat ALÇİÇEK 1

Tectonic meaning of the deformation in shallow marine region between Gaziköy-Mürefte (Sea of Marmara) by using seismic reflection data, NW Anatolia ..... Şule GÜRBOĞA, Aslı Zeynep YAVUZOĞLU, Recep GÜNEY, Fatma Betül KARCI, Ayhan YAVUZOĞLU, Özgür TÜRKMEN, Pir Çağatay KARTAL, Bahri Serkan AYDEMİR, Murat EVREN, Murat CENK, Barbaros ŞİMŞEK, Eyyüp ÖZBEK, Tuğrul Şükrü YURTSEVER, Füsun YİĞİT FETHİ, Eşref AYLAN and Uğur Zeki KIRAT 13

Using of GIS on field geology studies: An application on central-southern of Eskişehir ..... Coşkun GÜNEŞ, Emrah PEKKAN and Muammer TÜN 27

2D and 3D Structural Boundaries of the Tectonic Composition of the Anatolia and Surrounding Seas using by the Gravity (Satellite Data): Eastern Mediterranean ..... Ceyhan Ertan TOKER 39

Oligocene molasse sedimentation in the Central Taurides: Records of the onset of extensional tectonic regime ..... Ayhan ILGAR, Tolga ESİRTGEN, Banu TÜRKMEN-BOZKURT and Serap DEMİRKAYA 47

The internal structure of Beypazarı Blind Thrust Zone around Çayırhan ..... Anıl ARDAHANLIOĞLU, Gürol SEYİTOĞLU and Korhan ESAT 77

An approach for the application of energy-based liquefaction procedure using field case history data ..... Kamil KAYABALI, Levent SELÇUK and Turgay BEYAZ 99

Integration of the GNSS method and borehole camera to model the resulting spherical cavity generated by the main charge blast in clay ..... Denis TEŽAK, Nikola KRANJČIĆ, Bojan ĐURIN and Mihaela JURAS 115

A laboratory-scale investigation on freezing-thawing behavior of some natural stone samples manifactured in Turkey ..... Gökhan EROL and Ozan BAYRAM 131

The relationship of soils developed on different parent materials in Niğde province with lithological units and determination of their suitability for usage agricultural purposes ..... Harun TORUNLAR, Abdurrahman LERMİ and Emin ÇİFTÇİ 141

Evolution of slab tearing-related high potassium volcanism: Petrogenetic data from the Emirdağ and İscehisar volcanic units ..... Selin BİLGİÇ GENCER, Sibel TATAR ERKÜL and Fuat ERKÜL 167

An overview of the current seismicity of the Sultandağı Fault Zone (Afyonkarahisar-Konya) ..... Doğan KALAFAT, Yavuz GÜNEŞ, Mehmet KARA and Kıvanç KEKOVALI 187

Invited Article

The electric power production targeted Unconventional Geothermal Systems (UGS), some conceptual designs and their thermodynamics classification ..... Aydın ÇİÇEK 211

ACKNOWLEDGEMENT 229

Bulletin of the Mineral Research and Exploration Notes to the Authors 231

BULLETIN OF THE MINERAL RESEARCH AND EXPLORATION

Foreign Edition | 2020 | 163 | ISSN : 0026-4563 E-ISSN : 2651-3048

CONTENTS

Research Articles

First Turolian findings in the Neogene sequence of Denizli Basin (SW Anatolia) and its regional palaeobiogeographic significance
.....Adil DOĞAN, Serdar MAYDA and M. Cihat ALÇİÇEK 1

Tectonic meaning of the deformation in shallow marine region between Gaziköy-Mürefte (Sea of Marmara) by using seismic reflection data, NW Anatolia
Şule GÜRBOĞA, Aslı Zeynep YAVUZOĞLU, Recep GÜNEY, Fatma Betül KARCI, Ayhan YAVUZOĞLU, Özgür TÜRKMEN, Pir Çağatay KARTAL, Bahri Serkan AYDEMİR, Murat EVREN, Murat CENK, Barbaros ŞİMŞEK, ...Eyyüp ÖZBEK, Tuğrul Şükrü YURTSEVER, Füsun YİĞİT FETHİ, Eşref AYLAN and Uğur Zeki KIRAT 13

Using of GIS on field geology studies: An application on central-southern of Eskişehir
..... Coşkun GÜNEŞ, Emrah PEKKAN and Muammer TÜN 27

2D and 3D Structural Boundaries of the Tectonic Composition of the Anatolia and Surrounding Seas using by the Gravity (Satellite Data): Eastern Mediterranean
..... Ceyhan Ertan TOKER 39

Oligocene molasse sedimentation in the Central Taurides: Records of the onset of extensional tectonic regime
..... Ayhan ILGAR, Tolga ESİRTGEN, Banu TÜRKMEN-BOZKURT and Serap DEMİRKAYA 47

The internal structure of Beypazarı Blind Thrust Zone around Çayırhan
.....Anıl ARDAHANLIOĞLU, Gürol SEYİTOĞLU and Korhan ESAT 77

An approach for the application of energy-based liquefaction procedure using field case history data
.....Kamil KAYABALI, Levent SELÇUK and Turgay BEYAZ 99

Integration of the GNSS method and borehole camera to model the resulting spherical cavity generated by the main charge blast in clay
..... Denis TEŽAK, Nikola KRANJČIĆ, Bojan ĐURIN and Mihaela JURAS 115

A laboratory-scale investigation on freezing-thawing behavior of some natural stone samples manifactured in Turkey
.....Gökhan EROL and Ozan BAYRAM 131

The relationship of soils developed on different parent materials in Niğde province with lithological units and determination of their suitability for usage agricultural purposes
..... Harun TORUNLAR, Abdurrahman LERMİ and Emin ÇİFTÇİ 141

Evolution of slab tearing-related high potassium volcanism: Petrogenetic data from the Emirdağ and İscehisar volcanic units
..... Selin BİLGİÇ GENCER, Sibel TATAR ERKÜL and Fuat ERKÜL 167

An overview of the current seismicity of the Sultandağı Fault Zone (Afyonkarahisar-Konya)
.....Doğan KALAFAT, Yavuz GÜNEŞ, Mehmet KARA and Kıvanç KEKOVALI 187

Invited Article

The electric power production targeted Unconventional Geothermal Systems (UGS), some conceptual designs and their thermodynamics classification
.....Aydın ÇİÇEK 211

ACKNOWLEDGEMENT 229

Bulletin of the Mineral Research and Exploration Notes to the Authors..... 231

The translations of Güneş et al., Toker, Ardahanlıoğlu et al. were made by M. Kerem AVCI. The translation of Ilgar et al. was made by Alper BOZKURT. The translation of Çiçek was made by Emre Kaan BAŞARAN. The translation of Erol ve Bayram was made by Buğra ÇAVDAR. The translation of Bilgiç et.al. was made by Catherine YİĞİT. The translation of Torunlar et al. was made by Zehra DEVECİ ARAL. The translation of Kalafat et al. was made by Metin KOYUNCU.

Bull. Min. Res. Exp. is indexed and abstracted in TR Dizin, Emerging Source Citation Index (ESCI), Scopus, The ICI Journals Master List (Copernicus), Directory of Open Access Journals (DOAJ), Open Academic Journals Index (OAJI), Georef, MIAR, EBSCO and Zoological Record.

The Bulletin of the Mineral Research and Exploration is published in three issues in a year. Each bulletin is printed in Turkish and English languages as two separate issues. The English and Turkish issues of the "Bulletin of the Mineral Research and Exploration" can be obtained from "BDT Department" free of charge, either directly or ordered by adding postage fee from the correspondence address. Typesetting and printing operations are carried out and followed by the Publication Service of the Scientific Documentation and Publicity Department. Typesetting and Print Review: Yaşar ÖZKAN, Tuğba UĞUR AYDIN. e-mail: bdt@mta.gov.tr

The section of "notes to the authors", format, copyright and other information can be obtained from www.mta.gov.tr as PDF files.

Printed Date: 07.12.2020
Printing House: Kuban Matbaacılık - İvedik Organize Sanayi Matbaacılar Sitesi 1514. Sokak No: 20 Phone: 0312 395 2070 Fax: 0312 395 3723 www.kubanmatbaa.com
Periodical
ISSN: 0026-4563
E-ISSN: 2651-3048

Bulletin of the Mineral Research and Exploration

http://bulletin.mta.gov.tr

First Turolian findings in the Neogene sequence of Denizli Basin (SW Anatolia) and its regional palaeobiogeographic significance

Adil DOĞAN[a*], Serdar MAYDA[b] and M. Cihat ALÇİÇEK[c]

[a]*General Directorate Mineral Research and Exploration, 2nd Central Anatolian Regional Directorate, Konya, Turkey*
[b]*Ege University, Department of Biology, İzmir, Turkey*
[c]*Pamukkale University, Department of Geology, Denizli, Turkey*

Research Article

Keywords:
Terrestrial Neogene, Vertebrate, Turolian, Denizli, Western Anatolia.

Received Date: 20.07.2019
Accepted Date: 25.11.2019

ABSTRACT

The large fossil vertebrates obtained from the alluvial flood-plain deposits of the Kolankaya formation are determined as *Skoufotragus laticeps* (Andree, 1926) and *Hipparion brachypus* (Hensel, 1862), as representative elements of palaeomammal faunas spanning from the eastern Mediterranean to Iranian domains during the late Miocene (early-middle Turolian, MN11-12). These first Turolian records from the basin fill succession bear importance on reconstruction for the palaeobiogeographic diversity of relevant taxons as well as admit of interbasinal stratigraphic correlation for the Western Anatolian terrestrial Neogene basins.

1. Introduction

The Anatolian peninsula has a key position for migration and distribution of vertebrate groups due to its geographic location between Asia, Africa and Europe. Therefore, the rich fossil content of the terrestrial Neogene basins of Anatolia is of great importance in understanding inter-continental faunal changes and biodiversity (Sickenber and Tobien, 1971; Saraç, 2003; Alçiçek, 2010; Alçiçek et al., 2019; Krijsgman et al., 2019). Although there are already known vertebrate fossil records in the Neogene sequence of the Denizli Basin (Saraç, 2003), yet there is no record of Turolian time. On the other hand, the Turolian vertebrate fossil records are already known in many localities around the Denizli Basin such as Asarlık (Alçiçek et al., 2012, 2019; Alçiçek and Alçiçek, 2014), Mahmutgazi (Sickenberg et al., 1975; Pickford and Ertürk, 1979; Köhler, 1987; Saraç, 2003; Pickford, 2016; Geraads, 2017), Sazak (Saraç, 2003; Tuna, 1999), Elmalıyurt (Saraç, 2003; Alçiçek et al., 2005, 2006, 2019); Kemiklitepe (Şen et al., 1994; Saraç, 2003; Xafis et al., 2020), Karabeyli (Seyitoğlu et al., 2009), Karamusalar (Alçiçek, 2007; Alçiçek et al., 2019), Şerefköy (Saraç, 2003; Kaya et al., 2012; Mayda, 2014), Özlüce (Saraç, 2003; Alpagut et al., 2014; Mayda, 2014).

In this study, the presence of regional inter-basinal faunal connectivity and migration routes have been shown with support of the first Turolian vertebrates found in the Denizli Neogene sequence for the first time. These findings, which fill an important gap for a more detailed understanding of Turolian palaeobiogeography in Anatolia, also enable regional stratigraphic correlation among the basins.

2. Geological Setting

Since the Miocene, the western Anatolia has been consisted of horst-graben system driven by the

Citation info: Doğan, A., Mayda, S., Alçiçek, M. C. 2020. First Turolian findings in the Neogene sequence of Denizli Basin (SW Anatolia) and its regional palaeobiogeographic significance. Bulletin of the Mineral Research and Exploration 163, 1-12. https://doi.org//10.19111/bulletinofmre.651620.

**Corresponding author: Adil DOĞAN, adil.dogan@mta.gov.tr*

regional crustal extension and associated normal faults. The metamorphics of the Precambrian-Paleozoic Menderes Massif and tectonically overlying the Mesozoic carbonates and ophiolites of the Lycian Nappes are the basement rock suits. The regional extension was resulted in the subsidence of the Denizli Basin from the beginning of the early Miocene and initiated alluvial, fluvial and lacustrine sedimentation (Şimşek, 1984; Okay, 1989; Sun, 1990; Westaway, 1993; Konak and Şenel, 2002; Koçyiğit, 2005; Kaymakçı, 2006; Alçiçek et al., 2007; figure 1). Westaway (1993) states the Denizli Basin as a graben that subsided continually by the extension of western Anatolia, while Koçyiğit (2005) proposes a short term of compression interrupted the extension. Based on micro-mammal fossils Saraç (2003) attributes an early Miocene age to the oldest basin-fill deposits.

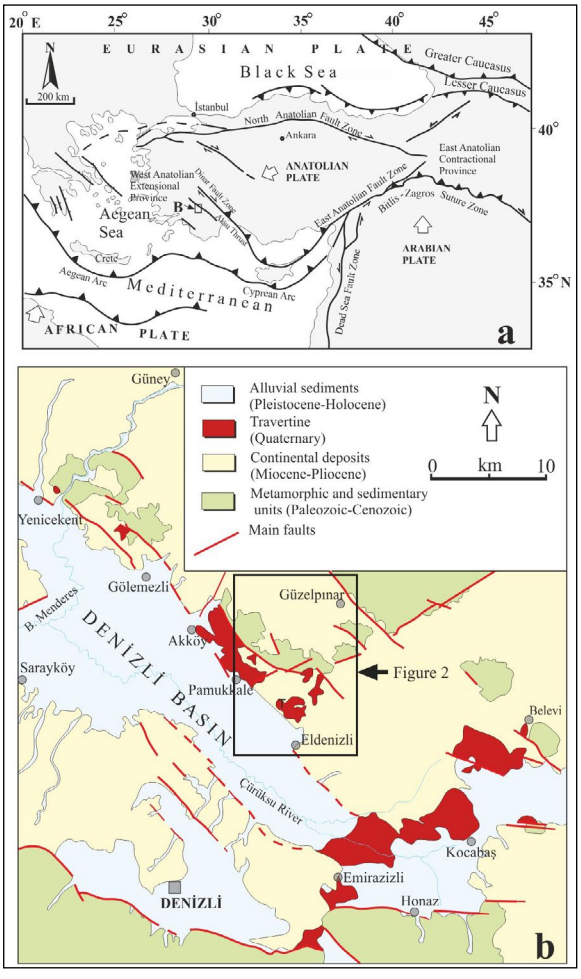

Figure 1- a) Regional tectonic setting of Anatolia (Bozkurt, 2003; Alçiçek et al., 2013; Kaymakçı et al., 2018) and b) geological map of the Denizli Basin (Sun, 1990).

Kaymakçı (2006) states that the extension in the basin was accompanied by transfer faults and documented a late Pliocene age of the basin based on micro-mammal fossils. According to Alçiçek et al. (2007) sedimentation in the basin has been constant until present in control of NW trending faults that limit the basin and accompanied by the climatic and lake-level changes.

In this study, a detailed geological map of the study area to the northeast of Denizli Basin framed in the Denizli M22-a2 sheet has been produced in 1/25.000 scale (Figure 2). The stratigraphy of the basin was elaborated by correlating the findings of the new Turolian fauna in the study area with the previously founded fossils in surrounding basins. The new fossils were found at Gölyeri (UTM 693655/4200295) within the Güzelpınar member of Kolankaya formation which consists of alluvial-fan deposits, tectonically elevated at the northeast margin of the basin.

3. Neogene Stratigraphy of the Denizli Basin

The Neogene units that unconformably overlie the basement in the study area were first described by Şimşek (1984) as the Denizli Group (Figure 3).

3.1. Kızılburun Formation

The unit forming the base of Denizli Neogene succession overlies unconformably the basement rocks. It is consisted of conglomerate at the base and sandstone, siltstone and mudstone alternations towards the top. The upper levels include clayey limestones, siltstones, mudstones and coal lenses. The unit is conformably overlain by lacustrine Sazak formation. The age of the unit was determined as early Miocene by Saraç (2003) according to the micro-mammalian remains (MN5-6).

3.2. Sazak Formation

The unit is mainly composed of lacustrine sediments, consists of limestones, marls, siltstones, claystones and organic mudstones, cherty limestones which contain gypsum, gypsum arenite and organic levels. The unit conformably overlies the Kızılburun formation as well as onlaps the basement units, and overlains by the Kolankaya formation. Saraç (2003) suggests a middle Miocene age for the unit according to the micro-mammalian associations (MN6-8).

3.3. Kolankaya Formation

The dominant lithology of the unit is yellowish-brown, gray coloured sandstones with alterated sandstones, marls and limestones at the base. Thin-medium to thick bedded sandstones are loosely cemented, dispersed and bright mica flakes within them are among the characteristics features in the field. Interlayers of clayey limestone are common in the unit and gypsum layers developed in the marshy environment towards the top. Fluvial deposits reaching

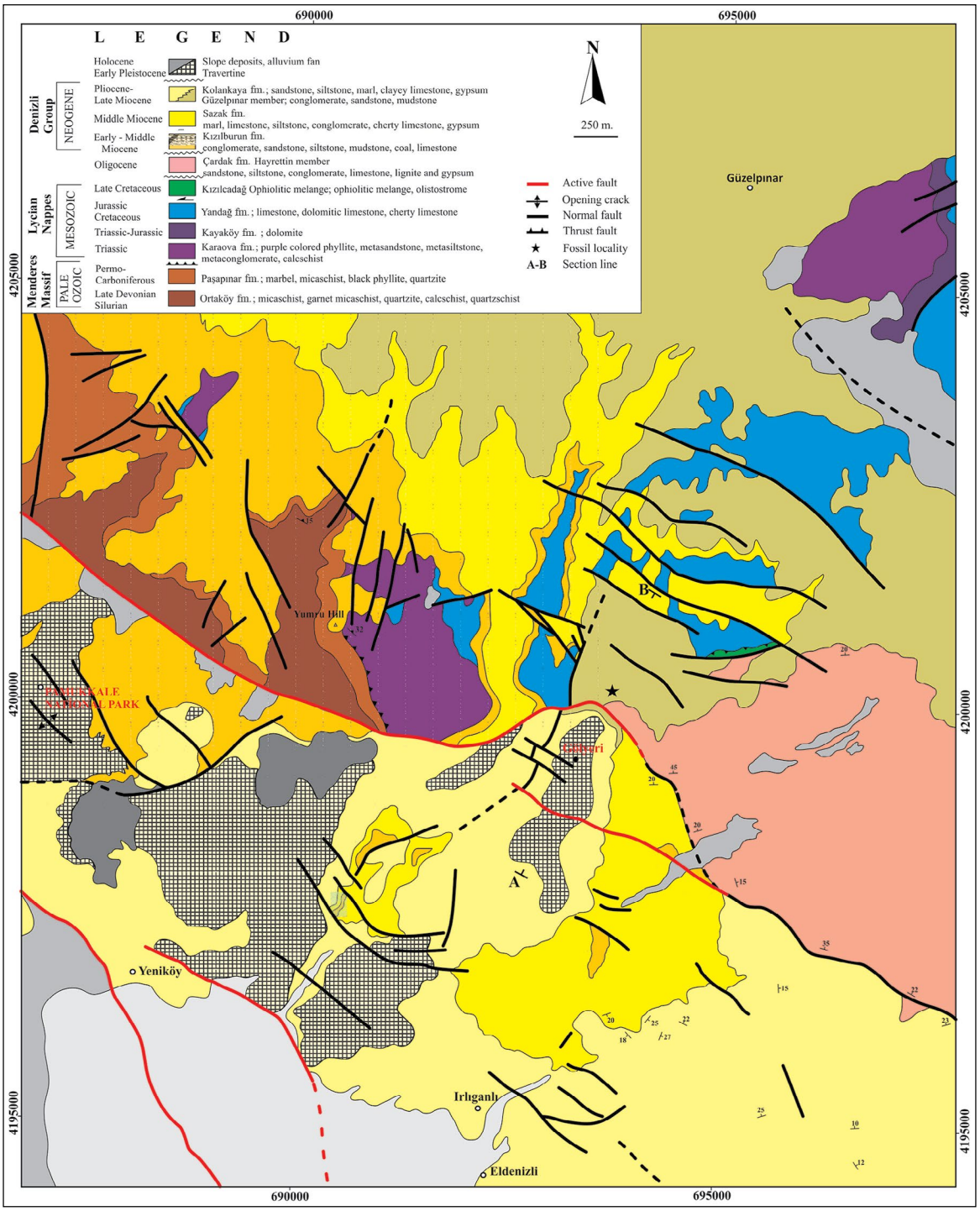

Figure 2- Detailed geological map of the study area (Denizli M22-a2). Based on the unpublished geological map of MTA in 1/25.000 scale compiled by N. Konak, and the active tectonic map of MTA (Emre et al., 2013).

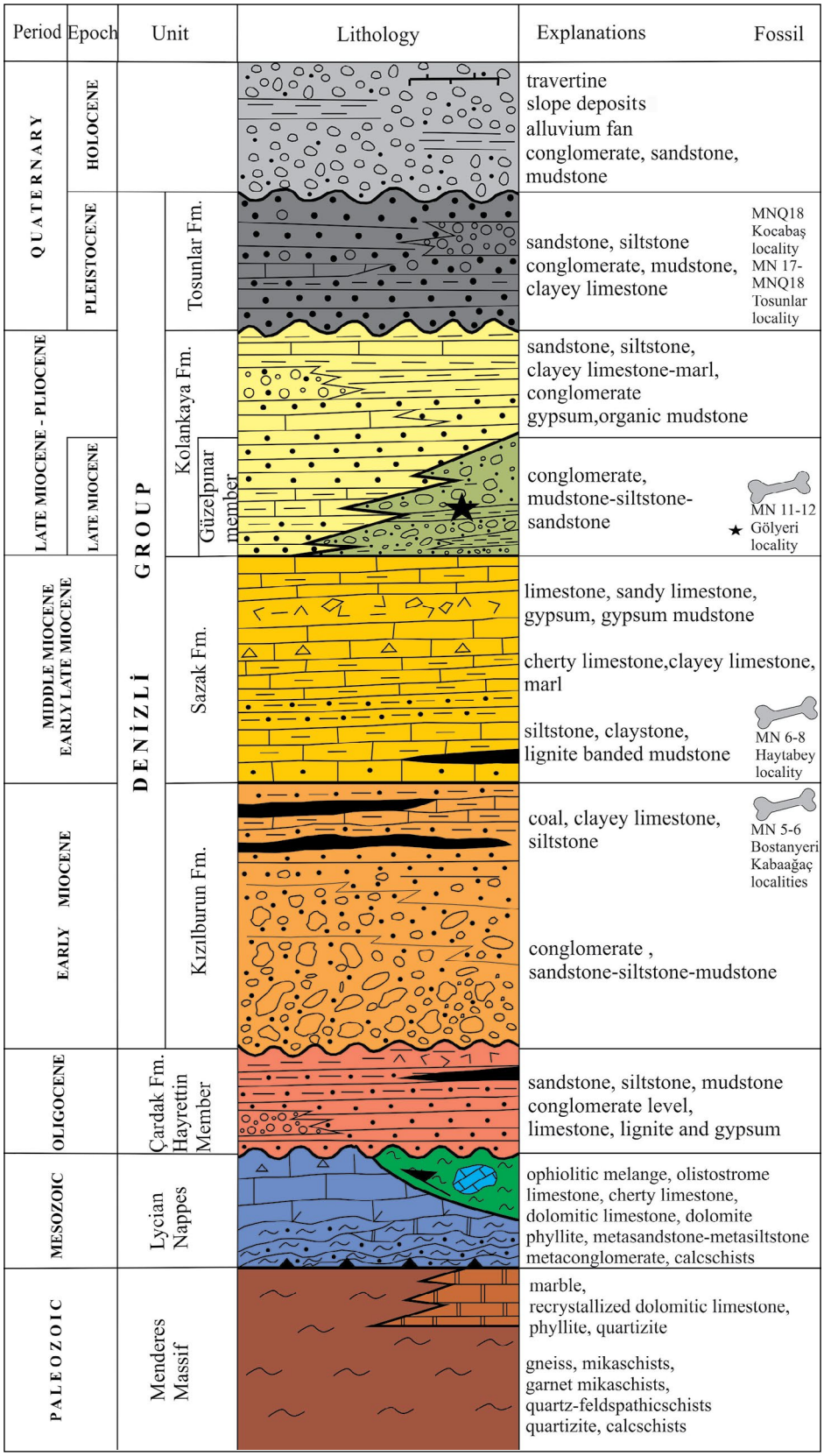

Figure 3- Stratigraphy of the Denizli Basin (Nebert, 1958; Şimşek, 1984; Okay, 1989; Sun, 1990; Alçiçek et al., 2007; Kaymakçı, 2006; Saraç, 2003; Lebatard et al., 2014*a, b*; Boulbes et al., 2014; Alçiçek et al., 2015, Rausch et al., 2019).

into the lacustrine part of the unit from the basin margins form shallow water deltaic successions. Saraç (2003) attributes a late Miocene-late Pliocene age to the unit based on the micro-mammal associations.

3.3.1. Güzelpınar Member

The fossil bearing unit presented in this study is defined as Güzelpınar member within the Kolankaya formation. The unit dominated by red, reddish brown coloured irregular alternation of conglomerate, sandstone, siltstone and mudstone. The pebbles are polygenic and rounded; angular to semi-angular pebbles are also observed. Sandstone-siltstone levels commonly contain caliches. The poorly-sorted, mass-transport dominated unit is mainly composed of alluvial flood deposits (Figure 4). The age of the unit is assigned to late Miocene (early-middle Turolian, MN11-12) according to the vertebrate fossils introduced in this study.

3.4. Tosunlar Formation

The dominant lithology of the unit is composed of yellowish-brownish sandstone and siltstones, conglomerate, mudstone and clayey limestones. It constitutes the uppermost reach of the Neogene sequence of the basin. The age of the unit has been determined as late Pleistocene based on the micro-mammal content of (MN17) by Kaymakçı (2006).

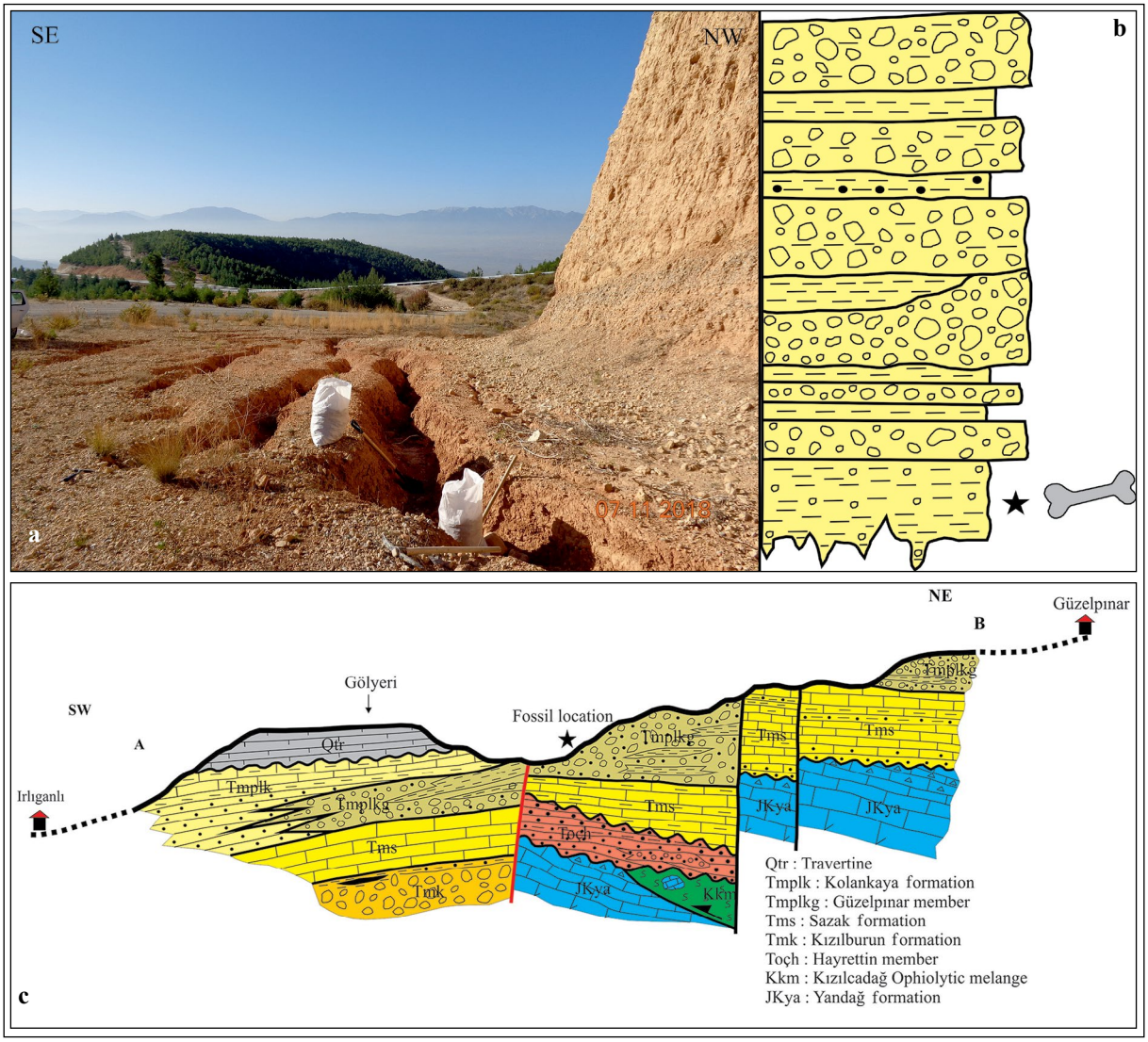

Figure 4- a) Field view of the Turolian fossil locality at Gölyeri, b) stratigraphic section of the fossil bearing unit and c) geological cross section through the fossil locality (not to scale).

The youngest units in the study area are the undifferentiated Quaternary alluvial-fan and scree and travertine deposits.

4. Material and Method

The fossil materials in this study (Figure 5) were found in situ and recorded in the inventory of Ege University Natural History Museum (EUNHM). The odontological study is based on a description of the structural elements of the tooth and comparison with the definitions in the previous studies. In this respect, for the dental terminology of the Bovidae, Gentry et al. (1999) has been followed. The upper teeth are indicated with M (upper case) and the measurements are obtained by measuring the maximum length and perpendicular width with a 0.1 mm precision calliper. All measurements are given in millimeters (mm). For the method and terminology of *Hipparion* metacarpal measurement, Eisenmann et al. (1988) has been followed. Measurements: M10 (maximum distal supra-articular diameter), M11 (maximum distal articular diameter), M12 (maximum diameter of the distal keel), M13 (minimum diameter of the distal lateral conduit), M14 (maximum diameter of the distal medial conduit) have been calculated and the values are depicted graphically in figure 6 and figure 7. Şen et al. (1978) suggested that the sagittal keel development observed in the distal third metapodials of Equidae family is an important morphological character to distinguish between the Vallesian and Turolian *Hipparion* forms, and they first revealed the index which was defined as the keel index. This index is obtained by (M12x100/M13) operation and this value increases from the Vallesian to Turolian. The development of the sagittal keel is directly related to the lateral mobility of horses, and it can be said that horses with larger keel values are runner forms that adapt to more open environments (Eisennmann, 1995; Koufos, 2016).

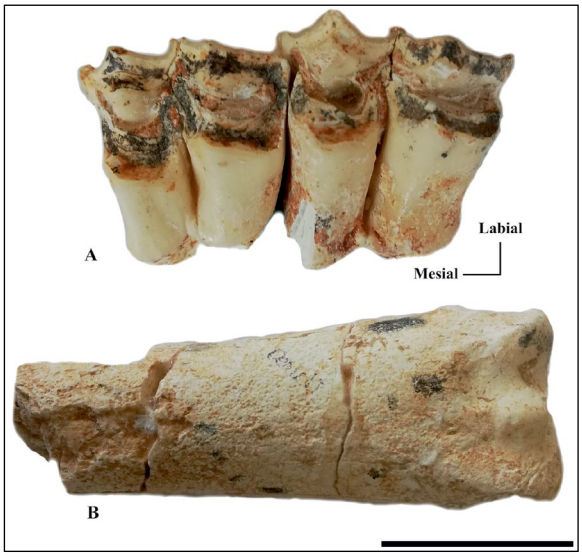

Figure 5- Fossil specimens of Denizli-Gölyeri fauna:
A. *Skoufotragus laticeps* upper letf M^{1-2} (EUNHM-PV-8000)
B. *Hipparion brachypus*: left distal MC3 (EUNHM-PV-8001) (Scale: 5a: 4 cm, 5b: 2 cm)

5. Systematic Paleontology

Ordo : ARTIODACTYLA Owen, 1848

Family : BOVIDAE Gray, 1821

Genus : *Skoufotragus* Kostopoulos, 2009

Type species : *Skoufotragus schlosseri* (Andrée, 1926)
Skoufotragus laticeps (Andrée, 1926)

Age: early-middle Turolian (MN12) (late Miocene**)**

Material: Upper left M^{1-2} (EUNHM-PV-8000) (Figure 5A)

Description: The specimen represents an upper left molar series of a semi-adult individual (length x width (mm): M1:20.3x19.2; M2:23.5x20.1). In both molars, entostyle is not observed with junction of the anterior and posterior medial lobes on the chewing surface. The protocon is angular and pointed, while the hypocon is larger and rounded. The basal pillar is not observed in the middle of the chewing surface of the tooth. Metastyle is the weakest and parastyle is the most developed style. M2 is larger than M1 and the proximal of the tooth is wider than its distal. Parastyle and mesostyle are equally developed.

Correlation/Comparison: 'Protoryxoid' bovids have been recorded in the SE Mediterranean region from the late-middle Miocene onwards (Gentry, 2000; Kostopoulos and Karakütük, 2015). During the late Miocene, especially in Anatolia, Greece and its environs, the group was widespread and many taxa co-exist in the same age. The taxonomy of the genera

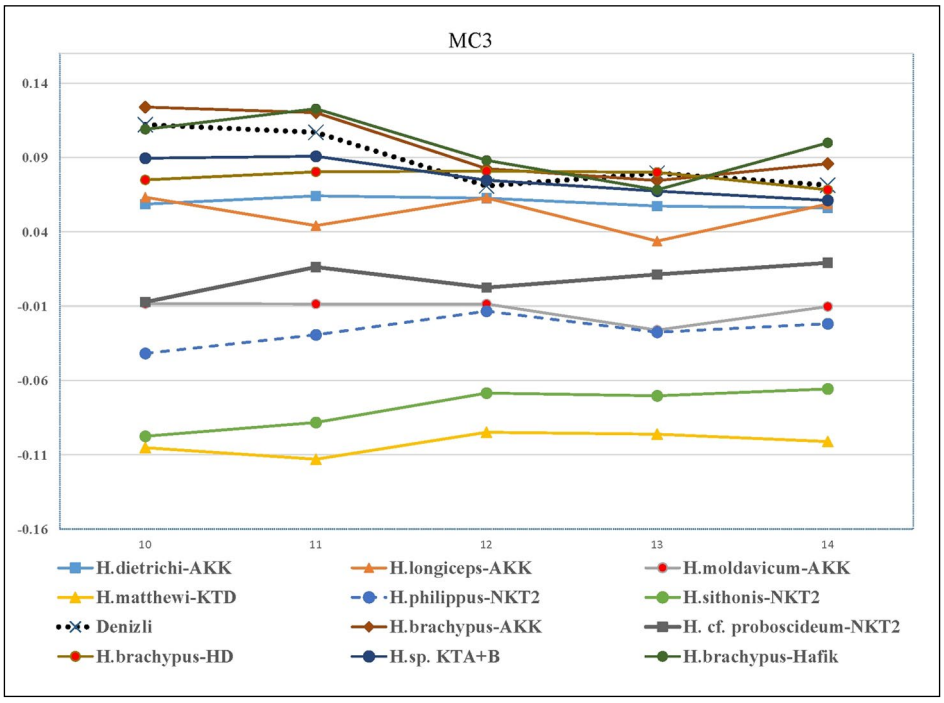

Figure 6- The logarithmic comparison diagram of the Denizli-Gölyeri fauna and various late Miocene *Hipparion* species presented by Hristova et al. (2003), Koufos and Kostopoulos (1994) and Koufos and Vlachou (2005) (Standard: *H. mediterraneum*, Pikermi-Greece, Koufos 1987). The M10-M14 measurements are compared with the findings by Hristova et al. (2003), Koufos and Kostopoulos (1994) and Koufos and Vlachou (2005).

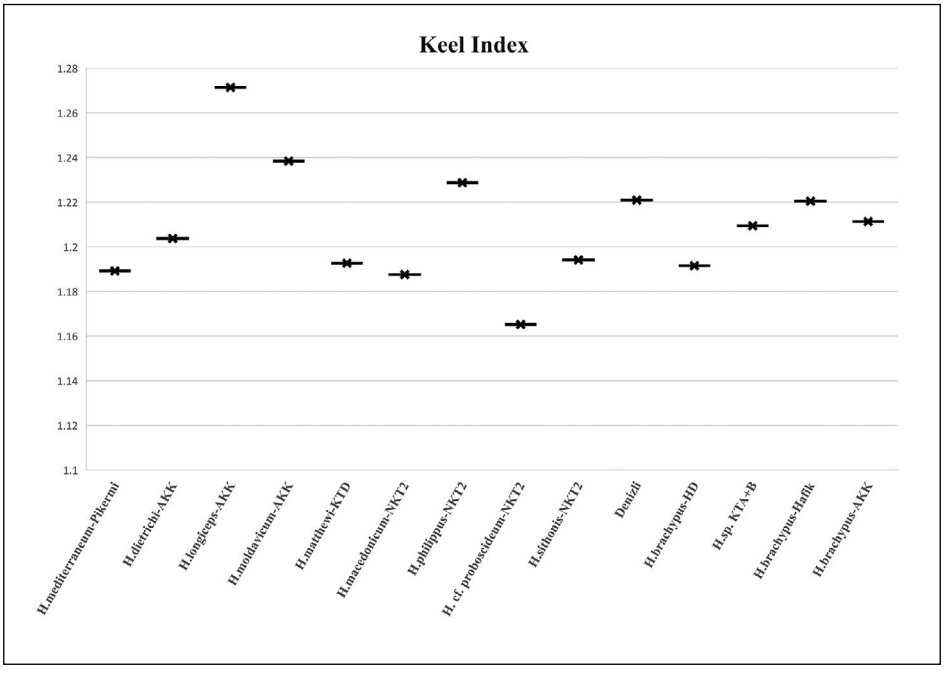

Figure 7- The MC3 keel index diagram including Denizli-Gölyeri fauna and various late Miocene Hipparion species presented by Hristova et al. (2003), Koufos and Kostopoulos (1994) and Koufos and Vlachou (2005).

involved was revised by Kostopoulos (2009), who suggested replacing the problematic *Pachytragus* by the new name *Skoufotragus*, keeping *Protoryx* only for *Protoryx carolinae* and *Pr. capricornis*. In Anatolia *Skoufotragus* is recorded in the localities of Kınık (*Skoufotragus sp.,* late Miocene, MN12) (Köhler, 1987), Kemiklitepe-A (*S. laticeps,* late Miocene, MN11) (Bouvrain, 1994), Akkaşdağı (*S. schlosseri,* late Miocene) MN12) (Kostopoulos, 2009) and Şerefköy-2 (*S.* cf. *schlosseri*, late Miocene, MN12) (Kostopoulos and Karakütük, 2015). In addition, this genus has been recorded in Greek (Samos, Kryopigi) (Kostopoulos, 2009; Lazaridis et al., 2018) and Iranian (Maragheh) localities (Kostopoulos and Bernor, 2011).

The Gölyeri specimen is similar to *S. laticeps* morphologically (absence of entostylid, narrow protocon in M1, relatively high hypsodonty (M1:102, M2:110 mm height/width) and biometrically, and larger than *S. schlosseri* and *S. zemalisorum* samples from neighbouring localities (Kostopoulos, 2009; Kostopoulos and Bernor, 2011).

Ordo : PERISSODACTYLA Owen, 1848

Family : EQUIDAE Gray, 1821

Genus : *Hipparion* de Christol, 1832

Hipparion brachypus Hensel, 1862

Age: early-middleTurolian (MN12) (late Miocene**)**

Material: Left distal metacarpal 3 (MC3) (EUNHM-PV-8001) (Figure 5B) (M10: 43.57, M11: 41.15; M12: 31.5; M13: 25.8; M14: 28.53

Description: The sample is a distal part of a large equid metacarpal. It is highly compatible with *H. brachypus* samples in size (Figure 6). In addition, the keel index (M12×100/M13) (Staesche and Sondaar, 1979; Şen et al., 1978, Eisenmann et al., 1988) value is compatible with *H. brachypus* values known from Anatolia and nearby regions (Akgün et al., 2000; Kaya et al., 2012) (Figure 7).

In Anatolia, large forms of late Miocene Equidae findings were grouped under *H. brachypus* species. To date, these findings are known in the localities of Kemiklitepe-A (late Miocene, MN11) (Koufos and Kostopoulos, 1994), Akkaşdağı (late Miocene, MN12) (Koufos and Vlachou, 2005), Şerefköy-2 (late Miocene, MN12) (Kaya et al., 2012) and Sivas-Hafik (late Miocene, MN12) (Akgün et al., 2000) (Figure 8). The species is also present in the late Miocene localities of Greece (Samos, Pikermi) (Koufos and Vlachou, 2005; Vlachou and Koufos, 2009), Bulgaria (Hadjidimovo, Kalimanci) (Hristova et al., 2003) and Iran (Maragha) (Bernor et al., 2016). The relatively short and coarse metapodials suggest that this species was adapted to living in more confined paleo-environments (Koufos and Vlachou, 2005; Vlachou and Koufos, 2009).

6. Discussion and Conclusions

The mammalian fossils known in the Neogene succession of the Denizli Basin have shown that the region is an important migration route for many terrestrial taxa during the Neogene period. In this study, the Turolian stage is defined for Denizli Basin for the first time in the regional paleobiogeographic context. These fossils are located in the Güzelpınar member which is composed of alluvial fan deposits and defined during this study within the Kolankaya formation which is tectonically uplifted on the northeastern margin of the basin. The Gölyeri vertebrate fossil fauna is composed of taxa within the Anatolia and Greco-Iranian bioprovince extending from Greece to Iran throughout the late Miocene (MN11-12, early-middle Turolian). Similar taxa are known in the context of Turolian faunas from Asarlik, Mahmutgazi, Sazak, Elmalıyurt (Pırnaz), Kemiklitepe and Karabeyli, Şerefköy, Özlüce and Karamusalar localities around Denizli Basin. Although the Gölyeri fauna contains a small number of specimens, it is of particular importance in terms of the stratigraphic correlation between the basins and the understanding of regional paleobiogeographic distributions as the first Turolian evidence in the Denizli Basin.

Acknowledgement

This study was framed within the Paleoseismology Research Project of Turkey supported by General Directorate of Mineral Research and Exploration, Directorate of Geology Research Department with grant number of 2018-30.14.05 We would like to thank the project director Hasan Elmacı, S.M. was supported by Ege University, İzmir (research projects:

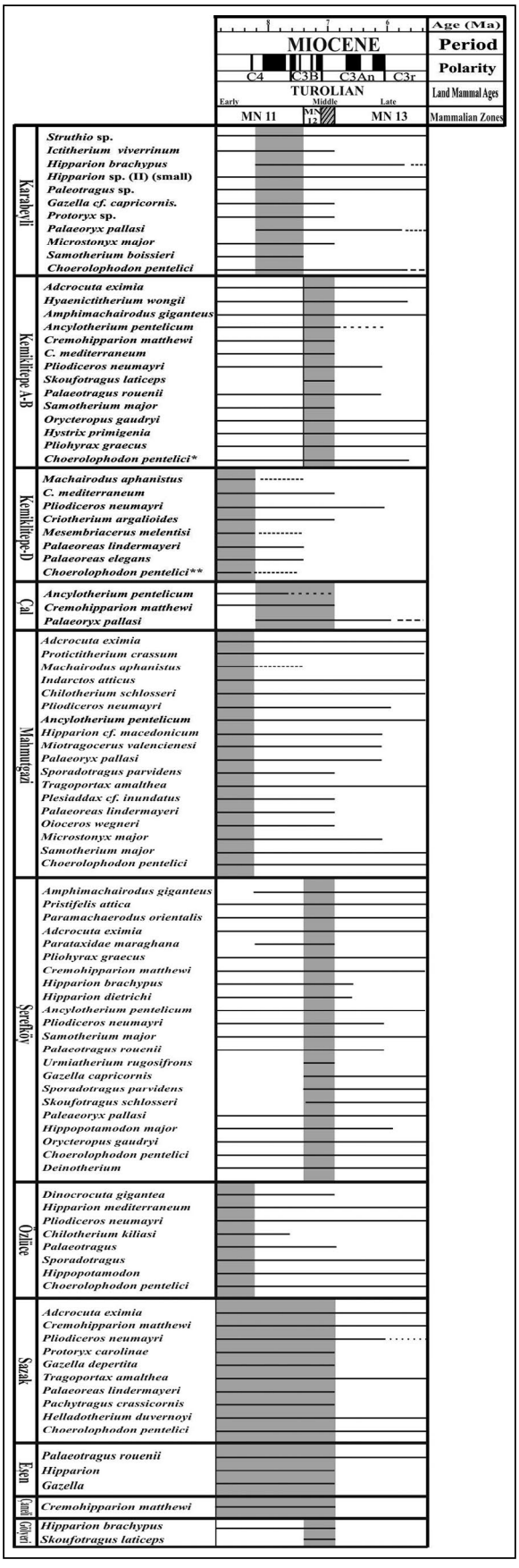

Figure 8- Biostratigraphic distribution and correlation of Turolian localities known in western Anatolia. Karabeyli (Seyitoğlu et al., 2009), Kemiklitepe (Şen et al., 1994; Saraç, 2003; Xafis et al., 2020), Çal-Asarlık (Alçiçek et al., 2012, Alçiçek and Alçiçek, 2014, Alçiçek et al., 2019), Mahmutgazi (Sickenberg et al., 1975; Pickford and Ertürk, 1979; Köhler, 1987; Saraç, 2003; Pickford, 2016; Geraads, 2017), Şerefköy (Saraç, 2003; Kaya et al., 2012; Mayda, 2014), Özlüce (Saraç, 2003; Alpagut, et al. 2014; Mayda, 2014), Sazak (Saraç 2003, Oruç, 2009, Tuna, 1999, Kaya, 1993), Eşen-Karamusalar (Alçiçek, 2007; Alçiçek et al., 2019), Çameli-Elmalıyurt (Saraç, 2003; Alçiçek et al., 2005, 2006, 2019), Sazak (Saraç, 2003; Tuna, 1999), Gölyeri (in this study).

TTM/001/2010, TM/001/2013, TTM/001/2014, TTM/001/2016, TTM/002/2016) during field and lab works. Constructive comments by T. Tanju Kaya (Ege Univ.) are appreciated. The manuscript was critically read and improved by Dimitris S. Kostopoulos (Aristotle University of Thessaloniki).

References

Akgün, F., Kaya, T., Forsten, A., Atalay, Z. 2000. Biostratigraphic data (Mammalia and palynology) for the late Miocene Incesu Formation in Düzyayla (Hafik-Sivas). Turkish Journal of Earth Sciences 9, 57-67.

Alçiçek, H. 2010. Stratigraphic correlation of the Neogene basins in Southwestern Anatolia: regional palaeogeographical, palaeoclimatic and tectonic implications. Palaeogeography, Palaeoclimatology, Palaeoecology 291, 297-318.

Alçiçek, H., Alçiçek, M.C. 2014. Palustrine carbonates and pedogenic calcretes in the Çal basin of SW Anatolia: Implication on the Plio-Pleistocene regional climatic pattern in the Eastern Mediterranean. Catena 112, 48-55.

Alçiçek, H., Varol, B., Özkul, M. 2007. Sedimentary facies, depositional environments and palaeogeographic evolution of the Neogene Denizli Basin of SW Anatolia, Turkey. Sedimentary Geology 202, 596-637.

Alçiçek, H., Wesselingh, F.P., Alçiçek, M.C. 2015. Palaeoenvironmental evolution of the late Pliocene-early Pleistocene fluvio-deltaic sequence of the Denizli Basin (SW Turkey). Palaeogeograpy, Palaeoclimatology, Palaeoecology 437, 98-116.

Alçiçek, M.C. 2007. Tectonic development of an orogen-top rift recorded by its terrestrial sedimentation pattern: the Neogene Eşen Basin of Southwestern Anatolia, Turkey. Sedimentary Geology 200, 117-140.

Alçiçek, M.C., Kazancı, N., Özkul, M. 2005. Multiple rifting pulses and sedimentation pattern in the Çameli Basin, Southwestern Anatolia, Turkey. Sedimentary Geology 173, 409-431.

Alçiçek, M.C., Ten Veen, J.H., Özkul, M. 2006. Neotectonic development of the Çameli Basin, Southwestern Anatolia, Turkey. In: A. H. F. Robertson, D. Mountrakis (Eds.), Tectonic Development of the Eastern Mediterranean Region. Geological Society London Special Publication 260, 591-611.

Alçiçek, M.C., Mayda, S., Alçiçek., H. 2012. Faunal and palaeoenvironmental changes in the Çal Basin, SW Anatolia: Implications for regional stratigraphic correlation of late Cenozoic basins. Comptes Rendus Geoscience 344, 89-98.

Alçiçek, M. C., Brogi, A., Capezzuoli, E., Liotta, D., Meccheri, M. 2013. Superimposed basin formation during Neogene- Quaternary extension in SW-Anatolia (Turkey): insights from the kinematics of the Dinar fault zone. Tectonophysics 608, 713-727.

Alçiçek, M.C., Mayda, S., Ten Veen, J.H., Boulton, S.J., Alçiçek, H., Tesakov, A., Saraç, G., Hakyemez, Y., Göktaş, F., Murray, A., Wesselingh, F.P., Jimenez-Moreno, G., Büyükmeriç, Y., Bouchal, J.M., Demirel, F.A., Kaya, T.T., Halaçlar, K., Bilgin, M., Van den Hoek Ostende, L.W. 2019. Reconciling the stratigraphy and sedimentation history of the Lycian orogen-top basins, SW Anatolia. Palaeobiodiversity and Palaeoenvironments 99, 551-570

Alpagut, B., Mayda, S., Kaya, T., Göktaş, F., Halaçlar, K., Kesici, S.D. 2014. Overview of Recent Research on Muğla-Özlüce Mammalian Fossil Locality. 67th Geological Congress of Turkey.15-18 April 2014, Ankara, pp. 732-733.

Bernor, R.L., Ataabadi, M.M., Meshida, K., Wolf, D. 2016. The Maragheh hipparions, late Miocene of Azarbaijan, Iran. Palaeobiodiversity and Palaeoenvironments 96, 453-488.

Boulbes, N., Mayda, S., Titov, V.V., Alçiçek, M.C. 2014. Les grands mammifères pléistocènes des travertins du Bassin de Denizli, Sud-ouest de l'Anatolie, Turquie (The large Upper Villafranchian mammals from the Denizli Basin travertines, Southwest Anatolia, Turkey). Anthropologie 118, 44-73.

Bouvrain, G. 1994. Les gisements de mammifères du Miocène supérieur de Kemiklitepe, Turquie. 9. Bovidae. Bulletin du Muséum national d'Histoire naturelle 16, 175-209.

Bozkurt, E. 2003. Origin of NE-trending basins in Western Turkey. Geodinamica Acta 16, 6 -81

Eisenmann, V. 1995. What metapodial morphometry has to say about some Miocene hipparions. In: E.S. Vrba, G.H. Denton, T.C. Partridge, and L.H. Burckle (eds.), Palaeoclimate and Evolution with Emphasis on Human Origins, Yale University Press. New Haven, 48-162.

Eisenmann, V., Alberdi, M.T., Giuli, C. de., Staesche, U. 1988. Methodology.In: M. Woodburne and P.Y. Sondaar (eds.), Studying Fossil Horses, Brill press. Leiden, 1-71.

Emre, Ö., Duman.T.Y., Özalp, S., Elmacı, H., Olgun, Ş., Şaroğlu, F. 2013. Türkiye Diri Fay Haritası. Maden Tetkik ve Arama Genel Müdürlüğü Özel Yayın Serisi-30. Ankara-Türkiye.

Gentry, A.W. 2000. Caprinae and Hippotragini (Bovidae, Mammalia) in the Upper Miocene. In: Vrba, E. S.; Schaller, G. B. (ed.), Antelopes, Deer, and Relatives. Fossil Record, Behavioral Ecology, Systematics, and Conservation. New Haven, CT, USA: Yale University Press, 65–83.

Gentry, A. W., Rössner, G. E., Heizmann, E.P.J. 1999. Suborder Ruminantia in: Rössner, G. & Heissig, K. (eds.), The Miocene Land Mammals of Europe, Verlag Dr. F. Pfeil, s. 225-249.

Geraads, D. 2017. late Miocene large mammals from Mahmutgazi, Denizli province, Western Turkey. Neues Jahrbuch für Geologie und Paläontologie, Abhandlungen 284, 241-257.

Hristova, L., Kovachev, D., Spassov, N. 2003. Hipparion brachypus Hensel, 1862 from Hadjidimovo, southwestern Bulgaria (late Miocene). Dokladi na Bulgarskata Akademiya na Naukite 56, 77-84.

Kaya, T. 1993. Late Miocene Perissodactyla from Sazak (Kale-Denizli). Bulletin of the Mineral Research and Exploration 115, 23-31.

Kaya, T., Mayda, S., Kostopoulos, D., Alçiçek, M. C., Merceron, G., Tan, A., Karakütük, S., Giesler, A. K., Scott, S. S. 2012. Şerefköy-2, a new late Miocene mammalian locality from the Yatağan formation, Muğla, SW Turkey. Comptes Rendus Palevol 11, 5-12.

Kaymakçı, N. 2006. Kinematic development and paleostress analysis of the Denizli Basin (Western Turkish): implications of spatial varition of relative paleostress magnitudes and orientations. Journal of Asian Earth Sciences 27, 207-222.

Kaymakçı, N., Langereis, C., Özkaptan, M., Özacar, A. A., Gülyüz, E., Uzel, B., Sözbilir, H., Koç, A. 2018. Paleomagnetic evidences for upper plate response to a STEP fault, SW Anatolia. Earth and Planetary Science Letters 498, 101-115.

Koçyiğit, A. 2005. The Denizli graben-horst system and the eastern limit of the Western Anatolian continental extension: basin fill, structure, deformational mode, throw amount and episodic evolutionary history, SW Turkey. Geodinamica Acta 18, 167-208.

Konak, N., Şenel, M. 2002. Geological map of Turkey in 1/500.000 scale: Denizli sheet. Maden Tetkik ve Arama Genel Müdürlüğü Ankara.

Kostopoulos, D.S. 2009. The late Miocene Mammal Faunas of the Mytilinii Basin, Samos Island, Greece: new collection. 13. Bovidae. Beiträge zur Paläontologie 31, 345-389.

Kostopoulos, D.S., Bernor, R.L. 2011. The Maragheh bovids (Mammalia, Artiodactyla): systematic revision and biostratigraphic-zoogeographic interpretation. Geodiversitas 33, 649-708.

Kostopoulos, D.S., Karakütük, S. 2015. late Miocene bovids from Şerefköy-2 (SW Turkey) and their position withinthe sub-Paratethyan biogeographic province. Acta Palaeontologica Polonica 60, 49–66.

Koufos, G.D. 1987. Study of the Pikermi hipparions. Part I: Generalities and taxonomy. Part II: Comparisons and odontograms. Bulletin Museum Nationale Histoire Naturelle Paris 4e ser. 9 sect. C 2: 197–252, 3: 327–363.

Koufos, G.D. 2016. Hipparion macedonicum revisited: New data on evolution of hipparionine horses from the late Miocene of Greece. Acta Palaeontologica Polonica 61, 519-536.

Koufos, G.D., Kostopoulos, D.S. 1994. The late Miocene mammal localities of Kemiklitepe (Turkey). 3. Equidae. Bulletin du Muséum National d'Histoire Naturelle Paris 4, 16C, 41-80.

Koufos, G.D., Vlachou, T.D. 2005. Equidae (Mammalia, Perissodactyla) from the late Miocene of Akkaşdağı. Geodiversitas 27, 633-705.

Köhler, M. 1987. Boviden des Türkischen Miozäns (Kanozoikum und Braunkohlen der Türkei). Paleontologia i evolució 28, 33–246.

Krijgsman, W., Tesakov, A., Yanina, T., Lazarev, S., Danukalova, G., Van Baak, G.C.G., Agustí, J., Alçiçek, M.C., Aliyeva, E., Bista, D., Bruch, A., Büyükmeriç, Y., Bukhsianidze, M., Flecker, R., Frolov, P., Hoyle, T.M., Jorissen, E.L., Kirscher, U., Koriche, S.A., Oms, O., Rausch, L., Singarayer, J., Stoica, M., Van de Velde, S.V., Titov, V.V., Wesselingh, F.P. 2019. Quaternary time scales for the Pontocaspian domain: interbasinal connectivity and faunal evolution. Earth-Science Reviews 188, 1-40.

Lazaridis, G., Tsoukala, E., Rae, T. C., Gómez-Olivencia, A., Nagel, D., Bartsiokas, A. 2018. Mesopithecus pentelicus from the Turolian locality of Kryopigi (Kassandra, Chalkidiki, Greece). Journal of Human Evolution 121, 128-146.

Lebatard, A.E., Bourlès, D.L., Alçiçek, M.C. 2014*a*. Datation des travertins de Kocabaş par la méthode des nucléides cosmogéniques 26Al/10Be (Dating of the Kocabaş travertines with the 26Al/10Be cosmogenic nuclide method). Anthropologie 118, 34-43.

Lebatard, A.E., Alçiçek, M.C., Rochette, P., Khatib, S., Vialet, A., Boulbes, N., Bourlès, D.L., Demory, F., Guipert, G., Mayda S., Titov, V.V., Vidal, L., de Lumley, H. 2014*b*. Dating the Homo erectus bearing travertine from Kocabaş (Denizli, Turkey) at at least 1.1 Ma. Earth and Planetary Science Letters 390, 8-18.

Mayda, S. 2014. The updated late Miocene mammalian faunas of Özlüce, Şerefköy and Salihpaşalar from Yatağan Basin, Muğla, SW Turkey. 8th International Symposium on Eastern Mediterranean Geology, 13-17 October 2014, Muğla, 176.

Nebert, K. 1958. Die Pliozanen Ablagerungen Von Denizli Und Ihre Bedeutung Fur Die Stratigraphie Des Westanatolischen Sosswasserneogens. Bulletin of the Mineral Research and Exploration 51, 7–20.

Okay, A.İ. 1989. Geology of the Menderes Massif and The Lycian Nappes South of Denizli, Western Taurides, Bulletin of the Mineral Research and Exploration 109, 45-58.

Oruç, S. 2009. The Fossils of Bovidae (Artiodactyla) From Denizli (Sazak) Neogene Mammalian Fauna and Their Biochronological, Paleobiogeographic and Paleoclimatologic Meanings. MSc Thesis. Ege University. İzmir. 154. (unpublished).

Pickford, M. 2016. Hippopotamodon erymanthius (Suidae, Mammalia), from Mahmutgazi, Denizli-Çal Basin, Turkey. Fossil Imprint 72, 183-201.

Pickford, M., Ertürk, Ç. 1979. Suidae and Tayassuidae from Turkey.Bulletin of the Geological Society of Turkey 22,141–154.

Rausch, L., Alçiçek, H., Vialet, A., Boulbes, N., Mayda, S., Titov, V.V., Stoica, M., Charbonier, S., Abels, H.A., Tesakov, A.S., Moigne, A-M., Andrieu-Ponel V., de Franceschi D., Wesselingh F.P., Alçiçek, M.C. 2019. An integrated reconstruction of the early Pleistocene palaeoenvironment of Homo erectus in Denizli Basin (Turkey). Geobios 57, 77-95.

Saraç, G. 2003. Türkiye omurgalı fosil yatakları. Maden Tetkik ve Arama Genel Müdürlüğü Rapor No:10609, 1-208, Ankara (unpublished).

Seyitoğlu, G., Alçiçek, M.C., Işık, V., Alçiçek, H., Mayda, S., Varol, B., Yılmaz, İ., Esat, K. 2009. The stratigraphical position of Kemiklitepe fossil locality (Eşme, Uşak) revised: Implications for the Late Cenozoic sedimentary basin development and extensional tectonics in Western Turkey. Neues Jahrbuch fur Geologie und Palaontologie-Abhandlungen 251, 1-15.

Sickenberg, O., Tobien, H. 1971. New Neogene and Lower Quaternary vertebrate faunas in Turkey. Newsletters on Stratigraphy 1, 51-61.

Sickenberg, O., Becker-Platen, J. D., Benda, L., Berg, D., Engesser, B., Gazlry, W., Heissig, K., Hünermann, K. A., Sondaar, P. Y., Schmidt-Kittler, N., Staesche, K., Staesche, U., Steffens, P., Tobien, H. 1975. Die Gliederung des höheren Jungtertiärs und Altquartärs in der Türkei nach Vertebraten und ihre Bedeutung für die internationale Neogen-Stratigraphie. Geologisches Jahrbuch, Reihe B, 15, 1-167.

Staesche, U., Sondaar, P.Y. 1979. Hipparion aus dem Vallesium und Turolium (Jungtertiar) der Türkei. Geologisches Jahrbuch B, 33, 35-79.

Sun, S. 1990. Denizli-Uşak arasının jeolojisi ve linyit olanakları. Maden Tetkik ve Arama Genel Müdürlüğü Rapor No 9985, 1-92, Ankara (unpublished).

Şen, S., Sondaar, P.Y., Staesche, U. 1978. The biostratigraphic application of the genus Hipparion with special references to the Turkish representatives. Proceedings of the Koninklijke Nederlandse Akademia van Wetenschappen Amsterdam B, 81, 370-385.

Şen, Ş, De Bonis, L., Dalfes, N., Geraads, D., Koufos, G. 1994. Les gisements de mammifères du Miocène supérieur de Kemiklitepe, Turquie: 1. Stratigraphie et magnétostratigraphie. Bulletin du Muséum national d'Histoire naturelle, Paris, 4e sér., section C, 16, 1, 5-17.

Şimşek, Ş. 1984. Denizli-Kızıldere-Tekkehamam-Tosunlar-Buldan-Yenice alanının jeolojisi ve jeotermal enerji olanakları. Maden Tetkik ve Arama Genel Müdürlüğü Rapor No: 7846, 85s, Ankara (unpublished).

Tuna, V. 1999. Late Miocene Artiodactylles (Mammalia) From Yukarısazak Village (Kale-Denizli). Bulletin of the Mineral Research and Exploration, 121, 73-82.

Xafis, A., Mayda, S., Alçiçek, M.C., Kaya, T., Halaçlar, K., Grimsson, F., Nagel, D. 2020. Large giraffid remains (Mammalia, Ruminantia) from the new late Miocene locality Kemiklitepe-E (Western Anatolia, Turkey) Palaeobiodiversity and Palaeoenvironments (https://doi.org/10.1007/s12549-020-00433-4).

Westaway, R. 1993. Neogene evolution of the Denizli region of Western Turkey. Journal of Structural Geology 15, 37-53.

Vlachou, T.D. Koufos, G.D. 2009. Equidae. In: G.D. Koufos and D. Nagel (Eds.), The late Miocene Mammal Faunas of the Mytilinii Basin, Samos Island, Greece: New Collection. Beitrage zur Paläontologie 31, 207-281.

Bulletin of the Mineral Research and Exploration

http://bulletin.mta.gov.tr

Tectonic meaning of the deformation in shallow marine region between Gaziköy-Mürefte (Sea of Marmara) by using seismic reflection data, NW Anatolia

Şule GÜRBOĞA[a*], Aslı Zeynep YAVUZOĞLU[a], Recep GÜNEY[b], Fatma Betül KARCI[a], Ayhan YAVUZOĞLU[a], Özgür TÜRKMEN[a], Pir Çağatay KARTAL[a], Bahri Serkan AYDEMİR[a], Murat EVREN[a], Murat CENK[a], Barbaros ŞİMŞEK[a], Eyyüp ÖZBEK[a], Tuğrul Şükrü YURTSEVER[a], Füsun YİĞİT FETHİ[a], Eşref AYLAN[a] and Uğur Zeki KIRAT[a]

[a]*General Directorate of Mineral Research and Exploration, Marine Research Department, Ankara, Turkey*
[b]*General Directorate of Mineral Research and Exploration, Department of Geophysical Studies, Ankara, Turkey*

Research Article

Keywords:
Gaziköy-Mürefte, Shallow marine deformation, Unconformity surface, North Anatolian Fault System, Sea of Marmara.

ABSTRACT

Within the scope of this paper, seismic reflection and bathymetry studies were carried out in the shallow marine area forming the westernmost part of the Tekirdağ Basin using the R/V Selen Research Vessel within the MTA Marine Research Department. In the study area, ~ 500 km length bathymetry data and ~191 km shallow seismic profiles (41 lines) were collected. By means of the data, tectonic structures and deformation textures of the North Anatolian Fault System (NAFS) in the marine area of Gaziköy were examined. As a result of the processing and interpretation of the seismic sections, compression structures occurring due to the SW rotation of the NAFS in the study area, the morphology of the Ganos depression that formed as a result of faulting and also three different stratigraphic units were distinguished. These units are separated from each other by distinct unconformity surfaces and each unit presents different deformation structures. One of the most significant results obtained from the seismic data is that the unconformity surface that separates the current sediments of the seafloor from the older units is represented by the overlapping structures indicate sea level changes. It has been assessed that this situation occurred as a result of the erosional process developed during sea level fall.

Received Date: 02.08.2019
Accepted Date: 20.08.2020

1. Introduction

The North Anatolian Fault System (NAFS) is a right-lateral strike-slip mega shear structure, which is approximately 1500 km length and has primary importance in the tectonic and morphological shaping of Turkey. With these features, the NAFS contains many characteristic structures and undoubtedly the most important one is the Sea of Marmara, which includes 3 huge basins (Çınarcık, Orta and Tekirdağ basins). The Sea of Marmara is the most remarkable inland sea of the world with an area of approximately 11.350 km^2 separated the Black Sea and Aegean Sea by the Istanbul and Çanakkale Straits, respectively (Figure 1). This geographic importance increases the effect of the North Anatolian fault System (NAFS) tectonically. The NAFS, which is a product of the plate motions around Turkey and surroundings, and shapes the region tectonically, enters the Sea of Marmara from the Izmit Bay in the east and crosses the entire marine area in the E-W direction up to the Gaziköy in the west. The effect of the NAFS, which

Citation info: Gürboğa, Ş., Yavuzoğlu, A. Z., Güney, R., Karcı, F. B., Yavuzoğlu, A., Türkmen, Ö., Kartal, P. Ç., Aydemir, B. S., Evren, M., Cenk, M., Şimşek, B., Özbek, E., Yurtsever, T. Ş., Yiğit Fethi, F., Aylan, E., Kırat, U. Z. 2020. Tectonic meaning of the deformation in shallow marine region between Gaziköy-Mürefte (Sea of Marmara) by using seismic reflection data, NW Anatolia. Bulletin of the Mineral Research and Exploration 163, 13-26. https://doi.org/10.19111/bulletinofmre.784476.

**Corresponding author: Şule GÜRBOĞA, sule.gurboga@mta.gov.tr*

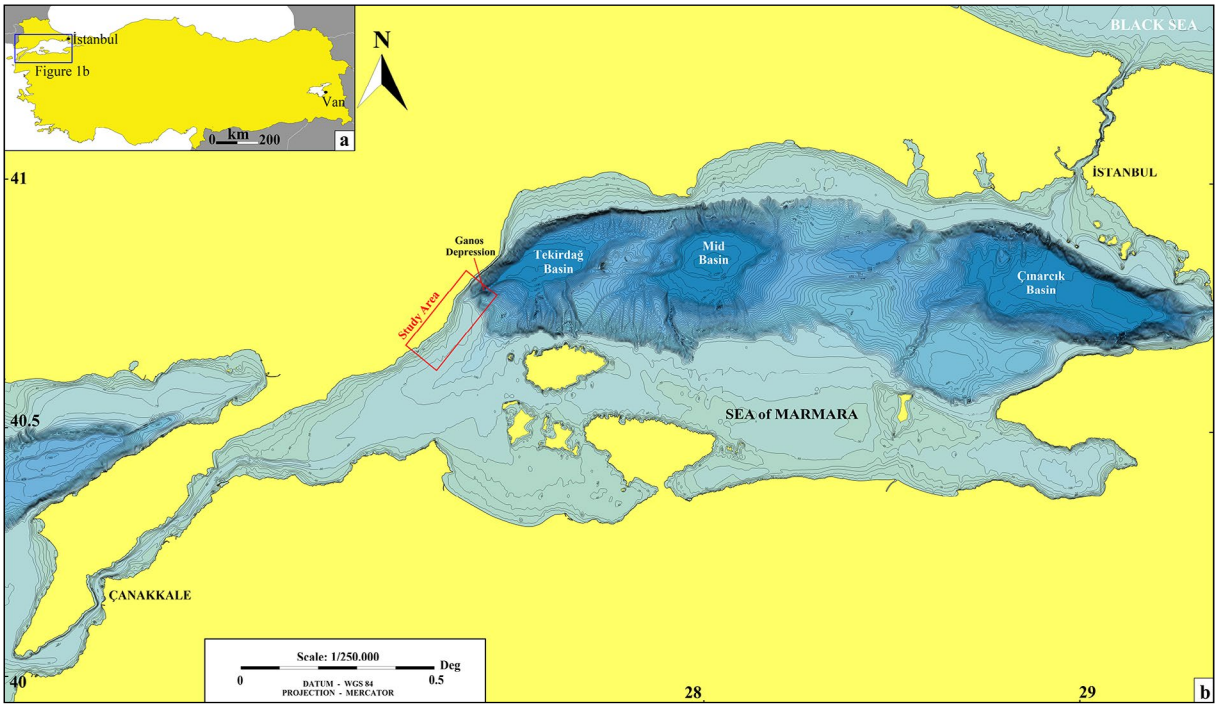

Figure 1- a) Location of the Sea of Marmara in Turkey and b) map showing the study area and bathymetry of the Sea of Marmara. The data was collected by R/V MTA SİSMİK-1 between 1995 - 2003 years under the control of Marine Research Department by using Atlas Deso Echo Sounder and Seisnet Integrated Navigation System (DGPS) with 25 - 50 m resolution of depth and coordinates values. Multibeam data collected from Navigation Hydrography and Oceanography Department (SHODB); MARMARA-2000 (R/V LE SUROIT and R/V ODIN FINDER) with MARMARA-2001 (R/V URANIA) data was used to prepare this map (Yanmaz, 2017).

has a right lateral strike-slip motion, on the formation of the Sea of Marmara has been tried to be explained with different models, and today there is no consensus between them (Pınar, 1943; Ketin, 1969; Kasar et al., 1983; Turgut et al., 1983, 1991; Crampin and Evans, 1986; Barka and Kadinsky-Cade, 1988; Yaltırak, 1995; Wong et al., 1995; Görür et al., 1997; Tüysüz et al., 1998; Armijo et al., 1999, 2005; Sakınç et al., 1999; Okay vd., 2000; Siyako et al., 2000; Aksu et al., 2000; Turgut ve Eseller, 2000; İmren vd., 2001; Gazioğlu et al., 2002; Gökaşan et al., 2003; Yaltırak et al., 2002). These models are not detailed as they are not included in the scope of this study.

The NAFS cuts the Tekirdağ basin, located in the westernmost part of the Sea of Marmara, in the E-W direction and reaches the land area in the near north of Gaziköy (Figure 2). The submarine depression created by the NAFS just before land area is called the Ganos depression. In addition, the fault segment continuing to the terrestrial area is called the Ganos fault (Gutzwiller,1923; Sieberg,1932; Pınar, 1943), and it continues by entering the Aegean Sea from Saros Bay (Yaltırak, 1996). The active faults, which are very dominant in this area, result a quite high earthquake activity (Soysal et al., 1981; Ambraseys and Finkel, 1991, 1995; Guidoboni et al., 1994). In addition to historical earthquakes, the most important earthquake that occurred in the region during the instrumental period was the 9 August 1912 Mürefte-Şarköy earthquake (Mw 7.4). This earthquake affected the Mürefte and Şarköy settlements and was felt very strongly in Tekirdağ, Gelibolu and Çanakkale regions. The damages and loss of life caused by the earthquake are included in an article "Marmara Havzası'nın Hareket-i Arzının Esbabı on 26-27 July 1328 (1912)" written by Doctor Lieutenant M. Sadi on August 28, 1912 (1328). The article also includes the news of Istanbul Newspaper in French, and it is stated that a 400 m long and 5 m deep surface rupture developed in Mürefte village. With the 1912 earthquake, it was determined that tsunamis occurred along the landslides in the Marmara (Altınok vd., 2003). While the earthquakes of 9 August 1912 (Mw 7.4) and 13 September 1912 (Mw 6.8) created some displacements varying between ~ 1.4 and 5.5 m, the amount fault slip (coseismic) and fault segmentation were determined. As a result of evaluating the historical records, the

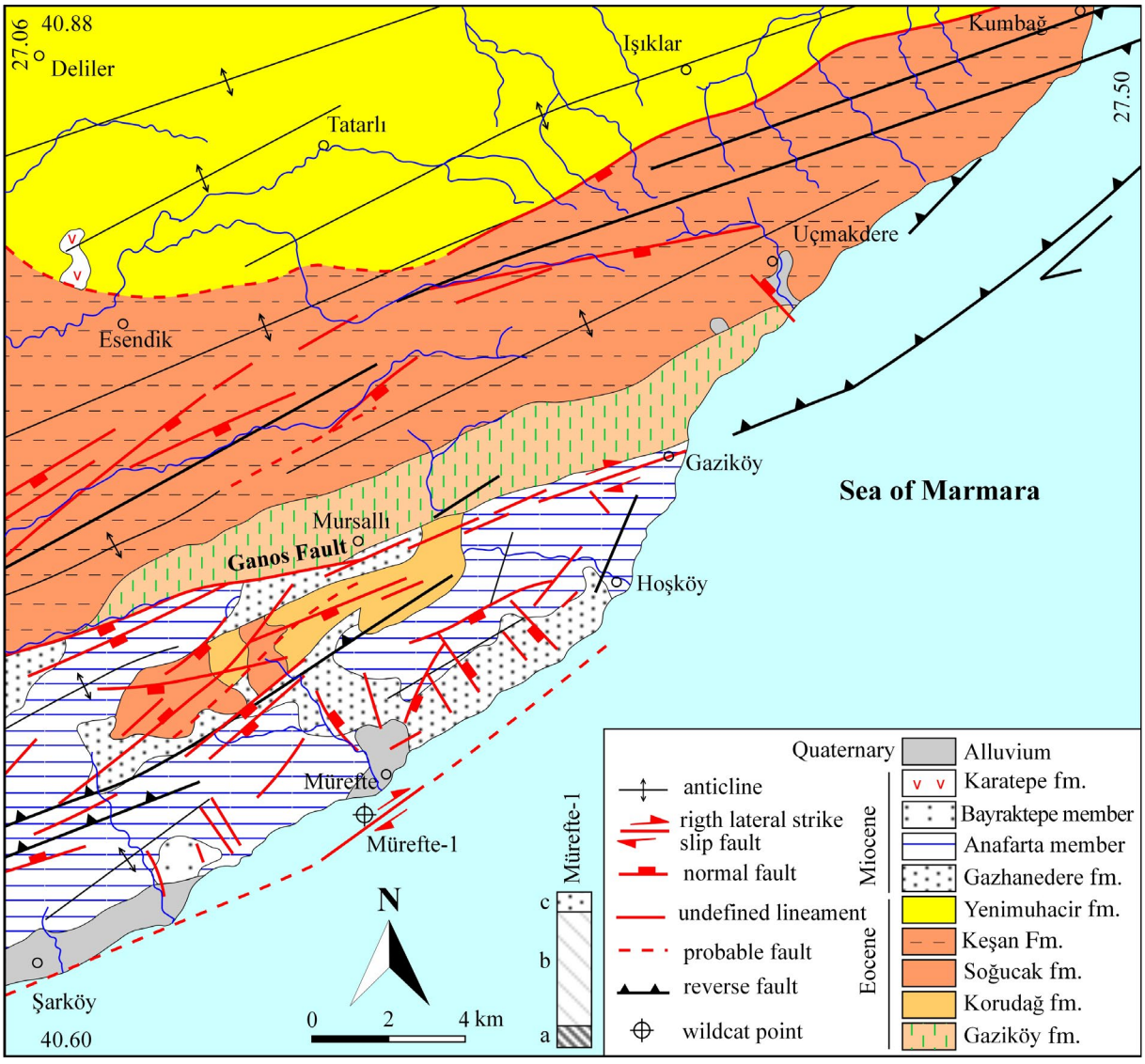

Figure 2- Geological map of the Ganos Fault and its vicinities (Yaltırak, 1996, 2002). the Mürefte-1 offshore wildcat is added in this map (simplified from Yaltırak, 1996). a) Mesozoic units, b) Paleogene units, and c) Gazhanedere formation.

total surface rupture length for two earthquakes was calculated as 150 ± 30 km (Aksoy et al., 2010).

Onshore deformational structures in the previous studies, considering the intensive earthquake activity and the facing of the units from different ages, displays very important evidences of surfacing of NAFS in Thrace region and its deformational imprints for earth sciences. Besides of these onshore studies, there are many researches carried on determining the geological features of the offshore segment of NAFS in the Sea of Marmara. These studies are on geometry and kinematics of NAFS (Tapırdamaz and Yaltırak, 1997; Alpar 1999; Okay et al., 1999, 2000; Halbach et al., 2002; Gürbüz et al., 2000; McClusky et al., 2000; Siyako et al., 2000; Ergin vd., 2000; İmren et al., 2001; Gökaşan et al., 2001, 2002, 2003; Le Pichon et al., 2001, 2003; Rangin et al., 2001, 2004; Armijo et al., 2002, 2005; Alpar and Yaltırak, 2002; Meade et al., 2002; Polonia et al., 2002, 2004; Yaltırak, 2002; Demirbağ et al., 2003), sea level changes and its comparison with Eastern Mediterranean Sea data (Imbrie et al.,1984; Aksoy et al., 1999) etc.

In almost every well cutting section near the study area, three different units have been described (Yaltırak, 1996). From older to younger; number 3 is pre-Miocene base units, number 2 is Miocene deposits and number 1 is late Quaternary to recent sediments. Three units with different ages were determined in

the Mürefte-1 offshore wildcat, which was drilled by TPAO. These units are defined as, Mesozoic (a), Paleogene (b) and Miocene (c) units.

Within the context of this study, determination of the deformation of NAFS, whose onshore and offshore stratigraphic and tectonic features are mostly known, between Gaziköy –Mürefte shallow marine area was aimed. Another aim of this study was to identify the erosional and depositional surfaces created by sea level changes, where the present sea level is very shallow.

2. Stratigraphy and Tectonics of the Study Area

2.1. Stratiraphy

Although there are different stratigraphic designations in the studies carried out in Gaziköy and its surroundings, it is seen that the units present similar stratigraphic sequences. The stratigraphic sequence of the region was simplified and presented as shown in figure 2 by Yaltırak (1996). The sequence package overlying the basic units starts with the Gaziköy Formation (Sümengen et al., 1987; Sümengen and Terlemez, 1991; Siyako, 2006), which contains sandstone, siltstone and silicified tuff series formed by the turbiditic sediments of lower-middle Eocene age and deposited in the deep sea environment (Figure 2). Gaziköy Formation (Şentürk et al., 1998), which is gradually transitive with the formations on it, is covered by the Korudağ formation, which is composed of intercalation of sandstone and claystone, with conglomerate of the upper Eocene (Figure 2). Korudağ formation, which consists of submarine fan deposits, is observed in the southern part of the Ganos Fault in the study area (Yaltırak, 1996). This unit is followed by Soğucak Formation (Holmes, 1961) consisting of upper Eocene aged limestones and the Keşan Formation (Gökçen, 1967), which are turbiditic deposits. Yenimuhacir formation (Şentürk et al., 1998), consisting of upper Eocene-lower Miocene aged claystone, siltstone and sandstone spreading in the drainage area of Anadere, which flows into the sea around Kumbağ (Şentürk et al., 1998), has been eroded and covered uncomformably with younger units (Siyako, 2006).

The middle Oligocene Danişment Formation, which is observed in limited areas in the southern part of the Thrace Region but where coal formations are densely observed in the Thrace basin, consists of sandstone layers containing lignites at different levels (Şentürk et al., 1998). This level is then unconformably covered by the middle-upper Miocene Çanakkale Group, in which there are different members (Gazhanedere Fm, Anafarta and Bayraktepe members). This group, which is unconformably covered by the Karatepe formation, consists of basalts observed in the form of lava flow, generally in the form of black, sometimes brown, massive and resistant agglomerates with calcite in places. These basalts, which show column and flow structures, have augite and olivine crystals and have augite, olivine, magnetite paste and have alkaline properties (Şentürk et al., 1998). According to the K/Ar absolute age determinations of the Karatepe formation, the age is upper Miocene (6-9 Ma) (Şentürk et al., 1998).

The top of the stratigraphic sequence is the Quaternary Marmara Formation, which represents various coastal facies and consists of loosely attached sandstones and beach rocks and tufa deposits. These sediments have been detected both in the vicinity of Mürefte, Marmara Ereğlisi and Uçmakdere on land, and in shallow and partially deep areas of more than 100 m in the sea (Siyako, 2006). The formation, which is unconformable with all the older units on land, is harmoniously located in the deep marine parts and unconformably in the shallow parts. According to radiometric age determinations, it was determined that this precipitation was between 240-40 thousand years on terresterial and 400-24 thousand years on sea areas (Siyako, 2006).

2.2. Tectonics

The Tekirdağ basin, located in the westernmost of the three major basins in the Sea of Marmara, is traversed by the NAFS in an approximately E-W direction. The land part of the fault, which comes ashore from the near north of Gaziköy, is called the Ganos fault. Using the earthquake activities recorded by Boğaziçi University Kandilli Observatory Earthquake Research Institute between 2003-2010, it was aimed to reveal the current behavior of the Ganos Fault (Yıldız et al., 2013). The focal mechanism solutions of 12 earthquakes ($M \geq 3.3$) selected from these events were calculated using three component waveform modeling and inverse methods with numerical analysis method. As a result, although the fault has a dominant right-lateral strike-slip motion,

it has been shown that there are some normal and thrust components due to some local changes (Yıldız et al., 2013). According to the focal mechanisms of the earthquakes obtained as a result of these analysis: in inverse solutions, the largest principal stress axis (σ1) and the smallest principal stress axis (σ3) are in the horizontal and outer arc; strike-slip stress regime is expressed in which the intermediate stress axis (σ2) is in the center and vertical position. Considering the status of the stress axes, it is clearly stated that the Ganos Fault is a right-lateral strike-slip fault that develops under a compression regime in NW-SE direction and is present in local normal faults with transtensional characteristics (Yıldız et al., 2013). This dominant compression direction is also expected to reveal the deformation structures associated with the tectonic regime in the hardened and unconsolidated sediments in the sea. Within the scope of this study, deformation patterns of units of different ages are interpreted with reference to current stress distributions.

3. Material and Methods

In the geophysical survey completed by the R/V MTA Selen Research Vessel in the study area, 41 (191 km) high resolution multi channel seismic and 500 km bathymetry data were gathered (Figure 3). After the data processing of the seismic profiles were completed, seismic profiles of sufficient quality were selected in order to carry out this study, in addition, all bathymetry data were combined and the sea floor morphology was obtained. In this context, the work plan was implemented in two main methods. The first of these methods is shallow seismic data acqusition phase. The seismic data penetration is minimum of 55 m. This situation have great importance for detecting and distinguishing shallow geological unit deformations under the sea floor. Seismic profiles that best represent both the data quality and structures, that will cross the coastline and the NE-trending Gaziköy fault, are evaluated within the scope of this study.

Seismic profiles were planned by creating a grid with one (1) kilometer intervals in a vertical and parallel position to the geological structures as much as possible. The seismic parameters given in table 1 was used during data collection.

Table 1- Seismic acqusition parameter.

Parameter	
Shot interval (m)	6.25
Group interval (m)	3.125
Number of channel	96
Offset (m)	50
Sample rate (ms)	0,5
Air gun	1x10 inch^3

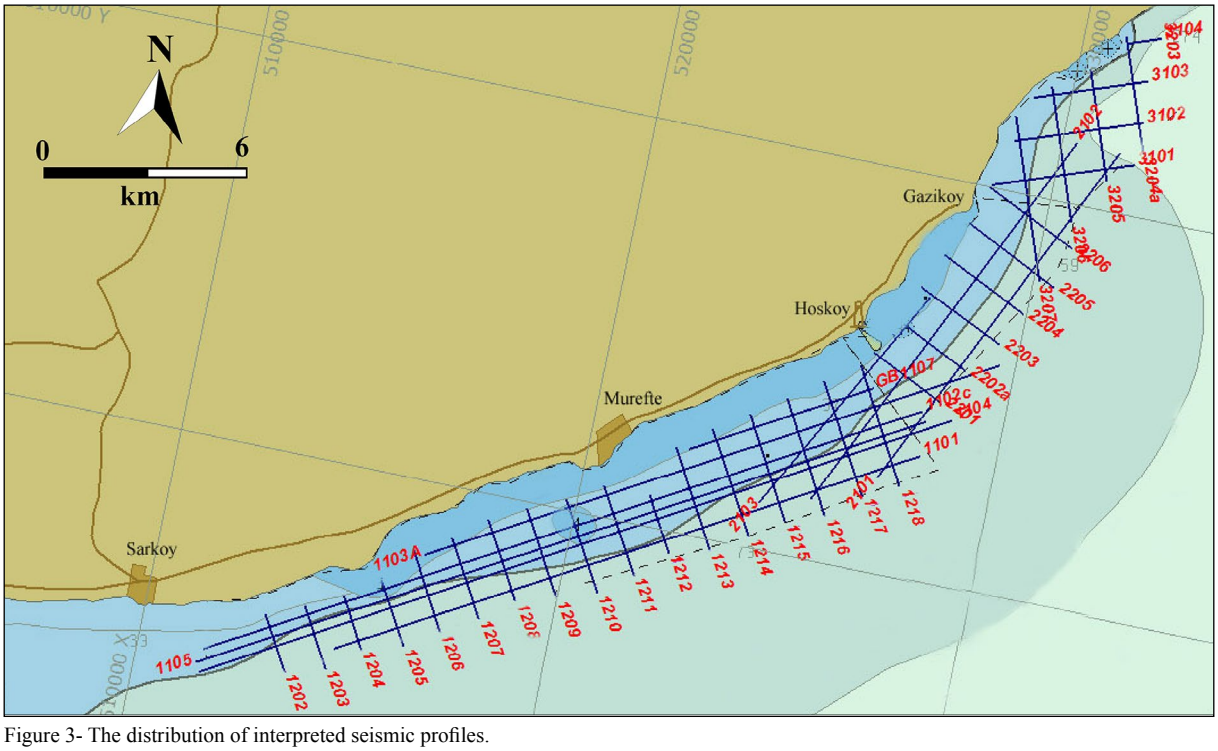

Figure 3- The distribution of interpreted seismic profiles.

Within the scope of this study; The data were processed using Halliburton (Landmark) ProMAX Seismic Processing Software in the MTA Marine Data Processing Laboratory, Department of Marine Research, MTA. A conventional seismic data processing flow was applied. After Kirchhoff time migration step, all seismic sections were converted from time domain (t-x) to depth (x-h) domain by using Dix (1955) interval velocity formula. The second method is to reveal the sea floor morphology within the study area. Bathymetry data of the study area were collected with an ELAC SEABEAM 1050D (30 kHz / 180 kHz) multibeam echosounder and data processing was done with the Hypack Hysweep software. Bathymetry map was prepared in metric system according to WGS84 horizontal datum and UTM Zone 35N (34E-30E) projection system.

As it is apparent in the created bathymetry map, the depth data are mostly compatible with the existing sea maps (navigation maps) (Figure 4). Bathymetric changes in the area (except Gaziköy-Uçmakdere near the shore) range from 10 to 70 m. In a short distance between Gaziköy and Uçmakdere coastal area vertical height difference reach up to 700 m or more. The area with the greatest difference in depth is known as the Ganos pit. The southwestern part of the Ganos depression is also clearly observed on the obtained bathymetry map (Figure 4b). Sharp change in seabed morphology and fault discontinuity are clearly observed in the NW-SSE oriented seismic sections in this area.

4. Seismic Data Interpretation

Within the scope of this study, seismic data were collected along 41 lines in the shallow marine area at the NW of the Sea of Marmara. Active fault traces and seismic stratigraphic data were interpreted from these seismic profiles. 7 seismic sections (Figure 5), which have the potential to provide sufficient data in between Mürefte and southwestern part of Ganos pit, were selected to interpretate soft sediment deformation structures and sediment packets. The geological comments and the information they contain related with these sections are presented in detail.

The stratigraphic equivalence of units a and b, were differentiated in previous studies, is to the unit number 3 in the seismic sections in this study; unit number 2 corresponds to unit c in previous studies (Figure 2). Unit number 1 is defined as current sediments deposited on the continental shelf close the shore.

In this study based on seismic sections, firstly, two longer lines (1101 and 2102) taken parallel to the shore were interpreted and units 1, 2 and 3 were identified in the study carried out. Although the boundary of units 2 and 3 is clearly seen in seismic section 1101 (red border), this boundary has not been determined exactly in seismic section 2102 (Figures 6 and 7). On the other hand, in both sections, the boundary between Miocene-recent units, indicated by green, and sediment overlap structures (red arrows) were observed as a result of the transgression. The common feature seen in both sections is quite a large

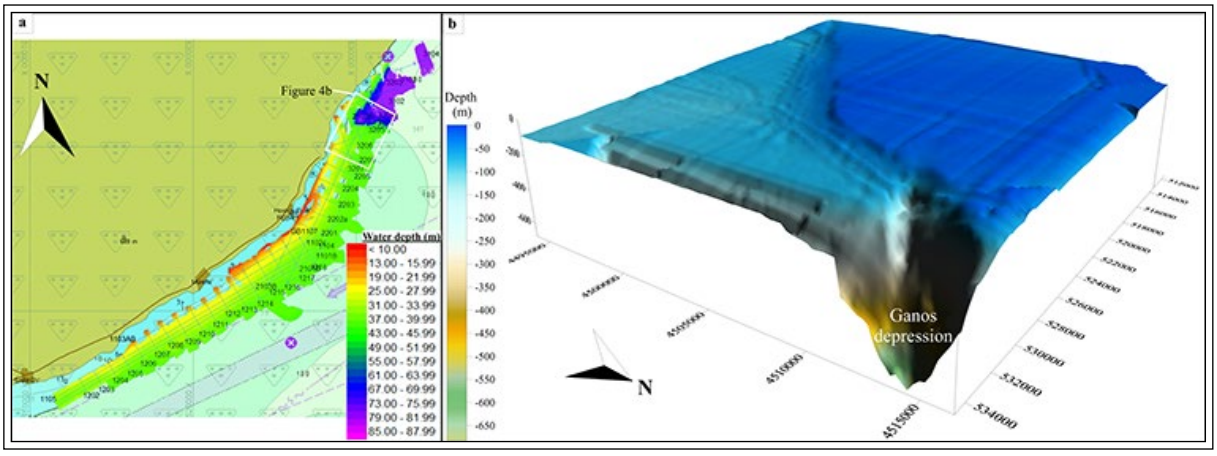

Figure 4- a) Distribution map of bathymetry data collected in the study area and b) 3D view of the area indicated by the white rectangle on figure 4a.

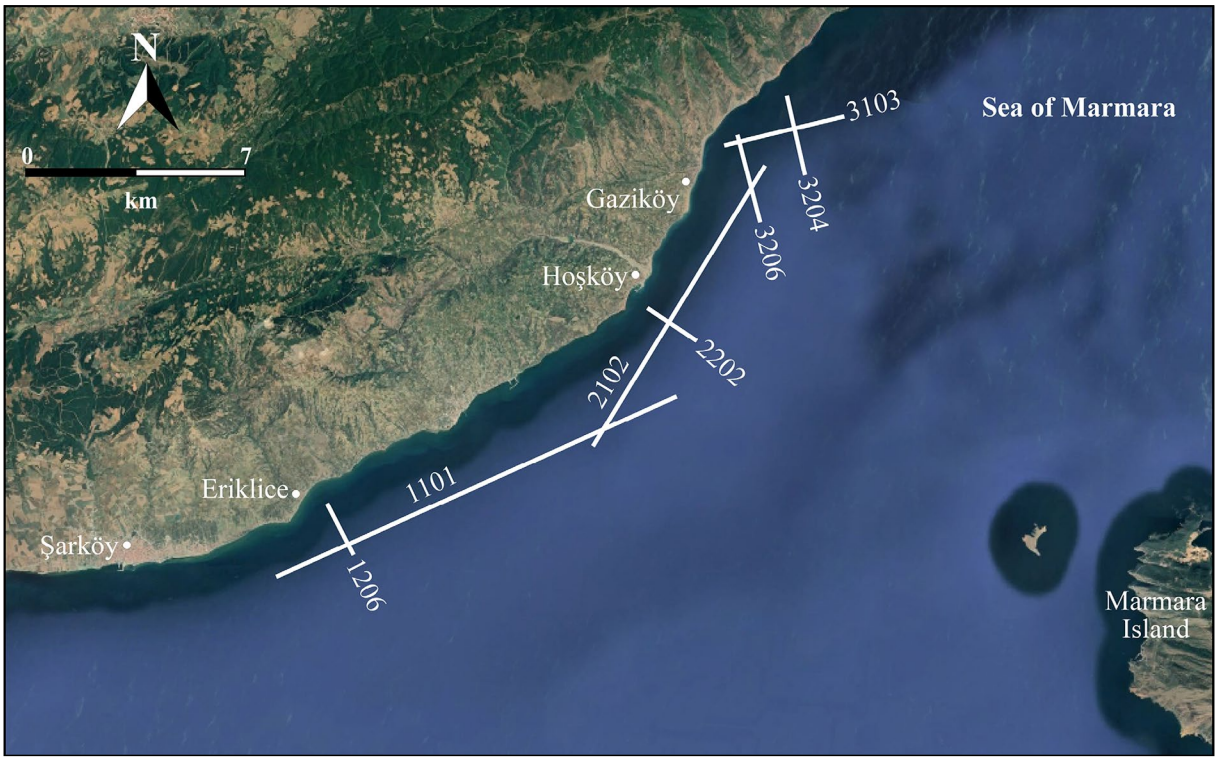

Figure 5- Map showing the locations of interpreted seismic profile.

number of strike-slip faulting structures developed within the older units. These mostly have reverse component and are observed as faulting and folding. The sharp elevation change observed in the NE part of 2101 represents the mostern SW section of the Ganos depression. The Ganos depression forms the SW part of the Tekirdağ basin and clearly shows the deformation texture of the NAFS.

Due to the distortion caused by multiples in section 2101, the boundary between units 2 and 3 could not be clearly distinguished. On the other hand, the boundary between units 1 and 2 and the transcendent structures (red arrows) thought to be connected to sea level could be clearly drawn. In each of the other sections, the boundaries between units 1, 2 and 3 and sediment overflow structures are observed and marked on the

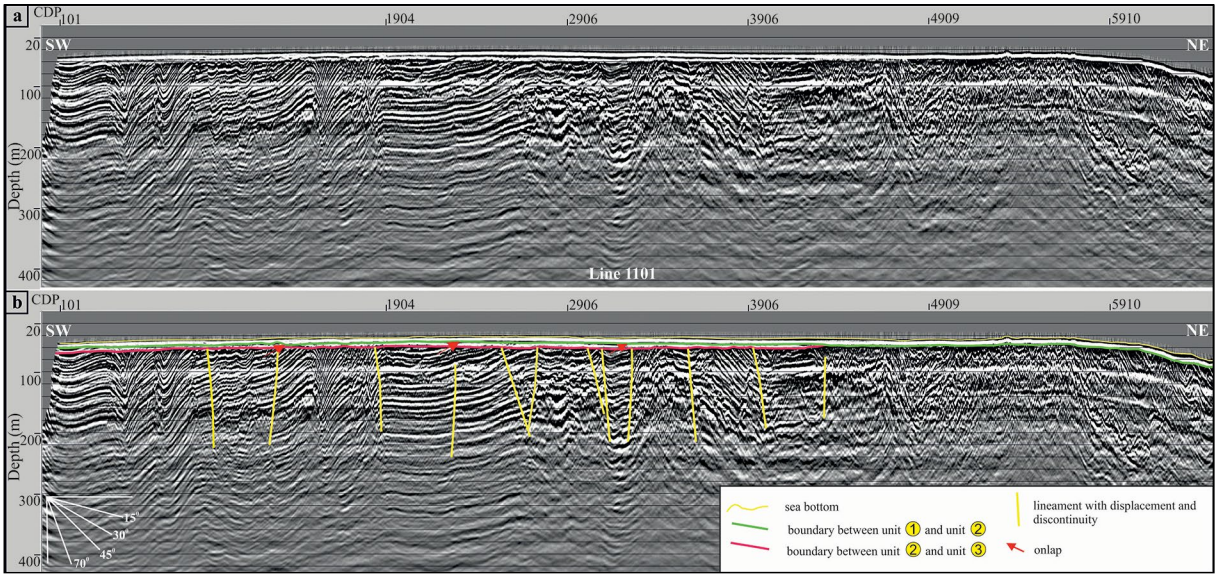

Figure 6- a) Seismic profile 1101 and b) geological interpretation of line 1101.

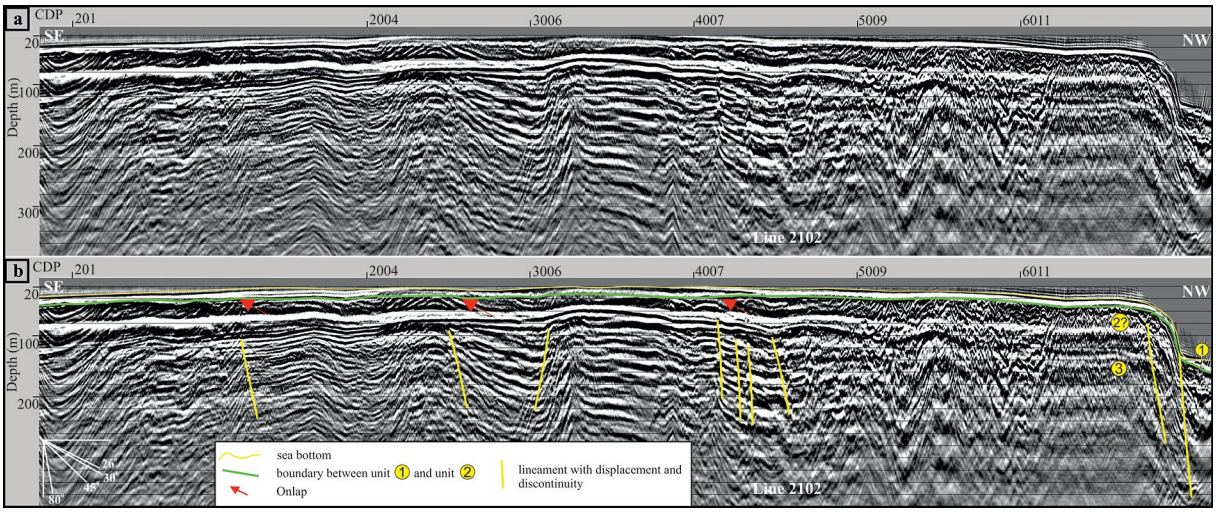

Figure 7- a) Seismic profile 2102 and b) geological interpretation of line 2102.

sections (1206 in figure 8, 2202 in figure 9, 3103 in figure 10, 3204 in figure 11, 3206 in figure12).

In the sections 1101 and 2102, the pre-Miocene units, which are interpreted as 3 units, have undergone extensive deformation. The most important indicator of deformations are faults and folds that observed frequently. The fact that most of these faults are observed only in units number 3 indicates that a tectonic phase quite different from the current tectonic regime was active in this time period. The folds observed in the section 1206 are another finding that supports this conditions (Figure 8). Although the boundary of the units 2 and 3 in the seismic section no. 2202 has not been identified, the slip and folds of the reverse faulting in the 3 unit show the older period

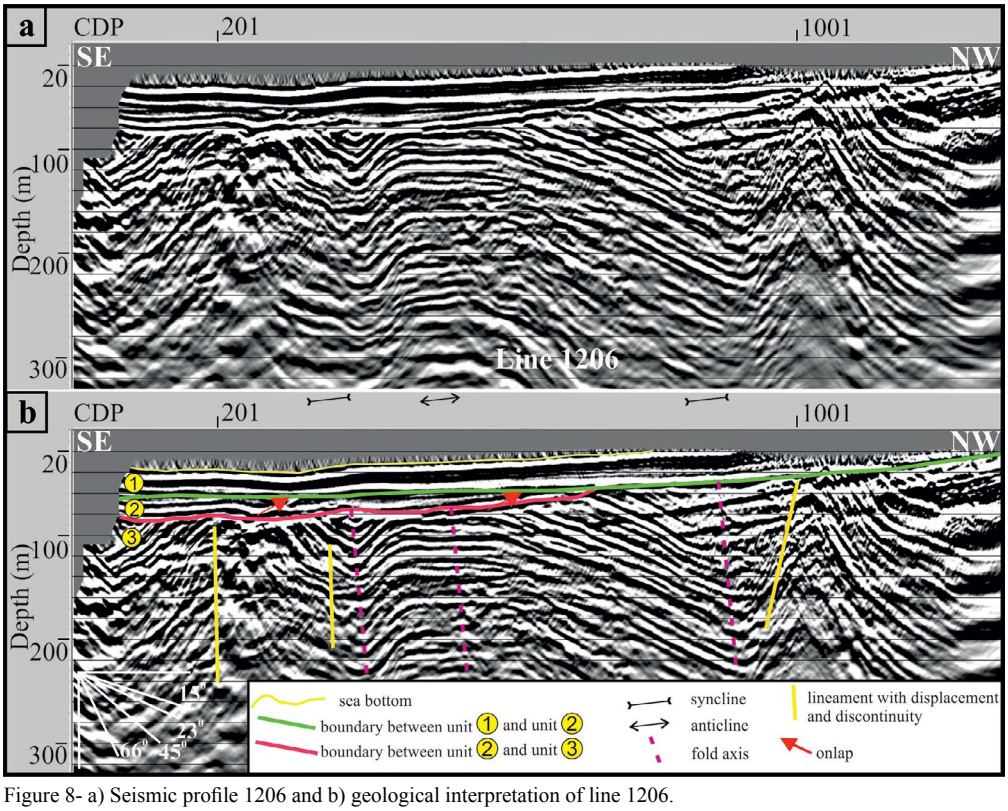

Figure 8- a) Seismic profile 1206 and b) geological interpretation of line 1206.

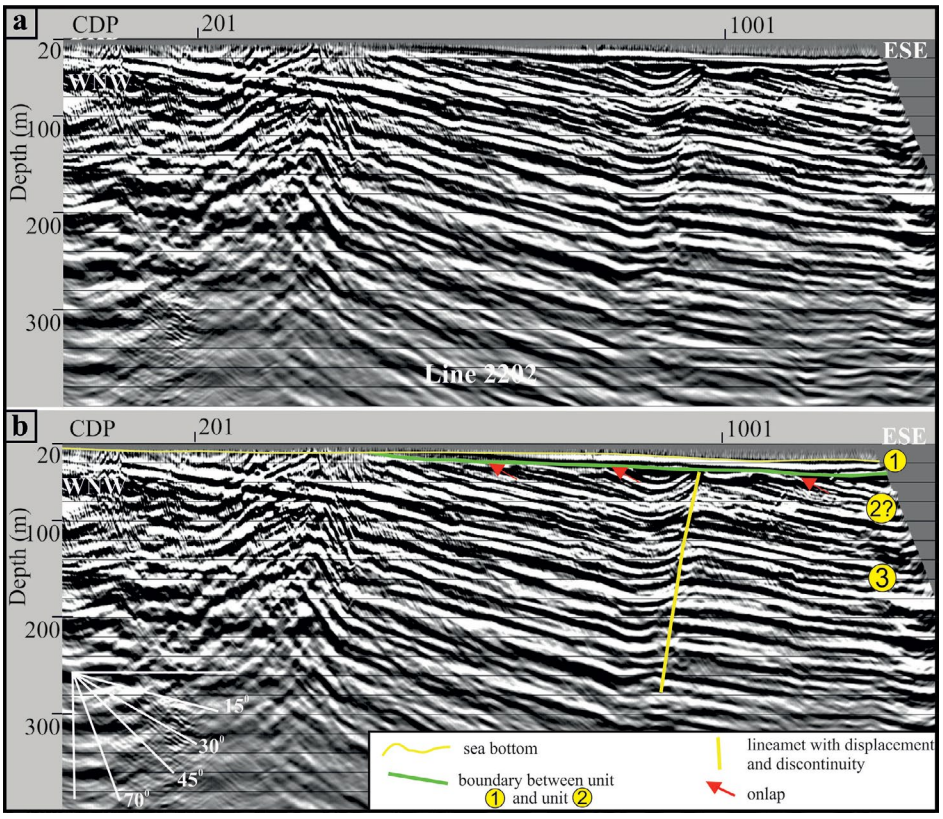

Figure 9- a) Seismic profile 2202 and b) geological interpretation of line 2202.

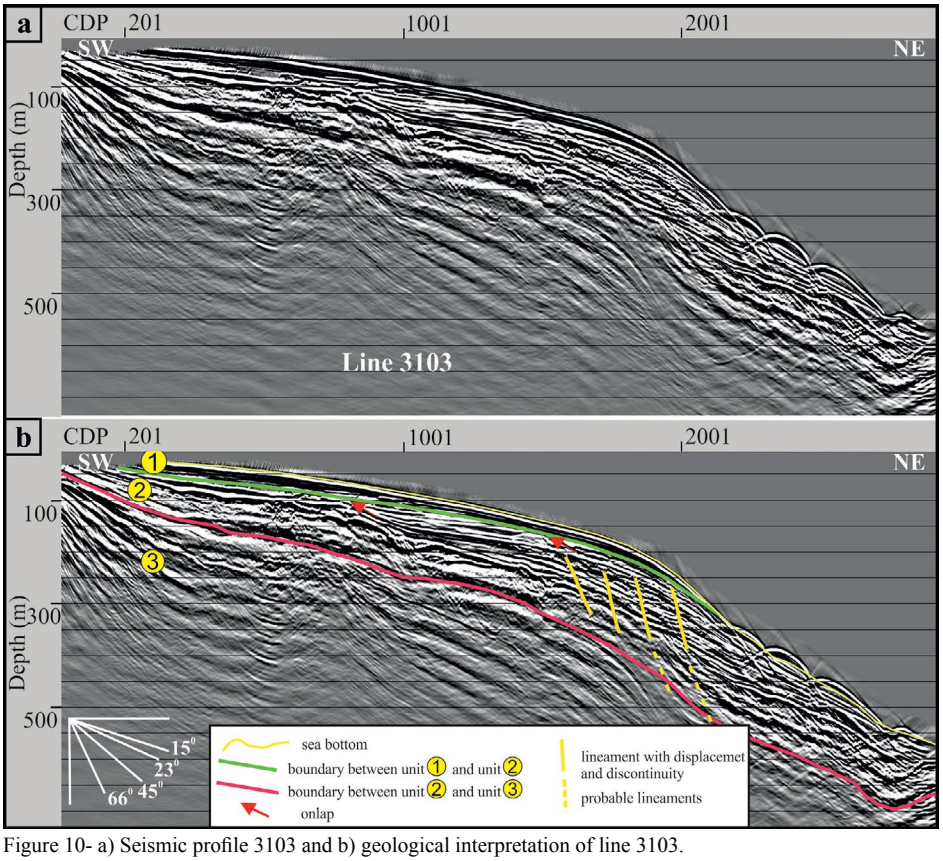

Figure 10- a) Seismic profile 3103 and b) geological interpretation of line 3103.

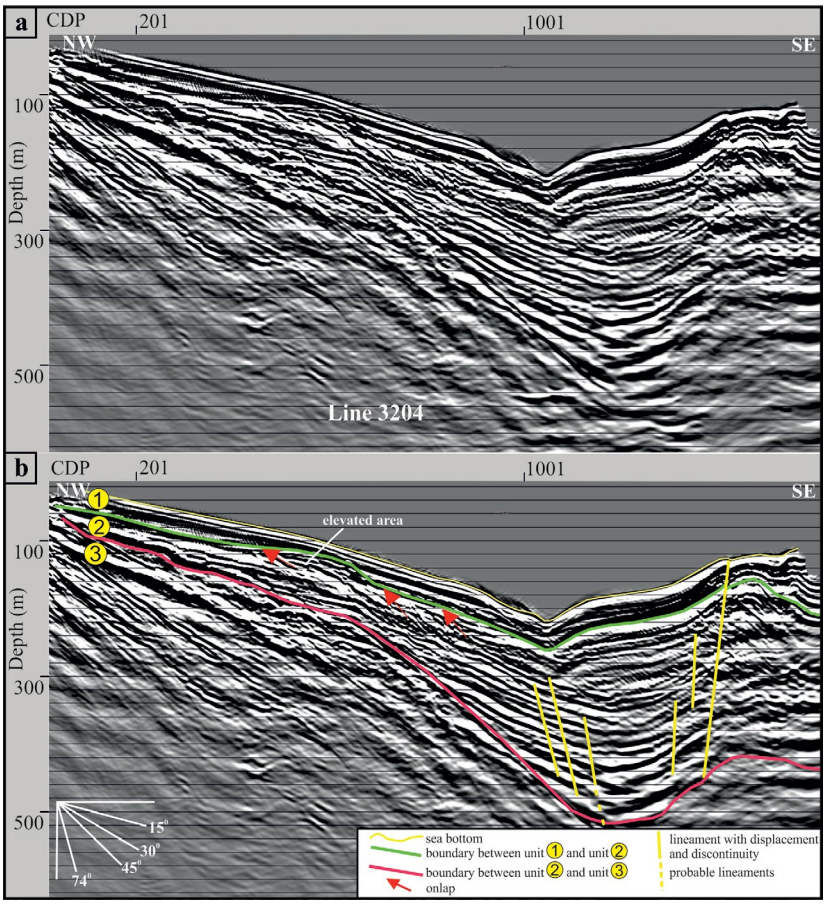

Figure 11- a) Seismic profile 3204 and b) geological interpretation of line 3204.

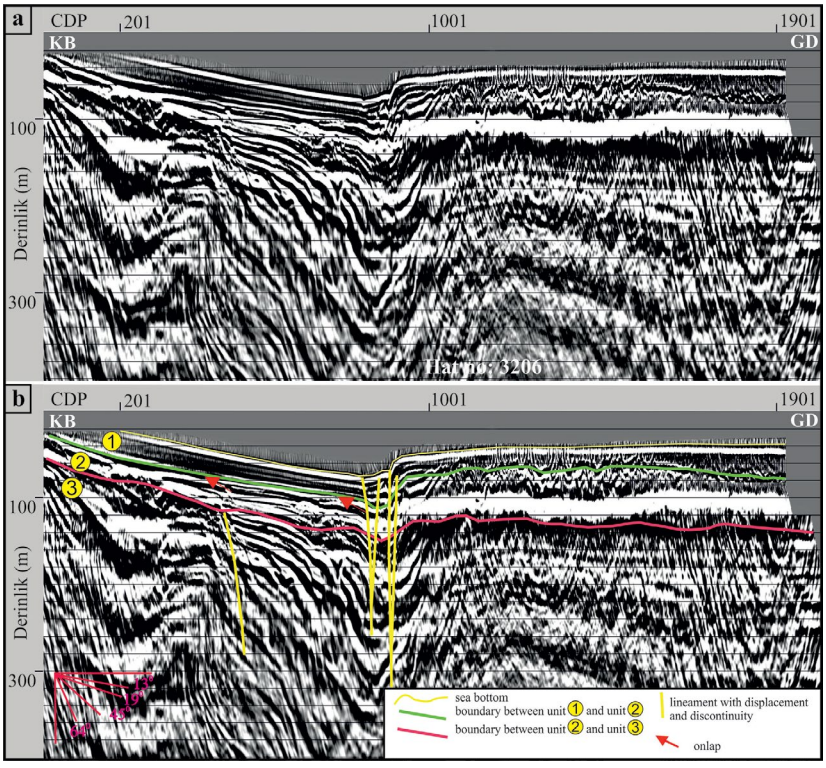

Figure 12- a) Seismic profile 3206 and b) geological interpretation of line 3206.

in this section, when the compressional phase was effective (Figure 9). In addition to these deformation structures that differ from the current tectonic regime, strike-slip faulting traces that still continue today, affecting units no. 2 and 1, are observable in sections. In the sections 2102, 3204 and 3206, a strike-slip faulting structure (with reverse component) indicating the current tectonic regime of the NAFS is observed (Figures 11-12).

In the seismic section number 3206, the faulting geometry with slight vertical offset is clearly observed in the soft sediment in the marine area where the NAFS rises from the Ganos depression to continental shelf and in the areas close to shoreline near Gaziköy that extends to the deep base units. In this section, it is clearly observable that NAFS has deformed by cutting all sediments from the basement units that have undergone dense deformation to the current units.

5. Discussions and Conclusions

Based on geological interpretation of shallow seismic and bathimetry data collected by R/V MTA Selen Reserach Vessel in the northwest of the Sea of Marmara and wildcat in the literature, 3 stratigraphic units were recognized, from older to younger, pre-Miocene basement, Miocene succession and Holocene shelf deposits.

The upper unit (Unit 1), which deposited during late Quaternary transgression, overlies on units (2 and 3) with an angular unconformity (the green lines on seismic sections). The thickness of the unit indicates some variations on different seismic sections with a range between 30-40 m, which is in accordance with the estimated sedimentation rate of 5 – 4 cm/kyr for northeast of the Sea of Marmara, reported by Ediger et al (2018). Having similar sediment source area characteristics, these two region are also easy to compare with each other, despite the considerable distance between them. The Ganos fault, which is a segment of NAFS and reaches to terresterial area in Gaziköy, is distinguisible on seismic sections indicating the recent tectonic activity. It can be proved by cutting through most recent deposits. On seismic section 3206, Ganos fault demonstrates upward branching “negative flower structure”, one of the characteristic features strike slip faults show in cross-sections.

The Unit 2 correspondings Miocene age. The unit is deformed and has an erosional boundary on top of it. There is an angular unconformity between the units and late Quaternary deposits. Near shoreline, the red colored erosional surface on seismic sections can be traced at 40-60 m water depth. According to the literature, 65 m sea level drop (Çağatay et al., 2003; Newman, 2003; Eriş et al., 2007) during Younger Dryas, 11.7 – 12.3 Cal kyr BP (Fairbanks, 1989), resulted in progressive decreasing of water flow from Black Sea to Sea of Marmara, which eventually transform the latter into a lake. The erosional surface interpreted from seismic sections probably indicates the aforementioned sea level drop and coincides with the sea bottom near shore line once exposed to atmospheric conditions.

The unit 3, which is distinguished in seismic sections and corresponding to the pre-Miocene basement units, is clearly different from the unit 2 in terms of structural and deformation pattern. This situation is the most important indicator that two units are subjected to different deformation processes. The discontinuities and folds defining the amount of deformation revealed that the unit 3 was exposed to a compressional tectonic regime more than the unit 2. It is an expected result to observe compression structures especially in transpressional areas in strike-slip regimes. However, the determination of different deformation amount in the unit number 2 and 3 indicates the differences in the dominant tectonic regimes. As a result, the recent strike-slip faulting with reverse component is different from the older tectonic regimes.

Acknowledgement

In this study, multibeam and shallow seismic data collected by R/V MTA Selen Research Vessel in the General Directorate of Mineral Research and Exploration (Research and Application Project, 2018-37-14-01) is used. Moreover, we would like to thanks to 3 refrees; anonymous, Prof. Dr. Hasan Sözbilir and Doç. Dr. Selim Özalp for their contributions to improve the quality of the manuscript.

References

Aksoy, E., Türkmen, İ., Turan, M., Meriç, E. 1999. Harami formasyonunun (Üst Kampaniyen-Maastrihtiyen) stratigrafik konumu ve çökelme ortamıyla ilgili yeni bulgular, Elazığ güneyi. Türkiye Petrol Jeologları Derneği Bülteni 11(1), 1-15.

Aksoy, M.E., Meghraoui, M., Vallée, M., Çakır, Z. 2010. Rupture characteristics of the A.D. 1912 Mürefte (Ganos) earthquake segment of the North Anatolian fault (Western Turkey). Geological Society of America 38/11, 991–994.

Aksu, A.E., Calon, T., Hiscott, R.N., Yaşar, D. 2000. Anatomy of the North Anatolian Fault Zone in the Marmara Sea, Western Turkey: extensional basins above a continental transform. GSA Today 37.

Alpar, B. 1999. Underwater signatures of the Kocaeli earthquake of 17 August 1999 in Turkey. Turkish Journal of Marine Sciences 5, 111-130.

Alpar, B., Yaltırak, C. 2002. Characteristic features of the North Anatolian Fault in the Eastern Marmara region and its tectonic evolution. Marine Geology 190/1-2, 329-350.

Altınok, Y., Alpar, B., Yaltırak, C. 2003. Şarköy-Mürefte 1912 Earthquake's Tusunami, extension of the associated faulting in the Marmara Sea, Turkey. Journal of Seismology 7, 329-346.

Ambraseys, N., Finkel, C. 1991. Long-term seismicity of Istanbul and of the Marmara Sea region. Terra Nova 3, 527-539.

Ambraseys, N.N., Finkel, C.F. 1995. Seismicity of Turkey and Adjacent Areas, A Historical Review, 1500–1800. Eren Yayıncılık ve Kitapçılık Ltd., Istanbul, 240 pp.

Armijo, R., Meyer, B., Hubert, A., Barka, A. 1999. Westward propagation of the North Anatolian fault into the northern Aegean: Timing and Kinematics. Geology 27, 3, 267-270.

Armijo, R., Meyer, B., Navarro, S., King, G. 2002. Asymetric slip partitioning in the Sea of Marmara pull-apart: a clue to propagation processes of the North Anatolian Fault? Terra Nova 13, 80-86.

Armijo, R., Pondard, N., Meyer, B., Uçarkuş, G., Mercier de Lepinay, B., Malavieille, J., Dominguez, S., Gustcher, M.A., Schmidt, S., Beck, C., Çağatay, N., Çakır, Z., Imren, C., Eris, K., Natalin, B., Özalaybey, S., Tolun, L., Lefevre, I., Seeber, L., Gasperini, L., Rangin, C., Emre, Ö., Sarıkavak, K. 2005. Submarine Fault scarps in the Sea of Marmara pull-apart (North Anatolian Fault): implications for seismic hazard in Istanbul. Geochemistry, Geophysics and Geosystems 6, 1-29.

Barka, A. A., Kadinsky-Cade, K. 1988. Strike-slip Fault Geometry in Turkey and its influence on earthquake activity. Tectonics 7/3, 663-684.

Crampin, S., Evans, R. 1986. Neotectonics of the Marmara Sea Region of Turkey. J Geol Soc Lond 143, 343-346.

Çağatay, N., Görür, N., Polonia, A., Demirbağ, E., Sakınç, M., Cormier, M.-H, Capotondi, L., Mc Hugh, C, Emre, Ö., Eriş, K. 2003. Sea level changes and depositional environments in the İzmit Gulf, Eastern Marmara Sea, during the Lateglacial-Holocene period. Marine Geology 202, 159-173.

Demirbağ, E., Rangin, C., Le Pichon, X., Şengör, A.M.C. 2003. Investigation of the tectonics of the Main Marmara Fault by means of deep-towed seismic data. Tectonophysics 361,1-19.

Dix, C. H. 1955. Seismic Velocities from Surface Measurements. Geophysics 20, 1, 68-86.

Ediger, V., Demirbağ, E., Ergintav, S., İnan, S., Saatçılar, R. 2018. Post-Glacial Terraces of The Marmara Sea and Water Exchange Periods. Bulletin of the Mineral Research and Exploration 157, 39-57.

Ergin, M., Özalaybey, S., Aktar, M.T., Tapırdamaz, C., Yörük, A., Biçmen, F. 2000. Aftershock analysis of the August 17, 1999 İzmit, Turkey, Earthquake. In: Barka, A., Kozacı, Ö., Akyüz, S., Altunel, E. (Eds.), The 1999 İzmit and Düzce earthquakes: preliminary results, İstanbul Technical Univ. Press, İstanbul, 171-178.

Eriş, K. K., Ryan, W. B. F., Çağatay, M. N., Sancar, U., Lericolais, G., Ménot, G., Bard, E. 2007. The timing and evolution of the post-glacial transgression across the Sea of Marmara shelf south of İstanbul. Marine Geology 243, 57-76.

Fairbanks, R.G. 1989. A 17,000-year glacioeustatic sea level record: Influence of glacial melting rates on the Younger Dryas event and deep ocean circulation. Nature 342, 637-642.

Gazioğlu, C., Gökaşan, E., Algan, O., Yücel, Z., Tok, B., Doğan, E. 2002. Morphologic features of the Marmara Sea from multibeam data. Marine Geology 190, 397-420.

Gökaşan, E., Alpar, B., Gazioğlu, C., Yücel, Z.Y., Tok, B., Doğan, E., Güneysu, C. 2001. Active tectonics of the İzmit Gulf (NE Marmara Sea): from high resolution seismic and multi-beam bathymetry data. Marine Geology 175/1-4, 271-294.

Gökaşan, E., Gazioğlu, C., Alpar, B., Yücel, Z. Y., Ersoy, Ş., Gündoğdu, O., Yaltırak, C., Tok, B. 2002. Evidences of NW extension of the North Anatolian Fault Zone in the Marmara Sea; a new approach to the 17 August 1999 Marmara Sea earthquake. Geo-Marine Letters 21, 183 -199.

Gökaşan, E., Ustaömer, T., Gazioğlu, C., Yücel, Z.Y., Öztürk, K., Tur, H., Ecevitoğlu, B. Tok, B. 2003. Active tectonics of the Marmara Sea. Morphotectonic evolution of the Marmara Sea inferred from multi-beam bathymetric and seismic data. Geo-Marine Letters 23/1, 19-33.

Gökçen, L.S. 1967. Keşan bölgesinde Eosen-Oligosen sedimantasyonu, Güneybatı Türkiye Trakyası. Bulletin of the Mineral Research and Exploration 69, 1-10.

Görür, N., Çağatay, M.N., Sakınç, M., Sümengen, M., Şentürk, K., Yaltırak, C., Tchapalyga, A. 1997. Origin of the Sea of Marmara as deduced from Neogene to Quaternary paleobiogeographic evolution of its frarne. International Geology Review 39, 342-352.

Guidoboni, E., Comastri, A., Trania, G. 1994. Catalogue of Ancient Earthquakes in the Mediterranean Area up to 10th Century, Instituto Nazionale di Geofisica, Rome.

Gutzwiller, O. 1923. Beitrage zur Geologie der Umgebung von Merfete (Mürefte) am Marmara Meer: Tez. Basel Üniversitesi, 25 s.

Gürbüz, C., Aktar, M., Eyidoğan, H., Cisternas, A., Haessler, H., Barka, A., Ergin, M., Türkelli, N., Polat, O., Üçer, S., Kuleli, S., Barış, S., Kaypak, B., Bekler, T., Zor, E., Biçmen, F., Yörük, A., 2000. The seismotectonics of the Marmara region (Turkey): Results from a microseismic experiment. Tectonophysics 316, 1-17.

Halbach, P., Kuşçu, İ., Inthorn, M., Kuhn, T., Pekdeğer A., Seifert, R. 2002. Methane in sediments of the deep Marmara Sea and its relation to local tectonic structures. In: Görür, N., Papadopoulos, G. A., Okay, N. (eds) Integration of Earth Science Research on the Turkish and Greek 1999 Earthquakes. Kluwer Academic Publishers, The Netherlands, NATO Science Series, IV. Earth and Environmental Sciences 9, 71-85.

Holmes, A.W. 1961. A stratigraphic review of Thrace. Turkish Petroleum Corporation unpubl techn rep 368, 1-56.

Imbrie, J., Hays, J.D., Martinson, D.G., McIntyre, A., Mix, A.C., Morley, J.J., Pisias, N.G., Prell, W.L., Shackleton, N.J. 1984. The orbital theory of Pleistocene climate: support from revised chronology of the marine N18O record. In: Berger, A.L., Imbrie, J., Hays, J., Kukla, G., Saltzman, B. (Eds.), Milankovitch and Climate, Part I. Reidel, Dordrecht 269-305.

İmren, C., Le Pichon, X., Rangin, C., Demirbağ, E., Ecevitoğlu, B., Görür, N. 2001. The NorthAnatolian Fault within the Sea of Marmara: a new interpretation based on multi-channel seismic and multi-beam bathymetry data. Earth and Planetary Science Letters 186, 143-158.

Kasar, S., Burkan, K.A., Siyako, M., Demir, O. 1983. Tekirdağ-Şarköy- Keşan-Enez bölgesinin jeolojisi ve Hidrokarbon olanakları. TPAO rap. 1171 (unpublished).

Ketin, İ. 1969. Über Die Nordanatolische Horizontalverschiebung. Bulletin of the Mineral Research and Exploration 72,1-25.

Le Pichon, X., Şengör, A. M. C., Demirbağ, E., Rangin, C., Imren, C., Armijo, R., Görür, N., Çağatay, N., Mercier de Le´pinay, B., Meyer, B., Saatçılar, R., Tok, B. 2001. The active main Marmara Fault. Earth and Planetary Science Letters 192, 595-616.

Le Pichon, X., Chamot-Rooke, N., Rangin, C., Şengör, A.M.C. 2003. The North Anatolian Fault in the Sea of Marmara. Journal of Geophysical Research 108 (B4), 2179.

McClusky, S., Balassanian, S., Barka, A., Demir, C., Ergintav, S., Georgiev, I., Gürkan, O., Hamburger, M., Hurst, K., Kahle, H., Kastens, K., Kekelidze, G., King, R., Kotzev, V., Lenk, O., Mahmoud, S., Mishin, A., Nadariya, M., Ouzounis, A., Paradissis, D., Peter, Y., Prilepin, M., Reilinger, R., Sanli, I., Seeger, H., Tealeb, A., Toksöz, N., Veis, G. 2000. GPS constraints on plate kinematics and dynamics in the Eastern Mediterranean and Caucasus. J of Geoph Res 105, 5695-5719.

Meade, B. J., Hager, B. H., McClusky, S. C., Reilinger, R. E., Ergintav, S., Lenk, O., Barka, A., Özener, H. 2002. Estimates of seismic potential in the Marmara Sea region from block models of secular deformation constrained by global positioning system measurements. Bulletin of the Seismological Society of America 92 (1), 208-215.

Newman, K. R. 2003. Using Submerged Shorelines to Constrain Recent Tectonics in the Marmara Sea, Northwestern Turkey, Department of Geology, Senior Thesis, Smith College 49 pp (unpublished).

Okay, A.I., Demirbağ, E., Kurt, H., Okay, N., Kuşçu, İ. 1999. An active, deep marine strike-slip basin along the North Anatolian fault in Turkey. Tectonics 18, 129-148.

Okay, A. I., Kaşlılar-Özcan, A., İmren, C., Boztepe- Güney, A., Demirbağ, E., Kuşçu, İ. 2000. Active faults and evolving strike-slip basins in the Marmara Sea, northwest Turkey: a multichannel seismic reflection study. Tectonophsics 321, 189-218.

Pınar, N. 1943. Marmara Denizi Havzasının sismik jeoloji ve meteorolojisi. İÜ. Fen Fakültesi Monografileri 5, 64.

Polonia, A., Cormier, M. H., Çağatay, N., Bortoluzzi, G., Bonatti, E., Gasperini, L., Seeber, L., Görür, N., Capotondi, L., Mc Hugh, C., Ryan, W. B.F., Emre, Ö., Okay, N., Ligi, M., Tok, B., Blasi, A., Busetti, M., Eriş, K., Fabretti, P., Fielding, E. J., İmren, C., Kurt, H., Magagnoli, A., Morazzi, G., Özer, N., Penitenti, D., Serpi, G., Sarıkavak, K. 2002. Exploring submarine Earthquake Geology

in the Marmara Sea. Eos, Transactions. American Geophysical Union 83 (21), 235-236.

Polonia, A., Gasperini, L., Amorosi, A., Bonatti, E., Bortoluzzi, G., Çağatay, M. N., Capotondi, L., Cormier, M. H., Görür, N., Mc Hugh, C.M.G., Seeber, L. 2004. Holocene slip rate of the North Anatolian Fault beneath the Sea of Marmara. Earth and Planetary Science Letters 227, 411-426.

Rangin, C., Demirbağ, E., İmren, C., Crusson, A., Normand, A., Le Drezen, E., Le Bot, A. 2001. Marine Atlas of the Sea of Marmara (Turkey). 11 plates and 1 booklet. Special publication (ISBN 2-84433-068-1) by IFREMER Technology Center, Brest, France.

Rangin, C., Le Pichon, X., Demirbağ, E., İmren, C. 2004. Strain localization in the Sea of Marmara: propagation of the North Anatolian Fault in a now inactive pull-apart. Tectonics 23, 1-18.

Sakınç, M., Yaltırak, C., Oktay, F.Y. 1999. Palaeogeographical evolution of the Thrace Neogene basin and the Tethys-Paratethys relations at northwestern Turkey (Thrace). Palaeogeogr Palaeoclimatol Palaeoecol 153, 17-40.

Sieberg, A. 1932. Untersuchgen über Erdbeben und Bruchschollenbau im östlichen Mittelmeer: Denkschr. Med. Naturw. Ges., Jena.

Siyako, M. 2006. Trakya Bölgesi Litostratigrafi birimleri. Stratigrafi Komitesi Litostratigrafi Birimleri Serisi 2, 70 s.

Siyako, M., Tanış, T., Şaroğlu, F. 2000. Marmara Denizi aktif fay geometrisi. TÜBITAK Bilim ve Teknik Dergisi 388, 66-71.

Soysal, H., Sipahioğlu, S., Kolçak D., Altınok, Y. 1981. A catalogue of earthquakes for Turkey and surrounding area (BC 2100-AD 1900). Final report, project number TBAG 341, The Scientific and Technical Research Council of Turkey (TUBİTAK), Ankara.

Sümengen, M., Terlemez, I. 1991. Güneybatı Trakya yöresi Eosen çökelleri stratigrafisi. Bulletin of the Mineral Research and Exploration 113,17-30.

Sümengen, M., Terlemez, I., Şentürk, K., Karaköse, C., Erkan, E., Ünay, E., Gürbüz, M., Atalay, Z., Şentürk, K. 1987. Gelibolu Yarımadası ve Güneybatı Trakya Tersiyer Havzasının Stratigrafisi, Sedimantolojisi ve Tektoniği. Maden Tetkik ve Arama Genel Müdürlüğü Rapor No: 8128,Ankara (unpublished).

Şentürk, K., Sümengen, M., Terlemez, İ., Karaköse, C. 1998. 1/100.000 ölçekli Açınsama Nitelikli Türkiye Jeoloji Haritaları Bandırma-D4 Paftası, Ankara. Maden Tetkik ve Arama Genel Müdürlüğü Raporu No: 64, Ankara (unpublished).

Tapırdamaz, C., Yaltırak, C. 1997. Trakya'da Senozoyik Volkaniklerinin Paleomanyetik Özellikleri ve Tektonik Evrimi. Bulletin of the Mineral Research and Exploration 119, 27-42.

Turgut, S., Eseller, G. 2000. Sequence stratigraphy, tectonics and depositional history in eastern Thrace Basin, NW Turkey. Mar Petrol Geol 17, 61-100.

Turgut, S., Siyako, M., Dilki, A. 1983. Trakya havzasının jeolojisi ve hidrokarbon olanakları. Türkiye Jeoloji Kongresi Bülteni 4, 35-46.

Turgut, S., Türkaslan, M., Perinçek, D. 1991. Evolution of the Thrace sedimantary basin and its hydrocarbon prospectivity: Generation, accumlation, and production of Europe's hydrocarbons (ed. A. M. Spencer) 415-437.

Tüysüz, O., Barka, A., Yiğitbaş, E. 1998. Geology of the Saros Graben: its implications on the evolution of the North Anatolian Fault in the Ganos-Saros region, NW Turkey. Tectonophysics 293, 105-126.

Wong, H.K., Lüdmann, T., Uluğ, A., Görür, N. 1995. The Sea of Marmara: a plate boundary sea in an escape tectonic regime. Tectonophysics 244, 231- 250.

Yaltırak, C. 1995. Gaziköy-Mürefte Arasının Sedimantolojisi ve Tektoniği. TPJD Bülteni 6/1, 93-112.

Yaltırak, C. 1996. Tectonic History of The Ganos Fault System (in Turkish with English abstract). Turk Assoc Pet Geol Bull 8, 137-156.

Yaltırak, C. 2002. Tectonic evolution of the Marmara Sea and its surroundings. Marine Geology 190/1-2, 493-530.

Yaltırak, C., Sakınç, M., Aksu, A.E., Hiscott, R., Galleb, B., Ülgen, U.B. 2002. Late Pleistocene uplift history along southwestern Marmara Sea determined from raised coastal deposits and global sea level variations. Mar Geol 190/ 1-2, 283-306.

Yanmaz, M. N. 2017. Marmara Denizi Batimetri Haritası. R/V MTA SİSMİK-1 Araştırma Gemisi ile 1995 - 2003 yıllarında yapılan çalışmaları sırasında Atlas Deso Echo Sounder ve Seisnet Integrated Navigation System (DGPS) kullanılarak 25 - 50 metre ölçü aralıklarıyla sayısal olarak kaydedilen derinlik ve koordinat değerleri derlenerek oluşturulmuş harita.

Yıldız, S., Özden, S., Tutkun, S.Z., Ateş, Ö., Altuncu Poyraz, S., Kapan Yeşilyurt, S., Karaca, Ö. 2013. Ganos Fayı Boyunca Geç Senozoyik Yaşlı Gerilme Durumları, KB Türkiye. Türkiye Jeoloji Bülteni 56, 1.

Bulletin of the Mineral Research and Exploration

http://bulletin.mta.gov.tr

Using of GIS on field geology studies: An application on central-southern of Eskişehir

Coşkun GÜNEŞ[a*], Emrah PEKKAN[a] and Muammer TÜN[a]

[a]*Eskişehir Technical University, Research Institute of Earth and Space Sciences, Eskişehir, Turkey*

Research Article

Keywords:
Eskişehir basin, Geographial information systems, Field geolgy, Stratigraphy.

ABSTRACT

Technological developments on Geographical Information Systems (GIS) make possible to use its applications on all departments of earth sciences. GIS based drill-hole data, lithological and structural maps are used integrated with field geolgy investigations in this study. The area where is bordered Batıkent-Yukarı Söğütönü districts on northwest and Vadişehir-Ihlamurkent districts on southeast is defined as study area. 44 water wells drilled by State Hydraulic Works (DSİ) are located in various points of Eskişehir region were transformed to GIS base. Geological cross-sections which were designed by drill-hole lithology are point out a disconformity zones between Paleogene and Neogene according to principle of lateral continuity. Neotechtonic researches on study area show thah right lateral strike slip shear zone dominates the region structurally. Searching these structural traces on the field and representing new field evidances by using GIS on the regions where there is no consensus stratigraphicly are the main purposes of the study. Geological map of the region where lies between Çankaya and Karapınar districts without consensus stratigrapichly was made by field observations on Miocene units. The other surface evidances include dilation fractures, strike-slip faults are support the idea which is suggested for Eskişehir region as right lateral strike-slip shear zone.

Received Date: 09.08.2019
Accepted Date: 23.12.2019

1. Introduction

The Geographical Information Systems (GIS), which allow the collection, analysis and storage of spatial data, can be used in all areas of geosciences. The integrated use of GIS on fields such as geology, geotechnics and seismology has become widespread in the last 20 years. Seyis et al. (2002), by taking into account the geological criteria have prepared a database Zonguldak coal basin on the GIS environment. Thanks to this database, the geological properties of coals of the region have become easily accessible and questionable. Kumsar et al. (2011) contributed to the control of urban development developing a geological and geotechnical urban information system in the GIS environment for Denizli province center. Tün et al. (2015) developed disaster management practices by interpreting earthquake data obtained from seismic networks in GIS environment. In this study, it is aimed to present new findings to the stratigraphy and neotectonic evolution of Eskişehir region by using GIS and field geology studies in an integrated manner. The study area, which consists mostly of the south of Eskişehir, is bordered by Batıkent-Yukarı Söğütönü districts in the northwest and Vadişehir-Ihlamurkent districts in the southeast (Figure 1).

The province of Eskişehir and its vicinity are located within the Anatolide platform, which is described by Ketin (1966) where all series between Paleozoic and Upper Cretaceous have been more or less metamorphosed and covered by an apparent angular unconformity and thick basal conglomerate by the lower Eocene. Okay (2011) defines that the

Citation info: Güneş, C., Pekkan, E., Tün, M. 2020. Using of GIS on field geology studies: An application on central-southern of Eskişehir. Bulletin of the Mineral Research and Exploration 163, 27-38. https://doi.org//10.19111/bulletinofmre.669305.

**Corresponding author: Coşkun GÜNEŞ, coskungunes226@gmail.com*

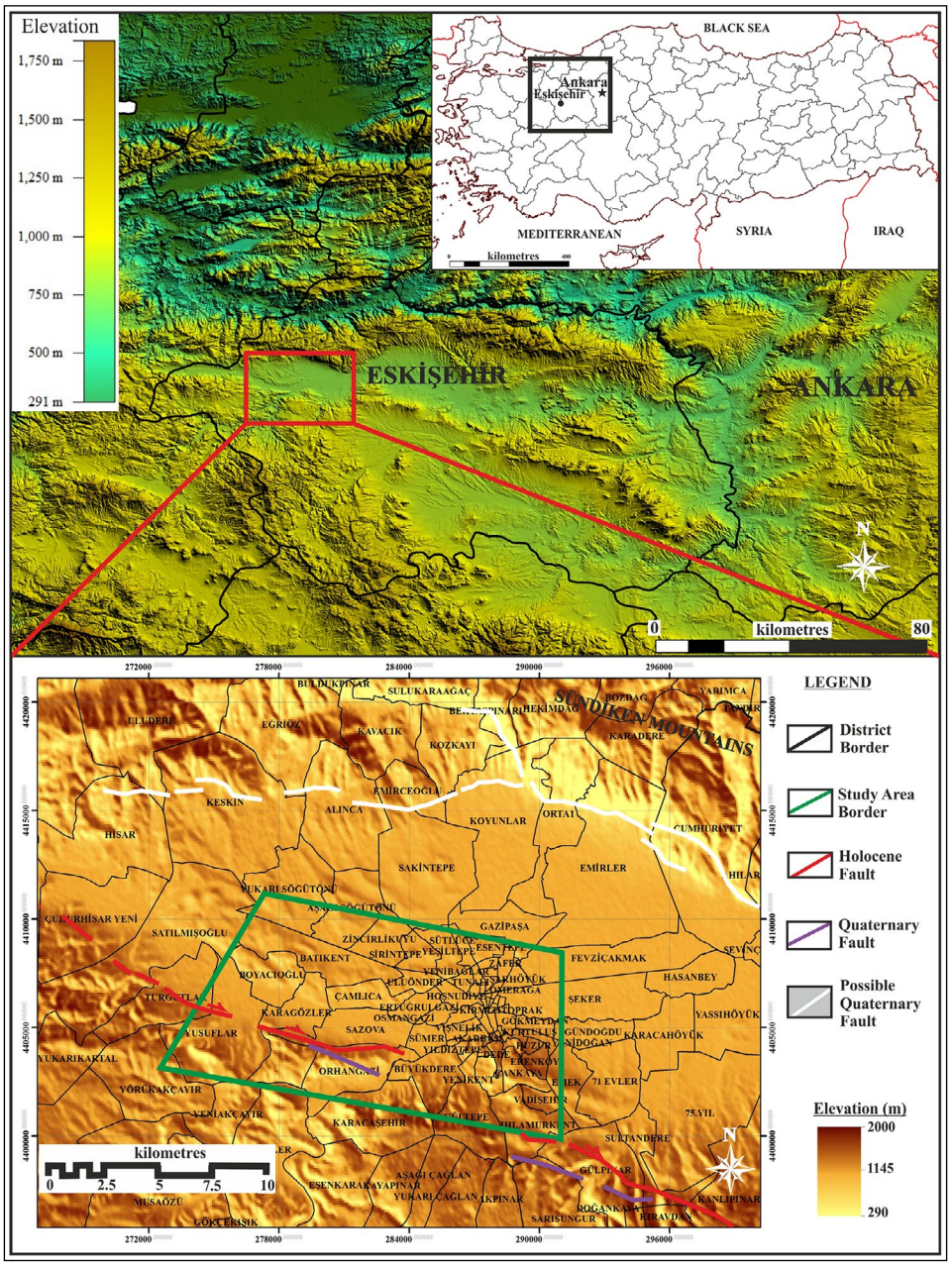

Figure 1- Morphology and location map of the study area [faults were projected from Emre et al., (2013)].

northern end of the Anatolide platform, which covers the study area, formed the portion which was located in subduction zone and again uplifted to the surface in the Late Cretaceous and named this region as the Tavşanlı Zone.

Gözler et al. (1996) explained that the basement rocks in Eskişehir area consisted of pre-Jurassic metamorphics and Triassic ophiolites. It is mentioned in many studies that Paleogene is unconformably deposited on this basement and the Paleogene and Neogene rocks are covered by Quaternary (Gözler et al., 1996; Ocakoğlu, 2007; Orhan et al., 2007; Şengüler and Izladı, 2013; Usta and Kutluk, 2014). The region is tectonically restricted by the Eskişehir Fault Zone (EFZ), which is a right lateral strike slip fault with normal component in south (Şaroğlu et al., 1992; Barka et al., 1995; Altunel and Barka, 1998; Seyitoğlu et al., 2015) and bordered by a probable Quaternary fault system and lineament (Emre et al., 2013) between the Bozdağ and Sündiken mountains that extend generally in NW-SE directions in the

north. In analyses carried out in the EFZ and its close vicinity; it is seen that there is a general consensus that the NW-SE trending shear zone shapes the structural geology of Eskişehir environment (Altunel and Barka 1998, Seyitoğlu et al., 2015).

2. Method

The study was carried out under the headings of GIS, Field Geology and Literature Survey. In the light of studies mentioned in the literature (Gözler et al., 1996; Ocakoğlu, 2007; Orhan et al., 2007; Şengüler and Izladı, 2013; Usta and Kutluk, 2014, Seyitoğlu et al., 2015), the stratigraphic relations, structural and tectonic traces of the geological units were investigated on the field. GIS studies consist of application steps of; i) the transformation of water drilling logs of DSİ into vector format in 1/1000 vertical scale, ii) the definition of point data by assigning coordinate to drilling logs in vector format and transferring them in to the GIS environment, iii) forming cross-section lines passing over point data and obtaining topographic sections of lines over digital elevation model (DEM), iv) the overlapping of the topographic cross-section generated in GIS environment with the vector-format drilling logs prepared on a scale of 1/1000, v) the completion of the design section and interpretation of the general geology criteria (lateral continuity, cross-cutting relationships, law of superposition) (Figure 2). Drilling data used in the study were distributed to various regions of Eskişehir province and obtained from 44 DSI water drilling logs and ASTERGDEM data with 30 m resolution.

3. General Geology of the Study Area

Geological evolution in Eskişehir region is considered to have been formed on the basement rocks which began to occur during the closure of Neotethys ocean in the Late Cretaceous (Göncüoğlu et al., 2000). The Paleotethyan relationship and Triassic age were also suggested for these basement rocks (Okay et al., 2002). It is known that the basement rocks are composed of rocks that show widespread blueschist metamorphism and serpentinized ultramafic rocks that overly them by tectonic contact (Okay, 2011). The region stratigraphically consists of Neogene and Quaternary, which relatively thins out towards younger units deposited on the metamorphic and ultramafic basement (Ocakoğlu, 2007). The basic rocks are overlain by the units of lower Eocene, upper Miocene and Pliocene in sequence (Gözler et al., 1996). The Pleistocene and all other rocks are covered by the Quaternary alluvium (Figure 3).

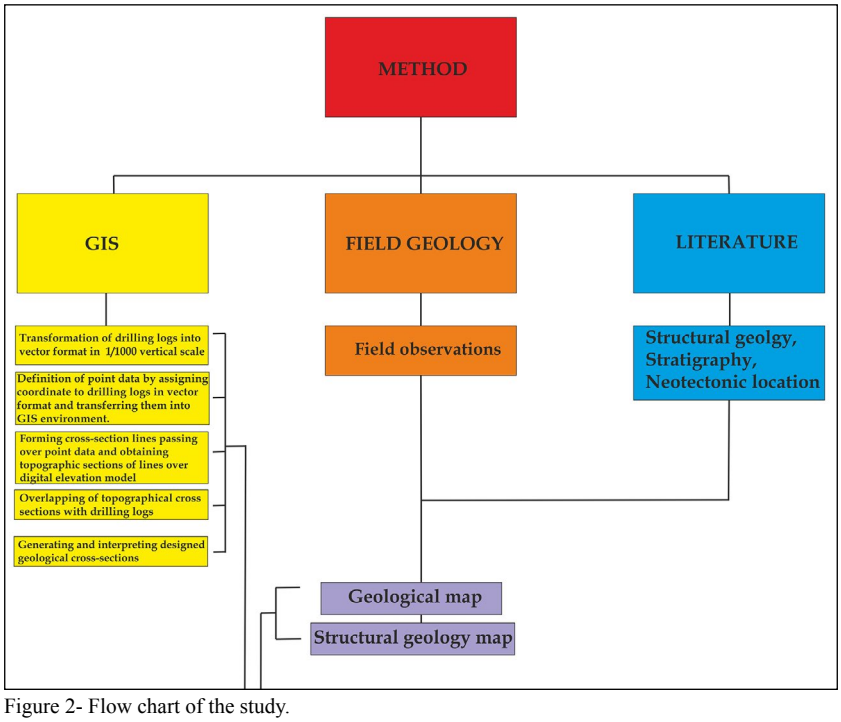

Figure 2- Flow chart of the study.

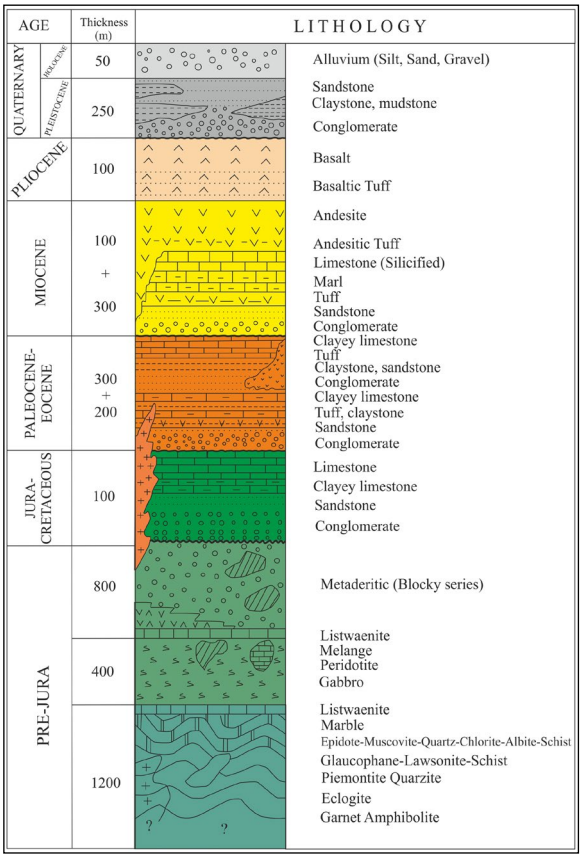

Figure 3- Generalized columnar section of Eskişehir and its vicinity [modified from Gözler (1996)].

The Mesozoic units located in and around Eskişehir are represented by radiolarites, radiolarian limestones, mudstones, serpentinite, diabase, limestone, schist blocks and occasionally serpentinized peridotite and partly metamorphosed diabases and gabbros (Gözler et al., 1996). Mesozoic units crop out with mudstones in the study area on a E-W extending hill between Karagözler and Sazova.

The Eocene, which unconformably overlies Mesozoic units present outcrops in south of Eskişehir with colors varying in red, dark pink, medium compacted, low-strength sandstone, conglomerate levels and the overlying pale yellow, low strength clayey limestones. The Eocene units in the region show clayey limestone layers over sandstone levels in the vicinity of Mamuca, while red-pink sandstone-conglomerate layers are common in the north of Aşağıçağlan and Kayapınar districts. The overall thickness of Eocene units is assumed to vary between 200-500 m.

The Miocene, which disconformably overlies the Eocene, cover large areas with conglomerate, sandstone, marl, limestone levels in the study area and in the south of Eskişehir. In west of the study area, it is possible to observe transitions between the green marl-limestone around Turgutlar-Yusuflar districts and the conglomerate-limestone levels in the central-east on highly elevated hills of Odunpazarı district.

The Pliocene, which covers very few area with respect to other units are represented by tuff and basalt units.

The entire study area to the north of the Sarisu River consists of Quaternary. The Quaternary in this area is composed of Pleistocene with lithologies of conglomerate, claystone, mudstone and sandstone and the Holocene cover (Figure 4).

The study area was assessed by broad literature survey, drilling logs and GIS based analyses (Figure 5). Field studies were carried out by using classical methods in an area of 10 km^2 restricted by Akarbaşı and Göztepe districts in northwest and Yenikent and Çankaya districts in southeast.

The most important tectonic element in Eskişehir region is the right lateral strike slip fault system, which extends between Uludağ in the northwest and Kaymaz (Eskişehir) in the southeast (Şaroğlu et al., 1992). A series of discrete faults in the stated area were mapped as the İnönü - Dodurga Fault Zone, the Eskişehir Fault Zone and the Kaymaz Fault Zone (Şaroğlu et al., 1992). The line, which is accepted as the northeastern border of the Western Anatolian block and the Central Anatolian block (Barka et al., 1995), was also mapped as the Eskişehir Fault (Şengör et al., 1985; Barka et al., 1995). Altunel and Barka (1998) defined the line formed by right lateral strike-slip fault between Uludag in the west and Kaymaz in the east as the Eskişehir Fault Zone (EFZ). In the study, the EFZ was defined as a trans-tensional zone based on detailed field analyzes in İnönü-Çukurhisar and Turgutlar Eskişehir segments. Seyitoğlu et al. (2015) stated that the Eskişehir region (Figure 6a) was shaped by the effect of right lateral shear zone along the 60 km long line of which its main axis is N60W as a result of field studies carried out around Bozüyük - İnönü in the northwest, Alınca-Muttalıp in the north, Kızılinler-Gökçekısık in the central-south, and Akçapınar in the southwest (Figure 6b).

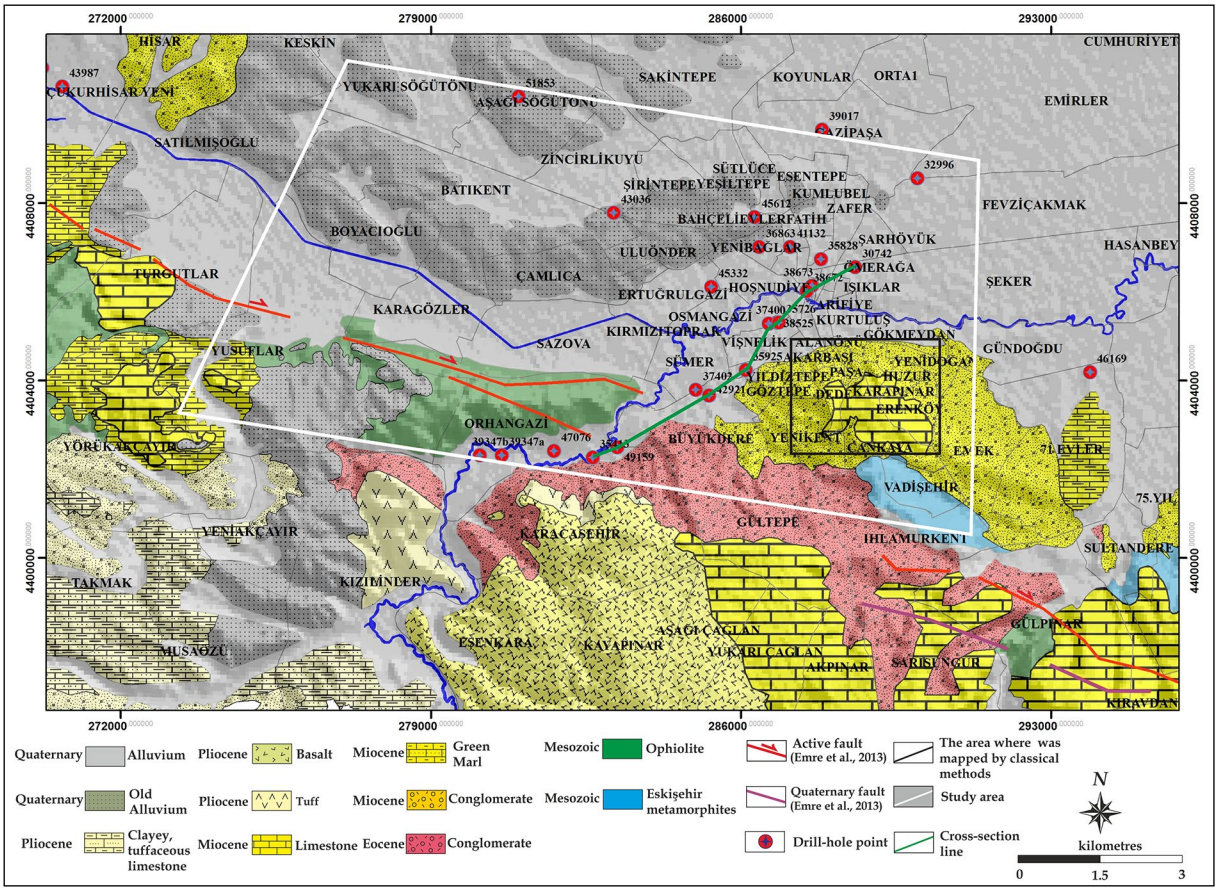

Figure 4- Geological map of the study area [modified from Gözler et al. (1996) and Orhan et al. (2007)].

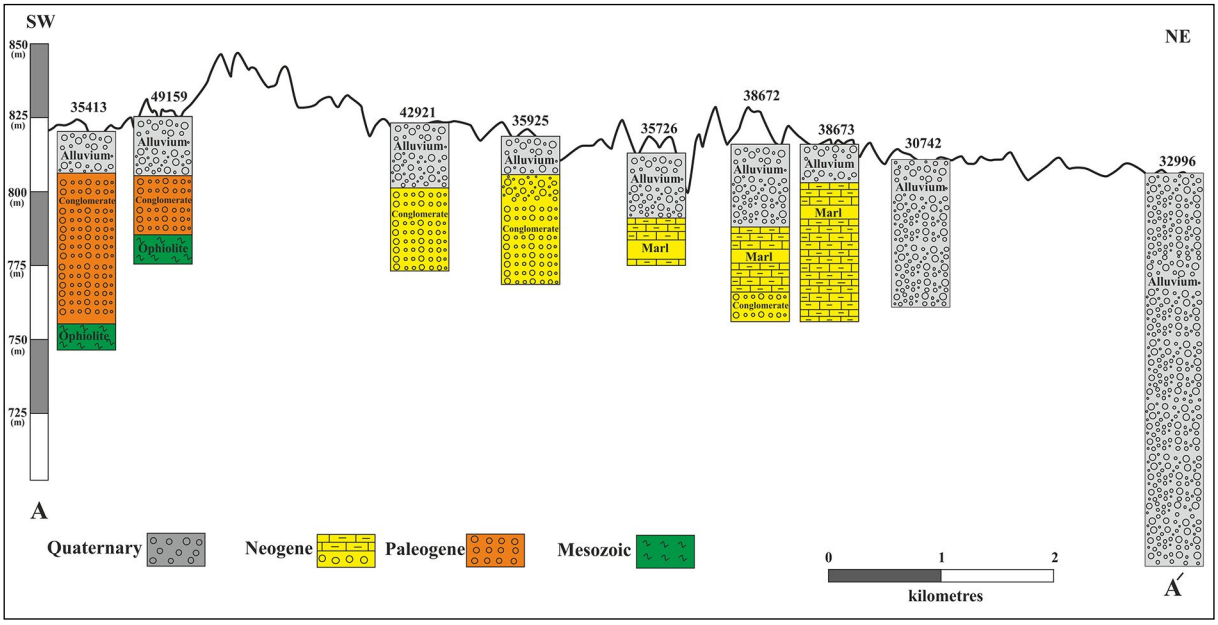

Figure 5- Topographic section of the study area with SW-NE direction and lithology logs of the drillings on the section.

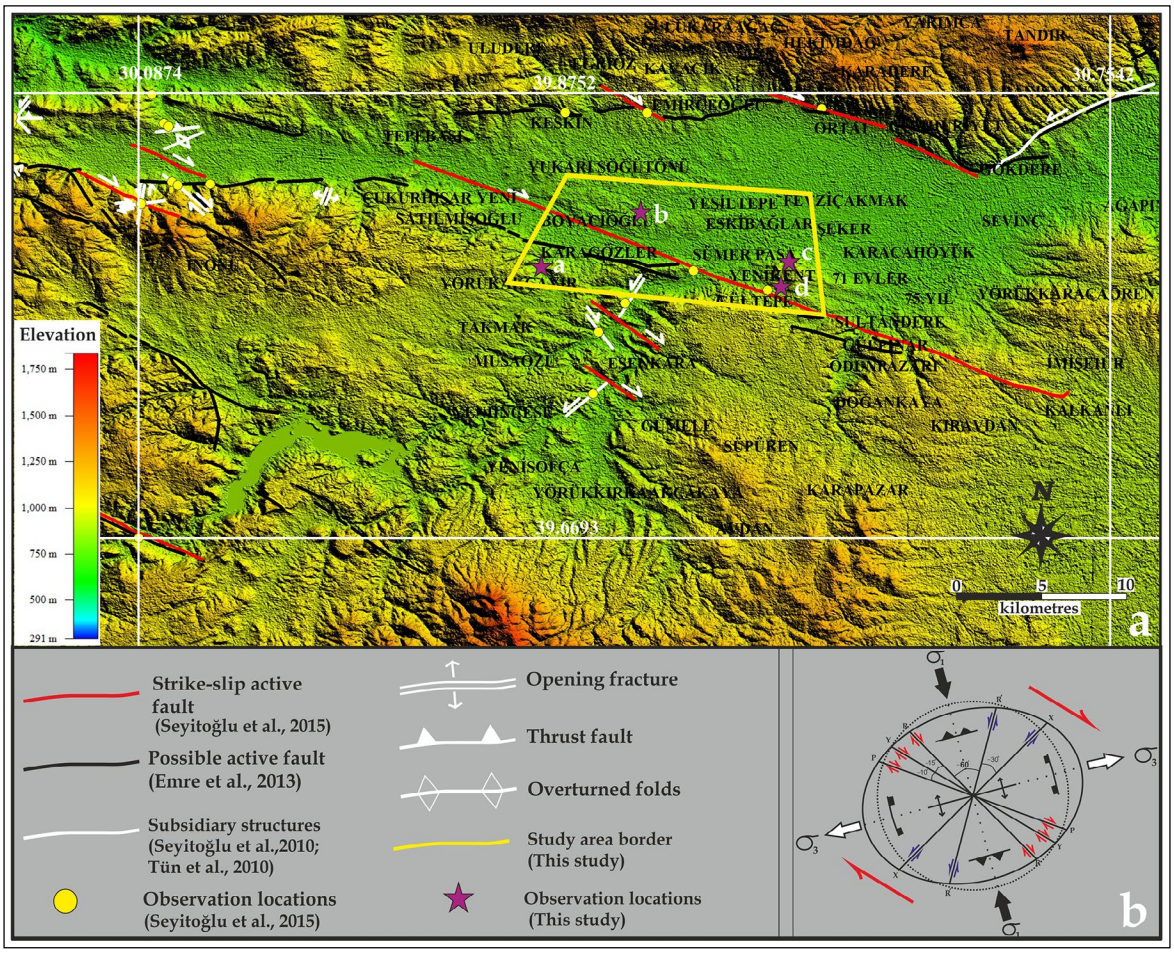

Figure 6-a) Structural geology map of Eskişehir region (modified from Seyitoğlu et al., 2015) and b) deformation axes proposed for Eskişehir region (Seyitoğlu et al., 2015).

The main structures likely to occur in simple shear zones (Figure 7) are; Y (corresponding to the main fault), R1 and P fractures that move in the direction of the main fault, and R2 and X fractures that move in opposite direction with the main fault. The internal friction angle (Φ) determines the geometry of the secondary faults with the main fault. Riedel shears (R1) develop at an angle of approximately Φ/2 with the main fault, while the opposite Riedel shears (R2) develop at an angle of approximately 90- Φ/2 with the main fault. When, Φ is considered to be approximately 300-400; then R1 fractures are expected to develop with the main fault at angles of 150-200, and R2 fractures at angles of 750-700 (Tchalenko and Ambraseys, 1970; Sylvester, 1988). The P fractures develop as symmetrical forms of R1 fractures with respect to the main fault (Woodcock, 1986).

It is sporadically possible to observe the traces of structures developed by NNW-SSE directional compressional and ENE-WSW directional extensional mechanism on the field in Eskişehir region. Approximately, at 1 km southeast of the Yusuflar district (Figure 8a), the presence of fracture sets varying from N30W to E-W are remarked in the green marl-limestone (Figure 8b) units (Figure 8c). The absence of opening in carbonate fillings in E-W extending fractures in the stratigraphically older green marl unit from these two units of which their ages are regarded as Miocene (Figure 8d) shows that the tectonic activity forming the sets in this direction does not continue today.

In observations made in clayey carbonate deposits and the overlying older alluvial units in the vicinity of the Çamlıca district (Figure 9a), (Figure 9b); the direction of opening fractures observed in light yellow-beige colored, medium strength, clay and carbonate containing unit varies between N30W / N-S (rotation measurement was performed in 21 fractures) (Figure

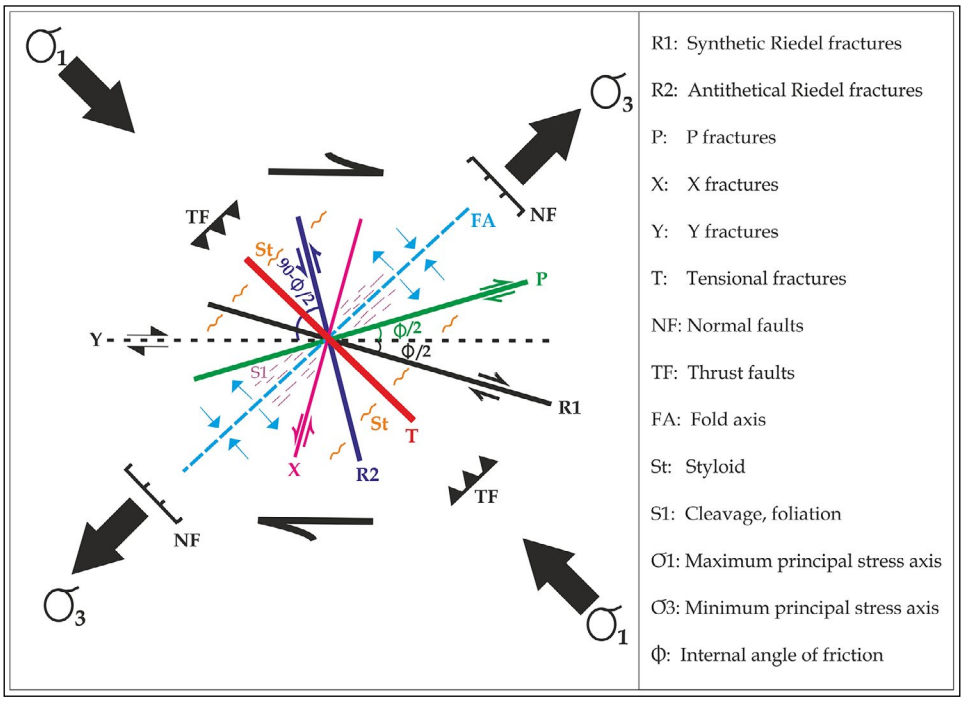

Figure 7- Possible structures likely to occur in simple shear zones (Harding, 1974; Bartlett et al., 1981; Hancock, 1985)

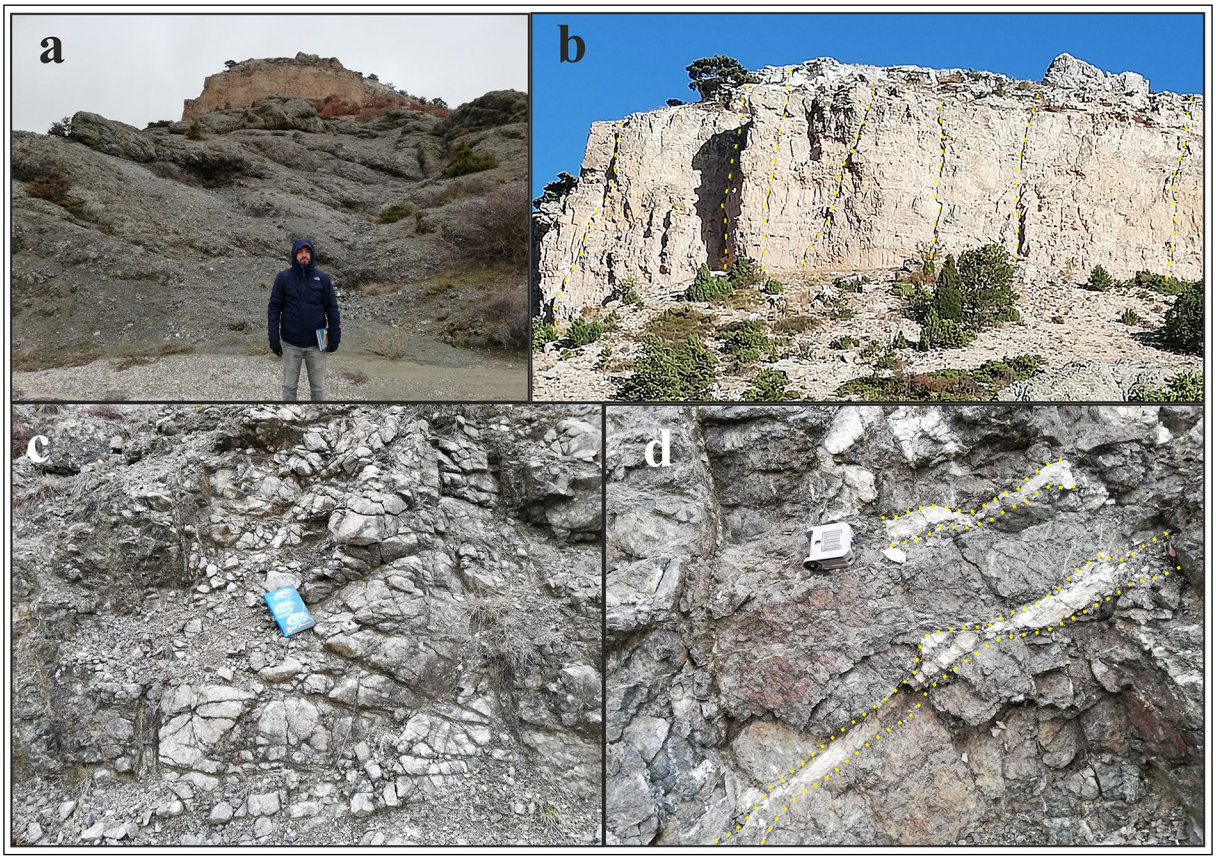

Figure 8- a) Green marl and limestone units showing traces of crustal deformation around the Yusuflar district, b) E-W trending fractures in the limestone unit, c) N30W / E-W fractures in the green marl unit and d) E-W trending, carbonate-filled fractures in the green marl unit (location: see Figure 6a: a, look direction of photos: ENE).

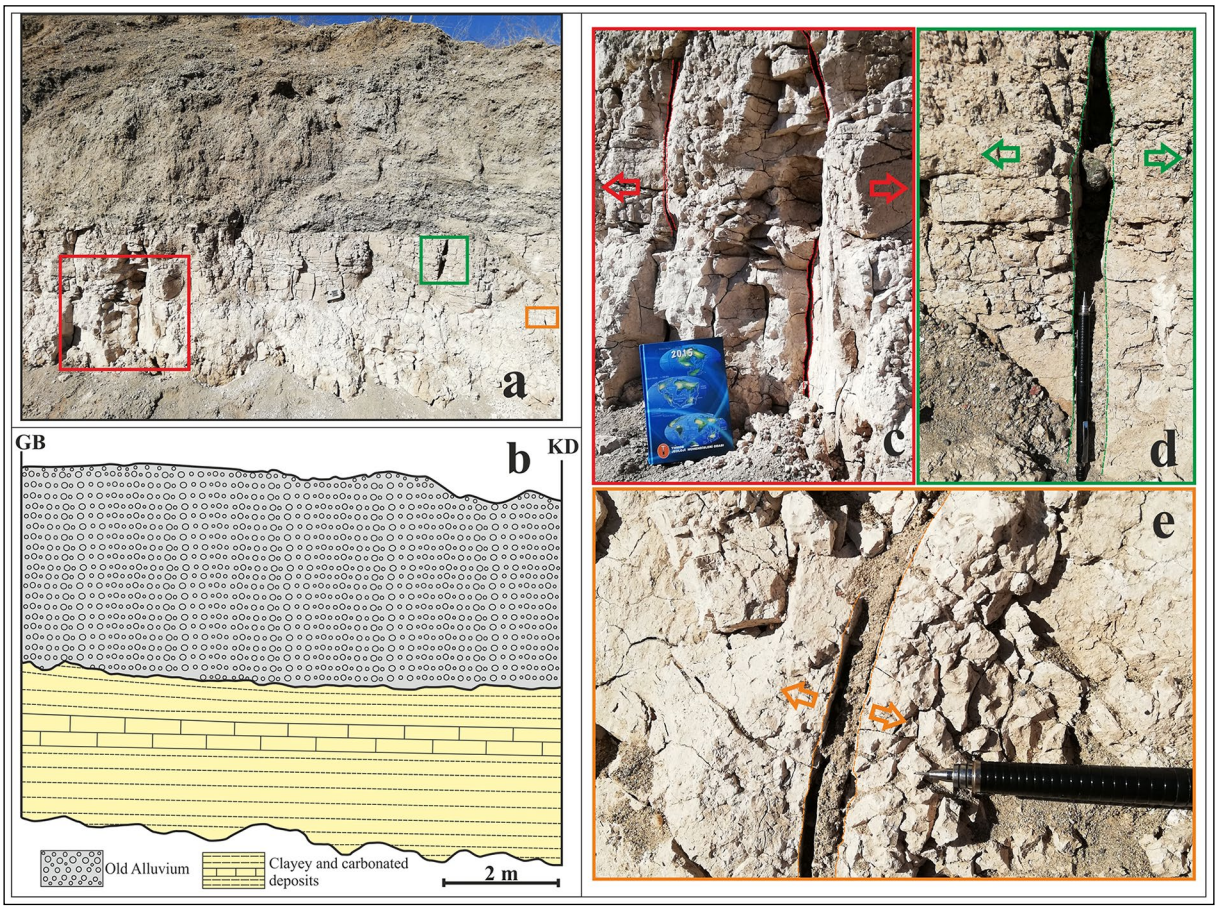

Figure 9- a) The older alluvium which overlies clayey and carbonated sediments in the vicinity of Çamlıca district, b) the stratigraphic relationship of clayey carbonate sediments and older alluvial units, c) opening fractures developed in N30W direction, d) opening fractures that developed in N-S direction and e) opening cracks developed in E-W direction and bear more center fill compared to other fractures (location: see Figure 6a: b, look direction of photos: NE).

9c) and forms systematic fracture sets. These sets can be observed in an area of approximately 20 km^2. The fact that the central opening in fracture systems are clearly observed, which developed in N20W/N-S directional interval (Figure 9d) and the openings are not completely covered with alluvial fill, indicate that the tectonic activity in the region continues to date. In addition to the indicated directions, the E-W trending fractures in the region (rotation measurement was made in 4 fractures) are also observed (Figure 9e).

The separation of Miocene clay and carbonate bearing sediments and Miocene conglomerates with a N40W/78SW directional plane (Figures 10a and 10b) contains field data related to probable faulting on surfaces observed around the Karapınar district. The fault related surfaces are also observed in the area between Büyükdere and Ihlamurkent districts, where EFZ is not continuous. To the east of the plane, which cut NE dipping, medium compacted clay, conglomerate and sandstone alternation with a strike of N10W/82NE, there is observed a different lithology, which is red-dark pink colored, poor to medium compacted, clay-silt grain sized and bear carbonate fillings in places (Figures 10c and d). The geometry on this surface (the cross cutting relationship, the appearance of units in different lithologies, the clays observed on the plane and no significant fall or rise in the topography) point out to a probable strike-slip fault mechanism. There is not observed enough field data to determine the types of F1 and F2 fault planes. F1 and F2 planes, which are assessed on the right lateral shear zone proposed for Eskişehir (Seyitoğlu et al., 2015) (Figure 11a), correspond to R/ and the geometry of Riedel shears, respectively. However, whether these planes cut the Quaternary can be considered as a matter of discussion (Figure 11b).

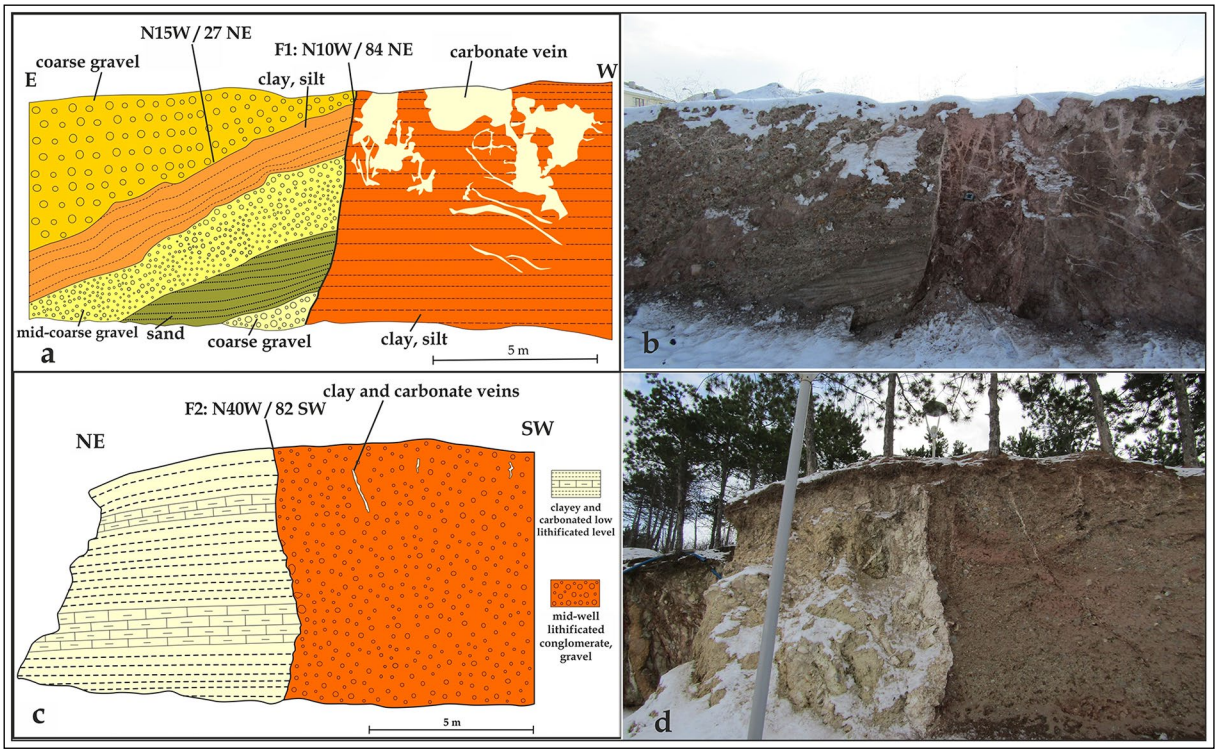

Figure 10- a) Plane with a dip direction of N10W in south of Çankaya district (F1) and its relationship with geological units, b) the field photograph of F1 plane; look direction: S, c) N40W directing plane (F2) and its relationship with geological units around Karapınar district and d) the field photo of F2 plane; look direction: EES (Location see Figure 6a: d and c).

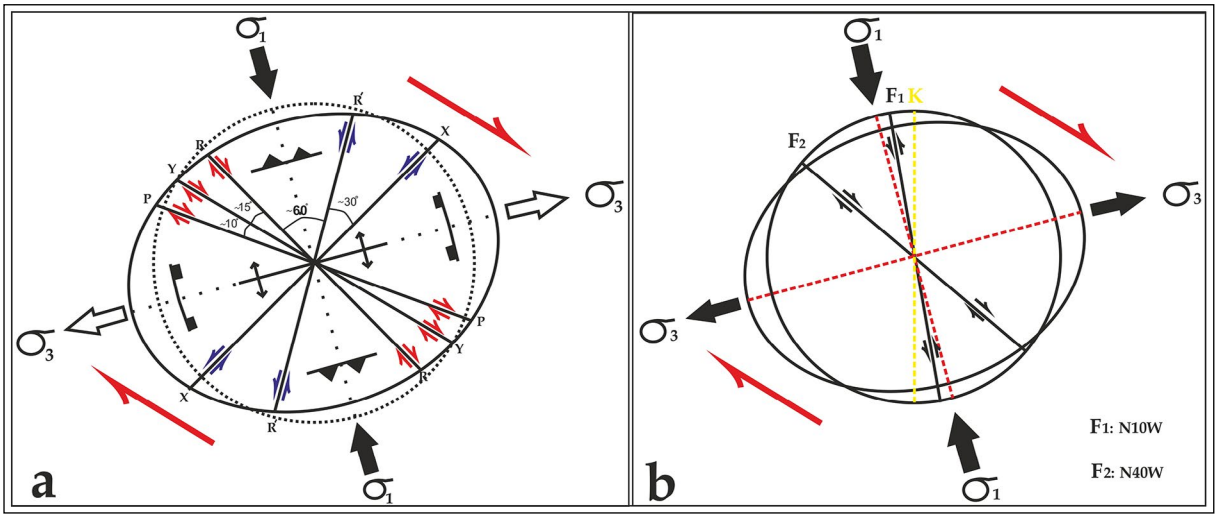

Figure 11- a) Right lateral strike-slip shear zone (Seyitoğlu et al., 2015) that shapes Eskişehir surround and b) locations of F1 and F2 planes which shape the region in the shear zone.

4. Discussions

There is not observed any consensus on the stratigraphic relations of Miocene units and the Miocene-Pliocene transition in the central-south region of Eskişehir. When geological maps in the literature are examined; the distribution of the Miocene conglomerate (Orhan et al., 2007; Ocakoğlu, 2007) and Pliocene limestone (Şengüler and Izladı, 2013; Usta and Kutluk, 2014) units in the region in Akarbaşı-Alanönü districts and in the vicinity of Çankaya-Göztepe districts located at further south

seems to be open to discussion. In order to present new findings to the general geology of the region, the field studies were carried out using classical methods in an area of approximately 10 km^2 which is bordered by Akarbaşı and Göztepe districts in the northwest and Yenikent and Çankaya districts in the southeast. The ages of units in field studies were taken as reference from Gözler et al. (1996).

The oldest unit in the identified region is composed of red colored, medium-well cemented Miocene conglomerates which sporadically crop out between Yenikent and Karapınar districts. The conglomerates are unconformably overlain by the carbonate bearing clayey sediments. As going towards south at higher latitudes through a line formed between Karapınar and Çankaya districts, it is possible to see the transitions of pale yellow-beige, medium-strength clayey-limestone that overly the carbonate bearing clay level and the beige-white well-strength limestone that overly the clayey limestone level (Figure 12).

Data obtained from field observations indicate the fault mechanism between Karapınar and Akarbaşı districts during Miocene. These are the presence of conglomerate pebbles cemented by clayey-limestone unit in the northeast of the Yenikent district (Figure 13a), the horizontal transition from conglomerate to clayey-limestone (Figure 13b), the separation of conglomerate and carbonate clay units with a N40W/78SW (Figure 13c) and the fact that this plane does not cut the younger limestone levels at higher elevations (Figure 13d).

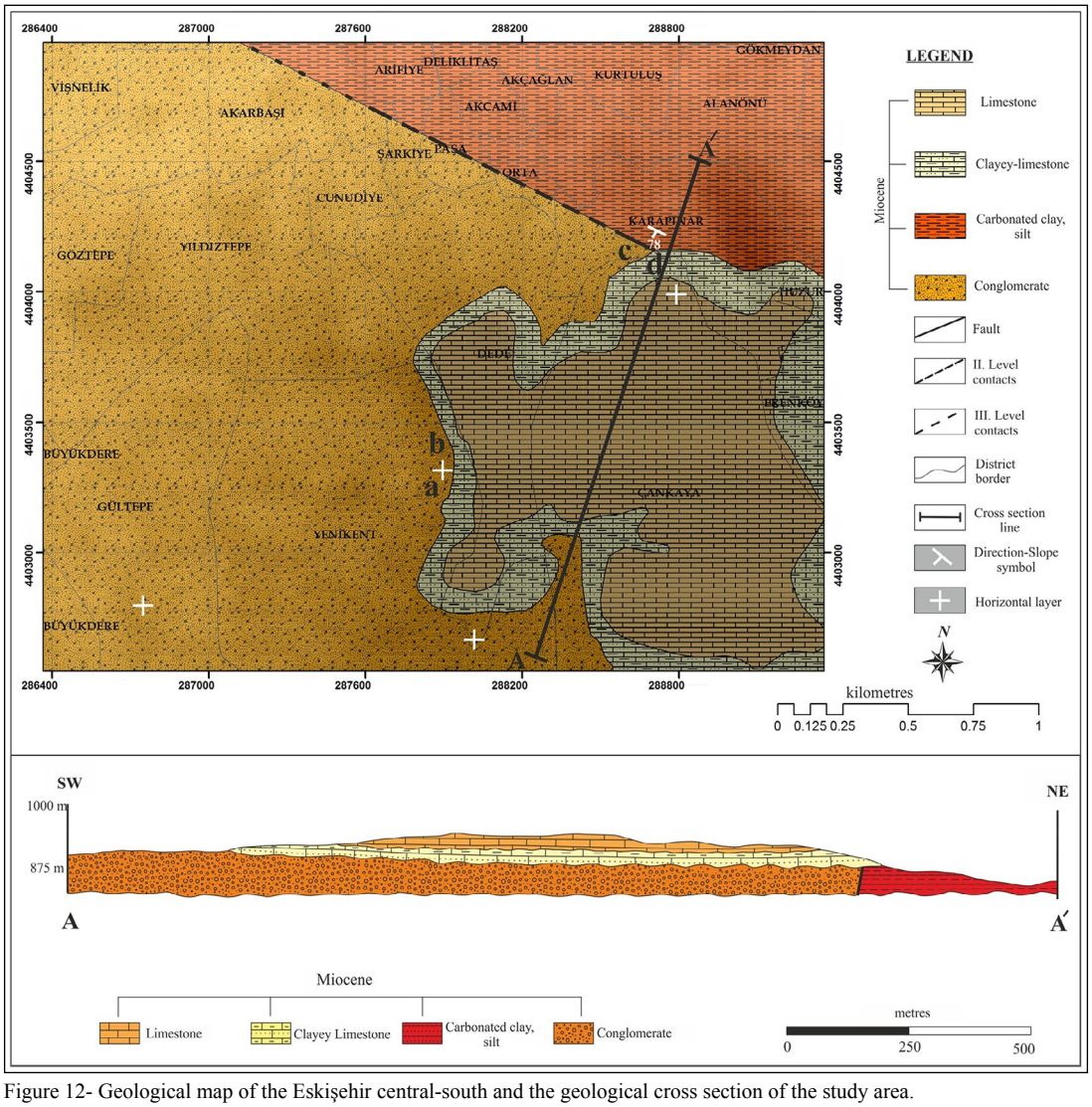

Figure 12- Geological map of the Eskişehir central-south and the geological cross section of the study area.

Figure 13- a) Clay and carbonate cemented conglomerate pebbles, b) clayey limestone which unconformably overlies pebble-conglomerates, c) conglomerate and clayey-carbonated units with an angle of 78° between them and d) clayey limestones that have no traces of fault (Location: see figure 12).

5. Conclusion

Total of 44 water drilling points, which were distributed to various regions of Eskişehir province and opened by DSI, were transferred to GIS environment. The analyses of points transferred to the GIS environment were carried out on the transverse geological cross sections. As a result of analyzes carried out by general geological principles (lateral continuity, cross cutting relationship, law of superposition), it is observed that there is no stratigraphic and geological consensus in an area of approximately 10 km^2 restricted by Akarbaşı and Göztepe districts in the northwest and Yenikent and Çankaya districts in the southeast. The studies in this area were carried out with the principle of transferring the classical geological mapping methods to GIS environment. As a result of completed field and GIS studies, the stratigraphic relationships of Miocene units in the study area were evaluated through field data. The carbonate-bearing clay levels deposited on conglomerate and the clayey limestone and limestone levels deposited on them, respectively, can be observed in the field. The horizontal transitional contact between the conglomerate-clayey limestone levels observed in the vicinity of Yenikent district, to be cut in the direction of N40W with dip amount of 78° in the Karapınar district (close to vertical) is the characteristic of field data for a fault that may develop at this point. Although the mentioned plane conforms to the proposed Riedel shear geometry for the region, the current activity of this plane could not be determined from field data due to the absence of Quaternary units in the region. In the Eskişehir region, where neotectonic activity is thought to be shaped by the effect of right lateral shear zone, the structural traces of this activity have been investigated by field studies. The opening cracks observed in Quaternary units in N-S direction around Çamlıca-Batıkent districts and the planes having the geometry

compatible with the R and R' planes developed on the Vadişehir-Ihlamurkent-Karapınar line support the right lateral strike-slip shear model proposed for the neotectonic activity of the Eskişehir region.

References

Altunel, E., Barka, A. 1998. Eskişehir fay zonimun İnönü-Sultandere arasında neotektonik aktivitesi. Geological Bulletin of Turkey 41(2), 41-52.

Barka, A., Reilinger, R., Şaroğlu, F., Şengör, A.M.C. 1995.The Isparta angle: Its importance in the neotectonics ofthe eastern Mediterranean region. IESCA-1995 Proce-edings

Bartlett, W.L., Friedman, M., Logan, J.M. 1981. Experimental folding andfaulting of rocks under confining pressure. Part IX. Wrench faults inlimestone layers. Tectonophysics 79, 255 – 277.

Emre, Ö., Duman, T. Y., Özalp, S., Elmacı, H., Olgun, Ş., Şaroğlu, F. 2013. 1/1.250.000 ölçekli Türkiye diri fay haritası. Maden Tetkik ve Arama Genel Müdürlüğü Özel Yayınlar Serisi, Ankara, Türkiye.

Göncüoğlu, M. C., Turhan, N., Şentürk, K., Özcan, A., Uysal, Ş., Yalınız, M. K. 2000. A geotraverse across northwestern Turkey: Tectonic units of the Central Sakarya region and their tectonic evolution. Geological Society, London, Special Publications 173(1), 139-161.

Gözler, M. Z., Cevher, F., Ergül, E., Asutay, H. J. 1996. Orta Sakarya ve güneyinin jeolojisi. Maden Tetkik ve Arama Genel Müdürlüğü Rapor No: 9973. Ankara (unpublished).

Hancock, P.L. 1985. Brittle microtectonics: Principles and practice. Journal of Structural Geology 7, 437 – 457.

Harding, T. P. 1974. Petroleum traps associated with wrench faults. AAPG Bulletin 58(7), 1290-1304.

Ketin, İ. 1966. Tectonic units of Anatolia (Asia Minor). Bulletin of the Mineral Research and Exploration 66, 23-33, Ankara.

Kumsar, H., Çelik, S. B., Mustafa, K. 2011. Denizli İl Merkezi Yerleşim Alanının Jeolojik, Jeoteknik Kent Bilgi Sistemi (JEO-KBS). Pamukkale Üniversitesi Mühendislik Bilimleri Dergisi 10(4), 25-31.

Ocakoğlu, F. 2007. A re-evaluation of the Eskişehir Fault Zone as a recent extensional structure in NW Turkey. Journal of Asian Earth Sciences 31(2), 91-103.

Okay, A. I. 2011. Tavşanlı Zone: The Northern Subducted Margin of the Anatolidetauride Block. Bulletin of the Mineral Research and Exploration 142, 195-226.

Okay, A. I., Monod, O., Monié, P. 2002. Triassic blueschists and eclogites from northwest Turkey: vestiges of the Paleo-Tethyan subduction. Lithos 64(3-4), 155-178.

Orhan, A., Seyrek, E., Tosun, H. 2007. A probabilistic approach for earthquake hazard assessment of the Province of Eskişehir, Turkey. Natural Hazards and Earth System Science 7(5): 607-614.

Seyis, C,. Yalçın, M.N., İnan, S. 2002. Coğrafi Bilgi Sistemine (CBS) Dayalı Jeolojik Veri Tabanı Yönetimine Zonguldak Bölgesinden Bir Örnek, Türkiye 13. Kömür Kongresi Bildiriler Kitabı, Zonguldak, 29-31 Mayıs 2002, 335-346.

Seyitoğlu, G., Ecevitoğlu, G. B., Kaypak, B., Güney, Y., Tün, M., Esat, K. 2015. Determining the main strand of the Eskişehir strike-slip fault zone using subsidiary structures and seismicity: A hypothesis tested by seismic reflection studies. Turkish Journal of Earth Science 24(1), 1-20.

Sylvester, A. G. 1988. Strike-slip faults. Geological Society of America Bulletin 100(11), 1666-1703.

Şaroğlu, F., Emre, Ö., Kuşçu, İ. 1992. 1/1.000.000 Türkiye diri fay haritası. Maden Tetkik ve Arama Genel Müdürlüğü, Ankara.

Şengör, A.M.C., Görür, N., Şaroğlu, F. 1985. Strike-slip faulting and related basin formation in zones of tectonicescape: Turkey as a case study. In: Strike-Slip Deformation, Basin Formation and Sedimentation (edited by Biddle, K.T. & Christie-Blick, N.). Soc of Eco Paleo and Min Spec Publ 37, 227-264.

Şengüler, İ., Izladı, E. 2013. Neogene stratigraphy of the Eskişehir graben and the investigation of coal deposition by seismic reflection method. Bulletin of the Mineral Research and Exploration 146, 105-116.

Tchalenko, J. S., Ambraseys, N. N. 1970. Structural analysis of the Dasht-e Bayaz (Iran) earthquake fractures. Geological Society of America Bulletin 81(1), 41-60.

Tün, M., Pekkan, E., Tunç, S. 2015. Yer Sarsıntı Haritalarının Üretilmesinde Sismik Ağ Yapısı: Eskişehir Örneği. Electronic Journal of Map Technologies 7(3), 1-14.

Usta, K., Kutluk, H. 2014. Eskişehir-Alpu Linyitlerinin Fiziksel ve Kimyasal Özellikleri. Anadolu University of Sciences and Technology-A: Applied Sciences and Engineering 15(1).

Woodcock, N. H. 1986. The role of strike-slip fault systems at plate boundaries. Philosophical Transactions of the Royal Society of London. Series A, Mathematical and Physical Sciences 317 (1539), 13-29.

Bulletin of the Mineral Research and Exploration

http://bulletin.mta.gov.tr

2D and 3D structural boundaries of the tectonic composition of the Anatolia and surrounding seas using by the gravity (Satellite Data): Eastern Mediterranean

Ceyhan Ertan TOKER[a*]

[a]*General Directorate of Mineral Research and Exploration, Department of Marine Researches, Ankara, Turkey*

Research Article

Keywords:
Gravity, Filter, Standart deviation, Long wavelength, East mediterranean, 2D, 3D.

ABSTRACT

Gravity data is processed and the problems of the earth are examined. The density of the data can be arranged to solve detail, semi-detail and regional problems. Here, the gravitational data obtained by processing the linearity of the 2D and 3D visuals in terms of plate size large wavelength structures are examined. 2D linearities determine important stress areas but they are affected at different rates with respect to the spatial distribution of source effect. Due to grid formation, these boundaries are affected at different rates from less dense and very dense structures. Different wavelengths in structure boundary analysis; derivative and phase elements and filters. Vertical change in 3D analysis can be made at the approach level with the analytical examination of 2D change. At this stage, the distribution of source effect and depth model structure parameters are calculated. When examining large wavelength structures, some of the buried structures appear due to cover removal. In search of solutions for tectonic structures that we may miss; The tectonic components that need to be confirmed in the Eastern Mediterranean have been tried to be elucidated in this study. 3D building solutions are important in this respect.

Received Date: 05.09.2019
Accepted Date: 20.10.2019

1. Introduction

The Anatolia, which resembles a horizontal rectangle extending from the Aegean coast to the Iranian border, has intracontinental movements and mobile microplate boundaries. These boundaries can be observed in processed gravity data (Figures 1 and 2). Roughly, the lower right corner (SE) of this rectangle is pushed northward by the Arabian plate. This pushing is stopped by the inverse forces on the upper right (NE) of the rectangle. While the main block escapes westward along the North Anatolian Fault (NAF) by 25 mm/year (Barka, 1992; McClusky et al., 2000; Reilinger et al., 2006) and the Eastern Anatolian Fault (DAF) by 10 mm/year (Nalbant et al., 2002; Barka and Reilinger, 1997) it is met by the shear zone in the Aegean plate (McKenzie, 1972). It then moves towards the left by the influence of Hellenic and Cyprus arcs (SW). The left north (NW) and south of the rectangle were compressed (SW) and enlarged. All of these movements caused large transformations and plate ruptures. The North Anatolian transform extends from the Anatolia to Greece and covers a large part of the geography which is the subject of the data. While there are many reasons for the rectangular structure to be cut in a north-south direction with large transforms, the discontinuities in this direction cannot be seen. The flattened structure of the Black Sea (NS) and the mid-Mediterranean ridges (EW) where discontinuities are covered by additional accretions and plains in the Central Anatolia show that they have stress lines of which the main axes are in north-south directions and accordingly developed lineaments in different times. Several deformations have developed along with the

Citation info: Toker, C. E. 2020. 2D and 3D structural boundaries of the tectonic composition of the Anatolia and surrounding seas using by the gravity (Satellite Data): Eastern Mediterranean. Bulletin of the Mineral Research and Exploration 163, 39-45. https://doi.org//10.19111/bulletinofmre.641237.

**Corresponding author: C. Ertan TOKER, ceyhanertan.toker@mta.gov.tr*

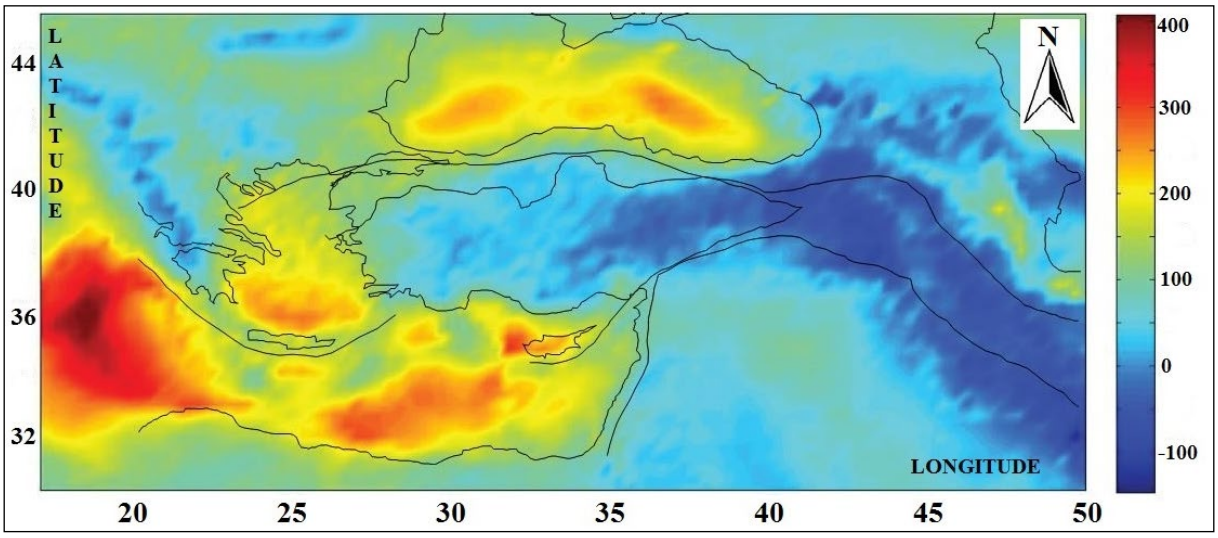

Figure 1- Bouguer gravity data.

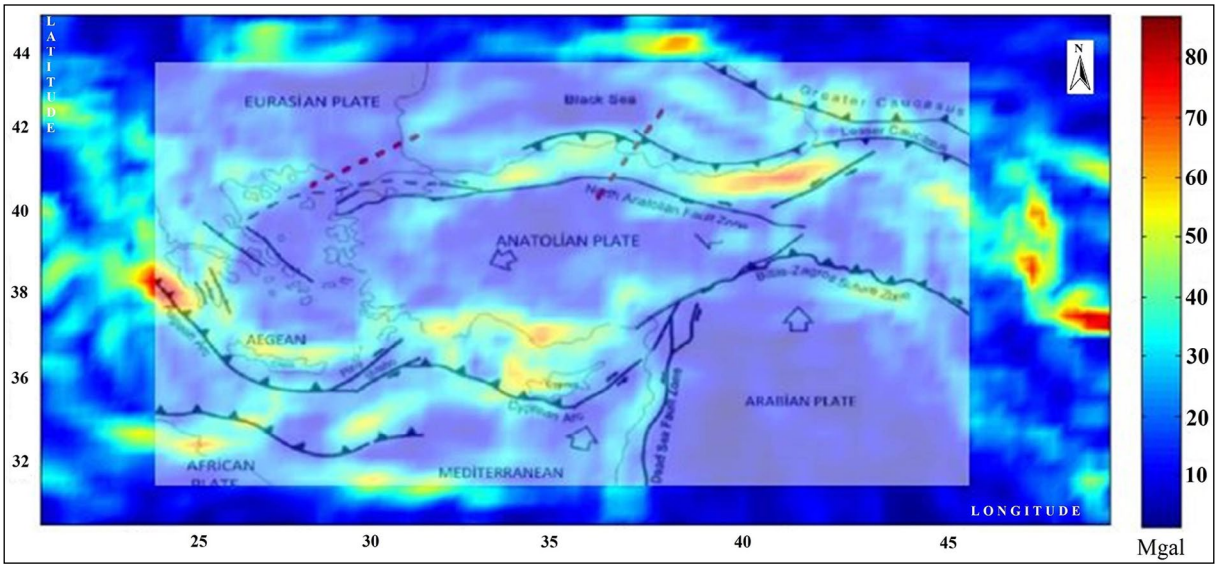

Figure 2- 2D, shifting window, non-derivative filter and tectonic elements (Toker, 2019).

Anatolian plate under big compressional load in the region among the Crimean shores in the north, the Egyptian shores in the south, Iran in the east and Greece in the west. The accompanying of the Eastern Mediterranean by subducting to the upward movement of the Arabian plate should indicate the presence of NS directing stress axis and/or plate boundaries. The tectonic activities in the continental crust have been investigated in previous studies [McClusky et al. (2000); Reilinger, et al. (2006); Aktuğ et al. (2009)] by global positioning (GPS) data. Özdemir and Karslıoğlu (2019) also investigated the microplate boundaries by classifying the vectorial slip rates in global positioning data.

The aim of this study is to reveal the unclear tectonic formations of regional tectonics and the Eastern Mediterranean. For this purpose, the 2D and 3D lineaments were examined.

2. Data and Method

Data set is a network data formed by satellite data that has a sampling point at each 7 km. (URL1). This data was filtered for 2D linearity (Toker, 2019). For 3D, Pham et al. (2018), a hybrid method developed by Cordell - Henderson inverse solution was applied. An algorithm, which quickly reaches the interface where the observed and calculated values overlap, is used to

identify the density contrast that does not need to be predicted for the target depth.

Non-linear filtering technique that can perform non-derivative boundary analysis by limiting the data neighbourhoods by shifting and shifting this limitation by controlling the deviation without using derivative (Figure 2) (Toker 2019).

3. Findings

Figure 1 shows the Bouguer gravity data and the generated grid. In figures 2 and 3, the discontinuities in the scale of long-wavelength plate obtained by the 2D filter and in figure 3; the microplate and longwave boundary relationships observed by the "0" contour of the tilt angle are seen. In figure 4, the structure boundaries of the inverse solution take place. Figure 5 shows the traces on the interface of the gravity foundation without cover, and figure 5b shows 3D lineaments looking from Southwest-Northeast directions. Figure 6 shows the three-dimensional shell structure of the Aegean region. Since the depths in the Aegean region are known as graben and sub-graben depths, the results representing the approximate upper crust and lower crust depth were reached. The fact that the region is a smaller area than the main data has enabled the depths to be seen as more sensitive. In figure 6, the "0" (zero) contour on the upper surface

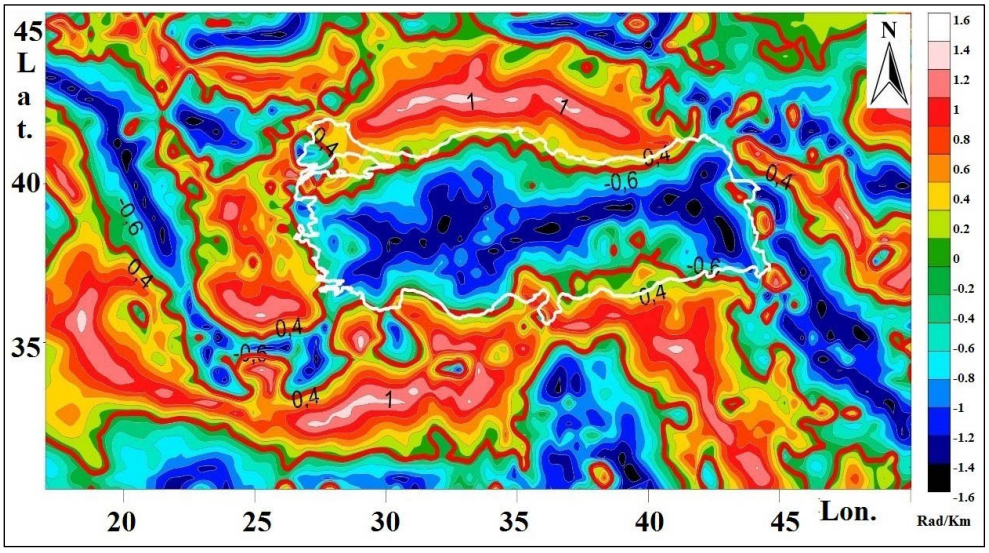

Figure 3- Tilt angle and its "0" contour (red line).

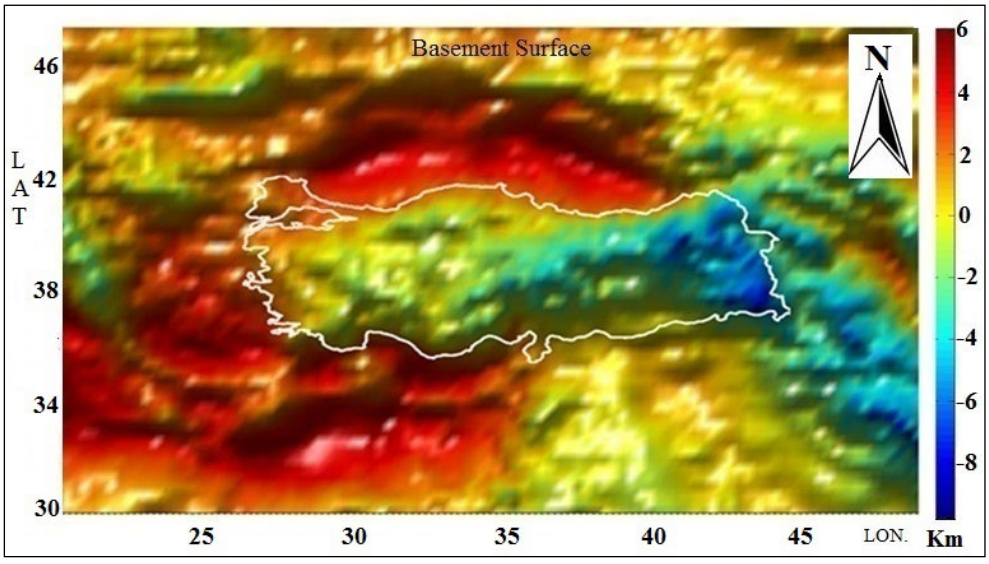

Figure 4- 3D, gravity inverse solution (no comment).

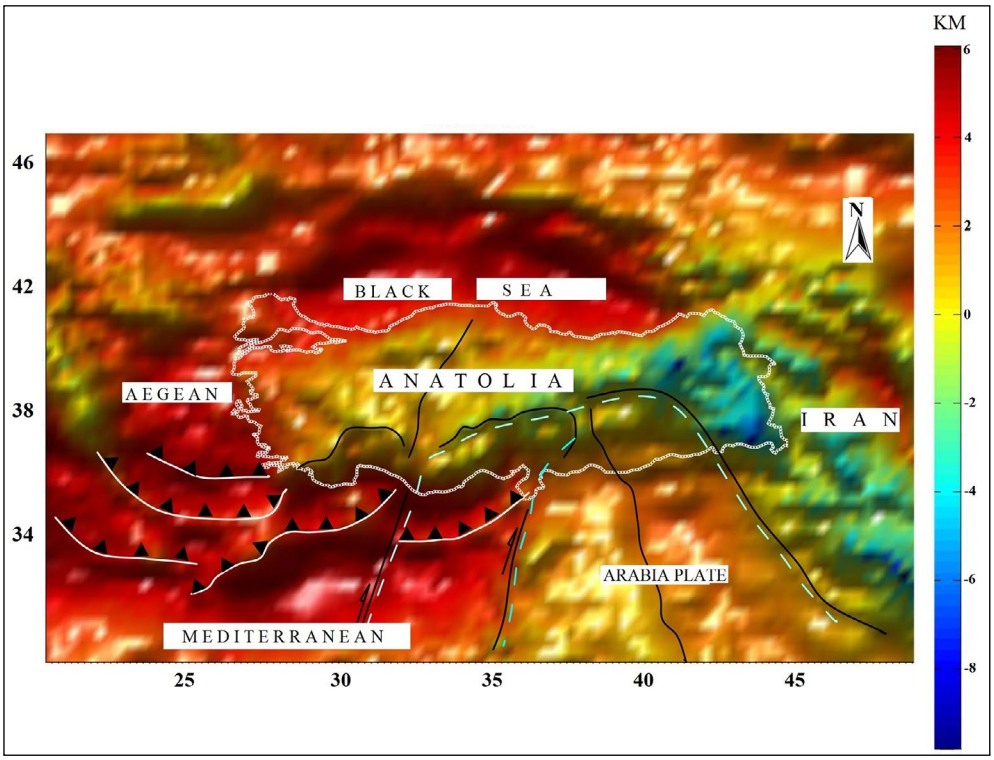

Figure 5- Main tectonic lineaments and the Antalya arc. (Özdemir et al., 2019) showed the anomaly which formed by the variations of GPS velocities in Antalya-Sinop axis.

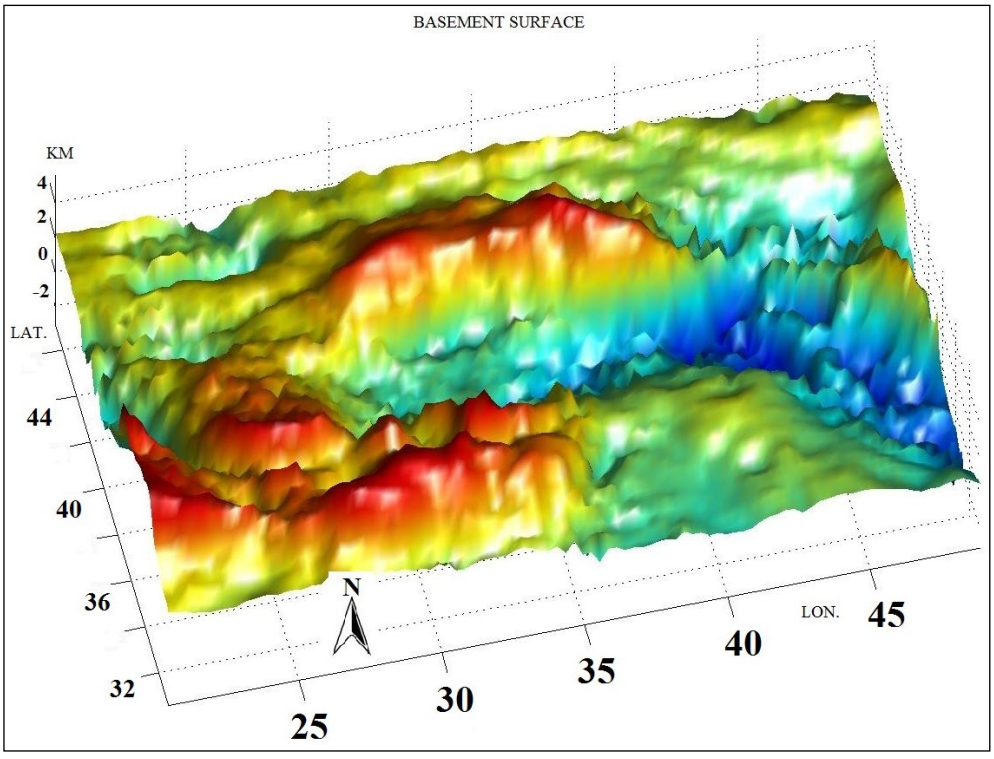

Figure 6- Look direction SW-NE. Angular 3D interface view. The regions in which the interface topography is dense due to gravitational magnitude present interface close the surface.

of the grabens is clearly observed. The depth contour (zero) and the tilt angle contour (zero) are concepts that should not be confused. Zero contour is the actual plate boundary. However, boundaries are actually zones of anomalies. The zero contours are the actual plate boundary. It is seen that the Thrace plate forms a microplate within the closed red line. It is seen that the plates converge as interlaced sequentially on the subduction boundary in the Hellenic arc. It is also seen that there is an offset with the northward movement of the Arabian plate along the Turkey-Iran border in the east and crust scale basins were developed in places where offsets are observed. The yellow-orange belt that represents high angular values along the border of the Arabian plate and Turkey is considered to have been the borders of the Neotethys remnants. Tilt angle values on the map in figure 3 vary between -1.57 and +1.57. However, the visual scale is defined by 0.2 colour ranges. It is seen that there is a block structure boundary closed under the sedimentary cover in the Thrace. The deep structure boundary extending from its southwestern part to the Black Sea with arc-shaped curvature indicates the great block structure. In figure 7, the displays in which the Moho interface was calculated and the lineaments sensed by software took place are seen. It is seen that the lineaments of Moho do not match with topographic lineaments.

Antalya - Sinop orienting lineament in figure 5 was shown as a large zone anomaly where GPS velocities vary by Özdemir et al. (2019). The density along this direction forms a boundary between east and west. Epellbaum (2017), defined the Southern Taurus belt extending from east of the Sırrı Erinç Plateau and the south of Cyprus to the northeast (İskenderun bay), as parallel to the Taurus mountain belt in the southern Anatolia and as a conjugate in the south. Le Pichon et al. (2019) stated that gravity data represented the continental crust in the southeast of the Eastern Mediterranean. The detailed data processing results show that tectonic events in the south of Antalya (Figure 2) are more complex. There is a covered and dense structure that draws an arc towards the east of the Antalya Bay. There is a third depth structure called the "Antalya subduction" between Cyprus and the Hellenic arcs.

The Geoid is called the equipotential surface formed by the gravitational field which best fits with the average sea surface. Another definition is the average earth surface ellipsoid (URL2). It is a dynamic (variable) interface sensitive to topographic changes. In spite of the data sets created at different times, it seems possible that the inverse solution and geoid structures can be related to shedding light on

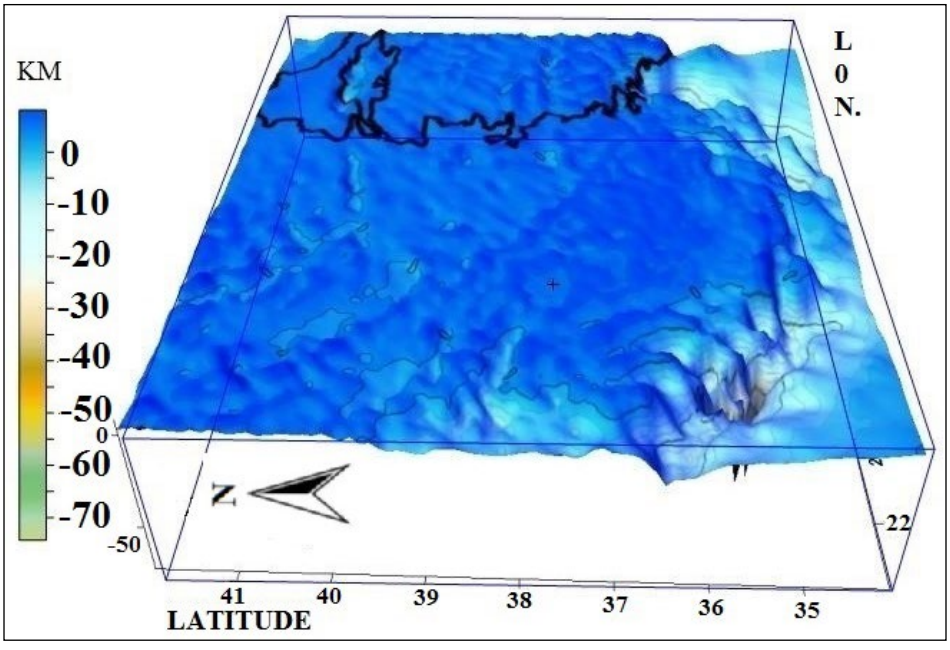

Figure 7- The interface topography of which the 3D, Aegean crust structure (inverse solution) is dependent on the magnitude. The Aegean region grabens, the lineaments of the Sea of Marmara and the North Anatolian Fault are clearly seen. The tectonic events overlap with the inverse solution.

the problem (Figure 8). In figure 8, the Geoid image created with open sources is correlated with the satellite data filtered by the non-derivative filter. In both maps, the harmony in tectonic structures in front of the Gulf of Antalya in the Eastern Mediterranean is observed. Since the geoid surface takes the average sea level as a reference, it has smooth transitions similar to the inverse solution interface and it is compatible with the inverse solution. Inverse solution depths are meaningful depths that require a reference depth and are relative to each other.

4. Discussion

The 3D lineaments and the known tectonic situation may not correspond exactly with tectonic elements and displacements. For example, the North Anatolian Fault (NAF) may not be displayed as a lineament. When the cover structure is removed by the 3D inverse solution, the lineaments may indicate different situations. For example; when lineaments in the depth map created by calculating the Moho interface are examined, it is seen that NAF is not really seen among the lineaments in Moho. However; it is a discontinuity called as the Paleotethys residual following the Black Sea coasts and/or as a discontinuity representing the Black Sea subductions. In the Mediterranean, there are two southwest-northeast oriented discontinuities belonging to two different subductions. The reference information here is that the crust deformations and discontinuities in Moho do not overlap. When the crust behaves as a ductile, there will be no lineament on the surface. The crust has to break away as it cannot keep up with the movement in the Moho (lower shell). This is reactive, but the movements at the Moho interface may not produce discontinuity. Moho discontinuities were determined by the software and an algorithm. Very deep structures aligned in the N-S direction in the east could be detected by the algorithm (Figure 9).

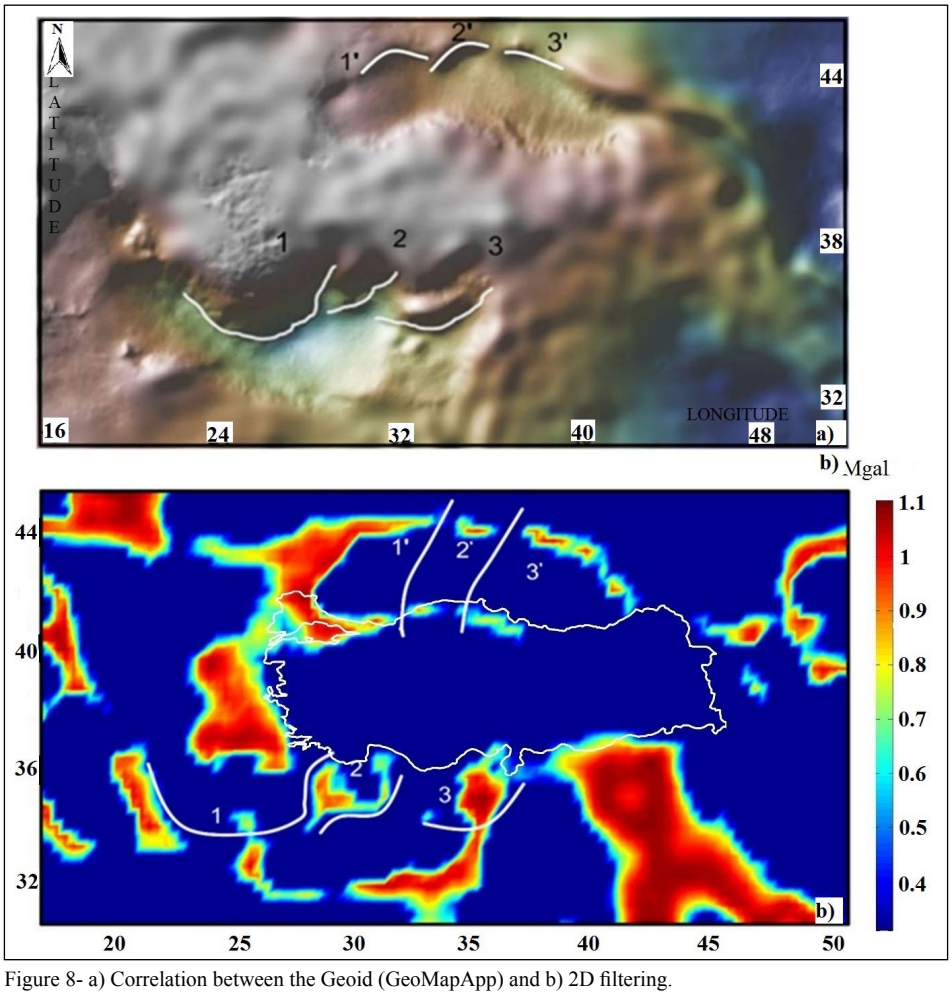

Figure 8- a) Correlation between the Geoid (GeoMapApp) and b) 2D filtering.

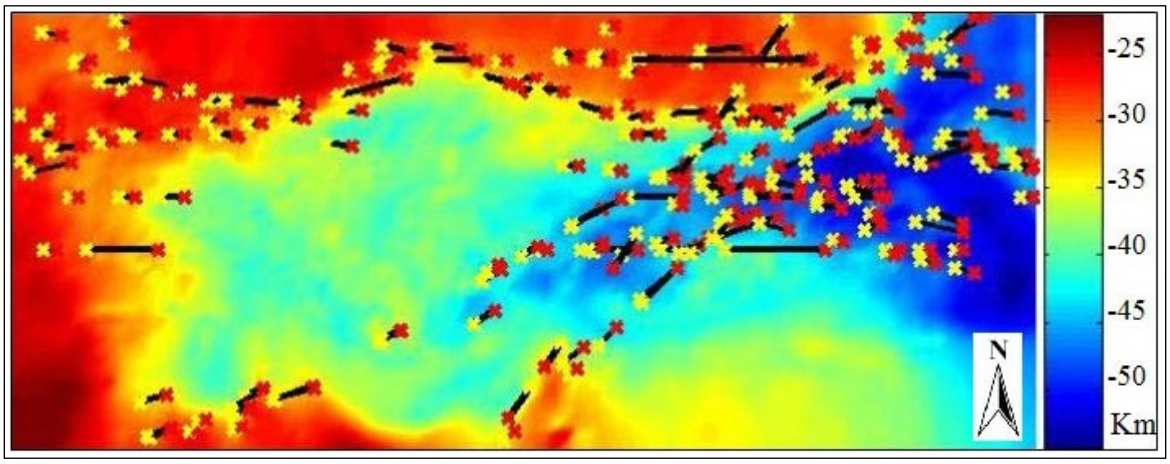

Figure 9- Moho interface and loop point. Discontinuities perceived by the software.

Acknowledgements

I am thankful to our General Directorate and all staffs of the Department of Marine Researches.

References

Aktuğ, B., Nocquet, J.M., Cingöz, A., Parsons, B., Erkan, Y., England, P., Lenk, O., Gürdal, M.A., Kılıçoğu, A., Akdeniz, H., Tekgül, A. 2009. Deformation of Western Turkey from a combination of permanent and campain GPS data: Limits to block-like behavior. Journal of Geophysical Research 114, B10404, doi:10.1029/2008JB006000

Barka, A. 1992. The North Anatolian Fault Zone. Annales Tectonicae VI, 164-195.

Barka, A., Reilinger, R. 1997. Active tectonics of the Eastern Mediterranean region: deduced from GPS, neotectonic and seismicity data. Annali di Geofisica XL(3), 587-610.

Epellbaum, V. L. 2017. Satellite Gravity ('Big Data') – a powerful tool for regional tectonic examination and reconstruction. Horizons in Earth science research Vol No:1-1.Chapter. Editors: Veress, B., Szigethy, J. Nova Science Publishers.

Le Pichon, X., Şengör, A.M.C., İmren, C. 2019. A new approach to the opening of the Eastern Mediterranean Sea and the origin of the Hellenic Subduction Zone Part 1: The Eastern Mediterranean Sea. Canadian Journal of Earth Sciences DOI:10.1139/cjes-2018-0128.

McClusky, S., Balassanian, S., Barka, A., Demir, C., Ergintav, S., Georgiev, I., Gürkan, O., Hamburger, M., Hurst, K., Kahle, H., Kastens, K., Nadariya, M., Ouzounis, A., Paradissis,D., Peter, Y., Prilepin, M., Reilinger, R., Şanlı, I., Seeger, H., Tealeb, A., Toksöz, M.N., Veis, G. 2000. GPS constraints on plate kinematics and dynamics in the Eastern Mediterranean and the Caucasus. Journal of Geophysical Research 105, 5695-5719.

McKenzie, D.P. 1972. Active tectonics of the Mediterranean region. Geophys J R Astr Soc 30, 109-185.

Nalbant, S.S., McCloskey, J., Steacy, S., Barka, A. 2002. Stress accumulation and increased seismic risk in eastern Turkey. Earth and Planet Sci Lett 195, 291-298.

Özdemir, S., Karslıoğlu, O. 2019. Soft clustering of GPS velocities from a homogeneous permanent network in Turkey. Journal of Geodesy 93, 1171–1195.

Pham, L, T., Öksüm, E., Thanh, D. D. 2018. GCH_gravinv: A MATLAB-based program for inverting gravity anomalies over sedimentary basins. Computers and Geosciences 120, DOI:10.1016/j.cageo.2018.07.009.

Reilinger, R., Mcclusky, S., Vernant, P., Lawrence, S., Ergintav, S., Çakmak, R., Özener, H., Kadirov, F., Guliev, I., Stepanyan, R., Nadariya, M., Hahubia, G., Mahmoud, S., Sakr, K., Arrajehi, A., Paradissis, D., Al-Aydrus, A., Prilepin, M., Guseva, T., Evren, E., Dmitrotsa, A., Filikov, S.V., Gomez, F., Al-Ghazzi, R., Karam, G. 2006. GPS Constraints on Continental Deformation in the Africa-Arabia-Eurasia continental collision zone and implications for the dynamics of plate interactions. Journal of Geophysical Research 111, BO5411, 1-26, DOI: 10.1929/2005JBOO4051.

Toker, C. E. 2019. A brief note on the effects of floating standard deviation (non-derivative) and horizontal gradient (derivative) filters. Bulletin of the Mineral Research and Exploration 159, 239-241.

URL1 (Gravity Data) Bureau Gravimetrique International (BGI). DOI:10.18168/BGI

URL2 (Geoid): https://tr.wikipedia.org/wiki/Geoit

Geoid Data: http://www.geomapapp.org

Bulletin of the Mineral Research and Exploration

http://bulletin.mta.gov.tr

Oligocene molasse sedimentation in the Central Taurides: Records of the onset of extensional tectonic regime

Ayhan ILGAR[a*], Tolga ESİRTGEN[a], Banu TÜRKMEN-BOZKURT[a] and Serap DEMİRKAYA[a]

[a]*General Directorate of Mineral Research and Exploration, Department of Geological Research, 06800, Ankara, Turkey*

Research Article

Keywords:
Taurus orogeny, Orogenic collapse, Lacustrine deposits.

ABSTRACT

The lacustrine units have been deposited in the Ermenek, Bucakkışla, Korucuk and Çamlıyayla basins in the Central Taurides since early Oligocene. In this study, structural features and stratigraphical properties of Oligocene basins have been described in detail and the lacustrine units have been dated. Regional geological interpretations have been made by using tectono-stratigraphic and age data of the basins. Lacustrine Oligocene sedimentation in these basins, which were opened on the tectonic units of Taurides due to normal faults, constitute the first records of the sedimentation occurring under the extensional tectonic regime after the orogeny of the Central Taurides. All the pre-Oligocene units that had been emplaced in the region due to a north-south compressional movement in the Central Taurides, continued to be compressed until the end of Eocene, and completed their orogenic development as napped structures. The bedrock units, reaching the maximum elevation, have been subjected to "orogenic collapse" due to the strain or gravity forces as a result of an interruption or termination of the compression which lasted until the end of Eocene. Thus, "orogenic collapse" basins have started to be formed in the Central Taurides since Oligocene. The orogeny and the compressional tectonic regime forming the Taurides lasted until late Miocene in the Eastern Taurides. On the other hand, extensional basin formation since early Oligocene on the Taurus units, which had been emplaced in the region due to nappe tectonics, indicates that a new tectonic period has started in the Central Taurides.

Received Date: 09.09.2019
Accepted Date: 26.01.2020

1. Introduction

Taurides which are the southern mountain range of Turkey, consist of plate fragments amalgamated between Eurasian and Afro-Arabian plates. Triassic to Eocene geological evolution of Taurides is the result of a series of events from opening of an ocean beginning with rifting, to the closure of an ocean due to subduction, and collision. As the beginning of rifting along the northern margin of Gondwana in Early-Middle Triassic, Africa-derived microcontinents and oceanic branches between them started to be developed (Şengör and Yılmaz, 1981; Robertson and Dixon, 1984; Okay and Tüysüz, 1999). The rifted basins maintained their presence during Mesozoic –early Tertiary period (Robertson et al., 2012). The convergence between Afro-Arabian and Eurasian plates which occurred in late Mesozoic-early Tertiary period, and the closure of the Neotethyan Ocean controlled the geological development of Anatolia during this period (Şengör and Yılmaz, 1981; Robertson and Dixon, 1984; Dewey et al., 1986). Northward subduction of branches of Neotethys caused the emplacement of subduction zone ophiolite and ophiolitic mélange over Taurus

Citation info: Ilgar, A., Esirtgen, T., Türkmen-Bozkurt, B., Demirkaya, S. 2020. Oligocene molasse sedimentation in the Central Taurides: Records of the onset of extensional tectonic regime. Bulletin of the Mineral Research and Exploration 163, 47-76. https://doi.org/10.19111/bulletinofmre.681218.

**Corresponding author: Ayhan ILGAR, ayhan.ilgar@mta.gov.tr*

carbonate platform in Late Cretaceous (Özgül, 1976; 1977; Ünlügenç et al., 1990; Dilek and Whitney, 1997; Parlak and Robertson, 2004). This process continued during the Paleocene-Eocene period (Şengör, 1987; Clark and Robertson, 2002), thus, ophiolite and ophiolitic mélange emplacement occurred in a wide area on Taurus platform (Monod, 1977; Polat and Casey, 1995; Parlak and Robertson, 2004).

The orogeny that formed Taurides, and the resulting deformation proceeded until the late Miocene in the Eastern Taurides, and the Misis structural heights was developed by folding and thrusting (Michard et al., 1984; Kelling et al., 1987; Aktaş and Robertson, 1990; Dilek and Moores, 1990; Yılmaz, 1993; Yılmaz et al., 1993; Robertson, 2000). At the transition between the Western and the Central Taurides, the Lycian Nappes collided with the Isparta Angle until the late Miocene (Collins and Robertson, 1998, 2000; Poisson et al., 2003; Nemec et al., 2018).

In the Central Taurides which is structurally located between Isparta Angle in the west and Ecemiş Fault in the east (Figure 1a), basins started to develop due to post-orogenic extensional tectonic. However, timing of the extensional tectonics, which follow the compressional deformations related to orogeny, and the tectonic processes causing in basinal opening are controversial. According to Şengör (1987) and Clark and Robertson (2002), orogenic activities and compressional deformations in the Central Taurides lasted until the end of Eocene. Andrew and Robertson (2002) stated that the compressional tectonics indicating last movement of the nappes continued until middle Oligocene. Robertson et al. (2012) also claimed that post-collisional compressional regime lasted until the end of Oligocene.

According to Koçyiğit (1977), normal faults were formed as a result of epirogenic movements and the Mut Basin started to open in the early Miocene. These movements caused a thick sediment deposition in the basin, lateral-vertical facies changes, and forming of the tectonic structure of the region (Koçyiğit, 1977). Şafak et al. (2005) claims that, in Ermenek-Mut region, basin formation started in early Oligocene by extensional collapse following nappe emplacement. However, they report that, lacustrine detrital units (Yenimahalle formation) were initially deposited in these basins, then the lacustrine carbonates (Fakırca formation) were sedimented on these units.

A thick Neogene sequence consisting of terrestrial and marine units was deposited in the Central Taurides after the development of Taurus orogenic belt (Figure 1b). However, small intermountain molasse basins were developed in the region prior to opening of Mut Basin. These basins which started to open in Oligocene and where lacustrine depositions were occurred, formed the first products of the post-orogenic extensional tectonics. It is important to reveal the formation time and mechanism of these basins in the interpretation of regional tectonics. For this purpose, Ermenek, Bucakkışla, Korucuk and Çamlıyayla basins which were opened on the nappes due to normal faults in the Oligocene period have been the subject of the study (Figure 1b). Structural features of these basins have been defined, stratigraphic sequences have been studied in detail and the dated. Thus, structural development of the Central Taurides leading to basinal opening after orogeny has been demonstrated.

2. Regional Geology and Stratigraphy

The units defined in Taurus orogenic belt by Özgül (1976) constitute the pre-Oligocene bedrock of the Central Taurides (Figure 2). Geyikdağı Unit, among them, consists of Cambrian-Eocene aged non-metamorphosed rock units (Figures 3a, b). Geyikdağı Unit is situated beneath the other units as parautochthon. Aladağ Unit consists of carbonate and clastic rocks deposited in Late Devonian-Late Cretaceous interval (Figures 3c, d). Aladağ Unit, except for the beginning of Late Triassic, has a continuous succession. The unit is allochthonous wherever it crops out throughout the belt, and it forms sheet-like bodies on other units (Figure 3e). However, sequences of Aladağ Unit in some regions in the Taurides have been obducted by ophiolite and ophiolitic mélange. Bolkardağı Unit contains lithostratigraphic units of Middle-Late Devonian to early Cenozoic age which mainly metamorphosed under greenschist facies conditions (Figure 4a). Effect of the metamorphism varies regionally and increases with depth. The youngest metamorphic unit is Paleocene aged (Özgül, 1976). Bozkır Unit consists of a large number of blocks and tectonic slices of various age, types and sizes which can be mapped and its stratigraphy can be defined (Figures 4b, c). Mersin ophiolite and ophiolitic mélange cropping out in the southwest of Ecemiş Fault is situated in the Bozkır Unit (Figure 4d). Bozkır Unit overthrusts the other units

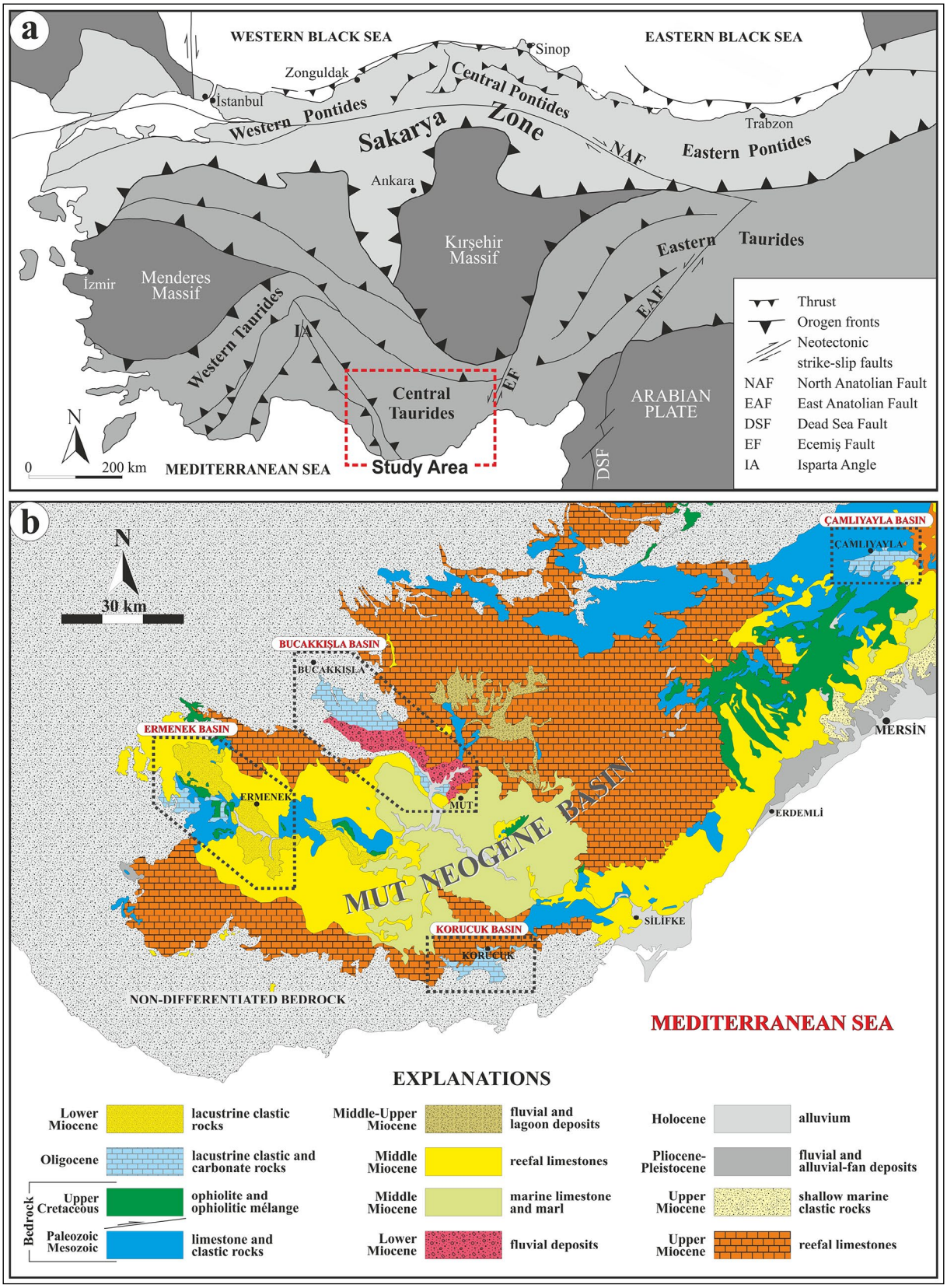

Figure 1- a) Tectonic map of the Anatolia showing Pontid and Taurus Orogenic Belts, and Menderes and Kırşehir massifs (Leren et al., 2007) and b) Simplified geological map of the Central Taurides showing Tertiary Units (modified after Şenel, 2002 and Ulu, 2002). This map shows the location and spatial distribution of the Oligocene Ermenek, Bucakkışla, Korucuk and Çamlıyayla basins and the Neogene Mut Basin.

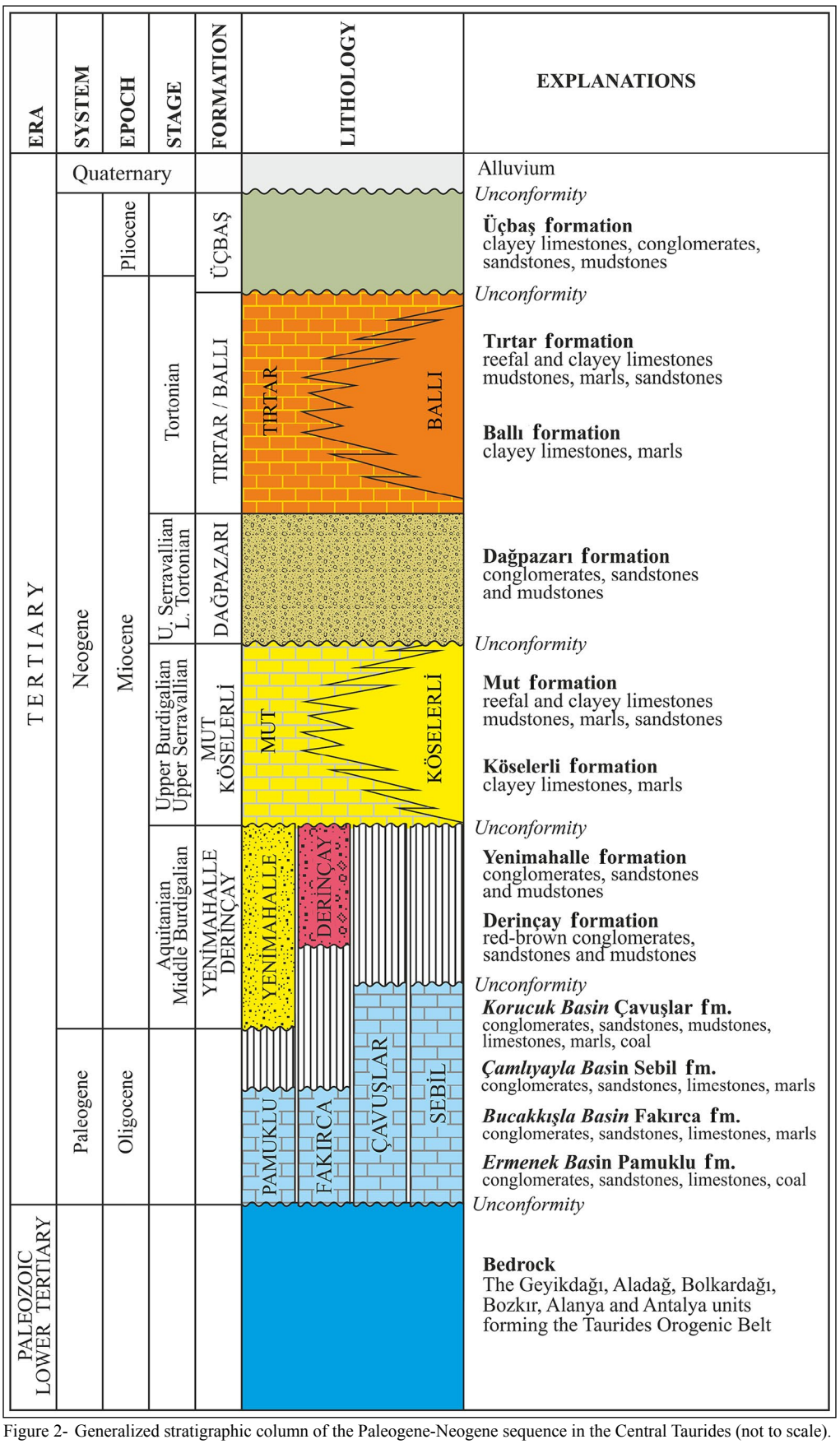

Figure 2- Generalized stratigraphic column of the Paleogene-Neogene sequence in the Central Taurides (not to scale).

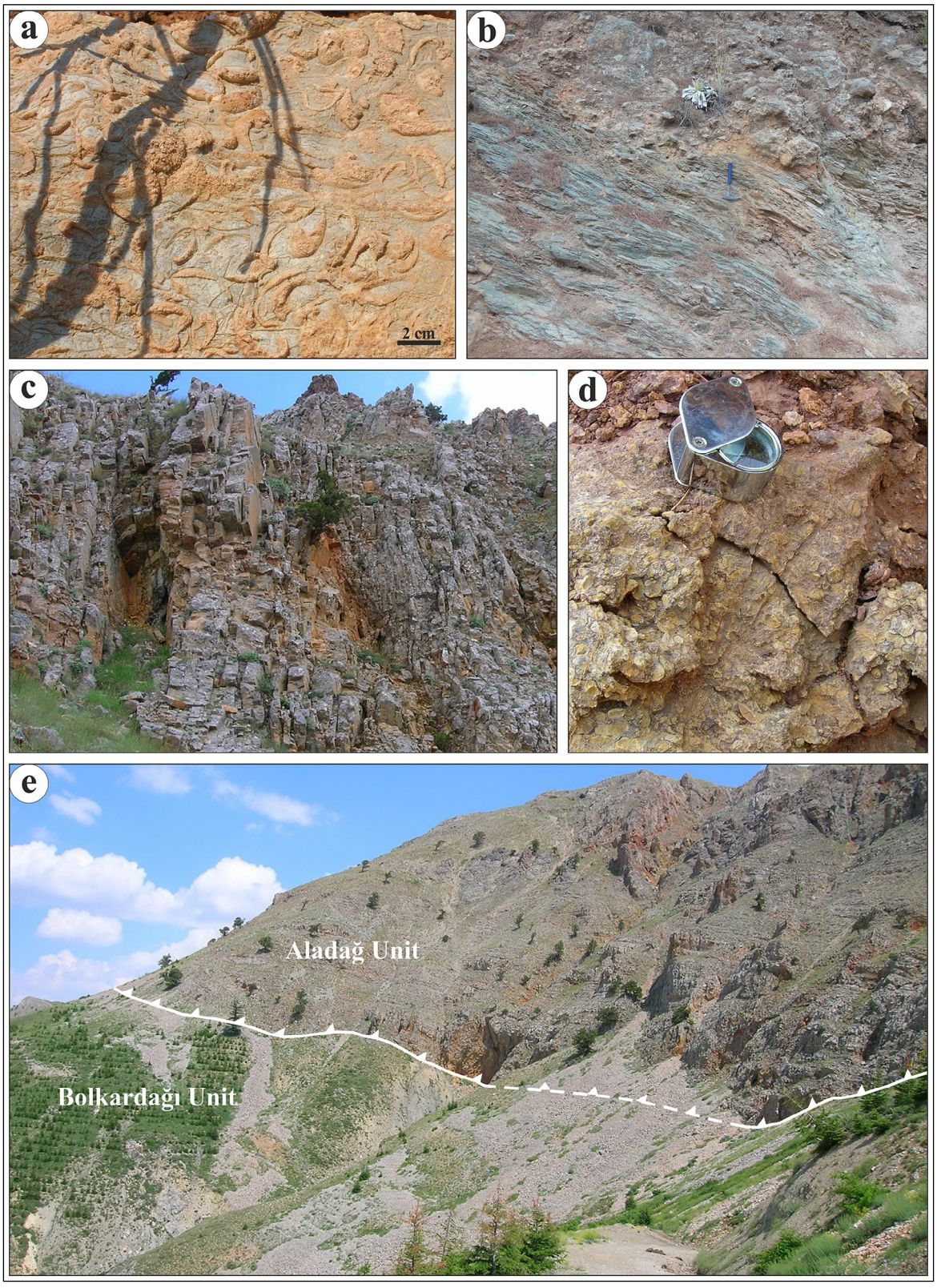

Figure 3- Bedrock of the study area consists of the rocks belonging to the Taurus units. a) Megalodon fossils observed in the Jurassic limestones of the Geyikdağı unit (N of Aydıncık), b) sandstones and conglomerates in Lutetian flysch (Mersin-Bozyazı, NW of Tekmen village) of the Geyikdağı unit, c) carbonate rocks of the Aladağ unit, d) Girvanella fossils determined in the Aladağ unit, e) Aladağ unit is allochthonous wherever it crops out throughout the belt and it is found as sheet-like bodies on other units. Note that (c), (d), and (e) images in this figure have been taken from Mersin, Cocak Valley.

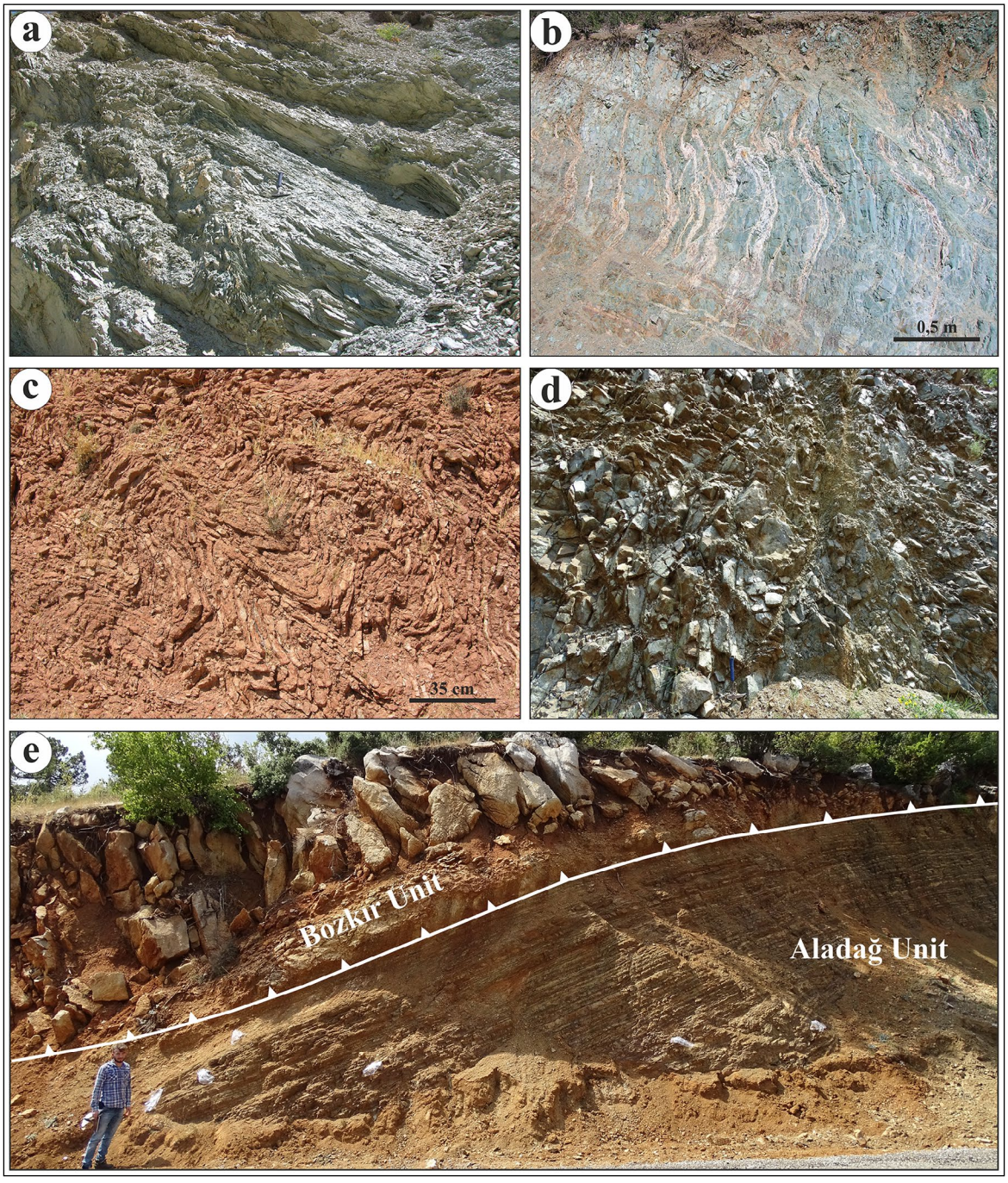

Figure 4- a) Early-Middle Triassic calcschists of Bolkardağı unit belonging to the Taurus units that constitute the bedrock (Mersin, Cocak Valley), b) Huğlu group defined in the Bozkır unit consists of green-colored thick tuffites (Karaman, S of Yollarbaşı village), c) the overlying Late Triassic-Senonian aged cherty pelagic limestone-mudstone-radiolarite alternation (Mut, Derinçay village), d) Ophiolites defined in the Bozkır unit (Mersin, Fındıkpınarı) and e) Ophiolitic mélange of the Bozkır unit which tectonically overlies Aladağ unit (Mersin, Kurudere village).

(Figure 4e). Mersin ophiolite which is the remnant of Mesozoic Neotethyan oceanic crust reflects the supra-subduction zone (Parlak et al., 1996). According to the $^{40}Ar/^{39}Ar$ hornblende ages, the initial detachment of the metamorphics from the oceanic crust during the closure of Neotethyan Ocean was occurred in late Cenomanian (Parlak et al., 1996). Metamorphism in Alanya Unit that consists of Permian, Triassic and lower Cenozoic rock units increases with depth. Lower Cenozoic rocks of this unit is transgressive

and have no traces of metamorphism. This unit forms allochthonous covers on Antalya Unit in Alanya and Gündoğmuş regions. Cambrian-Upper Cretaceous Antalya Unit bears the blocks of shallow and deep marine sediments up to a kilometer scale. It contains ophiolites and the rocks of Geyikdağ Unit, and is situated on Geyikdağ Unit as allochthonous.

Lacustrine depositions were occurred in the Oligocene molasse basins which are the subject of this study and were opened on the bedrock of the Central Taurides. From the west to east respectively, lacustrine clastic and carbonate rocks of the Pamuklu formation in Ermenek Basin, of the Fakırca formation in Bucakkışla Basin, of the Çavuşlar formation in Korucuk Basin, and of the Sebil formation in the Çamlıyayla Basin have been deposited (Figure 2). These formations are described in detail below.

In early Miocene, lacustrine clastic rocks of Yenimahalle formation were unconformably deposited on the Oligocene Pamuklu formation in Ermenek Basin (Ilgar and Nemec, 2005; figure 2). In Bucakkışla Basin, fluvial sediments of Derinçay formation were unconformably deposited on the carbonates of Fakırca formation in the middle Burdigalian (Ünay et al., 2001; figure 2). The marine transgression occurring in late Burdigalian in the Central Taurides caused the Mut Basin to drown and the initiation of marine deposition in the basin during the Neogene period (Ilgar et al., 2016). Thus, the reefal limestone and platform carbonates of Mut formation, and the marls and thin-bedded limestones which constitute the offshore sediments of Köselerli formation were deposited in the Mut Basin in late Burdigalian-Serravallian period (Figure 2). Shallow marine limestones of Mut formation which shows onlapping sedimentation pattern on the bedrock towards the north due to marine transgression and offshore sediments of Köselerli formation reflect the basinal deepening in late Burdigalian-late Serravallian. Relative sea level fall in the late Serravallian period led to the shoaling of the basin, migration of the reefal limestones of Mut formation on to Köselerli formation in basinward direction and to crop out on the basin margin. Thus, incised valleys, larger than a river channel, were formed upon the reefal limestone of Mut formation (Ilgar et al., 2019). In late Serravallian-early Tortonian period, sedimentary facies of Dağpazarı formation were deposited in this incised valley (Figure 2). Early Tortonian transgression caused re-flooding of the northern parts of the Mut Basin, deposition of the reefal limestones of Tırtar formation on the basin margins and of marls to thin-bedded limestones of Ballı formation inside the basin (Ilgar et al., 2016). The marine sedimentation in the Mut Basin terminated by the isostatic uplift of the Taurides in the late Tortonian, and the basin began to expose (Cosentino et al., 2012; Ilgar et al., 2013).

3. Oligocene Molasse Basins in the Central Taurides

The Mut Basin located in the Central Taurides is one of the Neogene basins opened after the Taurus orogeny. In Mio-Pliocene period, a thick sequence consisting mainly marine and terrestrial sediments was deposited in the Mut Basin. However, small molasse basins were developed prior to opening of the Mut Basin. These basins which began opening in Oligocene and where lacustrine depositions were occurred constitute the first products of the post-orogenic extensional tectonics. Formation of the Mut Basin occurred in the advanced stage of this extensional tectonic regime. The basins which are the subject of this study have been named as Ermenek, Bucakkışla, Korucuk and Çamlıyayla from west to eastward, respectively (Figure 1b). The locations and stratigraphy of these basins are described in this chapter and their structural features in detail in the fourth section.

3.1. Ermenek Basin

Ermenek Basin, located in the SW of Ermenek and extending in NW-SE direction, is approximately 42 km long and, in the largest place, 17 km wide (Figure 5). The rocks of Aladağ and Bozkır Units constitute the pre-Oligocene bedrock of the Ermenek Basin. Opening and development of the basin were mainly controlled by NW-SE normal and oblique faults (Figure 5). Geometry of the basin and the basin floor topography were also developed under the control of these fault systems.

The rocks, overlying the bedrock in the Ermenek Basin, consist of lacustrine carbonates at the bottom and lacustrine clastic deposits at the top. These rocks were defined and mapped under the name of Yenimahalle formation by Gedik et al. (1979),

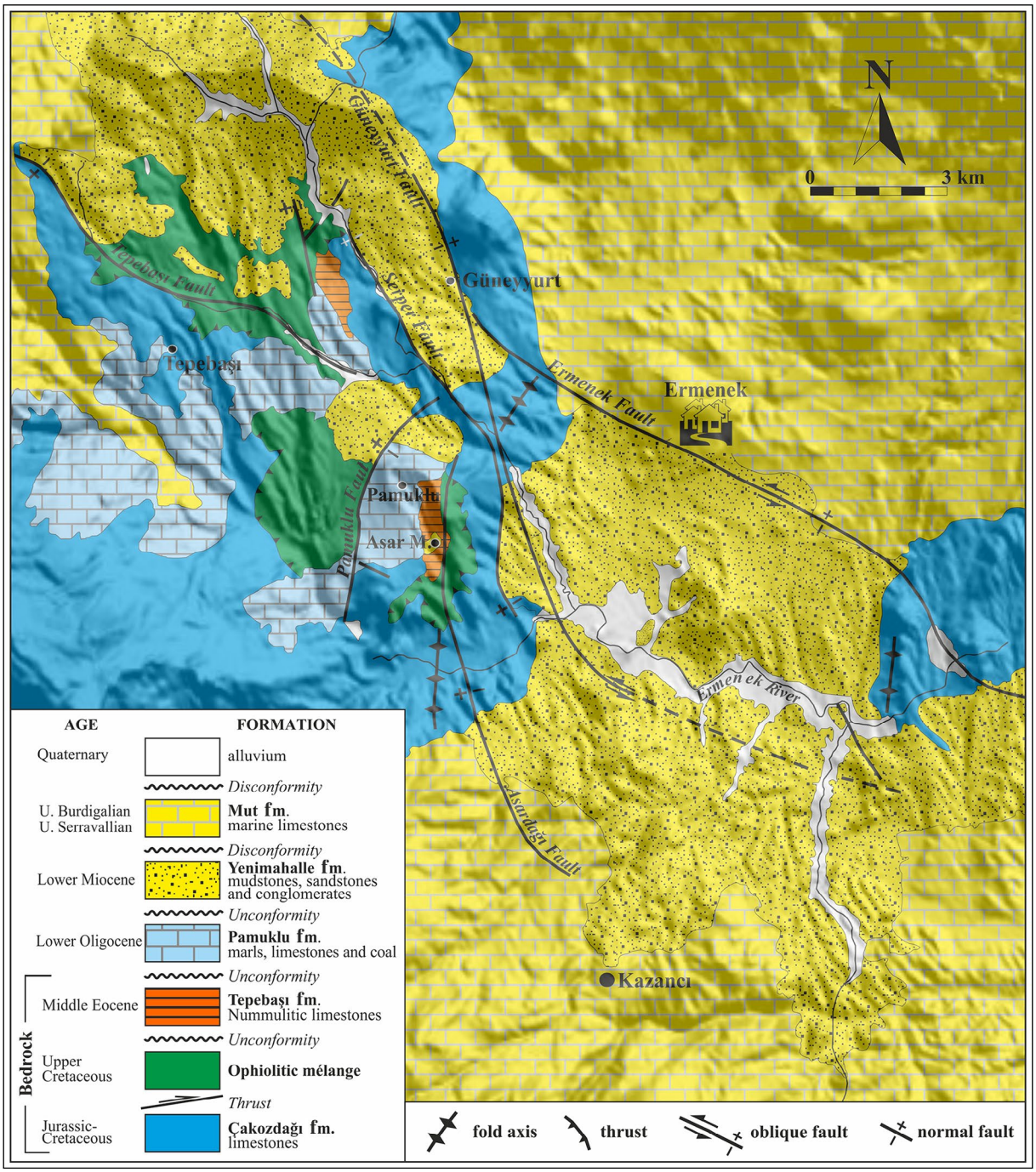

Figure 5- Detailed geological map of Ermenek Basin (Ilgar and Nemec, 2005). In this map, besides the Oligo-Miocene units, the faults that control the basin opening and development are seen.

Demirtaşlı et al. (1986), Demirel (1989). However, lithological features, age and stratigraphical position of these carbonates and their unconformable contact with the overlying lacustrine clastic rocks reveal that these carbonates had been formed and deformed before the clastic sediments. Therefore, Yenimahalle formation was divided into two formations, and the carbonates at the bottom were defined as Pamuklu formation by Ilgar (2002).

Pamuklu formation crops out in a limited area in the SW of Ermenek Basin. Location of type section of the formation is the former coal pit of the Central Coal Enterprise in Pamuklu (Cenne) coal field and

its vicinity. Other outcrops of the formation can be seen in the west of Asar Mountain and in the south of Tepebaşı village.

Pamuklu formation, which unconformably overlies the bedrock in the stratigraphic section (Figure 6a) is overlain with an angular unconformity by the clastic rocks of Yenimahalle formation.

Pamuklu formation consists mainly of conglomerate, sandstone, mudstone, limestone, marl alternation and coal (Figure 6). The Pamuklu formation

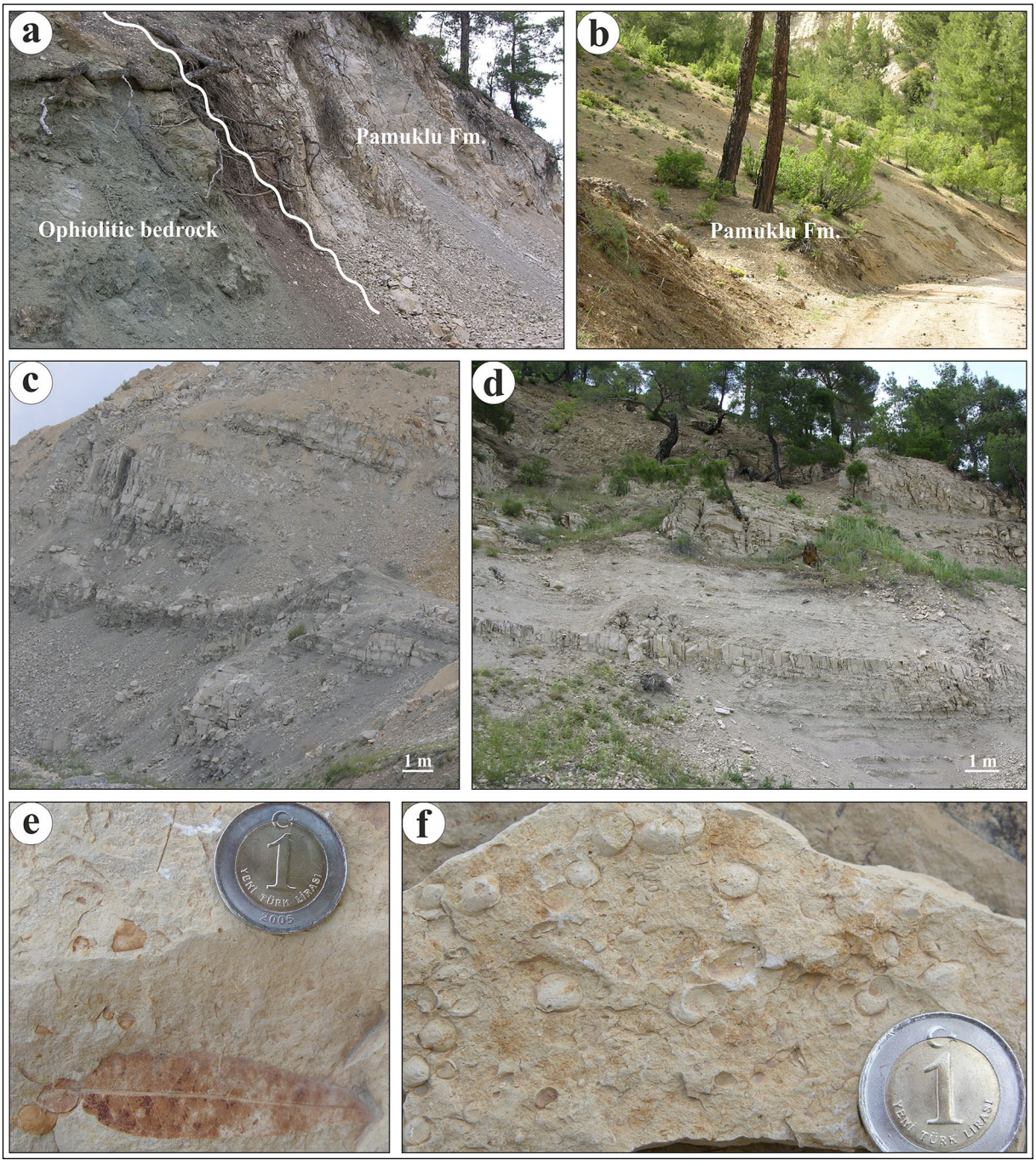

Figure 6- Early Oligocene aged Pamuklu formation which outcrops in Ermenek Basin. a) This formation unconformably overlies ophiolitic mélange of the bedrock, b) light brown colored conglomerates form the lowest levels of Pamuklu formation. There are brown-grey colored sandstones that reach several meters in thickness on the conglomerates. c) Planar-bedded sandstones pass upward into an alternation of mudstone-marl. d) Stratigraphic sequence passes upward into an alternation of thin- to thick-bedded, broken white-grey colored limestone and marl. There are (e) leaf fossils and (f) fresh-water gastropods such as *Planorbis* in the formation.

begins with a few meters thick, light brown colored, polygenic, matrix supported conglomerates with subrounded to rounded gravels on the bedrock (Figures 6a, b) Brown to grey colored sandstones that reach a few meters of thickness overlie the conglomerates (Figure 6b). Planar-bedded sandstones pass upward into an alternation of mudstone-marl (Figure 6c). There are economically operable coal deposits between these mudstone levels and their lateral continuation in the sequence. Thickness of the coal formations varies between 3 to 6 m. The thin-bedded limestone-marl alternations, 40-50 cm thick, are present between the coal bearing zones. The sequence grades upward into thin to thick-bedded, broken white-, pink-, beige-colored clayey limestones which occasionally bears leaf fossils (Figure 6d). In addition to leaf fossils, freshwater gastropods such as *Planorbis* are observed in the carbonate rocks (Figures 6e, f).

Pamuklu formation which is dispersedly situated between the paleoheights in the SW of Ermenek Basin, was significantly affected by the pre- to syn-depositional tectonism. Palynological investigations have been conducted on the samples of the formation collected from the coal pit around Pamuklu village. *Cupressacites cuspidateaformis* (ZANKL.) KRUTZS., *Tricolporopollenites megaexactus* (R.POT.) TH. and PF., *Tricolporopollenites microreticulatus* PF. and TH. in TH. and PF., *Monogemmites pseudostarius* (WEYL. and PF.) KRUTZS., *Tricolpopollenites microhenrici* (R.POT.) TH. and PF., *Pityosporites microalatus* (R.POT.) TH. and PF., *Inaperturopollenites dubius* (R.POT. and VENITZ.) TH. and PF., çok bol (% 14-20), *Caryapollenites simplex* (R.POT.) R.POT., *Tricolporopollenites cingulum* (R.POT.) TH. and PF., *Tricolporopollenites margaritatus* (R.POT.) TH. and PF., *Tricolpopollenites retiformis* PF. and TH. in TH. and PF., *Plicapollis pseudoexelsus* (KRUTZS.) KRUTZS., *Plicapollis* sp., *Arecipites* spp., bol (% 8-13), *Triatriopollenites exelsus* (R.POT.) TH. and PF., *Triatriopollenites rurensis* PF. and TH. in TH. and PF., *Triporopollenites densus* PF. in TH. and PF., *Momipites punctatus* (R.POT.) NAGY, *Triporopollenites simpliformis* PF. and TH. in TH. and PF., *Subtriporopollenites anulatus* PF. and TH. in TH. and PF., *Cycadopites* spp., *Compositoipollenites rhizophorus* (R.POT.) R.POT., *Polyporopollenites undulosus* (R.POT.) TH.and PF., *Intratriporopollenites instuructus* (R.POT. and VENITZ.) TH. and PF., *Polyvestibulopollenites verus* (R.POT.) TH. and PF., *Laevigatosporites haardti* (R.POT. and VENITZ.) TH. and PF., *Baculatisporites primarius* (WOLFF) TH. and PF., *Concavisporites concavus* PF. in TH. and PF. were determined from the samples as rare or slightly abundant (1-5%) (determination by Mine Sezgül Kayseri Özer, 9 Eylül University/İzmir, 2005).

Presence and abundance of lower Tertiary spores and pollens (*Tricolporopollenite exelsus, P. pseudoexelsus, Arecipites* sp., *Subtriporopollenite anulatus, Compositoipollenites rhizophorus* etc.) in Oligocene have been reported from various palynological studies from Turkey (Akgün et al., 1986; Akgün and Akyol, 1987, 1992, 1999; Akyol and Akgün, 1990; Akgün and Sözbilir, 2000, Akgün et al., 2002; Kayseri and Akgün, 2002, 2003). Percentage abundance of the sporomorphs tends to decrease from Oligocene to Miocene.

Age of the Pamuklu formation was assigned as early Oligocene due to the assemblage containing *Pityosporites microalatus, Inaperturopollenites hiatus, I. magnus, Triatriopollenites exelsus, Plicapollis pseudoexelsus, Caryapollenites simplex, Polyporopollenites undulosus, Compositoipollenites microechinatus, Intratriporopollenites instuructus, Compositoipollenites rhizophorus, Subtriporopollenites anulatus, Plicapollis* sp. and *Arecipites* spp. (Kayseri et al., 2006).

Age of the formation was determined as early-middle Oligocene according to the ostracod fauna containing *Lineocypris, Pseudocandona, Hemicyprideis montosa and Pokornyella limbata* obtained from the marls of Pamuklu formation, (Şafak et al., 2005). Pamuklu formation which contains leaf fossils and freshwater gastropods such as *Planorbis*, was deposited in a lacustrine basin in early Oligocene period.

3.2. Bucakkışla Basin

Bucakkışla Basin, located between Bucakkışla-Mut and extending in NW-SE direction, has a length of approximately 51 km and a width of 10 km (Figure 7). Rocks of the Bozkır Unit form the bedrocks of Bucakkışla Basin. The basin is bounded mainly by large scale NW-SE trending faults and smaller scale E-W trending normal faults. Geometry of the basin was correspondingly developed with these faults (Figure 7).

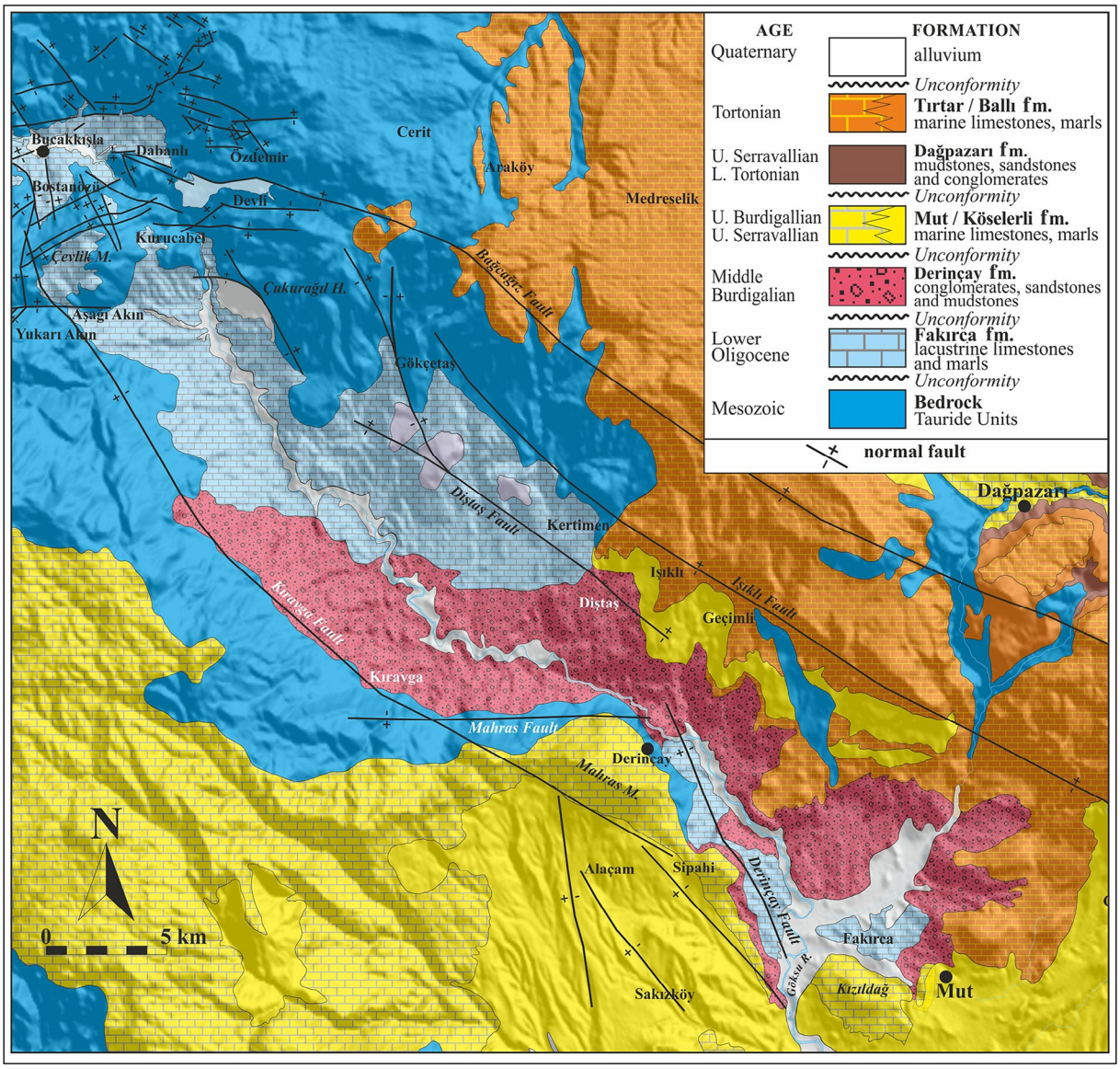

Figure 7- Detailed geological map of Bucakkışla Basin. In this map, besides the Oligo-Miocene units, the faults that control the basin opening and development are seen.

The conglomerate, sandstone, shale, marl assemblage overlying the Mesozoic bedrock with an angular unconformity in the Bucakkışla Basin, was named as Derinçay formation by Gedik et al. (1979). The shales and marls that are defined in this unit and outcropped in the Fakırca region in the NW of Mut are defined by the same researchers as the Fakırca member of the Derinçay formation. As being products of the terrestrial deposition systems, these sequences have been examined as two distinct formations depending on different facies features, relative stratigraphical position and erosional unconformity between the units. The rock assemblage, overlying the bedrock and consisting generally of lacustrine deposits, has been named as Fakırca formation. Fluvial deposits which overlie the Fakırca formation with an angular unconformity have been defined as Derinçay formation (Figures 2, 8a). Fakırca formation outcrops in a large area between Bucakkışla and Fakırca villages (Figure 7).

Fakırca formation begins with reddish conglomerates, sandstones and mudstones on the bedrock to the south of Derinçay village (Figures 8a, b). Conglomerates consist of rounded to surrounded gravels of serpentinite, limestone, chert and radiolarite. These conglomerates with clast-supported texture are massive or crude stratified. Sandstones that consist of medium to coarse grain size are planar-

parallel stratified, planar-cross stratified and trough-cross stratified, and graded bedded in less proportions (Figure 8c). This sequence, having a 20-50 m thickness in the basin margin, grades into marls and clayey limestones. Carbonized plant fragments and mudstones rich in organic matter are also observed in these levels.

Fakırca formation begins with thick-bedded sandstone-mudstone alternation in its type section located in Fakırca village. Sandstones with fine to medium grain size are planar parallel stratified. Claret red-colored thick mudstones are crude stratified. A thin-bedded rock assemblage consisting of marl-mudstone-clayey limestone and limestone alternation, with a thickness of 15 m, overlies these thick-bedded rocks (Figure 8d). The rocks constituting this assemblage are grey-colored and planar parallel stratified. Undulated and hummocky-cross stratified limestones are also present in different levels of the sequence (Figure 8e). The thickness of this rock assemblage increases towards the upper level of the

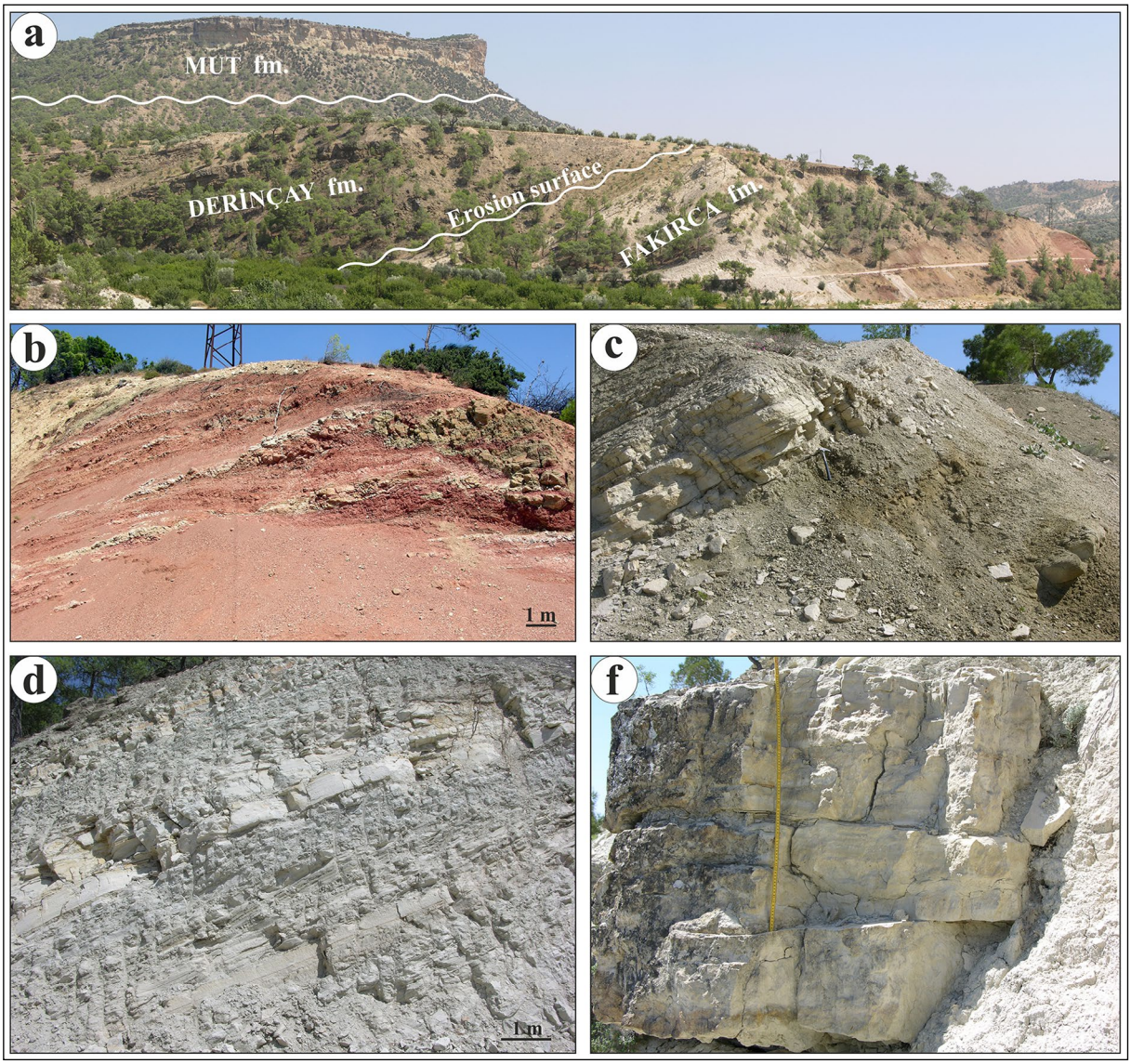

Figure 8- Oligocene aged Fakırca formation which outcrops in Bucakkışla Basin begins at the base with (a, b) reddish conglomerate, sandstone and mudstone on the bedrock. c) Overlying khaki sandstones are planar-bedded, planar-parallel stratified and locally normal-graded. This sequence grades into marls and clayey limestones. d) The formation in its type section located in Fakırca village, begins with thick-bedded sandstone-mudstone alternation and passes upward into an alternation of thin-bedded marl-mudstone-clayey limestone-limestone. e) Limestones defined in the sequence are generally planar-bedded or undulated.

sequence. There are occasionally very thick-bedded sandstones in this assemblage reaching approximately 35 m thickness. These limestones are generally planar parallel stratified, but occasionally hummocky-cross stratified and rippled-cross stratified. The hummocky-cross stratified sandstones are amalgamated and crudely normal-graded. Desiccation cracks are present at the base of some limestone beds.

The palynological investigations have been conducted on the samples collected from mudstones of Fakırca formation in Bucakkışla Basin, and results have shown that:

Pityosporites microalatus species is abundant,

Triatriopollenites coryphaeus, Momipites punctatus, Subtriporopollenites simplex, Tricolpopollenites microhenrici, Tricolpopollenites densus, Tricolporopollenites megaexactus species are regularly low,

Pityosporites libellus, Inaperturopollenites hiatus, Inaperturopollenites dubius, Spinizonocolpites prominatus, Spinizonocolpites echinatus, Triatriopollenites exelsus, Subtriporopollenites anulatus nanus, Polyporopollenites undulosus, Polyvestibulopollenites verus, Slowakipollis hipophäeoides, Tricolpopollenites retiformis, Tricolporopollenites microreticulatus, Tricolporopollenites margaritatus, Tetracolporopollenites sapotoides species are irregularly low. According to the obtained data, age of Fakırca formation outcropping in the Mut Basin is early Oligocene (determination by Mine Sezgül Kayseri Özer, 9 Eylül University/ İzmir, 2005).

The rock assemblage, situated at the base of Fakırca formation and consisting mainly of reddish conglomerate, sandstone and mudstone, constitutes the alluvial fan deposits. Massif or crude stratified conglomerates defined in these sediments reflect debris flow products. Medium to coarse-grained cross stratified sandstones, accompanying these rocks, indicate the bar deposits in active distributary channels within the alluvial fan. It is thought that, carbonized plant fragments and coal formations observed in relatively upper parts of the sequence indicate swamp environments occurred in floodplain or playa lake.

Thick-bedded, planar parallel stratified and wave rippled-cross stratified sandstones defined in Fakırca formation were deposited in the shoreface environment on the normal wave-base (Clifton, 1976; Walker and Plint, 1992; Ainsworth and Crowley, 1994). In addition to these deposits, amalgamated hummocky cross stratified sandstones in the sequence indicate a deposition within the shoreface environment due to storm processes.

Thin-bedded rock assemblage of marl-mudstone-clayey limestone and limestone alternation situated in the middle-upper parts of the sequence was deposited in the offshore- transition environment between the normal wave-base and the storm wave-base. Sand- and clay-sized materials were transported into the environment which has the calm water environment in the fair weather conditions and in which mud sedimentation occurred as from the suspension. The undulated and hummocky cross-stratified clayey limestones with sharp base defined at these levels of the sequence constitute the tempestites deposited due to storm processes (Dott and Bourgeois, 1982; Hunter and Clifton, 1982; Walker and Plint, 1992; Ainsworth and Crowley, 1994).

There are no fossil records suggesting a biogenic origin in planar-bedded marls and limestones that have gradational transition with mudstones. Despite having no isotopic data, these carbonate rocks are thought to be formed by inorganic precipitation due to gradational transition with mudstones. The absence of evaporitic sediments and the presence of *Planorbis* fossils in Fakırca formation reflect freshwater conditions. In this case, the waters that supply the lake have been enriched with calcium ions and hardened by probably passing through the limestone-rich rocks. As a result of the removal of CO_2 from the environment by photosynthesis of phytoplankton and picoplankton whose abundance level increased in the sedimentary environment, the pH of the water in the environment increased and $CaCO_3$ precipitation occurred (Kelts and Hsü, 1978; Wright, 1990; Talbot and Allen, 1996). Amount of the clastics that concurrently transported into the basin were also decreased in that period.

3.3. Korucuk Basin

Korucuk Basin, located in the W of Silifke in the S of Central Taurides and extending in E-W direction, has a length of approximately 22 km and a width of 10 km (Figure 9). Limestones of the Aladağ Unit, ophiolites and the mélange of Bozkır Unit form the

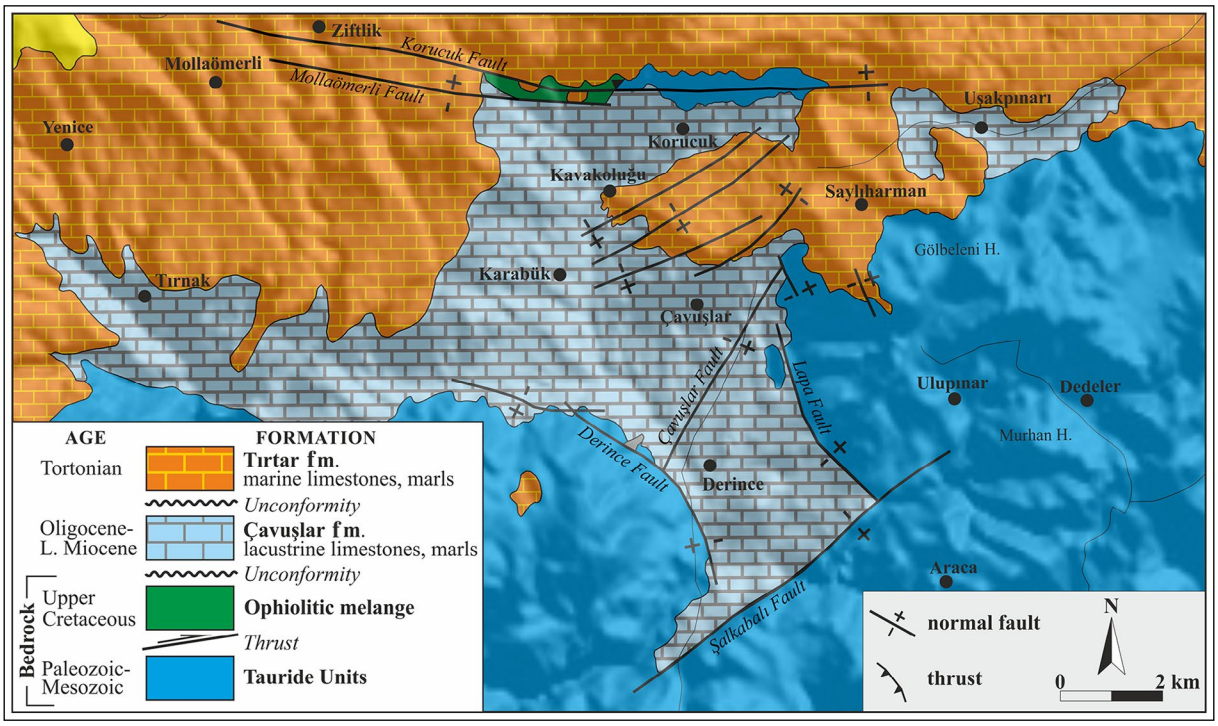

Figure 9- Detailed geological map of Korucuk Basin. In this map, besides the Oligo-Miocene units, the faults that control the basin opening and development are seen.

bedrocks of the Korucuk Basin. The basin has an irregular geometry and basin floor topography owing to being opened between faults developed in different directions (Figure 9).

Lacustrine sediments of Çavuşlar formation (Demirtaşlı, 1984) were deposited with an angular unconformity on the Mesozoic bedrock in the Korucuk Basin. Çavuşlar formation crops out in the vicinity of Bozağaç, Korucuk, Uşakpınarı, Kavakoluğu, Çavuşlar and Derince villages in the SE of Gülnar (Figure 9). Type section of the formation is located in the Kavakoğlu and Çavuşlar villages, and the reference section is in Korucuk village.

Çavuşlar formation, having approximately 100-400 m of thickness, unconformably overlies the Cretaceous limestones in the Korucuk village in the north (Figure 10a). In the west of Korucuk village, it unconformably overlies ophiolites. In the south, the formation overlies the Cretaceous limestone with an angular unconformity in Fıstık River in the vicinity of Derince neighborhood. Çavuşlar formation is overlain by late Miocene Tırtar formation with an angular unconformity between Kavakoğlu and Çavuşlar villages (Figure 10b).

Çavuşlar formation consists mainly of thin-bedded sandstone, mudstone, limestone, marl alternation (Figures 10c and d) and, in lesser proportions, conglomerate and coal. Yellow-, light-brown colored sandstones, consisting mainly of very fine to medium grain size, have bedding thickness varying between 1 to 20 cm. Normal grading, planar parallel stratification (Figure 10c), and sparse wave- and current ripples constitute the sedimentary structures of the sandstones which have laterally widespread planar bedding. Çavuşlar formation, in central and southern parts of the basin, consists mainly of the alternation of marl, mudstone, clayey limestone and limestone (Figure 10d). Marls and limestones of the formation are beige, and the mudstones are greyish-green colored. Planar-bedded mudstones are massif, and the limestones are generally planar parallel stratified and occasionally rippled-cross laminated. Coal formation is located in the immediate south of the E-W trending normal fault in the northern margin of the basin.

Conlomerates and pebbly sandstones observed in the northern margin of the basin consist of basinward inclined tabular beds towards the south (Figure 10a). Horizontally bedded conglomerates and pebbly sandstones overlie the tabular inclined beds (Figure 10a). Basinward inclined rocks and the

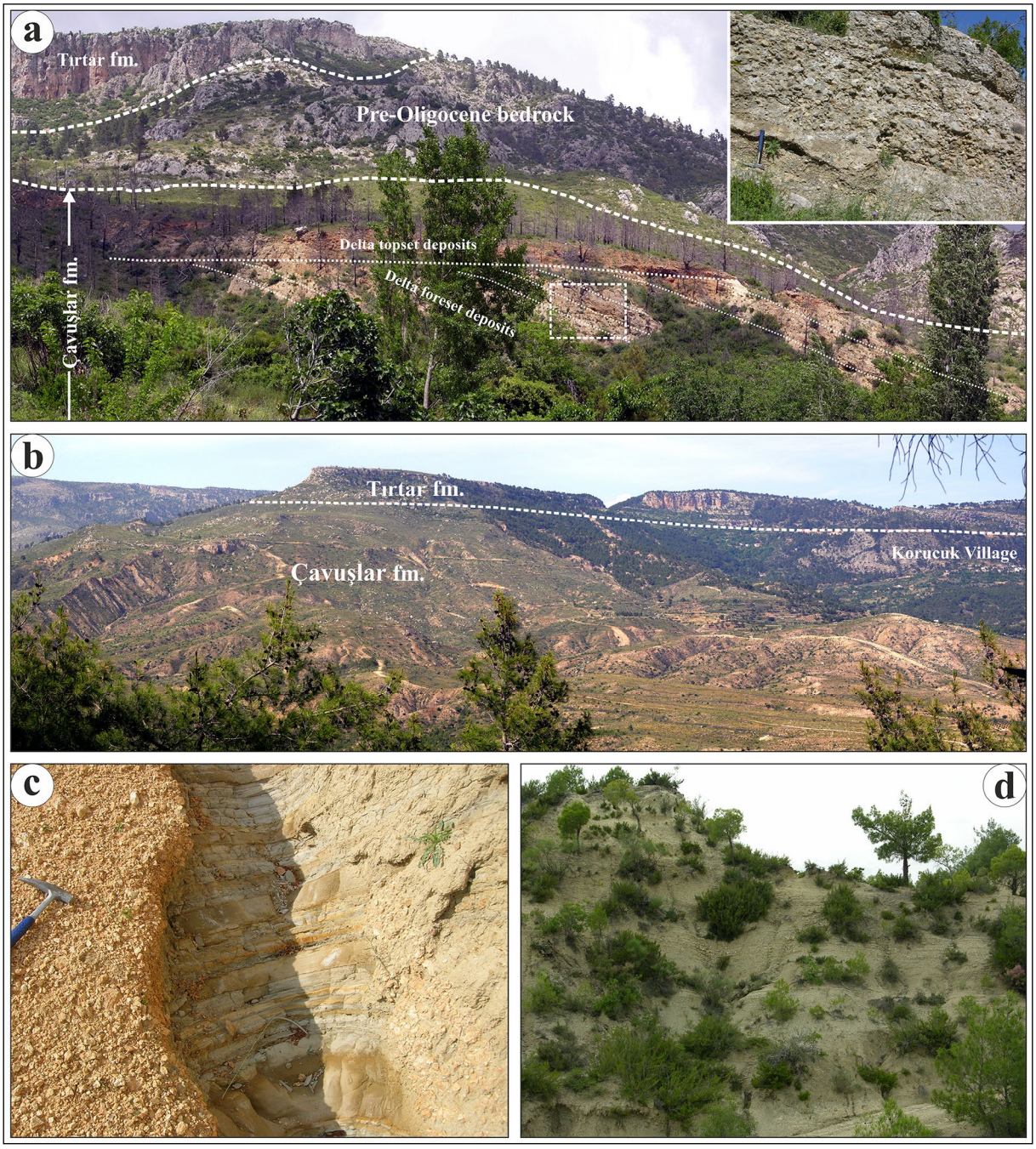

Figure 10- Oligocene-early Miocene aged Çavuşlar formation which outcrops in Korucuk Basin a) unconformably overlies the bedrock. Gilbert-type delta deposits, consisting of conglomerate and sandstone, crop out in front of the normal faults that limit the basin to the north of the basin. In this figure, besides the delta topset and delta foreset deposits which form the delta, there is also a close up view of the delta foreset deposits. b) Çavuşlar formation is overlain by the late Miocene Tırtar formation with an angular unconformity between Kavakoğlu and Çavuşlar villages. c- d) Çavuşlar formation consists mainly of thin-bedded sandstone, limestone, marl alternation.

overlying horizontally bedded sediments constitute the delta foreset and delta plain deposits that are typical for Gilbert-type delta (Barrell, 1912; Colella, 1988; Postma, 1990). These delta deposits have approximately 25 m of thickness.

Delta foreset deposits: Delta foreset deposits consist mainly of basinward inclined (<25°) conglomerates, and sandstones in less proportions (Figure 10a). Conglomerates that consist of granule to coarse pebble size grains are generally

15-120 cm thick, and planar-bedded. Cobbles, up to 15 cm in size, occur scattered in conglomerates. Grains are subrounded to rounded in these deposits which have clast-supported texture. The grains were mostly derived from Mesozoic limestones of the bedrocks. Intergranular cement consists of sand and granule sized grains that are well sorted. Massif conglomerates, showing generally no gradation or reverse grading, are planar shaped in longitudinal sections and mound-shaped in transverse sections. These have been interpreted as noncohesive debris flow deposits (Nemec and Steel, 1984; Nemec, 1990). Sandstones are commonly found in the lower parts of delta foreset deposits. Planar bedded, fine to very coarse grained sandstones have 10-30 cm of bedding thickness, and alternate with granule conglomerates. Planar parallel stratified sandstones show either normal grading or no gradation. Planar parallel stratified sandstones and granule conglomerates show the sediment transportation and deposition resulted from hyperpycnal turbidity currents (Bornhold and Prior, 1990; Nemec, 1990). Hyperpycnal turbidity currents indicate river-derived low-density turbidity currents (Lowe, 1982).

Delta topset deposits: The topset deposits, which are horizontally bedded on the delta foreset deposits, consist of fine-coarse pebble conglomerates and coarse-grained sandstones. These deposits form fining upward bedsets that have erosional bottom surfaces. The bedsets stacked upon one another and have a few meters wide, form the channel-fill deposits of braided stream (Miall, 1985; Collinson, 1996). Planar parallel-stratified and cross-stratified conglomerate and sandstone beds defined in the channel deposits, 10–45 cm thick, reflect the longitudinal and transverse midchannel bar deposits (Miall, 1985; Nemec and Postma, 1993).

Çavuşlar formation, containing coal and freshwater gastropods such as *Planorbis* in its marls and limestones, was deposited in a fault-controlled lacustrine basin. Coal deposition occurred due to normal faulting at the northern margin of the basin. Depending on the sediment transport carried from the north in a period that the basin was relatively deepening, Gilbert-type delta deposition was also developed in the northern margin.

According to the palynological investigations conducted to date lacustrine Çavuşlar formation, latest Oligocene-early Miocene (Burdigalian) age was assigned based on the findings of *Pinus indet* (for taxonomy see Benda, 1971), *-haploxylon-* group, silvestris group, *Picca*-type, *Cedrus*-type, *Magnus-dubius* group, *Taxodiaceaepoll.* hiatus (R.POT) KREMP, *Sequoiapoll. polyformosus* Thierg, Ineperturopoll. *emmaensis* (Murr. and pF.).pF, *Quercoidites* henrici (R.POT) R.POT., TH. and THIERG, *Quercoidites* microhenrici (R.POT) R.POT., TH. and THIERG, *Rhoipites dolium* R.POT, *Caprifoliipites microreticulatus* (Pf. and Th) R.POT, *Nyssoidites roddorensis* Thierg, Trivestibulopoll. betuloides PF., *Myricoides-bituitus-rurensis-* group, *Subtriporopoll simplex* (R.POT) Pf. and Th., *Alni-poll verus* R.POT, *Gramineae, Cyperaceae, Cicatricosisporites* corogeresis R.POT. and Gell, of Osmundaceae spores (Uğuz, 1989). Bilgin et al. (1994) accepted the age of Çavuşlar formation as early Oligocene-early Miocene (Burdigalian). In this study, the age of Çavuşlar formation has been accepted as Oligocene-early Miocene considering previous studies.

3.4. Çamlıyayla Basin

Çamlıyayla Basin, located in the eastern side of the Central Taurides and extending in the NE-SW direction, has a length of approximately 17 km and a width of 7 km (Figure 11). Bedrocks of the Çamlıyayla Basin are the rocks of Aladağ Unit and the ophiolite and mélange of Bozkır Unit. In the north of the basin, Eocene carbonate rocks of Kaleboynu formation are also found in the bedrock with a very limited distribution. Çamlıyayla Basin is bounded mainly by large scale NE-SW trending parallel faults and smaller scale E-W trending faults. Basin geometry was developed under the control of NE-SW trending fault systems (Figure 11).

The rock assemblage consisting mainly of sandstone, mudstone, marl, limestone and, in less proportions, conglomerate and coal deposited in Çamlıyayla Basin has been named as Sebil formation in this study. Sebil formation crops out between Çamlıyayla, Sebil, Boğazpınar and Korucuk villages in the south of Çamlıyayla (Figure 11). Sebil formation overlies the Jurassic to Cretaceous aged limestones and the Eocene aged nummulitic limestones with an angular unconformity around Çamlıyayla and Sebil. The formation is unconformably overlain by limestones of Mut formation and clastic rocks of Dağpazarı formation in the south of Çamlıyayla.

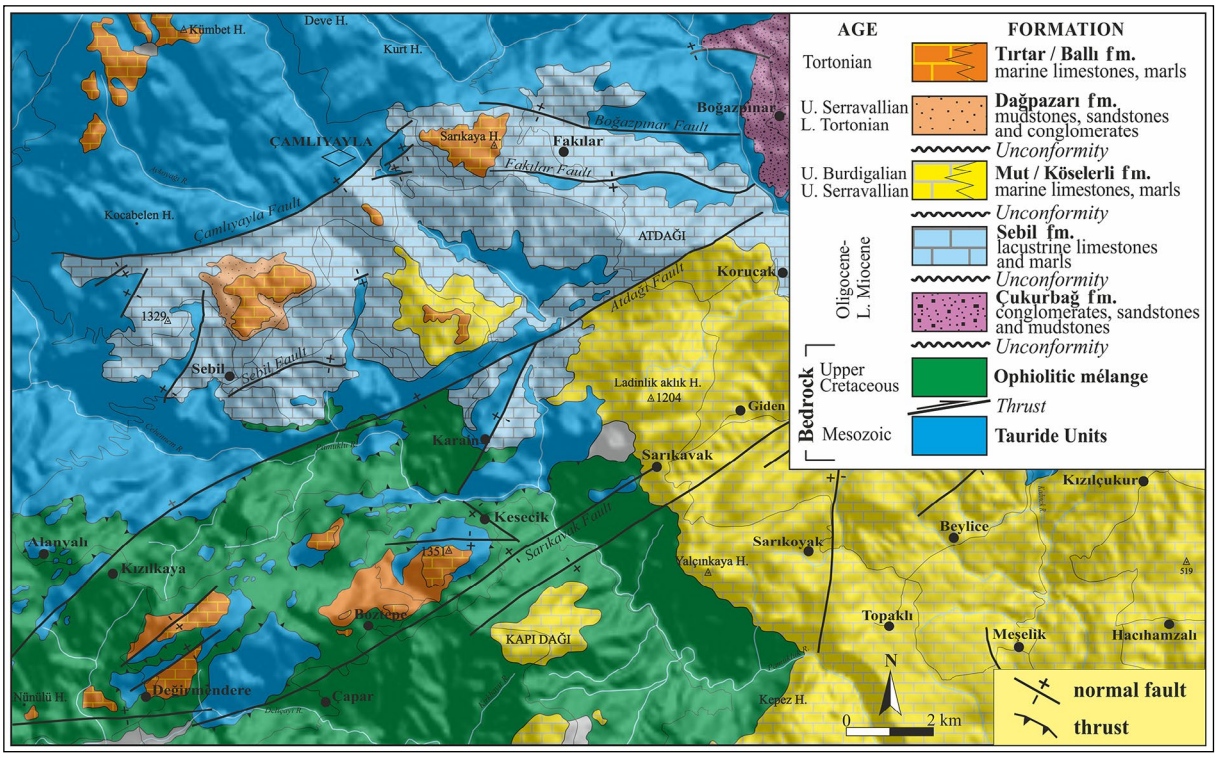

Figure 11- Detailed geological map of Çamlıca Basin. In this map, besides the Oligocene-Miocene units, the faults that control the basin opening and development are seen.

This formation consists of cream-light yellow colored sandstone, limestone, marl, mudstone alternation, coal and conglomerates in the vicinity of Sebil village (Figure 12). The sequence begins with the alternation of mudstones and marls at the bottom. Thin-bedded coal-bearing deposits that reach 150 cm in thickness, and organic matter-rich mudstones overlie these sediments (Figures 12a, b). The coal-bearing zones grade upward into an alternation of clayey limestone-marl. Thin-bedded, laterally continuous clayey limestones are overlain by fine-medium grained, planar bedded sandstones which reach 250 cm in thickness (Figures 12 a, b, c). Well sorted sandstones are planar parallel stratified, wave rippled and occasionally hummocky cross-stratified. Pebbly sandstones and fine pebble conglomerates, reaching 1 m in thickness, are present between these sandstones (Figure 12d). Well sorted and well-rounded conglomerates are planar parallel stratified. The sequence continues with the thin-bedded mudstone-sandstone alternation which reaches 4 m in thickness. These sandstones and mudstones have thickness varying between 5-20 cm. This sandstone-mudstone alternation continues upward with the alternation of marl, limestone and occasionally dark grey colored mudstone. These thin-bedded and laterally continuous sediments have an approximate thickness of 7 m. In the uppermost part of the sequence, there is an alternation of mudstone-sandstone. Sebil formation, which consists of clastic rocks as conglomerate, sandstone, siltstone in the basin margin, passes basinward into an assemblage of marl and limestone. Leaf fossils and freshwater gastropods such as *Planorbis* are present in the marls and limestones.

Planar parallel stratified and wave rippled-cross stratified sandstones defined in Sebil formation were deposited in the shoreface environment on the normal wave-base (Clifton, 1976; Walker and Plint, 1992; Ainsworth and Crowley, 1994). Hummocky cross-stratified sandstones defined in this sequence reflect the storm processes which occurred in the shoreface environment. Well sorted, planar parallel stratified conglomerates, accompanying the shoreface sandstones, indicate beach environment (Bluck, 1967, 1999; Clifton, 1973; Postma and Nemec, 1990). Marl, mudstone, clayey limestone, limestone alternation defined in different levels of the sequence were deposited in the offshore-transition environment

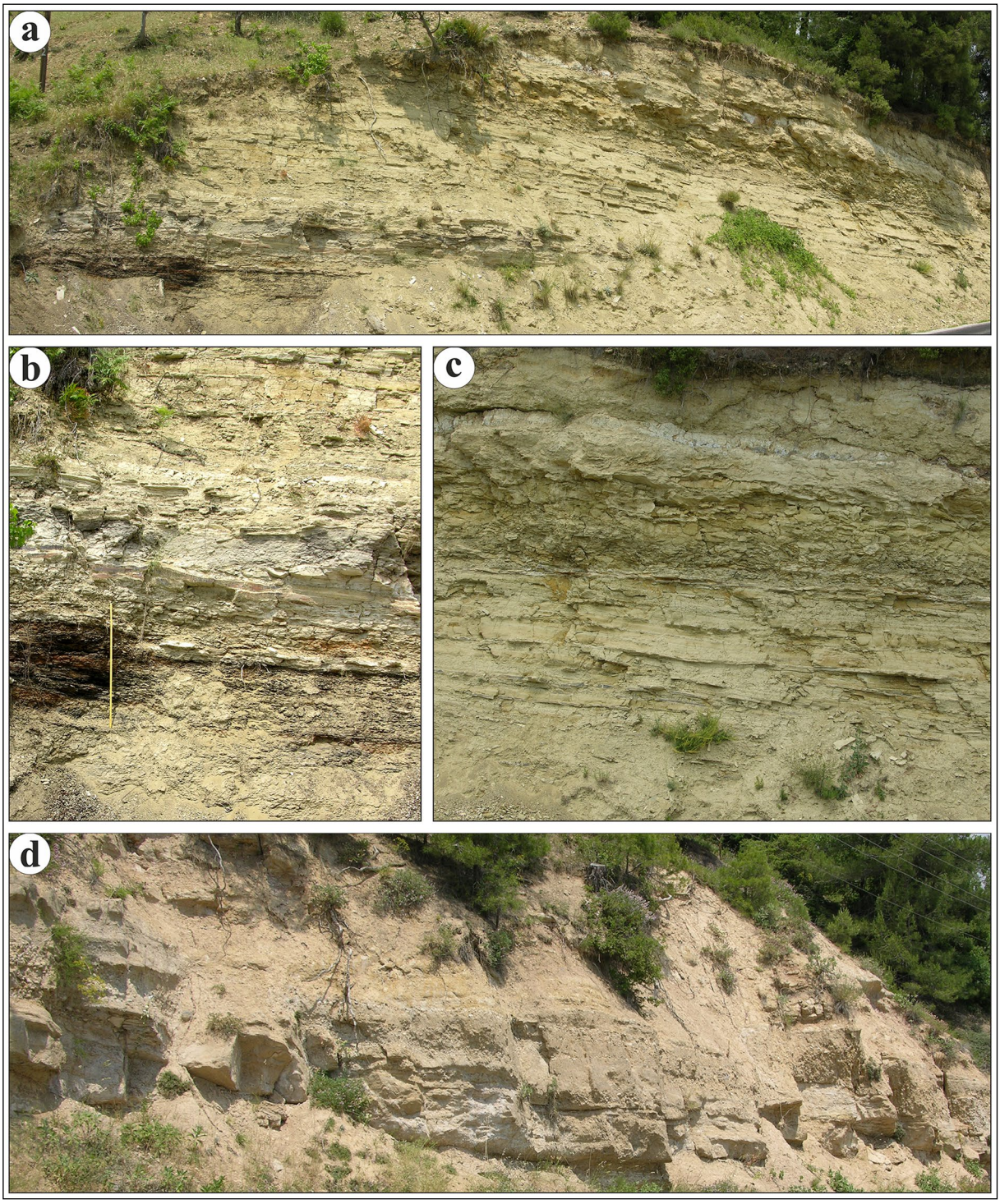

Figure 12- Oligocene-early Miocene aged Sebil formation which outcrops in Çamlıyayla Basin a) consists of cream-light yellow colored sandstone, limestone, marl, mudstone alternation, and coal and conglomerates. b) Coal-bearing zones and mudstones rich in organic matter grades upward into the alternation of clayey limestone-marl. c) There are fine to medium grained, planar-bedded sandstone on the limestones. d) Planar-parallel stratified, well sorted and well-rounded conglomerates and pebbly sandstones are seen between the sandstone beds.

between the normal wave-base and the storm wave-base. In this environment, while mud sedimentation occurred as from the suspension in the fair weather conditions; sand- and silt-sized materials transported into the environment depending on the storm processes, and were deposited in offshore-transition environment (Dott and Bourgeois, 1982; Hunter and Clifton, 1982; Walker and Plint, 1992; Ainsworth and Crowley, 1994).

No age data has been obtained from the mudstone samples collected from Sebil formation. However, based on its stratigraphical position between the Eocene Kaleboynu formation and the reefal limestones of late Burdigalian-late Serravallian Mut formation, and its close stratigraphical similarities with Fakırca formation defined in the Bucakkışla Basin, age of Sebil formation is thought to be Oligocene-early Miocene.

4. Structures and Deformations of Oligocene Basins

4.1. Ermenek Basin

Ermenek Basin, which is located in the SW of Ermenek and has a longitudinal geometry in NW-SE direction, is a tectonically controlled basin. There are faults of various sizes on the NE and SW margins of the basin and inside of the basin. NE margin of the Ermenek Basin is bounded by Ermenek fault which strikes N63W and dips 54ºSW (Figures 5 and 13a). Starting from Güneyyurt village towards the SE, trending of this 17 km long fault rotates in the east of the basin, and continues as striking N26W with dip of 62º SW. Slickenlines with +64º rake are present on the slickenside (Figure 13a). Trending of the 18 km long Tepebaşı fault, which is located in the NW margin of the basin, changes between N33W/60ºNE and N74W/65ºNE (Figure 5). Serper fault observed in the NW of the basin, bounds the bedrock and the

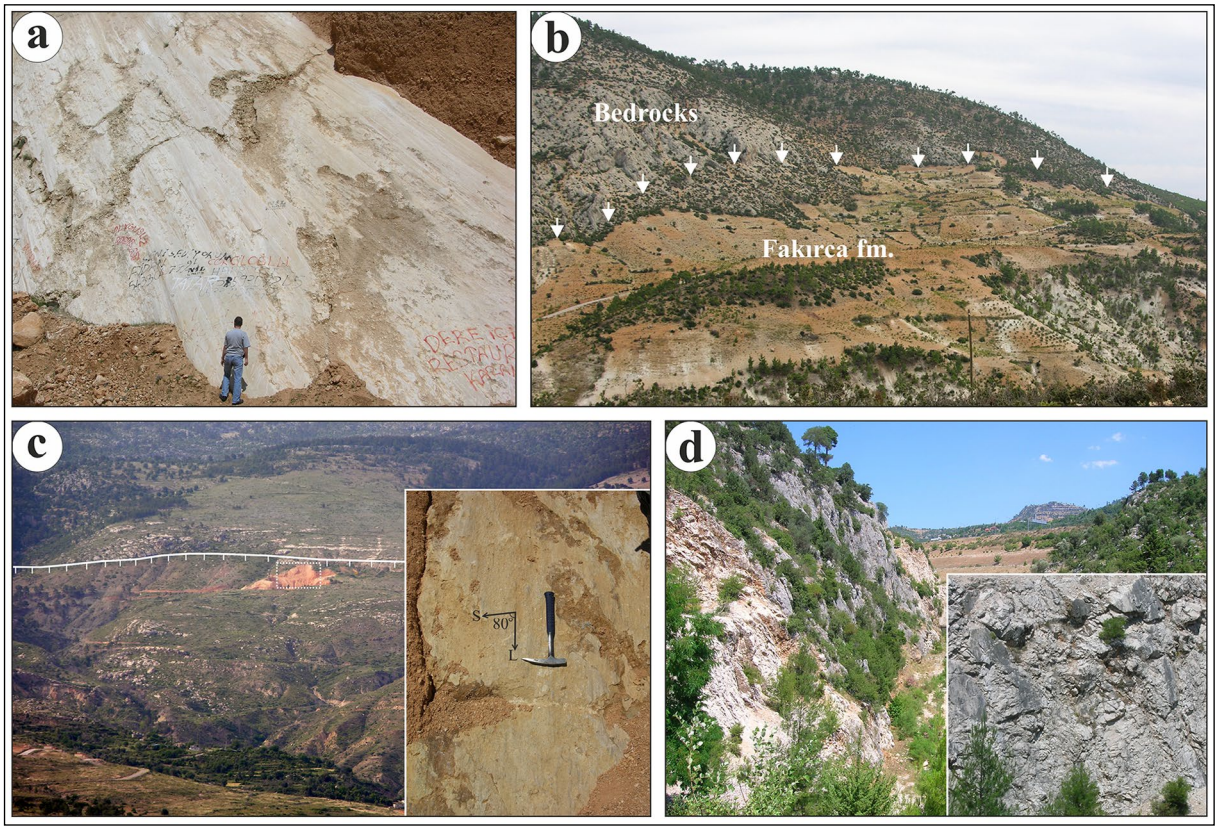

Figure 13- Examples of normal faults that limit the Oligocene basins in the Central Taurides. a) Ermenek fault which starts from Güneyyurt village in Ermenek Basin and extends 17 km towards the SE by limiting the NE margin of the basin. Note that the slickenlines are present on the fault planes. b) Dıştaş fault defined in the Bucakkışla basin, is a N60W striking and 82ºSW dipping fault. Fault plane forms a border between Oligocene Fakırca formation and the bedrock. c) Korucuk normal fault which limits the northern margin of Korucuk Basin. d) Atdağı normal fault, cutting the bedrock and Oligocene Sebil formation and Miocene Mut formation, is a fault defined in Çamlıyayla Basin.

early Miocene lacustrine deposits. This fault has a length of 10 km between the trending N32W/73ºNE and ~N-S/70ºE (Figure 5). Pamuklu fault, forming a boundary between the bedrock and the Oligocene lacustrine deposits in the west of Pamuklu village, has a total length of 8 km. Trending of the Pamuklu fault changes between N34E/55ºSE and N08E/58ºSE. Asardağı fault, 11 km long and located in the middle of the basin, extends along trends between the N-S/72ºE and N18W/68ºNE. Güneyyurt fault, a 28 km long oblique-slip fault, extends from the NW of the basin towards the SE along the trends N34W/66ºSW, N17W/73ºSW, N67W/64ºSW. Slickenlines with +57º rake are present on the slickenside.

Slickenlines and corrugation axis trends on the abovementioned faults are perpendicular or nearly perpendicular to the strike of the faults. In addition to the slickenlines and the corrugation axis trends, chatter marks also indicate normal faulting. Besides, two different normal faults with left lateral strike-slip component are seen in the north and inside of the basin.

Bedrock of the Ermenek Basin which consists of Jurassic-Cretaceous aged limestones, ophiolites, Eocene aged limestones were cut by normal faults. Ermenek, Güneyyurt, Tepebaşı, Pamuklu faults form boundaries between the bedrock and the Oligocene-early Miocene aged lacustrine deposits. Onlapping geometry is observed on fault planes in lacustrine depositions occurring along the faulted contacts. This depositional geometry indicates that normal faulting was occurred before the deposition.

While the faults bounding the NE of the basin dip to the SW, the faults located in the SW margin dip to the NE. Data obtained from stereographic projection analysis of the faults which limit the basin show that the Ermenek Basin was opened as being cut by normal faults under the effect of NE-SW directed stress after the Taurus Orogeny (Figure 14a).

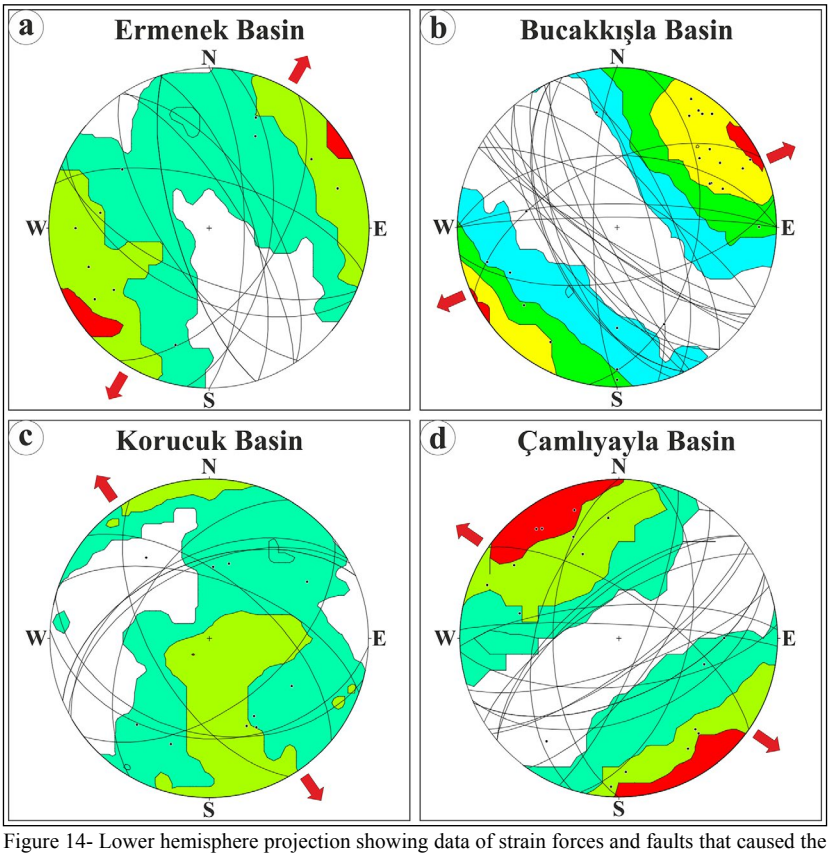

Figure 14- Lower hemisphere projection showing data of strain forces and faults that caused the opening of Ermenek, Bucakkışla, Korucuk, Çamlıyayla basins in the Central Taurides and later on affected the Tertiary marine sediments. Dataset including strikes and dip angles of faults, and the plots have been generated by using Stereonet 9.5 program (Allmendinger et al., 2013).

Ermenek Basin, which began opening in Oligocene and infilled with mainly lacustrine carbonates of Pamuklu formation, has continued to develop under the control of normal faults. In early Miocene period, lacustrine clastic rocks of Yenimahalle formation were deposited in this basin. While the lacustrine clastic rocks of early Miocene Yenimahalle formation are generally in almost horizontal or slightly inclined position, early Oligocene aged lacustrine carbonates have been tilted at angles between 20º to 25º. The angular unconformity observed between the early Oligocene and the early Miocene units have been interpreted as deformations occurred due to an ongoing basin formation under the gravity effect in late Oligocene.

4.2. Bucakkışla Basin

Bucakkışla Basin which is located in the NW of Mut and has a longitudinal geometry in NW-SE direction, is bounded by Bağcağız and Işıklı faults in the NE and by Kıravga and Derinçay faults in the SW (Figure 7). In addition to these major faults, there are large number of minor faults with various sizes both in the basin interior and in the margin. There are large number of faults with 1 to 5 km of lengths particularly in the NW edge of the basin (Figure 7). Bağcağız fault, which is a 51 km long fault and limits the NE margin of the basin, strikes N57W and dips 72º SW. Işıklı fault, which is another fault located in the northeast of the basin and runs parallel to Bağcağız fault, strikes N53W and dips 78ºSW, and has 33 km in length (Figure 7). Widespread colluvium cones have been developed in front of these faults. Kıravga fault which has a trending of N40W/65º NE in the region between Bostanözü and Sipahi villages and is located in the west of the basin, has 27 km of length (Figure 7). Derinçay fault, which limits the western margin of the basin and has 13 km of length, strikes N23W and dips 62º to NE. Mahras fault which limits the basin in the north of the Mahras Mountain, is 12 km in length, strikes E-W and dips 78ºN. Dıştaş fault defined in the basin, has an approximate length of 12 km. This fault strikes N60W and dips 82º SW, and bifurcates into two branches towards the northwestern end. Another fault bifurcated from Dıştaş fault strikes N25W and 76ºSW in the west of Gökçetaş village (Figures 7 and 13b).

Bucakkışla Basin forms a depression area between the faults bounding the basin to the NE and to the SW margins. Slickenlines and corrugation axis trends on the fault planes of Bağcağız, Işıklı, Kıravga, Mahras, Derinçay faults, which limit the depression area, are perpendicular or nearly perpendicular to the strike. While, as such in Ermenek Basin, the faults limiting the NE of the basin dip to the SW, the faults located in the SW margin dip to the NE. These faults, in many locations along the boundaries of the basin, forms a border between the bedrock and the Oligocene lacustrine sediments. The lacustrine sediments of Fakırca formation deposited upon the fault planes as onlapping geometry (Figure 13b). The onlapping geometry observed along the faulted contacts of the basin shows that normal faults which thought to have controlled the basinal opening had developed prior to the deposition. Data obtained from the stereographic projection analysis of the faults that limit the basin reveals that Bucakkışla Basin was opened as being cut by normal faults under the effect of NE-SW directed stress after the Taurus Orogeny (Figure 14b).

Lacustrine carbonates of Oligocene Fakırca formation deposited in the Bucakkışla Basin are overlain by the fluvial deposits of early Miocene Derinçay formation with an angular unconformity. In addition to the tectonic deformations, Fakırca formation is observed as being deeply eroded by fluvial processes in the basin. Fluvial erosion indicates the exposure of Bucakkışla Basin at the end of Oligocene and a fall in the base level. Tilting occurred after deposition in the units of Fakırca formation shows that tectonism, which leads to basinal opening due to normal faulting under the gravity effect, maintained its activity in also post-Oligocene period (Esirtgen, 2014).

4.3. Korucuk Basin

Korucuk Basin was opened in the S of Central Taurides between the faults with different strikes and dip directions (Figure 9). It is a smaller basin comparing with the Ermenek and Bucakkışla basins. Although the basin does not present a regular basin geometry, it generally has E-W trending. Northern margin of the Korucuk Basin is bounded by the south-dipping Korucuk and Mollaömerli faults which have 15 and 7 km of length, respectively. Korucuk fault which strikes N87W and dips 37ºSW in the south of Ziftlik village, continues in E-W trending down from the NW of Korucuk village (Figures 9 and 13c). On

the other hand, Mollaömerli fault strikes N75W and dips 40º SW (Figure 9). Southern margin of the basin is limited by ~8 km long Şalkabalı fault which strikes N67E and dips 50º NW. Lapa fault, striking N32W and dipping 58ºSW, is located in the east of the basin, and has approximately 5 km of length. In the west of the basin, 5 km long Derince fault which strikes N48W and dips 63º NE is situated. This fault continues towards the NW in 3 km distance as striking N69W and dipping 60º NE. Çavuşlar fault, striking N30E and dipping 54º NW, is approximately 5 km long and is located between Çavuşlar and Derince villages in the middle of the basin (Figure 9). Kavakoğlu faults, 4-5 km long and running parallel to each other, are seen between Çavuşlar and Korucuk villages. These faults are observed as in following trends: N60E/47º NW, N62E/53º NW, N67E/50ºNW from north to the south, respectively. Besides this, Saylıharman fault which strikes N52E and dips 54º SE is located in the NW of Saylıharman village.

Slickenlines and corrugation axis trends on the fault planes of Korucuk, Mollaömerli, Şalkabalı, Lapa and Derince faults which lead Korucuk Basin to opening and also limit the basin, are perpendicular or nearly perpendicular to the strike of the faults. Korucuk Basin was formed in front of these faults. Chatter marks on the fault planes indicate also normal faulting.

Coal deposition has been occurred in front of Mollaömerli fault under the control of normal faulting in the northern margin of the basin. A Gilbert-type delta has also been deposited under the control of particularly Korucuk fault in the northern margin of the basin. The development of Gilbert-type delta architecture on the northern margin of the basin is important in terms of showing the activities of the faults opening the basin during sedimentation. The dip slip magnitude on the Korucuk fault and the basin deepening allowed the drainage system from the north of the basin to develop Gilbert-type delta instead of the shallow water delta.

In addition to the Gilbert-type delta development in the fault-controlled basin margins, onlapping depositions, as in Ermenek and Bucakkışla basins, occurred on the bedrock cut by normal faults.

The faults in the northern margin of the basin are inclined towards the south, while the faults located in the east and south of the basin are inclined towards the NW. Data obtained from the stereographic projection analysis of the faults which led the Korucuk Basin to be opened, reflect that Korucuk Basin was opened as being cut by normal faults under the effect of NW-SE directed stress after the Taurus Orogeny (Figure 14c) and also that the development of an extensional tectonic regime was occurred following nappe emplacement.

4.4. Çamlıyayla Basin

Çamlıyayla Basin, which is located in the south of Çamlıyayla and has a NE-SW trending, is bounded mainly by large scale NE-SW trending faults and smaller scale E-W trending faults (Figure 11). These faults, cutting the bedrock and running nearly parallel to each other, have been developed as step faults. The NW margin of the basin is limited by Çamlıyayla fault. Çamlıyayla fault, striking N35E and dipping 69º SE in the south of Çamlıyayla, strikes E-W towards the west. Çamlıyayla fault forms a border between bedrock and Sebil formation. Boğazpınar and Fakılar faults are located in the NE margin of Çamlıyayla Basin (Figure 11). The fault which extends for 6 km between the SW of Boğazpınar village and the NW of Fakılar village, strikes N73W and dips 47º SW. Fakılar fault, which is located in the south of Fakılar village and is 6 km long, strikes almost E-W and dips 56º N. Atdağı fault, which is located in the south of the basin and extends from the NE of Atdağı towards the SW for approximately 17 km, cuts the ophiolite and mélange belonging to the Bozkır Unit, Oligocene aged Sebil formation, and Miocene Mut formation (Figures 11 and 13d). Atdağı fault is a N67E striking and 73º SE dipping fault. Sarıkavak fault, running almost parallel to Atdağı fault, is observed between Sarıkavak village and the SW of Çapar. This fault, striking N66E and dipping 59º SE, has 10 km of length. There are two other faults, running parallel to Sarıkavak fault, with 8 and 3 km lengths and with dip angles 50º - 55º in the south of Sarıkavak village. In addition to these larger faults, there are also N26E striking and 62º SE dipping Karain fault in the east of Karain village, and some other small-scale faults around Sebil village and in the SE of Çamlıyayla village in the basin.

Slickenlines and the corrugation axis trends on the fault planes defined in Çamlıyayla Basin are perpendicular or nearly perpendicular to the fault strikes so as indicating normal faulting.

The faults, which causes the Çamlıyayla Basin to be opened by cutting the bedrock and limits the northern and southern margins of the basin, are inclined towards the S and the SW. The NE-SW trending faults which are thought to have controlled basin opening and the development, have been developed as forming stair-stepping pattern from the NW towards the SE. Çamlıyayla Basin has been developed as a half-graben in front of these faults. Stereographic projection analysis of the faults which controlled the development of Çamlıyayla Basin has revealed that these faults were formed under the effect of NW-SE directed stress (Figure 14d). This data shows that Çamlıyayla Basin was opened as being cut by normal faults after the Taurus Orogeny.

5. Discussion

5.1. Pre-Oligocene Orogenic Development of the Central Taurides

Taurides, which is situated in the Eastern Mediterranean section of the Alpine-Himalayan mountain range and constitute the southern parts of Turkey, consist of both oceanic and continental plate fragments amalgamated between Eurasian and Afro-Arabian plates. Pre-Oligocene geological development of the Central Taurides is the result of a series of events that occurred in Triassic-Eocene time interval. This includes, from rifting to the collision, following events: opening of an ocean, obduction of ophiolites and ophiolitic mélanges, and mountain-building events depending on the closure, collision, and compressions.

Initiation of the rifting along the northern margin of Gondwana in Early-Middle Triassic provided the derivation of African-originated microcontinents and development of the oceanic branches between these microcontinents (Şengör and Yılmaz, 1981; Robertson and Dixon, 1984; Okay and Tüysüz, 1999). These oceanic braches maintained their existence during Mesozoic-early Tertiary interval (Robertson et al., 2012). Rock units such as limestone, cherty limestone, sandstone, mudstone, radiolarite and rift volcanism products belonging to the Taurus Units have been accumulated in these basins. These units which were deposited in shelf, slope, and deep marine environments, are vertically and horizontally transitional and reflect the deepening and the shallowing occurred in the basin (Esirtgen, 2014).

The convergence between Afro-Arabian and Eurasian plates which occurred in late Mesozoic-early Tertiary interval, and the closure of the Neotethyan Ocean dominated the geological development of Anatolia in this period (Şengör and Yılmaz, 1981; Robertson and Dixon, 1984; Dewey et al., 1986). Northward subduction of the branches of Neotethyan Ocean caused the subduction-zone ophiolites and the ophiolitic mélange to have been obducted over the Taurus carbonate platform in Late Cretaceous (Dilek and Whitney, 1997; Özgül, 1997; Parlak and Robertson, 2004). The compression between Eurasian and Afro-Arabian plates continued also in Paleocene-Eocene period, thus widespread ophiolite and mélange emplacement over the Taurus platform occurred. The subduction that began at the end of Mesozoic, and the compression which continued during early Tertiary caused forming of the napped structure in Taurus Units (Figures 3e, 4e, 15a, b) and the development of Taurus orogenic belt. The orogeny in the Taurus orogenic belt which had been shaped by subduction, collision and compressional movements, and had created napped structure, has been ended by the thickening of continental crust.

5.2. Formation of the Oligocene Molasse Basins in the Central Taurides

Although the depositions occurred in Oligocene on the Taurus orogenic belt in the Central Taurides have limited lateral extent, they host very important data in revealing regional tectonic changes. Signs of changing in regional tectonic manifest firstly itself by the opening of Oligocene basins. Lacustrine sedimentations within the Ermenek, Bucakkışla, Korucuk and Çamlıyayla basins, which were opened due to normal faulting upon the Taurus Units, constitute the first records of the depositions occurred under the extensional tectonic regime following the Taurus Orogeny. The Central Taurides have been shaped by the depositions occurred under this new tectonic regime which began in Oligocene and continued during Neogene.

Different basin models developed based on the compressional or extensional tectonism can be proposed for the Oligocene lacustrine basins defined in this paper within the Central Taurides. However, considering that the basins defined in the region are situated on the Taurus Units and were opened in front of normal faults under extensional tectonic conditions

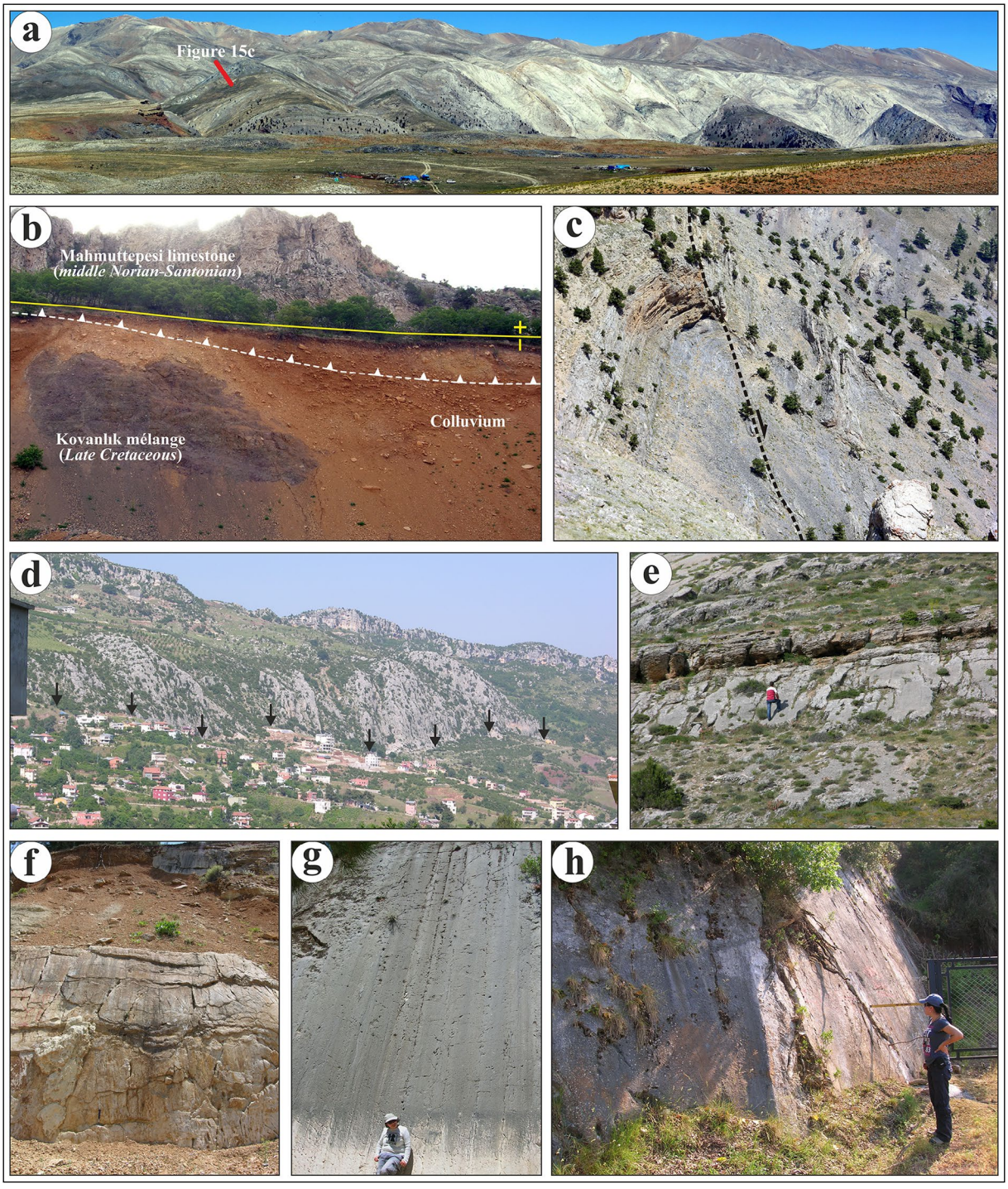

Figure 15- a, b) All the pre-Oligocene units in the Central Taurides gained a napped structure by the compression that lasted until the late Eocene due to Taurus Orogeny, and completed their orogenic developments (a- Mersin, Cocak Valley; b- Karaman, NE of Afgan Village). b, c, d) These units have been subjected to orogenic collapse as from Oligocene as a result of interruption or termination of the compression and have been cut by dip-slip normal faults (c- Mersin, Cocak Valley; d- Mersin, Bekiralanı Village). e, f, g, h) Normal faulting in the region continued after Neogene and the units deposited in the Neogene period were also cut by the larger normal fault systems (e- Mersin, NW of Çömelek Village; f- Mersin, S of Zeyne; g- Mersin, Sarıkavak, S of Gündüzler Village; h- Mersin, W of Ayvagediği).

and are absent of deformation data that reflect the compressional tectonism; it has been inferred that the compressional deformation and the basin development due to compressional regime have not been active in the region since Oligocene.

Mut Basin at regional scale is thought to be formed as a result of orogenic collapse developed in the extensional back-arc of Cyprus-arc located in the south (Kempler and Ben-Abraham, 1987; Robertson, 2000; Kelling et al., 2001; Ünlügenç et al., 2001). According to Le Pichon and Angelier (1981) and Gautier and Brun (1994), extensional tectonic regime was occurred as a consequence of northward-subducting Hellenic arc to migrate towards the south via back-arc spreading. However, the time discrepancy between the extensional tectonics beginning in late Oligocene-early Miocene within the Western Anatolia and the southward migration of subducting plate in middle Miocene-early late Miocene interval make the proposed models improbable (Seyitoğlu and Scott, 1996). Vertical uplift of the Central Taurides in the late Miocene (late Tortonian) (Cosentino et al., 2012; Ilgar et al., 2013) indicates that the formation of the Oligocene basins could not be related to vertical uplift of the Taurides. Kelling et al. (1995) suggested that this structural development was developed as a result of the orogenic collapse. The continental crust, overthickened in Eocene period, has caused basin opening by gravity effect due to disappearance of compression (Gautier et al., 1999; Dilek and Whitney, 2000).

All the pre-Oligocene units which had been emplaced in the region depending on the N-S compression in the Central Taurides, gained a napped structure by compression that lasted until the late Eocene, and completed their orogenic developments (Figures 3e, 4e, 15 a, b). These mountain ranges where the thickening of continental crust and the structural heterogeneity developed, are the post-orogenic extensional regions (Dewey, 1988; Seyitoğlu and Scott, 1996). Gravity collapse is expected to be occurred in the subduction zones where the crustal thickening observed and in the continent-to-continent collision regions. Gravitational collapse of the continental crust is a process which follows the crustal thickening. Inıtiation of the collapse is resulted from changes in the balance of forces that, during conversion and collision, generate crustal thickening and stabilize this thickness (Rey et al., 2001).

Pre-Oligocene units, reaching maximum elevation in the Central Taurides, have been subjected to strain or gravitational forces occurred in the region in consequence of interruption or termination of compression that lasted until the end of Eocene. Thus, the units which constitute nappes were cut by dip-slip normal faults due to orogenic collapse (Figures 15b, c, d), and in front of the faults, Ermenek, Bucakkışla, Korucuk, Çamlıyayla basins began to form upon the hanging wall blocks.

The fact that the Taurus orogenic belt has a napped structure and the presence of ophiolites and ophiolitic mélange in the Bozkır Unit have contributed significantly to the basin opening after the nappe emplacement. Nappe tectonics, at first, has caused the Taurus orogenic belt to be overthickened. The decrease in the horizontal compressional force that caused the crustal thickening allowed the orogenic collapse and a rapid basin formation under the effect of gravity. Besides, the nappe tectonics has caused the Taurus orogenic belt to have a heterogeneous structure and the development of weak zones between the nappes/thrusts. These weak zones have caused reduction of the basal shear stress between nappes and thrust sheets (Rey et al., 2001). It is thought that the reduction of the compressional force that creates orogeny and the re-activation of weakness zones in the form of normal faults or detachment planes under the effect of gravity facilitates the basin development due to extensional tectonics.

According to Robertson et al. (2012), Oligocene period in the Central Taurides is represented by the post-collisional compressional regime. However, the formation of Ermenek, Bucakkışla, Korucuk and Çamlıyayla basins, which take place in the form of grabenization, reflect the post-orogenic molasse basin development. The fact that the clastic and carbonate rocks deposited in the molasse basins in the Central Taurides are Oligocene aged indicate that the post-orogenic collapsing and basin formation occurred in the early Oligocene, just after collision and compression.

Formation of the basins related to extensional tectonics upon the units emplaced in the region due to nappe tectonics in the Central Taurides indicates that a new tectonic period has started in the region. This new period shows that the compressional tectonic regime did not have any effect in the region in early Oligocene,

but on the contrary, a new tectonic regime that could lead to basin development began to develop. It is observed that the Oligo-Miocene basins located in the Central Taurides, at first, began to open as independent small basins due to the orogenic collapse in the Oligocene period and lacustrine sedimentation was developed in these basins. The marine transgression that occurred in the Central Taurides during the late Burdigalian period caused the drowning of Mut Basin and marine sedimentation in this basin in the Neogene period. As a result of the migration of the northward-subducting Cyprus plate towards the south as from the end of the middle Miocene, the orogenic collapse continued in the extensional back-arc, and the units deposited in the Neogene period were cut by normal fault systems (Figures 15e, f, g, h).

6. Conclusions

In this study, four Oligocene lacustrine basins, namely Ermenek, Bucakkışla, Korucuk and Çamlıyayla basins, have been defined in the Central Taurus Mountains. Structural features and stratigraphic sequences of these basins have been studied in detail and the basins have been aged.

The tectono-stratigraphic and age data of the basins have been evaluated together, and the timing of formation of the basins and the tectonic processes controlling the basin opening have been discussed at the scale of Central Taurides.

The Oligocene lacustrine sediments deposited in Ermenek, Bucakkışla, Korucuk and Çamlıyayla basins reflect the first sedimentary sequences deposited on the Taurus Units. These units constitute the first records of deposition occurred under the extensional tectonic regime following the Taurus Orogeny in the Central Taurides.

Extensional basin formation on the Taurus Units which had been emplaced in the region due to nappe tectonics indicates the "orogenic collapse basins" developed under the effect of strain or gravity forces at a regional scale.

In previous studies, it was interpreted that Mut Basin was opened as a result of orogenic collapse in extensional back-arc of the Cyprus subduction arc in the south, or as the back-arc spreading as a result of migration of the northward subducting Cyprus plate towards the south. However, the time discrepancy between the southward migration of the subducting-plate in the late middle Miocene-early late Miocene interval and the basin opening that began in Oligocene in the Central Taurides makes the suggested models controversial.

The orogeny that built Taurides and the compressional deformation lasted until late Miocene in the Eastern Taurides. In the Central Taurides, extensional basin formation as from the early Oligocene on the Taurus Units that had been emplaced in the region due to nappe tectonics indicates a new tectonic period has started in the region.

Acknowledgements

This study was carried out in the scope of "*Geology and Paleogeographic Development of the Neogene Rocks in Adana-Mut Basin*" project conducted between 2009-2012 by the Department of Geological Research of the General Directorate of Mineral Research and Exploration (MTA). Palynological investigations were conducted by Assoc. Prof. Dr. Mine Sezgül Kayseri Özer. The first draft of the manuscript was reviewed by Prof. Dr. Cihat Alçiçek, Dr. Volkan Özaksoy, Dr. Oktay Parlak and Ali Ergen. Prof. Dr. Yaşar Eren, Prof. Dr. Ulvi Can Ünlügenç and Assoc. Prof. Dr. Serkan Üner made valuable contributions. We would like to thank to the Referees for carefully reading our article and for giving such constructive comments which substantially helped improving the quality of the paper.

References

Ainsworth, R.B., Crowley, S.F. 1994. Wave-dominated nearshore sedimentation and 'forced' regression: post-abandonment facies, Great limestone cyclothem, Stainmore, UK. Journal of the Geological Society of London 151, 681–695.

Akgün, F., Akyol, E. 1987. Akhisar (Çıtak) çevresi kömürlerinin palinolojik incelenmesi. Türkiye Jeoloji Kurumu Bülteni 30/1, 30–50.

Akgün, F., Akyol, E. 1992. Yukarıkaşıkara ve Yarıkaya (Isparta) kömürlerinin karşılaştırmalı palinostratigrafisi ve paleoekolojisi. Türkiye Petrol Jeologları Derneği Bülteni 4/1, 10–20.

Akgün, F., Akyol, E. 1999. Palynostratigraphy of the coal-bearing Neogene deposits, Graben in Büyük Menderes, Western Anatolia. Geobios 32, 3, 367–383.

Akgün, F., Sözbilir, H. 2000. A palynostratigraphical approach to the SW Anatolian Molasse Basin: Kale-Tavas and Denizli Molasse. Geodinamica Acta 14, 71–93.

Akgün, F., Alişan, C., Akyol, E. 1986. Soma Neojen staratigrafisine palinolojik bir yaklaşım. Türkiye Jeoloji Kurumu Bülteni 29, 13–25.

Akgün, F., Akay, E., Erdoğan, B. 2002. Terrestrial to shallow marine deposition in Central Anatolia: A palynological approach. Turkish Journal of Earth Sciences 11, 1–27.

Aktaş, G., Robertson, A.H.F. 1990. Tectonic evolution of the Tethys suture zone in SE Turkey: evidence from the petrology and geochemistry of Late Cretaceous and Middle Eocene extrusives. Malpas, J., Moores, E.M., Panayiotou, A., Xenophontos, C. (Ed.). Ophiolites – Oceanic Crustal Analogues. Proceedings of the International Symposium Troodos 1987, Cyprus Geological Survey, Nicosia, 311−328.

Akyol, E., Akgün. F. 1990. Palynology Of The Borate Bearing Neogene Sediments In Bigadiç, Kestelek, Emet And Kirka Regions. Bulletin of the Mineral Research and Exploration 111, 165–173.

Allmendinger, R.W., Cardozo, N.C., Fisher, D. 2013. Structural Geology Algorithms: Vectors & Tensors: Cambridge, England, Cambridge University Press, 289 pp.

Andrew, T., Robertson, A.H.F. 2002. The Beyşehir-Hoyran-Hadım nappes: genesis and emplacement of Mesozoic marginal and oceanic units of the northern Neotethys in southern Turkey. Journal of the Geological Society of London 159, 529−543.

Barrell, J. 1912. Criteria for the recognition of ancient delta deposits. Bulletin of the Geological Society of America 23, 377−446.

Bilgin, A. Z., Uğuz, M. F., Elibol, E., Güner, E., Gedik, İ. 1994. Mut-Silifke-Gülnar yöresinin (İçel ili) jeolojisi. Maden Tetkik ve Arama Genel Müdürlüğü Rapor No: 9715, 120, 4 Ek, Ankara (unpublished).

Bluck, B.J. 1967. Sedimentation of beach gravels: examples from South Wales. Journal of Sedimentary Petrology 37, 128–156.

Bluck, B.J. 1999. Clast assemblages, bed-forms and structure in gravel beaches. Transactions of the Royal Society of Edinburgh Earth Sciences 89, 291– 332.

Bornhold, B.D., Prior, D.B. 1990. Morphology and sedimentary processes of the subaqueous Noeick River delta, British Columbia, Canada. Colella, A., Prior D.B. (Ed.), Coarse-grained Deltas. International Association of Sedimentologists Special Publication l0, 169-181.

Clark, M., Robertson, A.H.F. 2002. The role of the Early Tertiary Ulukışla Basin, southern Turkey, in suturing of the Mesozoic Tethys Ocean. Journal of the Geological Society of London 159, 673–690.

Clifton, H.E. 1973. Pebble segregation and bed lenticularity in wave-worked versus alluvial gravel. Sedimentology 20, 173–187.

Clifton, H.E. 1976. Wave-formed sedimentary structures-a conceptual model. In: Davis Jr., R.A., Ethington, R.L. (Ed.), Beach and Nearshore Sedimentation. Society of Economic Paleontologists and Mineralogists Special Publication 24, 126– 148.

Colella, A. 1988. Pliocene–Holocene fan deltas and braid deltas in the Crati Basin, southern Italy: a consequence of varying tectonic conditions. Nemec, W., Steel, R.J. (Ed.). Fan Deltas-Sedimentology and Tectonic Settings. Blackie, London, 50–74.

Collins, A.S., Robertson, A.H.F. 1998. Processes of Late Cretaceous to Late Miocene episodic thrust-sheet translation in the Lycian Taurides, SW Turkey. Journal of the Geological Society of London 155, 759–772.

Collins, A.S., Robertson, A.H.F. 2000. Evolution of the Lycian allochthon, western Turkey, as a north-facing Late Palaeozoic to Mesozoic rift and passive margin. Geological Journal 34, 107–138.

Collinson, J.D. 1996. Alluvial sediments. Reading, H.G. (Ed.). Sedimentary Environments: Processes, Facies and Stratigraphy. Blackwell Science, Oxford, 37–82.

Cosentino, D., Schildgen, T.F., Cipollari, P., Faranda, C., Gliozzi, E., Hudáčková, N., Lucifora, S., Strecker, M.R. 2012. Late Miocene surface uplift of the southern margin of the Central Anatolian plateau, Central Taurides, Turkey. Bulletin of the Geological Society of America 124, 133–145.

Demirel, İ. H. 1989. Ermenek (Konya) yöresinde yer alan Tersiyer yaşlı istifin jeolojisi, sedimantolojisi ve bölgedeki kömür damarlarının ayrıntılı incelenmesi. Doktora Tezi, H.Ü. Fen. Bil. Enst., 173, Ankara.

Demirtaşlı, E. 1984. Stratigraphy and tectonics of the area between Silifke and Anamur, Central Taurus Mountains. Tekeli, O., Göncüoğlu, M.C. (Ed.). Geology of the Taurus Belt. Maden Tetkik ve Arama Genel Müdürlüğü Special Publication, 101–118.

Demirtaşlı, E., Gedik, İ., İmik, M. 1986. Ermenek batısında Göktepe-Dumlugöze ve Tepebaşı arasında kalan bölgenin jeolojisi, Maden Tetkik ve Arama Genel Müdürlüğü Rapor No: 5783, Ankara (unpublished).

Dewey, J.F. 1988. Extentional collapse of orogens. Tectonics 7, 1123–1139.

Dewey, J.F., Hempton, M.R., Kidd, W.S.F., Şaroğlu, F., Şengör, A.M.C. 1986. Shortening of continental lithosphere: The neotectonics of eastern Anatolia, a young collision zone. Coward, M.P., Ries, A.C. (Ed.). Collision tectonics. Geological Society of London Special Publication 19, 3–36.

Dilek, Y., Moores, E.M. 1990. Regional tectonics of the eastern Mediterranean ophiolites. Malpas, J., Moores, E.M., Panayiotou, A., Xenophontos, C. (Ed.). Ophiolites, oceanic crustal analogues: Proceedings of the symposium Trodos 1987: Geological Survey Department, Nicosia, Cyprus, 295–309.

Dilek, Y., Whitney, D.L. 1997. Counterclockwise P-T-t trajectory from the metamorphic sole of a Neo-Tethyan ophiolite (Turkey). Tectonophysics 280, 3–4, 295–310.

Dilek, Y., Whitney, D.L. 2000. Cenozoic crustal evolution in Central Anatolia: Extension, magmatism and landscape development. Panayides, I., Xenophontos, C., Malpas, J. (Ed.). Proceedings of the Third International Conference on the Geology of the Eastern Mediterranean: Geological Survey Department, Nicosia, Cyprus, p.183–192.

Dott, R. H., Bourgeois, J. 1982. Hummocky stratification: Significance of its variable bedding sequence. Geological Society of America Bulletin 93, 663–680.

Esirtgen, T. 2014. Tectono - Sedimentary Evolution of Bucakkifila Region (SW Karaman) In Central Taurides. Bulletin of the Mineral Research and Exploration 148, 19–42.

Gautier, P., Brun, J.P. 1994. Ductile crust exhumation and extensional detachments in the central Aegean (Cyclades and Evvia Islands). Geodinamica Acta 7, 57–85.

Gautier, P., Brun, J.P., Moriceau, R., Sokoutis, D., Martinod, J., Jolivet, L. 1999. Timing, kinematics and cause of the Aegean extention: A scenario based on a comparison with simple analogues experiments. Tectonophysics 315, 31–72.

Gedik, A., Birgili, Ş., Yılmaz, H., Yoldaş, R. 1979. Mut-Ermenek-Silifke yöresinin jeolojisi ve petrol olanakları. Türkiye Jeoloji Kurumu Bülteni 22, 7–26.

Hunter, R. E., Clifton, H. E. 1982. Cyclic deposits and hummocky-cross-stratification of probable storm origin in Upper Cretaceous rocks of Cape Sebastian area, southwestern Oregon. Journal of Sedimentary Petrology 52, 127–143.

Ilgar, A. 2002. Ermenek (Karaman) Miyosen yaşlı karasal çökel sistemlerinin sedimantolojik evrimi (Orta Toroslar-Türkiye), Doktora Tezi, H.Ü. Fen Bil. Enst., 125 s., Ankara.

Ilgar, A., Nemec, W. 2005. Early Miocene lacustrine deposits and sequence stratigraphy of the Ermenek Basin, Central Taurides, Turkey. Sedimentary Geology 173, 217–249.

Ilgar, A., Nemec, W., Hakyemez, A., Karakuş, E. 2013. Messinian forced regressions in the Adana Basin: a near-coincidence of tectonic and eustatic forcing. Çiner, A., Strecker, M.R., Bertotti, G. (Ed.). Late Cenozoic Evolution of the Central Anatolia Plateau. Turkish Journal of Earth Sciences Special Publication 22, 864–889. DOI: 10.3906/yer-1208-3.

Ilgar, A., Esirtgen, T., Türkmen Bozkurt, B., Demirkaya, S., Hakyemez, A., Culha, G., Danacı, F., Aydın, A., Gürler, G., Baykal Dölen, M., Çınar Durgut, S.N., Beşter Bengü, B., Akpınar, S., Karakuş, E. 2016. Adana-Mut (İçel) Arasında Yüzeylenen Neojen Yaşlı Kayaçların Jeolojisi ve Paleocoğrafik Gelişimlerinin Kurulması. Maden Tetkik ve Arama Genel Müdürlüğü, Rapor No: 11915, Ankara (unpublished).

Ilgar, A., Esirtgen, T., Hakyemez, A., Culha, G., Demirkaya, S., Türkmen Bozkurt, B. 2019. The control of sea-level changes on sedimentation in the Mut Basin: Late Serravallian-Early Tortonian incised valley-fill. Bulletin of The Mineral Research and Exploration 159, 1–28.

Kayseri, M.S., Akgün, F. 2002. Palynostratigraphic correlation of the Miocene sediments with Lignites and their depositional environments in the central Anatolia, Turkey. 6th European Paleobotany-Palynology Conference, Aug. 29 - Sep. 2, 2002 Athens, Greece.

Kayseri, M.S., Akgün, F. 2003. Palynofloristic correlation of Neogene sediments in western and central Anatolia (Turkey). Neclime Annual Meeting, p.12.

Kayseri, M.S., Akgün, F., Ilgar, A., Yurtsever, Ş., Derman, S. 2006. Palynostratigraphy and Palaeoclimatology of the Ermenek and Mut Regions (Southern Turkey) in the Earliest Oligocene Period. In Abstract 7th European Palaeobotany-Palynology Conference, Prague, 63.

Kelling, G., Gökçen, S., Floyd, P., Gökçen, N. 1987. Neogene tectonics and plate convergence in the eastern Mediterranean: new data from southern Turkey. Geology 15, 425–429.

Kelling, G., Şafak, Ü., Gökçen, N.S. 1995. Mid-Cenozoic evolution of the Mut Basin, south Türkiye, and

its regional significance. Abstracts Int. Earth Sci. Colloq. on the Aegean Region. İzmir Univ, İzmir, 30.

Kelling, G., Egan, S. E., Gürbüz, K., Şafak, Ü., Ünlügenç, U.C. 2001. Oligo-Miocene basins of south-central Turkey: Synthesis and appraisal. Abstracts 4th International Symposium on Geology of Turkey and Its Surroundings–Work in Progress. 24-28 Sept. 2001 Çukurova University, Adana, 17.

Kelts, K., Hsü, K.J. 1978. Freshwater carbonate sedimentation. Lerman, A. (Ed.). Lakes: Chemistry, Geology, Physics. Springer-Verlag, Berlin, 295–323.

Kempler, D., Ben-Abraham, Z. 1987. The tectonic evolution of the Cyprean Arc. Annales Tectonicae 1, 58–71.

Koçyiğit, A. 1977. Karaman-Ermenek (Konya) arasındaki bölgenin tektoniği. Türkiye Jeoloji Kurumu Bülteni 20, 1–8.

Le Pichon, X., Angelier, J. 1981. The Aegean sea. Philosophical Transactions of the Royal Society of London 300, 357–371.

Leren, B.L.S., Janbu, N.E., Nemec, W., Kırman, E., Ilgar, A. 2007. Late Cretaceous to Early Eocene sedimentation in the Sinop–Boyabat Basin, north-central Turkey: a deep-water turbiditic system evolving into littoral carbonate platform. Nichols, G., Williams, E.A., Paola, C. (Eds.). Sedimentary Processes, Environments and Basins: A Tribute to Peter Friend. IAS Special Publication 38, 401–456.

Lowe, D.R. 1982. Sediment gravity flows: II. Depositional models with special reference to the deposits of high-density turbidity currents. Journal of Sedimentary Petrology 52, 279–297.

Miall, A.D. 1985. Architectural-element analysis: a new method of facies analysis applied to fluvial deposits. Earth-Science Reviews 22, 261–308.

Michard, A., Whitechurch, H., Ricou, L.E., Montigny, R., Yazgan, E. 1984. Tauric subduction (Malatya-Elazığ provinces) and its bearing on tectonics of the Tethyan realm in Turkey. Dixon, J.E., Robertson, A.H.F. (Ed.). The Geological Evolution of the Eastern Mediterranean. Geological Society of London, Special Publications 17, 349–360.

Monod, O. 1977. Geological Investigations in Western Taurides to the South of Beyşehir (Turkey): [Dissertation]. University of Paris-Sud, Paris-Sud. 450.

Nemec, W. 1990. Aspects of sediment movement on steep delta slopes. Colella, A., Prior, D.B. (Ed.). Coarse-grained Deltas. International Association of Sedimentologists, Special Publication 10, 29–73.

Nemec, W., Steel, R.J. 1984. Alluvial and coastal conglomerates: their significant features and some comments on gravelly mass-flow deposits. Koster, E.H., Steel, R.J., (Ed.). Sedimentology of Gravels and Conglomerates. Canadian Society of Petroleum Geologists, Memoir 10, 1–31.

Nemec, W., Postma, G. 1993. Quaternary alluvial fans in southwestern Crete: sedimentation processes and geomorphic evolution. Marzo, M., Puigdefabregas, C. (Ed.). Alluvial Sedimentation. International Association of Sedimentologists, Special Publication 17, 235–276.

Nemec, W., Alçiçek, M.C., Özaksoy, V. 2018. Sedimentation in a foreland basin within synorogenic orocline: Palaeogene of the Isparta Bend, Taurides, SW Turkey. Basin Research 30, 650–670.

Okay, A.I., Tüysüz, O. 1999. Tethyan sutures of northern Turkey. Durand, B., Jolivet, L., Horváth, F., Séranne, M. (Ed.). The Mediterranean Basins: Tertiary Extension Within the Alpine Orogen. Geological Society of London, Special Publication 156, 475–515.

Özgül, N. 1976. Torosların bazı temel jeoloji özellikleri. Türkiye Jeoloji Kurumu Bülteni 19, 65–78.

Özgül, N. 1997. Stratigraphy of the Tectonostratigraphic Units Around Hadım-Bozkır-Taşkent Region (Northern Part of the Central Taurides, Turkey). Bulletin of the Mineral Research and Exploration 119, 113–174.

Parlak, O., Bozkurt, E., Delaloye, M. 1996. The Obduction Direction of the Mersin Ophiolite: Structural Evidence from Subophiolitic Metamorphics in Central Tauride Belt, Southern Turkey. International Geology Review 38, 778–786.

Parlak, O., Robertson, A.H.F. 2004. The ophiolite-related Mersin Melange, southern Turkey: Its role in the tectono-sedimentary setting of Tethys in the Eastern Mediterranean region. Geological Magazine 141, 257–286.

Poisson, A., Yağmurlu, F., Bozcu, M., Şentürk, M. 2003. New insights on the tectonic setting and evolution around the apex of the Isparta Angle (SW Turkey). Geological Journal 38, 257−282.

Polat, A., Casey, J.F. 1995. A Structural Record of the Emplacement of the Pozantı-Karsantı Ophiolite onto the Menderes-Taurus Block in the Late Cretaceous, Eastern Taurides, Turkey. Journal of Structural Geology 17, 1673–1688.

Postma, G. 1990. Depositional architecture and facies of river and fan deltas: a synthesis. Colella, A., Prior, D.B. (Ed.). Coarse-Grained Deltas. International Association of Sedimentologists, Special Publication 10, 13–27.

Postma, G., Nemec, W. 1990. Regressive and transgressive sequences in a raised Holocene gravelly beach, southwestern Crete. Sedimentology 37, 907–920.

Rey, P., Vanderhaeghe, O., Teyssier, C. 2001. Gravitational collapse of the continental crust: definition, regimes and modes. Tectonophysics 342, 435–449.

Robertson, A.H.F. 2000. Mesozoic-Tertiary tectonic-sedimentary evolution of a south Tethyan oceanic basin and its margins in southern Turkey. Bozkurt, E., Winchester, J.A., Piper, J.D.A. (Ed.). Tectonics and Magmatism in Turkey and the Surrounding Area. Geological Society of London Special Publication 173, 97–138.

Robertson, A.H.F., Dixon, J.E. 1984. Introduction: Aspects of the geological evolution of the Eastern Mediterranean. Dixon, J.E., Robertson, A.H.F. (Ed.). The geological evolution of the Eastern Mediterranean. Geological Society of London, Special Publication 17, 1–74.

Robertson, A.H.F., Parlak, O., Ustaömer, T. 2012. Overview of the Palaeozoic-Neogene evolution of Neotethys in the Eastern Mediterranean region (southern Turkey, Cyprus, Syria). Petroleum Geoscience 18, 381–404.

Seyitoğlu, G., Scott, B.C. 1996. The cause of N-S extensional tectonics in western Turkey: Tectonic escape vs back-arc spreading vs orogenic collapse. Journal of Geodynamics 22, 145–153.

Şafak, Ü., Kelling, G., Gökçen, N.S., Gürbüz, K. 2005. The mid-Cenozoic succession and evolution of the Mut basin, southern Turkey, and its regional significance. Sedimentary Geology 173, 121–150.

Şenel, M. 2002. 1/500.000 ölçekli Türkiye Jeoloji Haritası, Pafta No: 14 (Konya). Maden Tetkik ve Arama Genel Müdürlüğü (MTA), Ankara.

Şengör, A.M.C. 1987. Tectonics of the Tethysides: orogenic collage development in a collisional setting. Annual Review of Earth and Planetary Sciences 15, 213–244.

Şengör, A.M.C., Yılmaz, Y. 1981. Tethyan evolution of Turkey: a plate tectonic approach. Tectonophysics 75, 181–241.

Talbot, M.R., Allen, P.A. 1996. Lakes. Reading, H.G. (Ed.). Sedimentary Environments: Processes, Facies and Stratigraphy. Blackwell Science, Oxford, pp. 83–124.

Uğuz, M.F. 1989. Silifke-Ovacık-Gülnar (İçel İli) Arasının Jeolojisi: İstanbul Üniversitesi, Mühendislik Fakültesi, Yer Bilimleri Ana Bilim Dalı Doktora tezi. İstanbul.

Ulu, U. 2002. 1/500.000 ölçekli Türkiye Jeoloji Haritası, Pafta No: 15 (Adana). Maden Tetkik ve Arama Genel Müdürlüğü (MTA), Ankara.

Ünay, E., Atabey, E., Saraç, G. 2001. Small mammals and foraminifera from the Anatolian (Central Taurus) early Miocene. Annals of Carnegie Museum 70, 4, 247–256.

Ünlügenç, U.C., Kelling, G., Demirkol, C. 1990. Aspects of basin evolution in the Neogene Adana Basin, SE Turkey. Proceedings of the International Earth Sciences Congress on Aegean Regions, İzmir, 353-369.

Ünlügenç, U.C., Demirkol, C., Kelling, G., Williams, G.D., Kop, A. 2001. Timing and causes of Tertiary deformation in the Çukurova Basin Complex, southern Turkey: new seismic-sequence stratigraphic interpretations. Abstracts 4th International Symposium on Geology of Turkey and Its Surroundings–Work in Progress. Çukurova University, Adana, p. 281.

Walker, R.G., Plint, A.G. 1992. Wave- and storm-dominated shallow marine systems. Walker, R.G., James, N.P. (Ed.). Facies Models: Response to Sea Level Change. Geological Association of Canada, St. John's, pp. 219–238.

Wright, V.P. 1990. Lacustrine carbonates. Tucker, M.E., Wright, V.P. (Ed.). Carbonate Sedimentology. Blackwell Science, Oxford, 164–190.

Yılmaz, Y. 1993. New evidence and model on the evolution of the southeast Anatolian orogen. Geological Society of America Bulletin 105, 251–271.

Yılmaz, Y., Yiğitbaş, E., Genç, Ş.C. 1993. Ophiolitic and metamorphic assemblages of southeast Anatolia and their significance in the geological evolution of the orogenic belt. Tectonics 12, 1280–1297.

Bulletin of the Mineral Research and Exploration

http://bulletin.mta.gov.tr

The internal structure of Beypazarı Blind Thrust Zone around Çayırhan

Anıl ARDAHANLIOĞLU[a*], Gürol SEYİTOĞLU[a] and Korhan ESAT[a]

[a]*Ankara University, Department of Geological Engineering, Tectonics Research Group, Gölbaşı, Ankara, Turkey*

Research Article

Keywords:
Central Anatolia, Neotectonics, Blind thrust fault, Earthquake, Fault-propagation fold.

Received Date: 15.09.2019
Accepted Date: 19.11.2019

ABSTRACT

The Beypazarı Blind Thrust Zone, which is surrounded by the North Anatolian, the Eskişehir, and the Kırıkkale-Erbaa fault zones, is a recently defined neotectonic structure developed in the NW central Anatolia together with the Eldivan-Elmadağ and the Abdüsselam Pinched Crustal Wedges. In this study, the internal structure of the Beypazarı Blind Thrust Zone has been examined in detail around Çayırhan region. It has been defined that it consists of the Karaköy, Sekli, Nalçabayırı, Uzunbayır blind thrusts, Davutoğlan Back Thrust, and Beypazarı Blind Thrust I-II from north to south, respectively with help of the fault-propagation folds in the study area. The existence of economically important and operational resources such as lignite and trona in the Neogene sequence affected by these faults in the region and earthquake generating potential of the faults determined in previous studies increase the importance of this study.

1. Introduction

The Neogene Beypazarı-Çayırhan basin located in the central Anatolia region contains important mineral deposits. The basin has been subjected to geochemical studies due to its potential for geothermal resources as well as lignite and trona deposits (Helvacı et al., 1981; Özpeker et al., 1991; Suner, 1993; Kavuşan, 1993*a*; Karadenizli, 1995; Orti et al., 2002; Özçelik, 2002; Özgüm et al., 2003; Özçelik and Altunsoy, 2005; Diker et al., 2006; Şener, 2007; Garcia-Veigas et al., 2013; Bechtel et al., 2014; Pehlivanlı et al., 2014). Although the researches are mainly concentrated on mineral deposits, there are also engineering geology studies (Aksoy et al., 2006; Apaydın, 2010). When all these engineering and mineral deposits studies are taken into consideration, some researchers indirectly have mentioned about the tectonics and structural geology of the region (Yağmurlu et al., 1988; İnci, 1991; Kavuşan, 1993*b*). The studies based on the structural geology and tectonics of the region are less when compared with other subjects (Demirci, 2000; Seyitoğlu et al., 2017*a*; Şahin et al., 2019).

Major geological structures in the basin were defined as the "Beypazarı flexure" (Randot, 1956; Kalafatçıoğlu and Uysallı, 1964; Kavuşan, 1993*b*) and the "Beypazarı monocline" (Yağmurlu et al., 1988; Demirci, 2000). The same structures were defined by Seyitoğlu et al. (2017*a*) as fault propagation folds due to blind thrust faults. It was stated that the region remained under the influence of extensional tectonic regime in the early Miocene and the contractional tectonic regime in NW-SE direction between the North Anatolian and the Eskişehir Fault Zones in the early Pliocene (Yağmurlu et al., 1988). Kavuşan (1993*b*) stated that the basin has been developed under the NW-SE contractional tectonic regime since the beginning of the formation of the basin. Demirci (2000) mentioned about three different tectonic phases (contraction in

Citation info: Ardahanlıoğlu, A., Seyitoğlu, G., Esat, K. 2020. The internal structure of Beypazarı Blind Thrust Zone around Çayırhan. Bulletin of the Mineral Research and Exploration 163,77-97. https://doi.org/10.19111/bulletinofmre.651712.

**Corresponding author: Anıl ARDAHANLIOĞLU, a.ardahanli@gmail.com*

E-W direction, contraction and extension phases in N-S direction) that were active in the region.

Seyitoğlu et al. (2017*a*) revealed that the structures observed in the region were fault propagation folds related to blind thrust faults using the Erenler Back Thrust observed at the surface in the study carried out around Beypazarı. They defined the main factor affecting the formation of all observed structures in the region as the Beypazarı Blind Thrust Zone (Figure 1). The seismic activity distribution and focal mechanism solutions of this zone show that the zone is active today (Seyitoğlu et al., 2017*a*). The reason why such a structure is observed in the Beypazarı-Çayırhan basin is the contraction developed in the inverse triangle shaped area defined as the Northwest Central Anatolia Contractional Region (Esat and Seyitoğlu, 2010; Esat, 2011). They also emphasized that the Beypazarı Blind Thrust Zone should be assessed as a neotectonic structure together with the Eldivan-Elmadağ Pinched Crustal (Seyitoğlu et al., 2009) and the Abdüsselam Pinched Crustal Wedge (Esat et al., 2017) (Figure 1). Şahin et al. (2019) stated that the deformation in the region was directly related to the closure of the Intra-Pontide and İzmir-Ankara oceans, and emphasized the importance of deformation in the area bounded by young faults such as the North Anatolian Fault Zone and the Eskişehir Fault Zone.

With this study, it is aimed to reveal the internal structure of the Beypazarı Blind Thrust Zone with detailed field observations in the Beypazarı-Çayırhan basin that contains important underground resources such as lignite and trona and to reach a general tectonic model, which would be tested by the mining activities, drilling data and geophysical methods.

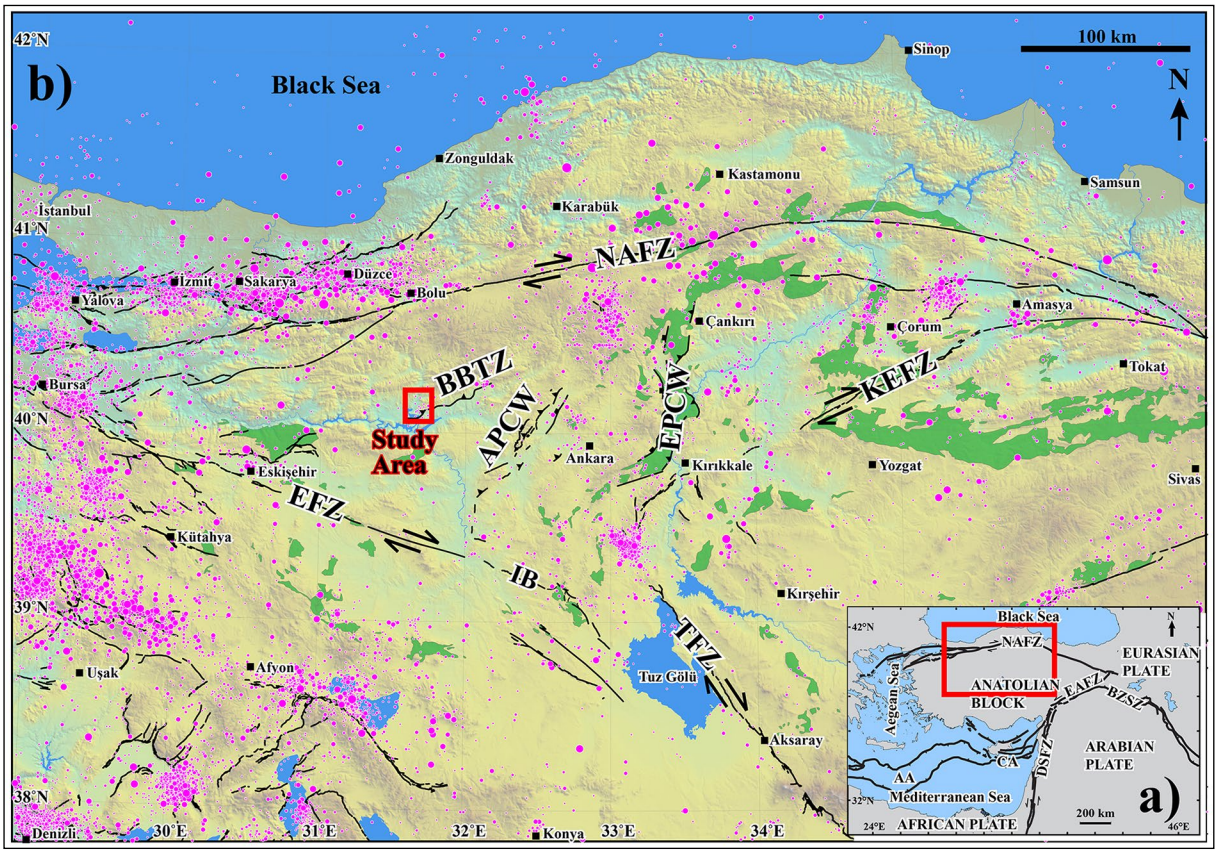

Figure 1- a) Neotectonic elements of the Eastern Mediterranean. DSFZ: Dead Sea Fault Zone; BZSZ: Bitlis-Zagros Suture Zone; EAFZ: Eastern Anatolia Fault Zone; NAFZ: North Anatolian Fault Zone; AA: Aegean Arc; CA: Cyprus Arc. b) The main neotectonic elements of the northwestern Central Anatolia and the location of the study area. KEFZ: Kırıkkale-Erbaa Fault Zone; TFZ: Tuzgölü Fault Zone; EFZ: Eskişehir Fault Zone; IB: Ilıca Branch; EPCW: Eldivan-Elmadağ Pinched Crustal Wedge; APCW: Abdüsselam Pinched Crustal Wedge; BBTZ: Beypazarı Blind Thrust Zone. Faults are taken from the following publications: Şaroğlu et al. (1992); Seyitoğlu et al. (2009; 2015; 2017*a*); Esat (2011); Emre et al. (2013); Esat et al. (2014; 2016; 2017). The distribution of the epicenters of earthquakes with magnitude 3 and above recorded in the instrumental period is shown in the UDİM catalog of Boğaziçi University Kandilli Observatory.

2. Stratigraphy of the Beypazarı-Çayırhan Basin

The stratigraphy of the basin has been studied by previous researchers (Siyako, 1983; Yağmurlu et al., 1988; Kavuşan, 1993*b*), and compiled and updated by Helvacı (2010). The basement rocks observed in the study area are metamorphic units consisting of mainly mica schists. The first sedimentary unit overlying the basement is the Kızılçay group. Paleocene age of the Kızılçay group (Helvacı, 2010) was updated by Şahin et al. (2019) as the middle-upper Eocene (Figure 2). The Kızılçay group consists of red, wine-colored conglomerate, sandstone, claystone and volcaniclastics. The unconformably overlying Çoraklar formation is composed of orange, red orange, yellowish red conglomerate, sandstone, siltstone and mudstone. This formation is economically important as it contains lower and upper lignite levels. The Hırka formation, which overlies the Çoraklar formation, contains white, dirty-white, beige mudstone, claystone, shale, siltstone and dolomitic limestones as well as trona. Radiometric dating studies from tuff levels yielded 21.5 ± 0.9 Ma (early Miocene) (Helvacı, 2010). The Akpınar formation transitionally overlies the Hırka formation. It consists of siliceous limestone, chert, claystone, tuff and mudstone alternations. The Bozbelen formation is composed of blue-green, dark green, reddish sandstone, conglomerate and mudstone. The Kirmir formation, which is the youngest Neogene unit, is composed of greenish gray, green colored claystones and gypsum levels (Figure 2).

The distinction of the Quaternary units of the region in this study is based on the classification proposed by Kazancı (2012). This makes it possible to create a more realistic mapping and interpretation of the geology of the region. For example, in all of the studies conducted in Uluköy and its vicinity in the study area (Yağmurlu et al., 1988; Kavuşan, 1993*b*; Helvacı, 2010), the area mapped as the Kızılçay formation was found to be covered by the alluvial fans (Figure 3).

The river channels with narrow Quaternary beds cut all across the study area. There are also flood plains that developed at low elevations belonging to

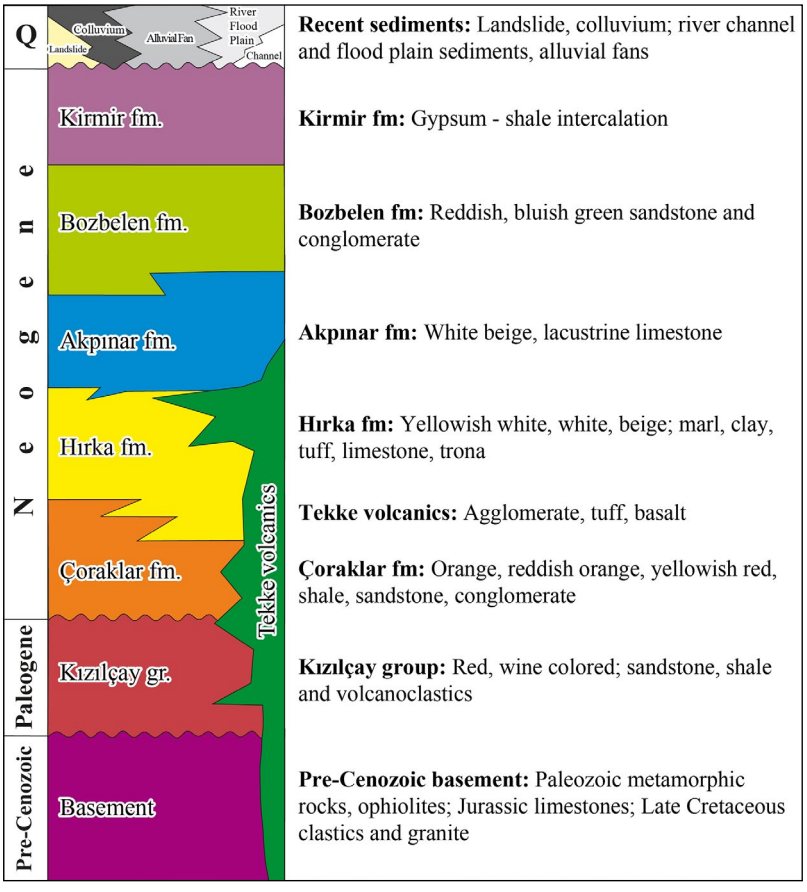

Figure 2- Stratigraphy of the study area (Helvacı, 2010).

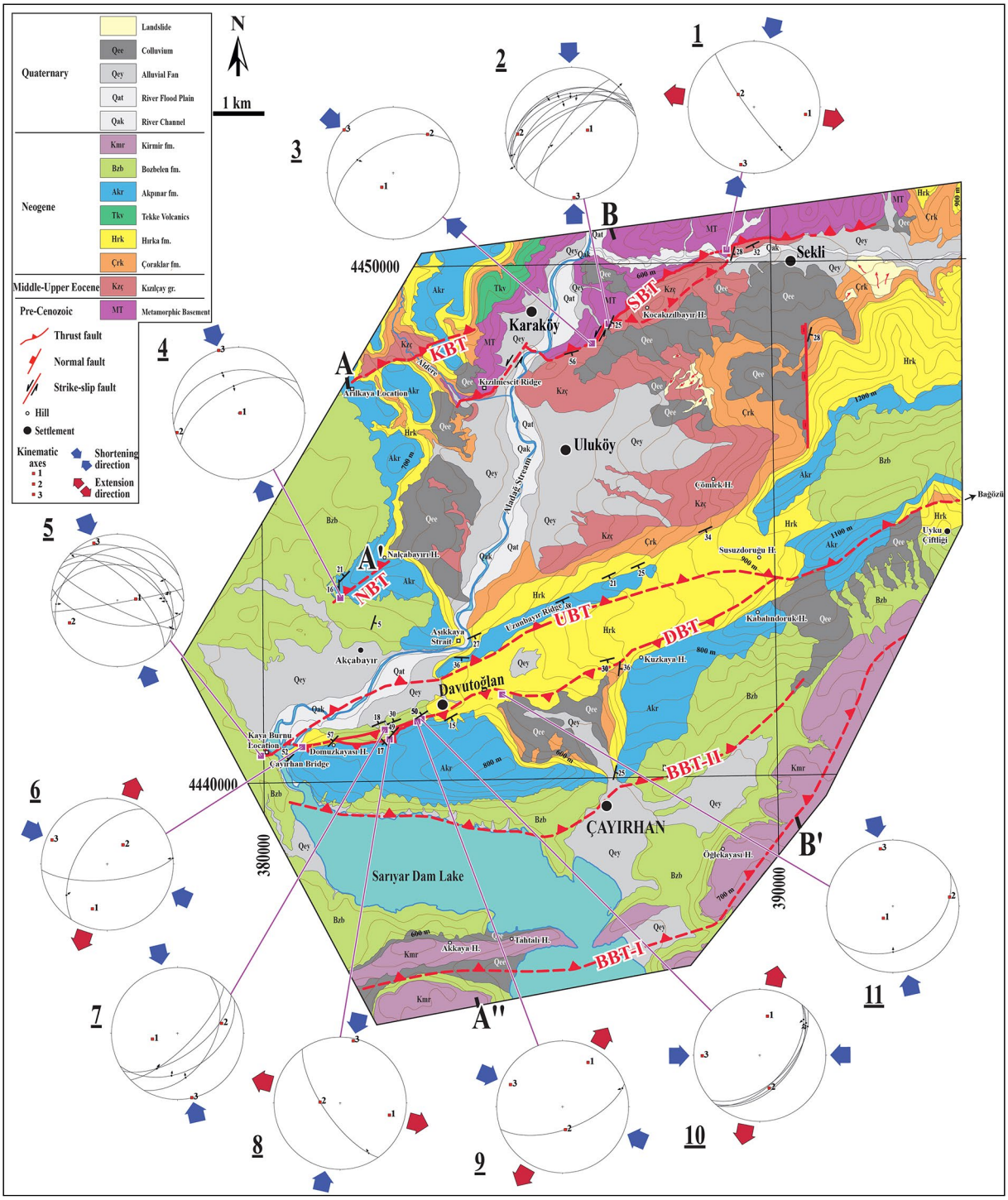

Figure 3- Geological map of the Çayırhan and surroundings. It was redrawn using the previous studies (Siyako, 1983; Kavuşan, 1993*b*; Helvacı, 2010). The circles around the map, the fault planes measured in the field and striations on them are the presentation of equal area lower hemisphere projection. This demonstration and kinematic analysis were performed using FaultKin (Marrett and Allmendinger, 1990; Allmendinger et al., 2012) software. See table 1 for kinematic data. BBT: Beypazarı Blind Thrust, DBT: Davutoğlan Back Thrust, KBT: Karaköy Blind Thrust, NBT: Nalçabayırı Blind Thrust, SBT: Sekli Blind Thrust, UBT: Uzunbayır Blind Thrust.

Table 1- Fault plane-striae data observed in the study area and orientations of the kinematic axes. See figure 3 for the spherical projection views of the data. "# on map" column refers to the spherical projection numbers on the figure 3.

Location (UTM-ED50)			Fault		Striae		Slip	Kinematic Axes					
								1		2		3	
# on Map	X (East)	Y (North)	Strike	Dip	Trend	Plunge		Trend	Plunge	Trend	Plunge	Trend	Plunge
1	389152	4450204	144	83	147	24	Reverse	98	22	309	65	193	12
2	386827	4448826	236	50	344	49	Reverse	78	70	269	19	178	4
			250	45	7	42	Reverse						
			244	36	340	36	Reverse						
			248	34	326	33	Reverse						
			255	40	358	39	Reverse						
			245	60	250	9	Normal						
			240	65	240	0	Normal						
			45	90	45	0	Normal						
			215	75	239	57	Reverse						
3	386532	4448438	242	50	290	42	Reverse	219	68	42	23	311	1
4	381541	4443574	260	35	338	34	Reverse	82	88	252	2	342	0
			242	57	350	56	Reverse						
5	379969	4440539	271	45	66	23	Reverse	86	68	245	21	338	7
			116	80	117	6	Reverse						
			100	60	103	4	Reverse						
			248	23	267	8	Reverse						
			315	26	83	21	Reverse						
			298	49	87	30	Reverse						
			305	42	91	27	Reverse						
			80	87	81	20	Reverse						
			315	65	315	0	Reverse						
6	380762	4440682	213	52	233	23	Reverse	198	29	40	59	294	9
			85	70	85	0	Reverse						
7	382352	4440981	55	62	210	39	Reverse	257	58	77	32	167	0
			30	44	169	32	Reverse						
			60	42	188	35	Reverse						
			45	72	210	38	Reverse						
8	382482	4440848	145	70	150	14	Reverse	104	24	273	65	12	4
9	383009	4441166	70	62	73	5	Reverse	30	23	173	61	293	16
10	383062	4441200	40	55	51	15	Reverse	11	40	164	47	269	14
			42	50	55	15	Reverse						
			47	54	59	16	Reverse						
			40	48	57	18	Reverse						
11	384608	4441680	60	35	180	31	Reverse	218	71	81	14	348	12

these channels. Alluvial fans that develop in the region also cover large areas. However, the slope debris and landslides in the Quaternary units, which are caused by not having sufficient strength of the older rocks, are also important. All of these Quaternary units are transitional with each other (Figure 2).

3. Structural Geology and Tectonics of the Beypazarı Çayırhan Basin

Geological mapping were done between the Çayırhan in the south, Sekli in the north, Çayırhan Bridge in the west, and Hırka in the east (Figure 3). Most of the thrust/blind thrust structures observed in the region are located just in the north of Çayırhan. The high angle limbs of asymmetrical anticlines were used following the criteria revealed by Seyitoğlu (2017*a, b*) when mapping the blind thrusts on to the geological map detected during field studies. During this, the indicators mentioned about blind thrusts and fault propagation folds and theoretical background were used. The structures identified as a result of field studies will be explained in a sequence from north to south.

3.1. Karaköy Blind Thrust

This structure, shown by Yağmurlu et al. (1988), Helvacı (2010) and Helvacı et al. (2014) as normal fault dipping southwest were mapped by Kavuşan (1993*b*) as thrust planes dipping northwest. The limestone layers belonging to the Akpınar formation inside the Aldere valley and near the Arılkaya location in the west of Karaköy acquire high dipping and thus the thrust line is encountered. This line carried conglomerate and volcaniclastics of the Kızılçay group to the same level with the units of the Akpınar formation elevating them in the axis of an asymmetrical anticline (Figure 3). The deformation on layers caused by the thrust line is clearly observed on Google Earth images and they were marked as blind thrust in front of the steeply dipping southern limb of the asymmetric anticline. The deformation caused by the thrust can no longer be traced to the west of Karaköy under the Hırka formation and younger formations (Figures 4a and b). According to field observations, it can be said that the Karaköy Blind Thrust were developed after the Akpınar formation, which is the youngest unit affected by deformation.

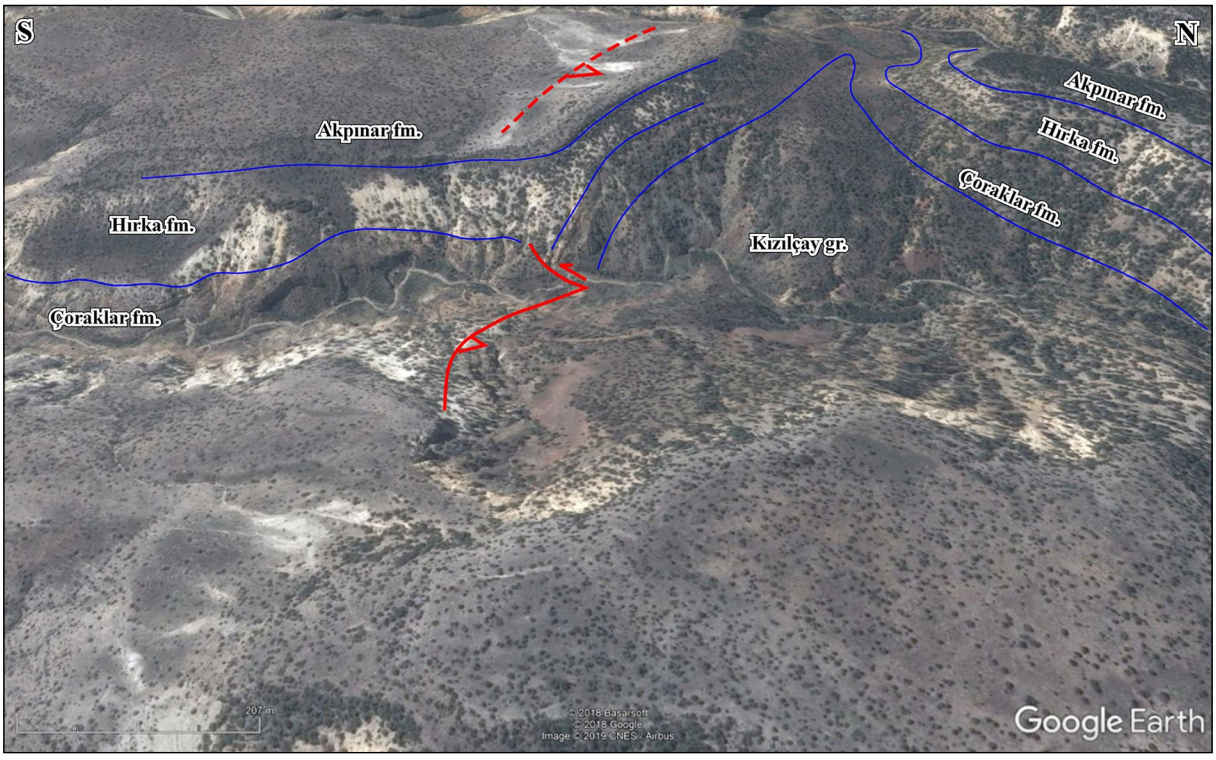

Figure 4- a) Karaköy Blind Thrust and south verging asymmetric anticline in the hanging wall. The boundaries of the units are marked on the inclined Google Earth image.

Figure 4- b) Field view of the steeply dipping southern limb of the asymmetric anticline used to determine the location of the Karaköy Blind Thrust. Note that the dipping of the units gradually decreases upwards.

3.2. Sekli Blind Thrust

The Sekli thrust has been noticed and mapped in almost all previous studies (Yağmurlu et al., 1988; Kavuşan, 1993*b*). To the north of Sekli village, the gray metamorphic rocks clearly thrusted on maroon-colored Kızılçay group sedimentary units (Figures 3 and 5a). The thrust zone was subjected to extensive shearing (Figure 5b). The Sekli thrust disappears under the Quaternary alluvium in east-northeast direction and continues in the west-southwest direction as blind thrust and back thrust. This feature was most clearly observed on the southwestern slopes of the Kocakızılbayır Hill (Figure 5c). It is observed that an asymmetric anticline is formed on the up thrown block of the fault affecting the Kızılçay group and the fault does not reach the surface (fault-propagation fold) (Figure 5c). The Sekli thrust, which is observed as a high angle reverse fault on the Uluköy - Karaköy road, is clearly observed on the Kızılmescit ridge on the western edge of the Aladağ stream. Here, it has deformed the Kızılçay group by thrusting with Çoraklar formation which unconformably overlies the metamorphic basement (Figure 5d). To the west of Aldere, it is clearly observed that the up thrown block of this thrust rises along the Çoraklar formation above the metamorphic basement (Figure 5e). Although the Sekli Blind Thrust is observed on the surface in some sections due to abrasion, it is a blind thrust as it is observed on the Kocakızılbayır Hill, and according to the field observations it can be said that it was developed at least after the Çoraklar formation.

3.3. Nalçabayırı Blind Thrust

This thrust has not been identified in previous studies (Figure 3). Only, Şahin et al. (2019) showed the presence of an asymmetric fold in Nalçabayır Hill. Looking from the east of Nalçabayır Hill to the west, the presence of the asymmetric anticline is clearly observed. As a coal quarry is active in this area, it is understood that the Hırka formation overlies

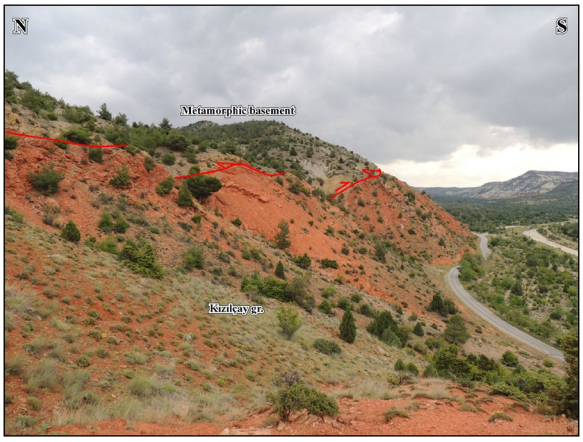

Figure 5- a) Field view of the Sekli Blind Thrust observed on the abraded surface. The north of Sekli village.

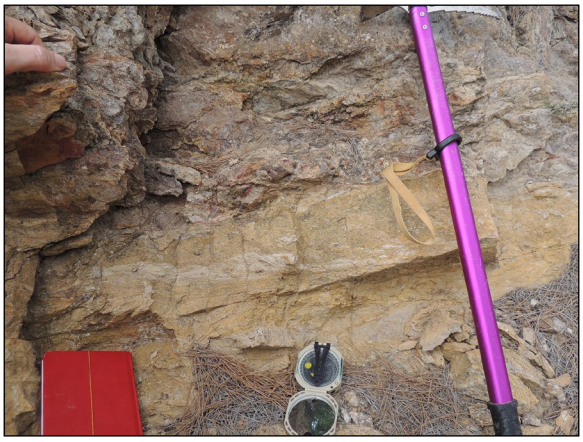

Figure 5- b) Intense shear zone belonging to the Sekli Blind Thrust. Looking north.

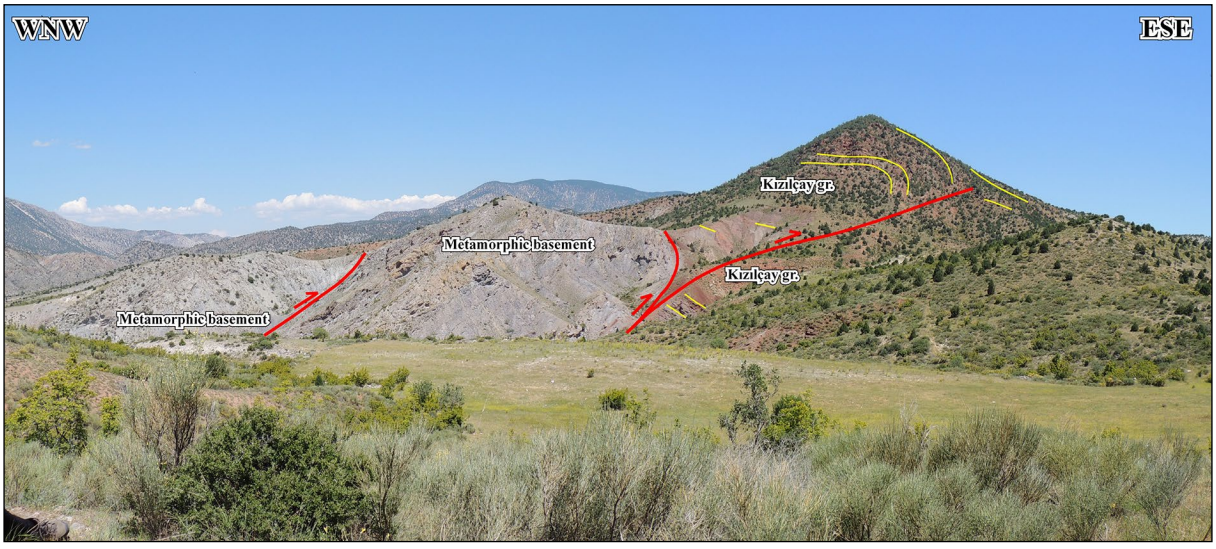

Figure 5- c) Field view of the Sekli Blind Thrust on the Kocakızılbayır Hill.

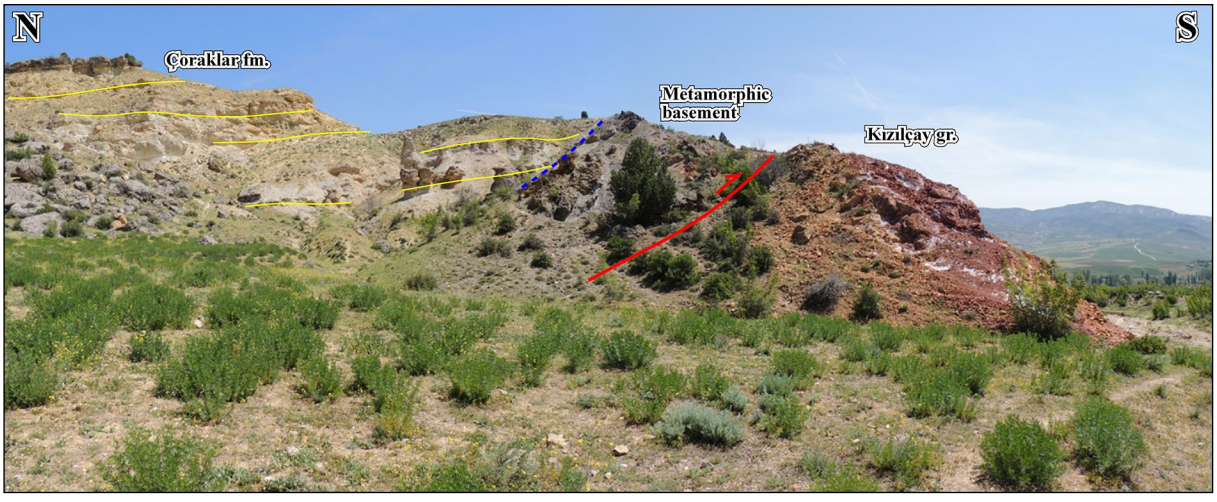

Figure 5- d) The tectonic contact between metamorphic basement together with overlying Çoraklar fm. and the Kızılçay group on the Kızılmescit ridge where the Sekli Blind Thrust can be observed on the surface.

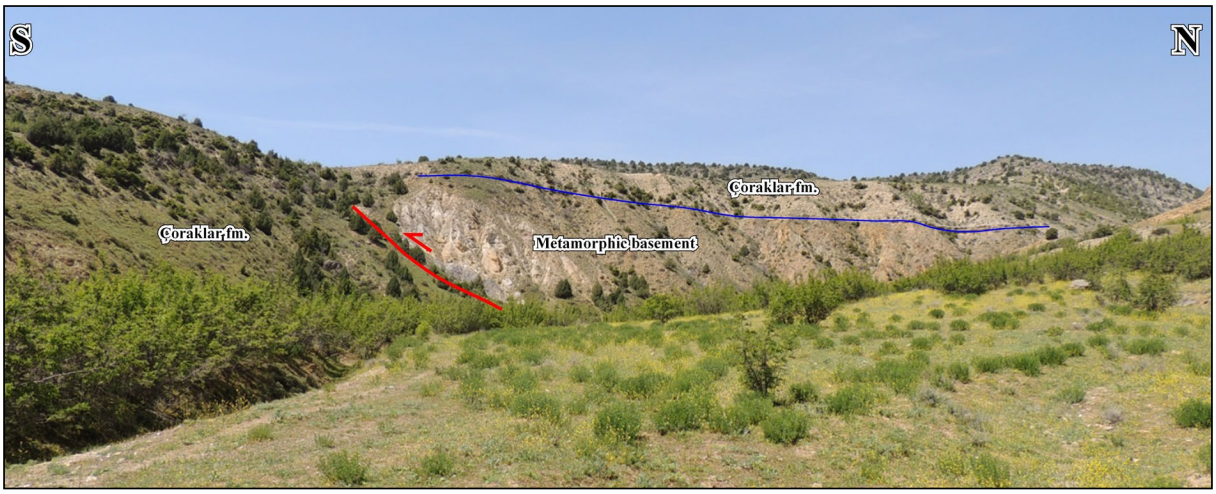

Figure 5- e) Sekli Blind Thrust in west of Aldere has brought the metamorphic basement over Çoraklar fm. To the west of this location, the thrust plane disappears under younger units.

the Çoraklar formation. The blind thrust can be hypothetically drawn just in front of the high angle southern limb of the asymmetric anticline (Figure 6a). The axis of the Nalçabayırı anticline is a structure plunging southwest. The asymmetric anticline also diminishes increasingly, as the movement on the blind thrust plane is most probably reduced laterally. It is possible to see the synthetic thrust planes and back thrust planes with hypothetical blind thrusts in the valley opening perpendicular to the axis in the area where the Nalçabayır anticline disappears (Figure 6b). They generally form a triangular zone (Figure 6c). The general position of the Nalçabayır asymmetrical anticline and the probable blind thrust were marked on the eastern slope of the valley opening perpendicular to the fold axis (Figure 6d). It is possible to say that the Nalçabayırı Blind Thrust was developed after the Akpınar formation.

3.4. Uzunbayır Blind Thrust

The north dipping Uzunbayır blind thrust passes through the Kaya Burnu locality to the southwest of the Akçabayır village and to the south of Aşıkkaya strait, and it extends to the north of the Uyku Çiftlik following the south of Uzunbayır ridge (Figure 3). In this area, the northwest dipping Çömlek Tepe normal Fault was defined by Yağmurlu et al. (1988) in previous studies. However, the Çoraklar formation overlies the Kızılçay group with an angular unconformity along the stated fault boundary, especially at the Çömlek Hill locality. On the other hand, when looking at the drainage lines on the southern and northern slopes of the Uzunbayır ridge, it is observed that the northward drainages are long and southward drainages are short. This shows that the Uzunbayır ridge is in fact an asymmetric fold. Its field evidence is located about 1.5 km northeast of

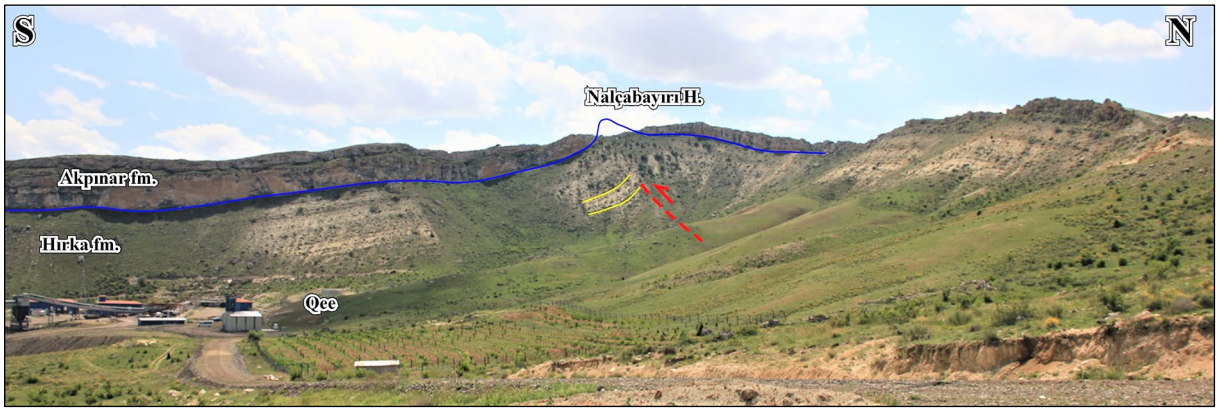

Figure 6- a) West plunging asymmetric anticline on the Nalçabayırı Tepe and the probable location of the Nalçabayırı Blind Thrust.

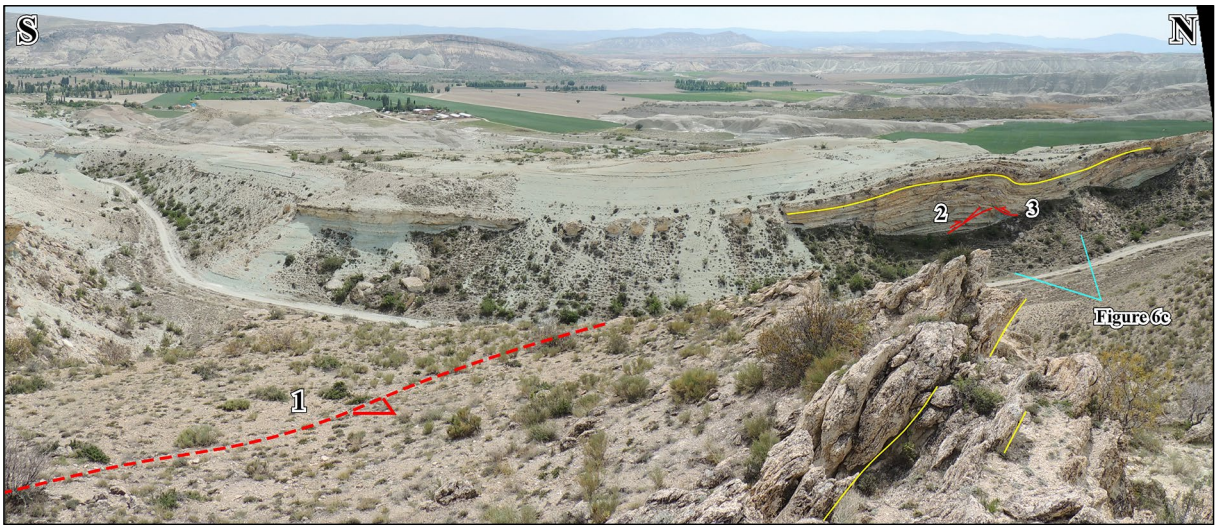

Figure 6- b) Triangle zone among (1) The Nalçabayırı Blind Thrust, (2) Back Thrust and (3) Synthetic Thrust. The position of the Nalçabayırı Blind Thrust was drawn in front of the steeply dipping limb of the asymmetric anticline.

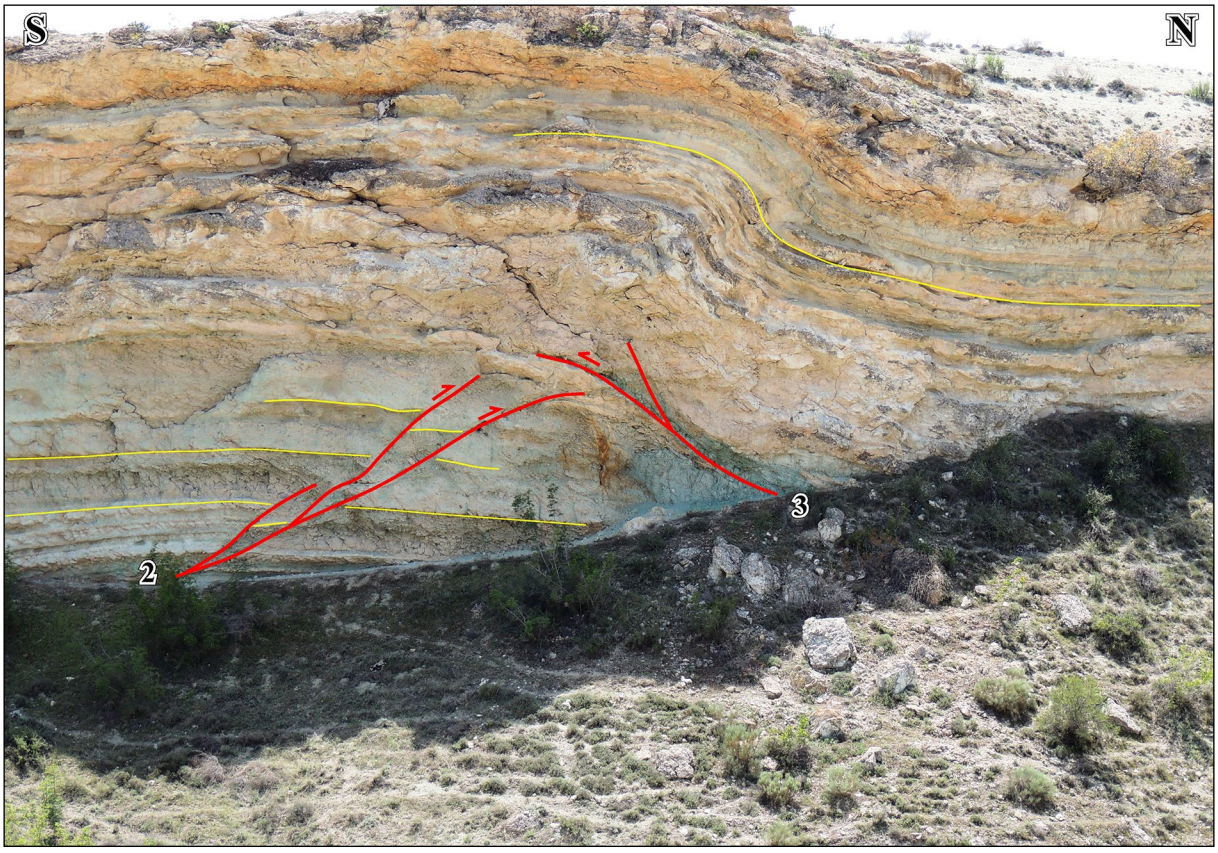

Figure 6- c) Close up view of; (2) the back thrust plane and (3) the synthetic thrust plane of the Nalçabayırı Blind Thrust.

the Davutoğlan in the Aşıkkaya strait opened by the Aladağ stream. The dipping increasing towards south can be easily observed in the layers (Figure 7a). The fault is named in this study as the Uzunbayır Blind Thrust, due to the name of the ridge.

Field observations related to the presence of Uzunbayır Blind Thrust are located at western and eastern ends of this fault in the study area. The shear zone observed in the west after passing the Çayırhan Bridge, 250 meters northwest in the direction of

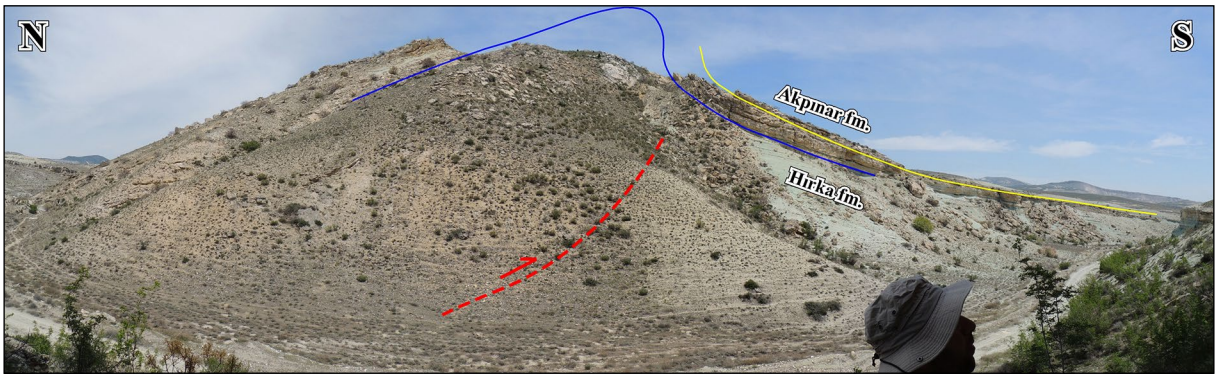

Figure 6- d) The probable position of the asymmetrical anticline and Nalçabayırı Blind Thrust on the Nalçabayırı Hill. This panoramic view shows the opposite slope of the figure 6c.

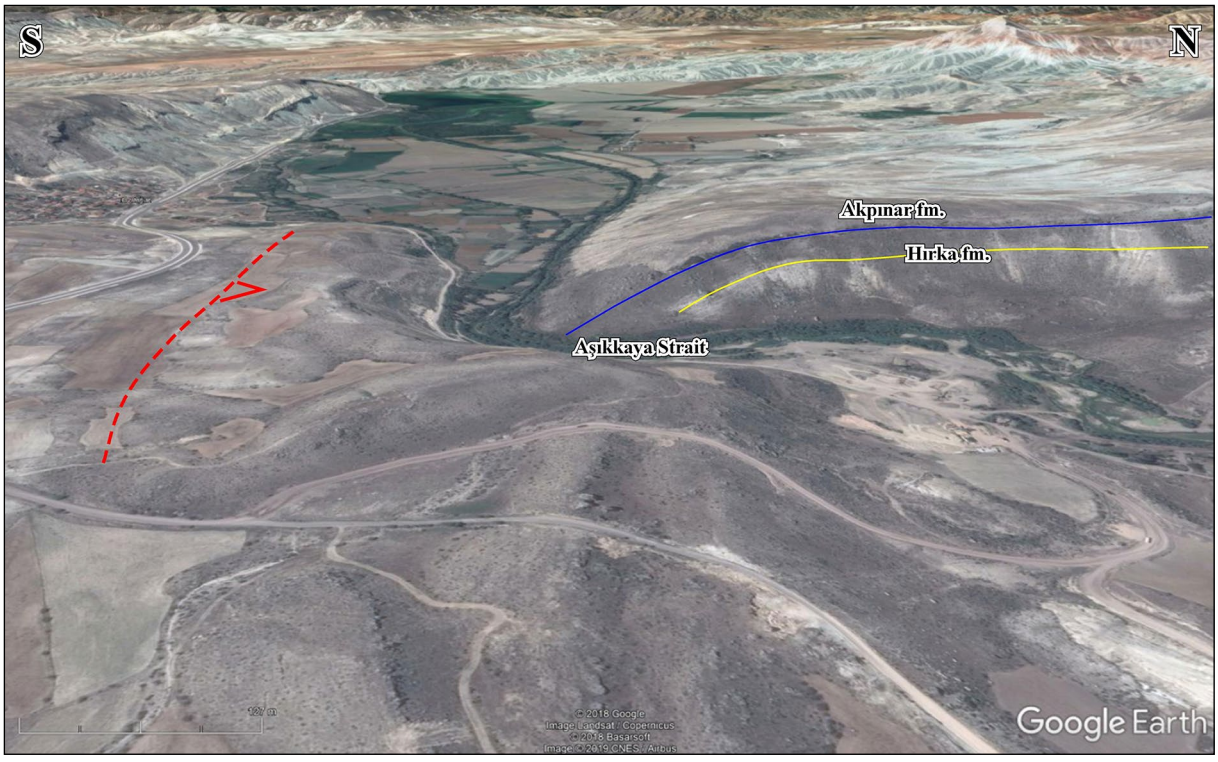

Figure 7- a) Inclined Google Earth image of the asymmetric anticline formed by the layers of the Akpınar and Hırka formations in the Aşıkkaya strait. The probable position of the Uzunbayır Blind Thrust in front of the 30° dipping limb is indicated by a dashed red line. The thrust planes can be traced on the surface at eastern and western edges of the study area. See figures 7b and c.

Nallıhan, belongs to the Uzunbayır Blind Thrust (Figure 7b).

It is interpreted that the Uzunbayır Blind Thrust and the Davutoğlan Back Thrust connect between the Kabalındoruk Tepe and Susuzdoruğu Tepe, which is located about 5 km northeast of Çayırhan and that the Uzunbayır Blind Thrust continues eastward towards the Bağözü (Figure 3). The observation point in east of the Uzunbayır Blind Thrust is in the valley opened by the Uyku Çiftlik creek, at 500 meters north of the Uyku Çiftlik, which is approximately 7 km northwest of Kuzkaya Hill (Figure 7c). In this position, which can be easily viewed on satellite images, the Uzunbayır Blind Thrust is observed on the surface, and the Çoraklar formation is placed over the younger Akpınar formation and disappears between the layers of the Akpınar formation (Figure 7d).

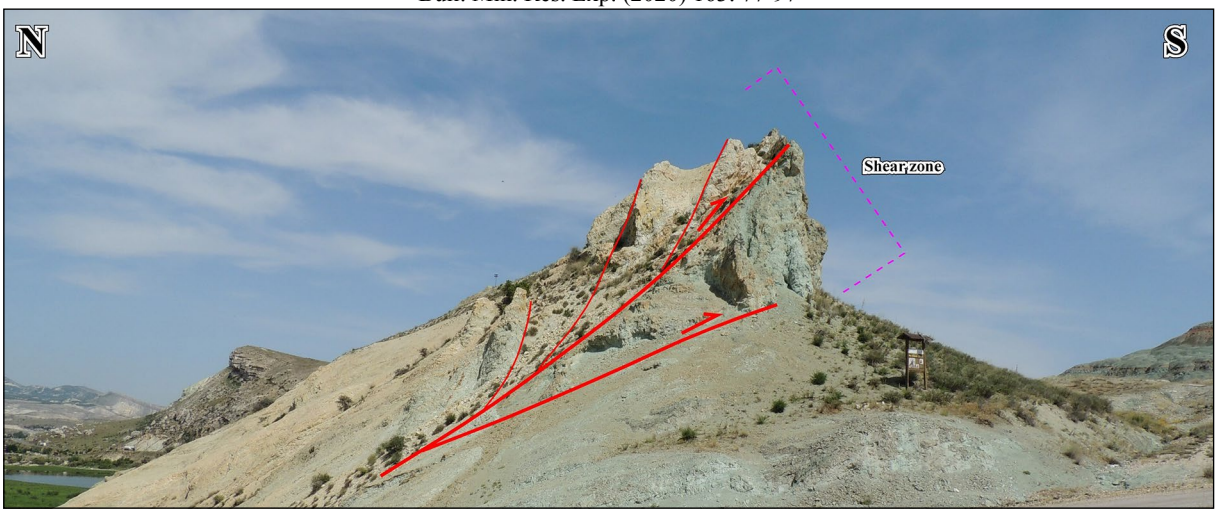

Figure 7- b) North dipping shear zone which can be traced on the surface as a continuation of the Uzunbayır Blind Thrust in the west of the study area. The west of the Çayırhan Bridge.

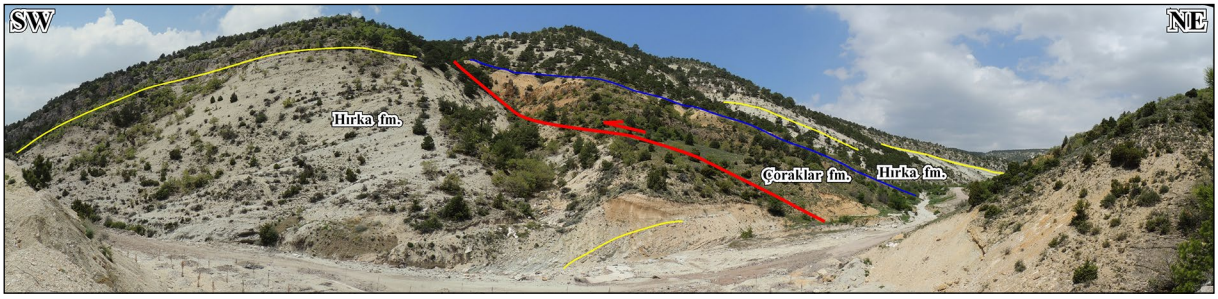

Figure 7-c) Panoramic view of the surface track of the Uzunbayır Blind Thrust in the Uyku Çiftlik creek in east of the study area. The Çoraklar fm. has been thrusted on the Hırka fm.

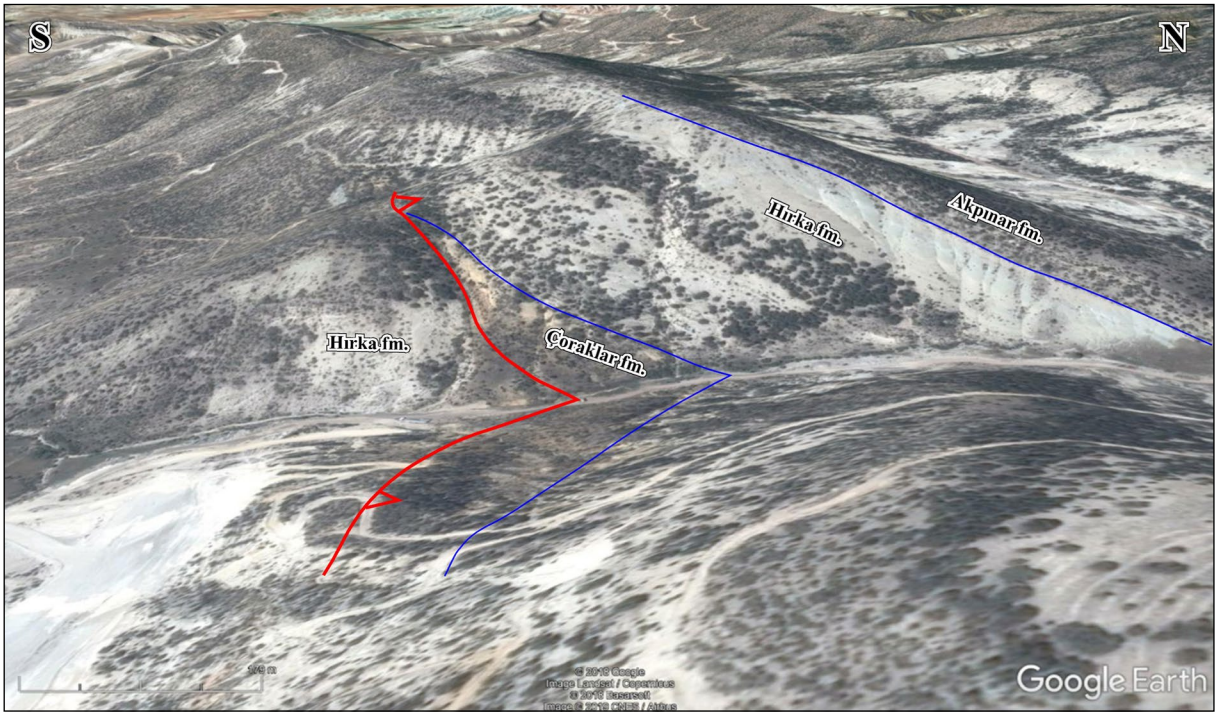

Figure 7-d) Inclined Google Earth image of the Uzunbayır Blind Thrust on the surface of the Uyku Çiftlik creek in the east of the study area.

3.5. Davutoğlan Back Thrust

It was named as the Davutoğlan Fault by previous investigators and defined as the northwest dipping normal fault by Yağmurlu et al. (1988) and Helvacı (2010), as northwest dipping reverse fault by Kavuşan (1993*b*) and as south dipping thrust fault by Şahin et al. (2019).

Helvacı (2010) starts the Davutoğlan Fault from the northwest of Beypazarı (near Zaviye) in the geological map and advances it towards west in reverse fault character. However, it is cut by the strike-slip fault near the Uyku Çiftlik, which is approximately 8 km northwest of Çayırhan, and continues from this point to the west as a normal fault character. On the other hand, Kavuşan (1993*b*) drew it as continuous, north dipping reverse fault. Lisenbee et al. (2010) defines the Davutoğlan Fault as a right-lateral strike-slip fault and explains folding around it by strike-slip faulting. According to this study, the fault passes to an anticline in the east and the offset becomes zero in the west. The recent study was carried out in the region by Şahin et al. (2019). They stated that the Davutoğlan Fault had gained the character of blind thrust in western end and dipped southward.

Our detailed field observations on the Davutoğlan Fault, which were evaluated in different ways in terms of both the fault character and the dip direction of the fault plane, are listed below.

The asymmetric anticline observed at the Kuzkaya Hill (Figure 3), approximately 2.5 km northeast of Çayırhan, indicates the presence of a south dipping blind thrust (Figure 8a). The kinematic indicators on the fault plane of the south dipping thrust are clearly observed in the road cut on the hill at 1 km east of the Davutoğlan Village (Figure 8b). Here, both the south dipping thrust plane and northward movement of the thrust were precisely determined by the position of the drag folds, and contrary to the southward thrusts dominantly observed in the region, it was named as the Davutoğlan Back Thrust (Figure 8b).

The northern slope of the Domuzkayası Hill located to the west of the Davutoğlan Village is another key location where all structural elements of the Davutoğlan Thrust are observed (Figure 8c). The Davutoğlan Back Thrust consists of the southern and northern branches. The southern branch is characterized by a well-developed ramp anticline, where the underlying Akpınar formation is uplifted and thrusted over the Bozbelen formation (Figure 8c). The northward movement on the southern branch of the Davutoğlan Thrust was clearly determined by the position of drag folds on the up thrown and down thrown blocks of the fault (Figure 8d). The northern branch of the Davutoğlan Thrust shows intense shearing, and the south dipping geometry of the shear plane is remarkable when looked at a closer distance (Figure 8e). The shear zone, which is more resistant to abrasion than its surroundings, forms an immediately noticeable elevation like a wall to the south of the Çayırhan - Nallıhan road (Figure 8f).

The northern branch of the Davutoğlan Back Thrust is also clearly observed between the Domuzkayası Hill and Davutoğlan village as a shear plane dipping

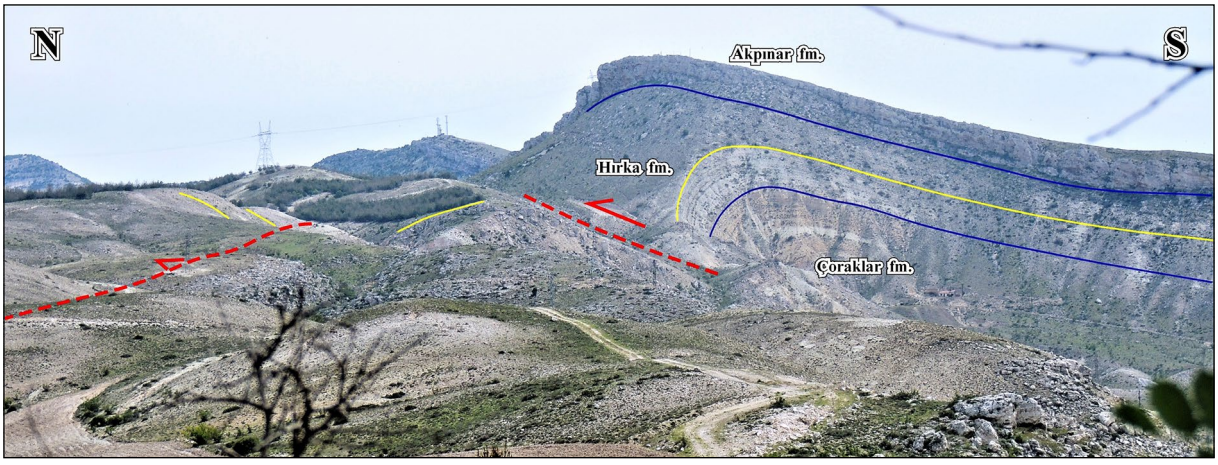

Figure 8- a) The location of the north verging asymmetric anticline on the Kuzkaya Hill and associated Davutoğlan Back Thrust. In the north, the traces of the Uzunbayır Blind Thrust on the surface are shown.

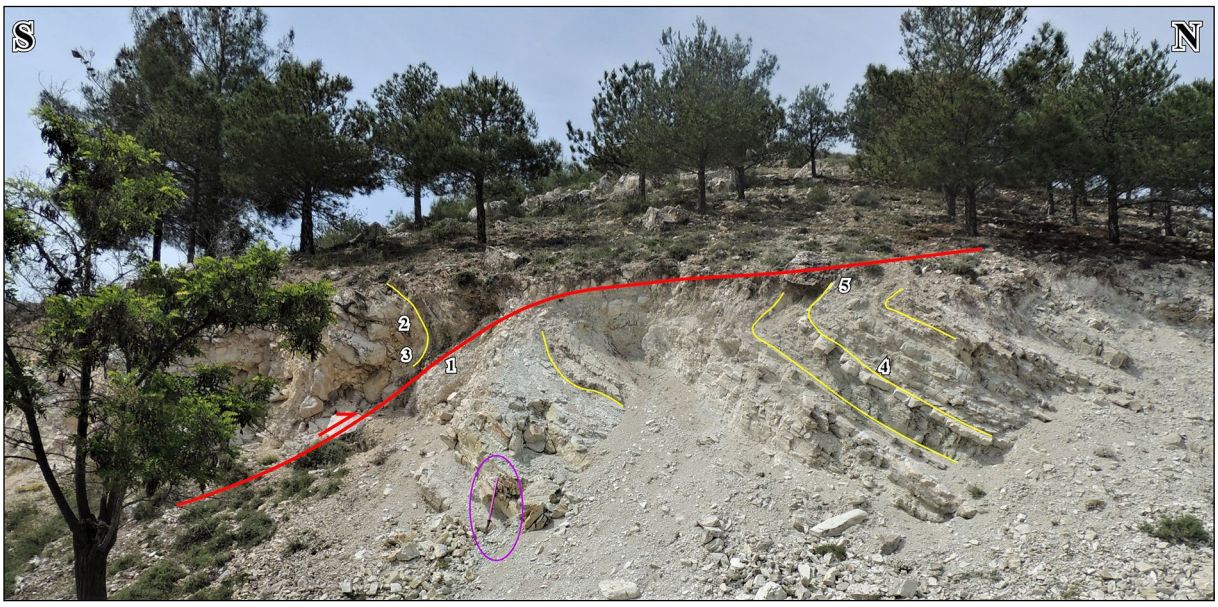

Figure 8-b) The Davutoğlan Back Thrust. The hanging wall has moved northward as drag folds show. The horizontal fold axis has E-W direction. (1) Fault plane: N 60 E, 35 SE; (2) Bedding: N 65 E, 65 NW; (3) Overturned bedding: N 30 E, 65 SE; (4) Bedding: E-W, 40N; (5) Overturned bedding: E-W, 55S.

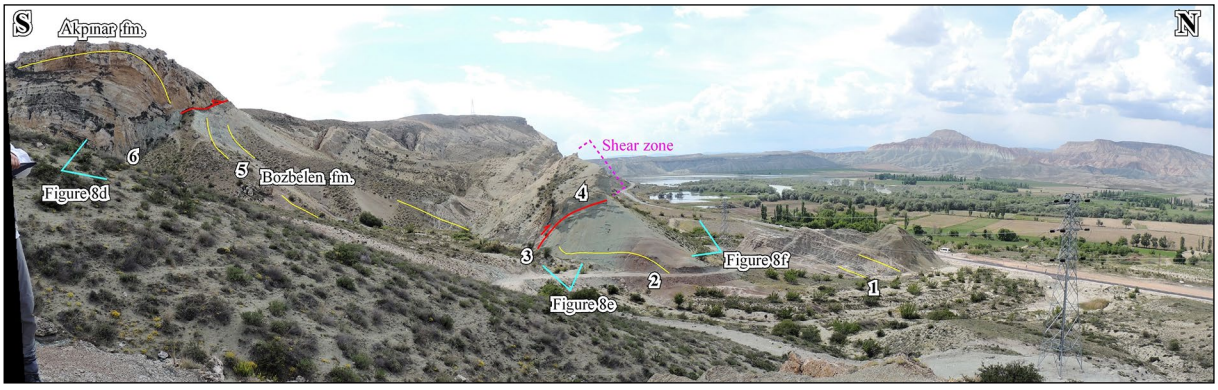

Figure 8- c) Panoramic photograph showing the position of the northern and southern branches of the Davutoğlan Back Thrust. The Akpınar fm. forming the north verging asymmetrical anticline on the up thrown block of the southern branch has been thrusted on the Bozbelen fm. The northern branch cuts the Bozbelen fm. (1) Bedding: N70E, 18NW; (2) Bedding: N60E, 30NW; (3) The fault plane of the northern branch: N70E, 55SE; (4) The location where the structural data is collected; (5) Bedding: N18E 55NW; (6) Bedding: N35E, 67NW.

south (Figure 3). Here, the asymmetric anticline created by the southern branch is clearly cut (Figure 8g). This relationship shows that the southern branch of the Davutoğlan Thrust was developed earlier than the northern branch and that an in-sequence thrust had taken place.

3.6. Beypazarı Blind Thrust

In previous studies, there has not been mentioned about main thrust passing through the south of Çayırhan except Seyitoğlu et al. (2017*a*), but the asymmetric fold axis has been shown in published geological maps (Yağmurlu et al., 1988; Kavuşan, 1993*b*; Helvacı, 2010; Şahin et al., 2019). Therefore, the structural relationship between the Beypazarı Blind Thrust and Davutoğlan Back Thrust has not been solved so far.

The criterion used for mapping of blind thrusts in the Southeastern Anatolia in Seyitoğlu et al. (2017*b*) was also applied to the Beypazarı blind thrust

Figure 8- d) Close-up view of the southern branch of the Davutoğlan Back Thrust. The northward movement of the fault is clearly observed from drag folds of up thrown and down thrown blocks. The photo was taken from the location (6) in figure 8c.

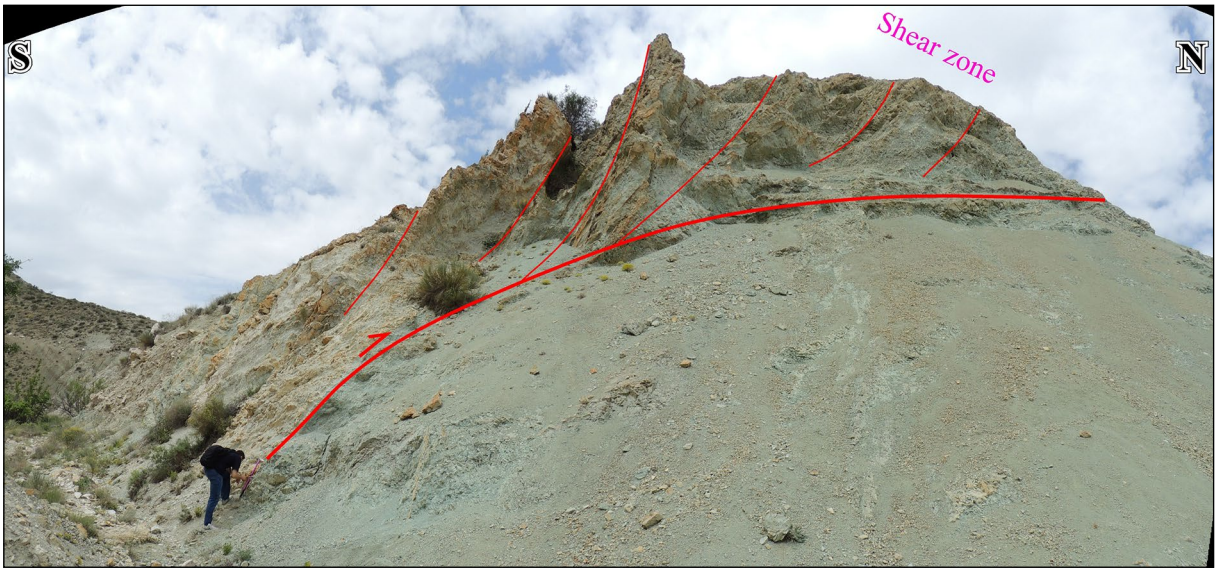

Figure 8- e) Close-up panoramic view of the northern branch of the Davutoğlan Back Thrust. The majority of the structural data of the fault was obtained from this location. The photo was taken from the location (3) in figure 8c.

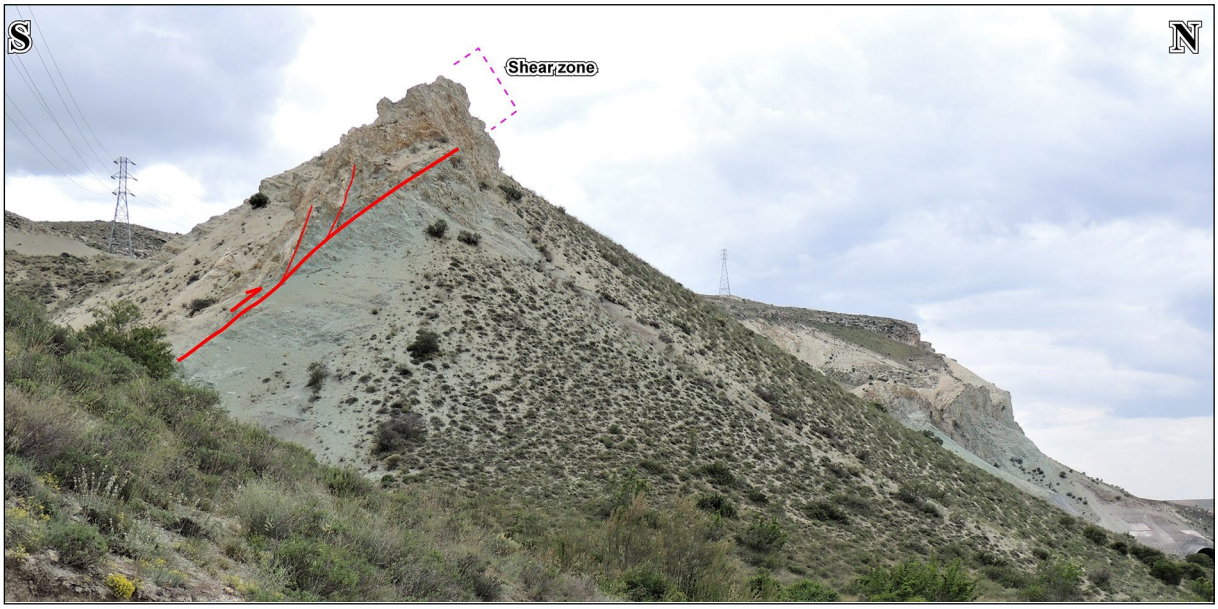

Figure 8- f) General view of the wall-like shear zone formed by the northern branch of the Davutoğlan Back Thrust in the Kuş Cenneti natural reserve area, south of the Çayırhan-Nallıhan highway.

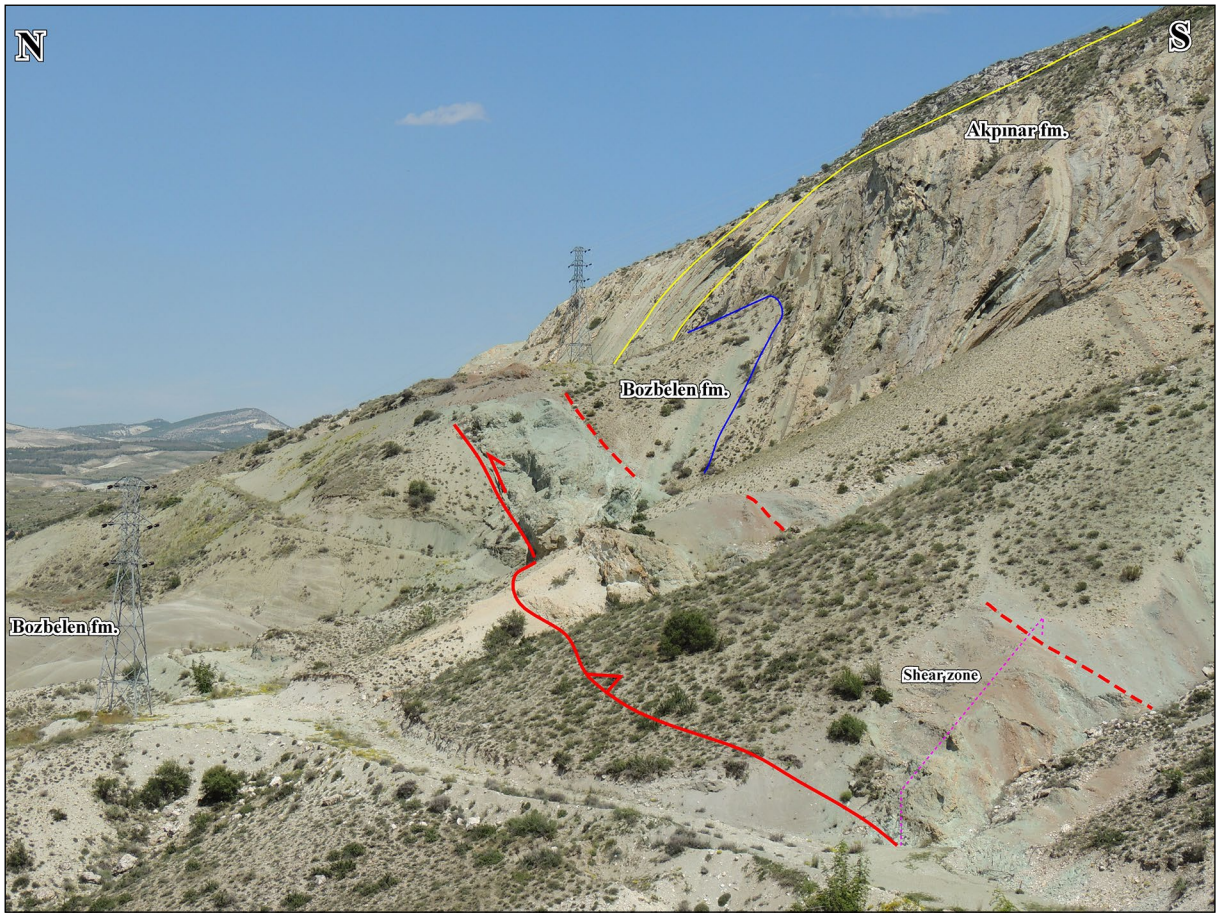

Figure 8- g) In the west of Davutoğlan village, photo showing the highly dipping limb of the asymmetric anticline formed by the southern branch of the Davutoğlan Back Thrust is cut by the northern branch. According to this observation, the Davutoğlan Back Thrust was evaluated as an in-sequence thrust.

(Seyitoğlu, 2017*a*) and a blind thrust line was drawn in front of the steeply dipping limb of the asymmetric anticline. Using the same criterion, it is observed that the Beypazarı blind thrust is divided into two branches when its continuity is observed by means of Google Earth images in the vicinity of Çayırhan to the southwest. The southernmost branch, Beypazarı Blind Thrust-I reaches Beypazarı passing from the south of 35° southeast dipping layers on the hills of Akkaya, Tahtalı and Öğlekayası. The northern branch, the Beypazarı Blind Thrust-II, on the other hand merges with the southern branch from Çayırhan following the northern coast of the Sarıyar Dam Lake.

The relationships of the faults and folds described above are shown on two geological cross-sections prepared from the geological map of the study area (Figure 3) (Figure 9a, b).

When all these observations are combined, it can be easily understood that the structures observed in the region between the Çayırhan-Davutoğlan and Sekli villages are the fault propagation folds of blind thrust systems.

4. Assessment of Structural Data

The fault plane and fault striation data collected from the field are shown on the map using the equal area lower hemisphere stereographic projection (Figure 3) and given as a table (Table 1). The FaultKin (Marrett and Allmendinger, 1990; Allmendinger et al., 2012) software was used for the kinematic analysis of fault data. Thus, the locations of the kinematic axes and the contraction and extension directions in relation to the faults were determined (Figure 3). Then, the fault plane solutions were generated utilizing the same software (Figure 10) and their compatibility with the structures in the field was evaluated in general.

The structural data obtained from thrust/reverse fault planes in the Kızılçay group, which are very close to the surface sections of the Sekli Blind Thrust and the data acquired from tear faults were shown on the stereonet plots 1, 2 and 3 in Figure 3. The combined assessment of these data shows that the Sekli Blind Thrust is NW dipping thrust with left lateral component which compensates NNW-SSE directing contraction (Figure 10a).

Striations obtained from the synthetic fault planes of the Nalçabayırı Blind Thrust (Figure 3; stereonet no: 4) show that NW-SE directing contraction is compensated by this fault (Figure 10b).

When data obtained from the location, which is considered as the section observed on the surface of the Uzunbayır Blind Thrust (Figure 3, stereonet no: 5)

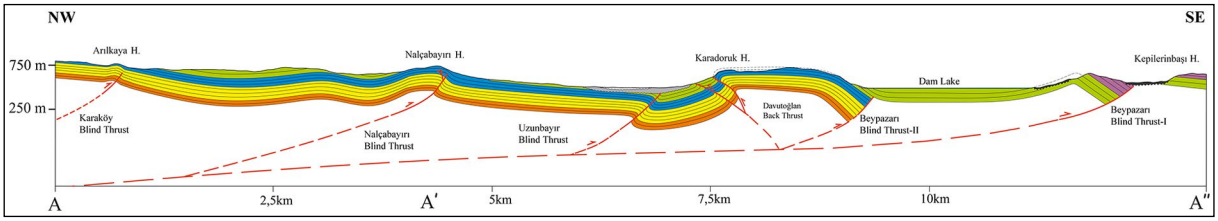

Figure 9- a) Geological cross section passing from the west of the study area that shows the internal structure of the Beypazarı Blind Thrust Zone. See figure 3 for location.

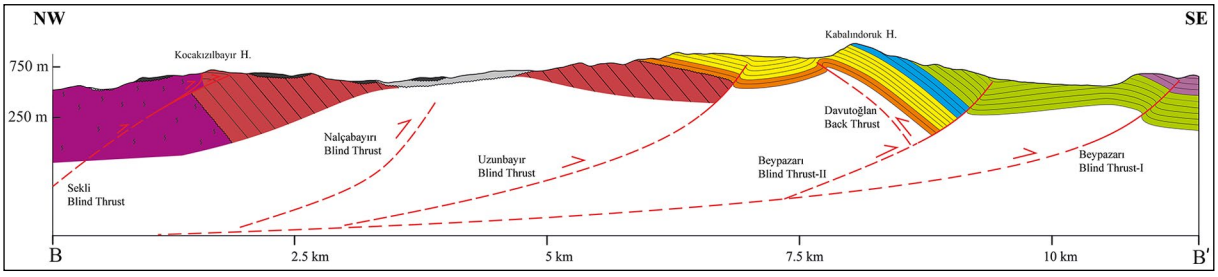

Figure 9- b) Geological cross section passing from the east of the study area that shows the internal structure of the Beypazarı Blind Thrust Zone. See figure 3 for location.

is assessed together, it shows that the Uzunbayır Blind Thrust, NW dipping thrust with left lateral component corresponds to the NW-SE contraction (Figure 10c).

The Davutoğlan Back Thrust is the structure in which the most kinematic data were collected in the study area (Figure 3; stereonet no: 6, 7, 8, 9, 10 and 11), and the combined assessment of the structural data shows that it is the thrust that has SW dipping, right lateral component meeting the NW-SE contraction (Figure 10d).

The overall evaluation of all data reveals the presence of a NW-SE-directed contraction in the region, such as individual thrusts (Figures 3 and 10 e), and this result is highly consistent with the overall assessment of data obtained from the focal mechanism solutions (Seyitoğlu et al., 2017*a*) (Figure 10f).

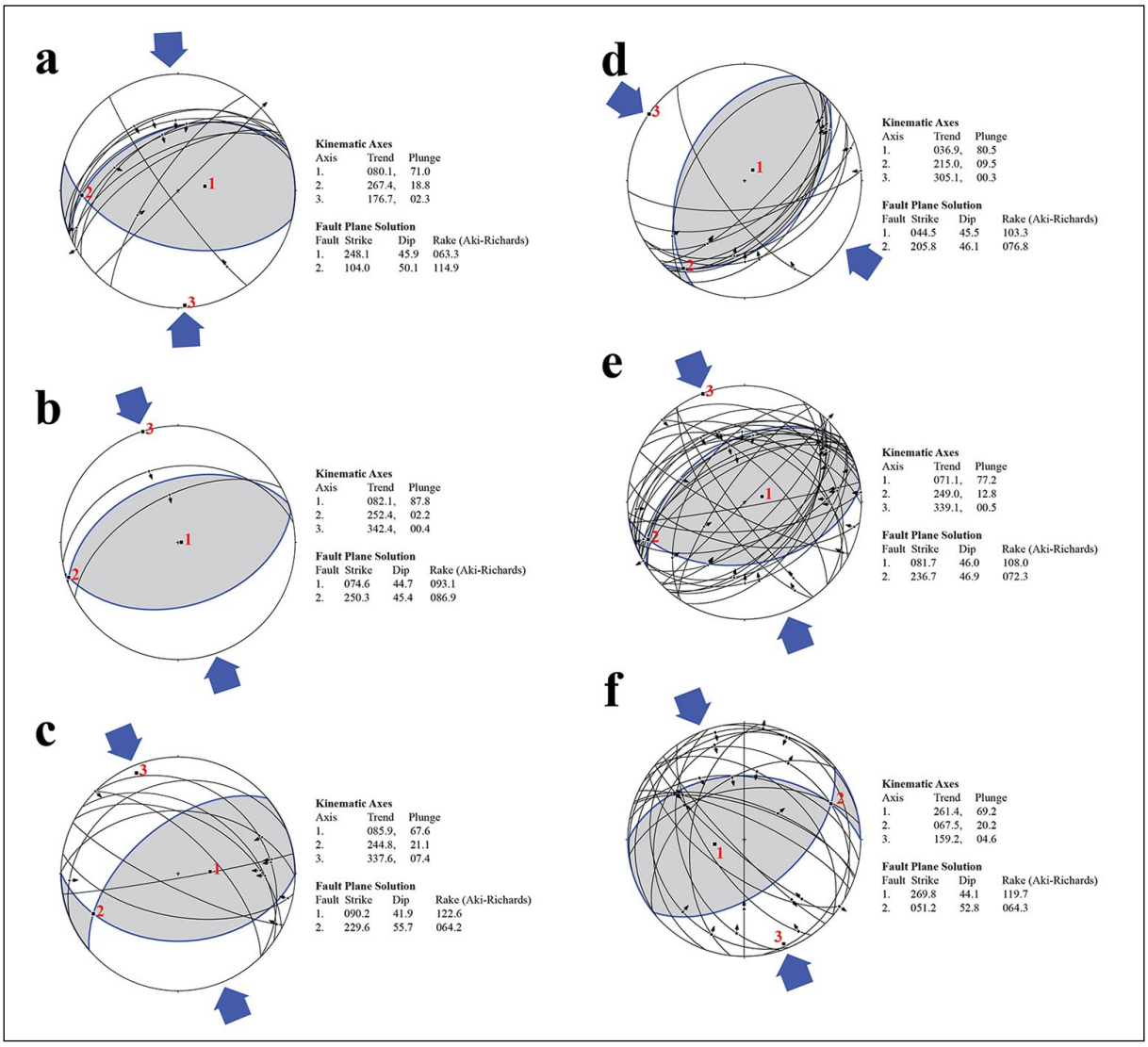

Figure 10- The analysis of kinematic data obtained from the faults in the study area. The gray area and the associated fault planes indicated by blue represent the fault plane solution. Accordingly, the blue arrows indicate the direction of contraction. This analysis was performed by FaultKin (Marrett and Allmendinger, 1990; Allmendinger et al., 2012) software. a) Fault planes of the Sekli Blind Thrust (Figure 3; measurements at locations 1, 2 and 3), b) Fault planes of the Nalçabayırı Blind Thrust (Figure 3; measurements at location 4), c) Fault planes of the Uzunbayır Blind Thrust (Figure 3; measurements at location 5), d) Fault planes of the Davutoğlan Back Thrust (Figure 3; measurements at locations 6, 7, 8, 9, 10 and 11), e) All fault planes measured in the region. See table 1 for kinematic data, f) The kinematic analysis of the fault data obtained from the focal mechanism solutions in the eastern part of the Beypazarı Blind Thrust Zone (Seyitoğlu et al., 2017*a*).

5. Discussion

In a recent study carried out in east-northeast of the study area (Seyitoğlu et al., 2017*a*), the Beypazarı Blind Thrust Zone has been defined and shown that this thrust has been formed by Başören and Kilci blind thrusts and the Erenler Back Thrust which can be traced on the surface. In this study, which was performed in the Çayırhan northern continuity of the Beypazarı Blind Thrust Zone, both the presence of blind thrusts from the outcrops in deep incised valleys and the sections that can be observed on the surface due to the erosion were proved. Besides, the structural data showing the movement directions of the faults were collected (presence of striations and drag folds). With the help of these data, the systematic relationships of the faults interpreted by different researchers in different ways in the study area were revealed and evaluated. Accordingly, the Beypazarı Blind Thrust Zone around Çayırhan consists of blind thrusts and back thrusts observed over a wide area. To order them from north to south, the Karaköy Blind Thrust was only noticed by the presence of the asymmetric anticline with a vergence to the south (Figure 4a, b). The Sekli Blind Thrust has been identified in previous studies and is clearly observed on the abraded surface (Siyako, 1983; Yağmurlu et al., 1988; Kavuşan, 1993*b*; Helvacı, 2010). However, the presence of fault propagation folds observed on the Kocakızılbayır Tepe in this study (Figure 5c) shows that this fault developed as a blind thrust. The Nalçabayırı Blind Thrust was also determined by the development of the asymmetric anticline and it was clearly observed that the back thrust and synthetic thrust planes formed a triangular zone (Figures 6b, c). The Uzunbayır Blind thrust was noticed by an asymmetric anticline in Aşıkkaya Boğazı and its presence was proved by the abrasion zone observed on the surface (Figure 7b) in the west and the thrust plane (Figure 7c) in the deep excavated valley in the east. The Davutoğlan Fault, which was the most emphasized by the previous studies in the study area and made different interpretations, was considered to be the Davutoğlan Back Thrust. When folding and faulting relations and structural data collected from the fault zone were evaluated together, it was understood that the character of the fault was thrust. However, it is also possible that this zone of weakness is used by a strike-slip fault. However, as Lisenbee et al. (2010) pointed out in their study that the Davutoğlan Fault disappeared within a relatively short distance for strike-slip faults on the surface. As a result, unlike all the thrusts in the region, the structure called the Davutoğlan Back Thrust, is south dipping and created north verging asymmetric folding (Figure 8c). It is considered that the Beypazarı Blind Thrust, the end most member of the Beypazarı Blind Thrust Zone, was developed as two separate branches (I and II) in the study area and that all the thrusts in deep were connected to a single shear zone (Figures 9a, b).

6. Results

The Beypazarı Blind Thrust Zone consists of Karaköy, Sekli, Nalçabayırı, Uzunbayır blind thrusts and the Davutoğlan Back Thrust and Beypazarı Blind Thrust I-II faults around Çayırhan. All of the asymmetric anticlines developed with blind thrusts show vergence to the south, except for those associated with the Davutoğlan Back Thrust. An anticline called the Çayırhan dome (Kavuşan, 1993*b*) in the literature developed between the Davutoğlan Back Thrust and Beypazarı Blind Thrust-II. The Beypazarı Blind Thrust Zone is seismically active and it is one of the neotectonic structures developed between the North Anatolian Fault Zone, Eskişehir Fault Zone and Kırıkkale-Erbaa Fault Zone (Seyitoğlu et al., 2017*a*).

Acknowledgements

This article is a part of the MSc thesis of the first author who is about to complete it in the Tectonics Research Group of Ankara University. It was benefited from the field support given by the Faculty of Engineering of Ankara University to the "Advanced Geological Mapping" courses. We appreciate a lot for this opportunity. In addition, we would like to thank to Efe Demirci, the member of the Tectonics Research Group, for his contributions during field studies and to referees Prof. Dr. Yaşar Eren and Assoc. Prof. Dr. Volkan Özaksoy for their constructive contributions.

References

Aksoy, C.O., Onargan, T., Yenice, H., Küçük, K., Köse, H. 2006. Determining the stress and convergence at Beypazarı trona field by three-dimensional elastic-plastic finite element analysis: A case study. International Journal of Rock Mechanics and Mining Sciences 43, 166-178.

Allmendinger, R.W., Cardozo, N.C., Fisher, D. 2012. Structural Geology Algorithms: Vectors and Tensors. Cambridge University Press, 289 p.

Apaydın, A. 2010. Relation of tectonic structure to groundwater flow in the Beypazarı region, NW Anatolia, Turkey. Hydrogeology Journal 18, 1343- 1356.

Bechtel, A., Karayiğit, A.İ., Sachsenhofer, R.F., İnaner, H., Christanis, K., Gratzer, R. 2014. Spatial and temporal variability in vegetation and coal facies as reflected by organic petrological and geochemical data in the Middle Miocene Çayırhan coal field (Turkey). International Journal of Coal Geology 134/135, 46-60.

Demirci, C.Y. 2000. Structural Analysis in Beypazarı-Ayaş-Kazan-Peçenek Area, NW of Ankara (Turkey). Doktora Tezi, Orta Doğu Teknik Üniversitesi Fen Bilimleri Enstitüsü, 178 s, Ankara.

Diker, S., Çelik, M., Kadıoğlu, Y.K. 2006. Fingerprints of the formation of geothermal springs on the granitoids: Beypazarı-Ankara, Turkey. Environmental Geology 51, 365-375.

Emre, Ö., Duman, T.Y., Özalp, S., Elmacı, H., Olgun, Ş., Şaroğlu, F. 2013. Türkiye Diri Fay Haritası. Maden Tetkik ve Arama Genel Müdürlüğü, Özel Yayın Serisi 30, Ankara.

Esat, K. 2011. Ankara çevresinde Orta Anadolu'nun neotektoniği ve depremselliği. Doktora Tezi, Ankara Üniversitesi Fen Bilimleri Enstitüsü, 144 s, Ankara.

Esat, K., Seyitoğlu, G. 2010. Neotectonics of North Central Anatolia: A strike-slip induced compressional regime. Tectonic Crossroads: Evolving Orogens of Eurasia-Africa-Arabia, 4-8 October 2010, Ankara, p.38.

Esat, K., Çıvgın, B., Kaypak, B., Işık, V., Ecevitoğlu, B., Seyitoğlu, G. 2014. The 2005-2007 Bala (Ankara, Central Turkey) earthquakes: a case study for strike-slip fault terminations. Geologica Acta 12(1), 71-85.

Esat, K., Kaypak, B., Işık, V., Ecevitoğlu, B., Seyitoğlu, G. 2016. The Ilıca branch of the southeastern Eskişehir Fault Zone: an active right-lateral strike-slip structure in central Anatolia, Turkey. Bulletin of the Mineral Research and Exploration 152, 25-37.

Esat, K., Seyitoğlu, G., Ecevitoğlu, B., Kaypak, B. 2017. Abdüsselam Kıstırılmış Tektonik Kaması: KB Orta Anadolu'da daralma rejimiyle ilişkili bir Geç Senozoyik yapısı. Yerbilimleri 38, 33-56.

Garcia-Veigas, J., Gündoğan, İ., Helvacı, C., Prats, E. 2013. A genetic model for Na-carbonate mineral precipitation in the Miocene Beypazarı trona deposits, Ankara province, Turkey. Sedimentary Geology 294, 315-327.

Helvacı, C. 2010. Geology of the Beypazarı trona field, Ankara, Turkey. Tectonic Crossroads: Evolving Orogens of Eurasia-Africa-Arabia, Ankara, Turkey. Mid-congress field exursions guide book, 1-33.

Helvacı, C., Yılmaz, H., İnci, U. 1981. Beypazarı (Ankara) yöresi Neojen tortullarının kil mineralleri ve bunların dikey ve yanal dağılımı. Jeoloji Mühendisliği Dergisi 32/33, 33-42.

Helvacı, C., Öztürk, Y.Y., Satır, M., Shang, K.C. 2014. U-Pb zircon and KAr geochronology reveal the emplacement and cooling history of the Late Cretaceous Beypazarı granitoid, central Anatolia, Turkey. International Geology Review 56(9), 1138-1155. DOI: 10.1080/00206814.2014.921795

İnci, U. 1991. Miocene alluvial fan-alkaline playa lignitetrona bearing deposits from an inverted basin in Anatolia: sedimentology and tectonic controls on deposition. Sedimentary Geology 71, 73-97.

Kalafatçıoğlu, A., Uysallı, H. 1964. Geology of The Beypazarı - Nallıhan - Seben Region. Bulletin of the Mineral Research and Exploration 62, 1-11.

Karadenizli, L. 1995. Beypazarı havzası (Ankara batısı) üst Miyosen-Pliyosen jipsli serilerinin sedimantolojisi. Türkiye Jeoloji Bülteni 38, 63-74.

Kavuşan, G. 1993*a*. Beypazarı-Çayırhan linyitleri hümik asitlerin IR-Spektrofotometrik incelenmesi. Bulletin of the Mineral Research and Exploration 115, 91-98.

Kavuşan, G. 1993*b*. Beypazarı-Çayırhan kömür havzası linyitlerinin yataklanmasında tektonizmanın önemi. Doğa-Türk Yerbilimleri Dergisi / Turkish Journal of Earth Sciences 2, 135-145.

Kazancı, N. 2012. Kuvaterner birimlerinin haritalanması. Kazancı, N., Gürbüz, A. (Ed.), Kuvaterner Bilimi. Ankara Üniversitesi Yayını 350, 463-470.

Lisenbee, A.L., Uzunlar, N., Terry, M. 2010. The Davutoglan Wrench Fault: Intra-Anatolian Plate, Neogene Deformation, Ankara Province, Turkiye. Tectonic Crossroads: Evolving Orogens of Eurasia-Africa-Arabia, 4-8 October 2010, Ankara, p.38.

Marrett, R., Allmendinger, R.W. 1990. Kinematic analysis of fault-slip data. Journal of Structural Geology 12(8), 973-986.

Orti, F., Gündoğan, İ., Helvacı, C. 2002. Sodium sulphate deposits of Neogene age: the Kirmir Formation, Beypazarı basin, Turkey. Sedimentary Geology 146, 305-333.

Özçelik, O. 2002. Beypazarı (Ankara) kuzeyinde Miyosen yaşlı bitümlü birimlerin organik jeokimyasal özellikleri. Türkiye Jeoloji Bülteni 45, 1-17.

Özçelik, O., Altunsoy, M. 2005. Organic geochemical characteristics of Miocene bituminous units in the Beypazarı basin, central Anatolia, Turkey. The Arabian Journal for Science and Engineering 30, 181-194.

Özgüm, C., Gökmenoğlu, O., Erduran, B. 2003. Ankara, Beypazarı doğal soda (trona) sahası izotop hidrolojisi çalışmaları. Jeoloji Mühendisliği Dergisi 27, 3-16.

Özpeker, I., Çoban, F., Esenli, F., Eren, R.H. 1991. Miyosen yaşlı Hırka formasyonundaki (Beypazarı-Ankara) dolomitlerin mineralojik özellikleri. Türkiye Jeoloji Bülteni 34, 23-26.

Pehlivanlı, B.Y., Koç, Ş., Sarı, A., Engin, H. 2014. Factors controlling low Uranium and Thorium concentrations in the Çayırhan Bituminous shales in the Beypazarı (Ankara) area, Turkey. Acta Geologica Sinica 88, 248-259.

Randot, J. 1956. 1/100.000 lik 39/2 (Güney kısmı) ve 39/4 nolu paftaların jeolojisi. Seben-Nallıhan-Beypazarı ilçeleri. Maden Tetkik ve Arama Genel Müdürlüğü, Rapor No: 2517, Ankara (unpublished).

Seyitoğlu, G., Aktuğ, B., Karadenizli, L., Kaypak, B., Şen, Ş., Kazancı, N., Işık, V., Esat, K., Parlak, O., Varol, B., Saraç, G., İleri, İ. 2009. A late Pliocene - Quaternary pinched crustal wedge in NW Central Anatolia, Turkey: a neotectonic structure accommodating the internal deformation of the Anatolian Plate. Geological Bulletin of Turkey 52(1), 121-154.

Seyitoğlu, G., Ecevitoğlu, B., Kaypak, B., Güney, Y., Tün, M., Esat, K., Avdan, U., Temel, A., Çabuk, A., Telsiz, S., Uyar Aldaş, G. 2015. Determining the main strand of the Eskişehir strike-slip fault zone using subsidiary structures and seismicity: a hypothesis tested by seismic reflection studies. Turkish Journal of Earth Sciences 24, 1-20

Seyitoğlu, G., Esat, K., Kaypak, B. 2017*a*. One of the main neotectonic structures in the NW central Anatolia: Beypazarı Blind Thrust Zone and related fault-propagation folds. Bulletin of the Mineral Research and Exploration 154, 1-14.

Seyitoğlu, G., Esat, K., Kaypak, B. 2017*b*. The neotectonics of southeast Turkey, northern Syria and Iraq: the internal structure of the South East Anatolian Wedge and its relationship with the recent earthquakes. Turkish Journal of Earth Sciences 26, 105-126.

Siyako, F. 1983. Beypazarı (Ankara) linyitli Neojen havzası ve çevresinin jeoloji raporu. Maden Tetkik ve Arama Genel Müdürlüğü, Rapor No: 7431, 46 s., Ankara (unpublished).

Suner, M.F. 1993. The Beypazarı trona deposits. Földtani Közlöny 123(3), 271-282.

Şahin, M., Yaltırak, C., Karacık, Z. 2019. A case study of compression to escape tectonic transition: Tectonic evolution of the Nallıhan Wedge and comparison with the Tercan Wedge (Eastern Mediterranean, Turkey). Journal of Asian Earth Sciences 174, 311-331.

Şaroğlu, F., Emre, Ö., Kuşçu, İ. 1992. 1/1.000 ölçekli Türkiye diri fay haritası. Maden Tetkik ve Arama Genel Müdürlüğü, Ankara.

Şener, M. 2007. Depositional conditions of the coal-bearing Hırka Formation beneath Late Miocene explosive volcanic products in NW central Anatolia, Turkey. Journal of Earth System Science 116, 125-135.

Yağmurlu, F., Helvacı, C., İnci, U., Önal, M. 1988. Tectonic characteristics and structural evolution of the Beypazarı and Nallıhan Neogene basin, central Anatolia. METU Journal of Pure and Applied Sciences 21, 127-143.

Bull. Min. Res. Exp. (2020) 163: 99-114

Bulletin of the Mineral Research and Exploration

http://bulletin.mta.gov.tr

An approach for the application of energy-based liquefaction procedure using field case history data

Kamil KAYABALI[a], Levent SELÇUK[b*] and Turgay BEYAZ[c]

[a]*Department of Geological Engineering, Ankara University, Gölbaşı-Ankara, Turkey*
[b]*Department of Geological Engineering, Van Yüzüncü Yil University, Tuşba-Van, Turkey*
[c]*Department of Geological Engineering, Pamukkale University, Denizli, Turkey*

Research Article

Keywords:
Soil liquefaction, Energy-based liquefaction method, Field case histories, Earthquake.

ABSTRACT

This paper presents an overview to the applicability of the "energy-based liquefaction approach" with regards to the new developments in the subject. The method involves comparing the strain energy for the soil liquefaction (capacity) with the strain energy imparted to the soil layer during an earthquake (demand). The performance of the method was evaluated by using a large database of SPT-based liquefaction case history. The energy-based method and the more commonly used stress-based method were compared in their capability to assess liquefaction potential under the same damaging historic earthquakes and geotechnical site conditions. In the procedure, the predictive strain energy equations were used to estimate the capacity energy values. These empirical equations have been developed based on the initial effective soil parameters. As for the energy of any given strong ground motion, it was computed from a velocity-time history of the ground motion and the unit mass of soil through utilization of kinetic energy concepts. The proposed energy-based method has effective way in evaluating the liquefaction potential based on the seismological parameters, contrary to the stress-based approach, where only peak ground acceleration (PGA) is considered.

Received Date: 27.09.2019
Accepted Date: 09.01.2020

1. Introduction

The soil liquefaction during a strong ground motion is a significant and ever-present phenomenon that threatens to damage or collapse buildings, bridges, highways, embankments, and other civil engineering structures. Catastrophic events such as Niigata (Japan) in 1964, Loma Prieta (California) in 1989, Kobe (Japan) in 1995, Kocaeli (Turkey) in 1999 indicated that the most striking failures on the ground are due to the soil liquefaction (e.g. sand boils/settlement-type ground deformations, lateral spreading and natural slope failures or flows).

The evaluation of the soil liquefaction is a complex problem in earthquake engineering, due to having numerous factors controlling the mechanism of the liquefaction (e.g. the magnitude, intensity, path effects, attenuation characteristics, types of soils, confining pressure, the distance from the source and other site-specific conditions) (Law et al., 1990). Numerous laboratory techniques and model tests, in-situ techniques and numerical approachs have been performed for assessment of the liquefaction potential (e.g. Finn et al., 1971; Seed and Idriss, 1971; Martin, 1975; DeAlba et al., 1976; Ladd et al., 1989; Elgamal et al., 1989; Tokimatsu et al., 1991; Oka et al., 1994; Youd et al., 2001; Zhang, 2001; Moss et al., 2006; Boulanger and Idriss, 2012). At the same time, several field procedures have been highlighted for more accurate assessment of liquefaction potential. The

Citation info: Kayabalı, K., Selçuk, L., Beyaz, T. 2020. An approach for the application of energy-based liquefaction procedure using field case history data. Bulletin of the Mineral Research and Exploration 163, 99-114. https://doi.org/10.19111/bulletinofmre.677626.

**Corresponding author: Levent SELÇUK, lselcuk@yyu.edu.tr*

available evaluation procedures for assessment of soil liquefaction include: 1) the Stress-based approach, 2) the strain-based approach, and 3) the energy-based approach (Green, 2001; Zhang et al., 2015).

The stress-based procedure for evaluation of liquefaction potential started with a basic approach defined by Seed and Idriss (1967), which has since been upgraded with many studies that have contributed the method. The contents of these studies, mostly quoted from Shahien (2007) can be summed up in to the following; a) update of the field case history data, b) deterministic or probabilistic treatments, and c) modification of some components of the liquefaction procedure (e.g. Seed et al., 1975; Seed, 1979,Tokimatsu and Yoshimi, 1983; Seed et al., 1984; Jamiolkowski et al., 1985; NRC, 1985; Ambraseys 1988; Lio et al., 1988; Hendron, 1990; Castro, 1995; Fear and McRoberts, 1995; NCEER,1997; Youd et al., 2001; Seed et al., 2001; Çetin et al., 2000 and 2004; Idris and Boulanger, 2006).

In the generalized framework, the cyclic stress ratio, CSR is compared with the cyclic resistance ratio, CRR of the soil. This procedure, however, involves some uncertainties. In the laboratory applications, the time-dependent irregular variation of shear stress should be converted to equivalent sequences of uniform shear cycles. As for the comparison of the earthquake-induced stress with the harmonic loading conditions, Seed et al. (1975) assumed the equivalent stress as "65% of the maximum shear stress. Ishihara and Yasuda (1975) concluded it's to be 57% (Zhang et al., 2015). Site response analysis is another approach for determination of cyclic resistance ratio. However, both a site response analysis and the procedure of Seed and Idriss (1967) require the determination of the a_{max} on the ground level of a project site as well. Determination of the a_{max} in a project site also brings with it some uncertainties such as the magnitude scale, site-to-source distance and the attenuation model itself in computing the a_{max}. Although the stress-based procedure has been re-evaluated with adequate studies and also updated with case histories, the limitation relating random loading still continue. (Baziar and Jafarian, 2007; Zhang et al., 2015).

Just like the stress-based liquefaction procedure, strain based approach has some similar limitations. The amplitude of the earthquake-induced cyclic shear strain (γ) is estimated from the cyclic stress (τ) and the shear modulus (G). The other variables are the similar components of cyclic stress as described by Seed and Idriss (1971). In the procedure introduced by Dobry et al. (1982), the cyclic threshold shear strain plays a significant role for pore-water pressure produced by cyclic loading. Upon a series of strain-controlled undrained cyclic tests on saturated sand specimens, Dobry et al. (1982) showed that the threshold shear strain for liquefaction to initiate is approximately 0.11%. Silver and Seed (1971) reported that this value has the range of approximately 0.020% - 0.030% for clean sands. Ladd et al. (1989) found this value to be roughly 0.011%. Vucetic (1994) and Hsu and Vucetic (2004) revealed that the cyclic threshold shear strain value of clayey soils is greater than those of sands. These researchers confirmed that this value was increased or decreased by soil characteristics (Kusumawardani et al., 2015).

As for the energy-based approach, the concept of strain energy and its applications for evaluation liquefaction potential has been described by the researchers (e.g. Davis and Berrill, 1982; Law et al., 1990; Figueroa et al., 1994; Liang 1995; Ostadan et al., 1996; Davis and Berrill 2001; Green, 2001; Baziar and Jafarian, 2007). Davis and Berrill (1982) found out that excess pore water pressure is quite relevant with the amount of strain energy. Thus, the strain energy has been compared with the strain energy imparted to liquefiable soil layer by an earthquake in order to predict the liquefaction. These affords has led to develop the concept of the energy-based liquefaction (Alavi and Gandomi, 2012).There has been a great deal of studies focusing on the strain energy and initial soil parameters in the form of empirical relationships. Figueroa et al. (1994) proposed a relationship relating initial soil properties to dissipated energy. Similarly, Baziar and Jafarian (2007) utilized from the artificial neural network model to suggest a statistical model relating soil parameters to strain energy. They also used a data recorded during earthquakes in addition to the centrifuge tests available to validate their model. They found a reasonable consistency between energy capacity and field observations. The energy-based method offers the following advantages;

1) Energy is related to both shear stress and shear strain;
2) Energy is a scalar quantity that is attributable to the characteristic main earthquake parameters

(e.g. the source-site distance, the earthquake magnitude), all the while considering the entire spectrum of ground motions, contrary to the stress-based approach, where only peak ground acceleration is considered;

3) It has accounting capabilities for the effects of a complex stress–strain history on pore water pressure (Zhang et al., 2015).

Although the energy-based liquefaction procedure offers great advantage, as mentioned here, its application is limited until now due to the fact that the basic principles and extensions of energy-based approach have not been discussed in detail with corresponding applications of stress-based liquefaction procedure. In several researches, the results obtained from the energy-based approach were compared to those of the stress-based approach under the same seismic motions, and some applications are available for actual liquefaction case histories (Kokusho, 2013; 2017; Kokusho and Mimori, 2015; Kokusho et al., 2015). Kokusho et al., (2015) investigated a liquefaction case by a far-field (M: 8.0) earthquake in order to compare the evaluations by stress-based method and energy-based method. It demonstrated a better applicability of energy-based method than stress-based method. Because the maximum acceleration in that case was only about 0.05 g, while its seismic wave energy enough to liquefy. Kokusho and Mimori (2015) pointed out that the energy-based method gives similar results as the stress-based method. Kokusho (2017) report that it is still necessary to apply energy-based method to more case histories to demonstrate its reliability in much more practical conditions. The aim of this study is to demonstrate a simplified procedure of the energy-based approach in accordance with further improvements. To demonstrate the consistency and reliability of the procedure, a large liquefaction database of past events compiled by several researchers (Seed et al., 1984; Idriss and Boulanger, 2004, 2008 and 2010; Çetin et al., 2000, 2004 and 2016) were used as a verification data in the proposed procedure.

2. Energy-Based Liquefaction Approach and Predictive Strain Energy Equations

There has been a great deal of studies relating the energy-based procedures. These procedures involve the different energy measurements in the terms of basic parameters to the demand and the capacity (Green, 2001). In the procedure, the amount of total strain energy for initial liquefaction is obtained from the laboratory testing (cyclic shear or cyclic triaxial testing) or field recorded data. The stress- strain time histories are recorded, and strain energy is given by the area inside the hysteresis loop generated from the stress and strain time histories (Figure 1). This area shows the dissipated energy per unit volume (Ostadan et al., 1996; Green, 2001; Alavi and Gandomi, 2012).

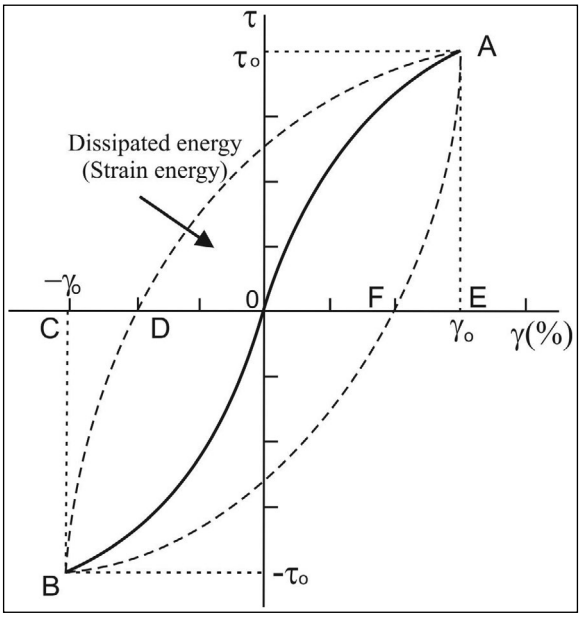

Figure 1- A typical shear stress–strain hysteresis loop.

The total energy (δW) gained by the soil specimen until the onset of liquefaction is computed as follows (Figueroa et al., 1994; Liang et al., 1995):

$$\delta W = \sum_{i=1}^{n-1} 0.5\left(\tau_i + \tau_{i+1}\right)\left(\gamma_{i+1} - \gamma_i\right) \quad (1)$$

Where, τ is shear stress, γ and n are shear strain and cycle numbers, respectively. The total amount of energy is considered as a measurement of the soil capacity against the initial liquefaction. The energy-based liquefaction approach is validated through laboratory testing or recorded field data. Numerous tests were performed to develop the energy-based models relating the energy capacity, confining pressure, strain amplitudes and soil initial parameters. Figueroa et al. (1994) conducted a series of tests

on sands using a hollow-cylinder torsional shear device. They utilized from initial soil properties in order to establish a relationship relating the strain energy. Some energy-based formulations developed for liquefaction assessment were given in table 1. These statistical models were mostly generated by the multiple linear regression analysis. In recent years, different statistical methods such as ANNs, artificial neural networks and SVM, support vector machines have been considered in order to provide more reliable results. In this context, Chen et al. (2005) proposed an energy-based method by using back-propagation neural networks to assess the soil liquefaction. These statistical methods perform sufficiently well in the evaluation liquefaction probability due to their prediction performance. However, they have some limitations. A major restriction of artificial neural network is that it is not satisfactory for generating practical predictive equations. Besides, the network model is not variable and identified in advance (Alavi et al., 2011).

3. The Approach in the Proposed Method

Calculation steps of soil capacity and demand were summarized fallowing subsections. Both two parameters is required for assessment of liquefaction potential.

3.1. Evaluation of the Seismic Demand

The total energy (E, Joule) resulted from a quake is given by the equation of Gutenberg and Richter (1956):

$$E = 10^{4,8+1,5M} \quad (2)$$

Only a part of energy propagates along the site-source distance. It's some part will be scattered by inelastic attenuation and energy attenuation is possible due to geometric spreading. (Law et al., 1990). The energy (W) imparted by an earthquake on a unit of mass of matter (e.g., soil) is computed as follows;

$$W = \frac{1}{2}mv^2 \quad (3)$$

Where, m is mass of liquefiable soil layer and v is velocity. As mentioned above, the dissipated energy is expressed in the unit volume of the soil mass. The unit soil mass is numerical value of the saturated density since the volume is 1 unit. To determine the total amount of the energy imparted to liquefiable soil layer by an earthquake, strong motion acceleration-time history of any event needs to be obtained from accelerograms. Thus, Eq.3 is performed to obtain the cumulative energy versus the time.

The general procedure for the evaluation of the soil liquefaction is to compare two parameters; 1) the seismic demand and 2) the soil capacity to induce liquefaction. In the proposed method, the strain energy equations were performed to compute the capacity of the soil, as expressed by following section.

3.2. Evaluation of the Soil Capacity

The predictive energy equations in table 1 require the calculation of the initial soil parameters. An exact determination of σ'_{mean} in-situ is very difficult and the initial effective overburden stress (σ'_v) is commonly preferred rather than the initial mean effective stress, σ'_{mean} or P'_o which could be interchangeably related as shown below (Seed et al., 1986). Thus, σ'_{mean} is

Table 1- Empirical strain energy equations between the dissipated energy and soil parameters.

Equation	Researcher	Expression	r
(I)	Figueroa et al. (1994)	$\log(W) = 2.002 + 0.00477\,\sigma'_{mean} + 0.0116D_r$	0.97
(II)	Liang (1995)	$\log(W) = 2.062 + 0.0039\,\sigma'_{mean} + 0.0124D_r$	0.96
(III)	Dief and Figueroa (2001)	$\log(W) = 1.164 + 0.0124\,\sigma'_{mean} + 0.0209D_r$	0.97
(IV)	Baziar and Jafarian (2007)	$\log(W) = 2.1028 + 0.00456\,\sigma'_{mean} + 0.005685D_r + 0.001821FC - 0.02868C_u + 2.0214D_{50}$	0.80
(V)	Jafarian et al. (2012)	$W = 0.1363P'_o\,(D_r^{4.925}) + 5.375\,(10^{-3}P'_o)$	0.80

W: measured strain energy density required for triggering liquefaction (J/m^3), P_o' and σ'_{mean}: initial effective mean confining pressure and initial mean stress (in kPa), D_r: initial relative density (%), FC : percentage of fines content, C_u : coefficient of uniformity and D_{50} = mean grain size (mm)

expressed by effective overburden stress (σ'_v) and coefficient of lateral earth pressure (K_o);

$$\sigma'_{ort} = \left(\frac{1 + 2K_0}{3}\right)\sigma'_v \quad (4)$$

Where, K_o and ϕ' are obtained using the following expressions (Eqs 5 and 6), ϕ' is the effective angle of internal friction, which is expressed in term of $(N_1)_{60}$ (Hatanaka and Uchida, 1996).

$$K_o = 1 - \sin(\phi') \quad (5)$$

$$\phi' = (20N_{1,60})^{0,5} + 20 \quad (6)$$

On the other hand, the relative density, (D_r) is defined for natural soils as follows (Skempton, 1986):

$$D_r = \left(\frac{N_{1,60}}{55}\right)^{0.5} \quad (7)$$

Eq.7 is employed to compute the relative density for clean sands. Herein $(N_1)_{60}$ is derived for clean sands and it should be modified to take into account fines content (FC) to obtain an equivalent clean sand value, $(N_1)_{60cs}$, as follows (Youd et al., 2001):

$$(N_1)_{60cs} = (N_1)_{60} + exp\left[1{,}63 + \frac{9{,}7}{FC + 0{,}1} - \left(\frac{15{,}7}{FC + 0{,}1}\right)^2\right] \quad (8)$$

Eq.8 is employed to find the "equivalent" relative density for fine-grained soils. Once σ'_{mean} and Dr are computed with the expressions defined above, the strain energy (i.e. capacity) is calculated by using any of the Equations I-V in table 1.To evaluate the soil liquefaction, the proposed method considers only a comparison between demand and capacity.

4. Examination of the Procedure for the Assessment of Soil Liquefaction

4.1. Database for Past Earthquakes

The SPT-based database was compiled and updated by several researchers (Seed et al., 1984; Idriss and Boulanger, 2004, 2008 and 2010; Çetin et al., 2000, 2004 and 2016) for liquefaction correlation of cohesionless soils. The first database was presented by Seed et al. (1984) which contained only 125 cases. Then, the first large database was presented by Idriss and Boulanger (2004). It includes both the compiled and updated data of Seed et al. (1984) and -Çetin et al. (2000, 2004). The total number of evidence is 230 and surface evidences of liquefaction were observed in only 115 case histories. Additionally, some of these cases were not approved by Çetin et al. (2016). In the end, the data set updated by Çetin et al. (2016) contains 210 cases with consistent screening standards enforced throughout. The values of earthquake and soil parameters such as magnitude (M), maximum ground acceleration (a_{max}), depths to the relevant layer and ground water table, the total (σ_v) and effective vertical stress (σ'_v), SPT-blow counts (N), correction factors (e.g. C_E, C_R, C_B and C_S), $(N_1)_{60}$, fines content (FC) and $(N_1)_{60cs}$ were presented in the updated data set of Çetin et al. (2016) for 20 major earthquakes.

This updated dataset was used to verify the proposed energy-based method in this investigation. For the calculation of the seismic demand on a soil layer, it is necessary to obtain the acceleration and velocity time histories of significant earthquakes. However, strong-motion data for many earthquakes prior to 1979 were not available. Therefore, only 115 cases with 9 major earthquakes in the data set of Çetin et al. (2016) were evaluated by using the existing acceleration records. The acceleration records are obtained from the seismic stations nearest to the sites of liquefaction/no liquefaction cases. Some information about seismic stations is given in table 2. The distances between the seismic stations and the sites of liquefaction/non-liquefaction cases are also given in table 3. Vertical (Up) acceleration component records of the ground motions are used to compute the cumulative energy of the earthquakes, because they can reach very high values at the surface close to the fault and compressive structural damage can occasionally be observed in the near field (Kunnath et al., 2008; Papazoglou and Elnashai, 1996; Riches, 2015; Tsaparli et al., 2016). High values was recorded during past earthquakes (e.g Northridge in 1994 and Kobe in 1995) where soil liquefaction events occurred (Shibata et al., 1996; Trifunac and Todorovska, 1996; Yasuda, 1996; Tsaparli et al., 2016). More recently, Canterbury earthquakes (New Zealand in 2010-11) are an important example for high records of vertical acceleration values and also soil liquefaction events (Bradley, 2012; Tsaparli et al., 2016).

Table 2- Strong motion stations and peak ground acceleration data for past major earthquakes.

Earthquake	Station			
	Code/ID	Lat/Long	Closest dist to epicenter (km)	PGA (cm/s^2)
1995 Hyogoken-Nambu (Kobe)	KJM (JMA, Japan Meteorological Agency)	34.6833/135.1800	1.5	336.13
1994 Northridge	Arleta Nordhoff Ave Fire Sta CGS - CSMIP Station 24087	34.2358/118.4398	9.5	539.39
1993 Kushiro-Oki	Kushiro Local Meteorological Observatory, JMA (KSR), Hokkaido	42.9786/144.3880	7.0	356.00
1989 Loma Prieta	CGS-47459 CGS-58483 CGS-58505 CGS-58117	36.9091/121.7575 37.7988/122.2582 37.9355/122.3434 37.8253/122.3739	17.0 89.0 105.0 97.0	647.00 42.00 29.00 20.00
1987 Superstition and Elmore Ranch	CGS-01336 CGS-11369	32.7735/115.4481 33.0370/115.6235	48.0 22.0	225.00 187.00
1981 Westmorland	CGS-11369	33.0370/115.6235	7.0	627.57
1979 Imperial Valley	CGS-01335	32.7933/115.5625	28.0	231.00
1971 San Fernando	C&GS241	34.2211/118.4711	22.0	167.00

4.2 Comparison of the Demand to the Capacity

The results of the strain energy imparted by strong ground motion (demand, W_{quake}) and the capacity of the soil to induce liquefaction (W_{liq}) are presented in table 3. The partial data in table 3, namely a_{max}, depths to layer of interest and water table, the total and effective vertical stresses on the layer, $(N_1)_{60}$, fines content (FC) and $(N_1)_{60cs}$ were taken from the updated database of Çetin et al. (2016). M_{sat} and M_t were deduced from the borehole logs and imported data in the database of Çetin et al. (2016). σ_{mean}, K_o, ϕ' and D_r were computed using Equations of 4-7. The capacities (W_{liq}) were calculated for 4 different empirical relationships (Equations I, II, III and V in Table 1) by employing the appropriate mean effective stresses and the relative densities. The ground motion records nearest to the site of interest were selected for the computation of demands.

To demonstrate how the proposed method works figure 2 was constructed, which covers field cases of 1995, Kobe/Hanshin (Hyogoken-Nanbu) Earthquake. It shows the acceleration-time history, velocity and the cumulative work for the first 2 cases (location #1 and 2 in table 3). The sites of no liquefaction cases were 15 km away from the epicenter of earthquake. The closest seismic station (KJM) to the site of cases was approximately 2.5 km. For these fields, the unit mass for the soil was taken as 1874 kg, which resulted in a demand of 2061 J/m^3 (Figure 2) when the Eq.3 was used along with the velocity time history. Since the demand for the station record is less than the soil capacities calculated using the 4 predictive equations, the liquefaction at these sites is verified from the perspective of the proposed method. Similarly, the location #5, as given in table 3, is a site of liquefaction in the same section. The unit mass of soil at this site is 1762 kg and thus the cumulative work or the demand is 1938 J/m^3, which is greater than all the capacities calculated using the 4 predictive equations. The comparison of the demand to capacity indicates that soil liquefaction should take place at location #5 as well.

The reliability and accuracy of the proposed method were examined for 115 cases in the data set of Çetin et al. (2016). The energy-based liquefaction method yields similar results with the stress-based liquefaction method for past events. Attempts have been made to provide more reliable seismic demand values by using near station records. However, the near station records for some case histories of past earthquakes are not available, and the use of the relatively far field ground motion records (>15km) resulted in a high seismic demand for a few non-liquefiable sites due to their site-to-source distances. The comparison between the demand values calculated from the nearest station and capacity values calculated for each site are given in figure 3. It shown that the results of the strain energy imparted by strong ground

Table 3- List of liquefiable/non-liquefiable cases used in this study (data source; updated data set of Çetin et al. (2016).

Location Name/Code	M	a_{max} (g)	Liquef.	Depth (m)	GWT (m)	σ_v	σ'_v	M_t (kg)	$(N_1)_{60}$	FC (%)	ϕ' (°)	K_o	σ'_{mean}	$(N_{1,60})_{cs}$	D_r (%)	W_{liq} (J/m³)				W_{quake} (J/m³)* St.Code	Distance Rcls **(km)
																a	b	c	d		
16 Jan. 1995, Kobe/Hanshin (Hyogoken-Nanbu) Earthquake, Mw= 7.2 (Japan)																				KJM	
1	6.9	0.4	No	6	2.4	122	86	1874	53.2	3.5	52.9	0.2	40.3	54.1	110.3	2978	3865	9317	9125	2061	2.5
2	6.9	0.4	No	8.5	2.9	173	118	1922	39.6	14.8	48.9	0.25	58.7	41.9	97.1	2560	3125	8334	7232	2114	2.5
3	6.9	0.4	No	5.5	2.5	103	73	1601	52.8	3.3	52.8	0.2	34.2	53.7	109.9	2757	3619	7692	7622	1761	2.5
4	6.9	0.4	No	4.3	2.1	79	57	1762	40.4	1.3	48.7	0.25	28.4	41.2	96.28	1797	2327	3381	3370	1938	2.5
5	6.9	0.4	Yes	8.8	3	160	104	1762	7	1.3	32.2	0.47	67	7.5	41.08	628	680	714	474	1938	2
6	6.9	0.4	No	5.8	2.3	112	78	1601	21.9	24.7	42.4	0.33	43	25	75	1194	1444	1838	1651	1761	2
7	6.9	0.4	Yes	2.8	3.2	48	51	1762	22.3	0.1	41.4	0.34	28.5	23	71.94	938	1162	1049	920	1938	2
8	6.9	0.5	Yes	5	3	87	66	1601	24	0.1	42.2	0.33	36.5	24.6	74.4	1094	1339	1482	1354	1761	2
9	6.9	0.5	Yes	4.3	2.8	73	58	1681	12.4	2.3	36.1	0.41	35.2	12.9	53.87	624	737	533	418	1849	2
10	6.9	0.6	No	7.5	4.5	144	114	1922	26.2	8.8	43.4	0.31	61.8	27.4	78.52	1612	1890	3724	2891	2114	1
11	6.9	0.5	Yes	6.8	1.5	125	73	1762	7.7	5	32.8	0.46	46.6	8.2	42.95	528	598	436	350	1938	1.5
12	6.9	0.5	yes	5.3	3.2	92	71	1762	26.2	14	43.7	0.31	38.3	28.1	79.51	1280	1575	1998	1894	1938	1
13	6.9	0.5	Yes	6.5	2.3	124	83	1922	12	15	36.6	0.4	50	13.7	55.52	767	882	881	645	2114	1.5
14	6.9	0.5	No	4.8	3.1	89	73	1842	21	18.5	41.6	0.34	40.7	23.3	72.41	1087	1314	1520	1350	2026	1
15	6.9	0.5	Yes	5.8	3.7	99	78	1601	19.6	4.7	40.1	0.36	44.5	20.2	67.42	992	1179	1333	1109	1761	1.5
16	6.9	0.6	No	4.5	2.5	83	62	1762	24.6	5	42.4	0.33	34.1	25.2	75.3	1092	1345	1448	1333	1938	1
17	6.9	0.5	Yes	4.5	0.8	84	47	1762	21.2	5	40.9	0.35	26.5	21.8	70.04	873	1081	904	767	1938	2
18	6.9	0.7	No	11	7.7	211	183	2002	36.7	0.1	47.3	0.26	93.3	37.4	91.73	3243	3658	17289	8813	2202	1
19	6.9	0.6	No	7.5	6.1	142	129	1922	20.8	10	41	0.34	72.6	22.1	70.52	1466	1657	3447	2160	2114	1.5
20	6.9	0.6	No	6	2	119	80	1762	65.5	0.1	56.5	0.17	35.5	66.5	122.3	3895	5217	14496	13258	1938	2
21	6.9	0.6	No	3.5	1.7	62	44	1601	36.8	0.1	47.4	0.26	22.4	37.5	91.86	1494	1943	2300	2131	1761	2
22	6.9	0.6	No	6	2.4	116	81	1922	38.9	6	48.2	0.25	40.7	39.8	94.63	1968	2479	4435	4450	2114	2
23	6.9	0.6	No	5	3	96	76	1601	23.3	10	42.1	0.33	42	24.5	74.25	1158	1401	1724	1547	1761	2.5
24	6.9	0.5	Yes	3.5	2.4	64	53	1842	24.8	0.1	42.5	0.32	29.1	25.4	75.6	1042	1297	1273	1157	2026	2.5
25	6.9	0.7	No	3.5	2.2	64	50	1762	39	2.5	48.2	0.25	25.1	39.8	94.63	1658	2155	2842	2747	1938	2
26	6.9	0.6	No	3.5	0.9	65	40	1601	41.2	0.1	49	0.25	19.9	42	97.21	1677	2213	2768	2464	1761	2.5
27	6.9	0.6	No	2.5	1.1	45	31	1766	50.4	10	52.3	0.21	14.7	52.1	108.3	2127	2895	4060	3033	1943	2
28	6.9	0.4	Yes	4	1.8	74	52	1601	21.5	8	41.2	0.34	29.2	22.5	71.15	926	1143	1030	900	1761	4
29	6.9	0.4	Yes	3.8	2	69	52	1762	18	0.1	39.3	0.37	30	18.6	64.69	787	958	774	641	1938	4
30	6.9	0.6	No	8.5	1.5	161	92	1601	39	10	48.5	0.25	46.1	40.5	95.46	2134	2664	5378	5245	1761	3.5
31	6.9	0.6	No	4	1.2	74	46	1601	57	0.1	54	0.19	21.2	57.9	114.1	2673	3630	6488	5651	1761	2.5
32	6.9	0.5	No	3.5	1.4	63	43	1601	30.5	6.3	45.1	0.29	22.7	31.4	84.05	1217	1559	1593	1438	1761	2.5
33	6.9	0.5	No	8	2	149	90	1601	27.8	50	45.5	0.29	47.2	32.6	85.64	1662	2032	3459	3251	1761	4
34	6.9	0.4	Yes	7	1.8	132	81	1681	23.5	9.3	42.2	0.33	44.7	24.7	74.55	1202	1448	1890	1675	1849	4.5
35	6.9	0.5	Yes	4.5	2.1	84	60	1762	17.7	6.3	39.2	0.37	34.7	18.4	64.34	820	989	870	726	1938	4.5
36	6.9	0.6	No	3.5	0.9	65	40	1601	33.7	2.5	46.2	0.28	20.7	34.4	87.98	1323	1713	1819	1616	1761	4

Table 3- (continue).

Location Name/Code	M	a_{max} (g)	Liquef.	Depth (m)	GWT (m)	σ_v	σ'_v	M_t (kg)	$(N_1)_{60}$	FC (%)	ϕ' (°)	K_o	σ'_{mean}	$(N_{1,60})_{cs}$	D_r (%)	W_{liq} (J/m³)				W_{quake} (J/m³)* St.Code	Distance **Rcls (km)
																a	b	c	d		
16 Jan. 1995, Kobe/Hanshin (Hyogoken-Nanbu) Earthquake, Mw= 7.2 (Japan)																				**KJM**	
37	6.9	0.4	Yes	5	4	95	85	1922	22.5	0.1	41.5	0.34	47.5	23.1	72.09	1161	1384	1816	1546	2114	5
38	6.9	0.5	Yes	8	3	152	103	1842	18.3	5	39.4	0.36	59.4	18.9	65.21	1101	1265	1833	1305	2026	5
39	6.9	0.6	No	4.5	2.6	89	71	1922	61.9	0.1	55.5	0.18	32	62.9	119	3425	4592	11149	10432	2114	5
40	6.9	0.6	No	3.5	2.8	67	60	1922	42.8	0.1	49.5	0.24	29.6	43.6	99.05	1959	2544	3988	4003	2114	4.5
41	6.9	0.4	Yes	4.1	2	71	51	1601	14.9	0.1	37.5	0.39	30.3	15.4	58.86	675	813	588	466	1761	5.5
42	6.9	0.4	Yes	5	1.2	92	55	1762	10.7	10	35.3	0.42	33.8	11.7	51.31	573	676	453	354	1938	5.5
43	6.9	0.4	Yes	4.7	2.2	82	57	1601	14.8	20	38.5	0.38	33.3	17.1	62.03	760	915	748	612	1761	6
44	6.9	0.4	Yes	4	1.6	69	45	1762	7.6	5	32.7	0.46	28.8	8.1	42.69	431	505	259	214	1938	6.5
Ashiyama A (Sand 1)	6.9	0.4	yes	5.2	3.5	94	77	1762	21.5	18	41.8	0.33	42.8	23.7	73.02	1131	1363	1663	1470	1938	1.5
Ashiyama A (M. Sand)	6.9	0.4	no	8	3.5	148	104	1762	30.6	2	45	0.29	55	31.3	83.92	1728	2075	3975	3454	1938	1.5
Ashi. C-D-E (Mnt Sand 2)	6.9	0.4	yes	13	3.5	247	154	1762	5.6	18	32.2	0.47	99.3	7.4	40.8	890	902	1773	698	1938	1.5
Ashi. C-D-E (M. Sand)	6.9	0.4	yes	8.8	3.5	164	112	1762	12.6	2	36.2	0.41	67.9	13.2	54.5	907	1006	1394	830	1938	1.5
Port Island BH Array St.	6.9	0.3	Yes	7.6	2.4	144	93	1762	7.1	20	33.5	0.45	58.8	9.1	45.25	642	712	690	477	1938	3.5
Port Is. Imp.St(Ikegaya)	6.9	0.4	No	8.5	5	155	121	1762	22.6	20	42.4	0.33	66.6	25.1	75.15	1554	1793	3635	2581	1938	4.5
Port Imp.St.(Tanahashi)	6.9	0.4	No	10	5	185	136	1762	19.1	20	40.8	0.35	76.8	21.6	69.71	1503	1682	3741	2183	1938	5
Port Imp St(Watanabe)	6.9	0.4	No	9.5	5	178	134	1762	32.8	20	46.7	0.27	69	35.6	89.5	2341	2760	7765	5817	1938	5.5
Port Island Site I	6.9	0.3	Yes	10	3	184	115	1762	11.1	20	36.2	0.41	69.7	13.2	54.5	926	1022	1469	852	1938	5.5
Rokko Island Building D	6.9	0.4	Yes	7.5	4	138	104	1762	17.6	25	40.3	0.35	59.2	20.6	68.08	1186	1371	2091	1532	1938	5.5
Rokko Island Site G	6.9	0.3	Yes	12	4	210	137	1762	12.5	20	37.1	0.4	81.8	14.7	57.51	1147	1243	2404	1172	1938	5.5
Torishima Dike	6.9	0.3	Yes	4.8	0	86	39	1762	15.2	20	38.7	0.37	22.7	17.5	62.75	689	849	572	435	1938	12
18 Jan. 1994, Northridge Earthquake, M=6.7 (USA)																				***ARLETA***	
Balboa Blv. Unit C	6,7	0,84	Yes	9	7,2	160	142	1762	19	48	41.6	0.34	79.2	23.3	72.41	1658	1856	4559	2625	2643	3
Potrero Canyon C1	6.7	0.4	Yes	6.5	3.3	120	88	1762	10.8	44	37.1	0.4	52.6	14.6	57.31	828	950	1034	745	2643	6
Wynne Ave Unit C1	6.7	0.5	Yes	6.3	4.2	112	92	1762	11.4	42.4	37.4	0.39	54.7	15.2	58.48	874	1001	1161	825	2643	11
15 Jan 1993, Kushiro-Oki Earthquake, M=7.6 (Japan)																				**KSR**	
Kushiro Port Quay Wall St. A	7.6	0.4	Yes	5.3	2	97	65	1681	16.5	2	38.5	0.38	38	17.1	62.03	800	954	855	698	2690	15
Kushiro Port Quay Wall Site D	7.6	0.4	No	11	1.6	210	120	1922	29.8	0.1	44.7	0.3	63.7	30.5	82.84	1849	2177	4849	3780	3075	15
Kushiro Port Seismo St.	7.6	0.5	Yes	3.6	2	66	50	1762	25.4	5	42.8	0.32	27.3	26.1	76.63	1050	1315	1272	1151	2819	15
18 Oct. 1989, Loma Prieta Earthquake, M= 6.9 (USA)																				**CGS-58483**	
Alameda Bay Farm Dike	6.9	0.2	No	6.5	3	125	91	2002	43.8	7	50	0.23	44.5	45	100.6	2408	3044	6594	6497	1401	6
POO7-2	6.9	0.3	Yes	6.2	3	181	88	1922	12.8	3	36.3	0.41	53.3	13.3	54.7	777	887	928	658	1345	1.5
POO7-3	6.9	0.3	yes	6	3	115	86	1922	16.4	5	38.4	0.38	50.4	17	61.85	911	1060	1205	915	1345	1.5
Farris Farm	6.9	0.4	Yes	6	4.5	99	84	1601	10.3	8	35	0.43	51.9	11.2	50.2	679	771	719	517	2081	1
SFOBB-1 & 2	6.9	0.3	Yes	6.3	3	120	89	1922	8.2	8	33.4	0.45	56.3	9	45	620	691	635	453	1345	10

Table 3- (continue).

Location Name/Code	M	a_{max} (g)	Liquef.	Depth (m)	GWT (m)	σ_v	σ'_v	M_t (kg)	$(N_1)_{60}$	FC (%)	ϕ' (°)	K_o	σ'_{mean}	$(N_{1,60})_{cs}$	D_r (%)	W_{liq} (J/m³) a	b	c	d	W_{quake} (J/m³)* St.Code	Distance **Rcls (km)
18 Oct. 1989, Loma Prieta Earthquake, M= 6.9 (USA)																				**CGS-58505**	
Hall Avenue	6.9	0.1	No	4.6	3.5	75	64	1601	5.1	30	32.6	0.46	41	8	42.43	489	560	362	302	320	2.5
POR-2 & 3 & 4	6.9	0.2	Yes	4.9	3.5	79	65	1601	3.5	50	31.7	0.48	42.3	6.8	39.12	454	515	320	284	320	2
																				CGS-58117	
Treasure Island	6.9	0.2	Yes	5.3	1.5	91	55	1601	7.7	20	34	0.44	34.5	9.8	46.96	514	601	374	299	190	0.2
																				CGS-47459	
MBARI No.3: EB-1	6.9	0.3	No	2.5	2	44	39	1762	22.9	1	41.7	0.34	21.7	23.5	72.72	889	1118	897	733	2291	10
MBARI No.3: EB-5	6.9	0.3	No	4.1	1.8	76	54	1762	17.8	1	39.2	0.37	31.3	18.4	64.34	790	959	788	654	2291	10
Miller Farm CMF3	6.9	0.4	Yes	6.6	5.7	117	108	1922	10.7	27.3	36.5	0.41	65.2	13.6	55.32	901	1005	1344	831	2499	5
Miller Farm CMF5	6.9	0.4	Yes	7	4.7	134	111	1922	20.6	13	41.1	0.34	62.4	22.2	70.68	1316	1519	2598	1874	2499	5
Miller Farm CMF8	6.9	0.4	Yes	6.5	4.9	107	91	1601	10	15.5	35.3	0.42	55.9	11.7	51.31	731	825	851	586	2081	5
Miller Farm CMF10	6.9	0.4	No	8.4	3	160	106	1762	20.1	20	41.3	0.34	59.4	22.6	71.31	1296	1506	2460	1850	2291	5
Sand holdt UC-B10	6.9	0.3	Yes	3.2	1.7	58	43	1762	14.3	2	37.2	0.4	25.7	14.8	57.71	622	754	488	371	2291	1.8
State Beach UC-B1	6.9	0.3	Yes	2.7	1.8	49	40	1762	7.9	1.7	33	0.46	25.5	8.4	43.47	425	502	245	194	2291	10
State Beach UC-B2	6.9	0.3	Yes	4.7	2.7	91	71	1922	17.4	1	39	0.37	41.2	18	63.64	865	1028	1012	828	2499	10
Wood Marine UC-B4	6.9	0.3	Yes	1.8	1	31	24	1762	8.3	35	35.4	0.42	14.7	11.9	51.74	470	577	268	157	2291	10
Wood Marine UC-B4	6.9	0.3	Yes	1.8	1	31	24	1762	8.3	35	35.4	0.42	14.7	11.9	51.74	470	577	268	157	2291	10
General Fish	6.9	0.3	No	2	1.7	36	32	1762	15.1	5	37.7	0.39	18.9	15.7	59.43	605	746	438	301	2291	12
M Laboratory UC-B1	6.9	0.3	Yes	4	2.4	72	57	1762	11.7	3	35.6	0.42	34.9	12.2	52.39	597	704	491	384	2291	10
M Laboratory UC-B2	6.9	0.3	Yes	3.5	2.5	63	53	1762	14.9	3	37.5	0.39	31.5	15.4	58.86	684	822	609	485	2291	10
M Laboratory F1-F7	6.9	0.3	Yes	4.6	1.5	89	59	1762	19.8	3	40.2	0.35	33.6	20.4	67.75	888	1079	993	854	2291	10
MBARI[B4/B5/EB2/ EB3]	6.9	0.3	No	5.1	2	98	67	1922	25.8	5	43	0.32	36.5	26.5	77.22	1180	1452	1701	1590	2499	10
Miller farm	6.9	0.4	No	6	4	108	89	1762	8.9	22	35	0.43	55	11.2	50.2	703	792	785	547	2291	5
23-24 Nov. 1987, Elmore Ranch and Superstition Hills Earthquakes Mw=6.2 and Mw=6.5 (USA)																				**CGS-11369**	
Radio Tower B1	6.2	0.1	No	4.3	2	72	50	1601	6.2	43.5	33.9	0.44	31.4	9.7	46.72	494	580	339	270	576	9
Wildlife B	6.2	0.1	No	4.7	0.9	86	49	1601	11.3	26.2	36.8	0.4	29.4	14.1	56.32	625	750	508	396	576	14
																				CGS-01336	
Heber Road A1	6.5	0.2	No	3.4	1.8	60	44	1601	46.5	13	51.2	0.22	21.1	48.7	104.7	2075	2770	4110	3722	256	6
Heber Road A2	6.5	0.2	No	3.2	1.8	53	39	1601	3.5	20.9	30.5	0.49	25.8	5.5	35.18	341	397	166	159	256	6
Heber Road A3	6.5	0.1	No	3.4	1.8	57	42	1601	18.6	25.3	40.8	0.35	23.7	21.7	69.87	842	1049	828	680	256	6
Mc Kim Ranch A	6.5	0.2	No	2.7	1.5	49	37	1762	7.9	19.8	34.1	0.44	23.2	10	47.43	460	550	277	205	282	7
																				CGS-11369	
Radio tower B1	6.5	0.2	No	4.3	2	72	50	1601	6.2	43.5	33.9	0.44	31.4	9.7	46.72	494	580	339	270	576	9
Radio tower B2	6.5	0.2	No	2.5	2	41	36	1601	16.6	18	39.3	0.37	20.8	18.7	64.87	714	886	599	448	576	9
Kornbloom B	6.5	0.2	No	4	2.7	68	55	1601	7.1	83	34.6	0.43	34.2	10.6	48.84	539	632	406	320	576	9
River Park A	6.5	0.2	No	1.1	0.3	18	10	1601	4	91	32.1	0.47	6.46	7.3	40.53	318	389	123	45	576	9
River Park C	6.5	0.2	No	4.3	0.3	76	38	1601	19.9	13.2	40.7	0.35	21.5	21.5	69.55	815	1019	765	605	576	9
Wildlife B	6.5	0.2	Yes	4.7	0.9	86	49	1601	11.3	26.2	36.8	0.4	29.4	14.1	56.32	625	750	508	396	576	17

Table 3- (continue).

Location Name/Code	M	a_{max} (g)	Liquef.	Depth (m)	GWT (m)	σ_v	σ'_v	M_t (kg)	$(N_1)_{60}$	FC (%)	ϕ' (°)	K_o	σ'_{mean}	$(N_{1,60})_{cs}$	D_r (%)	W_{liq} (J/m³) a	b	c	d	W_{quake} (J/m³)* St.Code	Distance **Rcls (km)
26 Apr. 1981, Westmorland Earthquakes, M=5.9 (USA)																				**CGS-11369**	
Kornbloom B	5.9	0.3	Yes	4	2.7	68	55	1601	7.1	83	34.6	0.43	34.2	10.7	49.07	542	636	410	323	256	9
Radio Tower B1	5.9	0.2	Yes	4.3	2	72	50	1601	6.2	43.5	33.9	0.44	31.4	9.7	46.72	494	580	339	270	256	9
Radio Tower B2	5.9	0.2	No	2.5	2	41	36	1601	16.6	18	39.3	0.37	20.8	18.7	64.87	714	886	599	448	256	9
River Park A	5.9	0.2	No	1.1	0.3	18	10	1601	4	91	32.1	0.47	6.46	7.3	40.53	318	389	123	45	256	9
River Park C	5.9	0.2	No	4.3	0.3	76	38	1601	19.9	13.2	40.7	0.35	21.5	21.5	69.55	815	1019	765	605	256	9
Wildlife B	5.9	0.3	Yes	4.7	0.9	86	49	1601	11.3	26.2	36.8	0.4	29.4	14.1	56.32	625	750	508	396	256	17
15 Oct. 1979, Imperial Valley Earthquakes, Mw=6.5 (USA)																				**CGS-01335**	
Heber Road A1	6.5	0.8	No	3.4	1.8	60	44	1601	46.5	13	51.2	0.22	21.1	48.7	104.7	2075	2770	4110	3722	8005	15
Heber Road A2	6.5	0.8	Yes	3.2	1.8	53	39	1601	3.5	20.9	30.5	0.49	25.8	5.5	35.18	341	397	166	159	8005	15
Heber Road A3	6.5	0.8	No	3.4	1.8	57	42	1601	18.6	25.3	40.8	0.35	23.7	21.7	69.87	842	1049	828	680	8005	15
Kornbloom B	6.5	0.1	No	4	2.7	68	55	1601	7.1	83	34.6	0.43	34.2	10.6	48.84	539	632	406	320	8005	25
Mc Kim Ranch A	6.5	0.5	Yes	2.7	1.5	49	37	1762	7.9	19.8	34.1	0.44	23.2	10	47.43	460	550	277	205	8810	17
Radio Tower B1	6.5	0.2	Yes	4.3	2	72	50	1601	6.2	43.5	33.9	0.44	31.4	9.7	46.72	494	580	339	270	8005	24
Radio Tower B2	6.5	0.2	No	2.5	2	41	36	1601	16.6	18	39.3	0.37	20.8	18.7	64.87	714	886	599	448	8005	24
River Park A	6.5	0.2	Yes	1.1	0.3	18	10	1601	4	91	32.1	0.47	6.46	7.3	40.53	318	389	123	45	8005	20
09 Feb. 1971, San Fernando Earthquake, Mw= 6.6 (USA)																				***C&GS-241***	
Juvenile Hall	6.6	0.5	Yes	5.4	4.3	94	84	1762	3.7	65.3	31.9	0.47	54.4	7.1	39.97	531	589	472	373	5568	5
Van Norman	6.6	0.5	Yes	6.2	5	110	97	1762	7.9	59.3	35.2	0.42	59.8	11.5	50.87	754	843	929	613	5568	5

Equations for Wlig (J/m³); a) Figueroa et al., 1994, b) Liang, 1995, c) Dief and Figueroa, 2001 and d) Jafarian et al., 2012

*This study [$W=0,5+(m*v^2)$] (Joule/m³) and Station Code (Exm.; KSR Kushiro Local Meteorological Observatory),

** Closest distance to station.

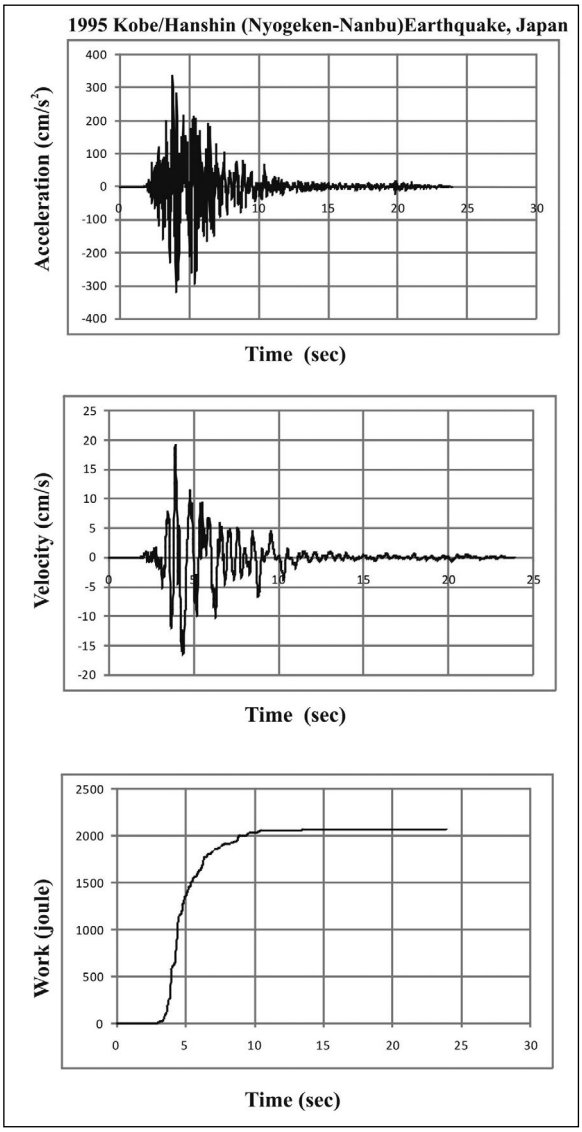

Figure 2- Time histories of acceleration, velocity and work for the 1995, Kobe/Hanshin (Hyogoken-Nanbu) Earthquake (Mw=6.9).

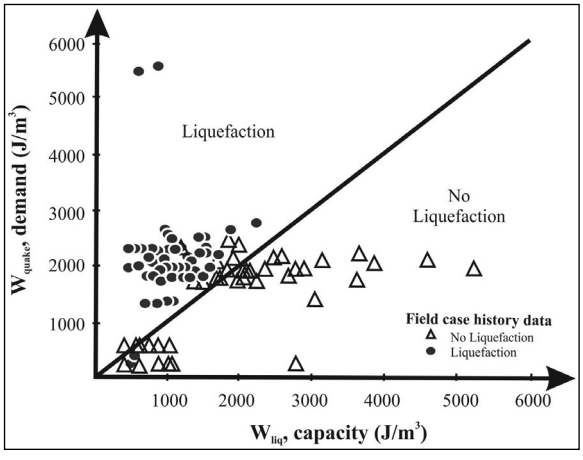

Figure 3- The comparison between the demand and capacity values for liquefiable/non liquefiable cases.

motion (demand, W_{quake}) and the soil capacity (W_{liq}) for liquefaction/no liquefaction case histories are quite consistent within the proposed method. The demand energy is larger than the capacity energy of the soil for liquefaction sites, or vice versa for non-liquefiable sites. Herein, the capacity values were calculated by using the equation of Liang (1995). Other models also provide partially same results. On the other hand, the method provides much more consistent results within the field observations of case histories. For example, the data base of Çetin et al. (2016) indicated that there is no surface evidence of liquefaction in the site of Treasure Island (Case#139) for 1989 Loma Prieta Earthquake. This observation is consistent with the result of the proposed method, that is, the demand for the station record is less than the soil capacities. For the stress-based approach, the liquefaction in this site was expressed by the change in the frequency of the ground motion (Çetin et al., 2016). Treasure Island is about 97 km away from the epicenter of the Loma Prieta Earthquake. Idris and Boulenger (2010) estimated the peak ground acceleration value to be 0.16g, whereas Çetin et al. (2016) suggested this value be 0.180 ± 0.027. These differences are even wider for some other historical cases. Considering that the ground acceleration values in the database compiled by different researchers are not consistent with each other and peak ground acceleration values are estimated using ground motion prediction models despite uncertainties still involved in these approaches, the proposed energy-based method seems to be much more capable for far-field ground motions in evaluating liquefaction potential with regards to the main earthquake parameters, such as magnitude and seismic source distances; contrary to the stress-based approach, where only peak ground acceleration value is considered.

5. Discussion

The reliability of proposed method was examined by utilizing a large database compiled and updated by several researchers. The results between the capacities and demands indicated that the proposed method appears to work in a reasonably good success. However, the seismic demands for some sites within the database were not checked by the near station records due to lack of available data. For these sites, the seismic demand values were calculated from far field station records (>15 km). The use of these records

provided partially high seismic demand values, due to their relatively close distance to source.

In this study, vertical acceleration records were used to determine the seismic demand values, because high vertical ground accelerations have been mostly recorded in past earthquake events and liquefaction events were observed at these sites, as given table 2 and 3. Bradley (2012) stated that there may be a relationship between the high vertical components of acceleration and soil liquefaction for the 2010-2011 Canterbury earthquake sequence in New Zealand. Extensive liquefaction and re-liquefaction of sandy deposits were observed at Christchurch and Compressive structural damage was evident due to the high vertical accelerations registered with peak surface amplitudes well exceeding a value of 1g (Riches, 2015; Lee et al., 2013; Tsaparli et al., 2016).

Some limitations of the energy-based method are associated with the computation of the capacity values. The predictive equations are based upon a series of laboratory tests and are within their specific data ranges; these generally allow the calculation of the liquefaction energy by employing basic soil parameters. However, these also ignore many soil criteria controlling the liquefaction probability (e.g. percentage of fines content (FC) and grains shape, D_{50}, C_u, etc.).

The liquefaction/non-liquefaction database indicated that the Dief and Figueroa (2001) and Jafarian et al. (2012) predictive equations result in greater capacities than those of Figueroa et al. (1994) and Liang (1995). Although some relationships relating some of soil initial parameters to energy capacity were developed by researchers, they were not utilized due to the limited parameters in the data set for the past earthquakes. Thus, the failure of the proposed method for past significant earthquakes is attributed to these uncertainties.

Yet still, considering that the stress and strain based approaches all have the requirement of determination of the a_{max} for a given site, the energy-based procedure has a clear advantage over those. Even though it is possible to utilize some attenuation relationships, those require correct employment of magnitude and distance values; which bring along some uncertainties like the type of the distance to be utilized (causative fault, hypocentral, epicentral distances) and the attenuation relationship itself. Furthermore, a_{max} at the depth of bedrock needs to be converted to the a_{max} of the surface level for the response analysis of a given site, even for an educated assumption. However the energy-based approach does not need this transformation as the total amount of energy passing through in a soil will remain the same. Finally, the stress and strain based approaches utilize one more parameter that is open to debate between researchers; the average shear stress value is assumed to be 65% for these methods, but some researchers claim that this value may not be correct. In the energy-based approach, on the other hand, no such coefficient is utilized, not even the depth correction and r_d corrections utilized by the stress and strain methods.

The ground acceleration values in the database compiled by different researchers were found to be inconsistent with each other. Besides, as mentioned before, peak ground acceleration values are mostly estimated from ground motion prediction models, despite uncertainties still involved in these models. The authors believe that these limitations in the assessment of liquefaction cannot be properly addressed without adequate consideration of seismological data and in-situ characterization of liquefiable fields. The proposed method seems to be much more capable for far-field ground motions in assessment of liquefaction, contrary to the stress-based approach, where only peak ground acceleration value is considered. This simplified method can be used for assessing the liquefaction potential at any sites by providing the near station records and in-situ characterization of soils.

6. Conclusion

A simplified energy-based approach for determination of soil liquefaction was presented. The proposed method was evaluated using a large database delineated by the previous researches. As a result, the proposed method was found to have great utility in making quick assessments of the liquefaction potential, using only the in-situ data and seismological records. The observations in liquefaction/non liquefaction sites are mostly consistent with the results of the calculations of the proposed method. The near station ground motion records provide reliable results in order to determine seismic demand values. In case of the use of long distance records for a project site, on

the other hand, high seismic demand values for non-liquefiable sites may emerge due to their distances to the source.

The borehole data of sites for liquefaction/non-liquefaction case histories were employed to compute the capacity energy values foreseen by predictive strain energy equations. Results indicate an acceptable performance of the equations to determine the capacity energy values of soils. Comparisons between demand and capacity energies confirmed the hypothesis of the method as well. The demand energy is larger than the capacity energy of the soil for liquefaction sites, or vice versa for non-liquefiable sites.

Different results for capacity values are likely to be obtained from these predictive energy equations, though, since the reliability and the accuracy of the derived equations are high only within their specific data ranges used. Although some other relationships relating soil initial parameters to energy capacity were developed by researchers, they were not utilized due to the limited parameters in the data set for the past earthquakes. The partial failure of the proposed method for those past significant earthquakes is thus attributed to these uncertainties. There is no doubt that the proposed method can be used for pre-design purposes, after checking more actual case histories to demonstrate its accuracy and reliability.

References

Alavi, A. H., Gandomi, A. H. 2012. Energy-based numerical models for assessment of soil liquefaction: Geoscience Frontiers 3(4), 541-555.

Alavi, A. H., Ameri, M., Gandomi, A. H., Mirzahosseini, M.R. 2011. Formulation of flow number of asphalt mixes using a hybrid computational method Construction and Building Materials 25, pp. 1338-1355.

Ambraseys, N. N. 1988. Engineering seismology, Journal of Earthquake Engineering and Structural Dynamics 17, 1, 1-105.

Baziar, M. H., Jafarian, Y. 2007. Assessment of liquefaction triggering using strain energy concept and ANN model, capacity energy: Soil Dynamics and Earthquake Engineering 27, 1056–1072.

Boulanger, R. W., Idriss, I. M. 2012. Probabilistic standard penetration test-based liquefaction-triggering procedure. J Geotech. Geoenviron. 138, 1185–1195.

Bradley, B. A. 2012. Recorded ground motions from the 22 February Christchurch earthquake. In Second Int. Conf. on Performance-Based Design in Earthquake Geotechnical Engineering Taormina, Italy, 28–30 May, pp. 2–13.

Castro, G. 1995. Empirical methods in liquefaction evaluation, Primer Ciclo d Conferencias Internationales, Leonardo Zeevaert, Universidad National Autonoma de Mexico, Mexico City.

Chen, Y.R., Hsieh, S.C., Chen, J.W., Shih, C.C. 2005. Energy-based probabilistic evaluation of soil liquefaction. Soil Dynamics and Earthquake Engineering 25 (1), 55-68.

Çetin, K.O., Seed, R.B., Der Kiureghian, A., Tokimatsu, K., Harder, L.F., Kayen, R.E. 2000. SPT-Based probabilistic and deterministic assessment of seismic soil liquefaction initiation hazard, Pacific Earthquake Engineering Research Report No. PEER-2000/05.

Çetin, K. O., Seed, R. B., Moss, R. E. S., Der Kiureghian, A. K., Tokimatsu, K., Harder, L. F., Kayen, R. E. 2000. Field Performance Case Histories for SPT-Based Evaluation of Soil Liquefaction Triggering Hazard, Geotechnical Engineering Research Report No. UCB/GT-2000/09, Geotechnical Engineering, Department of Civil Engineering, University of California at Berkeley.

Çetin, K.O., Seed, R.B., Der-Kiureghian, A., Tokimatsu, K., Harder, Jr. L.F., Kayen, R.E., Moss, R.E.S. 2004. Standard penetration test-based probabilistic and deterministic assessment of seismic soil liquefaction potential: Journal of Geotechnical and Geoenvironmental Engineering ASCE 130(12),1314–1340.

Çetin, K.O., Seed, R. B., Kayen, R. E,. Moss, R. E. S., Tolga Bilge, H., Ilgac, M., Chowdhury, K. 2016. Summary of SPT Based Field Case History Data. Report No: METU / GTENG 08/16-01, 703p.

Davis, R. O., Berrill, J. B. 1982. Energy Dissipation And Seismic Liquefaction in Sands, Earthquake Engineering And Structural Dynamics 10, 5948

Davis, R. O., Berrill, J. B. 2001. Pore pressure and dissipated energy in earthquakes-Field verification: Journal of Geotechnical and Geoenvironmental Engineering ASCE, 127(3), 269-274.

DeAlba, P. S., Seed, H. B., Chan, C. K. 1976. Sand liquefaction in large-scale simple shear tests: Journal of Geotechnical Engineering Division ASCE, 102(GT9): 909–927.

Dief, H. M., Figueroa, J. L. 2001. Liquefaction assessment by the energy method through centrifuge modeling. In: Zeng, X.W. (Ed.), Proceedings of the NSF International Workshop on Earthquake

Simulation in Geotechnical Engineering. CWRU, Cleveland, OH.

Dobry, R., Ladd, R., Yokel, F., Chung, R., Powell. D. 1982. Prediction of pore water pressure buildup and liquefaction of sands during earthquakes by the cyclic strain method: National Bureau of Standards Building Science Series, US Dept of Commerce, 138 p.

Elgamal, A.W., Dobry, R., Adalier, K. 1989. Small-scale Shaking Table Tests of Saturated Layered Sand-Silt Deposits, 2nd U.S-Japan Workshop on Soil Liquefaction, Buffalo N.Y., NCEER Rep. No. 890032, 233-245.

Fear, C. E., McRoberts, E. C. 1995. Report on liquefaction potential and catalogue of case records. Internal Research Report, Geotechnical Engineering Library, Department of Civil Engineering, University of Alberta, Edmonton, Alberta, Canada, 338.

Figueroa, J.L., Saada, A.S., Liang, L., Dahisaria, M.N. 1994. Evaluation of soil liquefaction by energy principles: Journal of Geotechnical Engineering ASCE, 120(9): 1554–1569.

Finn, W.D.L., Emery JJ, Gupta, Y.P. 1971. Liquefaction of Large Samples of Saturated Sand on a Shaking Table, Proceedings of the 1st Canadian Conference on Earthquake Engineering 97-110.

Green, R.A. 2001. Energy-based evaluation and remediation of liquefiable soils: PhD dissertation, Virginia Polytechnic Institute and State University, Blacksburg, VA.

Gutenberg, B., Richter, C.F. 1956. Magnitude and energy of earthquakes. Annali di Geofisica 9;1-15.

Hatanaka, M., Uchida, A. 1996. Empirical Correlation between Penetration Resistance and Internal Friction Angle of Sandy Soils: Soils and Foundations, 36(4): 1-9.

Hendron, A.J. 1990. The role of precedent, Soil Mechanics and Rock Mechanics in Geotechnical Engineering practice, Proceedings of H. Bolton Seed Memorial Symposium, Edt. J. M. Duncan, 2,83- 110.

Hsu, C., Vucetic, M. 2004. Volumetric threshold shear strain for cyclic settlement, Journal of Geotechnical and Geo environmental Engineering 130, 1, pp. 58-70.

Idriss, I. M., Boulanger, R. W. 2004. Semi-empirical procedures for evaluating liquefaction potential during earthquakes, in Proceedings, 11th International Conference on Soil Dynamics and Earthquake Engineering, and 3rd International Conference on Earthquake Geotechnical Engineering D. Doolin et al., eds., Stallion Press,1, pp. 32–56.

Idriss, I.M., Boulanger, R.W. 2006. Semi-empirical procedures for evaluating liquefaction potential duringearthquakes, Journal of Soil Dynamics and Earthquake Engineering 26, 115-130.

Idriss, I. M., Boulanger, R. W. 2008. Soil liquefaction during earthquakes. Monograph MNO-12, Earthquake Engineering Research Institute, Oakland, CA, 261 pp.

Idriss, I. M., Boulanger, R. W. 2010. SPT-Based Liquefaction Triggering Procedures. Center for Geotechnical Modeling Report NO. UCD/CGM-10/02, CA, 259p.

Ishihara, K., Yasuda, S. 1975. Sand liquefaction in hollow cylinder torsion under irregular excitation. Soils Found 15 (1), 45–59.

Jafarian, Y., Towhata, I., Baziar, M.H., Noorzad, A., Bahmanpour, A. 2012. Strain energy based evaluation of liquefaction and residual pore water pressure in sands using cyclic torsional shear experiments: Soil Dynamics and Earthquake Engineering 35, 13-28.

Jamiolkowski, M., Baldi, G., Bellotti, R., Ghionna V., Pasqualini, E. 1985. Penetration resistance andliquefaction of sands, Proceedings of 11th Int. Conf. Soil Mechanics and Geotechnical Engineering San Francisco, 3, 1891-1896.

Kokusho, T. 2013. Liquefaction potential evaluations: Energy-based method versus stress-based method. Can. Geotech J. 50,1088-1099.

Kokusho, T. 2017. Liquefaction potential evaluations by energy-based method and stress based method for various ground motions: Supplement. Soil Dynamics and Earthquake Engineering 95: 40–47.

Kokusho, T., Mimori, Y. 2015. Liquefaction potential evaluations by energy-based method and stress-based method for various ground motions. Soil Dynamics and Earthquake Engineering 75: 130–146.

Kokusho, T., Mimori, Y., Kaneko, Y. 2015. Energy-Based Liquefaction Potential Evaluation and its Application to a Case History. 6th International Conference on Earthquake Geotechnical Engineering 1-4 November, Christchurch, New Zealand.

Kusumawardani, R., Nugroho, U., Hanggoro Tri Cahyo, A., Lashari. 2015. Cyclic Shear Strain Threshold on Clean Sand due to Cyclic Loading. International Journal of Innovative Research in Science, Engineering and Technology 4(9); 8401-407.

Kunnath, S.K., Erduran, E., Chai, Y.H., Yashinsky, M. 2008. Effect of near-fault vertical ground motions on seismic response of highway overcrossings. J. Bridge Eng. 13, 282–290.

Law, K.T., Cao, Y.L., He, G.N. 1990. An energy approach for assessing seismic liquefaction potential: Canadian Geotechnical Journal 27, 320–329.

Ladd, R.S., Dobry, R., Yokel, F.Y., Chung, R.M. 1989. Pore water pressure buildup in clean sands because of cyclic straining. ASTM Geotechnical Testing Journal 12 (1), 2208-2228.

Lee, R.L., Franklin, M.J., Bradley, B.A. 2013. Characteristics of vertical ground motions in the Canterbury earthquakes. In New Zealand Society for Earthquake Engineering Annual Conf. (NZSEE2013). Wellington, New Zealand: University of Canterbury.

Liang, L. 1995. Development of an energy method for evaluating the liquefaction potential of a soil deposit: PhD dissertation, Department of Civil Engineering, Case Western Reserve University, Cleveland, OH.

Liao, S.C., Veneziano, D., Whitman, R.V. 1988. Regression models for evaluating liquefaction probability, Journal of Geotechnical EngineeringASCE, 114, 4, 389-411.

Martin, G. R. 1975. Fundamentals of Liquefaction Under Cyclic Loading, J. Geotech., Div. ASCE, 101:5, 423-438.

Moss, R.E.S., Seed, R.B., Kayen, R.E., Stewart, J.P., Der Kiureghian, A., Cetin, K.O. 2006. CPT-based probabilistic and deterministic assessment of in situ seismic soil liquefaction potential. J Geotech Geoenviron 132, 1032–1051.

NRC. 1985. Liquefaction of Soils During Earthquakes, National Research Council, National Academy Press, Washington, DC, 240 pp.

NCEER. 1997. Proceedings of the NCEER Workshop on Evaluating Liquefaction Resistance of Soils, Edited by Youd TL and Idriss IM, Technical Report No. NCEER-97-0022.

Oka, F., Yashima, A., Shibata, T., Kato, M., Uzuoka, R. 1994. FEM–FDM coupled liquefaction analysis of a porous soil using an elastic–plastic model Appl Sci Res, 52; 209-245.

Ostadan, F., Deng, N., Arango, I. 1996. Energy-based Method for Liquefaction Potential Evaluation, Phase I. Feasibility Study. U.S. Department of Commerce, Technology Administration, National Institute of Standards and Technology, Building and Fire Research Laboratory.

Papazoglou, A.J., Elnashai, A.S. 1996. Analytical and field evidence of the damaging effect of vertical earthquake ground motion. Earthq Eng Struct Dyn 25, 1109–1137.

Riches, L.K. 2015. Observed earthquake damage to Christchurch city council owned retaining walls and the repair solutions developed. In Proc. of the 6th Int. Conf. in Earthquake Geotechnical Engineering, Christchurch, New Zealand, 1--4 November.

Seed, H.B. 1979. Soil liquefaction and cyclic mobility evaluation for level ground during earthquakes, Journal of Geotechnical Engineering ASCE, 105, 2, 201-255.

Seed, H. B., Idriss, I. M. 1967. Analysis of liquefaction: Niigata earthquake. Proc., ASCE,93(SM3), 83-108.

Seed, H. B., Idriss, I. M. 1971. Simplified procedure for evaluating soil liquefaction potential, J. Soil Mechanics and Foundations Div ASCE 97(SM9), 1249–273.

Seed, H.B., Mori, K., Chan, C.K. 1975. Influence of seismic history on the liquefaction characteristics ofsands, Earthquake Engineering Research Center, University of California, Berkeley, Report No. EERC 75-25.

Seed, H.B., Tokimatsu, K., Harder, L.H., Chung, R. 1984 The influence of SPT procedures in soil liquefaction resistance evaluations, Earthquake Engineering Research Center, University of California, Berkeley, Report No. EERC 84-15.

Seed, H.B., Wong, R.T., Idriss, I.M., Tokimatsu, K. 1986. Moduli and damping factors for dynamic analyses of cohesionless soils: Journal of Geotechnical Engineering 112 (GT11), 1016-1032.

Seed, R. B., Cetin, K. O., Moss, R. E. S., Kammerer, A. M., Wu, J., Pestana, J. M., Reimer, M. F. 2001. Recent advances in soil liquefaction engineering and seismic site response evaluation, Proc. 4th Int. Conf. and Symposiumon Recent Advances in Geotechnical Earthquake Engineering and Soil Dynamics Paper SPL-2.

Shahien, M.,M. 2007. New Procedure To Estimate Liquefaction Resistance From Penetration Resistance Using Field Records. 4th International Conference on Earthquake Geotechnical Engineering June 25-28.

Shibata, T., Oka, F., Ozawa, Y. 1996. Geotechnical aspects of the January 17, 1995 Hyogoken-Nanbu earthquake: characteristics of ground deformation due to liquefaction. Soils Found. (Special Issue), 65–79.

Silver, M.L., Seed, H.D. 1971. Volume change in sands during cyclic loading, Journal Soil Mechanics and Foundation, Div. ASCE, 97, 9, 1171 – 1182.

Skempton, A.W. 1986. Standard penetration test procedures and the effects in sand of overburden pressure, relative density, particle size, aging, and overconsolidation: Geotechnique 21, 305-321.

Tsaparli, V., Kontoe, S., Taborda, D.M.G., Potts, D.M. 2016. Vertical ground motion and its effects on liquefaction resistance of fully saturated sand deposits Proc R Soc A, 472 (2192), p. 21.

Trifunac, M.D., Todorovska, M.I. 1996. Nonlinear soil response—1994 Northridge, California, earthquake. ASCE J. Geotech. Eng. 122, 725–735.

Tokimatsu, K., Yoshimi, Y. 1983. Empirical correlation of soil liquefaction based on SPT N-value and fines content. Soils and Foundations, 23(4), 56-74.

Tokimatsu, K., Kuwayama, S., Tamura, S. 1991. Liquefaction potential evaluation based on Rayleigh wave investigation and its comparison with field behavior, Proc.of 2nd Int. Conf. on Recent Advances in Geotechnical Earthquake Engineering and Soil Dynamics, St. Louis, Missouri, 1:357-364.

Yasuda, S. 1996. Geotechnical aspects of the January 17, 1995 Hyogoken-Nanbu earthquake: Effect of soil improvement on ground subsidence due to liquefaction. Soils Found. (Special Issue), 99–107.

Youd, T. L., Idriss, I. M., Andrus, R. D., Arango, I., Castro, G., Christian, J. T., Dobry, R., Finn, W. D.L., Harder, L. F., Hynes, M. E., Ishihara, K., Koester, J. P., Liao, S. S. C., Marcuson, W. F., Martin, G. R., Mitchell, J. K., Moriwaki, Y., Power, M. S., Robertson, P. K., Seed, R. B., Stokoe, K. H. 2001. Liquefaction resistance of soils: summary report from the 1996 NCEER and 1998 NCEER/NSF workshops on evaluation of liquefaction resistance of soils, J Geotechnical and Geoenvironmental Eng ASCE 127(10), 817–33.

Vucetic, M. 1994. Cyclic Threshold Shear Strain, Journal Geotechnic Engineering 120, pp. 2208-2228.

Zhang, G. 2001. Estimation of liquefaction-induced ground deformations by CPT and SPT-based approaches, Doctor of Philosophy Thesis in Geotechnical Engineering, University of Alberta

Zhang, W, Goh, A.T.C., Zhang, Y., Chen, Y.M., Xiao, Y. 2015. Assessment of soil liquefaction based on capacity energy concept and multivariate adaptive regression splines: Engineering Geology 188, 29-37.

Bulletin of the Mineral Research and Exploration

http://bulletin.mta.gov.tr

Integration of the GNSS method and borehole camera to model the resulting spherical cavity generated by the main charge blast in clay

Denis TEŽAK[a*], Nikola KRANJČIĆ[b], Bojan ĐURIN[c] and Mihaela JURAS[d]

[a]*Jalkovečka 104A, 42000 Varaždin, Croatia*
[b]*University of Zagreb, Faculty of Geotechnical Engineering, Hallerova aleja 7, 42000 Varaždin, Croatia*
[c]*University North, Department of Civil Engineering, Jurja Križanića 31b, 42000 Varaždin, Croatia*
[d]*Adolfa Wisserta 3, 42000 Varaždin, Croatia*

Research Article

Keywords:
GNSS, MASW, Borehole camera, Laser, Clay soil, Spherical cavity.

ABSTRACT

A depth camera was used to record the spherical cavity which occurred during blasting in clay soil. For this purpose, the integration of the Global Navigation Satellite System (GNSS) method was applied in addition to the depth camera and the laser, to determine the resulting spherical cavity. The expanded spherical cavity, formed after the blasting of the explosive charge in the bottom of the borehole, was measured by a depth camera-laser system. The GNSS measurement method was instrumental for obtaining the coordinates of the borehole. The Multichannel Analysis of Surface Waves (MASW) measurement method was also used during the study. Shear wave velocities (V_S) were calculated using MASW method to evaluate the dynamic properties of the clay soil along the in-situ profiles. The results obtained in this way, showed that there was an increase in the stiffness of the surrounding clay soil after blasting. The main objective of the study was to determine the resulting shapes and volume of the occurred cavities. For a more detailed graphical interpretation, an application was developed, which calculates the coordinates, shape and volumes of the formed spherical cavity.

Received Date: 23.10.2019
Accepted Date: 20.04.2020

1. Introduction

Expansions that occur when explosive charge is detonated, have not been sufficiently investigated in the view of the positive effects that its application can produce. This applies to blasting done in soft rocks at different depths below the soil surface to form a spherical cavity and at the same time activating a specific type and mass of the explosive charge. These cavities are most commonly used to install structural members for anchoring foundation and supporting walls and for anchoring underground structures in less solid and soft rocks (Težak, 2018; Težak et al., 2018; 2019).

A detonation of concentrated explosive charge in the clay soil, generates a shock wave supported by the expanding explosion product which creates intense strong pore excess pressure and oscillations in the surrounding area of the explosive charge (Qingwen et al., 2015; Težak et al., 2019). In that case, the natural structure of the clay soil is destroyed, a significant increase in the borehole volume is achieved, generating the spherical cavity and in the adjacent area, the clay soil is significantly compressed and has its density increased (Figure 1) (Zhongqi and Yong, 2003; Težak et al., 2019).

Citation info: Težak, D., Kranjčić, N., Đurin, B., Juras, M. 2020. Integration of the GNSS method and borehole camera to model the resulting spherical cavity generated by the main charge blast in clay. Bulletin of the Mineral Research and Exploration 163, 115-130. https://doi.org/10.19111/bulletinofmre.726391.

**Corresponding author: Denis TEŽAK, dtezak@gmail.com*

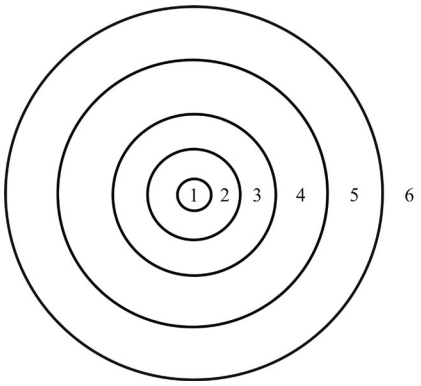

LEGEND:

1. Explosive charge - Area of the explosion
2. Area of the resulting spherical cavity
3. Area of the improvement soil
4. Area of the soil destruction
5. Area of the soil oscillation
6. Surrounding soil area without changes

Figure 1- Performance of explosion in soft rock (Težak et al., 2019).

The cavities generated by the explosive charge are used to incorporate the grout and geotechnical anchor, with the purpose of creating mechanical and adhesion bonds of the surrounding clay soil and grout. The efficiency rate of conducted blasting is measured by volume of the resulting expansion. The use of the standard field and laboratory methods can determine the expansion volume and the compaction of the clay soil, along with changes in the compressive strength, shear strength, density and elasticity modulus in the clay soil after blasting. This research will enable the determination of the improvement of the soil properties depending on the detonation parameters, quantity, and type of explosives. Accordingly, with the determination of the influence of the above-mentioned blasting parameters on the shape and volume of the implemented extension, suggestions will be proposed for recording and measuring the resulting expansion. (Težak, 2018).

Cavities resulting from blasting in clay soil were different in shape and size. In the case of homogeneous clay soils, it is basically a sphere-shaped extension (Araya et al., 1993). The spherical cavities for the given diameter and depth of the boreholes were a result of detonating of Permonex V19 and Pakaex explosives (Ester, 2005). During the research, it was necessary to determine the shape and calculate the volume of the formed cavity after activating the explosive charge at a certain depth of a 131 mm diameter borehole (Mesec et al., 2015; Težak, 2018; Težak et al., 2018).

The Multichannel Analysis of Surface Waves (MASW) is a seismic geophysical method which results allow the estimation of soil stiffness directly related to the shear modulus, which is one of the most important engineering parameters. This method was introduced into geophysical research in the late 1990s (Park et al., 1999) and became the subject of many researches and found application in many branches of science. Depending on the problem we need to solve, the MASW method is used in one dimension (1D) or sounding, two dimensions (2D) or tomography and in three dimensions (3D). The MASW method employs low-frequency (1-30 Hz) surface waves that have a dispersion property, and the depth of the survey ranges from several meters to several tens of meters. It is basically an engineering seismic method whose operating frequency range is from several Hz up to tens of Hz (3-30 Hz). Recording is done by multiple channels (24 or more), and the geophone layout can be set so that the distance between them is between several meters to several hundred meters (2-200 m). Passive and active MASW method can be distinguished. The passive MASW research method provides more depth of testing, while active method research is a more common type that gives 2D V_s profiles and is more prevalent in engineering projects than the passive method. The active MASW method adopts the conventional method of exploration with the use of an active seismic source (i.e. a hand hammer or a guide hammer) and fields of linear receivers (geophones), thus collecting data in a roll-along mode. It uses surface waves that propagate horizontally across the measurement surface, directly from the source to the receiver. Also, it provides V_s velocity information in 1D (depth) or 2D (depth and surface) formats in a cost-effective and time-efficient manner. The maximum depth of the survey is generally in the range of 10 to 30 m, but this may vary depending on the type of active seismic source used (Akgün et al. 2013; Pamuk et al. 2018). In this article, the MASW method was used to evaluate the dynamic properties of clay soil according to the depth of the profile before and after blasting.

For this purpose, a system for observation, measuring and calculating the shape and volume of the resulting cavities was designed and developed. The

system includes an instrumental and programming part, where a designed application enables detailed graphical interpretation of the cavity in 2D and 3D views, along with the borehole coordinates and resulting cavity volume calculations (Težak, 2018; Težak et al., 2018; 2019). The system also represents the integration of the GNSS measurement method (Official Gazette, 110/2004, 114/2004), a depth borehole camera (http://www.geovision.org/) and laser (EDS-C) (https://dimetix.com/en/?product=eds-c).

2. Previous Research

In the late 1980s, some research was carried out to determine the possibility of applying anchoring and anchoring extensions to structures built in soft soil (Hudec et al., 1989). Excavation through soft rock is one of the most complex tasks in the construction of underground structures and tunnels. Attempts have been made to develop procedures that can facilitate the fabrication of underground structures in rocks that, by their geotechnical characteristics, are soil. Almost all prior anchoring methods used reinforcing steel bars, pipes or prestressing cables, with the use of cement or plastics for injection and have not been sufficiently successful at anchoring to be made in clay, loam or similar soft or earthy materials. The anchors are made in the form of rigid profiles, or in the form of steel cables (Muhovec, 1987). The aforementioned procedure is protected by a patent, based on the fact that the explosion of a certain mass of explosives, located in a borehole of coherent soil, results in a limited expansion of the most commonly shaped sphere. Its volume depends on the mass and type of explosive used and of course on the geotechnical characteristics of the soil (Frgić et al., 1988; Bakr, 2019; Soltani et al., 2019).

Using generally known construction methods, it is possible to effectively improve the geotechnical characteristics of soft soils. Explosive Compaction (EC) is a soil modification technique where, in a borehole, energy released by detonation is used to compress soft soil. The effectiveness of EC depends on the type and size of soft soil grain and the type of explosive charge. The studies were conducted at thirteen work sites in the world where the EC method was successfully applied. It was concluded that the density, stability and strength of soft soil can be improved with the help of EC. Processing the field data obtained, EC efficiency was observed for unstable and liquefiable deposits with particle sizes ranging from gravel to dry sand with less than 10% clay (Shakeran et al., 2016; Težak et al., 2019).

However, EC is still less commonly used to improve the geotechnical features of soft soil than conventional construction methods, such as vibro methods, Deep Soil Mixing (DSM), Deep Dynamic Compaction (DDC) or jet grouting (Težak, 2018; Težak et al., 2019).

A review of the available literature has not documented systematic studies that define the impact of technical characteristics of explosives on the formation of spherical cavity at a certain depth of clay soil after blasting of explosive charge. No research has been found to define a method for determining the shape and volume of the resulting spherical cavity.

However, a new and 3D visualization in exploration borehole, to record natural discontinuities in rock, has been developed. The method is 3-D visualization of fracture distributions in volumes close to boreholes for well planning, reservoir-scale fracture model building, reservoir flow simulation, and hydraulic fracture control discontinuities (Wu and Pollard, 2002).

Also, Schepers et al. (2001) investigated characteristics of the rock structure, and defined the common meaning of core images and images of acoustic borehole wall.

The developed BoreIS application was studied and introduced. This software was developed as an extension to ESRI's ArcScene three-dimensional (3D) GIS environment. BoreIS interactive manipulation of terms in complex queries, simple addition of contoured surfaces, and masking by lithology or formation helps geologists find spatial patterns in their data, beyond the limits of data tables and flat maps (McCarthy and Graniero, 2006; Težak, 2018).

Based on available literature, it was imperative to develop an application and a unique method for computing the volume and 3D representation of the resulting spherical cavity. The described method demonstrates the integration of GNSS measurement data and data obtained by measuring with a borehole camera and laser (Težak, 2018; Težak et al., 2019).

3. Field Survey and Geotechnical Research

Survey and geotechnical field research were carried out on exploitation field Cukavec II during 2014, 2015 and 2016. The exploitation field Cukavec II is located in the vicinity of Varaždin (Figure 2). During the field research, the polygon in question was recorded and boreholes were staked out by the GNSS method. The modern blasting technique and technology was also used, and the newly developed application and AutoCad Civil 3D were used to processing the obtained data (Težak, 2018; Težak et al., 2019).

The importance and contribution of the application are reflected in the use of open source technology, and in compatibility with commercial tools and the ability to connect to other systems through a variety of interfaces. Additionally, the application involves using web technology that enables secure login to the system from any computer, tablet, cell phone, or other similar device connected to the internet. All the data that users collect and enter into the system are immediately available to all remaining process participants. The concept and possibilities of the application in the technical field are innovative. The application calculates and draws 2D and 3D models of the resulting cavity. The compatibility of the application with other CAD tools gives a more detailed 3D cavity expansion model. The presented method and application, measure and calculate the volume of the resulting cavity expansion, which helps engineers and geotechnicians to build and run overhead and underground structures in clay much more economically (Težak, 2018).

3.1. Survey Field Research

In order to define 3D coordinates of boreholes (MB1 to MB8, MB13 to MB45 and PMB1 to PMB6), a RTK GNSS method based on CROPOS (CROatian POsitioning System) was used. The positioned boreholes are shown in figure 3 (Težak, 2018; Težak et al., 2018; 2019).

Real-Time Kinematic (RTK) is a method where relative coordinates of an unknown point, in respect to the known one, are determined a moment after placing the rover on that point. The only limitation of the method is the distance range of radio connection which is resolved by implementing VRS (virtual reference stations) in CROPOS (Figure 4) (Pribičević and Medak, 2003; Težak et al., 2018).

The position of the boreholes is defined with the GNSS receiver TOPCON HiPer+ (Figure 5), with main technical features of the accuracy of RTK horizontal measurement H= 10mm+1ppm and accuracy of RTK vertical measurement V= 15mm+1ppm. The horizontal position of the surveying profile of boreholes is staked out in official reference coordinate system HTRS96/TM.

Figure 2- Location of exploitation field Cukavec II.

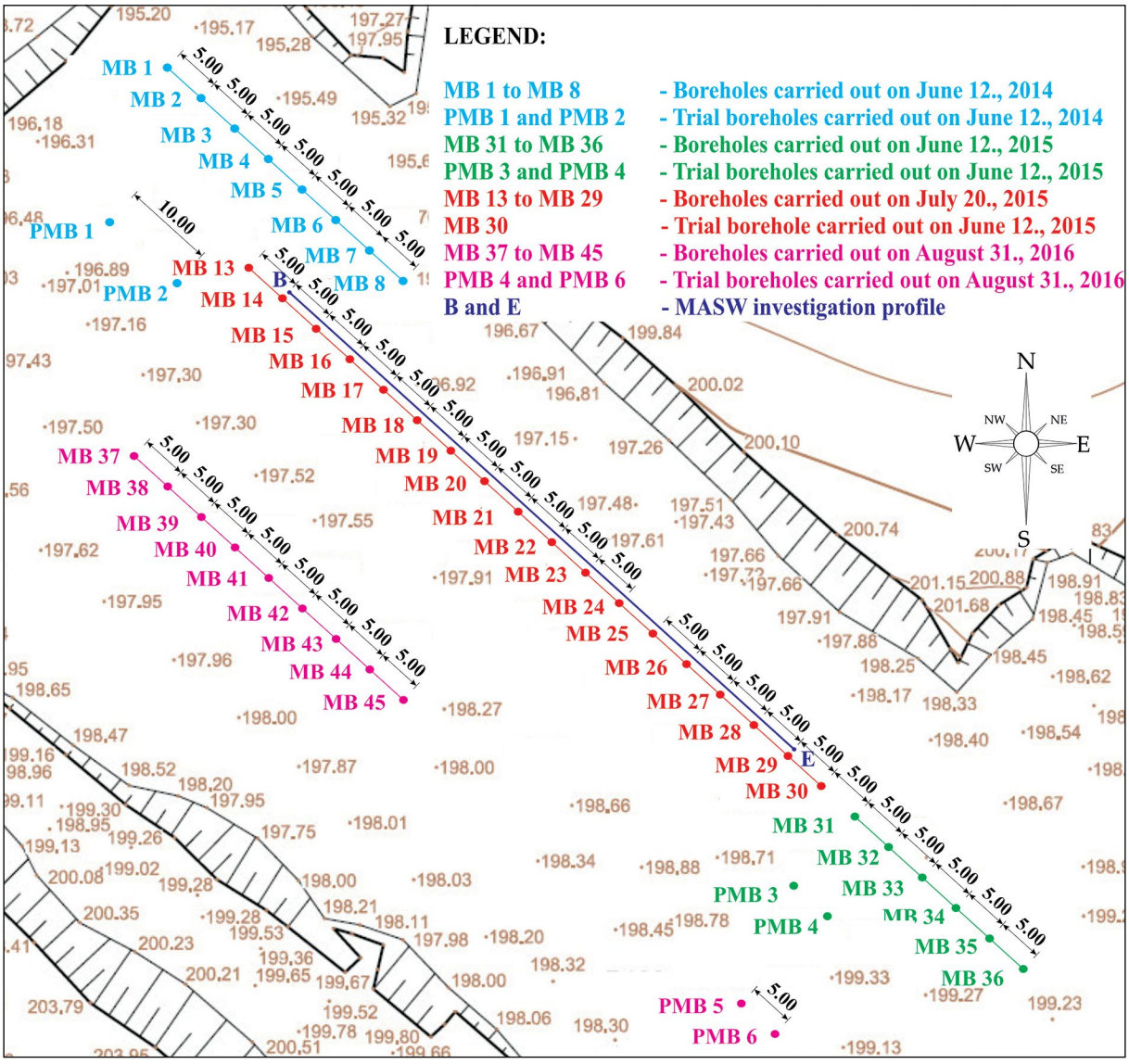

Figure 3- Exploitation field Cukavec II and positioned boreholes (Težak, 2018; Težak et al., 2019).

Preceding to blasting was the measurements of characteristic field points to make up a geodetic map. In order to stake out mine boreholes, they need to be defined on a surveying map. Boreholes are defined 5 meters apart and each has its own unique name. That way every borehole a has name, E and N coordinate. All boreholes are transferred to specific file in the format: NAME, E coordinate, N coordinate, h coordinate where the h coordinate is equal to zero for all entries.

Next step before blasting is staking out boreholes and evaluating the results of staking out. The processing of staked out data was done in TopoSURV v.8.2. Results are shown in table 1. From table 1 one can see that stake out points are almost the same as projected values. A conclusion based on the results from table 1 is that stake out points have great accuracy for blasting.

3.2. Geotechnical Field Research

Geotechnical field research has gathered useful data on soil layers at depth using geophysical seismic methods and in-situ testing of the dynamic properties of clay soil. Presented methods were implemented for better insight into the clay soil.

Before carrying out the investigations made at in the exploitation field Cukavec II, laboratory tests

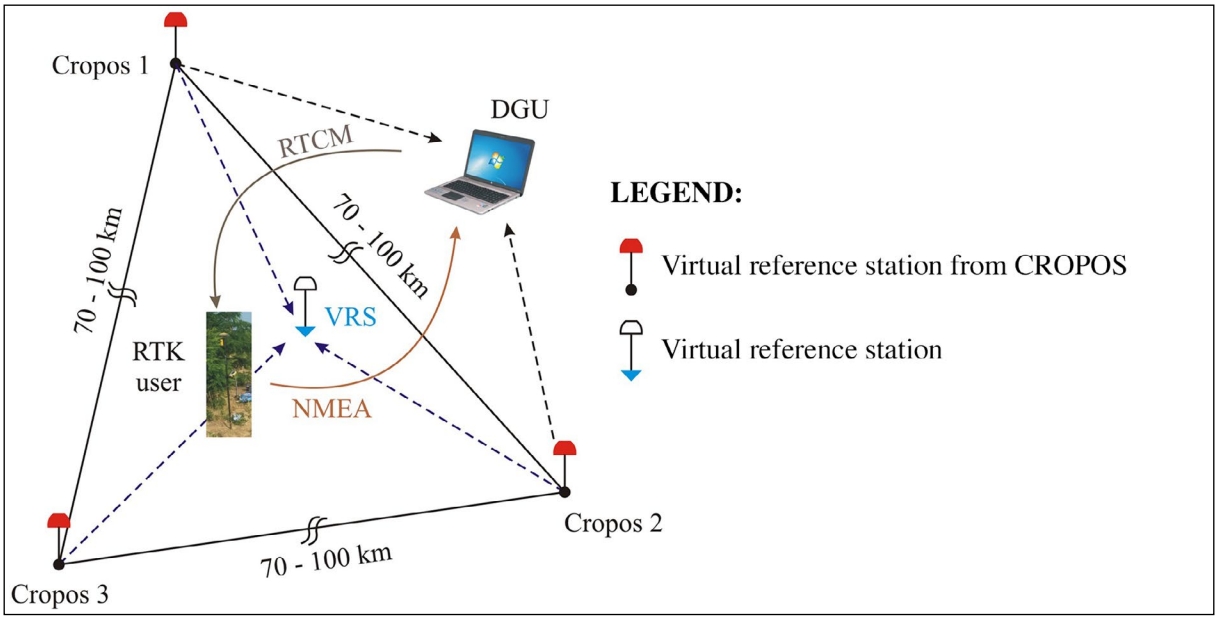

Figure 4- Principle of the virtual reference stations (Težak et al., 2018).

Figure 5- GNSS receiver-Topcon HiPer+.

were carried out on clay soil. Based on laboratory tests, a shear modulus G was obtained which, in small deformations, is directly related to the shear wave velocity V_s.

3.2.1. Geophysical Field Research

Shear wave velocity (V_s) was measured to estimate the dynamic properties of the soil by profile depth with Multichannel Analysis of Surface Waves (MASW) method (Gabriels et al., 1987; Park et al., 1999).

In refraction analysis, the travel times of the first arrival on each geophone was used. The geophones were arranged in a row along the profile (Figure 3 and 6). The record length and sample interval are the most sensitive parts of the measurement interpretation.

Investigation profiles were placed directly next to the line that connects the boreholes (Figure 6). Receiver spread for the MASW profile consisted of 24 vertical 4.5 Hz geophones, with the receiver spaced out 3.0 m. The depth of penetration for the surface wave for this particular survey was 30 m. For this purpose, fundamental mode and first higher mode of the dispersion curve are used. Experimental dispersion curve measured on the site was interpreted using SeisIMAGER 4.0.1.6. OYO Corporation 2004-2009 computer software (Strelec et al., 2019).

As typical seismic profiles shown are those which were performed in 2015. During field seismic surveys, a total of 2 seismic profiles were performed in 2015 using the MASW method. The profiles were placed in a line across the center of the borehole, and each profile included 15 boreholes with an average depth of 2.5 meters, and at a distance of 5 meters. MASW method was carried out before and after the activation of the explosive charge.

The MASW method gathered data, among other things, about the S wave velocities of the profiles. For the purpose of this article, changes in the velocity of S waves in profile 2 are presented. Figures 7 and 8 show 2D V_s - Depth graph on profile 2, before and after blasting.

Table 1- The comparison of projected and stake out values.

Borehole	Projected values		Stake out values		Distinction between projected and stake out values	
	E coordinate (HTRS96/TM) (m)	N coordinate (HTRS96/TM) (m)	E coordinate (HTRS96/TM) (m)	N coordinate (HTRS96/TM) (m)	ΔE (cm)	ΔN (cm)
MB1	489450.00	5122751.77	489449.97	5122751.77	-3	0
MB2	489453.79	5122748.40	489453.83	5122748.38	4	-2
MB3	489457.47	5122745.07	489457.46	5122745.05	-1	-2
MB4	489461.22	5122741.75	489461.23	5122741.75	1	0
MB5	489464.88	5122738.43	489464.84	5122738.44	-4	1
MB6	489468.61	5122735.08	489468.57	5122735.08	-4	0
MB7	489472.40	5122731.76	489472.41	5122731.77	1	1
MB8	489476.12	5122728.26	489476.14	5122728.24	2	-2
MB13	489075.02	5122634.35	489075.01	5122634.34	-1	-1
MB14	489078.74	5122631.02	489078.74	5122631.02	0	0
MB15	489082.47	5122627.68	489082.45	5122627.68	-2	0
MB16	489086.20	5122624.35	489086.21	5122624.35	1	0
MB17	489089.92	5122621.01	489089.93	5122621.01	1	0
MB18	489093.65	5122617.68	489093.64	5122617.65	-1	-3
MB19	489097.37	5122614.35	489097.39	5122614.36	2	1
MB20	489101.10	5122611.01	489101.10	5122611.00	0	-1
MB21	489104.83	5122607.68	489104.82	5122607.66	-1	-2
MB22	489108.55	5122604.34	489108.54	5122604.32	-1	-2
MB23	489112.28	5122601.01	489112.28	5122601.01	0	0
MB24	489116.00	5122597.68	489116.00	5122597.67	0	-1
MB25	489119.73	5122594.34	489119.76	5122594.34	3	0
MB26	489123.46	5122591.01	489123.46	5122590.98	0	-3
MB27	489127.18	5122587.67	489127.18	5122587.67	0	0
MB28	489130.91	5122584.34	489130.90	5122584.32	-1	-2
MB29	489134.63	5122581.00	489134.66	5122580.99	3	-1
MB30	489138.36	5122577.67	489138.35	5122577.65	-1	-2
MB31	489142.09	5122574.34	489142.09	5122574.35	0	1
MB32	489145.81	5122571.00	489145.81	5122570.99	0	-1
MB33	489149.54	5122567.67	489149.53	5122567.63	-1	-4
MB34	489153.26	5122564.33	489153.27	5122564.36	1	3
MB35	489156.99	5122561.00	489156.98	5122560.99	-1	-1
MB36	489160.72	5122557.67	489160.70	5122557.69	-2	2
MB37	489059.52	5122615.00	489059.48	5122615.04	-4	4
MB38	489063.24	5122611.74	489063.20	5122611.77	-4	3
MB39	489066.97	5122608.38	489066.96	5122608.40	-1	2
MB40	489070.71	5122605.03	489070.67	5122605.06	-4	3
MB41	489074.43	5122601.75	489074.40	5122601.77	-3	2
MB42	489078.13	5122598.39	489078.13	5122598.41	0	2
MB43	489081.86	5122595.05	489081.84	5122595.04	-2	-1
MB44	489085.61	5122591.71	489085.60	5122591.75	-1	3
MB45	489089.30	5122588.35	489089.26	5122588.39	-4	4
PMB1	489445.79	5122735.66	489445.79	5122735.62	0	-4
PMB2	489453.24	5122729.03	489453.24	5122729.04	0	1
PMB3	489127.98	5122573.54	489127.98	5122573.54	0	0
PMB4	489133.55	5122568.55	489133.55	5122568.55	0	0
PMB5	489126.59	5122555.03	489126.55	5122555.03	-4	0
PMB6	489130.32	5122551.69	489130.32	5122551.70	0	1

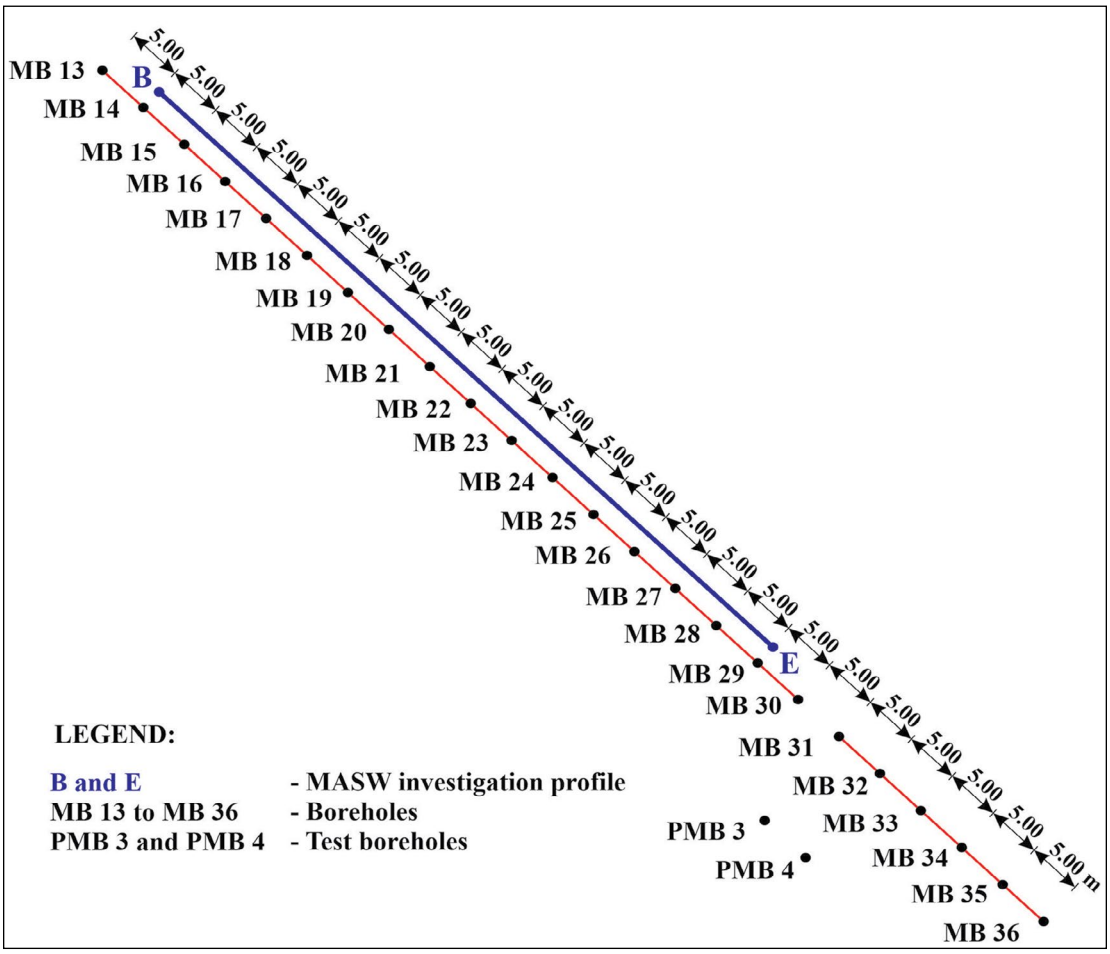

Figure 6- Geodetically determined MASW profile on the exploitation field Cukavec II in 2015.

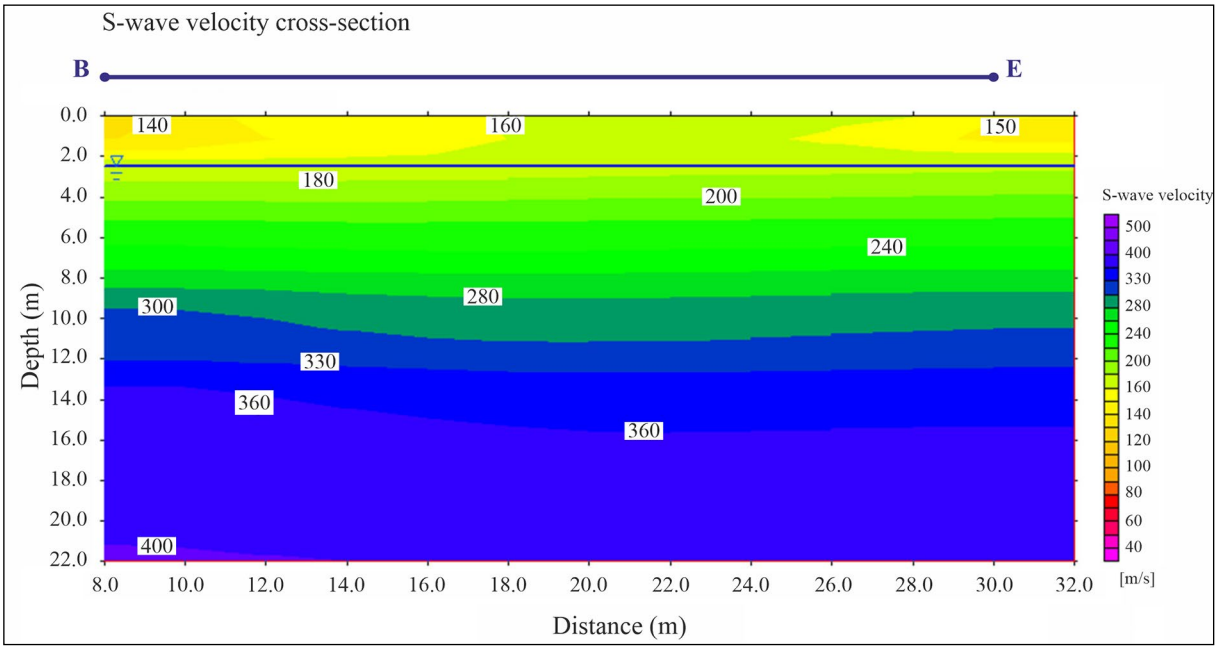

Figure 7- 2D V_s - Depth graph on profile 2 before blasting.

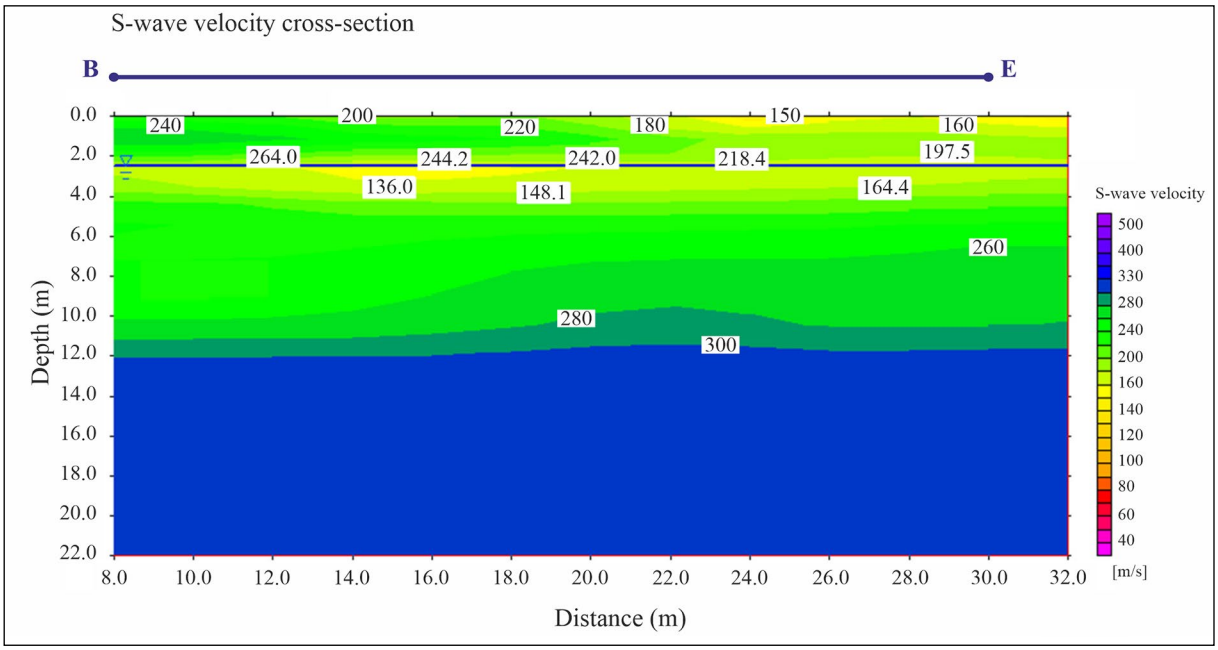

Figure 8 - 2D V_s - Depth graph on profile 2 after blasting.

Based on the above 2D V_s - Depth graph, figures 7 and 8, by comparison of the S wave velocities are shown before and after blasting. It shows that the activation of explosive charges resulted in an increase in S wave velocities at an average depth of 2.0 m to 3.0 m, which leads to a conclusion that there is an increase in the stiffness of the surrounding clay soil after blasting. A detailed MASW analysis is presented in the PhD thesis, Težak, 2018 and in a published article by Strelec et al., 2019.

3.2.2. Trial Blasting to Determine the Optimum Quantity of Explosive Charges Used to Produce Spherical Cavities in Clay Soil

During the trial blasting, effective quantities were determined for the used explosive charges, which produced spherical cavities in the clay soil. For a given borehole diameter of 131 mm and a depth of 2.00 - 3.00 m, a spherical cavity can be made with explosive charges Pakaex and Permonex V19 (Figure 9), ranging in mass from 0.2 to 1.6 kg. Detonation velocity for

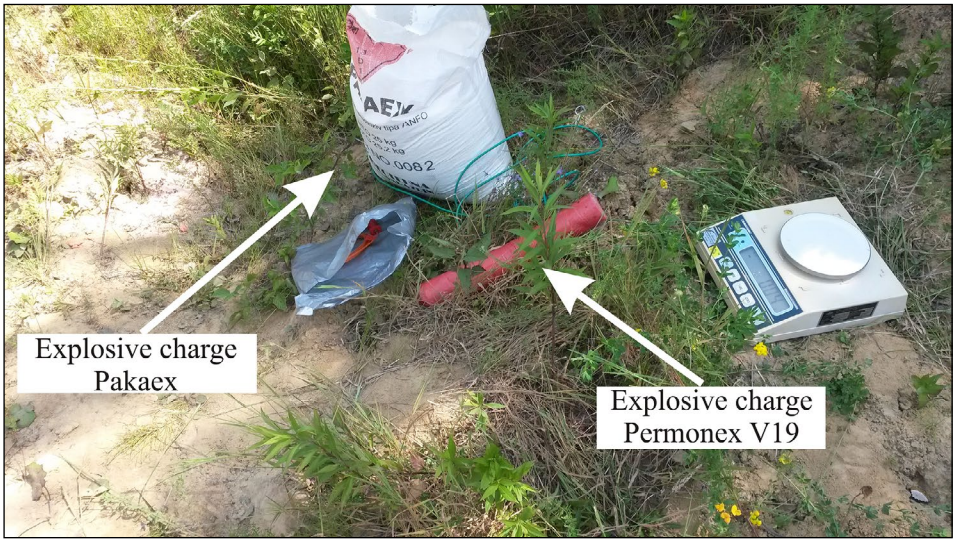

Figure 9- Explosive charge, Permonex V19 and Pakaex (Težak, 2018).

the Permonex V19 was determined in the accredited Explosive Materials Laboratory at the Faculty of Mining, Geology and Petroleum Engineering. The detonation velocity of Permonex V19 is 4500 m/s and that of Pakaex 2950 m/s (Ester, 2005). Activation of the blast field was performed by the NONEL system via instantaneous electric detonators (IED). The ideal size of the sand stem was 0.5 m, and made of stone material grain size of 0/4 mm. The construction of the borehole explosive loading is shown in figure 10a. Figure 10b shows the moment of activation of the explosive charge, and figure 10c shows a schematic representation of the resulting spherical cavity (Težak, 2018; Težak et al., 2018; 2019).

3.2.3. Determination of the spherical cavity

- Heavy Duty GeoVision Borehole Camera was used to record spherical cavities after blasting,

- EDS-c laser was used to determine the distances of the resulting expansion,

- The volumes of spherical cavities obtained by the activation of individual blastholes were determined by an integrated system, a Heavy Duty GeoVision Borehole Camera to which the EDS-C laser was added (Figure 11).

4. Integration of RTK GNSS Methods with Borehole Camera and Laser System

Determining the shape and volume of the spherical cavity was the main reason for developing a unique method of observation.

The integration of the RTK GNSS measurement method, depth camera and laser is the basis of the unique method of the observation. The application was developed to calculate the coordinates of boreholes based on the known E and N coordinates (obtained by GPS device) and the height H obtained by using a depth camera. In order to be able to calculate all the coordinates of boreholes at a certain depth of shooting, a laser was also used to obtain distances between the depth camera and the walls of boreholes. In this way, input data was obtained for the application, which calculated the coordinates, plotted the characteristic cross sections, and finally calculated the volume of the resulting spherical cavities of each borehole (Figure 12).

4.1. The Records of the Depth Camera and Laser

Depth camera shooting is designed in such a way that the depth camera rotates 360° clockwise at a

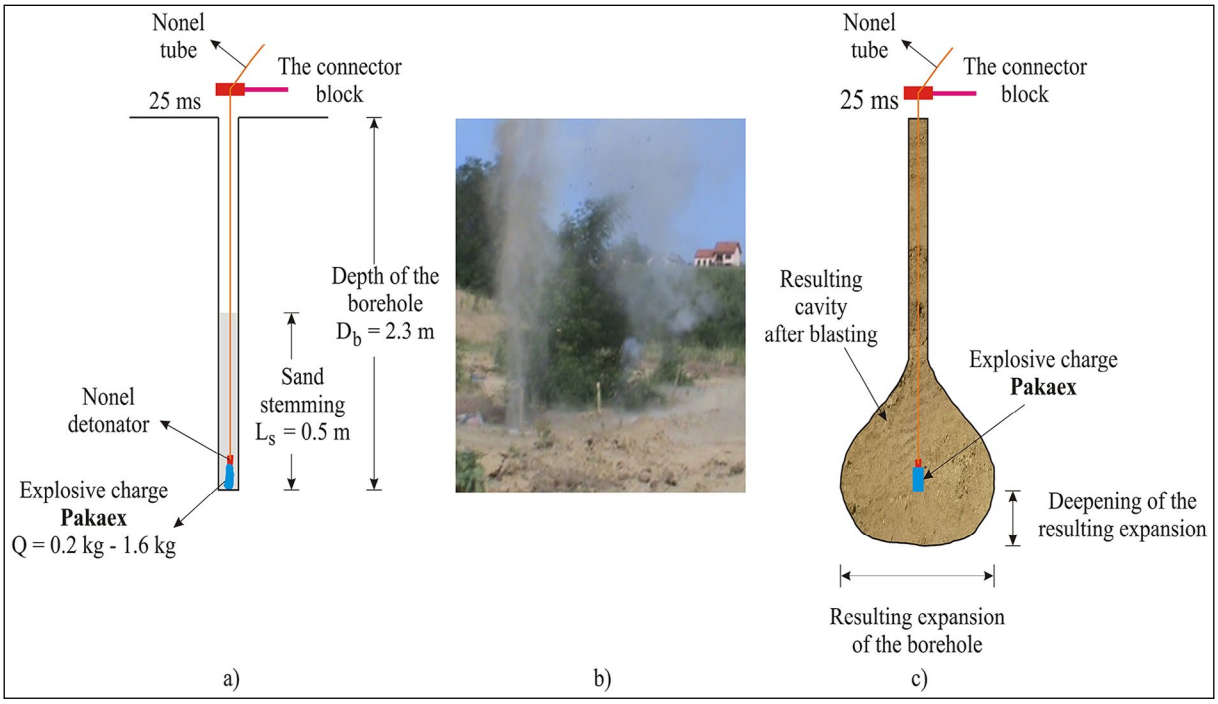

Figure 10- a) Shows the construction of the borehole, b) shows the moment of the activation of the explosive charge and c) shows the resulting spherical cavity after the explosive charge is activated (Težak et al., 2019).

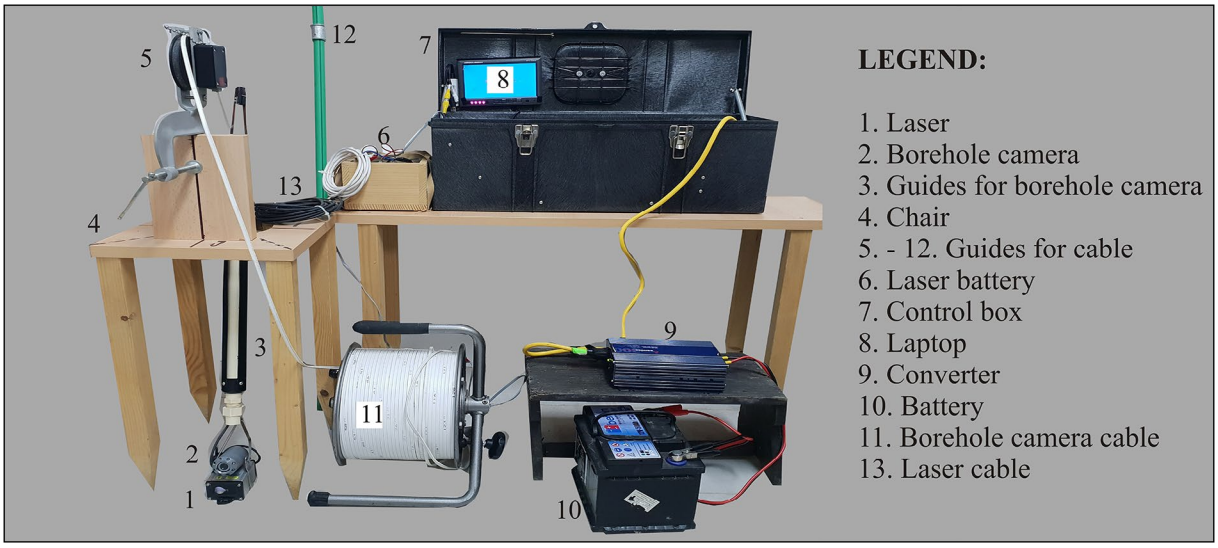

Figure 11- Spherical expansion measurement equipment (Težak, 2018).

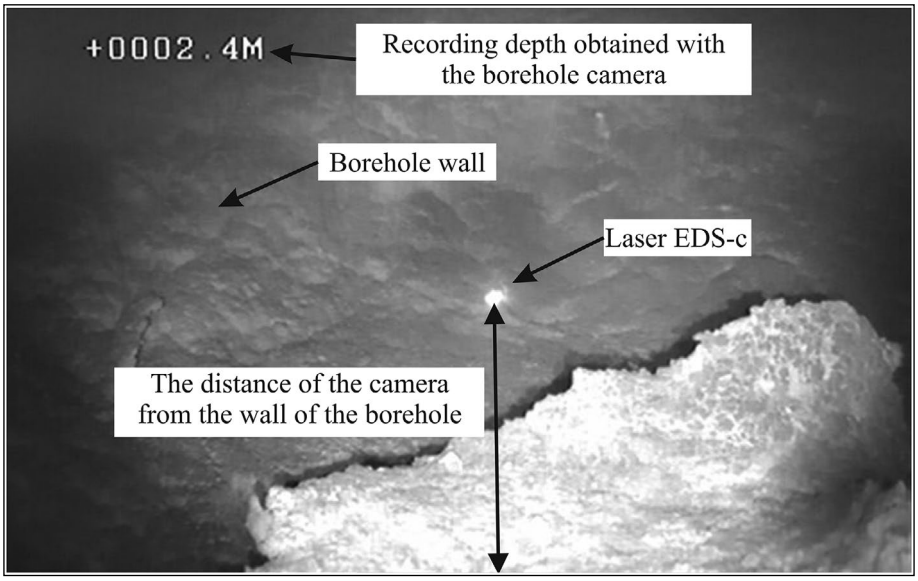

Figure 12- Depth camera snapshot of the spherical expansion (Težak et al., 2019).

shooting interval of 45° (Figure 9). The characteristic recording depths for every borehole was determined by detailed analysis of in-situ measurements. The result (Figure 12) and the laser-obtained distance, at characteristic recording depths, are recorded in the measurement log. The obtained data from the field, were entered into application for detailed processing. The application calculates the volume of the resulting spherical cavities and provides the ability to draw the entire borehole as well as the resulting cavity in 2D and 3D views. The application was defined to calculate and export coordinates of the cross section of the borehole in AutoCad Civil 3D. In this way, the accuracy of the application can be tested with AutoCad Civil 3D tools. More accurate 3D representation of the resulting extensions was obtained, i.e. an entire mine borehole with integration of measurement data, AutoCad Civil 3D tools, and designed applications (Težak, 2018; Težak et al., 2018; 2019).

5. Measurement Results Obtained and Processed

During the course of the research, encouraging field and cabinet results were achieved (Table 2). Knowledge about the effects of explosive charge in

Table 2- Obtained and processed data for spherical cavity after blasting (Težak et al., 2019).

Pakaex					Permonex V19				
Borehole	**Explosive charge mass**	**Volume of the resulting cavity**	**Resulting expansion of the borehole**	**Deepening of the resulting expansion**	**Borehole**	**Explosive charge mass**	**Volume of the resulting cavity**	**Resulting expansion of the borehole**	**Deepening of the resulting expansion**
	Q (kg)	**V_{rc} (m^3)**	**L_{re} (m)**	**D_{re} (m)**		**Q (kg)**	**V_{rc} (m^3)**	**L_{re} (m)**	**D_{re} (m)**
MB20	1.00	0.7100	1.1570	0.5200	MB24	0.80	0.6184	1.1900	0.3100
MB41	1.00	0.8095	1.1110	0.6000	MB26	0.80	0.5690	1.1310	0.3600
MB34	0.80	0.3935	0.9530	0.3300	MB45	0.80	0.7405	1.0700	0.4000
MB18	0.80	0.3440	0.8770	0.4600	PMB5	0.80	0.7227	1.0710	0.4200
MB19	0.80	0.3626	0.8750	0.4800	MB23	0.60	0.5276	1.1040	0.3500
MB40	0.80	0.5190	1.0600	0.4000	MB25	0.60	0.6330	1.0850	0.2900
MB35	0.60	0.2555	0.7830	0.2500	PMB6	0.60	0.6151	1.1520	0.3500
MB17	0.60	0.6160	1.0430	0.3400	MB36	0.40	0.1135	0.6930	0.2300
MB39	0.60	0.3785	1.0880	0.4000	MB21	0.40	0.2925	0.9360	0.2600
MB15	0.40	0.2445	0.6980	0.3100	MB27	0.40	0.2160	0.5850	0.3200
MB16	0.40	0.1945	0.7870	0.3000	MB43	0.40	0.2815	0.8660	0.3000
MB38	0.40	0.2980	0.8480	0.4000	MB22	0.20	0.0825	0.5570	0.2600
MB13	0.20	0.1005	0.5760	0.1800	MB28	0.20	0.0700	0.5050	0.2200
MB14	0.20	0.0645	0.5770	0.2200	MB42	0.20	0.1480	0.6620	0.2000
MB29	0.20	0.0980	0.6870	0.2400					
MB37	0.20	0.1175	0.6010	0.2500					

clay soil and the possibility of using a particular type of explosive in geotechnical practice were expanded. In particular, this relates to blasting in soft rocks at different depths below the soil surface by activating a specific type and mass of explosives to form spherical cavities. The conducted field research and innovation in the field data processing has led to a sufficient amount of quality data, which enabled the development of the presented application (Težak, 2018).

The development of CROPOS systems in the Republic of Croatia has led to a strong development of applications that use GNSS data. Since then, the data is obtained in real-time. Comparing the projected values and the field measurements, we can conclude that GNSS data can be used for the purposes of determining the coordinates of blasting in clay soil. The Heavy Duty GeoVision Borehole Camera and EDS-c laser is a system that integrates well with the GNSS measurement data. Such a system, along with its associated application, is an advanced system for modeling blasting in clay soil and blasting in general.

5.1. Examples of Resulting Volume of Spherical Expansion

Thanks to a well-established research plan, encouraging results of the spherical expansion were obtained by field research, and after processing of the results, the volumes of spherical expansion were calculated more accurately. The knowledge about the effect of explosive charge in clay soil and the possibility of using a particular type of explosive in geotechnical practice have also been expanded (Težak, 2018; Težak et al., 2018; 2019).

The significance and contribution of the application is reflected in the use of Open Source Technologies, and on the other hand, in its compatibility with commercial tools and the ability to connect to other systems through a number of interfaces. It adds value to the use of web technologies to enable secure login to the system from any computer, tablet, mobile phone or other similar device connected to the Internet. All data that users collect and enter into the system is immediately accessible to all remaining process participants (Težak, 2018).

Also, the compatibility of the application with other CAD tools will greatly contribute to the verification and more detailed 3D model of the resulting expansion (Težak, 2018).

Listed below are examples of measured spherical cavities after activation of explosive charge in the Cukavec II exploitation field in 2014, 2015 and 2016,

with the integration of RTK GNSS measurements, depth camera, and laser. Examples also show the accuracy of calculating the volume of a spherical cavity using an application and the AutoCad Civil 3D tool. In figures 13 and 14, an example from 2014 is given. Figures 15 and 16 show 2015 examples, and figures 17 and 18 show 2016 examples (Težak, 2018).

Example 1.

Borehole MB8 (*E 489476.12 N 5122728.26 H 196.24*). Explosive charge, Permonex *1.0 kg*, Stemming length *1.0 m* (*0.5 m* sand and *0.5 m* clay). Spherical cavity, AutoCad Civil V_{ACAD} = *842.00 dm³*, Application $V_{application=}$ *828.95 dm³*. **Distinction** $V_{distinction=} V_{ACAD}$- $V_{application}$=*13.05 dm³.*

Example 2.

Borehole MB31 (*E 489142.09 N 5122574.35 H 198.49*). Explosive charge, Permonex V19 *0.2 kg*, Stemming length *0.3 m* (sand). Spherical cavity, AutoCad Civil 3D V_{ACAD} = *81.00 dm³*, Application $V_{application=}$ *77.00 dm³*. Distinction $V_{distinction=}$ V_{ACAD}- $V_{application}$= *4 dm³*.

Example 3.

Borehole MB38 (*E 489063.24 N 5122611.74 H 197,45*). Explosive charge, Pakaex *0.4 kg*, Stemming length 0.5 m (sand). Spherical cavity, AutoCad Civil 3D V_{ACAD} = *304.00 dm³*, Application $V_{application=}$ *292.10 dm³*. Distinction $V_{distinction=}$ V_{ACAD}- $V_{application}$= *11.90 dm³*.

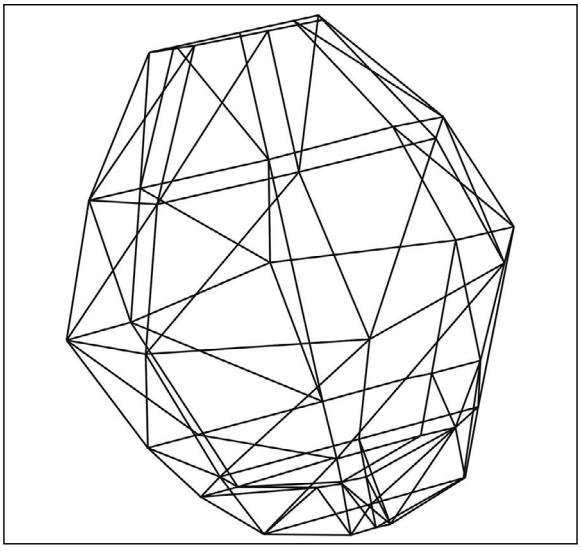

Figure 13- Linear 3D model of the resulting cavity, Borehole MB8, application.

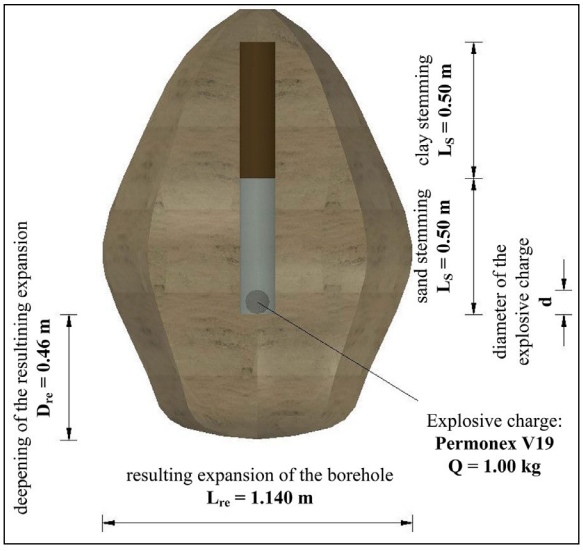

Figure 14- 3D model of the resulting cavity, Borehole MB8, AutoCad Civil 3D.

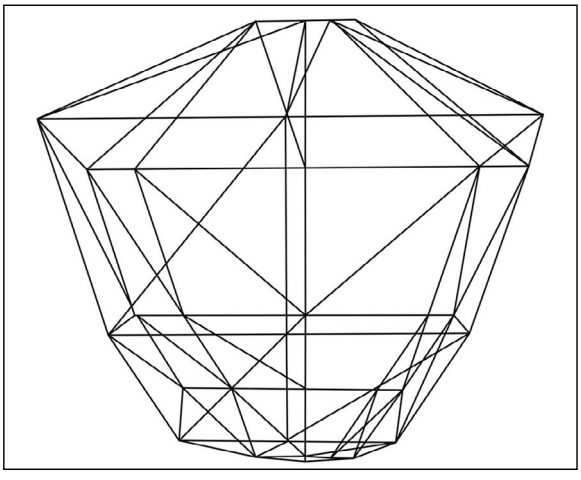

Figure 15- Linear 3D model of the resulting cavity, Borehole MB31, application.

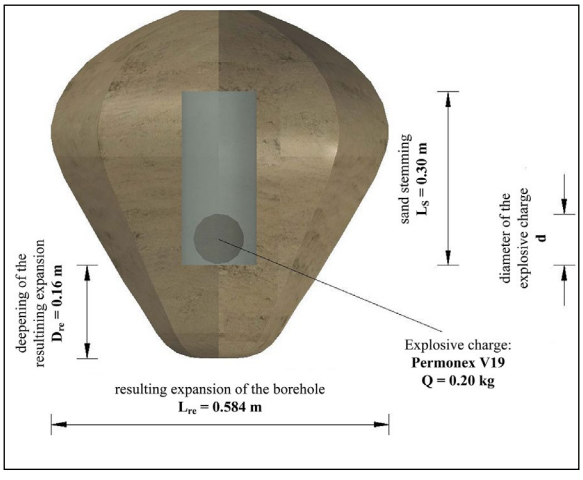

Figure 16- 3D model of the resulting cavity, Borehole MB31, AutoCad Civil 3D.

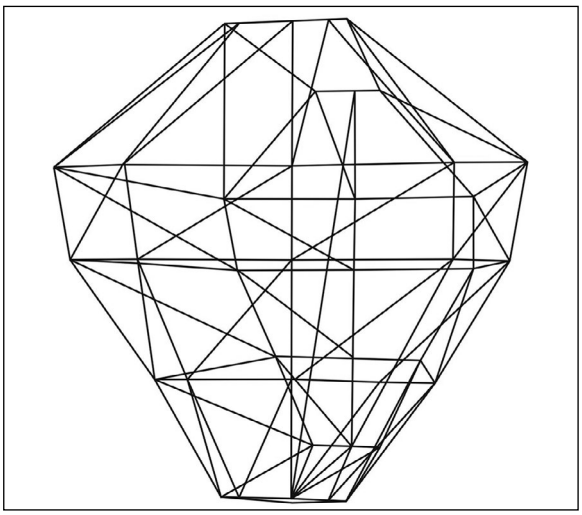

Figure 17- Linear 3D model of the resulting cavity, Borehole MB38, application.

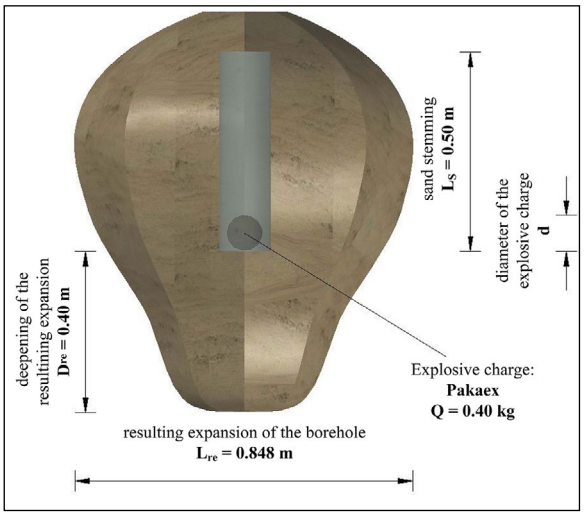

Figure 18- 3D model of the resulting cavity, Borehole MB38, AutoCad Civil 3D.

6. Conclusion

The paper presents an innovative method of measuring the resulting spherical cavities after the activation of an explosive charge, since spherical cavities in clay soil have not been studied widely.

The most significant results of the research presented in this paper are certainly the determination of the volume of cavities formed in the soft soil when blasting a series of boreholes set up on a certain profile. For this purpose, a unique system was designed and developed. The unique method of the observation is based on the integration of the RTK GNSS measurement method, depth camera and laser. An application is designed to calculate the resulting volume of the expansion. The concept and capabilities of the application in the technical field are innovative. In addition, the application draws 2D and 3D models of the resulting cavity. Also, the compatibility of the application with other CAD tools greatly contributes to the validation and more detailed 3D model of the resulting expansion.

The knowledge that it is possible to measure and calculate the volume of the resulting expansion will greatly help engineers to design and construct the overhead and underground structures more economically. The most important practical application of the research is in construction of structural elements for anchoring the foundation and retaining walls, the long-lasting slope stabilization in clay material and the stabilization of various structural objects. In conclusion, this paper clearly establishes the dependence of the volume of the formed spherical expansion on the mass of the explosive charge and the used explosive type and technical parameters. This way, the base for establishing the spherical formation model in different rocks and soil types has been laid, which is reflected in the application of the research results in the geotechnical practice of stabilizing and improving the properties of the working environment built of soil and rocks.

The aim of geophysical field research was to estimate the dynamic properties of the natural soil layers in depth, and to determine changes in the dynamic properties of the soil caused by the activation of explosive charges. To achieve this goal, the MASW method was implemented. It is a seismic geophysical method whose results allow estimation of soil stiffness. By comparing the 2D view of S wave velocities, before and after blasting, it was shown that activation of explosive charges led to an increase in S wave velocities at an average depth of 2.0 m to 3.0 m. It can also be concluded that at an average depth of 2.0 m to 3.0 m an increase in the stiffness of the surrounding clay soil after blasting occurs.

To improve this research, it is obligatory to perform supplementary researches that could bring new light to the technical characteristics of explosives and which type of soils have larger effect on the expansion diameter and volume. For this reason, it is also

recommended taking the process of detonation into account, where the shock wave front seems to play the most significant role (Sućeska, 2001; Dobrilović, 2008; Dobrilović et al., 2010).

References

Akgün, M., Gönenç, T., Tunçel, A., Pamukçu, O. 2013. A multi - approach geophysical estimation of soil dynamic properties in settlements: a case study in Güzelbahçe- İzmir (Western Anatolia). Journal of Geophysics and Engineering 10 (4), 045001,12.

Araya, K., Gao, R., Tsunematsu, S., Ochi, K. 1993. Loosening of dense clay soils by linear blasting, Journal of Agricultural Engineering Research 54 (2), 113-126.

Bakr, R.M. 2019. The Impact of the Unsupported Excavation on the Boundary of the Active Zone in Medium, Stiff and Very Stiff Clay. J Civ Environ Eng 9, 1-9.

Dobrilović, M. 2008. Raspoloživa energija tlačnog udarnog vala udarne cjevčice i njezina primjena u iniciranju elektroničkog detonatora, Doctoral thesis, University of Zagreb, Faculty of Mining, Geology and Petroleum Engineering, 264, Zagreb.

Dobrilović, M., Bohanek, V., Škrlec, V., Stanković, S., Dobrilović, I. 2010. Instructions for calibration method for measuring device of detonation velocity, 11th International Carpathian control conference, Miskolc: University of Miskolc, 285-288.

Ester, Z. 2005. Miniranje I - Eksplozivne tvari, svojstva i metode ispitivanja, University textbook, University of Zagreb, Faculty of Mining, Geology and Petroleum Engineering, 195, Zagreb.

EDS-C (Distance-Sensor measures). https://dimetix.com/en/?product=eds-c. Apr 12, 2019.

Frgić, L., Hudec, M., Krsnik, J., Krajcer, M., Mesec, J. 1988. Underground grounding by anchoring in soil, Proceedings of the I Yugoslavian symposium on tunnels, Brijuni, Croatia, 293-298.

Gabriels, P., Snieder R., Nolet, G. 1987. In situ measurements of shear-wave velocity in sediments using higher mode Rayleigh waves, Geophys Prospect 35, 187-196.

Heavy Duty Geo Vision Borehole Camera. http://www.geovision.org/. Apr 12, 2019.

Hudec, M., Krsnik, J., Abramović, V., Frgić, L., Krajcer, M., Gotić, I., Meštrić, M., Mesec, J., Fingerhut, L. 1989. Supporting with anchors in soft rock and soil. In Proceedings of the international Congress on Progress and Innovation in Tunneling, 111-117.

McCarthy, J.D., Graniero, P.A. 2006. A GIS-based borehole data management and 3D visualization system. Comput Geosci 32, 1699-1708.

Mesec, J., Težak, D., Grubešić, M. 2015. The use of explosives for improvement of clay soils. Environmental Engineering 2 (2), 95-101.

Muhovec, I. 1987. Uloga i karakter geotehničkih sidara s osvrtom na značenje injekcijskog zahvata. Geotehnička sigra i sidrene Konstr. 3-25.

Pamuk, E., Özdağ, C.Ö., Tunçel, A., Özyalın, Ş., Akgün, M. 2018. Local site effects evaluation for Aliağa/İzmir using HVSR (Nakamura technique) and methods. Natural Hazards 90 (2), 887-899.

Park, C.B, Miller, R.D., Xia, J. 1999. Multi-channel analysis of surface waves - active and passive methods, Geophysics 64 (3), 800-808.

Pribičević, B., Medak, D. 2003. Geodesy in civil engineering. University of Rijeka-Faculty of Civil Engineering: Zagreb, Croatia, 110.

Qingwen, L., Yuan, L., Gautam, D., Dongping, S., Lan, Q., Liping, W., Jianghui, D. 2015. Analysis of the Blasting Compaction on Gravel Soil. Journal of Chemistry 9.

Schepers, R., Rafat, G., Gelbke, C., Lehmann, B. 2001. Application of borehole logging, core imaging and tomography to geotechnical exploration. International Journal of Rock Mechanics and Mining Sciences 38, 867-876.

Shakeran, M., Eslami, A., Ahmadpour, M. 2016. Geotechnical aspects of explosive compaction. Shock and vibration, 14.

Soltani, D., Taheri, M., Vanapalli, S. 2019. Shrink behavior of rubberized expansive clays during alternate wetting and drying. Minerals 9, 224.

Strelec, S., Jug, J., Težak, D., Mesec, J. 2019. Improving rigidity of clay by using explosives and proofing by multichannel analysis of surface waves . IOP Conference Series: Earth and Environmental Science 221 (1), Prag, Czech Republic: IOP Publishing Ltd, 012056, 8.

Sućeska, M. 2001. Eksplozije i eksplozivi - njihova mirnodopska primjena, Brodarski institut, Zagreb, 305.

Težak, D. 2018. Influence of the blasting features on the expansion in clay soil, University of Zagreb, Faculty of Mining, Geology and Petroleum Engineering, Doctoral thesis, 236 s, Zagreb.

Težak, D., Kranjčić, N., Mesec, J. 2018. Integration of global navigation satellite system (GNSS) and borehole camera for purpose of modeling the blasting in clay soil, 18 International Multidisciplinary Scientific GeoConference SGEM 2018.

Težak, D., Stanković, S., Kovač, I. 2019. Dependence Models of Borehole Expansion on Explosive Charge in Spherical Cavity Blasting. Geosciences 9, 383, 18.

Official Gazette. 2004. Decision on Establishing Official Geodetic Data and Planar Projection of the Republic of Croatia. Official Journal of the Republic of Croatia 110/2004, 114/2004 Zagreb.

Wu, H., Pollard, D.D. 2002. Imaging 3-D fracture networks around boreholes. American Association of Petroleum Geologists Bulletin 4, 593-604.

Zhongqi, W., Yong, L. 2003. Numerical analysis on dynamic deformation mechanism of soils under blast loading, Soil Dynamics and Earthquake Engineering 23 (8), 705-714.

Bulletin of the Mineral Research and Exploration

http://bulletin.mta.gov.tr

A laboratory-scale investigation on freezing-thawing behavior of some natural stone samples manifactured in Turkey

Gökhan EROL[a*] and Ozan BAYRAM[a]

[a]*General Directorate of Mineral Research and Exploration, Mineral Analysis and Technology Department, 06800, Ankara, Turkey*

Research Article

Keywords:
Natural stone, Freezing and thawing, Water absorption, Thermal-mechanical behavior, Uniaxial compressive strength.

ABSTRACT

In the study, the changes in the mechanical properties of the natural stone samples, which had been obtained from different regions of Turkey, before and after the freeze-thaw test were examined. Within the scope of the study, 17 different natural stone samples were used and, after chemical and mineralogical-petrographical properties were determined. Water absorption at atmospheric pressure, real density, porosity, and uniaxial compressive strength tests were performed before and after freezing-thawing. The freezing and thawing test has been performed using TS EN 12371 standard from -12 °C to +20 °C in 56 cycles (2 cycles = 24 hours). After the test, the samples were subjected to uniaxial compressive strength test in order to identify the changes of the compressive strength values. The results of the physical and mechanical tests on these samples were evaluated by grouping according to chemical and mineralogical-petrographical properties of natural stones. It was aimed to determine which natural stone samples are resistant to freeze-thaw, and can be used in external cladding applications according to the findings obtained from the study.

Received Date: 30.10.2019
Accepted Date: 27.05.2020

1. Introduction

In this study, uniaxial compressive strength test was performed before and after the freeze-thaw test in order to determine the freeze-thaw effect on the natural stone samples manufactured, and it was aimed to examine the changes in the strength values according to the test results. Natural stones are the oldest construction materials that are mined from the surface by using suitable production methods and then cut-dimensioned and polished if necessary, and can also be mined economically. Since the early ages, natural stones have been used extensively by human beings in their buildings and monuments thanks to their visual beauty as well as their resistance to degradation. Due to the increase in usage of them, they are used especially in areas such as cladding, flooring, sculpture, construction, porcelain and glass industry, ornaments, optical industry, tombstone and stone chips production (T.C. Ekonomi Bakanlığı, 2016). Today, the usage rate of natural stones is increasing, this choice of use increases the reputation of some natural stones and enables new ones to be released. Natural stones create an ever-growing economic value for the region where they are found, and the country itself. However, natural resources and building blocks are not endless; reserves can be depleted, even affected by environmental conditions and degradable (Gökaltun, 2004; 2011).

As a result of this rising demand, mining activities have increased similarly and natural stone reserves with different origins, colors, textures and physical properties have started to be operated in Turkey where the richest natural stone deposits of the world are located. By commercial definition, natural stones

Citation info: Erol, G., Bayram, O. 2020. A laboratory-scale investigation on freezing-thawing behavior of some natural stone samples manifactured in Turkey. Bulletin of the Mineral Research and Exploration 163, 131-139. https://doi.org/10.19111/bulletinofmre.746486.

**Corresponding author: Gökhan EROL, gokhan.erol@mta.gov.tr*

include all natural rock materials produced for decorative usage (Onargan et al., 2006).

The properties sought in natural stones can be listed as color property and pattern homogeneity, block making feature and cutting and polishing, geomechanical and physical properties, resistance to atmospheric and chemical effects (Şentürk et al., 1995). These properties directly affect the suitability of these natural stones for building cladding depending on the usage place. All natural stones on the earth are constantly affected by physical and chemical processes such as freezing and thawing. However, the harmful effects of these processes are not the same everywhere and in every natural stone sample. The geological type and mineral composition of the natural stones, their resistance to abrasion, the climate conditions on the region where the stones are used, have a direct impact on the degradation; these harmful effects can be clearly seen especially on the surfaces of the materials used on cladding on exterior walls (Akbay et al., 2012). Along with the increase in the rate of natural stone use in building exterior cladding, the examination of the physical changes of natural stones exposed to effects such as rain and cold is an important parameter in terms of the choice of the usage area. In this process, especially in regions where the continental climate is dominant and the temperature difference is high during the day, the physical and mechanical properties of natural stones are weakened by the freeze-thaw effect. In natural stones used in long-term structures such as historical artifacts and monuments and exposed to freezing-thawing processes intensely, it is seen that the degradation that occurs as a result of these processes is very important in the change of physical and mechanical properties (Mutlutürk et al., 2004). Waters intruding by water absorption or capillary water absorption to the natural stones used in the regions where the day and night temperatures are quite different and the cold continental climate is dominant, freeze by increasing its volume by approximately 9% in sub-zero temperatures. As a result of this freeze-thaw cycle which is repeated over and over again and causing the most damage in natural stones, the cracks begin to form due to the increase in pore pressure when the absorbed water turns into ice, and over time, these cracks expand and grow. Thus, this situation causes degradation and fragmentation in the rock (Chen et al., 2004).

Beier and Sego (2009) and Proskin et al. (2010) showed that some engineering properties of rocks, such as stress and strength, are severely affected by the freeze-thaw cycles. Binal et al. (1997; 1998) investigated the changes in the physical and mechanical properties, after the freeze-thaw cycles, of volcano-sedimentary rocks in the Eskişehir region. Simonsen and Isacsson (1999), on the other hand, conducted a study on the dissolution resistance of paving stones laid in cold regions where the continental climate is dominant. In the study conducted by Binal and Kasapoğlu (2002), 30 freeze-thaw cycles have been applied on ignimbrite samples of the Aksaray region. At the end of these cycles, increases in some physical properties such as porosity and water absorption by volume and weight have been observed. On the other hand, it has been stated that some other mechanical properties like shear strength and uniaxial compressive strength decrease. Alyıldız (2003) and Altındağ and Alyıldız (2004) investigated the effects of freeze-thaw cycles on the physical and mechanical properties of tuff samples from Isparta region in a laboratory environment. As a result of the experiments carried out by applying 55 cycles in total, while the change of physical properties started to show differences after the 10th cycle, some other mechanical properties after 25th cycle; it has been stated that these differences are most effective in the point load strength index in mechanical test results and in water absorption values by weight through physical test results. Tuğrul (2004) examined the effect of degradation on the properties of rocks and stated that there is an increase in porosity and a decrease in strength values as a result of the experiments conducted on rock samples exposed to degradation at different levels. Nicholson and Nicholson (2000) examined the effect of defects (discontinuity etc.) on degradation by repeated freeze-thaw cycle tests on 10 sedimentary rock samples already having those structures. As a result, they have suggested that the defects existed before the test should also be evaluated in addition to rock strength and textural properties and that the loss of mass takes place due to the degradation in the structure of the rock. Binal et al. (2004) have used the Ankara ignimbrite rock in their study and compared the changes of physical parameters between the samples exposed to the freeze-thaw process due to the effect of atmospheric conditions in the nature and other samples, which the freeze-thaw test has been applied on, in laboratory environment. They stated that the changes in the physical results of the

samples that underwent freeze-thaw for one year under natural conditions and the samples that had 10 freeze-thaw cycles in the laboratory environment are closely compatible with each other. In addition, they stated that the uniaxial compressive strength results of the samples with 5 freeze-thaw cycles applied in the laboratory were similar to the results of the samples exposed to freeze-thaw process under the effect of atmospheric conditions in nature.

Martínez-Martínez et al. (2013) conducted freeze-thaw tests on 6 different carbonated rock samples with 12-24-48-96 cycles, respectively. P wave propagation velocity, macro and micro-textural properties, elasticity modulus, volume loss, porosity and uniaxial compressive strength results have been examined with the tests performed after the relevant cycle numbers on the samples. They have stated that there is a non-linear relationship between those properties and freeze-thaw cycle time. However, after the given cycles, they have showed that there is a slight increase in porosity values for all rock samples determined before the cycle. As a result, P wave velocity and uniaxial compressive strength have decreased.

2. Material and Method

2.1. Identification Process of the Material

Mineralogical and petrographic analyzes of the natural stone samples subjected to the relevant tests have been carried out in Mineralogy-Petrography laboratories operating under Department of Mineral Analysis and Technology, General Directorate of Mineral Research and Exploration. Mineralogical and petrographic analyzes of the samples (Table 1) were made on thin section based on TS EN 12407 standard. Chemical analyzes of natural stone samples were made in the geochemistry laboratories operating under

Table 1- Mineralogical and petrographic analyzes of the samples.

Sample Code	Petrographic Identification	Texture Type	Grain Size	Constituent Distribution	Rock Classification
AND-1	Andesite	Porphyritic	Fine grained	Homogeneous	Magmatic
AND-2	Andesite	Massive, Hipocrystalline- porphyritic	Medium-Fine grained	Homogeneous	Magmatic
AND-3	Andesite	Massive, Hipocrystalline- porphyritic	Fine-Medium grained	Homogeneous	Magmatic
BAZ-1	Basalt	Massive, porphyritic	Fine grained	Homogeneous	Magmatic
GRN-1	Granite	Massive, Holocrystalline grain texture	Fine grained	Homogeneous	Magmatic
İGN-1	Ignimbrite	Massive, Detritic	Mostly fine-medium grained, Occasionally very coarse grained	Homogeneous	Magmatic
RKRÇ-1	Recrystallized Limestone	Massive, Detritic	Fine grained	Heterogeneous	Metamorphic
RKRÇ-2	Recrystallized Limestone	Massive, Detritic	Fine grained	Heterogeneous	Metamorphic
RKRÇ-3	Recrystallized Limestone	Massive, fine grained Granoblastic texture	Medium-Coarse-Very coarse grained	Homogeneous	Metamorphic
RKRÇ-3	Recrystallized Limestone	Massive, Detritic	Fine grained	Homogeneous	Metamorphic
RKRÇ-5	Recrystallized Limestone	Massive, Cryptocrystalline detritic	Fine grained	Homogeneous	Metamorphic
MER-1	Marble	Massive, granoblastic occasionally heteroblastic	Fine grained	Homogeneous	Metamorphic
TRV-1	Travertine	Vesicular, Microcrystalline	Fine grained	Homogeneous	Sedimentary
TRV-2	Travertine	Massive porous, Fine grained	Fine grained	Homogeneous	Sedimentary
TRV-3	Travertine	Massive porous, Fine grained	Fine grained	Homogeneous	Sedimentary
TÜF-1	Glassy Tuff	Massive, Detritic	Fine grained	Homogeneous	Magmatic
TÜF-2	Glassy Tuff	Massive, Detritic	Fine grained	Homogeneous	Magmatic

the Mineral Analysis and Technology Department. Chemical analyzes of the samples (Tables 2 and 3) were made by using the XRF device based on the TS EN 15309 standard.

2.2. Method

2.2.1. *Sample Preparation Processes*

The rock samples to be analyzed were prepared in the accredited natural stone laboratory of Mineral Analysis and Technology Department affiliated to General Directorate of Mineral Research and Exploration. Samples were prepared to a cube block of 50x50x50 mm in the relevant standards with large and small cutting-sizing machines, respectively. The cube samples were prepared for the related tests by removing the roughness with the related devices (Figure 1).

Table 2- Chemical analyzes of the samples with magmatic origin.

Chemical Composition	**Sample Code**							
	AND-1	AND-2	AND-3	BAZ-1	GRN-1	İGN-1	TÜF-1	TÜF-2
Al_2O_3	15.61	15.51	15.65	21.39	17.17	16.88	15.10	15.83
CaO	1.42	1.87	1.79	9.14	4.13	3.32	3.16	1.11
Fe_2O_3	1.81	1.92	1.87	10.23	3.57	4.03	1.79	1.69
MgO	0.61	0.52	0.45	4.63	2.08	1.37	0.64	0.37
SiO_2	68.46	68.56	69.17	45.72	62.00	62.78	68.73	70.28

Table 3- Chemical analyzes of the samples with Sedimentary-metamorphic origin.

Chemical Composition	**Sample Code**								
	RKRÇ-1	RKRÇ-2	RKRÇ-3	RKRÇ-4	RKRÇ-5	MER-1	TRV-1	TRV-2	TRV-3
Al_2O_3	0.26	0.26	0.44	0.50	0.53	0.10	0.17	0.20	0.22
CaO	54.56	54.65	54.12	40.30	53.02	36.2	54.77	53.86	54.51
Fe_2O_3	0.11	0.09	0.21	0.30	0.24	0.10	0.07	0.60	0.11
MgO	0.51	0.50	0.45	12.1	0.89	17.10	0.27	0.68	0.41
SiO_2	0.62	0.66	1.69	1.80	1.20	0.30	0.44	0.80	0.87

Figure 1- The visuals of the natural stones used.

2.2.2. *Experiments on the Samples*

In order to determine the real density, total and open porosity of the rock samples, tests based on TS EN 1936 "Determination of Natural Stones-Experiment Methods-Real Density, Total and Open Porosity" standard were performed by using cube samples (Tables 4 and 5). The samples of natural stones were powdered (grounded, -63 µm) and the pycnometer method was used for the real density test. Tests based on TS EN 13755 "Natural Stones-Experiment Methods-Determination of Water Absorption at Atmospheric Pressure" were performed by using cube samples (Tables 6 and 7) to determine the water absorption coefficients of the samples.

In order to determine the uniaxial compressive strength of natural stone samples, tests based on TS EN 1926 "Natural Stones-Experiment Methods-Determination of Uniaxial Compressive Strength" standard were performed by using cube samples (Table 8 - 9). During the test, a uniformly distributed load was applied on 10 samples of each natural stone type in accordance with the relevant standards, the load was continuously increased until fracture occurred through the sample and the results were given in MPa units. Standard deviation was calculated by 10 results obtained for each natural stone sample after the compressive strength test. Tests based on TS EN 12371 "Natural Stones-Test Methods-Determination of Frost Resistance" standard were performed by using cube samples to determine the effect of freeze/thaw cycles in natural stones. The samples were tested in the freezing tank at temperatures between -12°C and +20°C in 56 cycles (2 cycles = 24 hours). After the test, uniaxial compressive strength tests were carried out after freezing to determine the compressive strength changes of the samples.

Table 4- Open-total porosity and real density values of the samples with magmatic origin.

Test Name	**Sample Code**							
	AND-1	AND-2	AND-3	BAZ-1	GRN-1	İGN-1	TÜF-1	TÜF-2
Open Porosity (%)	18.0	10.7	14.5	5.0	0.9	38.4	10.7	26.6
Total Porosity (%)	25.7	15.2	21.0	11.9	1.7	49.9	13.6	38.9
Real Density (gr/cm³)	2.6	2.6	2.6	3.0	2.7	2.5	2.5	2.5

Table 5- Open-total porosity and real density values of the samples with sedimentary and metamorphic origin.

Test Name	**Sample Code**								
	RKRÇ-1	RKRÇ-2	RKRÇ-3	RKRÇ-4	RKRÇ-5	MER-1	TRV-1	TRV-2	TRV-3
Open Porosity (%)	0.3	0.2	5.2	1.1	0.8	0.5	9.0	4.7	9.1
Total Porosity (%)	1.3	1.4	6.6	2.5	1.3	1.3	17.3	11.5	16.8
Real Density (gr/cm³)	2.7	2.7	2.7	2.8	2.7	2.9	2.7	2.7	2.7

Table 6- Water absorption rates of the samples with magmatic origin under atmospheric pressure by mass.

Test Name	**Sample Code**							
	AND-1	AND-2	AND-3	BAZ-1	GRN-1	İGN-1	TÜF-1	TÜF-2
Water absorption at atmospheric pressure (%)	10.6	5.1	7.8	1.5	0.4	32.9	5.0	10.4

Table 7- Water absorption rates of the samples with sedimentary and metamorphic origin under atmospheric pressure by mass.

Test Name	**Sample Code**								
	RKRÇ-1	RKRÇ-2	RKRÇ-3	RKRÇ-4	RKRÇ-5	MER-1	TRV-1	TRV-2	TRV-3
Water absorption at atmospheric pressure (%)	0.1	0.2	1.9	0.4	0.5	0.2	2.5	2.0	3.9

Table 8- Compressive strength values of the samples with magmatic origin before and after freezing.

Test Name	Sample Code							
	AND-1	AND-2	AND-3	BAZ-1	GRN-1	İGN-1	TÜF-1	TÜF-2
Before Freezing (MPa)	75	135	112	146	167	19	166	80
Standard Deviation	6	10	14.6	6	34	1	9	4
After Freezing (MPa)	65	131	114	142	185	16	160	80
Standard Deviation	12	18	12.4	3	8	1.1	8	6

Table 9- Compressive strength values of the samples with sedimentary and metamorphic origin before and after freezing.

Test Name	Sample Code								
	RKRÇ-1	RKRÇ-2	RKRÇ-3	RKRÇ-4	RKRÇ-5	MER-1	TRV-1	TRV-2	TRV-3
Before Freezing (MPa)	167	151	79	154	183	237	39	56	29
Standard Deviation	12	26	8	23	27	7	19	6	7.5
After Freezing (MPa)	165	156	80	130	171	224	30	55	29
Standard Deviation	8	18	8	28	14	5	13	6	8

3. Research and Results

3.1. Relationship Between Pressure Values and Water Absorption Rate Before and After Frost Resistance Test

According to the results of compressive strength tests before water absorption and frost resistance test, it has been determined that the pressure values before freezing decreased due to the increase of water absorption rates in natural stone samples of magmatic origin.

After the freeze-thaw determination test, it has been determined that there was no change in the compressive strength values of some samples and there was an increase or decrease in the compressive strength values of some other samples (Figure 2).

Similarly, it was found that pre-freezing pressure values decreased due to the increase of water absorption rates in natural stone samples of metamorphic and sedimentary origin. After freezing-thawing, just like the samples of magmatic origin, there was no change in the compressive strength values of some samples and there was an increase or decrease in the compressive strength values of some other samples (Figure 3).

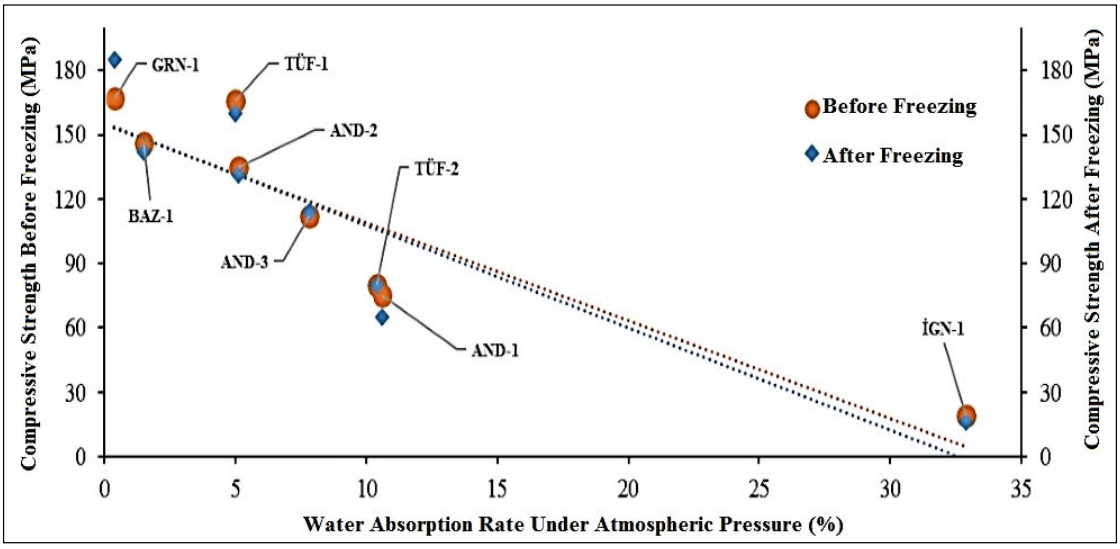

Figure 2- Water absorption rates and changes in compressive strength of the samples with magmatic origin, before-after freezing.

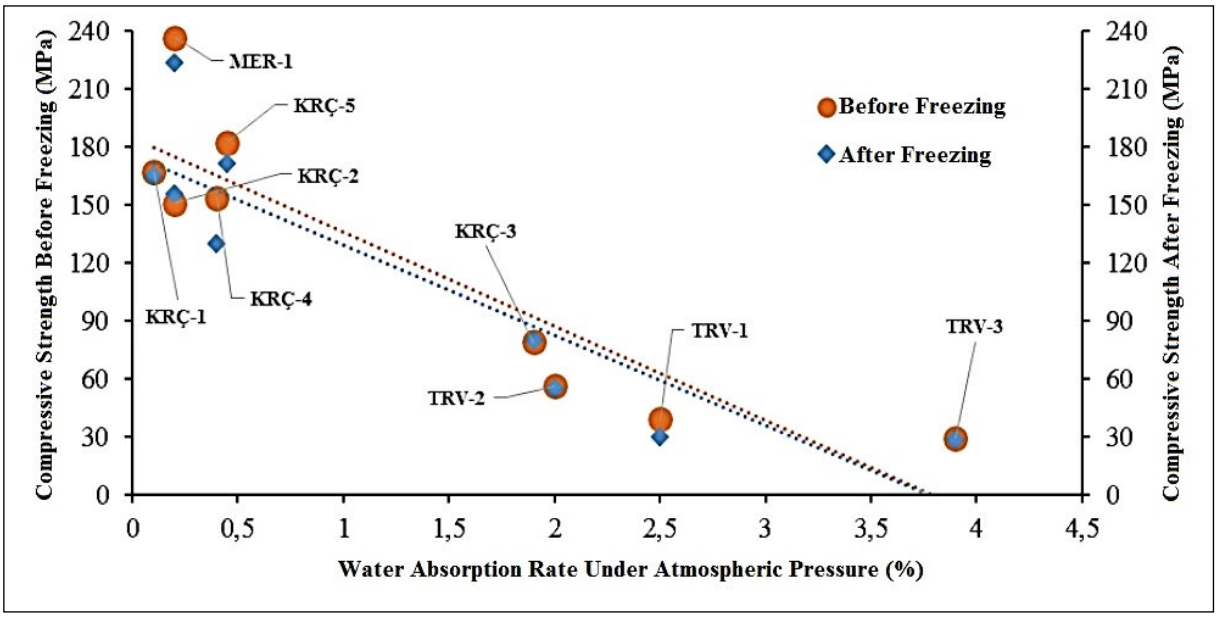

Figure 3- Water absorption rates and changes in compressive strength of the samples with sedimentary-metamorphic origin, before-after freezing.

4. Conclusion and Discussion

According to the results of water absorption and open-total porosity tests in magmatic, metamorphic and sedimentary origin stone samples, it has been determined that the open and total porosity rates increased due to increase in water absorption rates. According to the results of compressive strength tests performed before frost resistance tests, it has been concluded that the compressive strength values decreased due to the increase of water absorption rates in natural stone samples, therefore the compressive strength values would be lower in porous rocks. After the freeze-thaw test, there was a decrease in the compressive strength values of AND-1, BAZ-1, İGN-1, TÜF-1 and AND-2 samples with magmatic origin, however, increase in the values of AND-3 and GRN-1 samples. There was no change in compressive strength value of TÜF-2 sample. There was a decrease in the compressive strength values of RKRÇ-1, RKRÇ-4, RKRÇ-5, MER-1, TRV-1, TRV-2 samples with metamorphic-sedimentary origin, however, increase in the values of RKRÇ-2 and RKRÇ-3 samples and it has been observed that the value of the TRV-3 sample did not change.

The increase in water absorption and porosity ratio in atmospheric pressure is directly related. The reason for the decrease in pressure resistance values of some samples in both groups after frost resistance test is that the water is filled into the rock pores and subsequently expands the existing or newly formed cracks as a result of the water freezing and expanding at -12 °C and thus causes degradation through the rock structure. Compressive strength values of some samples in both groups at the end of freezing, no change was observed contrary to expectations or an increase was observed. From 20 samples prepared homogeneously for the test, 10 were selected for the pre-freezing compressive strength test and the rest for the post-freezing compressive strength test. During these selections, it is not possible to determine the ones having more or less compressive strength before the compressive strength test. After this sample selection, the sample or samples with high compressive strength were put into frost resistance test and they were not fully affected by the freeze-thaw cycle. As a result, it has been observed that the compressive strength values of these samples increased and the average compressive strength values increased slightly in the compressive strength tests performed after frost resistance tests. Momeni et al. (2015) have conducted uniaxial compressive strength tests on igneous rocks with different numbers of freeze-thaw cycles. In the related study, it has been revealed that compressive strength values increased after 50 cycles, but compressive strength values decreased at 100 cycles and over. In this study, it has been observed that some of the natural stone samples had some

increase (GRN-1 sample), some decrease (RKRÇ-4 sample) or remained constant (TRV-3 sample) in uniaxial compressive strength values after freezing-thawing. However, in this observation, it could not be concluded that the number of freeze-thaw cycles has a definite reducing effect on uniaxial compressive strength as expected. As a result, while applying the TS EN 12371 "Natural Stones-Test Methods-Determination of Frost Resistance" test standard, the samples should be subjected to frost resistance test for longer periods instead of 56 cycles to completely see the freeze-thaw effect. Such natural stones should not be used especially on the building exterior since the compressive strength values of natural stones resulted with degradation during the freeze-thaw cycle decrease over time. Natural stones with low porosity and low water absorption rate should be especially used in the regions where continental climate is dominant, with high temperature difference between day and night. Thus, the lifetime of natural stones used on exterior of buildings or over the areas that may be exposed to atmospheric conditions will increase and the most appropriate usage of the these stones will be economically provided.

5. Acknowledgement

We would like to thank the valuable staff of the Geochemistry Unit and Industrial Raw Materials Research Unit working under Mineralogy/Petrography Coordinatorship-Mineral Analysis and Technology Department-General Directorate of Mineral Research and Exploration for their contributions to the analyzes and experiments of the natural stones.

References

Akbay, D., Efe, T., Şengün, N., Demirdağ, S., Altındağ, R., Erinç Koççaz, C. 2012. Donma-Çözülme ve Termal Şok Koşullarının Bazı Mermerler Üzerindeki Etkilerinin İncelenmesi. MERSEM'2012 8. Uluslararası Mermer ve Doğaltaş Kongresi 13-15.

Altındağ, R., Alyıldız, I. S. 2004. Donma-Çözülme Periyotlarının Tüfün (Isparta-Dereboğazı) Fiziko-Mekanik Özellikleri Üzerine Etkisi, 5. Endüstriyel Hammaddeler Sempozyumu, 13-14 Mayıs 2004, 255-262, İzmir, Türkiye,

Alyıldız, I. S. 2003. Isparta-Derebogazı tüflerinde donma-çözülme periyotlarının fiziko-mekanik davranışlarına etkisi. Y. Lisans Tezi, S.D.Ü. Fen Bilimleri Enstitüsü, Isparta, 63 s.

Beier, N.A., Sego, D.C. 2009. Cyclic freeze-thaw to enhance the stability of coal tailings. Cold Regions Science and Technology 55, 278–285.

Binal, A., Kasapoğlu, K.E. 2002. Donma-Çözülme Sürecinin Aksaray-Ihlara Vadisi'nde Yüzeylenen Selime ignimbiritinin Fiziksel ve Mekanik Özellikleri Üzerindeki Etkisi, VI. Bölgesel Kaya Mekaniği Semp., Konya, 189-196.

Binal, A., Kasapoğlu, K.E., Gökçeoğlu, C. 1997. The Surficial Physical Deterioration Behaviour of Neogene Volcanosedimentary Rocks of Eskisehir-Yazılıkaya NW Turkey, Engineering Geology and The Environment, Yunanistan, 3065-3069.

Binal, A., Kasapoğlu, K.E., Gökçeoğlu, C. 1998. Eskisehir-Yazılıkaya Çevresinde Yüzeylenen Volkanosedimanter Kayaçların Donma-Çözünme Etkisi Altında Bazı Fiziksel ve Mekanik Parametrelerinin Degisimi, Hacettepe Üniv. Yayınları, Yerbilimleri 20, 41-54.

Binal, A., Kasapoğlu K.E., Seğmenoğlu, Ç. 2004. Donma-çözülme sürecinin Ankara İgnimbiritinin jeomekanik özellikleri üzerine etkisinin doğal ve laboratuvar ortamında karşılaştırmalı olarak incelenmesi. KAYAMEK′ 2004-VII. Bölgesel Kaya Mekaniği Sempozyumu, 59-66, Sivas.

Chen, T.C., Yeung, M.R., Mori, N. 2004. Effect of water saturation on deterioration of welded tuff due to freeze–thaw action. Cold Regions Science and Technology 38, 127–136.

Gökaltun, E. 2004. Atmosferik gaz ve asitlerin doğal taş yapı malzemeleri üzerindeki etkilerinin deneysel yöntemler ile analizi. Mimarlar Odası İstanbul Büyükkent Şubesi 2. Ulusal Yapı Malzemesi Kongresi ve Sergisi bildiriler kitabı, 149-160, İstanbul.

Gökaltun, E. 2011. The changes in the structre of limestones as a result of calcium sulfate (gypsum stone) formation caused by atmospheric polluters. World Applied Sciences Journal 13, 2082-2088.

Martínez-Martínez, J., Benavente, D., Gomez-Heras, M., Marco-Castaño, L., Garcíadel- Cura, M.A., 2013. Non-linear decay of building stones during freeze–thaw weathering processes. Construction and Building Materials 38, 443–454.

Momeni, A., Abdilor, Y. Khanlari, G. R., Heidari M., Sepahi A. A. 2015. The effect of freeze–thaw cycles on physical and mechanical properties of granitoid hard rocks. Bulletin of Engineering Geology and the Environment, doi: 10.1007/s10064-015-0787-9.

Mutlutürk, M., Altındağ, R., Türk, G. 2004. A decay function model for the integrity loss of rock when subjected to recurrent cycles of freezing–thawing

and heating–cooling. International Journal of Rock Mechanics and Mining Sciences 41(2), 237-244.

Nicholson, D. T., Nicholson, F. H. 2000. Physical deterioration of sedimentary rocks subjected to experimental freezing and thawing. Earth Surf Process Landforms 25, 1295-1307.

Onargan, T., Köse, H., Deliormanlı A.H. 2006. Mermer. TMMOB Maden Mühendisleri Odası Yayını, Yayın No: 95

Proskin, S., Sego, D., Alostaz, M. 2010. Freeze-thaw and consolidation tests on Suncor mature fine tailings (MFT). Cold Regions Science and Technology 63, 110–120.

Simonsen, E., Isacsson, U. 1999. Thaw Weakening of Pavement Structure in Cold Regions, Cold Regions Science and Technology, 29, 135-151.

Şentürk, A., Gündüz, L., Sarıışık, A. 1995. Yapı taşı olarak kullanılan endüstriyel kayaçlara teknik bir bakış. Endüstriyel Hammaddeler Sempozyumu, 21-22.

T.C. Ekonomi Bakanlığı, 2016 yılı Sektör Raporları, Doğal Taş Sektörü. Ankara.

TS EN 1926. 2007. Natural stone test methods-Determination of compressive strength. Turkish Standards Institute.

TS EN 1936. 2010. Natural stone test methods-Determination o f real density and apparent density and of total and open porosity. Turkish Standards Institute.

TS EN 12371. 2019. Natural stone test methods - Determination of frost resistance. Turkish Standards Institute.

TS EN 12407. 2019. Natural stone test methods - Petrographic examination. Turkish Standards Institute.

TS EN 13755. 2009. Natural stone test methods - Determination of water absorption at atmospheric pressure. Turkish Standards Institute.

TS EN 15309. 2008. Characterization of waste and soil - Determination of elemental composition by X-ray fluorescence. Turkish Standards Institute.

Tuğrul, A. 2004. The effect of weathering on pore geometry and compressive strength of selected rock types from Turkey. Engineering Geology 75 (3), 215-227.

Bulletin of the Mineral Research and Exploration

http://bulletin.mta.gov.tr

The relationship of soils developed on different parent materials in Niğde province with lithological units and determination of their suitability for usage agricultural purposes

Harun TORUNLAR[a*], Abdurrahman LERMİ[b] and Emin ÇİFTÇİ[c]

[a]*Field Crops Central Research Institute, Deparment of Geographic Information Systems, Ankara, Turkey*
[b]*Niğde Ömer Halisdemir University, Faculty of Engineering, Department of Geological Engineering, Niğde, Turkey*
[c]*Istanbul Technical University, Faculty of Mines, Geological Engineering Department, Istanbul, Turkey*

Research Article

Keywords:
Lithological units, Soil, Multi criteria decision making method.

ABSTRACT

In this study, general characteristics of soils formed on different parent materials in three different regions of Niğde province, their relationship with lithological units and the extent to which they are suitable for agricultural purposes were determined. Physical and chemical analysis values of rock and soil samples were used to reveal the relationship between lithological units and soils formed in the study area and correlation analysis was applied among the parameters. Multi Criteria Decision Making method was used to determine the suitability of these soils which are formed depending on the parent materials for agricultural use. In order to determine the effect rates among the main criteria of soil, topography, climate and geology and their sub criteria, Analytical Hierarchy Process of Multi Criteria Decision Making method was applied. According to this; Depending on the influence of the lithological units, the soils developed around Bor district are of basic character and the soils developed in Çiftlik and Gölcük districts and their vicinity are more acidic reaction. In addition, it has been determined that the soils of the Çiftlik district and its vicinity are developed by accumulation and in situ, while the soils around Gölcük and Bor districts are developed in situ. In determining the suitability of soils for agricultural use, it was calculated that the main criteria of geology was 5.5% and the criteria of lithological units, which is the sub-criterion of this, was 2.7% effective.

Received Date: 07.11.2019
Accepted Date: 17.05.2020

1. Introduction

The surface topography which is composed up the rocks are changed by various factors, and as a result of the change, soils that are an indispensable living environment and natural space for all biological entities are formed (Tarım ve Köyişleri Bakanlığı, 2008). The chemistry of the formed soils generally reflects the chemistry of the rocks of their origin. Kapur et al. (1996) concluded that basalt, as the main material, decomposes, the minerals it contains altered to clay and iron oxides, and due to the absence of quartz, the soils are brown or red-brown colored and enriched by iron-oxides. Yüksel (2003) studied the determination of the physical, chemical and mineralogical compositions of the soils formed on the rock materials (magmatic rocks and alluvial) under different environmental conditions of the Ağrı Mountain near Iğdır province and reveal the relationship between the soil, rocks, climate and mineralogical properties. It was determined that the dominant minerals for all soil samples are plagioclase, quartz, opal-CT and chlorite, while smectite is present in different amounts in all samples, and the smectite ratios in samples taken from the bottom lands are higher than other samples.

Citation info: Torunlar, H., Lermi, A., Çiftçi, E. 2020. The relationship of soils developed on different parent materials in Niğde province with lithological units and determination of their suitability for usage agricultural purposes. Bulletin of the Mineral Research and Exploration 163, 141-165. https://doi.org/10.19111/bulletinofmre.742137.

**Corresponding author:* Harun TORUNLAR, *htorunlar@hotmail.com*

Niğde and its territory is one of most important geological parts of Turkey (Göncüoğlu, 1981). In the study area, lithological units originating from Hasandağ, Keçiboyduran, Melendiz and Erciyes volcanics play an important role in gaining characteristic features of the developed and still developing soils. Determination of the suitability of these soils, which are sourced by regional lithology and have certain features for agricultural purposes, will play an important role both in establishing the relationship between lithological units and soils and in determining the intended use of soils developed on similar lithological units in different areas. In order to use a land for agricultural purposes, it must fulfil the conditions that the land is used for agricultural purpose. To obtain these suitable conditions, besides the soil, topography and climate factors, the geology of the region has also a great effect. Multiple Criteria Decision Making Method (MCDM), in which more than one of these factors are taken into consideration and can be applied in the easy solution of such complex problems, is effectively used (Malczewski, 2006).

By using Multi Criteria Decision Making Method, Feizizadeh and Blaschke (2012) evaluated soil, topography, climatic conditions and water adequacy factors for Tabriz region of Iran. They produced land use maps mainly consists of four classes for irrigated and dry agriculture (high, medium, marginal and unsuitable) and seven classes for land suitability (settlements, irrigated agriculture, dry agriculture, potential areas suitable for irrigated agriculture, potential areas suitable for dry agriculture, riverbed and areas unsuitable for agriculture) of the area. As a result of the land suitability analysis for agriculture, they determined that 100,028 hectares and 117.395 hectares of irrigated and dry farming areas, respectively, and they are the widest marginal suitability class area.

Torunlar and Nazlıcan (2018) applied land suitability analysis for determining the suitable areas where can be potential for producing soybean crops in Turkey by using Analytic Hierarchy Process of Multiple Criteria Decision Making Method. Based on soil, topography and climate data sets, they determined suitable areas where soybean plants can grow as land suitability classification consisting of four classes (Highly suitable, Moderate suitable, Marginally suitable and unsuitable). According to their study, the total area of 17.435.102,53 hectares, 22.34% of the study area, is highly and moderate suitable for the cultivation of the main product soybean, 15.56% (12.149.689,64 ha) of the area is marginally suitable, 62.10% (48.473.207,83 ha) of the area is not suitable for soybean cultivation.

In this study, three different areas in Niğde province are chosen and the characteristics of the soils developing on different rock materials, their relations with lithology and the classification of soils for agricultural use in three different areas of Niğde province were investigated.

2. Material and Method

2.1. Study Area

The study area has been selected as three different areas, each of which is 1/25,000 scaled size and represent the lithological units of the region within the borders of Niğde province (Figure 1). These areas are;

Çiftlik and its vicinity (L32c2); the study area is located northern side of the city, in the Çiftlik township and it is developed in the Turkey's recent geomorphological structure. The study area is in the Neogene-Quaternary, Melendiz-Quaternary volcano-sedimentary series (Beekman, 1966; Pasquare, 1968; Aydın et al., 2005). It is located on aglomerate, alluvium, andesite, basalt, ignimbrite, pyroclastics and slope debris cone units of Hasandağ-Melendiz mountains' foothills (Figure 2). The study area covers 14957.61 hectares (149.57 km^2) and covered by maquis or pastures, agricultural areas, settlements and non-agricultural areas.

Gölcük and its vicinity (L33c1); This area is located within the borders of the Central district in the north of the province and on the Neogene-Quaternary, Melendiz-Quaternary volcano-sedimentary series (Beekman 1966, Pasquare 1968, Aydın et al., 2005) and the Paleozoic-Mesozoic aged high temperature, medium pressure metamorphic rocks and cut by intrusive rocks. The study area covered by Niğde metamorphic units (Göncüoğlu, 1981) consisting of clastic and carbonate-based rocks is located on basalt, basalt-andesite, conglomerate-sandstone-mudstone, gabbro and ignimbrite (Figure 2). It is also covered by maquis or pastures, agricultural areas, settlement areas and located 15191.84 hectares (151.92 km^2) area.

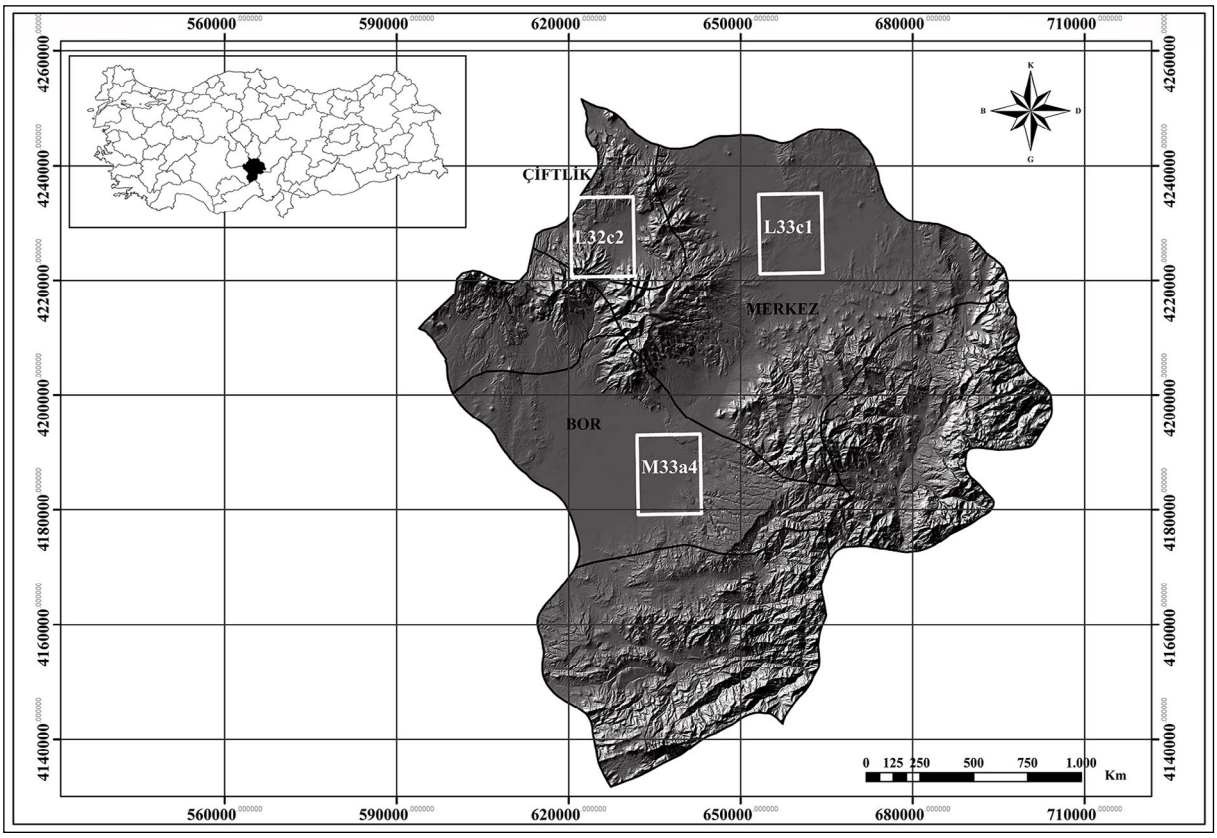

Figure 1- Study area.

Bor and its vicinity (M33a4); This area, on the other hand, is located in the Bor plain, and especially includes alluvium, ignimbrite, limestone, marble and pyroclastic rock-trachyandesite units (Figure 2). The study area is affected by Paleozoic-Mesozoic aged Niğde metamorphic units (Göncüoğlu, 1981). It covers 15266.06 hectares (152.66 km^2) in Niğde province and covered by macquis, pasture, agricultural, settlements and non-agricultural areas.

Different data sets were used in the study. These data sets;

2.2. Soil Data Set

Soil data set contains the physical and chemical analysis parameters of the sampled soils obtained from the study area. These parameters are water saturation, electrical conductivity, total salt, pH, lime, organic matter, total nitrogen, organic carbon, hydraulic conductivity (permeability), geochemical data of main and trace elements.

2.3. Topography Data Set

The maps are 1/25.000 scaled topographic maps with 10 meters accuracy in topographic contours, obtained from the General Directorate of Mapping. By using these maps, slope and land form of the area were obtained.

2.4. Climate Data Set

In this data set; The precipitation data obtained from meteorology stations in Niğde province and vicinity are used (Figure 3). For this purpose, long-year average monthly rainfall data obtained from the daily precipitation values recorded by the General Directorate of State Meteorology Affairs in the last 30 years were used (Table 1).

2.5. Geology Data Set

This data set consists of 1/25.000 scaled geology maps obtained from the General Directorate of Mineral Research and Exploration and geochemical analysis of rock samples from the study area (Figure 4).

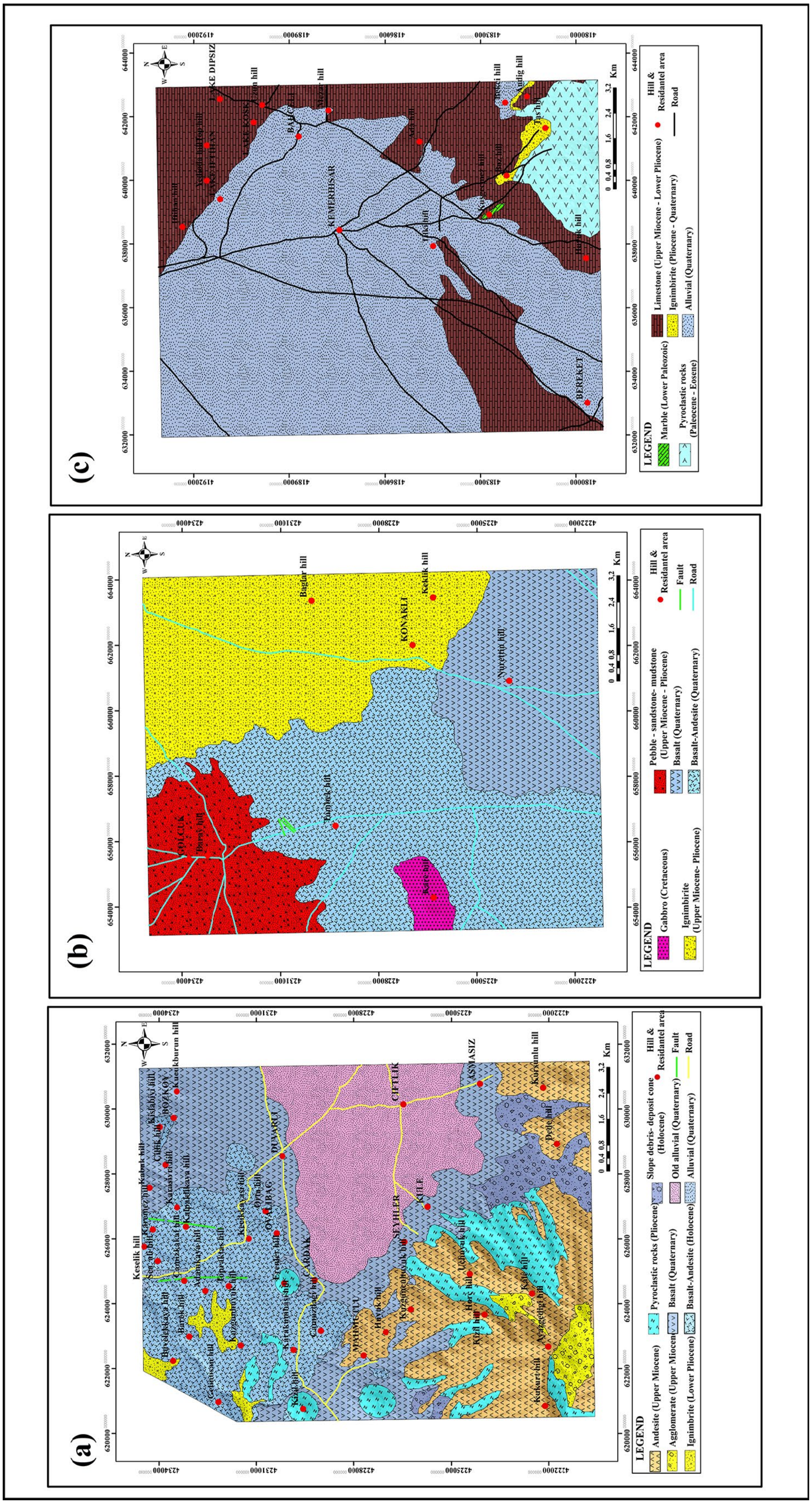

Figure 2- General geological map of (a) Çiftlik and its vicinity (L32c2, MTA 2010*a*), (b) Gölcük and its vicinity (L33c1, MTA2010*b*) and (c) Bor and its vicinity (M33a4, MTA2010*c*).

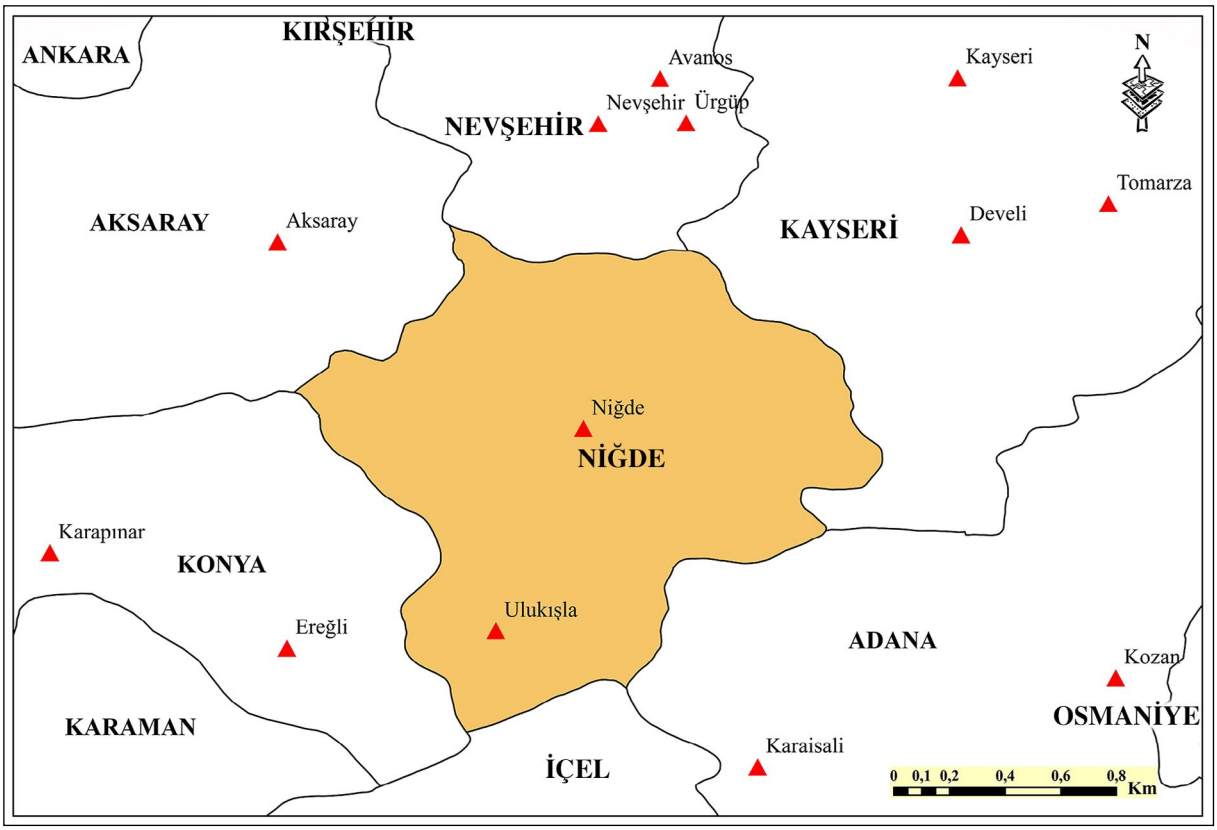

Figure 3- Meteorological stations in Niğde province and its vicinity.

Table 1- Monthly average precipitation datas for long term measured from Niğde province and surrounding meteorological stations.

CITY NAME	Station Name	Latitute	Longitude	Elevation	Station No	January	February	March	April	May	June	July	August	September	October	November	December	Annual Total Precipitation
ADANA	Karaisalı	35.0576	37.2499	235	17936	147.6	100.9	90.9	91.9	84.8	46.3	12.3	15.1	22.4	48.8	95.4	157.3	**913.8**
ADANA	Kozan	35.8210	37.4394	123	17908	107.6	80.1	90.9	96.1	87.8	59.3	22.6	21.4	33.6	57.5	83.1	109.5	**849.5**
AKSARAY	Aksaray	34.0341	38.3680	971	17192	37.2	31.1	36.3	52.5	43.8	22.7	7.0	3.7	7.5	26.8	33.0	41.6	**343.2**
KAYSERİ	Develi	35.4911	38.3831	1.233	17836	39.6	39.3	44.4	55.5	50.0	21.0	4.4	2.8	7.3	28.5	33.3	43.7	**369.8**
KAYSERİ	Kayseri	35.4835	38.7177	1.058	17196	31.9	32.3	39.8	56.3	59.1	35.8	12.3	5.8	10.3	32.5	37.9	40.6	**394.7**
KAYSERİ	Tomarza	35.8051	38.4493	1.394	17837	35.5	34.8	38.4	54.4	58.1	36.4	9.1	5.0	13.4	35.5	36.5	40.8	**397.9**
KONYA	Ereğli	34.0542	37.5029	1.054	17248	30.1	25.8	30.3	44.0	38.2	23.9	5.3	3.9	6.6	22.6	28.7	35.2	**294.6**
NEVŞEHİR	Avanos	34.8495	38.7157	928	17833	29.9	34.4	28.3	40.1	44.7	25.2	8.1	3.7	8.2	26.5	32.8	38.1	**320**
NEVŞEHİR	Nevşehir	34.7177	38.6196	1.199	17193	41.9	40.9	44.0	53.3	60.9	27.8	9.9	4.3	11.8	34.4	38.6	49.7	**417.5**
NEVŞEHİR	Ürgüp	34.9050	38.6215	1.092	17835	36.9	33.1	36.6	55.0	57.7	31.6	10.9	3.9	11.8	32.2	34.8	40.0	**384.5**
NİĞDE	Niğde	34.6860	37.9706	1.223	17250	30.6	31.0	33.8	47.8	47.4	25.2	5.3	3.4	7.1	27.2	33.2	39.7	**331.7**
NİĞDE	Ulukışla	34.4996	37.5399	1.409	17906	24.4	22.5	35.1	49.4	54.1	29.3	6.8	4.6	7.6	27.8	26.7	33.3	**321.6**

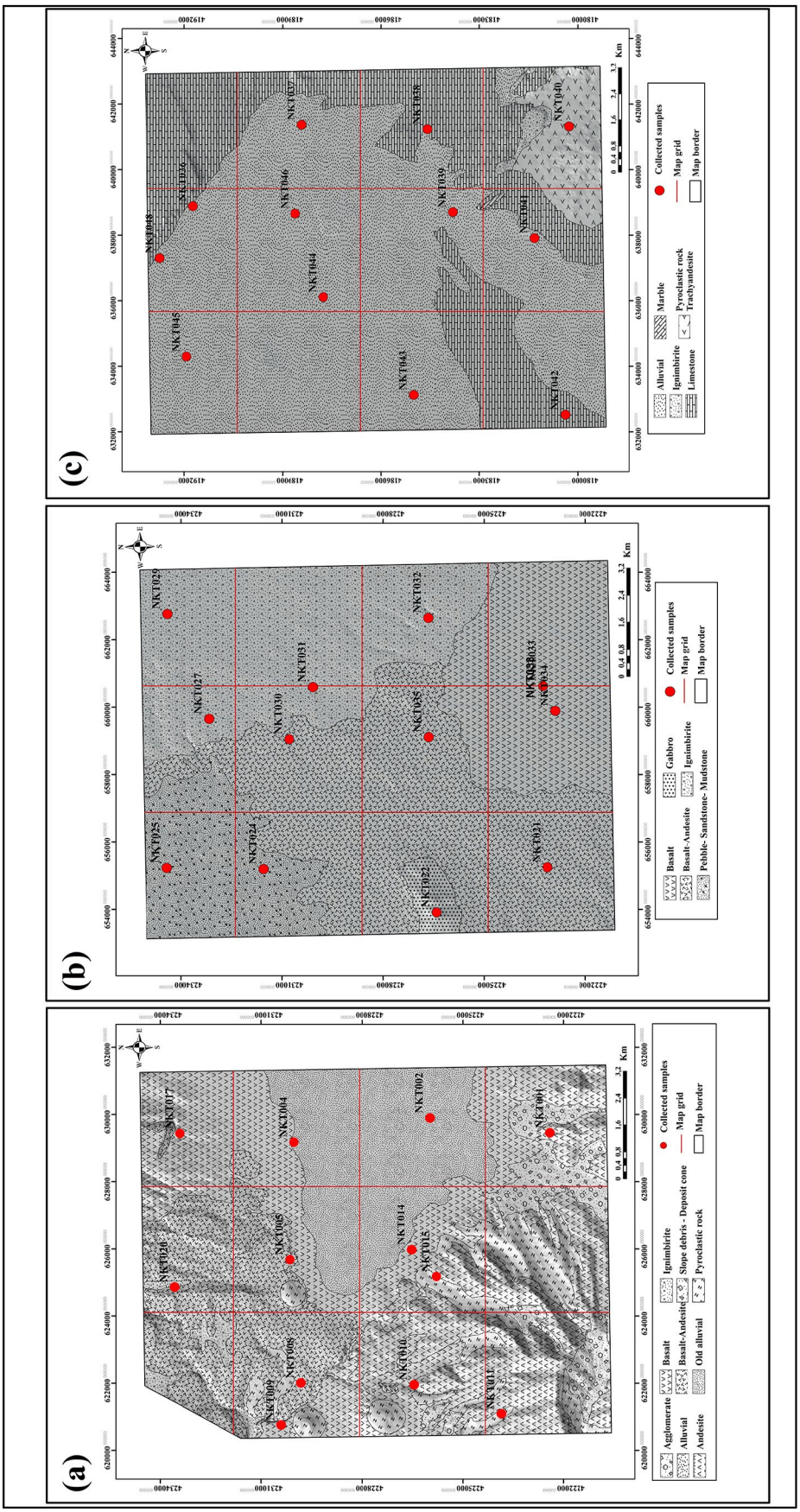

Figure 4- Soil and rock samples locations in (a) Çiftlik and its vicinity (L32c2), (b) Gölcük and its vicinity (L33c1), (c) Bor and its vicinity (M33a4)

2.6. Field Studies

In order to reveal the relationship between soils and the lithological units made up of different main materials, 12 soil and rock samples were taken from each study area and 36 samples in total. Within the reachable topographic conditions, dominant lithological units within each grid area was sampled. Rock samples were taken from points representing each different lithological unit, and soil samples were taken from 0-20 cm depth from the points where rock samples were taken (Figure 4).

In the study, both the lithological units and the soils formed on these lithological units, as well as determining the general characteristics of these soils and at the same time, the substrate data used as base data in determining the suitability of the soils for agricultural use were produced by applying different methods. Surface distribution maps of climate and soil parameters were created based on interpolation method. This method relies on the parameter values at the current measurement points in the calculation of values belonging to another unknown location (Esri, 2004). The Inverse Distance Weighting-IDW interpolation method, which is one of the local interpolation methods that uses the measured data at peripheral points, is one of the most used methods (Willmott and Matsuura, 1995; Dodson and Marks, 1997). This IDW interpolation method was used to create distribution maps of 9 different physical and chemical parameters and precipitation parameters obtained from soil samples taken from the study area.

X-Ray Fluorescence (XRF) analysis method was used for geochemical analysis of rock and soil samples. From the physical and chemical analysis of soil samples; Çağlar (1949) is used for the determination of lime ($CaCO_3$) ratio, Richards (1954) for soil reaction (pH), electrical conductivity (EC) and total salt ratio, Kaçar (1972) in determining the total nitrogen ratio, Ülgen and Ateşalp (1972) in determining the organic matter (OM) ratio, Kaçar (1994) in determining the organic carbon ratio, Klute (1965) in determining the hydraulic conductivity (permeability), and TS 8333 (1990) in determining the saturation ratio with water. Correlation Analysis, one of the statistical methods, was used to determine the relationships between rock and soil samples.

Topographic maps are used to create the slope and land forms data of the study area. The slope data was created using the Surface Analysis / slope menu in the Spatial Analyst module of the ArcGIS program (Mc Coy and Johnston, 2001), and the landform data was generated by using the Topograph Tools / Landform Classification module, which is an extension of the ArcGIS program (Jenness, 2005). Agricultural usage of an area is related to its ability to meet the requirements. The required many main criterias (soil, topography, climate and geology) and their sub-criterias (water saturation, electrical conductivity, total salt, pH, lime, organic matter, total nitrogen, organic carbon, hydraulic conductivity (permeability), precipitation, slope, land forms and lithological units) were evaluated together in the study area, The Multi Criteria Decision Making Method was used to determine the suitability classes for agricultural use. This method is combination of many complex spatial data and reveals how the data will be combined within different alternatives in the same evaluation dimension (Yu et al., 2011). Although it contains more than one different techniques in itself, the Weighted Linear Combination Method was used in this study (Patrono, 1998).In the Weighted Linear Combination method; For the criteria that affect the determination of the suitability for agricultural use, weight points were given by considering the relative importance. These criteria are divided into subcriteria, and the standardized subcriteria scores have been calculated with a separate numerical evaluation (Table 2).

Multiplying the subcriteria score and the weight values of each criteria provide that the criteria have been added to the same scale. The numerical equality provided by the method in determining the suitability classes for agricultural use is given below.

$$S = \sum_{i=1}^{n} W_i X_i \quad (1)$$

According to the equation, S: total score; Wi: weight value of the criterion; Xi: subcriteria score, n: total number of criteria. Using this numerical equation of the Weighted Linear Combination method, numerical values for each suitability class were calculated and reclassified according to the land suitability class ranges specified in (FAO, 1985), and the agricultural use classes of the soils formed on different main materials were determined. The weight points of the main and sub criteria used are effective on the distribution of the suitability classes within the field. Weighting scores of each criterion

Table 2- Classes and weight scores of Criteria and subcriteria (FAO, 1976, Dorronsoro, 2002, Chuong and Boehme, 2005, Jenness, 2005, Turoğlu 2005, Cengiz and Çelem, 2006).

CRITERIA	Suitability Classes			
	Highly suitable (S1)	Moderate suitable (S2)	Marginally suitable (S3)	Unsuitable (N)
	Weighted scores for subcriteria			
	4	3	2	1
SOIL MAIN CRITERIA				
pH	7.3-6.7	6.7-5.5 or 7.3-8.0	5.5-4.5 or 8.0-9.0	<4.5 or >9.0
Lime ($CaCO_3$) (%)	<7	7-15	15-25	>25
Total nitrogen (%)	> 0.2	0.1 – 0.2	< 0.1	----
Total salt (%)	<2	2-6	6-12	>12
Electrical conductivity (EC) (dS/m)	< 4	4 - 8	8 - 16	> 16
Organic matter (%)	>5	5-2	2-1	<1
Organic carbon (%)	> 2.5	1.0 – 2.5	< 1.0	-----
Permeabilite (cm/hour)	>2	2-0.5	0.5-0.1	<0.1
Saturation (%)	>75	75-50	50-25	<25
TOPOGRAPHY MAIN CRITERIA				
Slope (%)	0 - 2	2 - 6	6 - 12	> 12
Landforms	Plains - Open slope areas	Hollow valleys	Canyons, deeply incised streams, Midslope drainages, shallow valleys, Upland drainages, headwaters	Upper slope areas, local ridges, hills in valley, midslope ridges, mountain tops, high ridges
CLIMATE MAIN CRITERIA				
Precipitation (mm)	>1000	1000-600	600-300	<300
GEOLOGY MAIN CRITERIA				
Lithological units	Alluvial, Old alluvial	----	Slope debris, deposit cone, pebble-sandstone-mudstone	Ignimbrite, pyroclastic rocks, basalt-andesite, agglomerate, gabbro, limestone, trachyandesite, marble

were calculated according to the Analytical Hierarchy Process (AHS) technique of the Weighted Linear Combination Method (Satty, 1980).

The Analytical Hierarchy Process (AHP) technique allows the criteria to be compared with each other in pairs based on priority level. Pairwise comparisons of criteria with each other were made using the binary comparison scale developed by Satty (1980) (Table 3).

In order to measure whether the paired comparison matrix made between the criteria is consistent or not, the Consistency Ratio (CR) is calculated in the AHS technique. The consistency ratio, which is accepted as the 10% threshold value, must be equal to or less than the threshold value. If it is greater than 0.10 (10%), paired comparisons between criteria are inconsistent and in this case, the paired comparison matrix has to be reconstructed (Armacost et al., 1994). The consistency ratio is obtained using the equation below.

Table 3- The AHS scales for paired comparisons (Satty, 1980).

Numerical values	Description
1	Items are equally important
3	1st criterion is slightly more important than 2nd
5	1st criterion is more important than 2nd
7	1st criterion is much more important than 2nd
9	1st criterion has the strongest significance than 2nd
2,4,6,8	It is the intermediate value between two close criterions. Used when compromise needed

$$CR = \frac{CI}{RI} \quad (2)$$

CI = Consistency index, RI = Random index,

Consistency index (CI) is calculated using the formula below.

$$CI = \frac{(\lambda max - n)}{(n-1)} \quad (3)$$

CI: Consistency index

n: the number of compared elements

λmax: Maximum eigenvalue;

Maximum eigenvalue is the arithmetic mean of the values obtained by dividing each element of the weighted total vector obtained by multiplying the normalized weight values with the matrix of paired comparisons belonging to the criteria, by the corresponding normalized weight values. Random index (RI) refers to the average consistency index of randomly generated matrices of binary comparisons. RI values take the following values depending on the number of compared elements (n) (Table 4).

3. Findings and Discussion

There is a close relationship between soil and geological units. In soil formation process, firstly the rocks turn into the soil parent material and then the soil is formed from the soil parent material (Brady, 1990). Main soil material is only one of the factors that affect the formation of soils. However, its effect should be considered together with climate, topography, organism and time factors (Akalan, 1983). One or few of these factors, especially in local areas, main material and topography, climate and vegetation have dominant effect in large geographical areas. For this reason, the same soils do not always occur from the same parent material. Very different soils from similar parent materials occur in different parts of the world. In this study, the relationship between the soils of the region and lithological units developed on the main materials composed of different lithological units is revealed. For this purpose, the characterization of soils and their relationship with lithology is determined by using parameters obtained from physical, chemical and geochemical analysis of soil and rock samples collected from the field (Table 5, 6, 7, 8, 9, 10, 11, 12, 13).

Accordingly it was observed that the soils around Çiftlik and Bor districts were medium fine soils in the clay soils group, while Gölcük and vicinity soils were medium-very coarse soils in the loamy-sandy soils group. It has been determined that the soils observed in all three areas are salt-free soils, the soils in Çiftlik and its vicinity are generally very slightly acidic - medium alkaline soils, and the soils around Bor and Gölcük are light alkali - strongly alkaline soils.

At the same time, it has been determined that the soils around Çiftlik and Gölcük are generally lime-free-very little calcareous soils, while the soils around Bor are very calcareous - marly soils due to the fact that the soils around the region are developed on the upper Miocene-lower Pliocene limestones. Although some of the Çiftlik and its vicinity soils are slightly higher in terms of organic matter content compared to the soils observed in the other two areas, it has been determined that the soils of the region in general terms contain low and medium levels of organic matter. Due to the fact that Gölcük and its vicinity soils are medium-very coarse soils in the loamy-sandy soils group, Çiftlik and Bor soils are with higher permeability compared to other soils. Accordingly it was determined that the soils around Gölcük and its vicinity are generally fast, while the soils around Çiftlik and Bor districts are medium permeable soils.

The geochemical analysis of the main rock and the sampled soils in all three regions of the study area were done and the relations of the soils with lithology were revealed by using the obtained main and trace element contents and some element ratios calculated in soils. As an example of geochemical analysis for soil and rock samples belong to Çiftlik and its vicinity is given in table 6 and table 8. According to these tables, major oxide contents of soil samples from Çiftlik and its vicinity area: SiO_2 content is 52.78 -

Table 4- Random index values that vary according to matrix sizes (Satty, 1980).

n	1	2	3	4	5	6	7	8	9	10	11	12	13	14	15
RI	0.00	0.00	0.58	0.90	1.12	1.24	1.32	1.41	1.45	1.49	1.51	1.48	1.56	1.57	1.59

Table 5- Physical and chemical analysis of the soils samples from study areas.

Çiftlik (L32c2)	X (Latitute)	Y (Longitute)	Elevati. (m)	Text. Clas.	EC dS/m	T.T %	pH	Lime %	O.M %	T.A %	O.K %	Per. cm/hour	Sat. %	Lithology
NKT1	629454.81	4222400.49	1744.69	CL	0.983	0.039	6.77	0.00	1.10	0.06	0.64	16.52	62	Andesite
NKT2	629896.00	4225982.00	1551.16	CL	0.951	0.033	6.67	0.00	1.23	0.06	0.71	9.85	55	Old alluvial
NKT4	629177.00	4230026.00	1556.06	L	0.442	0.013	4.33	0.00	0.80	0.04	0.46	1.81	45	Old alluvial
NKT5	625681.00	4230145.00	1542.72	CL	0.911	0.041	7.36	0.59	3.36	0.17	1.95	4.57	70	Basalt-Andesite
NKT8	622009.00	4229815.00	1503.56	CL	1.013	0.035	7.69	12.19	3.31	0.17	1.92	2.20	54	Basalt-Andesite
NKT9	620757.00	4230410.00	1471.11	L	0.797	0.024	7.71	3.40	4.24	0.21	2.46	2.02	48	Basalt
NKT10	621956.00	4226448.00	1664.58	CL	0.819	0.029	7.28	0.37	1.16	0.06	0.67	16.89	55	Basalt
NKT11	621094.07	4223854.08	1917.36	L	0.603	0.019	7.60	0.59	1.39	0.07	0.81	1.55	48	Pyroclastic rock
NKT14	625977.00	4226518.00	1548.49	L	0.417	0.011	5.75	0.00	0.90	0.05	0.52	7.69	42	Basalt
NKT15	625179.00	4225786.00	1640.62	C	0.944	0.043	7.12	0.00	0.97	0.05	0.56	2.27	71	Pyroclastic rock
NKT17	629435.00	4233419.00	1678.06	L	0.902	0.027	7.91	1.92	0.87	0.04	0.50	2.47	46	Basalt
NKT20	624865.00	4233582.00	1713.07	CL	1.179	0.043	7.69	0.74	0.84	0.04	0.49	1.43	57	Basalt-Andesite
Gölcük (L33c1)	**X (Latitute)**	**Y (Longitute)**	**Elevati. (m)**	**Text. Clas.**	**EC dS/m**	**T.T %**	**pH**	**Lime %**	**O.M %**	**T.A %**	**O.K %**	**Per. cm/hour**	**Sat. %**	**Lithology**
NKT21	655250.00	4223122.00	1358.48	S	0.571	0.009	7.94	0.59	1.13	0.06	0.66	1.77	25	Basalt-Andesite
NKT22	653909.97	4226416.04	1455.07	L	0.843	0.022	7.87	0.59	1.01	0.05	0.59	12.25	41	Gabbro
NKT24	655197.00	4231537.00	1313.33	L	0.844	0.020	7.91	0.74	1.20	0.06	0.70	6.17	37	Pebble-sandsto-ne-mudstone
NKT25	655231.00	4234416.00	1317.17	S	0.348	0.006	8.23	1.63	1.09	0.05	0.63	2.83	26	Pebble-sandsto-ne-mudstone
NKT27	659650.00	4233159.00	1360.04	L	0.593	0.015	7.35	0.15	2.42	0.12	1.40	14.06	39	Ignimbrite
NKT29	662760.00	4234396.00	1387.30	L	1.185	0.024	7.74	0.37	2.12	0.11	1.23	10.82	32	Ignimbrite
NKT30	659048.00	4230781.00	1338.90	L	0.702	0.017	7.42	0.30	1.08	0.05	0.63	12.35	37	Basalt-Andesite
NKT31	660592.00	4230079.00	1355.06	L	0.687	0.018	7.61	0.15	1.54	0.08	0.89	9.27	42	Ignimbrite
NKT32	662645.00	4226663.00	1370.00	CL	0.632	0.022	7.89	1.26	1.14	0.06	0.66	1.97	55	Ignimbrite
NKT33	660623.00	4223256.00	1340.08	S	0.715	0.013	7.83	0.30	0.97	0.05	0.56	23.98	28	Basalt
NKT34	659888.00	4222888.00	1339.45	L	0.892	0.026	7.74	1.26	0.93	0.05	0.52	17.98	46	Basalt
NKT35	659110.00	4226652.00	1335.00	S	0.625	0.011	8.02	4.95	1.06	0.05	0.61	3.02	28	Basalt-Andesite
Bor (M33a4)	**X (Latitute)**	**Y (Longitute)**	**Elevati. (m)**	**Text. Clas.**	**EC dS/m**	**T.T %**	**pH**	**Lime %**	**O.M %**	**T.A %**	**O.K %**	**Per. cm/hour**	**Sat. %**	**Lithology**
NKT36	638883.00	4191734.00	1104.57	L	0.757	0.018	8.02	35.17	1.64	0.08	0.95	1.47	38	Alluvial
NKT37	641367.00	4188417.00	1137.89	L	0.811	0.020	8.10	33.18	2.14	0.11	1.24	12.75	39	Alluvial
NKT38	641234.00	4184589.00	1122.05	C	1.541	0.082	8.62	16.70	1.72	0.09	1.00	0.00	83	Limestone
NKT39	638703.00	4183810.00	1093.56	CL	1.749	0.071	7.72	29.56	0.58	0.03	0.34	3.54	63	Alluvial
NKT40	641315.00	4180267.00	1173.94	L	0.705	0.018	8.01	14.33	2.30	0.12	1.33	4.84	40	Pyroclastic rock Trachyandesite
NKT41	637908.00	4181325.00	1094.25	L	0.754	0.020	7.98	18.55	1.04	0.05	0.60	2.02	41	Alluvial
NKT42	632522.89	4180374.00	1060.00	C	1.427	0.065	8.60	24.75	0.87	0.04	0.50	0.91	71	Limestone
NKT43	633126.00	4185001.00	1069.55	L	0.834	0.024	8.11	29.56	1.39	0.07	0.81	0.80	45	Alluvial
NKT44	636111.00	4187762.00	1083.10	CL	0.871	0.034	8.14	39.90	2.03	0.10	1.18	2.24	61	Alluvial
NKT45	634298.00	4191933.00	1087.42	CL	1.502	0.065	7.74	32.66	2.00	0.10	1.16	3.60	68	Alluvial
NKT46	638656.00	4188620.00	1106.13	L	0.873	0.027	7.93	41.23	2.02	0.10	1.17	4.00	49	Alluvial
NKT48	637300.00	4192751.00	1100.00	L	0.657	0.019	8.00	40.49	1.68	0.08	0.97	1.11	44	Alluvial

L: Loam, CL: Clayey Loam, C: Clayey, S: Sandy, EC: Electrical conductivity, TS: Total salt, OM: Organic matter, TN: Total nitrogen, OC: Organic carbon, Per .: Permeability (Hydraulic conductivity) Sat .: Water Saturation

70.74%, TiO_2 content is 0.24 - 1.05%, Al_2O_3 content is 12.66 - 22.16%, Fe_2O_3 content is 1.74 - 7.89%, MnO content is 0.07 - 0.15%, MgO content is 0.69 - 2.79%, CaO content varies between 1.73 - 15.58%, Na_2O content is 0.93 - 2.45%, K_2O content is 1.86 - 4.76%, P_2O_5 content is between 0.09 - 1.07%. Similarly, SiO_2 content of the main oxides of rock samples is 53.82 - 68.83%, TiO_2 content is 0.13 - 1.22%, Al_2O_3 content is 9.23 - 24.7%, Fe_2O_3 content is 1.11 - 7.77%, MnO content is 0.07 - 0.14%, MgO content is 2.81 - 0.42%,

Table 6- Geochemical analysis of soil samples taken from Çiftlik and its surrounding area.

	ÇT-1	ÇT-2	ÇT-3	ÇT-4	ÇT-5	ÇT-6	ÇT-7	ÇT-8	ÇT-9	ÇT-10	ÇT-12_1	ÇT-12_2
X1	621094	625179	629455	621956	625977	629896	622009	625681	629177	620757	629435	629435
Y1	4223854	4225786	4222400	4226448	4226518	4225982	4229815	4230145	4230026	4230410	4233419	4233419
Elevation	1917	1641	1745	1665	1548	1551	1504	1543	1556	1471	1678	1678
%												
SiO_2	67.12	66.28	65.05	61.58	65.58	66.22	52.78	60.46	70.74	60.8	63.03	68.43
TiO_2	0.65	0.7	0.87	0.84	0.80	0.80	1.04	1.05	0.45	0.89	0.81	0.24
Al_2O_3	18.57	16.3	18.91	22.16	16.98	17.68	16.66	19.97	16.61	16.66	19.7	12.66
Fe_2O_3	4.27	5.19	5.72	6.17	5.07	5.32	7.43	7.89	3.06	6.39	5.57	1.74
MnO	0.1	0.1	0.13	0.13	0.13	0.13	0.15	0.15	0.07	0.14	0.14	0.08
MgO	1.28	2.11	1.37	1.41	1.4	1.23	2.79	2.31	0.80	2.57	1.21	0.69
CaO	2.82	4.6	3.24	3.24	4.32	3.56	15.58	4.32	1.73	7.42	4.39	8.75
Na_2O	1.83	1.1	1.68	1.67	2.45	2.02	1.28	1.21	1.96	0.93	1.27	2.34
K_2O	3.05	3.22	2.59	2.43	2.68	2.6	1.86	2.27	4.26	2.89	3.55	4.76
P_2O_5	0.11	0.23	0.23	0.13	0.36	0.2	0.16	0.12	0.17	1.07	0.09	0.09
Total	99.80	99.83	99.79	99.76	99.77	99.76	99.73	99.75	99.85	99.76	99.76	99.78
ppm												
Nb	17	8	14	18	11	10	16	17	24	16	25	15
Rb	91	91	91	91	82	91	71	91	183	91	183	183
Ba	1000	700	700	1000	800	800	700	700	600	800	900.00	1500.00
Sr	400	300	500	500	600	500	700	400	200	500.00	400	300
Zr	200	200	300	300	200	200	400	300	200	200	400	100
Fe	29900	36300	40000	43200	35500	37200	52000	55200	21400	44700	39000	12200
Mn	800	800	1000	1000	1000	1000	1200	1200	500	1100	1100	600
Cr	65	137	68	68	137	137	274	205	68	205	137	50
Cu	34	58	63	55	51	57	64	57	40	68	70	30
Ni	68	73	79	76	62	64	157	157	35	79	79	37
Zn	66	77	80	80	80	76	80	80	59	80	80	47
As	19	27	3	23	14	26		19	2	14	26	23
Y		16	20		17	18		23	17		27	9
Ca/Mg	2.20	2.18	2.36	2.30	3.09	2.89	5.58	1.87	2.16	2.89	3.63	12.68
Ba/Sr	2.50	2.33	1.40	2.00	1.33	1.60	1.00	1.75	3.00	1.60	2.25	5.00

CaO content varies between 3.41 - 23.88%, Na_2O content is 2.16 - 4.03%, K_2O content is 1.64 - 4.96%, P_2O_5 content is 0.14 - 0.52%.

The Ca/Mg ratios of the soils from the Çiftlik and its vicinity vary between 1.87 and 12.68 and the lime ratios measured from the same soils between 0 - 12.19% (Table 5, 6), the study area under the influence of magmatic origin region lithology which is an indicator of the low lime content of the soils. In the correlation analysis applied to the parameters of Çiftlik and its vicinity soils (Table 7), it was determined that the main elements showed low positive and negative values among themselves and especially with Si. This indicates that magmatic and sedimentary lithology are observed predominantly in soils of the study area, especially alkali (such as Ca, Na, K) elements in the soil are washed due to alteration (Price and Velbel, 2003) and it indicates that they are formed by developing locally (Gürel, 2006).

Normalized value means that each geochemical parameter obtained from a soil profile relative to the fresh bedrock on which the profile is developed (Soil/Rock; S/R). These values provide very useful data to better interpretation of the elemental distribution-enrichment in the soil profile formed in the region (Tijani et al., 2006). The normalized values of the

Table 7- Correlation matrix of parameters obtained from the soils of the Çiftlik and its nearby area ($p<0.01$).

	SiO_2	TiO_2	Al_2O_3	Fe_2O_3	MnO	MgO	CaO	Na_2O	K_2O	P_2O_5	Rb	Ba	Sr	Zr	Cr	Cu	Ni	Zn	As	EC	T.Salt	pH	$CaCO_3$	O.M.	T.N	O.C.	Perm.	Sat.
SiO_2	1.00																											
TiO_2	-0.79	1.00																										
Al_2O_3	-0.29	0.62	1.00																									
Fe_2O_3	-0.82	0.98	0.61	1.00																								
MnO	-0.81	0.93	0.53	0.91	1.00																							
MgO	-0.81	0.76	0.12	0.81	0.65	1.00																						
CaO	-0.71	0.20	-0.43	0.24	0.31	0.56	1.00																					
Na_2O	0.58	-0.59	-0.31	-0.67	-0.48	-0.76	-0.24	1.00																				
K_2O	0.73	-0.93	-0.58	-0.90	-0.83	-0.69	-0.22	0.37	1.00																			
P_2O_5	-0.17	0.22	-0.17	0.21	0.24	0.46	0.13	-0.36	-0.13	1.00																		
Rb	0.51	-0.71	-0.32	-0.68	-0.57	-0.66	-0.17	0.25	0.88	-0.27	1.00																	
Ba	0.24	-0.60	-0.35	-0.57	-0.33	-0.47	0.15	0.43	0.51	-0.19	0.39	1.00																
Sr	-0.74	0.71	0.23	0.63	0.78	0.52	0.51	-0.07	-0.80	0.23	-0.69	-0.18	1.00															
Zr	-0.72	0.72	0.62	0.71	0.69	0.42	0.27	-0.52	-0.57	-0.22	-0.16	-0.42	0.47	1.00														
Cr	-0.82	0.72	0.00	0.75	0.70	0.88	0.65	-0.60	-0.60	0.35	-0.45	-0.46	0.57	0.48	1.00													
Cu	-0.64	0.79	0.43	0.78	0.81	0.61	0.20	-0.69	-0.59	0.38	-0.35	-0.54	0.51	0.70	0.63	1.00												
Ni	-0.86	0.81	0.35	0.86	0.75	0.80	0.51	-0.59	-0.74	-0.05	-0.52	-0.38	0.53	0.68	0.79	0.51	1.00											
Zn	-0.63	0.93	0.65	0.89	0.86	0.63	0.02	-0.55	-0.84	0.28	-0.66	-0.62	0.64	0.66	0.57	0.87	0.58	1.00										
As	-0.28	0.05	0.06	0.11	0.20	0.13	0.32	-0.17	-0.06	-0.22	-0.06	0.43	0.06	0.04	0.21	0.09	0.16	0.09	1.00									
EC.	-0.03	-0.27	-0.34	-0.25	-0.06	-0.01	0.31	0.15	0.19	0.12	-0.01	0.71	0.13	-0.33	-0.01	-0.21	-0.20	-0.19	0.70	1.00								
T.Salt	-0.13	-0.18	-0.20	-0.14	-0.01	0.12	0.29	0.02	0.07	0.32	-0.15	0.65	0.18	-0.33	-0.01	-0.18	-0.16	-0.11	0.55	0.92	1.00							
pH	-0.27	0.07	-0.05	0.11	0.28	0.12	0.29	0.03	-0.03	-0.02	0.04	0.39	0.19	0.00	0.36	0.01	0.17	0.03	0.77	0.68	0.55	1.00						
$CaCO_3$	0.11	0.07	-0.06	-0.04	0.18	-0.17	-0.11	0.56	-0.14	0.06	-0.17	-0.03	0.39	-0.14	0.05	-0.01	-0.17	0.21	0.02	0.27	0.11	0.35	1.00					
O.M.	0.02	0.20	0.30	0.14	0.25	-0.14	-0.24	0.41	-0.39	-0.06	-0.40	-0.02	0.39	-0.11	-0.03	0.05	-0.11	0.29	0.33	0.16	0.14	0.39	0.58	1.00				
T.N	0.02	0.20	0.30	0.14	0.24	-0.14	-0.24	0.42	-0.39	-0.05	-0.41	-0.04	0.40	-0.12	-0.03	0.03	-0.11	0.29	0.31	0.16	0.14	0.38	0.59	1.00	1.00			
O.C.	0.02	0.20	0.30	0.14	0.25	-0.14	-0.24	0.41	-0.39	-0.06	-0.40	-0.02	0.39	-0.11	-0.03	0.04	-0.11	0.29	0.34	0.17	0.14	0.40	0.58	1.00	1.00	1.00		
Perm.	-0.25	0.05	-0.05	0.05	-0.16	0.29	0.35	-0.18	-0.19	-0.22	-0.26	-0.17	0.12	0.19	0.18	-0.20	0.25	-0.07	0.03	0.06	0.10	-0.11	-0.30	-0.25	-0.23	-0.25	1.00	
Sat.	-0.28	0.07	0.06	0.12	0.12	0.32	0.23	-0.19	-0.18	0.49	-0.37	0.38	0.27	-0.20	0.06	-0.03	-0.01	0.09	0.31	0.63	0.87	0.30	-0.10	0.13	0.14	0.13	0.16	1.00

T.N: Total Nitrogen. **OC:** Organic Carbon. **OM:** Organic Matter. **T.SALT:** Total Salt . **PERM.:** Permeability. **SAT:** Saturation.

Table 8- Geochemical analysis of bedrock samples taken from Çiftlik and its surrounding area.

	ÇK-1	ÇK-2	ÇK-3	ÇK-4_1	ÇK-4_2	ÇK-5	ÇK-7	ÇK-8	ÇK-10	ÇK-11	ÇK-12_1	ÇK-12_2
X_1	621094	625179	629455	621956	621956	625977	622009	625681	620757	624865	629435	629435
Y_1	4223854	4225786	4222400	4226448	4226448	4226518	4229815	4230145	4230410	4233582	4233419	4233419
Elevation	1917	1641	1745	1665	1665	1548	1504	1543	1471	1713	1678	1678
%	**Pyroclastic**	**Pyroclastic**	**Andesite**	**Basalt**	**Basalt**	**Basalt**	**Basalt Andesite**	**Basalt Andesite**	**Basalt**	**Basalt Andesite**	**Basalt**	**Basalt**
SiO_2	62.66	58.19	64.45	63.25	57.26	61.54	57.6	57.58	53.82	59.2	68.83	58.38
TiO_2	0.66	0.84	0.54	0.69	0.84	0.71	0.71	0.99	1.22	0.85	0.43	0.13
Al2O3	17.08	20.3	16.57	18.17	24.7	20.1	18.14	19.43	18.02	16.01	15.64	9.23
Fe_2O_3	4.53	5.7	4.06	5.06	5.32	4.71	5.17	6.17	7.77	5.87	2.64	1.11
MnO	0.09	0.11	0.07	0.1	0.09	0.11	0.11	0.14	0.13	0.12	0.09	0.07
MgO	1.81	1.78	2.06	1.44	1.01	1.45	1.66	1.87	2.81	2.81	0.42	0.6
CaO	6.44	7.07	6.29	4.95	5.56	5.18	10.34	7.2	9.44	8.22	3.41	23.88
Na_2O	3.82	3.88	3.59	3.23	2.78	3.07	3.82	3.87	4.03	3.98	3.21	2.16
K_2O	2.51	1.64	2.05	2.67	1.84	2.37	1.82	2.22	1.95	2.61	4.96	4.03
P_2O_5	0.24	0.27	0.19	0.23	0.3	0.52	0.38	0.26	0.52	0.14	0.16	0.18
Total	**99.84**	**99.78**	**99.87**	**99.79**	**99.7**	**99.76**	**99.75**	**99.73**	**99.71**	**99.81**	**99.79**	**99.77**
ppm												
Nb	10	11	7	8	12	10	10	9	10	10	16	12
Rb	65	33	56	75	46	59	13	32	34	70	183	183
Ba	600	800	400	900	1200	800	1000	1200	700	600	1000	1200
Sr	600	700	500	500	700	600	800	400	900	300	300	500
Zr	200	400	100	200	400	300	400	200	400	200	300	0,03
Fe	31700	39900	28400	35400	37200	32900	36200	43200	54300	41100	18500	7800
Mn	700	900	500	800	700	900	900	1100	1000	900	700	500
Cr		60	30	68		38	53	68	65	137		
Cu	36	56	36	69	37	72	47	37	73	60	32	26
Ni	45	79	41	61	157	79	63	79	52	71	19	28
Zn	59	66	63	63	80	72	68	72	80	67	58	60
As				11	11	11						20
Y	13			19	15		22	24	26	20	17	9

main and trace elements observed in Çiftlik and its vicinity soils with the bedrock are given in Table 9. Accordingly, among the trace elements proportional to the bedrock of the soil of the region; Nb is 0.75 - 2.36, Rb is 1 - 5.57, Ba is 0.58 - 1.75, Sr is 0.22 - 1.67, Zr is 0.50 - 3, Fe is 0.39 - 1.56, Mn is 0.50 - 2, Cr is 1 - 5.19, Cu is 0.54 - 2.20, Ni is 0.39 - 4.17, Zn is 0.73 - 1.39, As 0.00 - 3.31 and Y is 0.64 - 1.55 times higher (Table 9).

The abundance of these elements in the soil is result of the decomposition of the volcanic rocks predominant basalt andesite magmatism in the study area.

Major oxides of soil samples from Gölcük and its vicinity; SiO_2 content is 39.6 - 69%, TiO_2 content is 0.45 - 1.08%, Al_2O_3 content is 11.53 - 18.18%, Fe_2O_3 content is 3.27 - 9.6%, MnO content is 0.08 - 0.18%, MgO content is 1.06 - 4.76% from the soil samples of Gölcük and its vicinity. The CaO content varies between 3.02 - 37.01%, Na_2O content is 0.35 - 2.39%, K_2O content is 1.67 - 4.26%, P_2O_5 content is 0.09 - 0.26%. SiO_2 content is 19.4 - 93.9%, TiO_2 content is 0.16 - 1.14%, Al_2O_3 content is 0.38 - 19.93%, Fe_2O_3 content is 0.11 - 14.4%, MnO content is 0.04 - 0.14%, MgO content is 0.08 - 14.01% in rock samples

Table 9- Normalized values of major and trace elements with bedrock in Çiftlik and its nearby area soils (Soil/Rock).

	ÇT-1	ÇT-2	ÇT-3	ÇT-4	ÇT-5	ÇT-6	ÇT-7	ÇT-8	ÇT-9	ÇT-10	ÇT-11	ÇT-12
	Pyroclastic	**Pyroclastic**	**Andesite**	**Basalt**	**Basalt**	**Basalt**	**Basalt Andesite**	**Basalt Andesite**	**Basalt**	**Basalt Andesite**	**Basalt**	**Basalt**
SiO_2	1.07	1.14	1.01	0.97	1.15	1.08	0.92	1.05	1.31	1.03	0.92	1.47
TiO_2	0.98	0.83	1.61	1.22	0.95	1.13	1.46	1.06	0.37	1.05	1.88	1.85
Al_2O_3	1.09	0.80	1.14	1.22	0.69	0.88	0.92	1.03	0.92	1.04	1.26	1.37
Fe_2O_3	0.94	0.91	1.41	1.22	0.95	1.13	1.44	1.28	0.39	1.09	2.11	1.57
MnO	1.11	0.91	1.86	1.30	1.44	1.18	1.36	1.07	0.54	147	1.56	1.14
MgO	0.71	1.19	0.67	0.98	1.39	0.85	1.68	1.24	0.28	0.91	2.88	1.15
CaO	0.44	0.65	0.52	0.65	0.78	0.69	1.51	0.60	0.18	0.90	1.29	0.37
Na_2O	0.48	0.28	0.47	0.52	0.88	0.66	0.34	0.31	0.49	0.23	0.40	1.08
K_2O	1.22	1.96	1.26	0.91	1.46	1.10	1.02	1.02	2.18	141	0.72	1.18
P_2O_5	0.46	0.85	1.21	0.57	1.20	0.38	0.42	0.46	0.33	7.64	0.56	0.50
Nb	1.79	0.75	2.00	2.36	0.94	0.93	1.53	1.94	2.27	1.53	1.57	1.29
Rb	1.41	2.78	1.64	1.22	1.80	1.55	5.57	2.86	5.41	1.30	1.00	1.00
Ba	1.67	0.88	1.75	1.11	0.67	1.00	0.70	0.58	0.86	1.33	0.90	1.25
Sr	0.67	0.43	1.00	1.00	0.86	0.83	0.88	1.00	0.22	1.67	1.33	0.60
Zr	1.00	0.50	3.00	1.50	0.50	0.67	1.00	1.50	0.50	1.00	1.33	0.33
Fe	0.94	0.91	1.41	1.22	0.95	1.13	1.44	1.28	0.39	1.09	2.11	1.56
Mn	1.14	0.89	2.00	1.25	1.43	1.11	1.33	1.09	0.50	1.22	1.57	1.20
Cr		2.27	2.27	1.00		3.64	5.19	3.00	1.05	1.50		
Cu	0.96	1.03	1.76	0.80	1.39	0.79	1.36	1.54	0.54	1.13	2.20	1.19
Ni	1.53	0.93	1.92	1.26	0.39	0.81	2.50	2.00	0.67	1.11	4.17	1.34
Zn	1.12	1.17	1.27	1.28	1.01	1.06	1.18	1.11	0.73	1.19	1.39	0.77
As	1.58	3.31	0.61	2.07	1.27	2.43	0.00	1.89	0.25	2.06	1.72	1.15
Y					1.11			0.97	0.64		1.55	1.00

corresponding to soil samples. The CaO content varies between 1.65 - 74.9%, Na_2O content is 0.03 - 3.66%, K_2O content is 0.04 - 4.56%, P_2O_5 content is 0.05 - 0.83% in the same samples.

The Ca/Mg ratios of the soils taken from Gölcük and its vicinity vary between 1.50 and 14.51 and the lime ratios measured from the same soils vary between 0.15 and 8.17% (Table 5). The low lime contents observed in the study area indicates that they developed in situ from the dominant magmatic lithology in the region. In the correlation analysis applied to soil parameters (Table 10), the main elements shows low but positive values among themselves which the developed soils in this study area are less washed, less transported and in situ developed (Gürel, 2006).

In normalized values with the bedrocks of Gölcük and vicinity soils; the main and trace element values have variable values at low rates and according to the bedrock Nb is 0 - 1.50, Rb is 0.50 - 4.54, Ba is 0.43 - 1.20, Sr is 0.23 - 2.50, Zr is 0.01 - 1.54, Fe is 0.27 - 4.73, Mn is 0.83 - 3, Cr is 1.67 - 9.12, Cu is 0.49 - 1.63, Ni is 0.69 - 4.25, Zn is 1 - 2.62, As is 0.25 - 2.26 times higher. Cr, with values between 1.67 and 9.12, is the most observed element in the soils of the study area, indicates the predominance of the basic lithology observed in the region (Table 11).

Major oxides values belong to soil samples from Bor and its vicinity: SiO_2 content is 28.2 - 51.92%, TiO_2 content is 0.48 - 1.01%, Al_2O_3 content is 7.03 - 15.31%, Fe_2O_3 content is 3.67 - 8.78%, MnO content is 0.08 - 0.18%, MgO content is 1.53 - 11.4%, CaO content varies between 16.86 - 55.19%, Na_2O content is 0.35 - 1.46%, K_2O content is 1.37 - 3.21%, P_2O_5 content is between 0.09 - 0.64%. Major oxides of the rock samples from this region: SiO_2 content is 0.38 - 70.03%, TiO_2 content is 0.06 - 1.06%, Al_2O_3 content is 0.12 - 13.89%, Fe_2O_3 content is 0.06 - 7.58%, MnO

Table 10- Correlation matrix of parameters obtained from the soils taken from Gölcük and its nearby area ($p<0.01$).

	SiO_2	TiO_2	Al_2O_3	Fe_2O_3	MnO	MgO	CaO	Na_2O	K_2O	P_2O_5	Rb	Ba	Sr	Zr	Cr	Cu	Ni	Zn	As	EC	T.Salt	pH	$CaCO_3$	O.M.	T.N	O.C.	Perm.	Sat.
SiO_2	1.00																											
TiO_2	-0.41	1.00																										
Al_2O_3	0.51	0.43	1.00																									
Fe_2O_3	-0.47	0.92	0.43	1.00																								
MnO	-0.59	0.84	0.27	0.96	1.00																							
MgO	-0.53	0.71	0.26	0.91	0.92	1.00																						
CaO	-0.93	0.10	-0.77	0.13	0.27	0.23	1.00																					
Na_2O	0.81	-0.61	0.18	-0.65	-0.68	-0.71	-0.66	1.00																				
K_2O	0.77	-0.82	-0.10	-0.91	-0.90	-0.87	-0.50	0.85	1.00																			
P_2O_5	-0.42	0.23	-0.45	-0.02	0.01	-0.15	0.51	-0.39	-0.13	1.00																		
Rb	0.88	-0.60	0.30	-0.69	-0.77	-0.74	-0.72	0.88	0.86	-0.43	1.00																	
Ba	0.30	-0.45	-0.07	-0.58	-0.66	-0.54	-0.12	0.25	0.51	0.34	0.38	1.00																
Sr	0.02	0.56	0.35	0.35	0.25	0.03	-0.17	0.13	-0.20	0.15	0.07	-0.16	1.00															
Zr	-0.07	0.34	0.10	0.09	-0.03	-0.27	0.06	-0.02	-0.14	0.40	0.02	0.04	0.65	1.00														
Cr	-0.27	0.37	0.09	0.49	0.52	0.64	0.11	-0.43	-0.46	-0.36	-0.28	-0.59	-0.05	-0.43	1.00													
Cu	-0.68	0.76	0.10	0.71	0.74	0.55	0.47	-0.71	-0.80	0.34	-0.66	-0.42	0.37	0.43	0.19	1.00												
Ni	-0.95	0.36	-0.52	0.40	0.52	0.47	0.91	-0.84	-0.71	0.43	-0.84	-0.30	-0.18	0.02	0.27	0.69	1.00											
Zn	-0.66	0.85	0.05	0.79	0.83	0.70	0.43	-0.78	-0.84	0.38	-0.74	-0.51	0.35	0.25	0.52	0.83	0.62	1.00										
As	-0.81	0.14	-0.49	0.32	0.42	0.54	0.78	-0.77	-0.60	0.25	-0.81	-0.12	-0.51	-0.35	0.22	0.37	0.86	0.34	1.00									
EC.	0.19	-0.60	-0.48	-0.65	0.61	-0.65	0.07	0.41	0.56	0.14	0.28	0.16	-0.27	0.03	-0.56	-0.32	-0.04	-0.58	-0.02	1.00								
T.Salt	0.11	-0.54	-0.33	-0.61	-0.61	-0.63	0.11	0.25	0.47	0.22	0.27	0.48	-0.24	0.16	-0.70	-0.16	0.01	-0.58	0.04	0.80	1.00							
pH	-0.04	-0.11	-0.04	0.12	0.18	0.34	-0.01	-0.01	-0.07	-0.39	-0.14	-0.12	-0.40	-0.72	0.40	-0.44	-0.03	-0.17	0.29	-0.28	-0.38	1.00						
$CaCO_3$	0.29	-0.44	0.04	-0.32	-0.23	-0.22	-0.22	0.45	0.37	-0.47	0.44	0.02	-0.23	-0.32	0.15	-0.49	-0.36	-0.35	-0.28	-0.25	-0.30	0.52	1.00					
O.M.	0.06	-0.02	-0.01	-0.07	-0.18	-0.18	-0.02	0.16	-0.03	-0.05	0.10	-0.04	0.32	0.64	-0.36	0.08	-0.10	-0.07	-0.20	0.24	0.13	-0.55	-0.33	1.00				
T.N	0.09	-0.03	-0.02	-0.10	-0.23	-0.24	-0.04	0.20	0.02	-0.01	0.14	0.01	0.36	0.65	-0.41	0.04	-0.13	-0.12	-0.23	0.30	0.19	-0.55	-0.37	0.99	1.00			
O.C.	0.05	-0.01	-0.01	-0.06	-0.18	-0.18	-0.02	0.15	-0.04	-0.04	0.09	-0.04	0.32	0.63	-0.35	0.08	-0.09	-0.07	-0.19	0.24	0.12	-0.55	-0.33	1.00	0.99	1.00		
Perm.	-0.11	-0.07	-0.43	-0.18	-0.09	-0.21	0.23	-0.03	0.16	0.42	-0.10	-0.13	0.18	0.22	-0.15	0.18	0.10	0.15	-0.09	0.39	0.33	-0.50	-0.43	0.07	0.09	0.06	1.00	
Sat.	0.03	-0.23	0.00	-0.32	-0.39	-0.39	0.07	0.01	0.21	0.29	0.18	0.72	-0.04	0.31	-0.63	0.06	-0.01	-0.34	0.02	0.22	0.75	-0.36	-0.22	0.03	0.07	0.03	0.07	1.00

T.N.: Total Nitrogen. **OC:** Organic Carbon. **OM:** Organic Matter. **T.Salt:** Total Salt . **Perm.:** Permeability. **Sat:** Saturation.

Table 11- Normalized values of major and trace elements with bedrock in Gölcük and its nearby area soils (Soil/Rock).

	GT-1	GT-2	GT-3	GT-4	GT-5	GT-6	GT-7	GT-8	GT-9	GT-10	GT-11	GT-12
	Andesite	Sandy Limestone	Basalt Andesite	Andesite	Basalt Andesite	Andesite	Sandy Limestone	Basalt	Andesite	Sandy Limestone	Andesite	Andesite
SiO_2	1.29	0.67	1.31	1.17	0.89	0.94	3.28	1.02	1.08	2.80	0.94	0.92
TiO_2	2.38	0.86	0.92	2.26	0.96	1.61	5.06	1.43	1.93	3.39	1.81	2.04
Al_2O_3	1.08	0.65	1.14	1.14	1.12	1.13	8.01	1.06	1.24	4.98	1.17	1.20
Fe_2O_3	0.91	0.93	0.95	1.21	1.28	1.35	4.73	1.38	0.27	2.66	1.86	2.22
MnO	0.93	1.08	0.99	1.28	0.81	1.14	2.60	1.30	1.60	3.00	1.80	1.29
MgO	0.33	1.23	0.95	0.57	1.39	1.22	2.37	0.94	0.71	1.75	1.87	1.41
CaO	0.35	5.08	0.16	0.47	1.64	2.15	0.06	0.75	1.24	0.13	1.49	1.97
Na_2O	1.04	0.10	0.44	0.70	0.45	0.77	7.93	0.61	1.58	4.39	0.62	0.74
K_2O	2.53	0.71	1.16	1.60	0.99	0.94	7.80	0.70	1.41	5.15	0.91	0.94
P_2O_5	1.22	0.58	0.44	0.61	0.63	2.14	1.05	0.40	2.10	2.00	2.17	2.80
Nb	1.14	1.50	0.00	0.00	1.10	0.00	1.40	0.00	0.00	1.50	1.07	0.00
Ba	0.75	0.44	0.75	0.54	0.64	0.89	0.74	0.43	1.00	1.20	1.13	0.90
Rb	1.04	1.28	1.19	0.59	1.02	1.00	4.54	0.85	1.00	2.27	1.00	0.50
Sr	1.70	0.43	0.23	1.13	0.51	2.00	0.40	0.82	1.33	0.45	2.50	2.00
Zr	0.02	0.67	0.64	0.01	1.54	1.00	1.00	1.00	1.00	0.67	1.00	1.00
Fe	0.91	0.93	0.95	1.21	1.28	1.36	4.73	1.38	0.27	2.66	1.86	2.20
Mn	0.91	1.11	0.99	1.27	0.83	1.20	2.50	1.33	1.50	3.00	1.75	1.40
Cr	2.42	2.00	2.34	2.42	4.00	3.42	6.84	6.67	1.67	9.12	4.28	5.07
Cu	0.73	0.89	0.63	0.81	1.10	0.92	1.08	0.64	0.49	0.77	1.63	1.24
Ni	1.08	4.25	1.14	1.16	2.16	1.98	1.32	1.36	0.69	1.03	2.32	1.19
Zn	1.38	1.06	1.00	1.38	1.18	1.50	1.79	1.20	1.14	1.42	1.88	2.62
As	1.26	1.52	1.70	2.26	0.25	0.97	1.39	0.76	1.01	0.87	2.14	0.50

content is 0.05 - 1.59%, MgO content is 0.12 - 4.56%, CaO content varies between 4.31 - 96.1%, Na_2O content is 0.05 - 3.85%, K_2O content is 0.03 - 5.27%, P_2O_5 content is between 0.05 - 0.25%.

It has been determined that the Ca / Mg ratios of the soils of this region vary between 2 and 25, and the lime ratios measured from the same soils vary between 9 - 41% (Table 5) and these soils have calcite content. It is understood that the soils are derived from the carbonate-rich rocks that crop out in the region rather than being transported. In the correlation analysis applied to soil parameters (Table 12), the main elements show high positive (Ca high negative correlation) among themselves, and this indicates that soils were formed by similar processes and from similar lithogenic origin. Likewise, it was determined that there is very weak positive or negative correlation between trace elements and pH which plays an important role on the mobility of metals. Pb has poor mobility in neutral and alkaline soils, but Cu, As and Zn complexes are more common in such soils. It is seen that it coincides with the results of the researches that show that it has high mobility (Lee et al., 2001; Fernandez-Turiel et al., 2001).

Normalized values of Bor and its vicinity soils lithology, Rb is 0.41 - 3.57, Ba is 0 - 2, Sr is 0.03 - 3.67, Zr is 0.01 - 1.67, Fe is 0.44 -84.20, Mn is 0.10 - 2.40, Cu is 0.95 - 2.86, Ni is 0.19 - 10.48, Zn is 0.97 - 3.14, As is 1.91 - 6.67 times higher than the bedrock. It is quite enriched by Fe, Ni and As elements than lithology (bedrock) (Table 13). This shows that it was lithologically originated from the basaltic andesites in the region. The phosphate source of these soils, which are also rich in phosphate, increases the possibility of being pesticides and other fertilizers used in agricultural activities rather than lithology.

In addition, the relationships between the rock materials developed due to the effect of the volcanism

Table 12- Correlation matrix of parameters obtained from the soils taken from Bor and its nearby area ($p<0.01$).

	SiO_2	TiO_2	Al_2O_3	Fe_2O_3	MnO	MgO	CaO	Na_2O	K_2O	P_2O_5	Rb	Ba	Sr	Zr	Cu	Ni	Zn	As	EC	T.Salt	pH	$CaCO_3$	O.M.	T.N	O.C.	Perm.	Sat.
SiO_2	1.00																										
TiO_2	-0.08	1.00																									
Al_2O_3	0.73	0.49	1.00																								
Fe_2O_3	0.69	0.61	0.85	1.00																							
MnO	0.40	0.59	0.73	0.81	1.00																						
MgO	0.34	-0.32	-0.17	0.22	0.00	1.00																					
CaO	-0.95	-0.12	-0.76	-0.85	-0.56	-0.45	1.00																				
Na_2O	0.71	0.33	0.87	0.79	0.67	0.02	-0.77	1.00																			
K_2O	0.71	0.33	0.54	0.79	0.48	0.40	-0.80	0.61	1.00																		
P_2O_5	-0.23	0.24	-0.29	0.03	-0.11	0.09	0.14	-0.32	0.27	1.00																	
Rb	0.73	0.05	0.65	0.61	0.49	0.16	-0.72	0.50	0.53	-0.28	1.00																
Ba	0.71	0.42	0.63	0.88	0.64	0.38	-0.84	0.59	0.94	0.22	0.66	1.00															
Sr	0.14	-0.27	-0.32	0.11	-0.05	0.94	-0.27	-0.10	0.31	0.17	0.09	0.30	1.00														
Zr	0.11	0.36	0.02	0.39	0.00	0.41	-0.27	0.15	0.67	0.55	-0.05	0.55	0.40	1.00													
Cu	0.03	0.55	0.31	0.47	0.32	0.03	-0.19	0.04	0.17	0.27	0.30	0.43	0.09	0.32	1.00												
Ni	0.42	0.42	0.44	0.77	0.68	0.46	-0.63	0.57	0.80	0.15	0.45	0.84	0.44	0.62	0.35	1.00											
Zn	-0.02	0.58	0.47	0.40	0.31	-0.26	-0.11	0.40	0.05	-0.16	0.31	0.10	-0.19	0.09	0.43	0.19	1.00										
As	-0.01	-0.42	-0.15	-0.27	-0.39	0.03	0.10	-0.38	-0.32	0.07	0.21	-0.23	-0.06	-0.20	0.21	-0.36	0.08	1.00									
EC.	-0.24	0.11	-0.34	-0.25	-0.48	-0.17	0.29	-0.38	0.04	0.63	-0.43	-0.06	-0.04	0.35	0.08	-0.30	-0.30	-0.19	1.00								
T.Salt	-0.22	0.19	-0.30	-0.16	-0.34	-0.16	0.25	-0.35	0.12	0.73	-0.41	0.02	-0.04	0.33	0.07	-0.22	-0.33	-0.23	0.97	1.00							
pH	0.36	-0.03	0.06	0.31	0.33	0.38	-0.38	-0.01	0.49	0.51	0.15	0.52	0.26	0.16	-0.02	0.33	-0.58	-0.05	0.11	0.30	1.00						
$CaCO_3$	-0.44	0.12	-0.25	-0.30	-0.11	-0.15	0.42	-0.50	-0.53	-0.40	-0.05	-0.35	-0.06	-0.38	0.23	-0.33	0.14	0.09	-0.12	-0.19	-0.36	1.00					
O.M.	-0.39	0.55	0.10	0.22	0.56	-0.20	0.19	0.08	-0.01	0.04	0.00	0.09	-0.14	0.09	0.26	0.45	0.43	-0.13	-0.48	-0.39	-0.07	0.20	1.00				
T.N	-0.36	0.57	0.13	0.25	0.56	-0.20	0.17	0.11	0.03	0.08	0.03	0.14	-0.15	0.15	0.29	0.49	0.46	-0.12	-0.46	-0.37	-0.06	0.15	1.00	1.00			
O.C.	-0.39	0.56	0.10	0.22	0.56	-0.20	0.20	0.08	-0.01	0.04	0.00	0.09	-0.14	0.09	0.27	0.45	0.44	-0.12	-0.48	-0.39	-0.07	0.20	1.00	1.00	1.00		
Perm.	0.02	0.36	0.31	0.23	0.19	-0.21	-0.08	0.21	0.12	-0.29	0.09	0.20	-0.31	0.30	0.35	0.32	0.23	-0.02	-0.26	-0.35	-0.31	0.21	0.42	0.44	0.42	1.00	
Sat.	-0.27	0.24	-0.29	-0.15	-0.19	-0.22	0.29	-0.39	0.07	0.74	-0.40	0.00	-0.12	0.18	0.00	-0.24	-0.36	-0.24	0.85	0.95	0.45	-0.13	-0.24	-0.23	-0.23	-0.44	1.00

T.N.: Total Nitrogen. **OC:** Organic Carbon. **OM:** Organic Matter. **T.Salt:** Total Salt . **Perm.:** Permeability. **Sat:** Saturation.

Table 13- Normalized values of major and trace elements with bedrock in Bor and its nearby area soils (Soil / Rock).

	BT-1	BT-2	BT-3	BT-4	BT-5	BT-6	BT-7	BT-8	BT-9	BT-11	BT-12
	Calcite	Sandy Limestone	Ignimbrite	Ignimbrite	Calcite	Calcite	Ignimbrite	Ignimbrite	Ignimbrite	Sandy Limestone	Ignimbrite
SiO_2	5.35	1.13	0.69	0.66	115.24	25.08	0.63	0.62	0.59	0.67	0.56
TiO_2	2.13	0.83	3.37	2.81	14.20	11.83	1.96	1.90	3.31	0.81	2.67
Al_2O_3	4.51	1.60	1.00	0.86	96.17	18.45	0.57	0.67	0.33	0.79	0.86
Fe_2O_3	4.60	1.04	4.08	2.76	100.33	17.07	2.10	2.22	2.95	0.48	2.54
MnO	0.09	0.28	2.25	1.14	3.00	2.50	1.43	1.13	2.14	0.16	2.00
MgO	12.26	142	13.09	7.47	35.50	11.44	16.93	16.70	4.88	0.63	3.48
CaO	0.25	0.61	4.00	6.26	0.30	0.18	7.08	7.38	7.37	1.75	8.95
Na_2O	1.96	0.75	0.28	0.21	2.17	29.20	0.10	0.10	0.18	0.26	0.18
K_2O	3.27	1.65	0.61	0.46	87.00	36.00	0.41	0.35	0.41	0.82	0.27
P_2O_5	1.13	1.15	2.56	5.40	ae	1.80	7.40	1.48	3.80	2.15	0.72
Rb	3.57	1.10	0.50	0.50	0.83	1.13	0.41	0.50	0.49	0.65	0.50
Ba	0.53	2.00	1.20	0.75	1.03	0.91	0.63	0.40	0.63	0.00	0.40
Sr	2.11	1.17	3.33	2.33	0.03	5.00	3.67	3.67	1.33	1.17	1.67
Zr	1.33	1.67	1.67	1.33	ae	0.01	1.00	1.00	0.67	1.33	0.33
Fe	4.13	0.94	3.68	2.48	84.20	15.31	1.89	2.00	2.66	0.44	2.29
Mn	0.10	0.27	2.33	1.20	ae	2.40	1.60	1.17	2.40	0.16	2.00
Cu	0.95	1.30	2.86	2.73	1.21	1.36	2.33	2.60	2.36	1.13	2.86
Ni		0.50	5.72	4.24	10.48	4.91	4.76	2.46	4.76	0.19	2.86
Zn	3.14	0.97	1.28	1.61	2.13	1.46	1.58	1.28	1.61	0.97	1.28
As	2.04	3.96	2.03	2.55	2.73	2.51	2.24	6.67	1.91	2.78	3.33

of the region and the soils developed on them were revealed using the diagram obtained with SiO_2 (%) - $Na_2O + K_2O$ (%) parameters used in the classification of volcanic rocks developed by Cox et al. (1979) (Figure 5). Based the diagrams; Subalkaline tholeiitic magma series, which are poor in total alkali ($Na_2O + K_2O$) and rich in Fe content, are defined as basaltic andesite, andesite, trachy-andesite, dacite and rhyolite with medium and acid content. It was observed that most of the soils formed on these rocks developed in situ due to the effect of magmatism of the region and overlapped with the main rock materials. The main rock materials outcropping in Bor and its vicinity are defined as basic-ultrabasic rocks under the effect of regional metamorphism as alkaline magma series that are richer in total alkali content but poorer in SiO_2 composition. The similarity of the sample distributions in the diagram revealed that the soils observed in this area were also developed in situ by deriving from the rocks of calcic composition rich in Ca content.

There are many studies conducted to support the relationship between lithology and soil. One of them is Özdemir et al. (2008) which was conducted in Erzurum region. Four different main materials (andesite, alluvial, gypsum and basalt) and soil samples are taken from areas under three different land use types and based on the Mn, Fe, Cu and Zn element contents They determined that the distribution of these elements was significantly affected by the type of the rock material and the land use. Accordingly, they determined that the distributions of total microelement contents and fractions were generally higher in soils composed of andesite rocks than others.

The lithology of an area is an important parameter for agricultural use, not directly but indirectly. Lithological units constitute the main material of the soil, which is one of the most important parameters for agricultural use. The fact that the soils that can be cultivated are soils that develop on certain lithological units or developed on some lithological units do not have any importance for agricultural use, reveal the importance of lithological unit types for agricultural use. In this study, besides the soil, topography and climate factors, effects of geological factors of the selected areas on the determination of the suitability classes for agricultural use are determined. The effect level was determined by the normalized weight scores of the main parameters and their sub-parameters among themselves. Normalized weight scores for

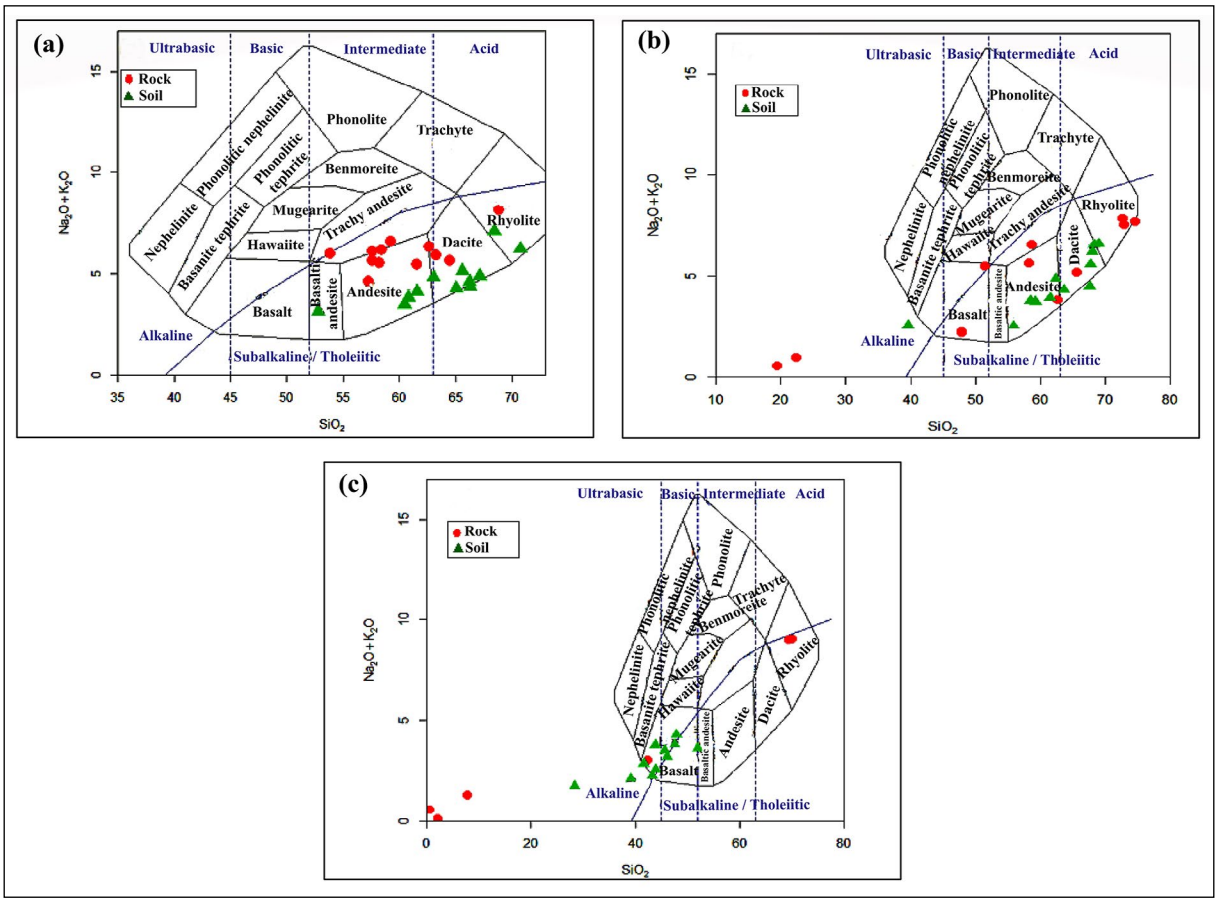

Figure 5- SiO_2-Na_2O + K_2O diagrams of a) Çiftlik, b) Gölcük, c) Bor and its vicinity rock and soil samples (Cox et al., 1979).

main and sub-parameters were calculated using the AHP technique (Table 14).

A consistent matrix of 0.028 consistency rate was created for the main parameters. In the matrix, it was determined that the soil main parameter has the highest weight (53.4%) on the determination of the agricultural suitability classes of the study area. This was followed by the main parameters of topography (30.3%), climate (10.8%) and geology (5.5%). Maddahi et al. (2014) made the agricultural land suitability classification of the rice product of economic importance in the Amol region of Iran. In this study, which they conducted by using the main parameters of soil, topography, climate and irrigation water and their sub-parameters, Analytical Hierarchy Process technique was used in the calculation of the weight values of the parameters. While they calculated the consistency ratio of the paired comparisons of the main parameters as 0.06, they determined that the soil, which is one of the most important parameters in terms of agriculture, was the factor with the greatest impact with 60.2% weight ratio. In this study, in which the topography is 11.3%, the climate is 4.7% and the irrigation water is 23.8% by weight, they have made land suitability classification consisting of 4 (four) classes in terms of agriculture as high suitable, suitable, moderate suitable and not suitable.

For the sub-parameters, consistent comparison was made with consistency ratio of 0.08 in the paired comparison matrix. When the normalized weight scores of the sub-parameters were evaluated, the slope was determined as the sub-parameter with the highest weight with value of 21.2%. Effective parameters in determining the suitability classes for agricultural use based on the weight values, after the slope are landforms (19.5%), pH (13.8%), organic matter (10.5%), lime (8.5%), precipitation (6.1%), total salt (4.6%) , hydraulic conductivity (permeability) (3.4%), electrical conductivity (EC) (3.2%), water saturation (2.8%), lithological units (2.7%), total nitrogen (2.4%) and organic matter (1.3%) parameters, respectively.

Table 14- Paired comparison matrix and normalized weight values of the main and subcriteria.

Paired comparison matrix of the main criteria					
	Soil	Topography	Climate	Geology	*Normalized Weight*
Soil	**1**				0.534
Topography	0.5	**1**			0.303
Climate	0.166	0.250	**1**		0.108
Geology	0.125	0.200	0.333	**1**	0.055

λ_{max} *:* 4,080*; Rİ:* 0.90*; TO:* 0,028 < 0,10 $\sum = 1$

Paired comparison matrix of the subcriteria														
	1	*2*	*3*	*4*	*5*	*6*	*7*	*8*	*9*	*10*	*11*	*12*	*13*	*Normalized Weight*
1	**1**													0.085
2	0.25	**1**												0.024
3	0.16	0.25	**1**											0.013
4	0.14	0.50	2	**1**										0.032
5	3	5	6	4	**1**									0.105
6	4	6	7	4	3	**1**								0.138
7	0.33	3	4	3	0.50	0.25	**1**							0.046
8	0.50	2	3	0.50	0.25	0.20	0.50	**1**						0.034
9	0.33	2	2	0.50	0.25	0.20	0.50	0.50	**1**					0.028
10	0.20	4	5	2	0.20	0.25	2	3	3	**1**				0.061
11	6	7	8	6	3	4	5	6	6	5	**1**			0.212
12	6	6	7	6	3	3	6	5	5	4	1	**1**		0.195
13	0.33	3	3	0.33	0.20	0.16	0.50	0.33	0.33	0.20	0.16	0.20	**1**	0.027

λ_{max} : 14.66 ; Rİ : 1.56 ; TO : 0.08 < 0.10 $\sum = 1$

1: Lime, 2: Total nitrogen, 3: Organic carbon, 4: EC, 5: Organic matter, 6: pH, 7: Total salt, 8: Hydraulic conductivity (Permeability), 9: Water saturation, 10: Precipitation, 11: Slope, 12: Terrain shapes, 13: Lithological units

Dengiz and Sarıoğlu (2013), on the agricultural land suitability map of the lands covering Dedeli and Çetinkaya villages and their close vicinity in the Bafra district of Samsun province, is determined the lands based on the suitability classification consisting of 4 (four) classes (Highly suitable, Moderate suitable, Marginally suitable and Not suitable). While they calculated the consistency ratio of the paired comparisons of the parameters used in determining these classes as 0.07, they revealed the slope parameter as the parameter with the highest weight with a weight value of 23.3%. The slope parameters are respectively drainage (16.2%), constituent (15.7%), pH (14.1%), depth (10.3%), EC (10%), efficiency (4.4%) and lime (0.8%), respectively.

Turoğlu (2005) evaluated the suitability of Kayaköy (Fethiye) polje for ecotourism, settlement and agriculture together with the geomorphology, slope, aspect, hydrography, vegetation, soil and land use parameters in his study, in which he used the lithology factor as an important parameter. In determining areas suitable for agriculture; While no weighted multiplier was used for limestones, one of the sub-classes of lithology parameter, the weighted multiplier for alluviums was used as 10 points. As a result of the evaluation, he divided the agricultural suitability classification of the study area into 5 (five) general suitability classification (Very suitable, Suitable, Moderately suitable, Less suitable and Inappropriate).

The main and sub-parameters used in the determination soils in the study area, developing on different main materials and the agricultural use classes were combined according to the normalized weight values assigned using the AHP technique, according to the weighted linear combination method, and the suitability classes map of the study area was created (Figure 6). The general distribution rates

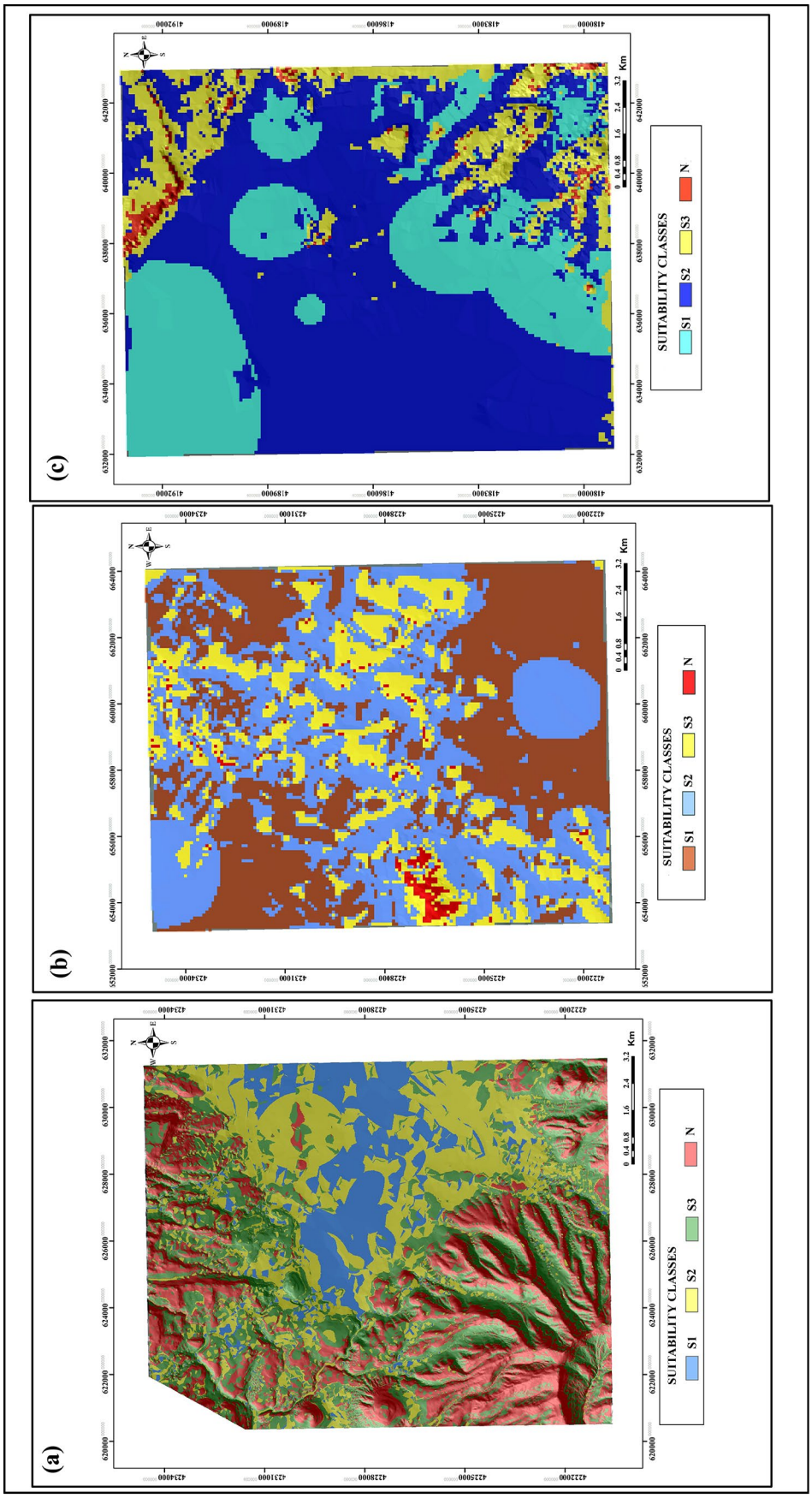

Figure 6- Suitability classes for agricultural use of a) Çiftlik and its vicinity, b) Gölcük and its vicinity, c) Bor and its vicinity.

of suitability classes in all three study areas were calculated as areal and percentage and given in table 15. It has been determined that the lands developed in Gölcük and its vicinity are much more suitable for agricultural use with a rate of 38.31% compared to the lands seen in the other two areas. Different from the other two areas of Çiftlik and its vicinity lands, due to the restrictive effects such as the excess of areas with a slope greater than 12%, the excessive observation of magmatic origin lithological units that are not agriculturally suitable and the excess of agriculturally unsuitable land forms (Table 2), the highest amount of agriculturally unsuitable soils with a rate of 27.93%. (Table 15).

Likewise, the distribution of agricultural suitability classes of developed soils on lithological units in each area was calculated as a percentage and given in Table 16. The calculated percentages express the ratio of each suitability class in its total area. While most of the arable lands around Çiftlik and Bor are alluvium units, the arable lands in Gölcük and its vicinity have formed the basalt-andesite unit. In addition, it has been determined that the soils developed on basalt-andesites in Çiftlik and its vicinity, gabbros in and around Gölcük, and limestones in and around Bor are not suitable for agriculture (Table 16).

4. Conclusions

In the research, the general characteristics of the soils that have developed and continued to develop on different rock materials, the relationships of these soils with lithological units observed in the area and also the quality of the soils derived from different various rock materials for their suitability in agricultural activity have been tried to be investigated. During the research, the geochemical analysis of the soil and rock samples collected from the study area, the physical and chemical analysis of the soils integrated with the topographic and climatic factors were evaluated. According to the results; depending on the lithological features of the units alkaline characteristics of the soils has been developed around Bor district and the soils developed around Çiftlik and Gölcük districts and their vicinity are more acidic reaction. The results of geochemical analysis from soil and rock samples indicated that the soils are developed by both in situ and accumulation around Çiftlik district and vicinity, while the soils around Gölcük and Bor districts are developed in situ. It has been calculated that the main criterion of geology is 5.5% and the criterion of lithological units, which is its' sub-criterion, is 2.7% effective in determining the agricultural suitability of the soils in the study area.

When the distribution of suitability classes for agricultural use is compared with lithological units, most of the suitable area for agricultural purposes around Çiftlik and Bor is alluvium and basalt-andesite units in and around Gölcük district. In addition, the unsuitable classes for agriculture are found to be distributed on basalt-andesites in and around Çiftlik, gabbros in and around Gölcük, and limestones in and around Bor districts.

Consequently, the soils developed around Gölcük and Bor are more suitable for agriculture than the soils developed in Çiftlik and its vicinity.

Table 15- Area and percentage rates of suitability classes for agricultural use in the study area.

Study areas	Suitability Classes for Agricultural Use			
	S1 (Highly suitable) (km^2)	**S2** (Moderate suitable) (km^2)	**S3** (Marginally suitable) (km^2)	**N** (Unsuitable) (km^2)
Çiftlik and its nearby area	18496.717 **%12.41**	37634.490 **%25.25**	51303.096 **%34.41**	41639.939 **%27.93**
Gölcük and its nearby area	57486.326 **%38.31**	62614.022 **%41.72**	27881.142 **%18.58**	2084.933 **%1.39**
Bor and its nearby area	44698.648 **%29.34**	85595.006 **%56.18**	19616.688 **%12.87**	2458.639 **%1.61**

Table 16- Distribution ratios of suitability classes for agricultural use on the lithological units in study area.

Study areas	Suitability Classes for Agricultural Use			
	S1 (Highly suitable) (%)	**S2 (Moderate suitable) (%)**	**S3 (Marginally suitable) (%)**	**N (Unsuitable) (%)**
Çiftlik and its nearby area	Alluvial %63.65	Basalt. Andesite %53.08	Basalt. Andesite %71.37	Basalt. Andesite %81.24
	Basalt. Andesite %19.61	Alluvial %36.51	Pyroclastic rock %13.92	Pyroclastic rock %11.77
	Pyroclastic rock %8.81	Slope debris. deposit cone %5.77	Alluvial %3.52	Alluvial %0.43
	Slope debris. deposit cone %4.50	Pyroclastic rock %2.70	Ignimbrite %1.68	Ignimbrite %0.42
	Agglomerate %2.10	Ignimbrite %1.71	Agglomerate %3.53	Agglomerate %3.01
	Ignimbrite %1.33	Agglomerate %0.23	Slope debris. deposit cone %5.98	Slope debris. deposit cone %3.13
Total	%100	%100	%100	%100
Gölcük and its nearby area	Basalt-Andesite %61.68	Basalt-Andesite %57.22	Basalt-Andesite %48.63	Gabbro %60.51
	Peble-sandstone-mudstoneı %18.18	Ignimbrite %29.62	Ignimbrite %43.49	Basalt-Andesite %23.96
	Ignimbrite %20.14	Peble-sandstone-mudstone %12.75	Peble-sandstone-mudstone %3.65	Ignimbrite %12.83
		Gabbro %0.41	Gabbro %4.23	Peble-sandstone-mudstone %2.70
Total	%100	%100	%100	%100
Bor and its nearby area	Alluvial % 85.88	Alluvial %68.32	Limestone %71.40	Limestone %75.70
	Limestone %10.17	Limestone %26.63	Pyroclastic rock Trachyandesite %14.90	Pyroclastic rock Trachyandesite %17.58
	Pyroclastic rock Trachyandesite %3.87	Pyroclastic rock Trachyandesite %4.65	Ignimbrite %4.13	Ignimbrite %2.77
	Ignimbrite %0.03	Ignimbrite %0.34	Alluvial %9.43	Alluvial %3.26
	Marble %0.05	Marble %0.06	Marble %0.138	Marble %0.69
Total	%100	%100	%100	%100

References

Akalan, İ. 1983. Toprak Bilgisi, A.Ü. Ziraat Fakültesi Yayını: 878, Ders Kitabı: 234, 346, Ankara.

Armacost, L.R., Componation, P.J., Mullens, M.A., Start, W. 1994. An AHY framework for prioritizing customer requirements in QFD: an industrialized housing application, IIE Transactions, 26 (4), 72-79.

Aydın, F., Karslı, O., Şen, C., Sadıklar, M.B., Uysal, İ. 2005. Orta Anadolu volkanitlerindeki (Niğde-Çiftlik-Altunhisar) dengesiz kristallenme dokuları ve fenokristallerin kimyasal bileşimleri. KTÜ 40. Yıl Jeoloji Sempozyumu, Trabzon, 51-52.

Beekman, P.H. 1966. The Pliocene and Quarternary volcanism in the Hasandağ-Melendizdağ region. Bulletin of the Mineral Research and Exploration 66, 99 – 106.

Brady, N. C. 1990. The nature and properties of soils (10 th edition). Macmillan Publishing Company, New York.

Cengiz, T., Çelem, H. 2006. Land use potential and suitability for areas of arable and garden farming, Meadow-Pasture and Recreation-Tourism in Alpağut Village, Journal of Applied Sciences 6 (8), Asian Network for Scientific Information, Bolu, Turkey, 1641 - 1651, ISSN 1812 – 5654.

Chuong, H.V., Boehme, M. 2005. Evaluation of physical land suitability for the Thanh Tra pomelo crop in Hue, Vietnam, In Conference on International Agricultural Research for Development, Stuttgart-Hohenheim.

Cox, K.G., Bell, J.D., Pankhurst, R.J. 1979. The Interpretation of Igneous Rocks. Allen and Unwin, London, 450. http://dx.doi.org/10.1007/978-94-017-3373-1

Çağlar, K.Ö. 1949. Toprak Bilgisi, (10. Basım), Ankara Üniversitesi Ziraat Fakültesi Yayınları, Ankara.

Dengiz, O., Sarıoğlu, F.E. 2013. Arazi değerlendirme çalışmalarında parametrik bir yaklaşım olan doğrusal kombinasyon tekniği, Ankara Üniversitesi Ziraat Fakültesi Tarım Bilimleri Dergisi 19, 101, 112, Ankara.

Dodson, R., Marks, D. 1997. Daily air temperature interpolated at high spatial resolution over a large mountainous region. Climate Research 8, 1 - 20.

Dorronsoro, C. 2002. Soil evaluation the role of soil science in land evaluation, International symposium on sustainable use and management of soils in arid and semiarid regions. Cartagena Spain, http://www.edafologia.net/comun/congres.htm,.. September 22- 26.

Esri. 2004. Using arcview gis. Environmental System Research Institute. Inc. Redlans, California.

FAO. 1976. A framework for land evaluation, Soils Bulletin, 32, Soils resources, management and conservation service, FAO Land and Water Development Division, Rome.

FAO. 1985. Guidelines land evaluation for irrigated agriculture. FAO, Rome.

Feizizadeh, B., Blaschke, T. 2012. Land suitability analysis for Tabriz County, Iran: a multi-criteria evaluation approach using GIS. Journal of Environmental Planning and Management 1-23.

Fernandez-Turiel, J. L., Acenolaza, P., Medina, M. E., Llorens, J. F., Sardi, F. 2001. Assessment of smelter impact area using surface soils and plants, Environ Geochem Health 23, 65-78.

Gürel, A. 2006. Adsorption characteristics of heavy metals in soil zones developed on spilite. Environmental Geology 51(3), 333-340.

Göncüoğlu, M.C. 1981. Niğde masifinin jeolojisi, İç Anadolu'nun Sempozyumu, Bildiriler Kitabı 16 – 19, Maden Tetkik ve Arama Genel Müdürlüğü, Ankara.

Jenness, J. 2005. Landform classification (Topography Tools 9.1.tbx) extension for ArcGIS 9.1 Jenness Enterprises. http://www.jennessent.com.

Kaçar, B. 1972. Bitki ve Toprağın Kimyasal Analizleri II. Bitki analizleri, (646. Basım), Ankara Üniversitesi Basımevi, Ankara.

Kaçar, B. 1994. Bitki ve Toprağın Kimyasal Analizleri III, Toprak Analizleri, (3. Basım) Ankara Üniversitesi, Ziraat Fakültesi Eğitim Araştırma ve Geliştirme Vakfı Yayını, Ankara.

Kapur, S., Sakarya, N., Akça E., Karaman, C. 1996. Alternative use of non arable soils in ceramics industry, Agriculture-Enviroment Symposium, Mersin, 670 – 678.

Klute, A.1965. Laboratory measurement of hydraulic conductivity of saturated soil, In: Black CA (ed), Methods of Soil Analysis, Part 1. ASA, Madison, WI, 210 -221.

Lee, C., Chon, H., Jung, M. 2001. Heavy metal contamination in the vicinity of the Daduk Au-Ag-Pb-Zn mine in Korea, Appl. Geochem 16, 1377 - 1386.

Maddahi, Z., Jalalian, A., Zarkesh, M.M.K., Honarjo, N. 2014. Land suitability analysis for rice cultivation using multi criteria evaluation approach and GIS. European Journal of Experimental Biology 4(3): 639-648.

Malczewski, J. 2006. GIS-based multicriteria decision analysis: a survey of the literature. Int. J of Geog In Sci 20:703–726.

Mc Coy, C., Johnston, K. 2001. Using ArcGis Spatial Anayst, ESRI, Redlands, USA.

MTA, 2010*a*. L33 c2 paftası 1/25.000 ölçekli jeoloji haritası. Maden Tetkik ve Arama Genel Müdürlüğü Türkiye Jeoloji Veri Tabanı, Ankara.

MTA, 2010*b*. L33 c1 paftası 1/25.000 ölçekli jeoloji haritası. Maden Tetkik ve Arama Genel Müdürlüğü Türkiye Jeoloji Veri Tabanı, Ankara.

MTA, 2010*c*. M33a paftası 1/25.000 ölçekli jeoloji haritası. Maden Tetkik ve Arama Genel Müdürlüğü Türkiye Jeoloji Veri Tabanı, Ankara.

Özdemir, N., Öztürk, E., Yakupoğlu, T. 2008. Anamateryal ve arazi kullanım şeklinin topraktaki bazı mikroelement fraksiyonlarının dağılımına etkileri, OMÜ Ziraat Fakültesi Dergisi Samsun, 23 (2) 92-97.

Patrono, A. 1998. Multi-Criteria Analysis and Geographic Information Systems: Analysis of Natural Areas and Ecological Distributions. Multicriteria Analysis for Land-Use Management, Edited

by Euro Beinat and Peter Nijkamp, Kluwer Academic Publishers, Environment and Management-Volume: 9, 271-292, AA Dordrecht, The Netherlands.

Pasquare, G. 1968. Geologie of the Senozoic volkanic area of Central Anatolia, Atti della Acad.No.delince; menorie serie VIII, vol.IX, Roma, 55 – 204.

Price, J. R., Velbel, M. A. 2003. Chemical weathering indices applied to weathering profiles developed on heterogeneous felsic metamorphic parent rocks. Chemical Geoology 202(3-4), 397-416.

Richards, L.A, 1954. Diagnosis and improvement of saline and alkali soils, US Salinity Lab., US Department of Agriculture Handbook 60, California, USA.

Satty, T.1980. The Analytical Hierarchy Process. McGraw Hill, New York.

Tarım ve Köyişleri Bakanlığı, 2008. Toprak ve Arazi Sınıflaması Standartları Teknik Talimatı ve İlgili Mevzuatı, Ankara.

Tijani, M. N., Okunlola, O. A., Abimbola, A. F. 2006. Lithogenic concentrations of trace metals in soils and saprolites over crystalline basement rocks: a case study from SW Nigeria. Journal of African Earth Sciences 46(5), 427-438.

Torunlar, H., Nazlıcan, A.N. 2018. Türkiye'de ana ürün olarak yetiştirilecek soyanın (glycine max l.merrill) çok kriterli karar verme yöntemiyle arazi uygunluk analizinin yapılması, Ondokuz Mayıs Üniversitesi, Ziraat Fakültesi, Anadolu Tarım Bilimleri Dergisi 33(3), 270-281, Samsun.

TS 8333, 1990. Toprağın su ile doygunluk yuzdesinin tayininde kullanilan metod. ICS Code: 13.080.40. 11 Nisan.

Turoğlu, H. 2005. Fiziksel planlama ve coğrafi bilgi sistemleri, Ege Üniversitesi, Ege Coğrafi Bilgi Sistemleri Sempozyumu, Bildiri Özetleri Kitabı 51, 27 - 29 Nisan. İzmir.

Ülgen, N., Ateşalp, M. 1972. Toprakta organik madde tayini, Tarım ve Köyişleri Bakanlığı, Topraksu Genel Müdürlüğü, Toprak Gübre Araştırma Enstitüsü, Teknik Yayını, 23.

Yu, J., Chen, Y., Wu, J. 2011. International Journal of Geographical Information Science, 25 (1), 131-148.

Yüksel, M. 2003. Farklı yükseklik, iklim ve ana materyaller üzerinde oluşmuş toprakların fiziksel, kimyasal ve minerolojik özellikleri, Ankara Üniversitesi, Tarım Bilimleri Dergisi Sayı 9 (3), Sayfa 365-369

Willmott, C.J., Matsuura, K. 1995. Smart interpolation of annually averaged air temperature in the United States, Journal of Applied Meteorology 34, 2577-2586.

Bulletin of the Mineral Research and Exploration

http://bulletin.mta.gov.tr

Evolution of slab tearing-related high potassium volcanism: Petrogenetic data from the Emirdağ and İscehisar volcanic units

Selin BİLGİÇ GENCER[a], Sibel TATAR ERKÜL[b*] and Fuat ERKÜL[c]

[a]*Çiftay Construction, Divriği Iron Ore Mine, Sivas, Turkey*
[b]*Akdeniz University, Department of Geological Engineering, Antalya, Turkey*
[c]*Akdeniz University, Vocational School of Technical Sciences, Antalya, Turkey*

Research Article

Keywords:
Afyon high potassium volcanism, Sr-Nd isotopes, Slab tearing, Slab roll-back.

ABSTRACT

Volcanism that has been active since the early Miocene along a N-S trending line from Eskişehir to Isparta displays calc-alkaline and alkaline character and is closely associated with slab tearing processes. However, the geodynamic setting of these volcanic units between Afyon and Emirdağ is still poorly known. In this study, petrological characteristics of the Emirdağ and İscehisar volcanic units have been investigated using petrography, whole-rock geochemistry and Sr-Nd isotopes. The Emirdağ and İscehisar volcanic units overlap the SeydileIgnimbrites. The Emirdağ volcanic unit is trachyandesite and the İscehisar volcanic unit is trachyte, basaltic trachyandesite and trachydacite in composition. The Emirdağ volcanic unit displays calc-alkaline character, while the İscehisar volcanic unit is alkaline but the rocks from both the units have shoshonite character defined by their high K_2O contents. The Emirdağ volcanic unit has $^{87}Sr/^{86}Sr$ ratios of 0.706790-0.706284 and $^{143}Nd/^{144}Nd$ ratios of 0.512472-0.512463, while these ratios in the İscehisar volcanic unit are of 0.707650-0.706527 and 0.512464-0.512424, respectively. Data revealed by this study indicate that these volcanic units were affected by crustal contamination, fractional crystallization and magma mixing. Rising of asthenosphere in the region due to the extensional regime in the Early Miocene appears to have caused formation of volcanism that pass from calc-alkaline to alkaline in character. The Emirdağ and İscehisar volcanic units are the products of the volcanism that developed in the late stages of southward slab roll-back and in the extensional regime prior to the slab tearing event.

Geliş Tarihi: 12.11.2019
Kabul Tarihi: 24.02.2020

1. Introduction

Magmatic rocks in Western Anatolia are observed in belts that occurred from north to south beginning in the Eocene until the middle Miocene following closure of the northern branch of the Neotethys. Volcanic and plutonic rocks developed in this time interval have high-K calc-alkaline, shoshonitic and ultrapotassic character. Though different opinions about the source of magmatism, stated to have developed under compressional or extensional regime, have been proposed such as delamination-related orogenic collapse, slab roll-back of subducted oceanic slab at different rates and back-arc extension, the idea that the southward roll-back of the African plate being subducted to the north caused core complex formation and development of magmatic belts has gained acceptance (Seyitoğlu and Scott, 1996; Dewey, 1988; Agostini et al., 2008; Dilek and Altunkaynak, 2009). Volcanism in the region

Citation info: Gencer, S.B., Erkül, S.T., Erkül, F. 2020. Evolution of slab tearing-related high potassium volcanism: Petrogenetic data from the Emirdağ and İscehisar volcanic units. Bulletin of the Mineral Research and Exploration 163, 167-185. https://doi.org/10.19111/bulletinofmre.693353.

**Corresponding author: Sibel TATAR ERKÜL, sibel582@gmail.com*

developed along NE-SW striking fault systems under the effect of transtensional regime within nearly E-W belts (Erkül et al., 2005*a, b,* 2006; Ersoy et al., 2008; Karaoğlu et al., 2010; Karaoğlu and Helvacı, 2012, 2014). Deep seismic tomography studies in recent years indicates that the African oceanic slab subducted under Anatolia has very fragmented structure and that slab-tear processes were effective in formation of orogenic and anorogenic volcanism in the region (Biryol et al., 2011; Mahatsente et al., 2017; Portner et al., 2018). This prediction is largely supported by geochemical and geochronologic data (Karaoğlu and Helvacı, 2014; Prelević et al., 2015). The volcanic units located in the eastern section of the magmatic belts in Western Anatolia extend nearly 250 km along a line from Kırka, Afyon and Isparta and give varying ages from the early Miocene to the present day (Keller and Villari, 1972; Besang et al., 1977; Sunder, 1980; Keller, 1983; Yağmurlu et al., 1997; Savaşçın and Oyman, 1998; Akal, 2003, 2008; Platevoet et al., 2008; Elitok et al., 2010; Prelević et al., 2015; Seghedi and Helvacı, 2016) (Figure 1a ,b). Volcanic rocks in the Kırka, Afyon and Isparta regions occur to have more pronounced alkaline character compared to Miocene high potassium volcanic units in Western Anatolia (Francalanci et al., 2000; Innocenti et al., 2005; Prelević et al., 2010, 2012). These volcanic units developed in parallel with regional convergence direction above the intersection between the Cyprus and Hellenic subduction zones (Yağmurlu et al., 1997; Savaşçın and Oyman, 1998; Dilek and Altunkaynak, 2009). As a result, many studies attributed magmatic

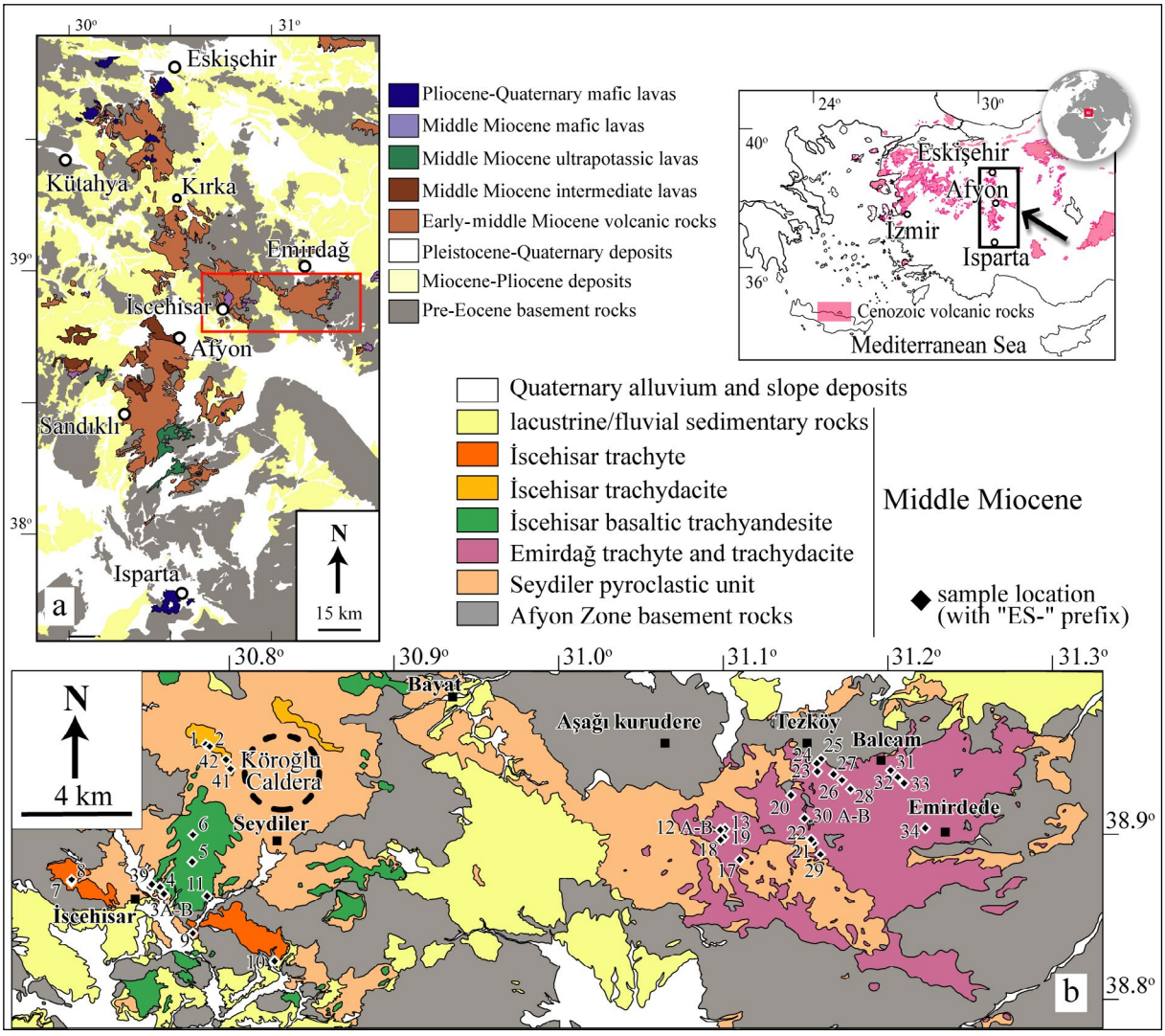

Figure 1- a) Simplified geologic map showing distribution of volcanic rocks outcropping along the Eskişehir-Afyon-Isparta line. Adapted from the 1/500.000 scale MTA (2002) geologic map. b) Geologic map of the İscehisar and Emirdağ volcanic units.

activity to the asthenospheric heat source owing to mantle upwelling between these two subducted plates (Yağmurlu et al., 1997; Savaşçın and Oyman, 1998). Petrological studies, especially on ultrapotassic volcanic rocks, indicate that these rocks probably derived from a highly metasomatized mantle source and the asthenospheric contribution increased with an advancing slab tear (Aydar and Beyhan, 1995; Aydar et al., 1998; Savaşçın and Güleç, 1990; Francalanci et al., 1990, 2000; Innocenti et al., 2005; Akal, 2008; Prelević et al., 2015; Erkül et al., 2019).

There are many studies to decipher the magma source characteristics of calc-alkaline, alkaline, shoshonitic and ultrapotassic volcanism developing along a N-S line extending from Eskişehir to Isparta (Aydar et al., 1996, 2003; Savaşçın and Oyman, 1998; Tonarini et al., 2005; Kumral et al., 2006; Çoban and Flower, 2006; Dilek and Altunkaynak, 2009; Doğan Külahcı et al., 2016; Prelević et al., 2010, 2012, 2015). However, the relationships between geodynamic processes of slab roll-back and tear, and the magma sources remain unknown for volcanic units extending on a NW-SE line from north of Afyon to Emirdağ regions. Within the scope of this study, geology, petrography, whole rock geochemistry and Sr-Nd isotope geochemistry of the Emirdağ and İscehisar volcanic units were investigated in an attempt to contribute to understanding the geodynamic evolution of the region.

2. Methods

A variety of analytical studies were performed to-define the geological characteristics and mineralogic-petrographic, geochemical and isotopic composition of the Emirdağ and İscehisar volcanic units. Collection of fresh or, if possible, least weathered samples was completed for petrographic identification, characterising all facies and geochemistry of the volcanic units. Samples taken from the Emirdağ and İscehisar volcanic units were investigated in terms of mineralogic composition and textural characteristics. After petrographic investigations, selected samples were broken to less than 0.4 cm size with the aid of a jaw crusher, then ground to less than 200 mesh size with a tungsten carbide vibrating mill. Whole-rock major and trace element analyses were completed for 28 chosen samples in ACME Laboratories, Vancouver, Canada. During major and trace element analyses, two hundred milligrams rock power was mixed with 1.5 g $LiBO_2$ fuser in a graphite bowl. Later the mixture was heated at 1050°C for 15 minutes in an oven. The melted samples were dissolved in 5% HNO_3 acid. Correction calculations used international standards and blank sample measurements. For major and some trace elements (Ba, Nb, Ni, Sr, Sc, Y, Zr), solutions were loaded into an ICP Emission Spectrometer and measured (Jarrel Ash AtomComb 975). For measurement of rare earth elements, solutions were loaded into an ICP Mass Spectrometer and measured (Perkin-Elmer Elan 6000). Sensitivity for major elements was less than 2%, while it was better than 10% for trace elements.

Seven samples representing the volcanic units had strontium and neodymium isotope analyses performed in Middle East Technical University, Radiogenic Isotope Laboratory. During measurement of Sr-Nd isotope ratios, TLM-ARG-RIL-01 (Sr Isotope Ratio Analysis Experiment Procedure) and TLM-ARG-RIL-02 (Nd Isotope Ratio Analysis Experiment Procedure) were applied. Details of these procedures are given in Köksal and Göncüoğlu (2008). Weighing, chemical solution and chromatography procedures were completed under clean laboratory conditions to 100 cleaning standards with ultra-pure water and chemicals. Approximately 80 mg of each rock powder sample was weighed and transferred to PFA bottles. Samples were left in 4 mL 52% HF for 4 days on a 160 °C heating table until fully dissolved. Samples dried on the heating table were first dissolved in 4 mL 6 NHCl for one day. Samples were later evaporated on the heating table again and placed in 1 mL 2.5 NHCl and prepared for chromatography. For strontium, Teflon columns were separated using 2.5 NHCl acid at 2 mL with Bio Rad AG50 W-X8 100-200 mesh resin. After collecting strontium, 6 NHCl and rare earth element fractions were collected. Strontium was loaded to single Re filaments on Ta-activator and 0.005 NH_3PO_4 and measured in static mode.

$^{87}Sr/^{86}Sr$ data were normalized to $^{86}Sr/^{88}Sr$ = 0.1194. During measurements, Sr NBA 987 standard was measured as 0.710251±10 (n=2). Neodymium was separated from the other rare earth elements using 0.22 NHCl acid in Teflon columns with 2 mL HDEHP (bis-ethyexyl phosphate)-covered biobeads by passing through Bio-Rad resin. The separated neodymium was measured in static mode using the double-filament

technique loaded on refilaments with 0.005 NH_3PO_4. During analyses, $^{143}Nd/^{144}Nd$ data were normalized to $^{146}Nd/^{144}Nd = 0.7219$, while the Nd La Jolla standard was measured as 0.511851±10 (n=2). No bias correction was made for the measurement results for strontium and Nd isotope ratios. Measurements were completed with multiple collection using Triton Thermal Ionisation Mass Spectrometer (Thermo-Fisher). Analytic uncertainty was at 2 sigma level. Results obtained for major, trace and isotope geochemistry were evaluated using GCDkit software (Janousek et al., 2006).

3. Geology

Lithostratigraphic units around the Emirdağ and İscehisar areas comprise, from oldest to youngest, basement rocks of the Palaeozoic metamorphic rocks and Afyon Zone, Miocene volcanic units and lacustrine/fluvial sedimentary deposits. The Afyon Zone around İscehisar and Emirdağ was formerly named the Afyon Metamorphics, consisting of Palaeozoic low-grade metamorphic rocks of phyllite, mica schist and quartzite with marble successions and Mesozoic carbonate and chert sequences (Metin et al., 1987).

Fluvial and lacustrine sedimentary rocks are located southwest and southeast of İscehisar and west and southwest of Emirdağ (Metin et al., 1987). The sequence covers metamorphic basement with basal conglomerate and continues upward into volcaniclastic rocks with clay and marl intercalations and ends with lacustrine limestone on top of the succession.

Thick pyroclastic deposits around Emirdağ and İscehisar were named the Seydiler tuff/agglomerate (Metin et al., 1987) and Seydiler Ignimbrite (Aydar et al., 1998) in previous studies, comprising nearly 200-250-metres thick pyroclastic layers dominated by ignimbrites, occasionally intercalated with epiclastic sediments passing laterally into lacustrine and fluvial sediments in distal sections. Trachydacite, trachyte and basaltic trachyandesites occurred on stratigraphically upper levels of the pyroclastic rocks around İscehisar and Emirdağ areas. Two samples from the İscehisar volcanic unit were dated 15.37 and 16.08 Ma using the $^{40}Ar/^{39}Ar$ method (Prelević et al., 2012). These ages are comparable to $^{40}Ar/^{39}Ar$ ages of the Emirdağ volcanic unit (16.5 My, unpublished). The volcanic rocks occurring as domes, dykes and massive lava flows were named as the Emirdağ volcanic unit and İscehisar volcanic unit in this study.

The Emirdağ volcanic unit is represented by domes, dykes and lava flows. Domes and lava flows overlap intercalations of ignimbrites, block and ash flow and debris flow deposits (Figure 2 a-c). Domes and lava flows contain large sanidine phenocrysts with lengths reaching up to 4 cm (Figure 2d). Dykes are lithologically similar to lava flows and domes, strike NW-SE in direction and their thickness reaches up to 2 metres.

Around İscehisar, lava flows are relatively more common than domes (Figure 2e). Lava flows occur above ignimbrites that are locally overlain by thin and cross-bedded fluvial sediments, suggesting a short time gap after deposition (Figure 2f). Massive lava flows are recognised by blackish, pinkish, dark grey colours, occasional weathering, breccia structure, flow bands and abundant vesicles. Their thickness reaches up to 50 metres.

4. Mineralogy-Petrography

The Emirdağ volcanic unit is mainly trachyandesite, trachyte and trachydacite in composition but trachydacites also occur. Trachyandesites are distinguished by the abundance of amphibole and biotite phenocrysts, while trachytes contain large sanidine crystals. Trachydacites are recognised by quartz phenocrysts in hand specimen. All rocks have hyalopilitic and occasional microlitic flow texture and consist of quartz, plagioclase, sanidine, biotite, augite, kaersutite, hornblende and apatite minerals. Large quartz phenocrysts are anhedral and display embayments, representing renewed reactions with magma. Biotites contain plagioclase and groundmass inclusions. Reddish-brownish kaersutite crystals are euhedral, opacified along their rims and are commonly embayed. Zoned plagioclase phenocrysts and melt inclusions in olivine, pyroxene and biotite are suggestive of magma mixing processes (Figure 3a-h).

The İscehisar volcanic unit is formed by contrasting mineral assemblages owing to varying compositions of lavas. Basaltic trachyandesites that consist of plagioclase, olivine, augite, kaersutite and biotite phenocrysts are defined by hyalopilitic and

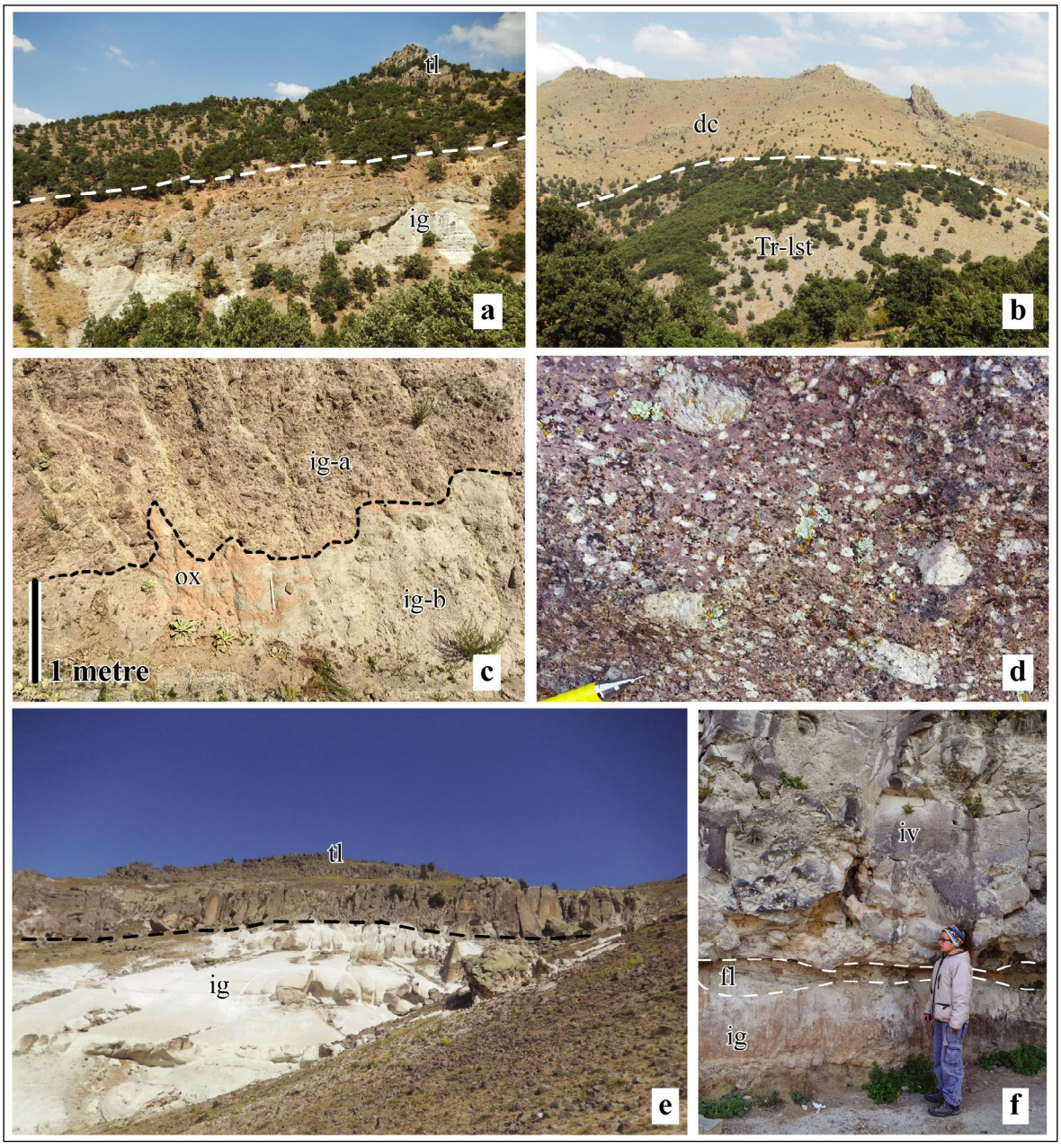

Figure 2- a) Trachydacites (tl) above ignimbrites and block and ash flow deposits near Emirdağ (31.148°/38.926°), b) trachydacite dome and dyke system emplaced by cutting Triassic recrystallized limestones south of Tezköy. Abbreviations; dc: dome and dyke complex, Tr-lst: Triassic limestones (31.154°/ 38.922°), c) contact between lithic-rich (ig-a) and lower lithic-poor (ig-b) pyroclastic flow deposits within Emirdağ volcanic unit and oxidized (ox) zone suggesting hot emplacement of the overlying ignimbrites (31.116°/38.915°), d) large sanidine crystals observed in a pink-coloured matrix in trachydacites of the Emirdağ volcanic unit. Length of sanidines reach up to 4 cm (31.104°/38.901°), e) columnar-jointed trachydacites conformably above light-coloured diffusely stratified ignimbrites (ig) (30.780°/38.951°) and f) basaltic trachyandesites of the İscehisar volcanic unit (iv) above ignimbrites (ig) and thin-bedded fluvial sediments (fl) in İscehisar area (30.752°/38.860°).

occasional trachytic texture. Olivine phenocrysts display common iddingsitization, carbonatization and opacification. Clinopyroxene phenocrysts, locally occurring as cumulates, are more common compared to orthopyroxene. Pyroxenes with polysynthetic twinning have embayed margins, indicating interaction with magma. Trachytes comprise plagioclase, olivine, biotite, augite and kaersutite phenocrysts and microlites. They have typical trachytic texture and occasional radial microlite

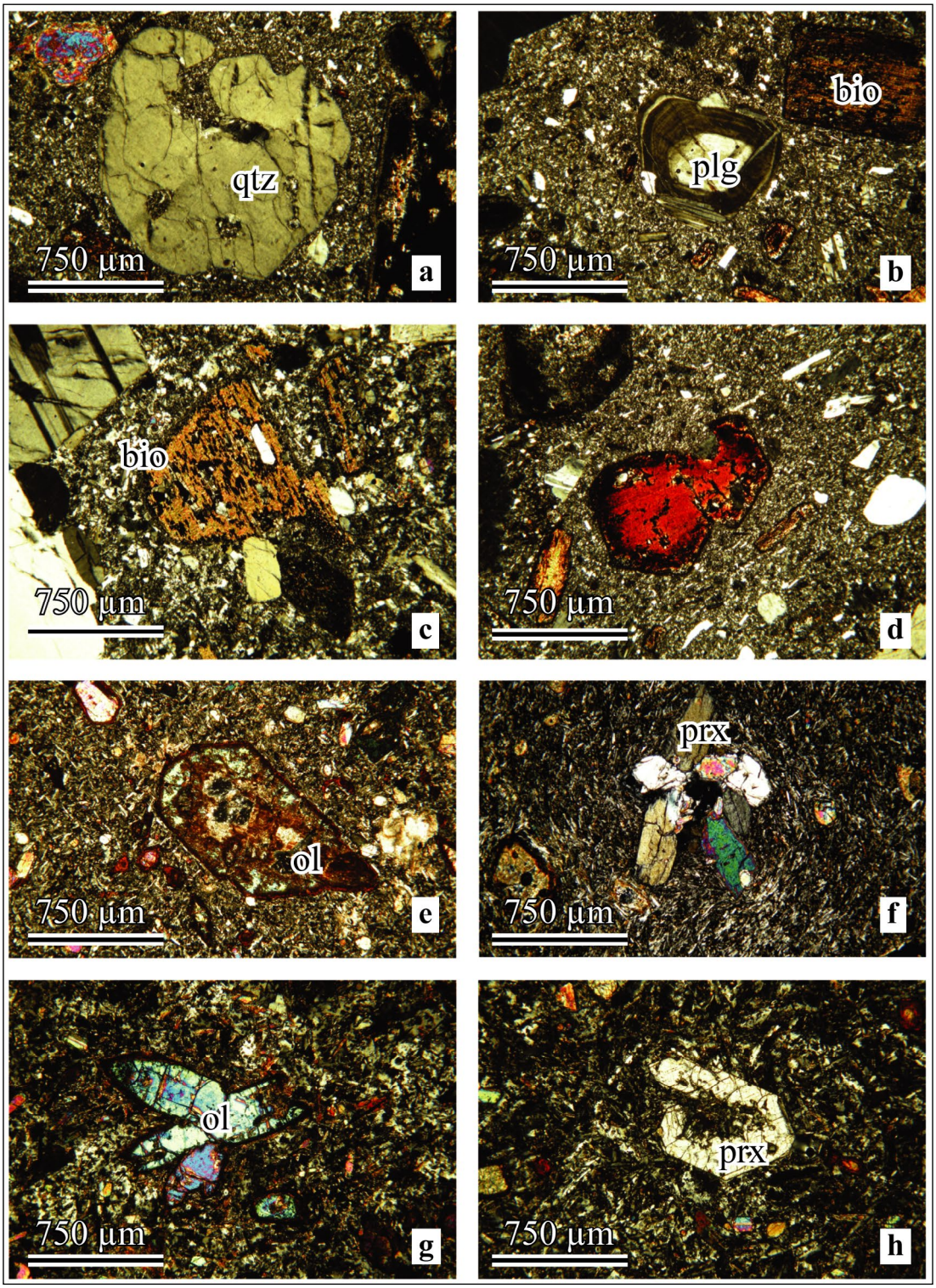

Figure 3- a) Embayed quartz phenocrysts within trachydacites of the Emirdağ volcanic unit, b) zoned plagioclase phenocrysts within trachydacites of the Emirdağ volcanic unit, suggesting the presence of magma mixing processes, c) enclosed plagioclase crystals and matrix in biotite (bio) phenocrysts having opaque rim observed in trachydacites of the Emirdağ volcanic unit, d) a reddish, embayed kaersutite phenocryst with opacified rims in trachydacites of the Emirdağ volcanic unit, e) iddingsitzed and opacified subhedral olivine (ol) phenocrysts within basaltic trachyandesites of the İscehisar volcanic unit, f) Clinopyroxene (prx) cumulates in basaltic trachyandesites of the İscehisar volcanic unit, g) Olivine cumulates in basaltic trachyandesites of the İscehisar volcanic unit and h) Embayed pyroxene phenocrysts in trachytes of the İscehisar volcanic unit.

growths are observed. Ferromagnesian minerals of biotite, augite and kaersutite are largely altered to opaque phases and olivine phenoscrysts are almost completely iddingsitized. Basaltic trachyandesites have almost the same mineralogical composition as trachytes whilst they may be texturally contrasting. Trachyandesites commonly exhibit hyalopitic texture. Minor amount of olivine phenocrysts is almost completely iddingsitized. Kaersutites are in the form of laths and are altered to opaque phases. Augites contain common matrix inclusions. Trachydacites comprise plagioclase, augite, kaersutite, biotite and hornblende phenocrysts. Plagioclase crystals are in the form of long thin laths shaped. Kaersutite and augite phenocrysts are largely altered to opaque phases. In the lava flows of the İscehisar volcanic unit, matrix inclusions within pyroxene and olivine phenocrysts indicate the effects of magma mixing processes.

5. Geochemistry

After petrographic studies, major and trace element analyses of 27 fresh whole-rock samples have been performed in order to, classify and define petrogenetic features of the volcanic rocks exposed in the Emirdağ and İscehisar regions. Analytical results are given in table 1. Attempts were made to determine the geochemical characteristics of early-middle Miocene volcanism using classification and tectono-magmatic discrimination diagrams. On the total alkali-silica diagram (Figure 4a), samples of the İscehisar volcanic unit fall in the basaltic trachyandesite, trachyte and trachydacite fields, while samples from the Emirdağ volcanic unit fall in the trachyandesite and trachyte-tachydacite transition. According to the alkaline-subalkaline differentiation diagram of Le Bas et al. (1986), the İscehisar volcanic unit is alkaline, while trachydacites from the Emirdağ volcanic unit are subalkaline in character. According to Peccerillo and Taylor's (1976) K_2O versus SiO_2 diagram, the İscehisar and Emirdağ volcanic units have shoshonitic character (Figure 4b). Mg# values vary from 46 to 75 for the İscehisar volcanic unit and from 26 to 57 for the Emirdağ volcanic unit. Volcanic rocks with MgO>3, K_2O>3, K_2O/Na_2O>2 and $(K_2O+Na_2O)/Al_2O$>1 were defined as ultrapotassic by Foley et al. (1987). Samples from the İscehisar and Emirdağ volcanic units were assessed according to the criteria recommended by Foley et al. (1987). Samples from the Emirdağ volcanic unit have K_2O and MgO contents varying from 4.37 to 6.09 wt.% and 0.71 to 3.90 wt.%, while samples from the İscehisar volcanic unit have 4.34-8.61wt.% and 3.28-9.44 wt.% for the same elements (Table 1). K_2O/Na_2O ratio for the Emirdağ volcanic samples is 1.34-2.30, while it varies between 1.61 and 5.38 in the İscehisar volcanic samples. $(K_2O+Na_2O)/Al_2O$ ratio is 0.48-0.61 for the Emirdağ volcanic samples and 0.46-0.88 for the İscehisar volcanic samples. The abovementioned element contents and ratios show that samples from the Emirdağ and İscehisar volcanic units cannot be classified as ultrapotassic.

The İscehisar volcanic unit differs from the Emirdağ volcanic unit with high SiO_2, Fe_2O_3, TiO_2, MgO, K_2O, and P_2O_5 and low CaO and Na_2O values. The major and trace element contents of the İscehisar volcanic unit have great similarities to the geochemistry of lamprophyres described in Afyon and surroundings (Aydar et al., 2003; Dedeoğlu and Yılmaz, 2016) and on Kos (Soder, 2017). On the variation diagrams, Fe_2O_3, CaO, MgO, TiO_2, P_2O_5, Rb, Th, U, and Nb increase with increasing SiO_2 content, while Al_2O_3, Zr and V contents decrease. Na_2O is low in trachytes of the İscehisar volcanic unit, while is high in other volcanic rocks. K_2O is high in the İscehisar volcanic unit and is low in the Emirdağ volcanic unit (Figure 5a-l).

Primitive mantle normalized multi-element spider diagrams (Sun and McDonough, 1989) are given in figure 6. The Emirdağ and İscehisar volcanic samples appear to be depleted in Nb, Pb and Ti. Basaltic trachyandesites of the İscehisar volcanic unit are enriched in U, K and Zr, while trachytes are enriched in K and Zr. The Emirdağ volcanic unit is enriched in Cs, U and Nd (Figure 6a). Chondrite-normalized rare earth element spider diagrams (Boynton, 1984) are shown in figure 6b. All samples show depletion from light rare earth elements to heavy rare earth elements. Light rare earth elements have 200-500 times enrichment, while enrichment in heavy rare earth elements is from 7 to 15 times relative to Chondrite.

6. Sr-Nd Isotope Ratios

$^{87}Sr/^{86}Sr$ isotope ratios of the Emirdağ volcanic unit vary from 0.706790 to 0.706284, while

Table 1- Major and trace element content of bulk rock samples from Emirdağ and İscehisar volcanic units.

Unit	**İscehisar Volcanic Unit**													**Emirdağ Volcanic Unit**												
Sample (ES)	**Basaltic Trachyandesite/Trachyandesite**							**Trachyandesite**				**Trachydacite**		**Trachydacite**												
	2	**5**	**6**	**7**	**10**	**11**	**40**	**3B**	**9**	**8**	**4**	**41**	**1**	**15**	**16**	**17**	**21**	**27**	**31**	**32**	**33**	**14**	**18**	**19**	**23**	**29**	**35**
Major element (weight %)																											
SiO_2	53.03	50.12	52.96	53.05	51.52	54.21	53.86	54.52	55.08	53.19	54.02	60.77	60.37	61.52	64.63	65.75	65.26	61.16	62.77	61.41	63.40	58.40	57.53	58.61	59.91	60.37	59.27
TiO_2	1.350	1.290	1.520	1.960	1.520	1.550	1.340	1.720	1.910	1.930	1.700	1.040	1.050	0.780	0.620	0.530	0.580	0.900	0.780	0.830	0.770	0.780	0.800	0.800	1.010	0.790	0.750
Al_2O_3	13.10	12.54	13.58	11.13	14.58	13.91	15.56	13.46	11.66	11.36	13.35	14.34	14.36	15.61	15.35	15.40	16.23	14.32	15.23	15.60	15.11	14.96	14.91	15.22	14.23	16.50	14.69
Fe_2O_3	7.190	7.530	7.290	5.990	8.150	7.170	7.660	7.400	6.480	6.090	7.310	4.590	4.760	5.370	4.560	3.770	4.080	4.900	4.830	5.070	4.920	5.730	5.750	6.010	5.090	5.420	5.770
MgO	5.020	8.680	6.760	9.050	4.980	3.480	3.280	3.870	5.630	9.440	4.510	3.370	2.910	2.220	1.360	0.920	0.710	2.720	1.910	1.650	2.110	3.900	3.720	3.290	2.890	2.090	3.730
CaO	7.440	7.320	6.660	5.470	8.790	6.410	6.880	5.870	5.620	5.400	6.270	4.460	4.740	4.470	3.400	3.120	2.460	4.810	3.750	3.680	4.060	6.060	5.890	5.260	4.960	4.120	5.960
Na_2O	2.100	1.930	2.160	2.510	2.330	2.220	2.790	2.100	1.600	2.230	2.110	2.810	2.770	3.270	3.230	3.270	2.980	2.770	3.040	3.020	3.040	2.980	2.900	2.920	2.650	3.080	2.930
K_2O	6.160	4.830	5.840	6.490	4.340	5.990	4.500	6.830	8.610	6.690	6.780	5.850	5.690	4.370	4.560	4.890	5.140	5.480	5.110	5.530	4.970	4.400	4.420	4.840	6.090	4.780	4.680
MnO	0.120	0.130	0.110	0.100	0.100	0.090	0.100	0.080	0.110	0.090	0.090	0.070	0.080	0.070	0.090	0.070	0.060	0.090	0.090	0.090	0.090	0.090	0.120	0.090	0.060	0.070	0.090
P_2O_5	1.050	0.980	1.070	0.670	0.790	1.060	0.680	1.070	0.930	0.650	1.070	0.680	0.700	0.460	0.410	0.350	0.360	0.640	0.490	0.550	0.470	0.480	0.470	0.560	0.750	0.540	0.520
LOI*	2.700	3.700	1.300	2.800	2.300	3.000	2.800	2.400	1.300	2.100	2.100	1.500	2.100	1.300	1.300	1.500	1.700	1.600	1.500	1.900	0.600	1.500	2.800	1.600	1.700	1.600	0.800
TOTAL	99.26	99.21	99.29	99.37	99.41	99.15	99.46	99.36	98.99	99.33	99.36	99.49	99.51	99.48	99.48	99.53	99.52	99.45	99.50	99.39	99.52	99.30	99.31	99.25	99.41	99.39	99.25
Trace Element (ppm)																											
Sc	24.00	23.00	22.00	17.00	28.00	22.00	22	22	18	17	22	13	14	13	10	8	8	15	12	13	12	15	16	16	15	13	16.00
Cu	44.30	48.50	43.40	45.70	34.50	22.90	36.0	35.7	32.8	38.0	19.7	8.5	19.8	9.9	7.9	7.3	5.5	14.9	15.3	17.7	12.4	24.2	18.9	15.7	14.0	9.3	31.00
Pb	4.200	3.600	4.200	11.10	4.100	2.300	3.8	5.2	12.7	9.5	1.0	0.8	0.9	2.4	1.7	3.8	4.5	3.6	2.6	2.4	1.4	8.3	2.7	4.7	8.7	5.6	11.20
Zn	52.00	68.00	62.00	54.00	67.00	48.00	58	59	50	51	57	18	41	36	30	42	42	46	24	34	19	49	35	23	48	40	46.00
Ni	31.20	280.9	122.2	328.5	56.60	97.40	109.1	85.3	90.2	319.2	69.4	5.7	8.7	8.8	4.0	3.4	2.7	7.6	10.4	13.5	5.7	12.3	14.4	7.5	8.6	4.2	10.00
Co	55.40	97.90	62.30	64.20	47.30	53.00	71.1	136.5	49.4	55.3	114.5	69.2	43.4	70.2	53.6	53.8	105.1	55.4	58.8	57.2	52.7	54.1	51.7	53.0	60.4	46.6	54.30
Mo	1.700	1.200	1.200	0.200	1.400	1.200	1.5	1.2	0.5	0.2	0.7	0.2	0.7	0.9	1.1	0.8	0.3	2.3	0.5	0.5	0.4	1.6	0.8	1	2.1	1	1.500
Cs	6.500	8.000	3.300	9.300	3.000	4.900	14.3	10.6	3.2	11.0	5.8	8.8	8.5	15.9	18.0	18.2	19.9	13.7	16.5	14.3	17.9	10.6	10.8	12.5	15.5	11.1	9.600
Nb	24.60	24.70	27.80	62.60	32.90	28.70	30.8	29.1	38.2	61.2	27.8	23.6	23.9	31.2	34.9	33.3	36.0	28.4	29.6	30.0	30.1	25.1	25.8	27.8	29.5	32.2	25.40
Ga	17.50	17.00	18.20	20.00	16.50	18.20	17.6	20.5	20.0	19.4	18.6	18.9	18.0	17.7	18.3	18.0	18.6	17.9	17.2	18.4	17.7	17.3	17.6	18.3	18.2	18.9	16.90

Table 1- (Continuie).

V	182.0	171.0	174.0	132.0	237.0	158.0	165	153	113	142	177	85	100	111	92	74	69	116	92	114	89	131	128	113	122	124	127.0
W	195.6	421.8	256.1	226.1	165.5	196.0	234.2	441.3	158.0	148.2	304.5	354.2	182.2	380.6	324.3	337.3	414.9	336.0	329.3	315.8	278.6	261.8	228.1	240.0	300.5	251.8	243.0
Ba	2214	2709	2293	829.0	18700	3974	1695	1719	2157	1175	1791	1533	1539	1283	1445	1521	1571	1704	1358	1863	1219	2315	2325	2636	1886	2065	2636
Rb	206.3	129.1	158.5	332.7	129.6	167.2	141.7	211.7	258.3	333.8	211.7	218.0	214.9	190.6	227.9	243.3	250.4	220.4	214.2	214.6	210.8	166.9	168.9	187.0	231.0	189.2	166.6
Sr	1690	1019	1061	748.0	941.0	1170	934	990	1480	751	992	902	934	1313	1149	1063	955	1179	1203	1562	1166	1688	1624	1773	1257	1369	1782
Hf	14.90	13.90	17.90	31.80	12.90	18.10	12.3	19.6	27.1	31.3	18.8	13.6	13.2	8.0	8.0	6.8	7.5	11.0	9.7	10.4	10.4	7.3	7.2	8.4	12.6	8.4	7.700
Y	27.70	28.40	27.60	23.30	26.20	31.30	26.1	24.9	27.6	23.7	27.6	21.7	19.9	27.8	31.2	28.1	31.6	21.9	24.4	27.4	26.6	27.9	31.6	29.4	23.2	30.6	26.90
Zr	570.0	507.0	659.0	1174	470.0	674.0	477	725	947	1144	729	488	481	295	294	248	279	417	370	378	388	272	285	316	468	321	286.0
Th	18.40	14.40	16.10	25.10	14.80	17.20	15.8	15.2	32.0	23.6	14.7	17.2	16.5	42.0	53.2	44.9	47.3	35.2	35.4	43.9	39.7	45.4	43.9	55.4	33.2	45.8	52.20
U	6.500	5.000	5.000	2.600	2.500	5.300	4.9	5.1	5.1	1.9	5.2	6.8	6.7	17.3	18.1	13.7	17.7	17.2	15.5	16.0	15.6	17.3	12.5	18.6	16.1	18.6	18.40
Ta	1.400	1.500	1.600	3.600	1.900	1.800	1.7	1.7	2.1	3.7	1.8	1.7	1.9	2.6	2.9	2.8	3.0	2.1	2.3	2.3	2.3	2.0	1.9	2.0	2.0	2.5	2.100
La	80.10	63.00	71.00	105.9	56.70	77.90	64.2	70.9	162.2	102.9	71.9	64.0	62.4	110.3	119.3	93.2	04.1	76.5	87.3	114.9	96.3	122.0	131.6	139.5	80.3	123.7	133.9
Ce	166.4	124.2	146.0	230.7	112.5	159.3	122.0	144.2	337.1	223.3	148.1	129.8	125.7	193.9	217.6	166.4	178.7	146.3	167.3	219.9	186.2	229.7	229.4	257.6	151.3	222.5	257.2
Pr	19.05	14.39	16.72	25.52	12.62	18.18	13.80	17.19	38.87	25.03	17.28	14.42	14.14	20.89	22.62	17.54	19.44	15.83	18.48	22.65	19.31	24.64	26.33	27.32	16.16	24.06	27.16
Nd	73.30	55.20	62.30	93.40	46.50	68.30	51.1	66.5	144.3	91.0	68.0	55.2	53.7	71.8	80.3	62.9	68.0	56.6	68.0	79.1	69.7	88.9	97.9	99.2	59.7	87.0	96.70
Sm	12.87	10.37	10.44	13.65	8.520	11.64	8.58	11.16	19.56	13.21	11.34	8.75	8.87	11.34	12.67	9.72	10.49	9.01	10.53	11.74	10.79	13.78	15.30	15.26	9.83	13.78	15.13
Eu	3.120	2.560	2.570	2.860	2.230	2.670	2.14	2.58	4.10	2.72	2.64	1.99	1.97	2.58	2.60	2.06	2.23	2.07	2.41	2.65	2.47	3.12	3.42	3.32	2.29	2.95	3.350
Gd	9.370	8.300	8.460	9.330	7.070	9.130	6.98	8.31	12.48	9.06	8.45	6.76	6.43	8.53	9.51	7.41	7.91	6.99	7.47	8.40	7.86	9.78	11.15	10.61	7.19	9.75	10.16
Tb	1.190	1.080	1.110	1.110	0.990	1.190	0.96	1.04	1.31	1.08	1.10	0.87	0.84	1.10	1.18	0.99	1.06	0.89	0.95	1.03	0.98	1.10	1.24	1.24	0.88	1.19	1.170
Dy	5.800	5.600	5.760	5.620	5.110	5.850	5.06	5.22	5.91	5.10	5.81	4.25	4.05	5.52	6.12	4.98	5.54	4.53	4.87	5.01	4.78	5.57	6.17	5.75	4.40	5.99	5.680
Ho	0.970	1.000	1.000	0.820	0.940	1.080	0.92	0.90	0.92	0.83	0.95	0.68	0.68	0.98	1.08	0.91	1.02	0.76	0.88	0.91	0.86	0.88	1.06	0.95	0.83	1.04	0.880
Er	2.640	2.670	2.630	2.180	2.660	2.910	2.50	2.35	2.46	2.11	2.67	1.95	1.81	2.48	2.98	2.62	3.00	2.06	2.47	2.44	2.55	2.74	3.20	2.65	2.06	2.77	2.560
Tm	0.380	0.380	0.380	0.290	0.340	0.430	0.38	0.34	0.36	0.28	0.37	0.26	0.28	0.39	0.46	0.40	0.43	0.30	0.33	0.36	0.38	0.38	0.44	0.41	0.30	0.43	0.380
Yb	2.300	2.220	2.370	1.920	2.280	2.540	2.24	2.02	2.29	1.72	2.25	1.67	1.57	2.66	3.04	2.58	3.11	2.09	2.32	2.40	2.50	2.44	2.81	2.57	2.10	2.72	2.420
Lu	0.320	0.360	0.350	0.260	0.360	0.400	0.37	0.30	0.31	0.24	0.34	0.24	0.26	0.36	0.47	0.42	0.44	0.31	0.35	0.36	0.38	0.36	0.40	0.37	0.32	0.42	0.360
Mg#	58.00	70.00	65.00	75.00	55.00	49.00	46.00	51.00	63.00	75.00	55.00	59.00	55.00	45.00	37.00	33.00	26.00	52.00	44.00	39.00	46.00	57.00	56.00	52.00	53.00	43.00	56.00

*LOI: loss on ignition

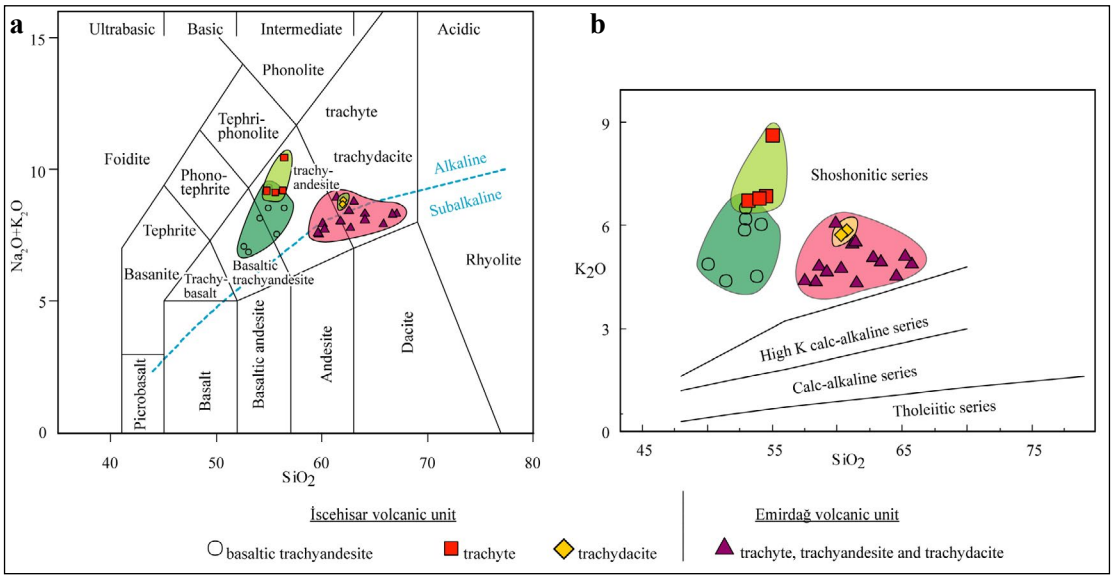

Figure 4- a) Total alkali-SiO_2 variation diagram (Le Bas et al., 1986) showing sample plots belonging to the İscehisar and Emirdağ volcanic units. Alkaline-subalkaline differentiation line taken from Irvine and Baragar (1971). b) Distribution of samples on K_2O-SiO_2 diagram (Peccerillo and Taylor, 1976).

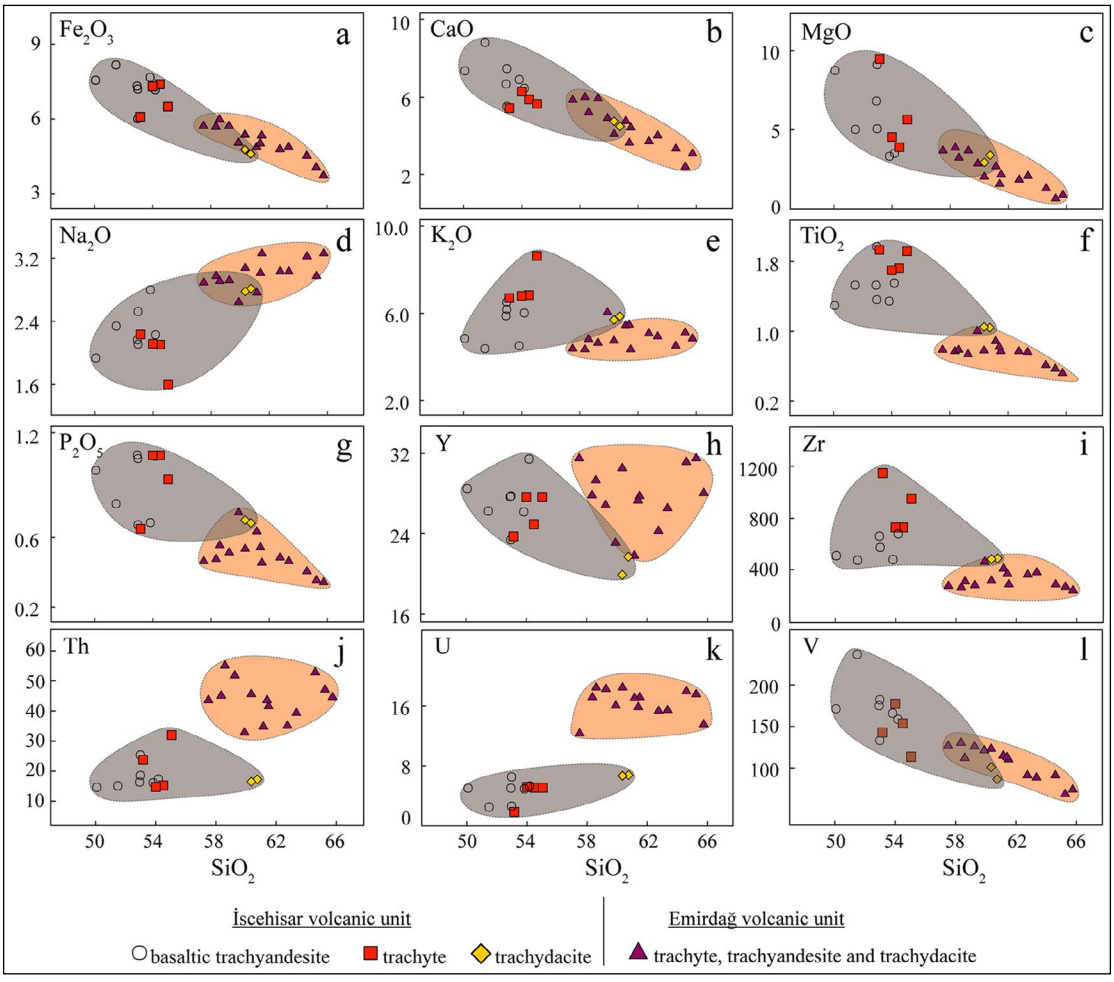

Figure 5- Major and trace element variation diagrams against SiO_2 for samples from İscehisar and Emirdağ volcanic units. Contents are weigth % for major elements and ppm for trace elements.

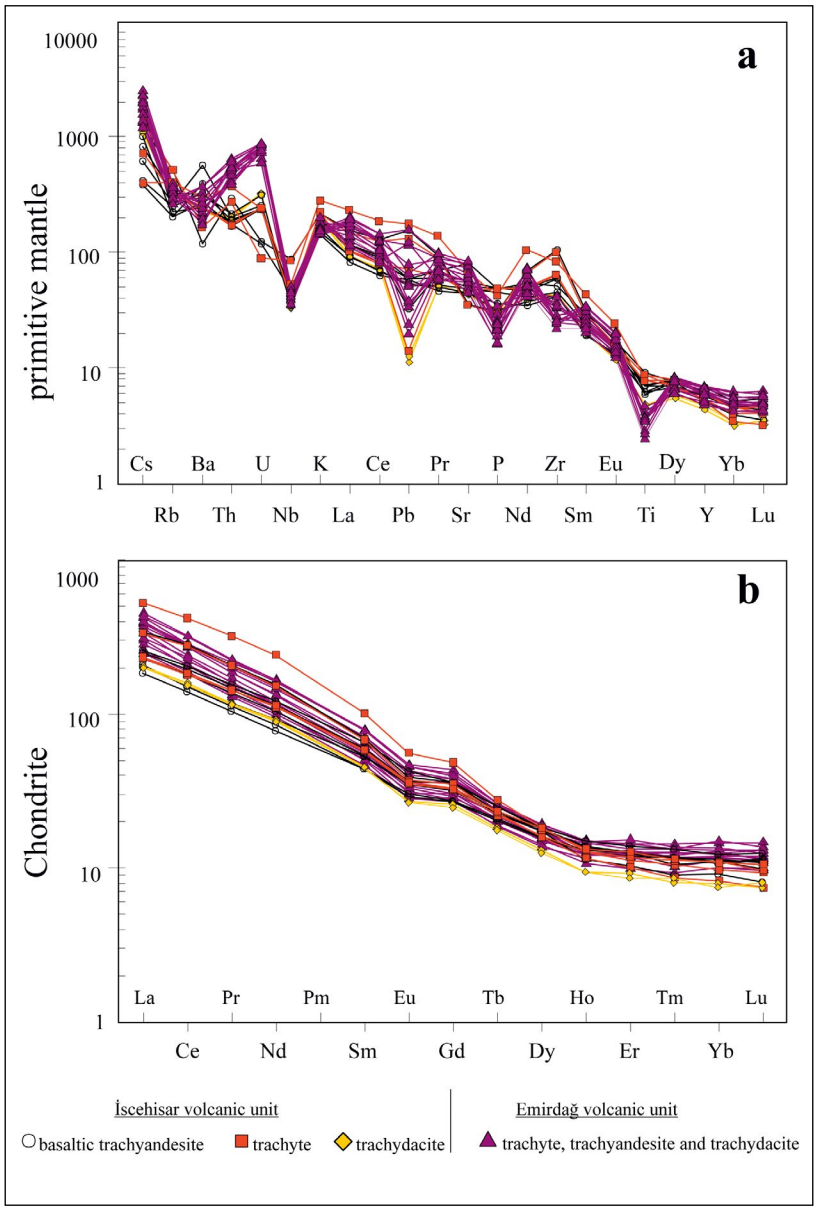

Figure 6- a) Spider diagrams normalized to primitive mantle (Sun and McDonough, 1989) and b) chondrite for samples from the İscehisar and Emirdağ volcanic units (Boynton, 1984).

$^{143}Nd/^{144}Nd$ isotope ratios is between 0.512472 and 0.512463. The same isotope ratios of the İscehisar volcanic unit are 0.707650-0.706527 and 0.512464-0.512424, respectively (Table 2) (Figure 7). The Sr and Nd isotope ratios for samples from the Emirdağ and İscehisar volcanic units are similar to the Sr-Nd isotope ratios of high-K and ultrapotassic volcanic rocks from Afyon and surroundings (Innocenti et al., 2005; Dilek and Altunkaynak, 2010; Chakrabarti et al., 2012; Prelević et al., 2012, 2015). When compared with silica-saturated and undersaturated volcanic rocks of the Afyon volcanic complex, (Prelević et al., 2015), the Emirdağ and İscehisar volcanic units have overlapping $^{87}Sr/^{86}Sr$ and $^{143}Nd/^{144}Nd$ ratios.

7. Magma Source and Evolution Processes

The Emirdağ volcanic unit display a compositional variation from trachyandesite to trachydacite, the majority of the samples are trachydacite in composition. Most samples are calc-alkaline and

Table 2- Sr-Nd isotope ratios for bulk rock samples from the Emirdağ and İscehisar volcanic units.

Sample	Unit	Rock type	Rb (ppm)	Sr (ppm)	Nd (ppm)	$^{87}Sr/^{86}Sr$	Std. error	$^{143}Nd/^{144}Nd$	Std. error
ES-16	Emirdağ volcanic unit	Trachydacite	227.9	1148.6	80.3	0.706790	9	0.512463	2
ES-23		Trachydacite	231.0	1256.6	59.7	0.706284	6	0.512466	3
ES-31		Trachydacite	214.2	1203.1	68.0	0.706342	6	0.512472	3
ES-41	İscehisar volcanic unit	Trachydacite	218.0	902.7	55.2	0.707650	7	0.512424	3
ES-9		Trachyte	258.3	1479.8	144.3	0.706881	5	0.512454	3
ES-6		Basaltic Trachyandesite	158.5	1061.2	62.3	0.707514	5	0.512449	2
ES-10		Basaltic Trachyandesite	129.6	941.4	46.5	0.706527	5	0.512464	4

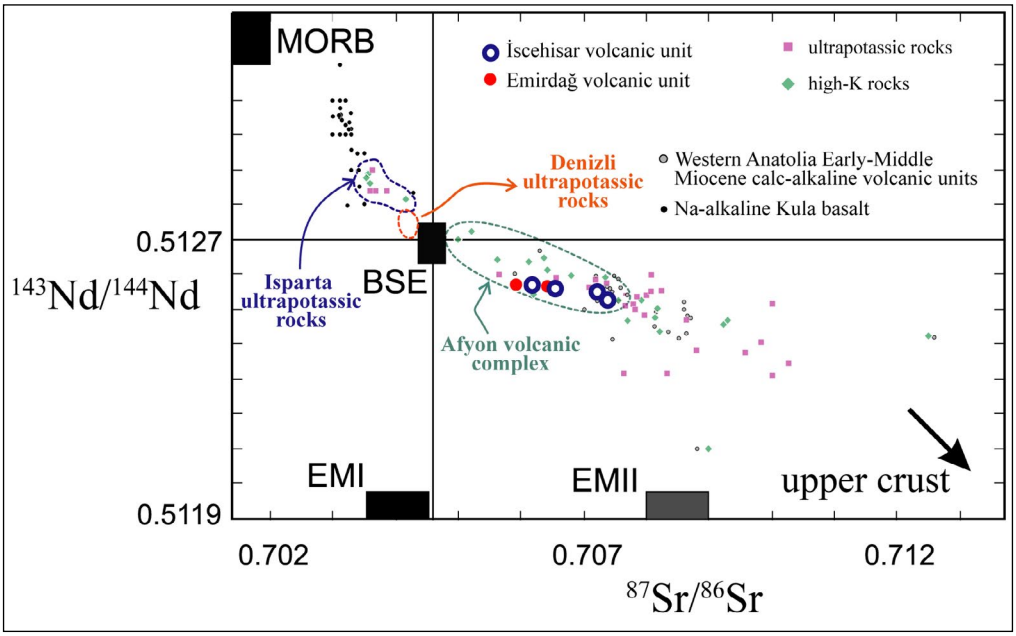

Figure 7- $^{87}Sr/^{86}Sr$ versus $^{143}Nd/^{144}Nd$ isotope diagram for the İscehisar and Emirdağ volcanic units. Comparisons with other rocks outcropping in western Anatolia included on the diagram. Isotope ratios were taken from Aldanmaz et al. (2000), Akal (2008), Alıcı et al. (1998, 2002) Chakrabarti et al. (2012), Çoban et al. (2012), Dilek and Altunkaynak (2010), Güleç (1991), Innocenti et al. (2005), Karaoğlu et al. (2010) and Prelević et al. (2012). MORB: mid-ocean ridge basalt, BSE: bulk silicate earth, EMI: enriched mantle I, EMII: enriched mantle II.

lesser amount of samples are alkaline in character. In terms of the K_2O content of volcanic rocks, they have high-K calc-alkaline and shoshonitic character. The İscehisar volcanic unit have variable compositions from basaltic trachyandesite through trachyte and trachydacite. The İscehisar samples have alkaline and shoshonitic character and display geochemically different trends with respect to the Emirdağ volcanic samples. Primitive mantle and Chondrite normalized spider diagrams show that the İscehisar and Emirdağ volcanic units have variable degrees of enrichment and/or depletion in some elements.

Somewhat variable mineralogical and geochemical features, varying from basic to acidic members, of the İscehisar and Emirdağ volcanic units indicate that these units have experienced fractional crystallisation and contamination (Figure 8). La/Sm increases with Th/Nb in the Emirdağ volcanic unit, while significant correlation in these ratios is absent in the İscehisar volcanic unit. Increasing Th/Nb in the Emirdağ volcanic unit indicates the role of crustal contamination or magma mixing processes. On the other hand, increasing La/Sm with almost constant Th/Nb imply the prominent role of fractional

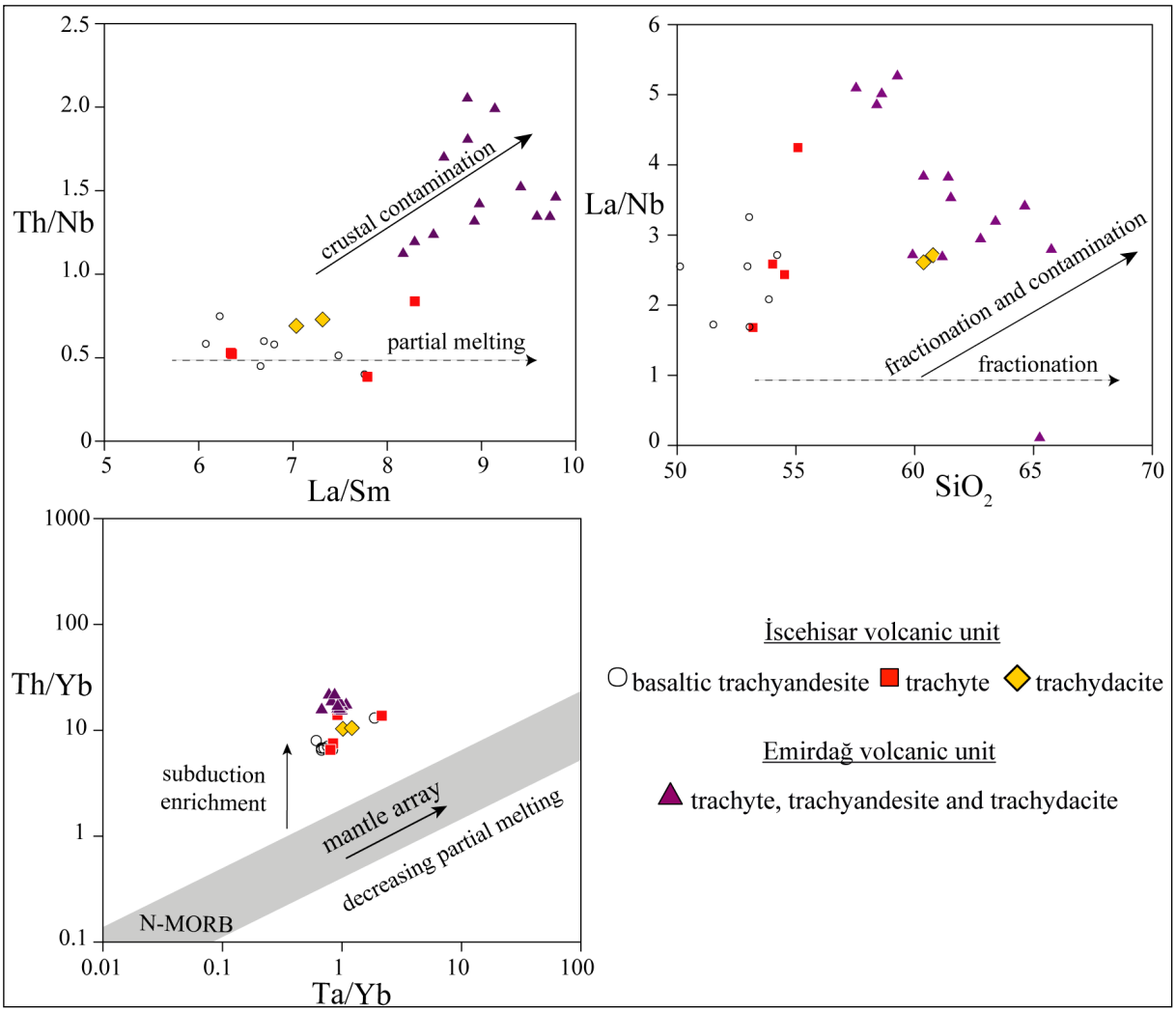

Figure 8- Variations diagrams for a) Th/Nb against La/Sm, (b) La/Nb against SiO_2 and c) Th/Yb against Ta/Yb.

crystallisation or different degrees of partial melting processes, leading to the transition from basaltic trachyandesite to trachydacite compositions in the İscehisar volcanic unit. The positive trend on the La/Nb versus SiO_2 variation diagram shows that the Emirdağ and İscehisar volcanic units were affected by fractional crystallization and fractional crystallisation-crustal contamination during their formation. Plagioclase and matrix inclusions within biotites, and zoned and spongy cellular texture plagioclase phenocrysts in the Emirdağ lava samples and matrix inclusions in pyroxene and olivine phenocrysts in the İscehisar lava samples indicate the presence of magma mixing processes. Clinopyroxene needles mantled by quartz phenocrysts in the lava samples of the İscehisar volcanic unit can be interpreted as a marker for magma mixing processes (Dedeoğlu and Yılmaz, 2016).

When all data are evaluated together, contribution of mantle and crustal sources at varying degrees occurred during formation of the Emirdağ and İscehisar volcanic units. All volcanic units have low to moderate $^{87}Sr/^{86}Sr$, Nb/U and Ce/Pb, and relatively high $^{143}Nd/^{144}Nd$ ratios. Enrichment of large-ion lithophile elements in subduction-related volcanic rocks is expected in addition to enrichment of Pb. However, the Emirdağ and İscehisar volcanic units do not appear to have enriched in Pb content identical to subduction setting, and even depletion of Pb in some samples is observed on multi-element spider diagrams. Although a negative Pb anomaly indicates asthenospheric mantle source, the behaviour of elements in the volcanic units support addition of subduction-related metasomatic solutions infiltrated into an enriched mantle source. The higher Mg# values

in the İscehisar volcanic unit compared to the Emirdağ volcanic unit indicates more mantle input during the formation of İscehisar volcanic unit. The increasing Th/Yb ratios indicate progressively metasomatized mantle source by subduction-related solutions. The higher Th/Nb ratios in the İscehisar volcanic unit compared to the Emirdağ volcanic unit imply that the subduction-related contribution occurred at higher rates during its formation.

8. Tectono-Magmatic Evolution

Geodynamic models involving orogenic collapse and associated lithospheric delamination (Aldanmaz et al., 2000; Dilek and Altunkaynak, 2009), slab roll-back resulting in mantle upwelling, and subducted lithospheric thinning and subsequent slab tearing have been proposed for the geodynamic environment that controlled Anatolian magmatism since Late Oligocene. As partial melting of the mantle wedge showing advanced degree of metasomatism due to infiltration of solutions and melts derived from the rolled-back slab causes development of K-rich magma (Lustrino et al., 2011 and references therein). Slab tear causes upwelling of juvenile, sub-slab asthenospheric mantle (Gasparon et al., 2009; Miller and Lee, 2008; Russo et al., 2010). The upwelled asthenospheric mantle may be partially melted itself, or may cause partial melting of the lithospheric mantle and lower crust owing to the induced high heat flow. In this scenario, nature of magmatism passes from high-K calc-alkaline to Na-rich alkaline in the advanced stages of slab tear (Doglioni et al., 2002; Tokçaer et al., 2005).

Early-middle Miocene magmatic belts in western Anatolia are represented by calc-alkaline, shoshonitic and ultrapotassic rocks with different compositions. Miocene magmatic rocks are locally observed as volcanic assemblages represented by the association of coeval calc-alkaline and mildly alkaline rocks. The distribution of these rocks is typically restricted to the Neogene basins, suggested to have developed under the NE-SW-directed extensional regime (Erkül et al., 2005*a, b*; Altunkaynak et al., 2010; Ersoy et al., 2008). During the early-middle Miocene, calc-alkaline volcanism in western Anatolia were resulted from the interaction between lower crust and metasomatized lithospheric mantle-derived magmas. These processes inferred to have been active since 12.2 Ma (Erkül et al., 2013). After the volcanic quiescence until 8.5 Ma, alkaline volcanism with geochemical signatures of asthenospheric contribution around Denizli, Selendi and Kula became active and this activity continued to the present day (Alıcı et al., 2002; Ersoy et al., 2011; Innocenti et al., 2005; Yılmaz, 2010).

Calc-alkaline, shoshonitic and ultrapotassic rock assemblages occurred during 20 to 16 Ma are exposed around Eskişehir, Afyon and Isparta. Calc-alkaline volcanic rocks crop out in a NW-SE-trending belt from Eskişehir towards Emirdağ (Figure 9a). Along this belt, widespread calc-alkaline pyroclastic deposits are accompanied by alkali trachydacites, trachytes, basaltic trachyandesites, lamprophyres and lamproites. All volcanic rocks to the south of Emirdağ and İscehisar have alkaline character. Lamproites emplaced after 12 Ma display geochemical evidences of asthenospheric input (Prelević et al., 2015) and this contribution in volcanic units increased in Senirkent, Isparta and Bucak (Çoban and Flower, 2006) towards south (Dilek and Altunkaynak, 2010; Elitok, 2019). The Emirdağ and İscehisar volcanic units can be accounted for the final products of orogenic volcanism developed within this belt. Calc-alkaline volcanism in western Anatolia is considered to have developed under the NE-SW oriented extensional regime since early Miocene. The extensional regime in western Anatolia was widely accepted to have occurred in response to roll-back of the subducting African oceanic lithosphere (Brun and Sokoutis, 2010; Gessner et al., 2013; Jolivet et al., 2013). Middle Miocene shoshonitic volcanism derived from lithospheric mantle and crustal sources around Emirdağ and İscehisar regions along with the roll-back of the subducting oceanic slab. The roll-back of the subducting slab triggered the upwelling of the asthenosphere as a heat source in the overlying mantle wedge, causing elevation and expansion in the crust. The rise of the asthenosphere during subduction processes might have caused partial melting of the metasomatized mantle wedge. The upwelling of asthenosphere also caused partial melting of the lower crust (Figure 9b). Coeval lithospheric mantle and crustal derived magmas may have mixed with each other at different rates (Figure 9c). Continental crust-derived melts at the initial stage were emplaced in the upper crust and are inferred to have formed the widespread Seydiler Ignimbrite associated with a caldera system. In advancing stages, the lithospheric mantle and lower crust-derived magmas might have mixed with each other. When compared to the

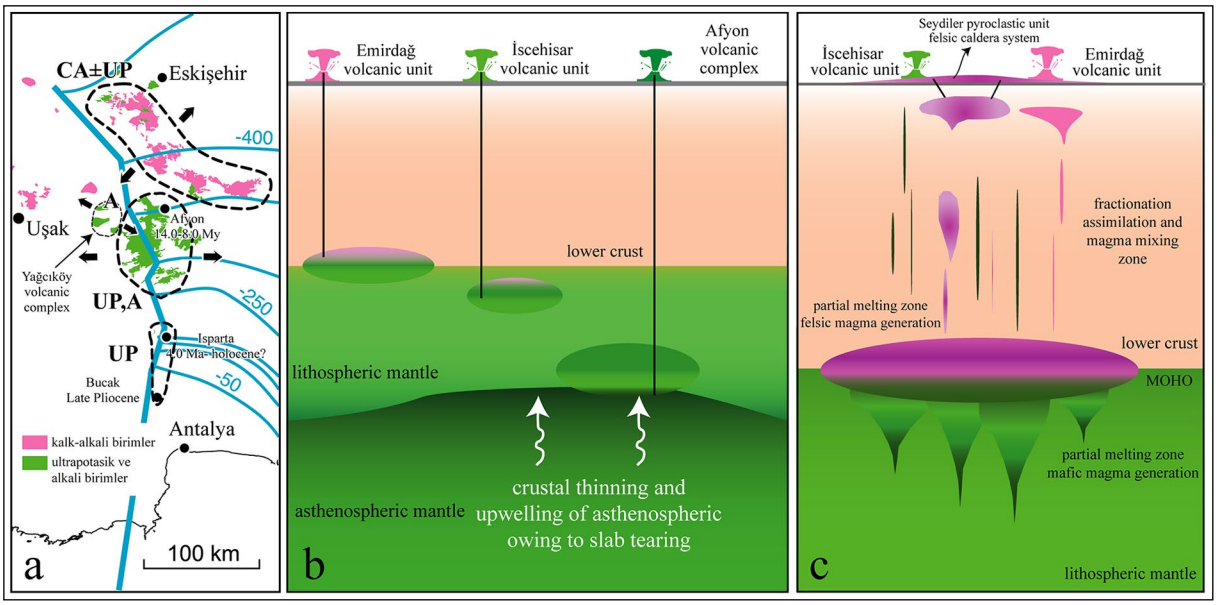

Figure 9- a) Map showing distribution of Miocene volcanic complexes outcropping between Afyon-Eskişehir (areas bounded by dashed lines). Yağcıköy volcanic complex comprises alkaline rocks located west of the Afyon volcanic complex and is outside the N-S striking emplacement axis (Erkül et al., 2019). Thin blue lines represent contours showing depth of the upper surface of the subducted lithosphere slab (depth in km). Thick blue line is equivalent to the projection on the surface of the edge of the torn slice. Data were taken from Biryol et al. (2011). CA: calc-alkaline, A: alkaline, UP: ultrapotassic volcanic rock assemblages. b) Schematic section showing location of the magma chamber forming the Emirdağ, İscehisar and Afyon volcanic units. c) Schematic section showing mixing of magmas in the lithospheric mantle and lower crust, fractionation and contamination by the upper crust.

İscehisar volcanic unit, crustal contribution to the Emirdağ volcanic unit is greater and the İscehisar volcanic unit appear to have greater contribution from metasomatized lithospheric mantle under the extensional regime. This extensional regime occurred immediately before tearing of the subducting oceanic slab. Oceanic slab tearing event is represented by voluminous alkaline volcanic rocks within the Afyon volcanic complex.

9. Conclusions

(1) Coeval calc-alkaline and alkaline volcanism occurs in the around Emirdağ and İscehisar areas. Calc-alkaline volcanism has dominantly trachydacite composition in Emirdağ and surroundings. Alkaline volcanism begins with basaltic trachyandesite and ends with trachydacite in İscehisar and surroundings.

(2) Geochemical data show that the Emirdağ and İscehisar volcanic units were affected by crustal contamination, fractional crystallisation and magma mixing processes. The magma mixing processes and crustal contamination was greater in the Emirdağ volcanic unit compared to the İscehisar volcanic unit.

(3) The extensional regime that has been active in the middle Miocene might have been caused by upwelling of the lithospheric mantle metasomatized during pre-Miocene former subduction events. Interaction of mantle- and crust-derived magmas at transition from slab roll-back to tearing stages resulted in a shift in geochemical character of the volcanism from calc-alkaline to alkaline character. The Emirdağ and İscehisar volcanic units are inferred to represent the transitional volcanism between two geodynamic episodes.

Acknowledgements

This study was supported by the Akdeniz University Scientific Research Projects Coordination Unit (project number FYL-2015-823).

References

Agostini, S., Ryan, J.G., Tonarini, S., Innocenti, F. 2008. Drying and dying of a subducted slab: Coupled Li and B isotope variations in western Anatolia Cenozoic Volcanism. Earth and Planetary Science Letters 272 (1-2), 139-147.

Akal, C. 2003. Mineralogy and geochemistry of melilite leucitites, Balçıkhisar, Afyon (Turkey). Turkish Journal of Earth Sciences 12 (3), 215-239.

Akal, C. 2008. K-richterite–olivine–phlogopite–diopside–sanidine lamproites from the Afyon volcanic province, Turkey. Geological Magazine 145 (4), 570-585.

Aldanmaz, E., Pearce, J.A., Thirlwall, M.F., Mitchell, J.G. 2000. Petrogenetic evolution of Late Cenozoic, post-collision volcanism in western Anatolia, Turkey. Journal of Volcanology and Geothermal Research 102 (1), 67- 95.

Alıcı, P., Temel, A., Gourgaud, A., Kieffer, G., Gündoğdu, M.N. 1998. Petrology and geochemistry of potassic rocks in the Gölcük area (Isparta, SW Turkey): Genesis of enriched alkaline magmas. Journal of Volcanology and Geothermal Research 85, 423-446.

Alıcı, P., Temel, A., Gourgaud, A. 2002. Pb–Nd–Sr isotope and trace element geochemistry of Quaternary extension-related alkaline volcanism: A case study of Kula region (western Anatolia), Turkey. Journal of Volcanology and Geothermal Research 115 (3–4), 487–510.

Altunkaynak, S., Rogers, N.W., Kelley, S.P. 2010. Causes and effects of geochemical variations in late Cenozoic volcanism of the Foça volcanic centre, NW Anatolia, Turkey. International Geology Review 52 (4–6), 579–607.

Aydar, E. 2003. Les lamprophyres du stratovolcan d'Afyon, Anatolie de l'Ouest, Turquie: Description et genèse. Comptes Rendus Geosciences 335 (3), 279-288.

Aydar E., Bayhan H. 1995. Le volcanisme alcalin d'Afyon, Anatolie de l'ouest, Turquie: Approche volcanologique et pétrologique. Bulletin Section Volcanologique Soc Géol France 36, 1-5.

Aydar, E., Bayhan, H., Zimitoğlu, O. 1996. Afyon stratovolkanının volkanolojik ve petrolojik gelisiminin incelenmesi. Yerbilimleri 18, 87-107.

Aydar, E., Bayhan, H., Gourgaud, A. 1998. Köroğlu caldera, mid-west Anatolia, Turkey: Volcanological and magmatological evolution. Journal of Volcanology and Geothermal Research 85 (1), 83-98.

Besang, C., Eckhardt, F.J., Harre, W., Kreuzer, H. Müller, P. 1977. Radiometrische altersbestimmungen an Neogenen eruptivgesteinen der Türkei. Geologisches Jahrbuch 25, 3-36.

Biryol, C.B., Beck, S.L., Zandt, G., Özacar, A.A. 2011. Segmented African lithosphere beneath the Anatolian region inferred from teleseismic P-wave tomography. Geophysical Journal International 184 (3) 1037-1057.

Boynton, W.V. 1984. Cosmochemistry of the rare earth elements; meteorite studies. Elsevier 63-114, Amsterdam.

Brun, J. P., Sokoutis, D. 2010. 45 m.y. of Aegean crust and mantle flow driven by trench retreat. Geology 38, 815–818.

Chakrabarti, R., Basu, A., Ghatak, A. 2012. Chemical geodynamics of western Anatolia. International Geology Review 54 (2), 227-248.

Çoban, H., Flower, M.F. 2006. Mineral phase compositions in silica undersaturated 'leucite' lamproites from the Bucak area, Isparta, SW Turkey. Lithos 89 (3), 275- 299.

Çoban, H., Karacık, Z., Ece, Ö.I. 2012. Source contamination and tectonomagmatic signals of overlapping Early to Middle Miocene orogenic magmas associated with shallow continental subduction and asthenospheric mantle. Lithos 140, 119-141.

Dedeoğlu, D., Yılmaz, K. 2016. Geochemistry of lamprophyres in Karakaya (İscehisar, Afyon), western Anatolia, Turkey. IOP Conference Series, Earth and Environmental Science 44 (4).

Dewey J.F. 1988. Extensional collapse of orogens. Tectonics 7, 1123-1139.

Dilek, Y., Altunkaynak, Ş. 2009. Geochemical and temporal evolution of Cenozoic magmatism in western Turkey: mantle response to collision, slab breakoff and lithospheric tearing in an orogenic belt. Geological Society of London Special Publications 311, 1, 213-233.

Dilek, Y., Altunkaynak, Ş. 2010. Geochemistry of Neogene–Quaternary alkaline volcanism in western Anatolia, Turkey and implications for the Aegean mantle. International Geology Review 52 (4-6), 631-655.

Doglioni, C., Agostini, S., Crespi, M., Innocenti, F., Manetti, P., Riguzzi, F., Savaşcın, Y., 2002. On the extension in western Anatolia and the Aegean sea. In: (Eds.) Gideon Rosenbaum and Gordon Lister, Journal of the Virtual Explorer 8, DOI: 10.3809/jvirtex.2002.00049.

Doğan Külahcı, G.D., Temel, A., Gourgaud, A., Demirbağ, H. 2016. Afyon volkanik kayaçlarının (Batı Anadolu, Türkiye) mineralojik-petrografik özellikleri ve P-T Hesaplamaları. Yerbilimleri/

Hacettepe Üniversitesi Yerbilimleri Uygulama ve Araştırma Merkezi Dergisi 36 (3), 137-162.

Elitok, Ö. 2019. Geology and petrology of the potassic and ultrapotassic rocks from the northern part of Senirkent (Isparta-SW Turkey): Evidence of magma–carbonate wall-rock interactions. Arabian Journal of Geosciences 12 (9).

Elitok, Ö., Özgür, N., Druppel, K., Dilek, Y., Platevoet, B., Guillou, H., Poisson, A., Scaillet, S., Satır, M., Siebel, W., Bardintzeff, J.M., Deniel, C., Yılmaz, K. 2010. Origin and geodynamic evolution of Late Cenozoic potassium-rich volcanism in the Isparta area, southwestern Turkey. International Geology Review 52 (4-6), 454–504.

Erkül, F., Helvacı, C., Sözbilir, H. 2005*a*. Evidence for two episodes of volcanism in the Bigadiç borate basin and tectonic implications for western Turkey. Geological Journal 40 (5), 545–570.

Erkül, F., Helvacı, C., Sözbilir, H. 2005*b*. Stratigraphy and geochronology of the Early Miocene volcanic units in the Bigadiç borate basin, western Turkey. Turkish Journal of Earth Sciences 14 (3), 227–253.

Erkül, F., Helvacı, C., Sözbilir, H. 2006. Olivine basalt and trachyandesite peperites formed at the subsurface/surface interface of a semi-arid lake: An example from the Early Miocene Bigadiç basin, western Turkey. Journal of Volcanology and Geothermal Research 149 (3–4), 240–262.

Erkül, F., Erkül, S. T., Ersoy, Y., Uysal, İ., Klötzli, U. 2013. Petrology, mineral chemistry and Sr–Nd–Pb isotopic compositions of granitoids in the central Menderes metamorphic core complex: Constraints on the evolution of Aegean lithosphere slab. Lithos 180-181, 74-91.

Erkül, F., Çolak, C., Erkül, S.T., Varol, E. 2019. Geology and geochemistry of the Middle Miocene Yağcıköy volcanic complex, western Turkey: Wide-rift alkaline volcanism associated with incipient stages of slab tearing. Journal of Asian Earth Sciences 179, 112-126.

Ersoy, Y., Helvacı, C., Sözbilir, H., Erkül, F., Bozkurt, E. 2008. A geochemical approach to Neogene-Quaternary volcanic activity of western Anatolia: An example of episodic bimodal volcanism within the Selendi Basin, Turkey. Chemical Geology 255 (1-2), 265-282.

Ersoy, Y.E., Helvacı, C., Palmer, M.R. 2011. Petrogenesis of the Neogene volcanic units in the NE–SW-trending basins in western Anatolia, Turkey. Contributions to Mineralogy and Petrology 163(3), 379–401.

Foley, S., Venturelli, G., Green, D.H., Toscani, L. 1987. The ultrapotassic rocks: Characteristics, classification and constraints for petrogenetic models. Earth Science Reviews 24 (2), 81-134.

Francalanci, L. 1990. Tertiary-Quaternary alkaline magmatism of the Aegean western Anatolian area: A petrological study in the light of new geochemical and isotopic data. International Earth Sciences Colloqium on the Aegean Region 385-396, 1-6 October, Dokuz Eylül University, İzmir.

Francalanci, L., Innocenti, F., Manetti, P., Savasçın, M.Y. 2000. Neogene alkaline volcanism of the Afyon-Isparta area, Turkey: Petrogenesis and geodynamic implications. Mineralogy and Petrology 70 (3-4), 285-312.

Gasparon, M., Rosenbaum, G., Wibranjs, J.R., Manetti, P. 2009. The transition from subduction arc to slab tearing: Evidence from Capraia Island, northern Tyrrhenian Sea. Journal of Geodynamics 47 (1), 30–38.

Gessner, K., Gallardo, L. A., Markwitz, V., Ring, U., Thomson, S. N. 2013. What caused the denudation of the Menderes Massif: Review of crustal evolution, lithosphere structure, and dynamic topography in southwest Turkey. Gondwana Research, 24, 243–274.

Güleç, N. 1991. Crust–mantle interaction in western Turkey: Implications from Sr and Nd isotope geochemistry of Tertiary and Quaternary volcanics. Geological Magazine 128 (5), 417-435.

Innocenti, F., Agostini, S., Di Vincenzo, G., Doglioni, C., Manetti, P., Savaşçın, M.Y., Tonaini, S. 2005. Neogene and Quaternary volcanism in western Anatolia: magma sources and geodynamic evolution. Marine Geology 221 (1), 397-421.

Irvine, T.N., Baragar, W.R.A. 1971. A Guide to the Chemical Classification of the Common Volcanic Rocks. Canadian Journal of Earth Science 8, 523-548.

Janousek, V., Farrow, C. M., Erban, V. 2006. Interpretation of whole-rock geochemical data in igneous geochemistry: Introducing geochemical data Toolkit *(GCDkit)*. Journal of Petrology 47 (6), 1255-1259.

Jolivet, L., Faccenna, C., Huet, B., Labrousse, L., Le Pourhiet, L., Lacombe, O., Lecomte, E. Burov, E., Denéle, Y., Brun, J.-P., Philippon, M., Paul, A., Salaün, G., Karabulut, H., Piromallo, C., Monié, P., Gueydan, F., Okay, A.I., Oberhansli, R., Pourteau, A., Augier, R., Gadenne, L., Driussi, O. 2013. Aegean tectonics: Strain localisation, slab tearing and trench retreat. Tectonophysics 597–598, 1–33.

Karaoğlu, Ö., Helvacı, C. 2012. Structural evolution of the Uşak-Güre supra-detachment basin during Miocene extensional denudation in western Turkey. Journal of the Geological Society 169 (5), 627-642.

Karaoğlu, Ö., Helvacı, C. 2014. Isotopic evidence for a transition from subduction to slab-tear related volcanism in western Anatolia, Turkey. Lithos 192-195, 226-239.

Karaoğlu, Ö., Helvacı, C., Ersoy, Y. 2010. Petrogenesis and $^{40}Ar/^{39}Ar$ geochronology of the volcanic rocks of the Uşak-Güre basin, western Turkey. Lithos 119 (3-4), 193-210.

Keller, J. 1983. Potassic lavas in the orogenic volcanism of the Mediterranean area. Journal of Volcanology and Geothermal Research 18 (1), 321-335.

Keller, J., Villari, L. 1972. Rhyolitic ignimbrites in the region of Afyon (Central Anatolia). Bulletin Volcanologique 36 (2), 342-358.

Köksal, S., Göncüoğlu, M.C. 2008. Sr and Nd isotopic characteristics of some S-, I and A-type granitoids from Central Anatolia. Turkish Journal of Earth Sciences 17 (1), 111-127.

Kumral, M., Çoban, H., Gedikoğlu, A., Kılınç, A. 2006. Petrology and geochemistry of augite trachytes and porphyritic trachytes from the Gölcük volcanic region, Isparta, SW Turkey: A case study. Journal of Asian Earth Sciences 27 (5), 707- 716.

Le Bas, M.J., Le Maitre, R.W., Streckeisen, A., Zanettin, B. 1986. A chemical classification of volcanic rocks based on the total alkali-silica diagram. Journal of Petrology 27 (3), 745-750.

Lustrino, M., Duggen, S., Rosenberg, C.L. 2011. The central-western Mediterranean: Anomalous igneous activity in an anomalous collisional tectonic setting. Earth-Science Reviews 104, 1-40

Mahatsente, R., Alemdar, S., Çemen, İ. 2017. Effect of slab-tear on crustal structure in Southwestern Anatolia Active Global Seismology 103-119.

Metin, S., Genç, Ş., Bulut, V. 1987. Afyon ve dolayının jeolojisi. Maden Tetkik ve Arama Genel Müdürlüğü Raporu No: 8103, Ankara (unpublished).

Miller, M.S., Lee, C.-T.A. 2008. Possible chemical modification of oceanic lithosphere by hotspot magmatism seismic evidence from the junction of Ninety East Ridge and the Sumatra-Andamanarc. Earth Planetary and Science Letters 265, 386–395.

MTA, 2002. 1/500.000 ölçekli jeoloji haritası. Maden Tetkik ve Arama Genel Müdürlüğü, Ankara.

Peccerillo, A., Taylor, S.R. 1976. Geochemistry of Eocene calc-alkaline volcanic rocks from the Kastamonu area, Northern Turkey. Contrubutions to Mineralogy and Petrology 58, 63-81.

Platevoet, B., Scaillet, S., Guillou, H., Blamart, D., Nomade, S., Massault, M., Poisson, A., Elitok, Ö., Özgür, N., Yağmurlu, F., Yılmaz, K. 2008. Pleistocene eruptive chronology of the Gölcük volcano, Isparta angle, Turkey. Quaternaire. Revue de l'Association Française Pour L'étude du Quaternaire 19 (2), 147-156.

Portner, D. E., Delph, J. R., Biryol, C. B., Beck, S. L., Zandt, G., Özacar, A.A., Sandvol, E., Turkelli, N. 2018. Subduction termination through progressive slab deformation across eastern Mediterranean subduction zones from updated P-wave tomography beneath Anatolia. Geosphere 14 (3), 907-925.

Prelević, D., Akal, C., Romer, R.L., Foley, S.F. 2010. Lamproites as indicators of accretion and/or shallow subduction in the assembly of Southwestern Anatolia, Turkey. Terra Nova 22 (6), 443-452.

Prelević, D., Akal, C., Foley, S.F., Romer, R.L., Stracke, A., Van Den Bogaard P. 2012. Ultrapotassic mafic rocks as geochemical proxies for postcollisional dynamics of orogenic lithospheric mantle: the case of Southwestern Anatolia, Turkey. Journal of Petrology 53 (5), 1019-1055.

Prelević, D., Akal, C., Romer, R. L., Mertz-Kraus, R., Helvacı, C. 2015. Magmatic response to slab tearing: Constraints from the Afyon alkaline volcanic complex, western Turkey. Journal of Petrology 56 (3), 527-562.

Russo, R.M., Gallego, A., Comte, D., Mocanu, V.I., Murdie, R.E., Van Decar, J.C. 2010. Source-side shear wave splitting and upper mantle flow in the Chile Ridge subduction region. Geology 38, 707-710.

Savaşçın, Y., Güleç, N. 1990. Relationship between magmatic and tectonic activities in western Turkey. International Earth Sciences Colloqium on the Aegean Region 300-313, 1-6 October, Dokuz Eylül University, İzmir.

Savasçın, M.Y., Oyman, T. 1998. Tectono-magmatic evolution of alkaline volcanics at the Kırka-Afyon-Isparta structural trend, SW Turkey. Turkish Journal of Earth Sciences 7 (3), 201-214.

Seghedi, I., Helvacı, C. 2016. Early Miocene Kırka-Phrigian Caldera, western Turkey (Eskisehir province), preliminary volcanology, age and geochemistry data. Journal of Volcanology and Geothermal Research 327, 503-519.

Seyitoğlu, G., Scott, B.C. 1996. The age of the Alaşehir graben (west Turkey) and its tectonic implications, Geological Journal 31, 1-11.

Soder, C. 2017. Geochemistry and petrology of lamprophyres from the Hellenides and the European Variscides. MsC Thesis, Heidelberg University, 185s.

Sun, S.S., McDonough, W.S. 1989. Chemical and isotopic systematics of oceanic basalts: Implications for mantle composition and processes. Geological Society of London Special Publications 42 (1), 313-345.

Sunder, M.S. 1980. Geochemistry of the Sarıkaya borate deposits (Kırka-Eskişehir). Bulletin of the Geological Society of Turkey 2, 19-34.

Tokçaer, M., Agostini, S., Savaşçın, M.Y., 2005. Geotectonic setting and origin of the youngest Kula volcanics (western Anatolia), with a new emplacement model. Turkish Journal of Earth Sciences 14, 145–166.

Tonarini, S., Agostini, S., Innocenti, F., Manetti, P. 2005. Delta11B as tracer of slab dehydration and mantle evolution in western Anatolia Cenozoic Magmatism. Terra Nova, 17 (3), 259-264.

Yağmurlu, F., Savasçın, Y., Ergün, M. 1997. Relation of alkaline volcanism and active tectonism within the evolution of the Isparta Angle, SW Turkey. The Journal of Geology 105 (6), 717-728.

Yılmaz, K. 2010. Origin of anorogenic 'lamproite-like' potassic lavas from the Denizli region in western Anatolia extensional province, Turkey. Mineralogy and Petrology 99 (3), 219–239.

Bulletin of the Mineral Research and Exploration

http://bulletin.mta.gov.tr

An overview of the current seismicity of the Sultandağı Fault Zone (Afyonkarahisar-Konya, Western Anatolia)

Doğan KALAFAT[a*], Yavuz GÜNEŞ[a], Mehmet KARA[a] and Kıvanç KEKOVALI[a]

[a]*Kandilli Observatory and Earthquake Research Institute, RETMC, Boğaziçi University, İstanbul, Turkey*

Research Article

Keywords:
Western Anatolia, Sultandağı Fault Zone, Micro-earthquake, Seismic network, Digital broadband earthquake stations

ABSTRACT

Western Anatolia is one of the most seismically active regions in Turkey. The high seismic activity is a result of a complex tectonic deformation dominated by the N-S extensional tectonic regime in Western Anatolia. This tectonic deformation is also a result of the relative movement of the African-Arabian plates towards the north, which causes the Anatolian plate to shift 2.5 cm per year towards W-SW. One of the largest fault zones in the Western Anatolia, Sultandağı Fault Zone (SFZ) has a northwest-southeast trend. SFZ, approximately 120 km long, is an important tectonic structure, which produced three major earthquakes (Mw> 6.0) between the years of 2000 -2002. Therefore, the most significant goals of this study were to monitor the micro-earthquakes along SFZ, to enrich the current seismic network and to increase the earthquake detection threshold in the region (Mc <2.5). Within the scope of the study, 3 digital broadband earthquake stations were installed in the region. The analysis of the data obtained in the research indicated that the central and western parts of SFZ are active and there is intense seismic activity especially in the vicinity of Sultandağı, Çay, Çobanlar, and Afyonkarahisar. Fault plane solutions revealed that the earthquakes in the region generally occur with normal faulting with oblique components. Seismic stations installed within the scope of the study contributed positively to the increase of the sensitivity (Mc = 1.3) of the earthquake detection threshold (Mc) in the region and increased the detection capacity.

Received Date: 05.12.2019
Accepted Date: 13.04.2020

1. Introduction

Sultandağı Fault Zone (SFZ) is one of the most important tectonic structures in Western Anatolia and has produced 3 important earthquakes in the last two decades (Figure 1). Between the years 2000 and 2002, 3 major earthquakes (Mw> 6.0) occurred on the Sultandağı Fault Zone, also called as Afyon-Akşehir Graben. The first earthquake (Eber-Sultandağı earthquake Mw = 6.0) occurred in 2000, followed by the Sultandağı (Mw 6.5) and Çay-Sultandağı earthquakes (Mw = 6.0) on February 3, 2002.

The last two earthquakes occurred consecutively on the Sultandağı Fault Zone (SFZ) on the same day, and the main shocks were followed by extensive aftershock activity. In this context, seismic activity in the form of an earthquake series in the region in recent years has revealed that the faults around the northwestern end of SFZ, especially the ones around Çay-Sultandağı-Afyonkarahisar, are each an active fault segment that can be considered within this fault zone. NW-SE and NE-SW trending faults play an important role in the tectonic development of the region. This makes it necessary to monitor regularly and precisely both the micro-earthquake activity and

Citation info: Kalafat, D., Güneş, Y., Kara, M., Kekovalı, K. 2020. An overview of the current seismicity of the Sultandağı Fault Zone (Afyonkarahisar-Konya, Western Anatolia). Bulletin of the Mineral Research and Exploration 163, 187-210. https://doi.org/10.19111/bulletinofmre.721796.

**Corresponding author:* Doğan KALAFAT, kalafato@boun.edu.tr

Figure 1- Study Area (Sultandağı Faut Zone), active fault zones and major tectonic plates across and in the vicinity of Turkey (active faults were taken from Emre et al., 2013; the figure was drawn using the GMT software; topography data was obtained from NASA-SRTM).

the recent earthquake activity which continues as series of earthquakes. The fact that the seismic stations in the region were not sufficient before the study, and, therefore, that the current seismic activity could not be followed properly made up the key motivational elements for the necessity to conduct a study in the region.

Therefore, monitoring the micro-earthquakes along SFZ, enriching the current seismic network and increasing the earthquake detection threshold in the region (Mc <2.5) were the most important goals of this study.

2. General Geological Structure and Seismicity

The region is under the influence of the extension regime which is dominant in Western Anatolia, and earthquake activity occurs as a result of this extension regime. However, this region, known as Turkish Lake District or Isparta Bend, where the Central and Western Taurus Mountains meet, contains different rock groups in terms of stratigraphic and structural features. Therefore, there are two basic views regarding the neotectonic regime of the region. The first one is that it is a compression regime, which is suggested by various researchers (Boray et al., 1985; Barka et al., 1995; Uysal, 1995; Altunel et al., 1999). In the second one, it is argued that no compression tectonic regime has occured in Isparta Bending after the early Messinian (upper Miocene) compression deformation phase, and that the neotectonic regime in Isparta Bending is extensional (Koçyiğit, 1996; Glover and Robertson, 1998; Koçyiğit and Özacar, 2003).

Turkish Lake District is roughly bordered by Denizli, Fethiye, Antalya, Alanya, Akseki, Ahırlı, Seydişehir, Beyşehir, Afyon, Sandıklı and Çivril. This section generally consists of many blocks of different sizes which are located between NE-SW, NW-SE and N-W trending dip-slip normal faults (Figure 2). Some of them represent depression and some represent elevation areas. Compression stress concentrating in different directions along the edges of the Anatolian-

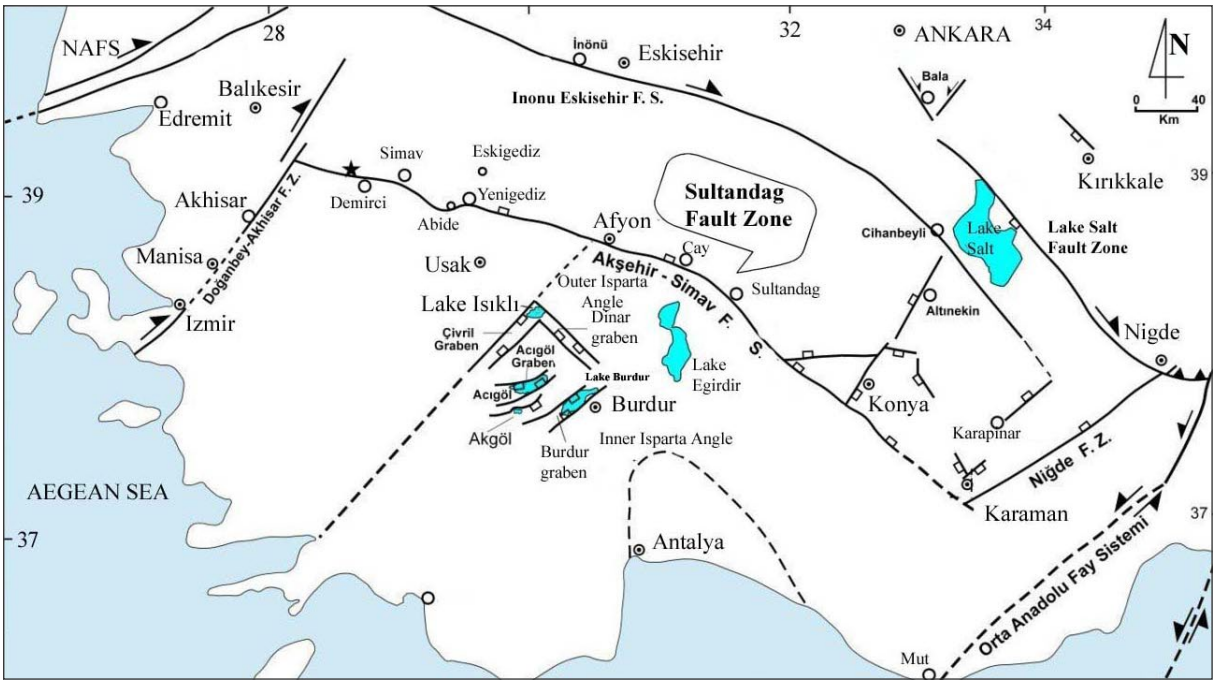

Figure 2 - Active tectonic elements in the region (taken from Koçyiğit, 2008; Akşehir-Simav Fault System, Dinar-Acıgöl-Burdur-Çivril Grabens: Normal Faults; Lake Salt FZ, İnönü Eskişehir FS, Middle Anatolian FS: Strike-Slip faults and between both systems are thrust fault).

Aegean plates was released in the form of tensional stress also in different directions in the inner shell, which led to the formation of the faults mentioned above (Koçyiğit, 1984; Şengör et al., 1985; Seyitoğlu and Scott, 1996; Kaya et al., 2014).

Turkish Lake District was significantly fragmented by dip-slip normal faults that had developed before the Neogene period and remained active throughout it (Koçyiğit, 2008; Özgül et al., 1991). It is also claimed that the region is dominated by a compression system that causes large thrust and lateral strike-slip movements (Boray et al., 1985; Barka et al., 1995; Uysal, 1995). However, it is considered that local releases and, accordingly, pull-apart basins may have developed in this compression system (Koçyiğit, 1984, 1996; Koçyiğit et al., 2000). Turkish Lake District, which has been controlled by block faultings (normal) since the late middle Oligocene, continues its tectonic activity under the control of normal block faulting (grabens), especially in the vicinity of Burdur-Dinar-Afyon-Akşehir (Koçyiğit, 2008; Koçyiğit and Özacar, 2003). Therefore, geological and geomorphological findings indicate Holocene activity along the Sultandağı Fault Zone (Atalay, 1975; Şaroğlu et al., 1987, 1992; Öğdüm et al., 1991; Koçyiğit et al., 2000). The February 3, 2002 Earthquakes occurred at SFZ as a result of this tectonic activity (Kalafat and Öz, 2001; Emre et al., 2003). Blumenthal, 1963 described the Sultandağı Fault as a large normal fault at the top of Isparta Bend. This region is the southeastern part of the extensional tectonics of western Anatolia (Emre et al., 2003).

It is quite intense in terms of earthquake activity and significant earthquakes in the last century are listed below (Table 1).

The recent earthquakes in the region reveal that NW-SE and NE-SW trending faults cause the current seismic activity. It was mentioned in the Turkish Active Fault Map (Emre et al., 2013) published by the MTA in 2003 that the 2002 earthquake occurred on the Çay segment (Table 1, Event 9), defined as Afyon-Akşehir Graben, with an extension to the northwest. The previous earthquake happened on this fault system on 15 December, 2000 (Figure 3). The fault system causing earthquakes has been defined as Sultandağı fault zone by various researchers (Kalafat and Öz, 2001; Kalafat et al., 2002, 2003; Emre et al., 2002; Ulusay et al., 2002).

Table 1- Major Earthquakes in the region (1900-2002).

Date (D/M/Y)	Time (h/m)	Lat. (N°)	Lon (E°)	Intensity (Io-MSK)	Mag. (M)	Location	Event No.
03.10.1914	22:07	38.00	30.00	IX	6.9	Burdur	1
07.08.1925	06:46	37.40	30.50	VIII	5.9	Dinar-Afyon	2
19.07.1933	20:07	38.20	29.80	VIII	5.7	Çivril- Denizli	3
22.11.1963	20:26	37.20	29.70	VII	5.1	Tefenni-Burdur	4
12.05.1971	06:25	37.60	29.72	VIII	5.9	Burdur	5
29.07.1978	04:34	37.57	30.02	VII	5.0	Burdur	6
01.10.1995	15:57	38.11	30.05	VIII	6.1	Dinar-Afyon	7
15.12.2000	16:44	38.63	31.19	VII	5.8	Sultandağı-Afyon	8
03.02.2002	07:11	38.58	31.25	VII	6.4	Sultandağı-Afyon	9
03.02.2002	09:26	38.68	30.38	VII	5.6	Sultandağı- Afyon	10

Source: Eyidoğan et al., 1991; Kalafat, 1996; Kalafat et al., 2000.

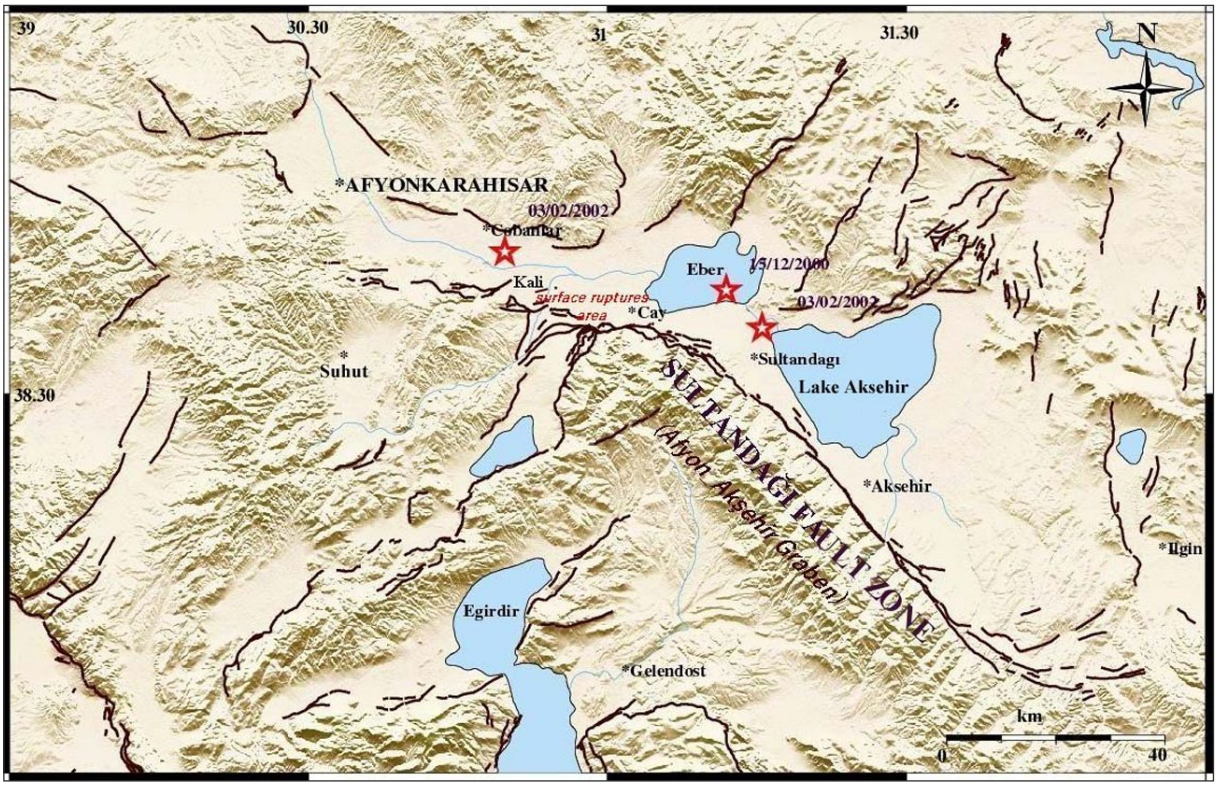

Figure 3- Distribution of the outer centers of the 2000 and 2002 Earthquakes [Active faults were taken from Emre et al., 2013; (The figure was drawn with the GMT software; the topography data is from NASA-SRTM)].

Land observations showed that, in the 2002 earthquakes, the WNW-ESE trending fault had damaged and affected the villages and towns located in this direction, especially to the S-SW of Eber Lake. Maltepe, Çobanlar and nearby villages of Çay and Sultandağı districts are the most affected settlements (Figure 4). The surface ruptures caused by the earthquake were observed to the SW of Eber, and generally between Çay and Maltepe Villages. The general direction of the surface rupture is N 80° W. The surface rupture is divided into two as Maltepe and Çay fault segments (Kalafat et al., 2002; Kalafat and Görgün, 2017; figure 4).

The general direction of the fractures dominantly varies as EW, NE-SW / NW-SE. Vertical strike ranges

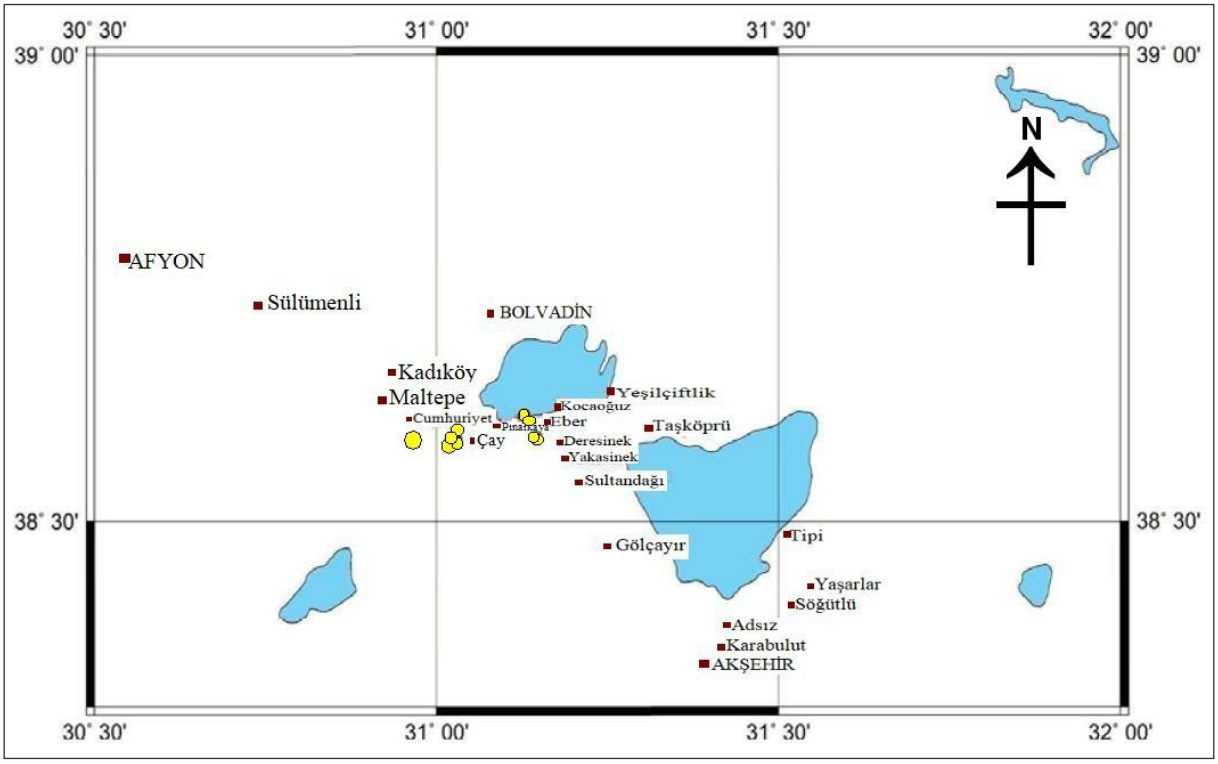

Figure 4- Locations of the surface ruptures and deformations (circles show the locations of the surface ruptures).

between 25 and 35 cm. The downthrown block is towards N-NE and the surface rupture resulting from the earthquake is approximately 18.5 (± 1.5) km (Kalafat et al., 2002; figure 5).

Various researchers supported these results, stating that the 2002 earthquakes caused a 26-km-surface rupture with a vertical displacement of up to 30 cm between Çay and Sultandağı and to the west of Çay (Emre et al., 2003; Akyüz et al., 2006). Emre et al (2003) stated that the rupture was 20 km long with

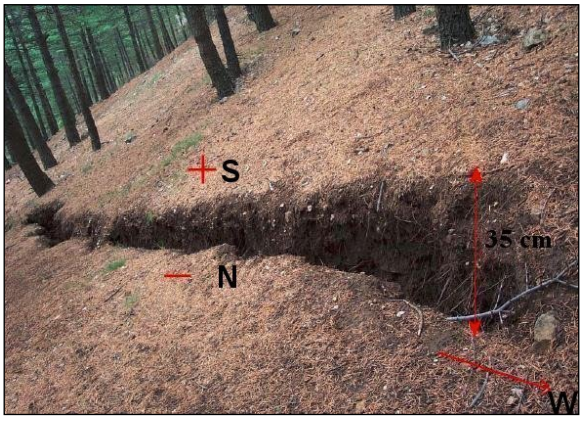

Figure 5- An example of surface ruptures observed in the field (Yaka district of Çay town; Kalafat et al., 2002).

a generally east-west trend and consisted of three distinct sections separated from each other, and that, during the earthquake, two conjugate normal surface faultings, called as Çay and Kali Çayı segments respectively, occurred.

The earthquake (Mw = 6.0) that occurred at 11:26 am, 2 hours after the main shock, was considered to be an earthquake and rupture which was triggered by the main shock (Kalafat et al., 2002). It hit the western part of Sultandağı fault, the area between Çay, Işıklar, and Çobanlar. Fault solutions revealed that earthquakes in the region generally occurred with oblique vertical strike normal faultings (Kalafat and Öz, 2001; Kalafat et al., 2002; Li et al., 2002; Kalafat and Görgün, 2017; figure 6, table 2).

The 3 February 2002 Sultandağı Earthquakes (Table 2, No=2-4) revealed that the earthquake activity continues in the region today under the influence of the extension regime. The extension regime is released by the formation of normal faults, which causes deformation and expansion. The Sultandağı earthquakes occurred as a result of the breaking of Sultandağı / Çay-Maltepe segments in the Sultandağı-Akşehir Fault system, stretching in a major E-W, NW-

Table 2- Fault Plane Solutions of important earthquakes in the region (1995-2019).

Eq. No.	Date G/A/Y	Time UTC	Lat. Deg.	Lon. Deg.	Depth. Km	Mag. Mw	FAULT PARAMETERS			REGION	Source
							Strike(°) Azimuth	Dip Angle	Rake Angle		
1	01.10.1995	15:57	38.06	29.68	15	6.4	310	60	-88	Dinar-Afyonkarahisar	HRV
2	15.12.2000	16:44	38.4	31.35	15	6	118	49	-81	Sultandağı-Afyonkarahisar	HRV
3	03.02.2002	07:11	38.62	31.21	15	6.5	66	55	-104	Sultandağı-Afyonkarahisar	HRV
4	03.02.2002	09:26	38.23	30.56	15	5.8	15	53	-118	Senirkent-Tatarlı-Isparta	HRV
5	03.02.2002	11:40	38.52	31.22	15	5.3	229	50	-108	Sultandağı-Afyonkarahisar	HRV
6	13.05.2002	11:42	38.59	31.12	5	4.3	288	88	-129	Eber-Çay-Afyonkarahisar	DK
7	26.06.2002	21:31	38.66	31.18	10	4.2	136	60	-105	Bolvadin-Afyonkarahisar	DK
8	05.08.2002	04:57	38.68	31.2	5	4.3	282	50	-113	Bolvadin-Afyonkarahisar	DK
9	03.07.2004	20:29	38.5	31.33	13	4.5	255	70	-85	Sultandağı-Afyonkarahisar	DK
10	08.08.2004	15:30	38.7	31.35	7	3.8	294	46	-116	Sultandağı-Afyonkarahisar	DK
11	07.09.2004	18:05	38.69	31.2	10	4.5	313	78	-32	Bolvadin-Afyonkarahisar	DK
12	16.09.2004	05:07	38.69	31.19	10	4.3	265	45	-65	Bolvadin-Afyonkarahisar	DK
13	08.11.2004	21:17	38.67	30.92	6	4.2	273	77	-76	Çay-Afyonkarahisar	DK
14	15.05.2005	10:54	38.61	30.78	6	4.2	296	43	-122	Çobanlar-Afyonkarahisar	DK
15	08.11.2006	12:09	38.59	30.75	10	3.3	334	33	-91	Kızıldağ-Afyonkarahisar	DK
16	19.04.2007	13:21	38.58	31.24	6	4	300	65	-60	Sultandağı-Afyonkarahisar	DK
17	06.05.2007	19:55	38.66	30.86	13	3.3	304	77	-39	Çay-Afyonkarahisar	DK
18	18.01.2009	19:39	38.81	31.4	15	3.5	218	74	-102	Emirdağ-Afyonkarahisar	DK
19	15.09.2009	09:54	38.71	31.28	7	3.5	230	35	-106	Bolvadin-Afyonkarahisar	DK
20	21.12.2009	21:09	38.68	31.21	10	3.7	225	32	-87	Bolvadin-Afyonkarahisar	DK
21	07.09.2013	23:59	38.45	30.63	16	3.9	300.2	36.4	-41.5	Şuhut-Afyonkarahisar	DK
22	28.11.2015	03:23	38.98	31.23	20	3.5	340	78	-89	Emirdağ-Afyonkarahisar	DK
23	18.10.2016	20:33	38.69	31.04	7	3.5	260	42	-74	Bolvadin-Afyonkarahisar	DK
24	18.10.2016	22:54	38.69	31.04	9	4.1	307	56	-32	Bolvadin-Afyonkarahisar	DK
25	08.08.2019	20:50	37.85	29.75	16	3.6	220	66	-129	Dazkırı-Afyonkarahisar	DK

Source: HRV, Harvard CMT Solutions; DK, Kalafat, 2018*a, b*.

SE / NE-SW direction. This segment is the part of the main fault system which passes near Sultandağı-Çay. Field observations support that an approximately 20 km-break occurred due to this earthquake (Kalafat et al., 2002). Emre et al. found out the following similar results in 2003: the Çay segment is the primary surface faulting caused by the earthquake; it is 20 km long and generally in the east-southwest / west-northwest trending between Maltepe and Pınarkaya villages; Kali Stream segment consists of scattered faults in the northeast-southwest region which runs 6 km long along the edge north of the Kali Stream graben.

The distribution of aftershocks is towards western and northwestern parts of the Sultandağı fault zone and they are generally shallow earthquakes about 10 km depth (Figure 7). The available data support that the energy released as a result of the earthquake move ESE-WNW and NE-SW.

3. Current Data Analysis

The lack of seismic stations in the region and inadequacy of broadband stations in particular have been the most important motivation for the study (Table 3). Though limited, studies were initiated in

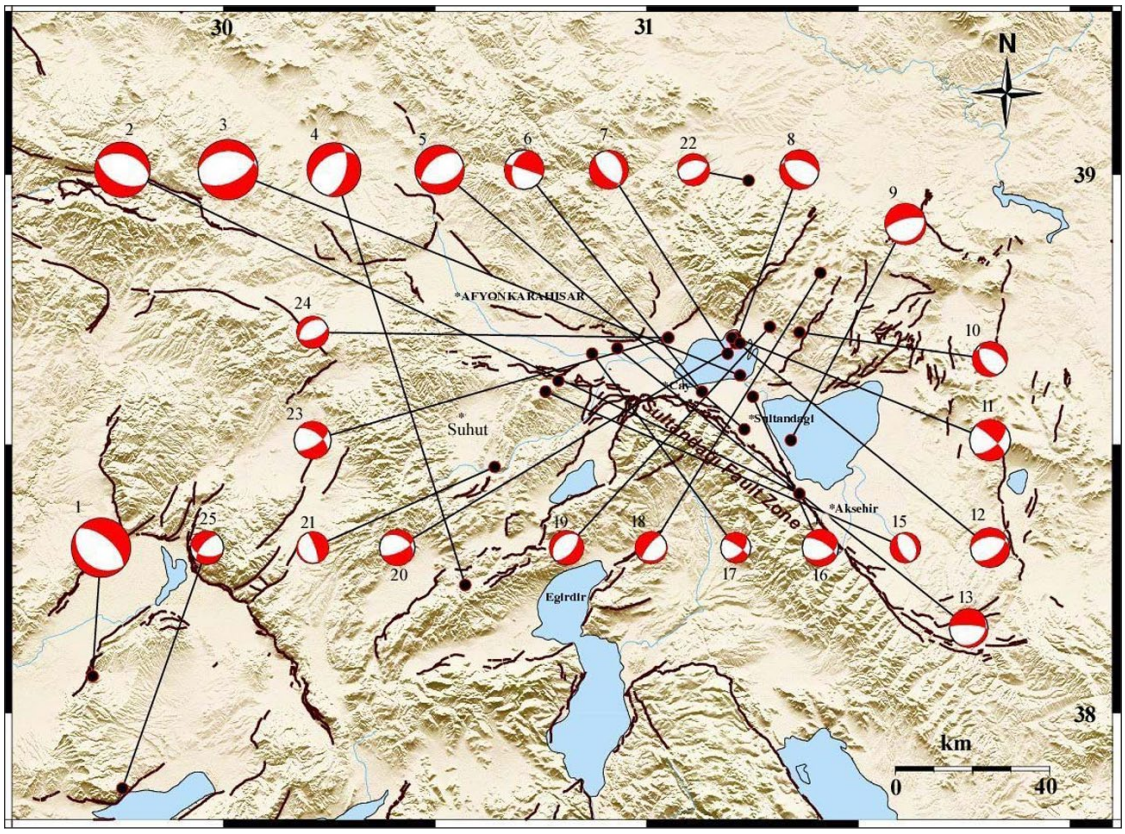

Figure 6- Faulting mechanisms of the earthquakes occurring in the region [of the 25 solutions in the figure, 21 give normal faulting, 4 of them (6, 11, 17 and 23 numbered earthquakes) oblique faulting; active faults were taken from Emre et al., 2013].

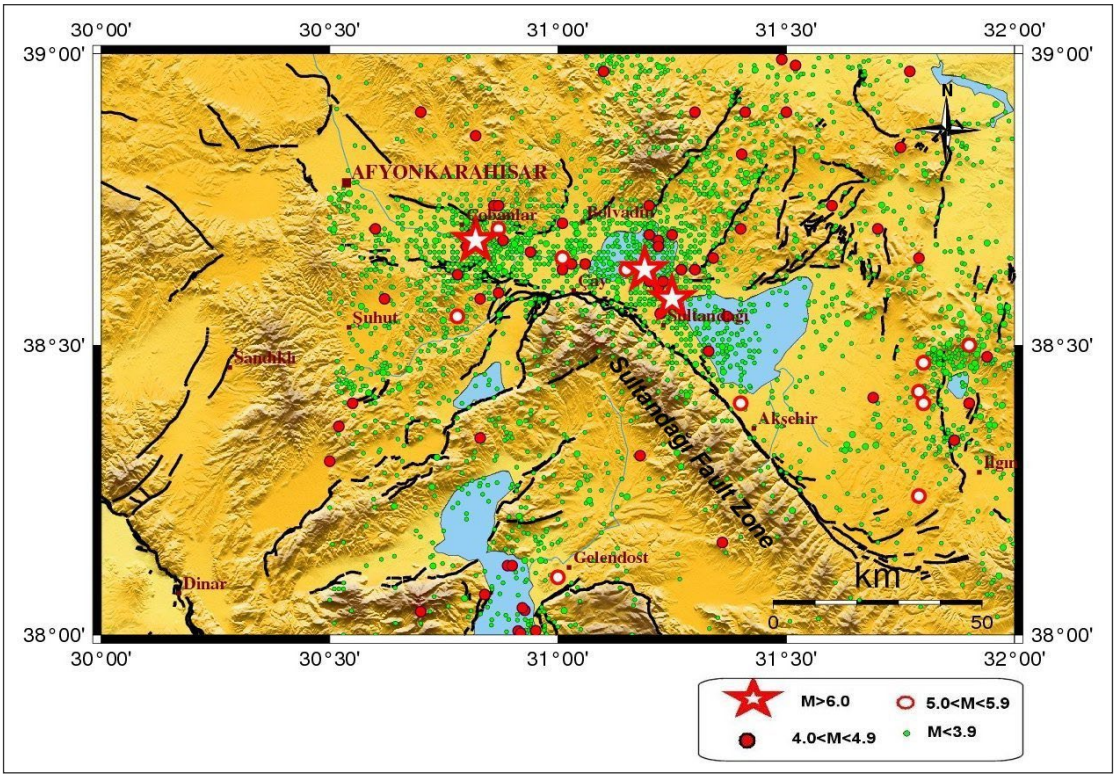

Figure 7- Earthquake activity of the region after the 2000-2002 earthquakes (All of the earthquake focal depths are approximately 10 km. are around and all earthquakes occurred in the shallow depth in the crust; active faults were taken from Emre et al., 2013).

November, 2016. First of all, the locations of 3 new seismic stations were determined. As the 3 major earthquakes (Mw = 6.0-6.5) between 2000 and 2002 occurred in the W-NW segment of the Sultandağı fault zone, this particular segment was selected as the location of the stations (Figure 8). While choosing the location, criteria such as safety, ground properties, noise level, logistics were taken into consideration.

Table 3- The stations installed in the region.

Station Name	Station Code	Station Coordinates (deg.)	Sensor Type	Frequency
Koçbeyli	KOCB	38.439513 K - 30.917470 D	Guralp 6-TD	100 Hz
Kırca	KIRC	38.509946 K - 31.232061 D	Guralp 6-TD	100 Hz
Taşağıl	TASA	38.794600 K - 31.095050 D	Guralp 6-TD	100 Hz

Data analyses were done in different time periods. The data obtained from each field study were evaluated. The 1st and 2nd Period data sets cover from 18 July 2017 until 27 March 2018. During this period, both the calculations of the data obtained from the stations installed within the scope of the study and the data obtained from the fixed earthquake station network operated by the Kandilli Observatory and Earthquake Research Institute (KOERI) were compared, and the parameters of the common earthquakes were recalculated. In addition, only the data obtained from the stations which had been installed within the scope of the study were evaluated. When analyzed statistically, the number of 139 events recorded by the KOERI Seismic network during this period (natural earthquakes due to tectonics + unnatural blasting events). The number of 496 events obtained from the stations installed within the scope of the study (Figure 9a, b). The data set obtained in the study is 3.57 times more than the seismic data of KOERI. Therefore, the stations installed within the scope of the study contributed significantly to the seismic monitoring of the region.

Data Set within the Scope of Study: 1st Period of Field Work (17-19 July 2017)

Data Set Date Range: 18 July 2017 (14:23 GMT) - 16 November 2017 (07:13 GMT)

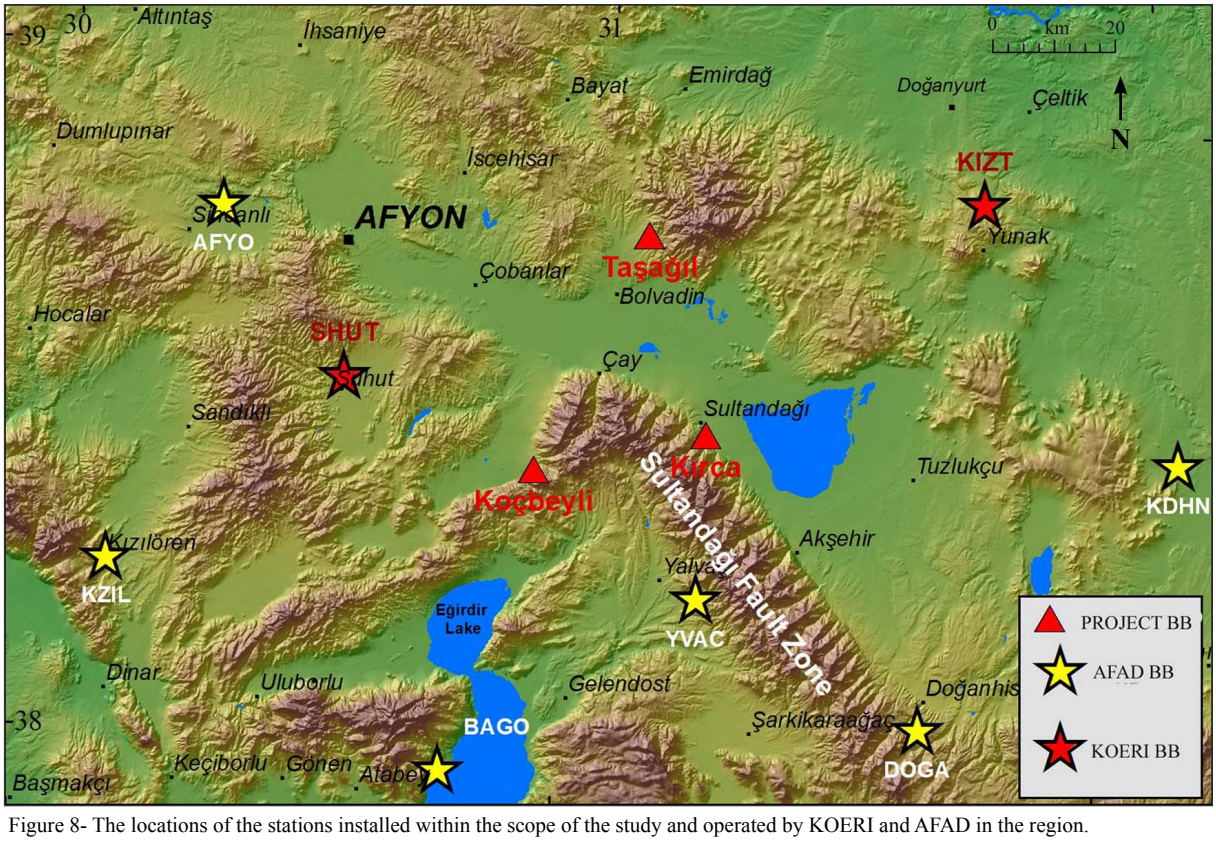

Figure 8- The locations of the stations installed within the scope of the study and operated by KOERI and AFAD in the region.

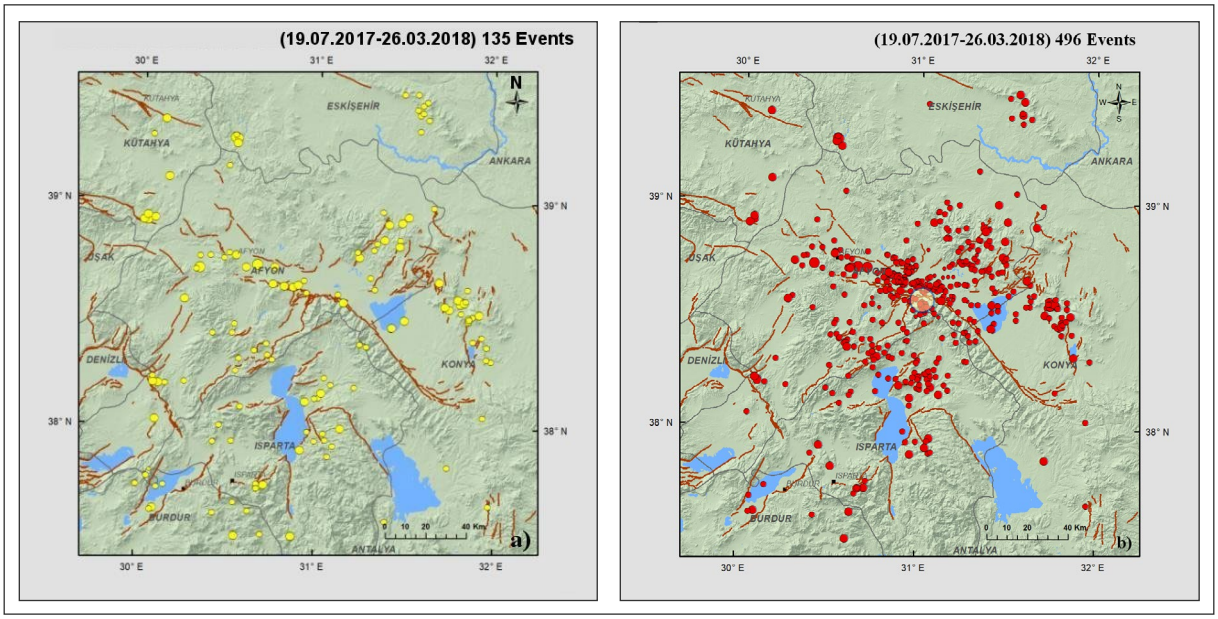

Figure 9- a) Distribution of events recorded by KOERI in the region during the 1st and 2nd periods in which data analysis was conducted (135 events) and b) distribution of events recorded by the stations installed within the scope of the study in the region during the 1st and 2nd periods in which data analysis was conducted (496 events), and light color circle indicates the blast area.

Data Range Coordinates Kandilli Catalog: KOERI 37.5-39.5 º N Latitude 30.0-32.0 º E Longitude

KOERI Total Number of Data: 71 (Earthquake and Blasting)

Data Set within the Scope of Study: 2nd Period of Field Work (25-27 March 2018)

Data Set Date Range: 15 November 2017 (10:15 GMT) - 27 March 2018 (07:00 GMT)

Data Range Coordinates Kandilli Catalog: KOERI 37.5-39.5 º N Latitude 30.0-32.0 º E Longitude

KOERI Total Number of Data: 68 (Earthquake and Blasting)

The stations installed within the scope of the study also contributed very positively to the determination of the epicenters of earthquakes whose solutions were obtained by KOERI. The parameters of the common earthquakes recorded by KOERI and the

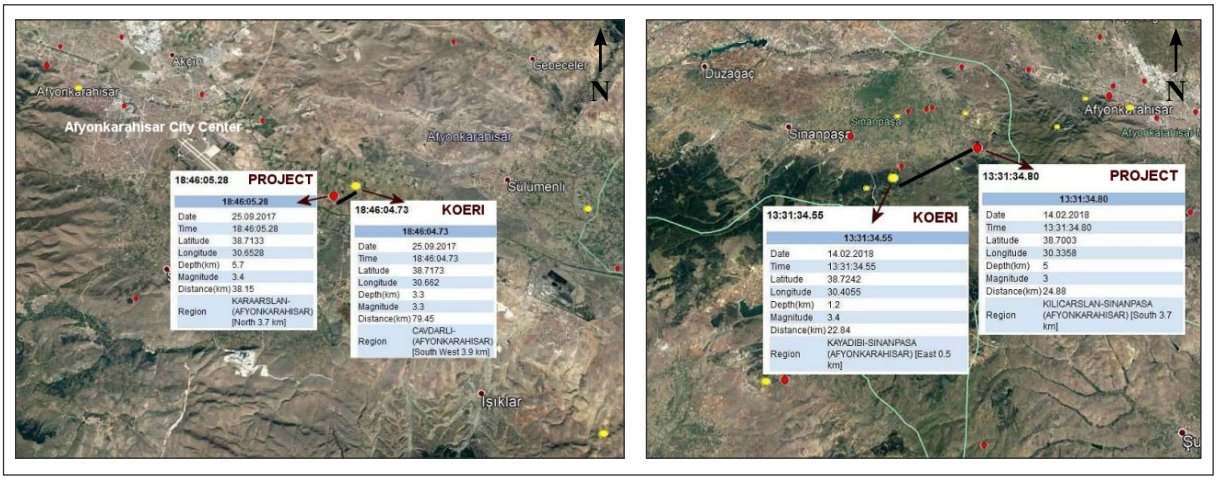

Figure 10- An example which shows how the epicenters of the two different events whose solutions were obtained by KOERI and the stations installed within the scope of the study have changed.

stations installed within the scope of the study were recalculated (Figure 9b). As a result, it was discovered that the epicenters of the earthquakes changed approximately ± 0.8-6 km in average (Figure 10). In addition, the study revealed positive changes in the depth distributions of the earthquakes. As a result, the horizontal and vertical error margins of the events in the region have been reduced thanks to the newly installed stations. The evaluation of the data obtained within the scope of the study indicated that the middle and northwest part of the Sultandağı-Akşehir fault zone has intense seismic activity. In addition, a significant NW-SE trending seismic activity was determined to the north of Isparta (province).

Figure 11a and 11b shows the distributions and numbers of the earthquakes the data sets obtained by KOERI (a) and within in the study (b) in the same period. It is clearly seen in figure 11a,b that the number of the earthquakes in the data set obtained within the study is much higher.

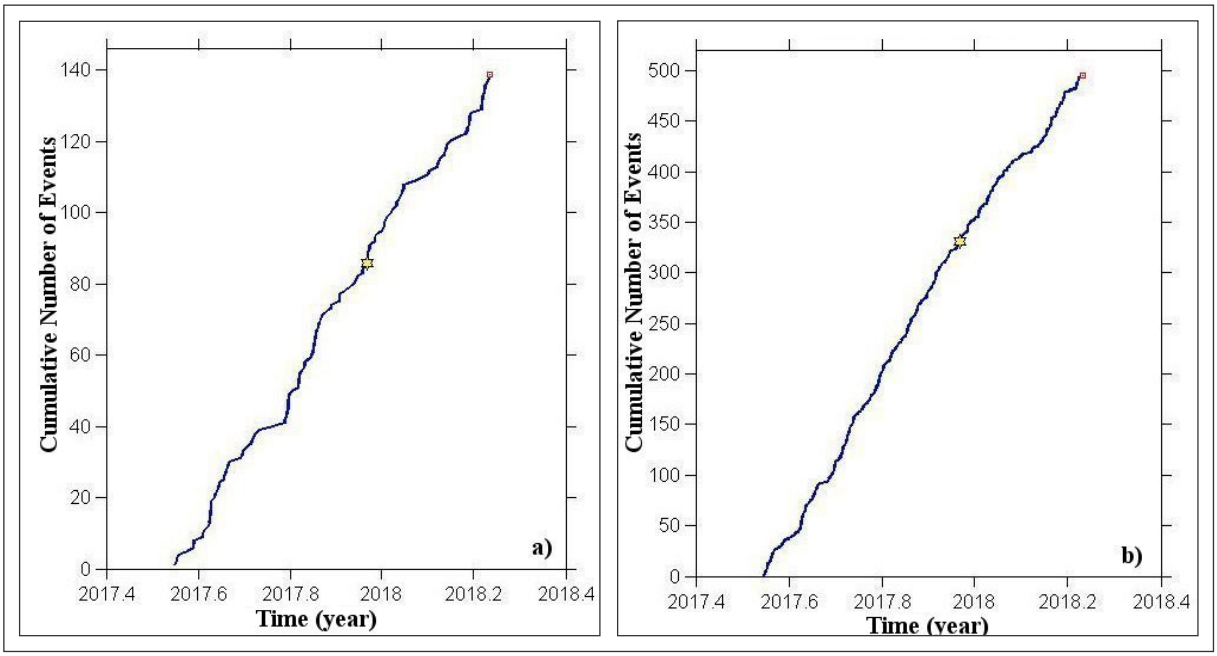

Figure 11- a) KOERI data set b) distribution of the number of the earthquakes in the data set obtained within the study.

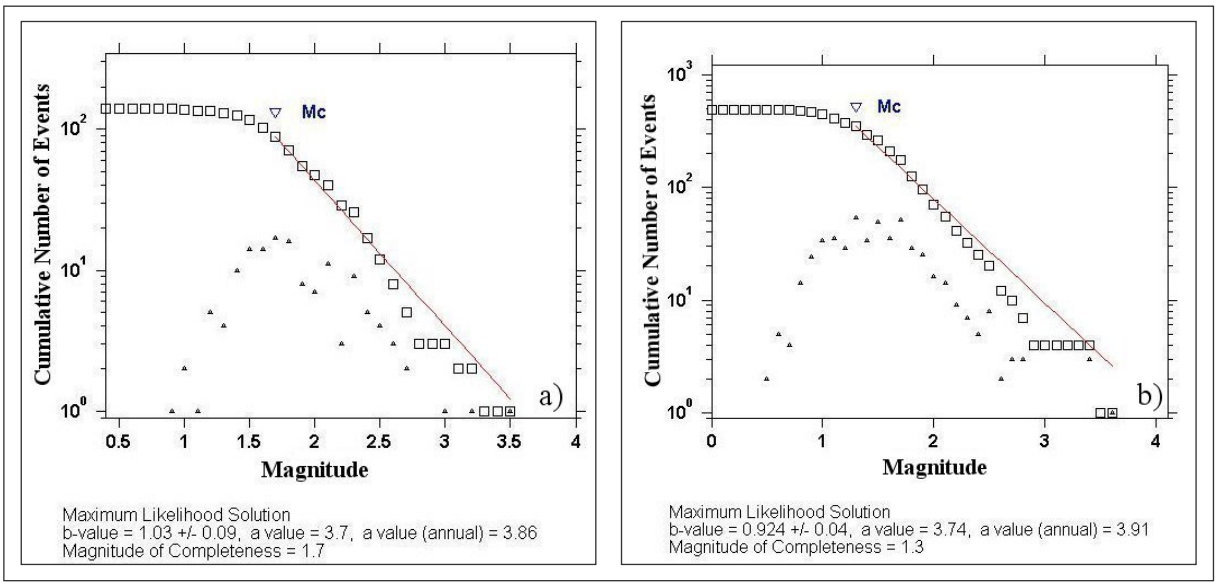

Figure 12- (a) KOERI data set (Mc = 1.7), (b) study data set (Mc = 1.3).

In the figures below (Figure 12a, b), the lowest magnitude threshold in the KOERI dataset (a) is Mc = 1.7; the lowest magnitude threshold in the data set obtained within the study (b) is Mc = 1.3. This means that the detection capacity of the fixed seismic network available in the region of KOERI is low (Mc = 1.7), and the seismic stations installed within the scope of the study contributed to the increase of the earthquake detection threshold (Mc) sensitivity in the region (Mc = 1.3) and increased the detection capacity, revealed that the seismic activity of the region was tracked more precisely.

In the region, especially in some areas, very small events occurring during the day were recorded. During the analysis of the data recorded in the field study, it was concluded that some intense micro-earthquake activity in the study area might have occurred due to the blasts, and therefore some locations where the events took place were detected during the field study. During these visits, we found out that a huge hydroelectric power plant and, therefore, a dam were being constructed in the area, and that quarry blasts were carried out to supply material in the region. Then, we visited some coordinates present in our records during the data analysis and observed the blasts in these areas (Figure 13).

It was observed that the blasts generally took place at 12:00-13:30/18:00-19:30 LT during the day and this data matches with the seismic records. Therefore, it was also statistically clear that the quarry blasts were carried out at certain time intervals during the day. The magnitude range of the blasts varies between M= 0.7-2.5. In the histogram below, the lower part of the red line shows the average number of events that could occur during the day, while the upper part of the red line indicates the number of blasts in the region. Therefore, the hours that display anomalies in the number of earthquakes during the day generally reflect the blasts (Figures 14, 15).

Figure 13 - Blast locations conducted for the embankment of Çay Dam.

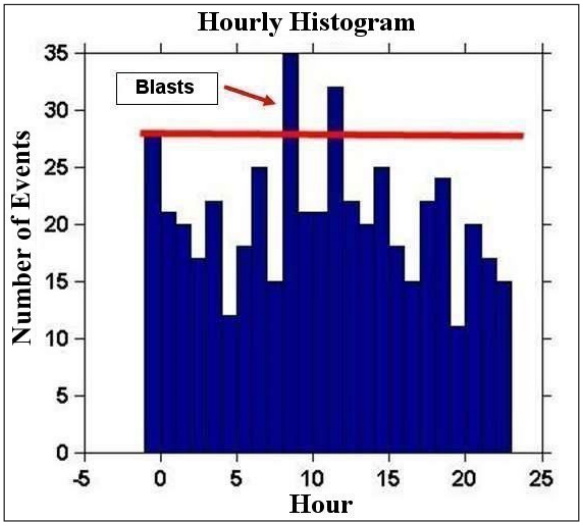

Figure 14- Hourly change of the events and blasts in the region during the day (GMT).

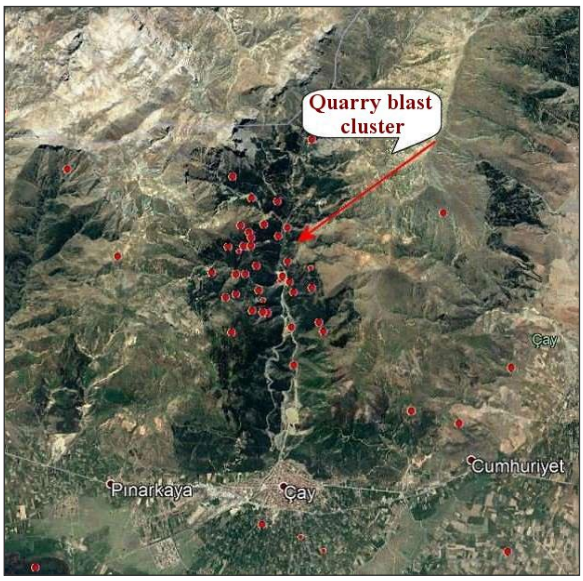

Figure 15- Blasting cluster analyzed within the scope of the study (south of Çay district, dam construction area).

The third data set analysis covers the period between 20 March 2018 and 15 March 2019. During this period, both the calculations of the data obtained from the stations installed within the scope of the study and the data obtained from the fixed earthquake station network operated by KOERI were compared, and earthquake parameters (coordinates, depth, magnitude, RMS root mean square residual, ERH horizontal error, and ERZ vertical error) of the common earthquakes were recalculated. This study evaluated only the data obtained from the stations which had been installed within the scope of the study. The statistics show that the number of events recorded by the KOERI seismic network during this period (natural earthquakes due to tectonics + unnatural blasting events) is 341. The number of events detected in the study is 480 (Figure 16a, b). In short, the data obtained within the scope of the study was approximately 41% higher than the seismic data of KOERI. Therefore, the stations

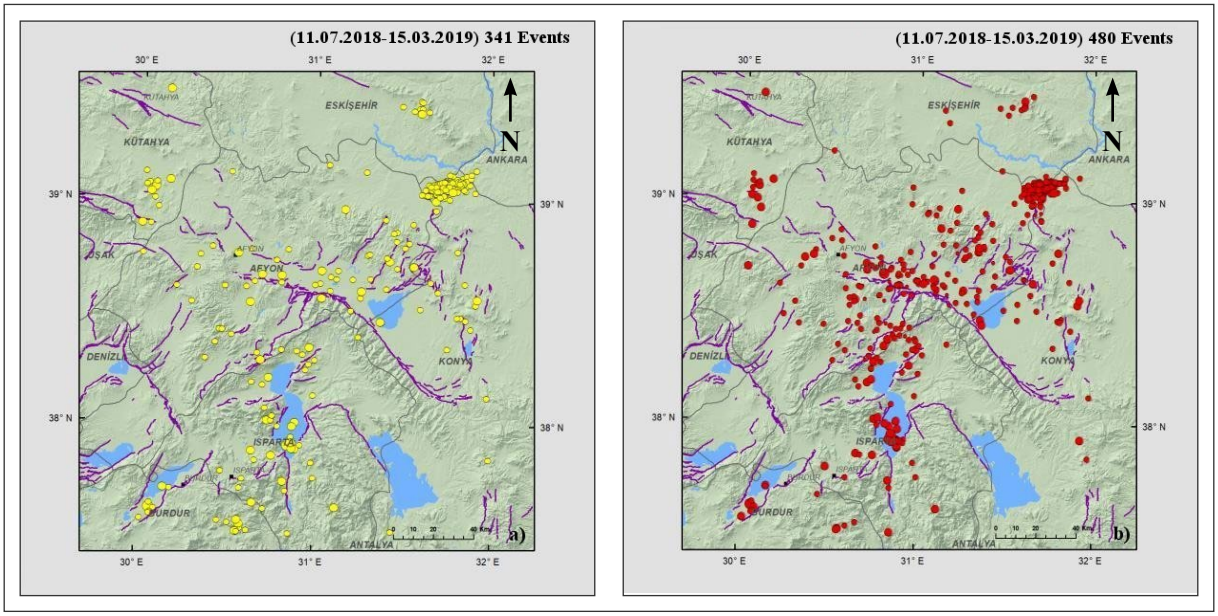

Figure 16 - a) Distribution of events recorded by KOERI in the region during the 3rd period in which data analysis was conducted (341 events). b) Distribution of events recorded in the scope of the study in the 3rd period (480 events).

installed within the scope of the study have made a great contribution to the seismic monitoring of the region and to the seismotectonics.

It was observed that the earthquake epicenters that were recalculated changed approximately ± 0.5-2.6 km on average (Figure 17). In addition, the study revealed some positive changes in the depth distributions of the earthquakes. As a result, the horizontal and vertical error margins of the events in the region were reduced thanks to the newly installed stations. As a result of the evaluation of all data, it was observed that especially the NE of Doğanyurt, the vicinity of Eğirdir Lake, Altıntaş-Kütahya, Çobanlar-Bolvadin-Çay, especially the middle and northwestern part of the Sultandağı-Akşehir Fault Zone have intense seismic activity.

Figure 17 is given as an example of how the epicenters of three different events changed with the new data obtained in the study. In the 3rd period, it was observed that there were no intense quarry blasts in the region. Local micro-earthquake activities, blasts and tele-seismic (distance earthquake) records were monitored in the 3rd period data set evaluated within the scope of the study.

4. Related Theories and Methods Used

Different software and techniques were used in this study. The most important of them were the software that are still widely used by the world's major seismology centers for the calculation of earthquake parameters (Hypo71, HypoInv, Hypocenter; Lee and Lahr, 1975; Klein, 1985; Lienert et al., 1986). Station distribution and density are of great importance in determining the locations of earthquakes. Earthquake locations can be calculated very accurately with a well-designed station distribution considering the intended target. The stations installed within the scope of the study were designed for these purposes. Three component digital data obtained from the stations were used in the Hypocenter program used within the scope of the study. All prepared data which were entered into the program as an input file, so all parameters such as occurrence time, geographic coordinates, size and depth of earthquakes were determined by inverse solution algorithm. The program attempted to determine the location of the earthquake in a way that can minimize the difference between the theoretical P- and S-arrival times created according to a given ground seismic velocity structure (Kalafat et al., 1987) and the observational times read from the data.

Another method targeted and used within the scope of the study was to enable the magnitude of earthquakes to be given by different methods. In this study, M_L Local magnitude was given to all earthquakes in general, and M_w Moment magnitude calculation was made for earthquakes with M > 3.3 in general. Richter (1936, 1948) magnitude, also defined as Local magnitude (M_L), is the magnitude type used by all seismology centers in local earthquake studies. The definition of the method was made according to the Wood-Anderson (WA) seismometer used at that time. In this study, the calculation method determined by KOERI was used. The earthquake records obtained

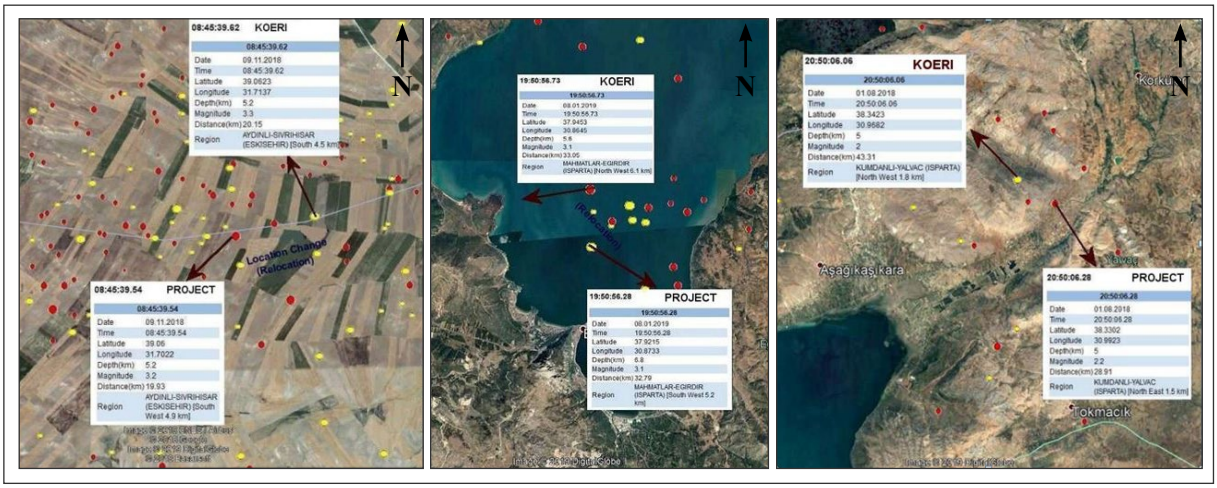

Figure 17- Examples showing both the new solutions of three earthquakes aside from the changes in their locations thanks to the stations installed within the scope of the study and the solutions obtained from KOERI.

within the scope of the project were converted into WA record with signal analysis methods and used in accordance with this definition. Briefly, they were simulated to the original WA seismometer. In the Richter approach, the basic expression is the ratio of the maximum amplitude (A) observed at the station to the reference amplitude (A_0):

$$M_L = \log \frac{A}{A_0}$$

A is the maximum (in mm) zero-to-peak amplitude (+ or -) recorded by a WA seismograph. A_0 is the amplitude of the zero magnitude earthquake as a function of the epicentral distance. Moment magnitude (M_w) was generally given as a result of the determination of earthquake source parameters or by using S wave spectrum technique. Below are the Moment Magnitudes (Mw) given by the BLVD and SDAG stations used within the scope of the study and their contribution to the solution of the Darıcılar-Dazkırı (Afyonkarahisar) earthquake on 8 August 2019 (Figure 18).

In addition, these stations also contributed to the determination of the Earthquake Source Parameters, and the digital data obtained enabled the calculation of fault plane solutions of earthquakes with a magnitude M > 3.5. Relevant programs were used for the analysis of the data obtained from the digital three-component records collected in the study (Dreger 2002; Sokos and Zahradník, 2013; Figure 19).

Within the scope of the study, Earthquake Source Parameters of the Acıpayam earthquakes that occurred in the region in 2019 were calculated through the Moment Tensor Inversion (MTI) technique (Figure 20; Table 3). In addition, regional stress analysis was performed using the stress analysis method (Gephard, 1990). In the stress analysis of 15 earthquakes using P

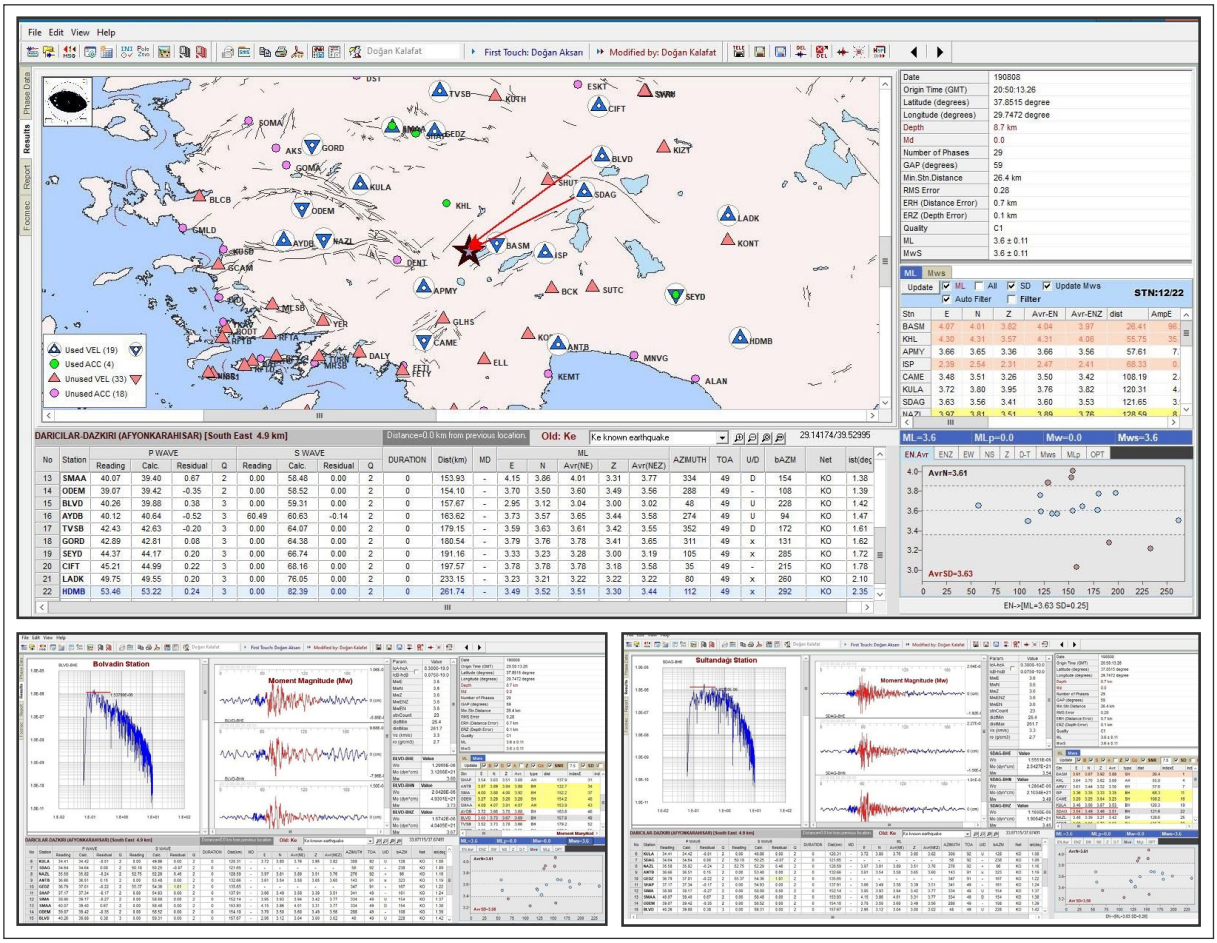

Figure 18- The contribution of the Bolvadin (BLVD) and Sultandağı (SDAG) stations to the solution of Darıcılar-Dazkırı (Afyonkarahisar) earthquake on 8 August 2019.

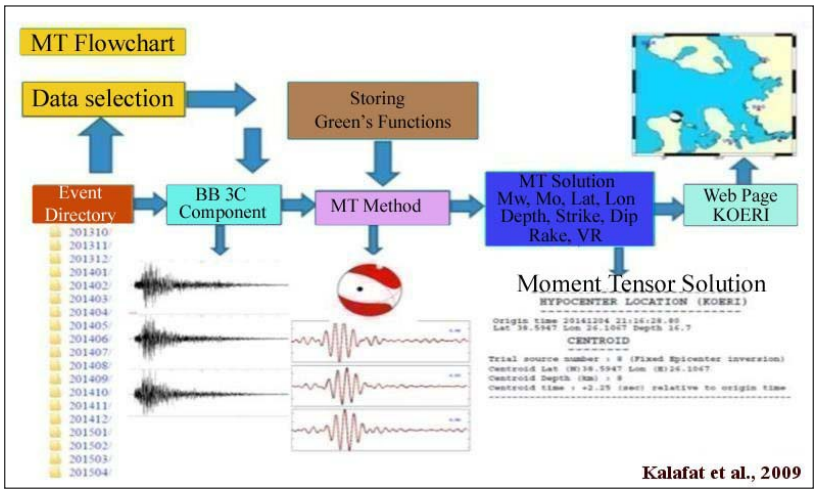

Figure 19 - Fault plane/MT solution flowchart (Kalafat et al., 2009; Kalafat, 2016).

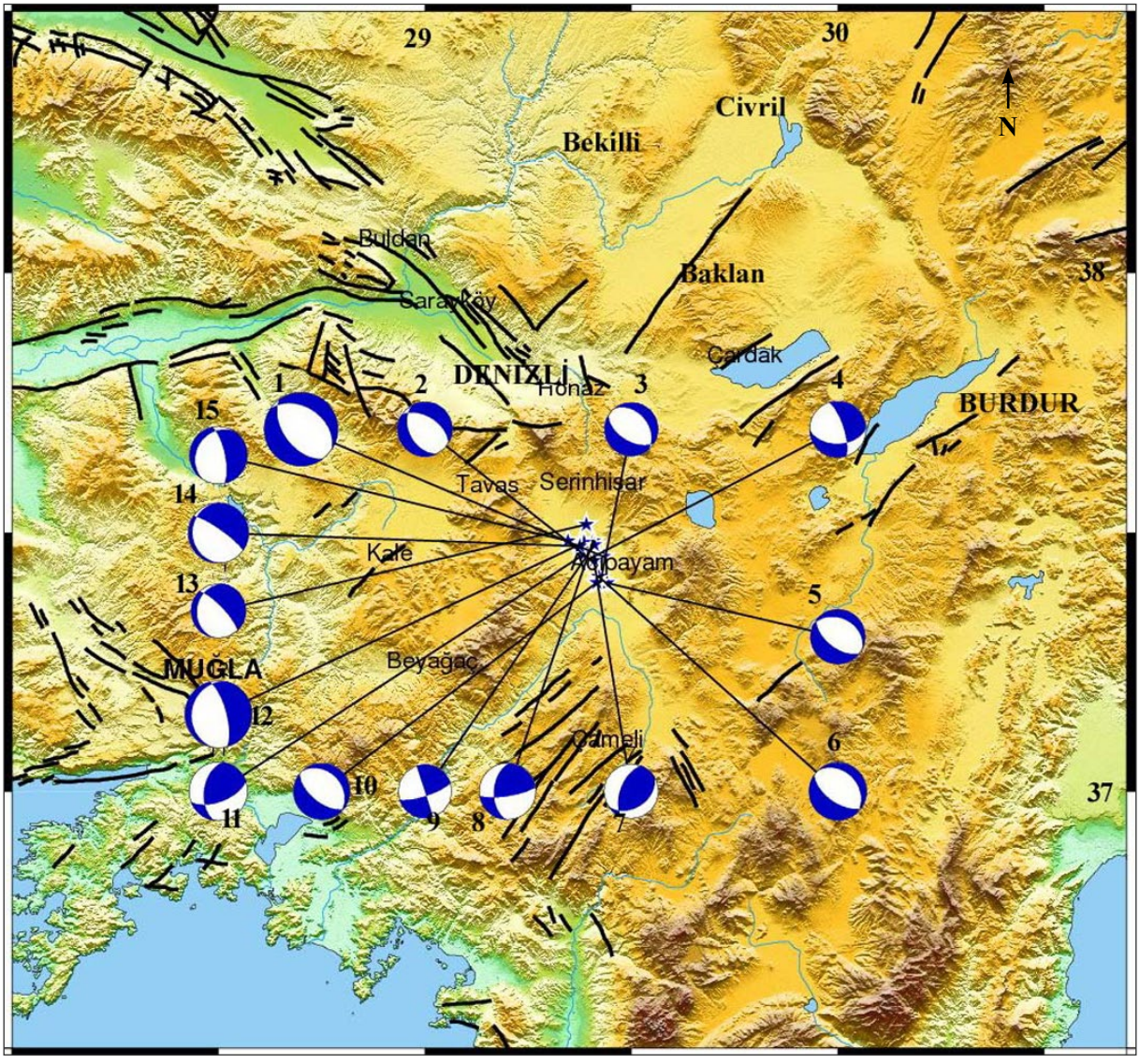

Figure 20 - Fault plane solutions of Denizli-Acıpayam earthquakes that occurred in the region in 2019.

Table 3- Fault Plane Solutions of the 2019 Acıpayam-Denizli earthquakes.

EQ. No.	Date	Time	Lat.	Lon.	Depth. km.	Mw	Str.	Dip A.	Rake A.
1	20.03.2019	06:34	37.4545	29.4317	12	5.5	304	40	-105
2	20.03.2019	06:51	37.446	29.405	6	4.1	302	52	-110
3	20.03.2019	08:00	37.4075	29.4252	6	4	121	54	-102
4	20.03.2019	12:45	37.4523	29.4025	6	4.2	89	47	-156
5	20.03.2019	17:04	37.4035	29.441	8	4.1	296	33	-100
6	20.03.2019	17:42	37.4163	29.421	8	4.3	317	31	-80
7	22.03.2019	08:20	37.4475	29.4098	20	4.1	201	57	68
8	22.03.2019	15:32	37.4845	29.4075	14	4.2	183	50	18
9	24.03.2019	16:17	37.4777	29.4105	8	4	72	76	-180
10	25.03.2019	06:15	37.4047	29.4163	8	4.2	129	60	-94
11	27.03.2019	11:27	37.4592	29.3848	15	4.4	188	49	40
12	31.03.2019	11:30	37.4815	29.385	8	5	345	71	-99
13	31.03.2019	11:45	37.5167	29.3905	8	4.1	316	76	-108
14	01.04.2019	01:49	37.4747	29.3745	8	4.5	305	80	-101
15	04.04.2019	15:01	37.4848	29.3468	8	4.3	348	72	-107

and T axes (azimuth – plunge), the general direction of the main axes is E-W (P) trending compression and N-S (T) trending extension.

In general, stress tensors are obtained by using fault plane solutions. These are the directions of the three principal stress axes (Sigma1 > Sigma2 > Sigma3) and the relative quantities explained by the Stress ratio (R) for the principal stress axes. The stress regime is expressed according to which of them is in the vertical plane. When the greatest principal stress axis (Sigma1) is vertical, this indicates extensional tectonics; when the intermediate principal stress axis (Sigma 2) is vertical, this indicates strike-slip tectonics; and when the minimum principal stress axis (Sigma 3) is vertical, this indicates compressional tectonics.

The fact that the dips of the principal stress axes Sigma 1 and Sigma 3 are close to horizontal and the dips of Sigma 2 are close to vertical indicates a dominant Strike-slip Faulting regime. The solution

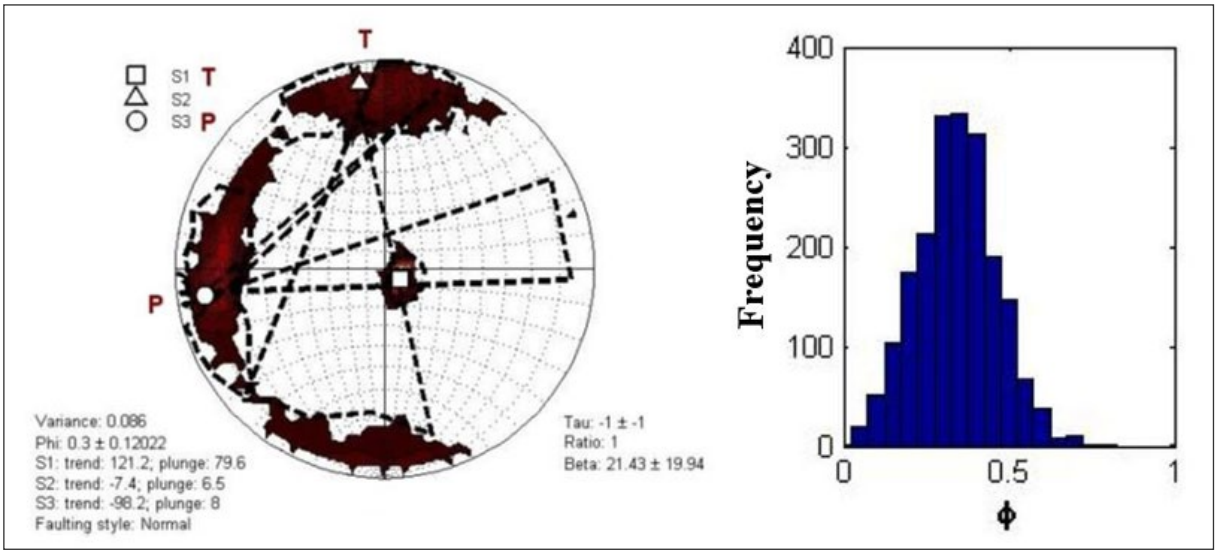

Figure 21 - Stress analysis performed in the study (The dominant directions of the principal stresses, the value of the R stress ratio).

from the study is the opposite and shows that the vertical slip normal faulting regime is dominant in the region (Figure 21).

Sigma2 – Sigma1 / Sigma3 – Sigma1 = R shows the amplitude values of the principal stress axes in the region. R_{max} = stress ratio R shows the relationship between the 3 principal stress axes. The fact that $0 \leq R \leq 1$ and R (ϕ) is between 0-0.5 indicates that an extensional tectonic regime is dominant in the region, and that this extensional regime continues its current evolution with vertical slip normal faults.

5. Results and Discussion

The study showed that the stations installed within the scope of the study decreased the earthquake detection threshold (Mc) in the region to M_c = 1.3 (Figure 22). This made a significant contribution to the monitoring of micro-earthquake activity very sensitively especially in the Sultandağı Fault Zone (SFZ) and its surrounding. It has been observed that as the sensitivity of the seismic network increases and the detection threshold (M_c) decreases, the number of earthquakes detected from the region increases significantly. The number of earthquakes that occurred in the region only during the study period is 1442 (Figure 23).

All Data Set in the Study Period (Between 19.07.2017 and 11.07.2019); while the number of Total KOERI Solutions is 638, the number of total solutions within the study is 1442 (Table 4; Figure 23; 24a, b). The comparison of the data obtained by KOERI and the study is below.

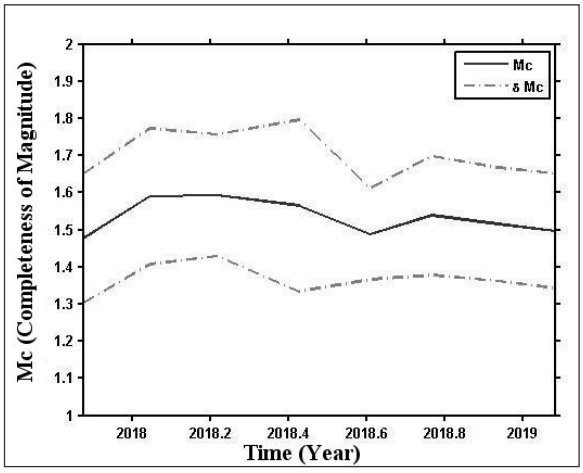

Figure 22- Mc range of earthquake detection threshold within the project.

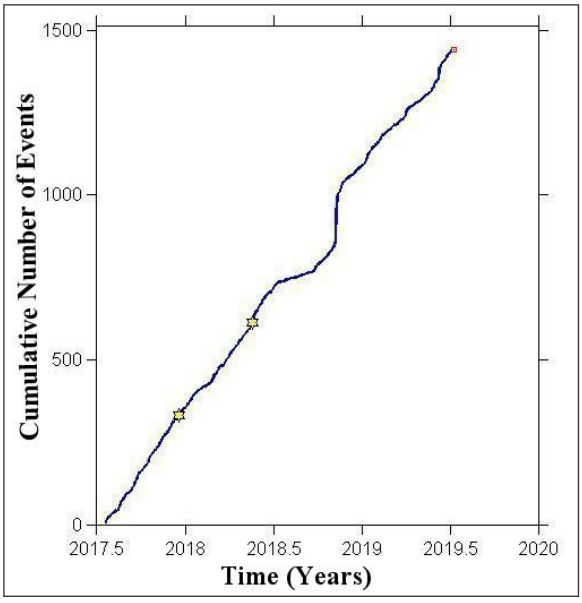

Figure 23- The cumulative increase in the number of events evaluated within the study.

Table 4- Comparison of data obtained by KOERI and the study.

PERIOD	DATE RANGE	KOERI SOLUTIONS	WITHIN THE STUDY AFTER EVALUATION	INCREASE
		Number of Events	Number of Events	Number of Events
1.-2.	**19.07.2017-26.03.2018**	135	496	361
3	**27.03.2018-10.07.2018**	79	236	157
	11.07.2018-14.03.2019	341	481	140
	15.03.2019-11.07.2019	83	229	146
TOTAL		**638**	**1442**	**804**

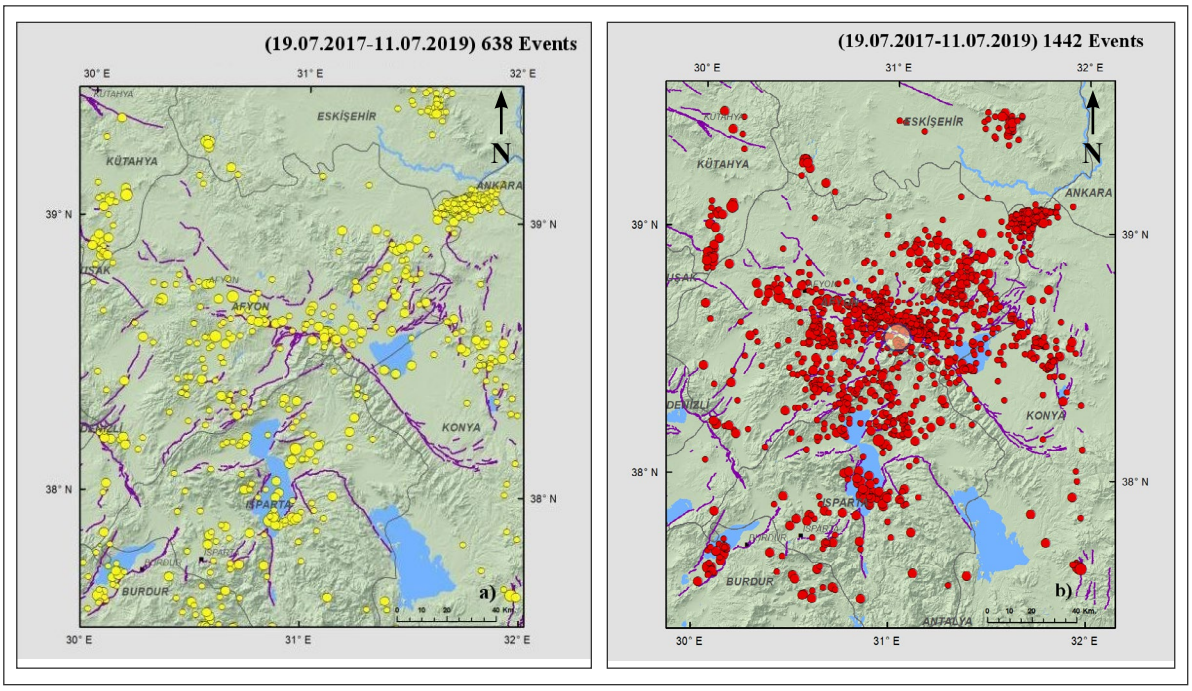

Figure 24- a) KOERI Solutions during the study period and b) solutions obtained with the contribution of the stations installed within the scope of the study (Active faults are from Emre et al., 2013; topography data is from NASA-SRTM).

In short, the number of earthquakes in the region whose parameters were calculated increased 2.26 times during the study. This has made a significant contribution to eliminating the lack of data in earthquake catalogs, monitoring the pre-earthquake process of earthquake generating sources, revealing the earthquake occurrence patterns, monitoring the energy discharge of the region, and calculating the cumulative seismic moment (Figure 25).

During the study, we recorded quarry blasts during the day conducted to supply material for the construction of the dam in the region. Thus, the sensitivity of the unnatural events catalog data set was increased by entering the coordinates of the blast areas into the existing database in the earthquake analysis of KOERI regarding the detection of the blast areas throughout the country (Figure 26a, b).

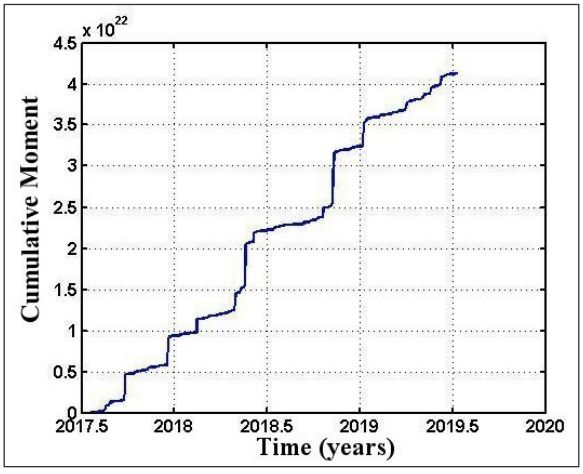

Figure 25 - Cumulative moment increase in the scope of the study.

As a result of the study, it was observed that the central and western parts of the SFZ are active, and that especially the vicinity of Sultandağı, Çay, Çobanlar and Afyonkarahisar have intense seismic activity. It was observed that there was a cluster of events owing to blasts during the construction of the Çay Dam to the south of Çay district. In addition, intensive seismic activities were observed along the south-southeast of Eğirdir Lake and to the south of Burdur Lake (Figure 24b).

The greatest contribution of the study is that two of the stations installed within the project were integrated into the National Seismic Network of Turkey operated by KOERI after the project was completed, enabling the existing network to serve more precisely across the country (Figure 27, 28).

The data obtained by the two stations installed within the scope of the study flow to RETMC

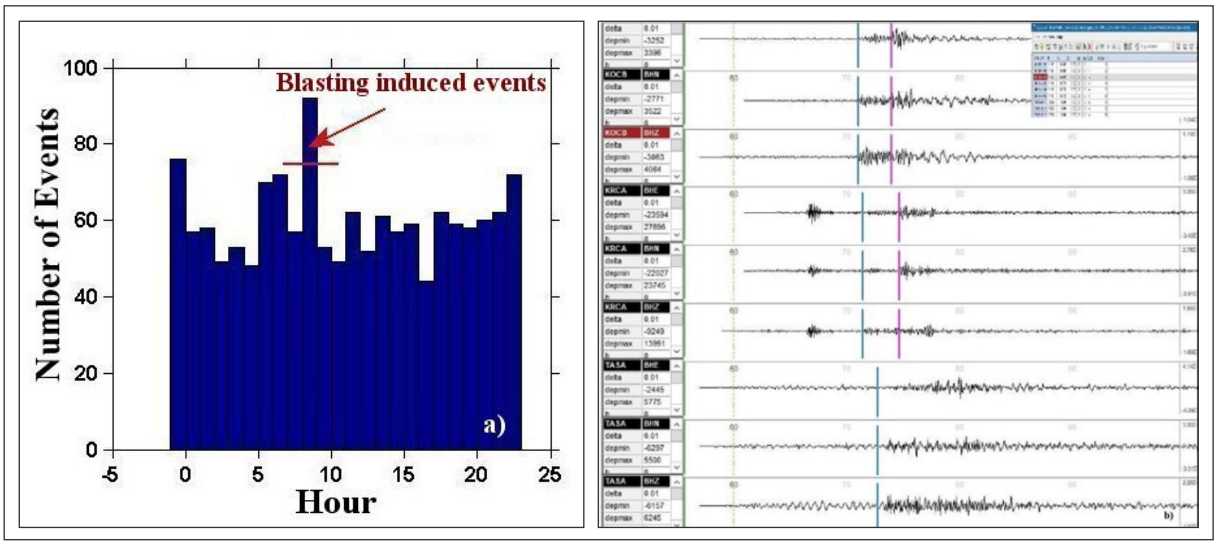

Figure 26- Unnatural blast event in the study area a) the distribution during the day and b) example of blast waveforms recorded by the installed stations (14.04.2018 15:11 GMT Çay-Afyon M= 0.9).

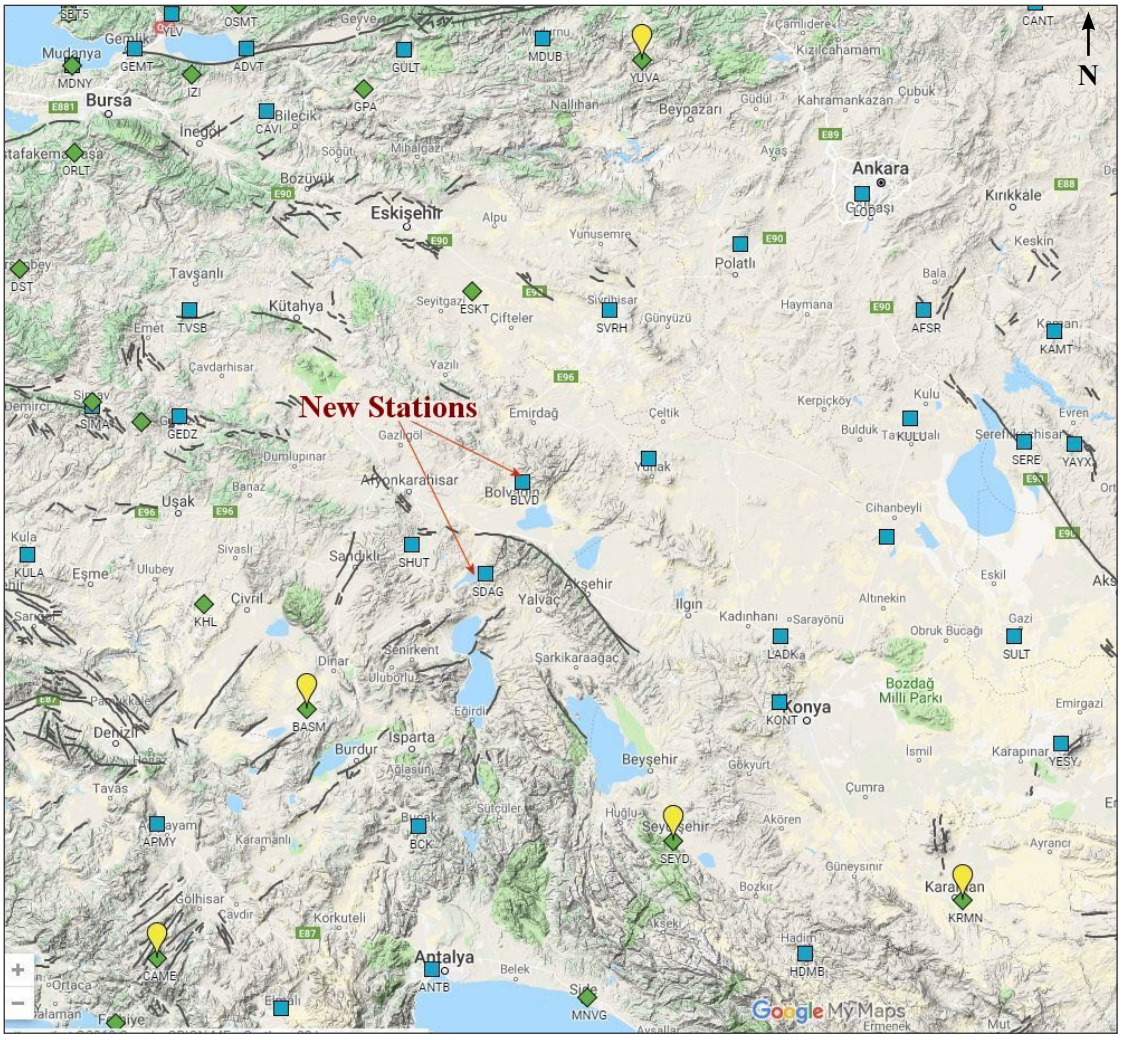

Figure 27- Two project stations, which are KOCB Koçbeyli and TASA Taşağıl, are integrated into National Seismic Network of Turkey. These stations are registered by ISC as BLVD and SDAG.

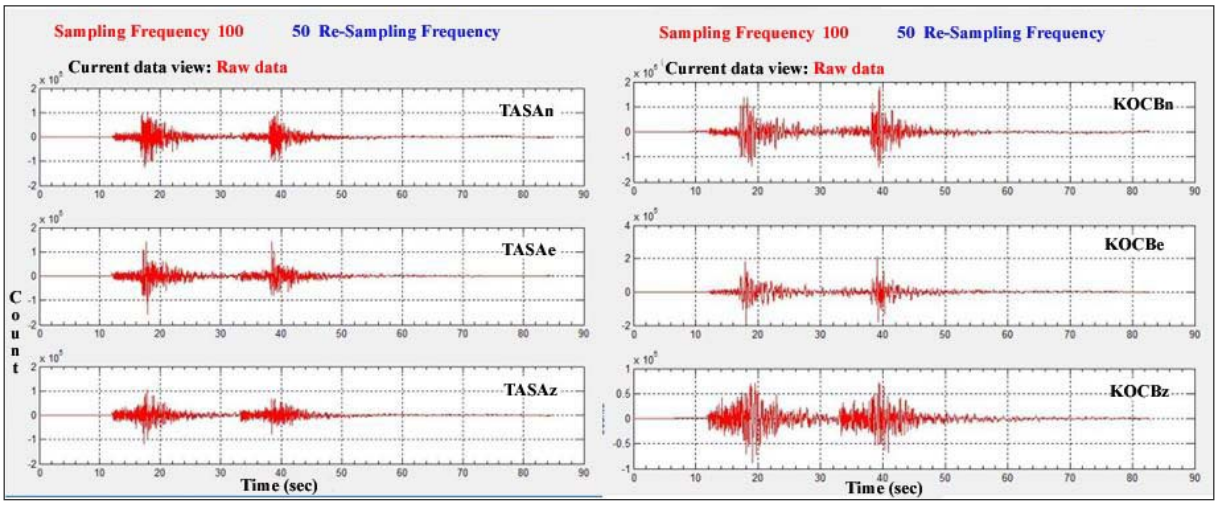

Figure 28- An example of sequential earthquakes recorded by the stations installed.

(Regional Earthquake-Tsunami Monitoring Center) in real-time. The stations installed were registered with the International Seismology Center (ISC); their International Station Codes were assigned (SDAG and BLVD) and they were included in the Global Seismic Network List. These stations contributed greatly to the solutions of the earthquakes that occurred in Western Anatolia recently. The 8 August 2019 Denizli Earthquakes can pose the best example for this. In the examples below (Figure 29), the contributions of these stations installed within the scope of the study to the Denizli Earthquake activity can be seen.

It was found that the locations of the earthquakes which were relocated by the installed stations changed with an average of ± 0.5-2.6 km. In addition, the study revealed positive changes in the depth distributions of the earthquakes. As a result, the horizontal and vertical error margins of the events in the region reduced thanks to the stations installed, and these stations greatly contributed to the development of the existing seismic network sensitivity. Therefore, the stations installed will have a remarkable contribution to find the answer to the questions whether the earthquake activity that might occur in the period after the three major earthquakes in the region in 2000 and 2002 will continue towards the NW or in a different direction. In this context, seismic monitoring in SFZ is crucial and it should not be ignored that the active fault segments to the west of Çay and northwest of Çobanlar carry a high seismic risk in the future.

Acknowledgements

This study was supported by Boğaziçi University under BAP Project No: 12280. Hereby, we would like to express our thanks to the Boğaziçi University Research Fund Commisson and its valuable members. The authors would also like to thank Dr. Selim Özalp (the referee), Dr. Asuman Kahya (the technical editor), Assoc. Prof. Dr. Şule Gürboğa (the assistant editor), Dr. Narumi Takahashi and the anonymous referee for their constructive contributions and critiques they provided throughout the examination of the article.

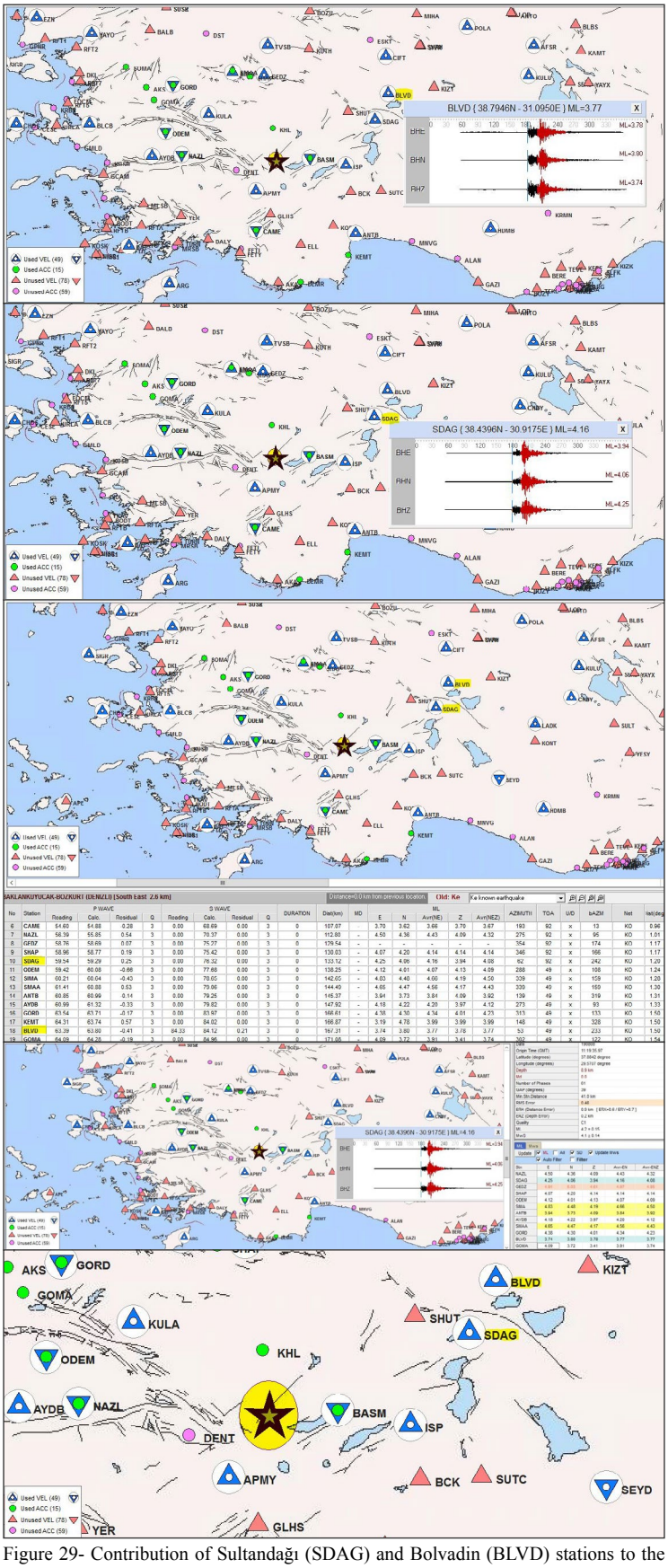

Figure 29- Contribution of Sultandağı (SDAG) and Bolvadin (BLVD) stations to the solutions of the 8 August 2019 (11:19 and 20:50 GMT) Denizli earthquakes.

References

Akyüz, S., Uçarkuş, G., Şatır, D., Dikbaş, A., Kozacı, Ö., 2006. 3 Şubat 2002 Çay depreminde meydana gelen yüzey kırığı üzerinde paleosismolojik araştırmalar. Yerbilimleri, 27 (1), 41-52.

Altunel, E., Barka, A., Akyüz, S. 1999. Palaeoseismicity of the Dinar fault, SW Turkey. Terra Nova- 11, 297-302.

Atalay, I. 1975. Tektonik hareketlerin Sultandağları'nın jeomorfolojisine olan etkileri, Türkiye Jeoloji Kurumu Bülteni 18, 21-26.

Barka, A.A., Reilinger, R.E., Şaroğlu, F., Şengör, A.M.C. 1995. Isparta Angle: its importance in the neotectonics of the Eastern Mediterranean Region. In: Pişkin, D., Ergün, M., Savaşçın, M.Y. and Tarcan, G. (eds), International Earth Science Colloquium on the Aegean Region Proceedings-3-18.

Blumenthal, M. M. 1963. Le systeme structural du Taurus sud Anatolien, Paul Fellot, 2, Societe Geologique de France, 611-662.

Boray, A., Şaroğlu, F., Emre, Ö. 1985. Isparta büklümünün kuzey kesiminde doğu-batı daralma için veriler. Jeoloji Mühendisliği Dergisi 23, 9-20.

Dreger, D. 2002. Time-Domain Moment Tensor INVerse Code (TDMT_INVC) Version 1.1, Berkeley Seismological Laboratory, 18.

Emre, Ö., Duman, T. Y., Doğan, A., Özalp, S., Tokay, F., Kuşçu, İ. 2002. 3 Şubat 2002 Sultandağı Depremi Ön Değerlendirme Raporu (Mw=6.3), Maden Tetkik ve Arama Genel Müdürlüğü, (http://www.mta.gov.tr/v3.0/bilgi-merkezi/afyon).

Emre, Ö., Duman, T. Y., Doğan, A., Özalp, S., Tokay, F., Kuşçu, İ. 2003. Surface Faulting Associated with the Sultandağı Earthquake (Mw 6.5) of 3 February 2002, Southwestern Turkey, Seismological Research Letters 74, 4, 382-392.

Emre, Ö., Duman, T. Y., Özalp, S., Elmacı H., Olgun, Ş., Şaroğlu, F. 2013. Açıklamalı Türkiye Diri Fay Haritası. Ölçek 1:1.250.000, Maden Tetkik Arama Genel Müdürlüğü, Özel Yayın Serisi-30, Ankara.

Eyidoğan, H., Güçlü, U., Utku, Z., Değirmenci, E. 1991. Türkiye Büyük Depremleri Makro-Sismik Rehberi (1900-1988), İTÜ MF Jeofizik Mühendisliği Bölümü Yayınları s. 200.

Gephard, J.W. 1990. FMSI: A FORTRAN program for inverting fault/slickenside and earthquake focal mechanism data to obtain the original stress tensor. Comput Geosci 16, 953-989.

Glover, C., Robertson, A. 1998. Neotectonic intersection of the Aegean and Cyprus tectonic arcs: extensional and strike-slip faulting in the Isparta Angle, SW Turkey. Tectonophysics 298, 103-132.

GMT v4 The Generic Mapping Tools, http://gmt.soest.hawaii.edu/gmt4/.

HRV Harvard Centroid-Moment Tensor Project CMT, Harvard University, MA, USA (1977-2017) https://www.globalcmt.org/.

Kalafat, D. 1996. 1 Ekim 1995 Dinar Depremi ve Saha Gözlemleri. Deprem Araştırma Bülteni 74, 95-113.

Kalafat, D. 2016. Türkiye ve Çevresi Faylanma-Kaynak Parametreleri (MT) Kataloğu (1938-2015) / A Catalogue of Source Parameters of Moderate and Strong Earthquakes for Turkey and its Surrounding Area (1938-2015), Tubitak Technical Report, 2016.

Kalafat, D. 2018*a*. Türkiye ve Çevresi Moment Tensör-Faylanma Bilgi Bankasının Oluşturulması ve Bölgesel Gerilme Analizleri, Türkiye Ulusal Jeodezi Jeofizik Birliği Bilimsel Kongresi – Scientific Congress of the Turkish National Union of Geodesy and Geophysics, Bildiri Kitabı-Abstract Book p. 462-469, 30 Mayıs-02 Haziran 2018, İzmir-Turkey.

Kalafat, D. 2018*b*. Source Parameters of Moderate and Strong Earthquakes for Turkey and its Surrounding Area (1938- 2017), JpGU Meeting 2018 Japan Geoscience Union, Presentation Number: S-SS08, 20-24 Mayıs 2018 Makuhari Messe Chiba, Japan.

Kalafat, D., Öz, G. 2001. 15 Aralık 2000 Sultandağı-Bolvadin (Afyon) Depremi, Türkiye 14. Jeofizik Kurultayı ve Sergisi, Genişletilmiş Sunu Özetleri Kitabı (Extended Abstracts Book) 26-31, MTA Kültür Merkezi, 8-11 Ekim 2001, Ankara (in Turkish).

Kalafat, D., Görgün, E. 2017. An example of triggered earthquakes in western Turkey: 2000–2015 Afyon-Akşehir Graben earthquake sequences, Journal of Asian Earth Sciences 146 (2017) p.103-113.

Kalafat, D., Gürbüz, C., Üçer, S.B. 1987. Batı Türkiye' de Kabuk ve Üst Manto Yapısının Araştırılması, Deprem Araştırma Bülteni 59, 43-64 (in Turkish).

Kalafat, D., Öz, G., Kara, M., Öğütçü, Z., Kılıç, K., Pınar, A., Yılmazer, M. 2000. 1981-1997 Türkiye ve Dolayları Deprem Kataloğu (M>4.0), B.Ü. Yayınları 2000, Bebek, İstanbul.

Kalafat, D., Kuleli, S., Li, X., Toksöz, M. N., Gulen, L. 2002. The Afyon Turkey Earthquake: Source Characteristics and Implications for Earthquake Triggering, Eastern Section of the Seismological Society of America, Program and Abstracts p.16,

74th Annual Meeting October 20-22, 2002 Boston College, Chestnut Hill, MA.

Kalafat, D., Li, X., Kuleli, H.S., Toksöz, M.N. 2003. The Afyon, Turkey Earthquake: Source Characteristics and Implications for Earthquake Triggering, Geophysical Research Abstracts, Vol. 5, 13694, European Geophysical Society EGS - AGU - EUG Joint Assembly, Nice, France, April 2003.

Kalafat, D., Yılmazer, M., Kekovalı, K., Görgün, E., Poyraz, A. S. 2009. Türkiye Deprem Ağına ait Genişbantlı (BB) Deprem İstasyonları Kullanılarak Yapılan Yakın Gerçek Zamanlı Bölgesel Moment Tensör Değerlendirmeleri – Near Real Time Regional Moment Tensor Estimation Using Turkish Seismic Network's Broadband Stations, International Earthquake Symposium, Abstracts Book p. 62, 17-19 August 2009, Kocaeli-Turkey.

Kaya, S., Esat, K., Ecevitoğlu, B., Işık, V., Kaypak, B., Aldaş, G.U., Can, Z.A., Baksı, E.E., Akkaya, İ., Seyitoğlu, G. 2014. Afyon-Akşehir Grabeni Batı Kenarının Tektonik Özellikleri Üzerine Jeolojik ve Jeofizik Gözlemler: İki Evreli Genişleme Modeli Hakkında Tartışmalara Bir Katkı (Geological and Geophysical Observations on the Tectonic Features of Western Part of the Afyon-Akşehir Graben: A Contribution to the Arguments on the Two-stage Extension Model), Hacettepe Üniversitesi Yerbilimleri Uygulama ve Araştırma Merkezi Bülteni, Yerbilimleri 35(1),1-16.

Klein, F. W. 1985. User's guide to HYPOINVERSE, a program for VAX and Professional 350 computers to solve for earthquake locations: U.S. Geological Survey Open-File Report 85-515, 53p. http://pubs.usgs.gov/of/1985/0515/report.pdf

Koçyiğit, A. 1984. Güneybatı Türkiye ve yakın dolayında levha içi iki yeni tektonik gelişim, TJK Bülteni C 27, 1-15.

Koçyiğit, A. 1996. Lakes region graben-horst system, SW Turkey: differential stretching and commencement age of the extensional neotectonic regime. In: Görür, N. (coordinator), National Marine Geological and Geophysical Programme, Workshop-1, İstanbul, Extended Abstracts, 99-103.

Koçyiğit, A. 2008. Orta Anadolu'nun aktif tektoniği ve jeotermal Enerji potansiyeli. Orta Doğu Teknik Üniversitesi, Müh. Fakültesi, Jeoloji Müh. Bölümü, Proje No. 07-03-09-1-00-23, Final Raporu, 135 (unpublished).

Koçyiğit, A., Özacar, A. 2003. Extensional neotectonic regime through the NE edge of outer Isparta Angle, SW Turkey: new field and seismic data. Turkish Journal of Earth Sciences 12, 67-90.

Koçyiğit, A., Onay, E., Saraç, G. 2000. Episodic graben formation and extensional neotectonic regime in west Central Anatolia and the Isparta Angle: A case study in the Akşehir-Afyon graben, Turkey, in E. Bozkurt, J. A. Winchester, and J. D. A. Piper (editors), Tectonics and Magmatism in Turkey and the Surrounding Area, Geological Society, London, Special Publication 173, 405-421.

Lee, W.H.K., Lahr, J.C. 1975. HYPO71 (revised): a computer program for determining hypocenter, magnitude, and first motion pattern of local earthquakes, U.S. Geol. Surv., Open-File Rept. 75-3111, 1-113.

Li, X., Kalafat, D., Kuleli, S., Toksöz, M. N. 2002. Complex Source Process of the February 3, 2002 Afyon Turkey Earthquake, EOS Trans. AGU 83 (47), Fall Meeting Suppl., Abstract , S71C-1111 0830h Poster, MCC: Hall C Sunday 0830h Presiding, Boston.

Lienert, B. R., Berg, E., Frazer, L. N. 1986. HYPOCENTER: An earthquake location method using centered, scaled, and adaptively damped least squares: Bulletin of the Seismological Society of America 76, 771-783.

NASA/USGS (https://earthexplorer.usgs.gov/) 30m SRTM Shuttle Radar Topography Mission (SRTM) – JPL-NASA topoğrafya verisi.

Öğdüm, F., Kozan, T., Bircan, A., Bozbay, E. 1991. Sultandağları ile çevresindeki havzaların jeomorfolojisi ve genç tektoniği, Maden Tetkik ve Arama Genel Müdürlüğü Report no. 9123, Ankara (unpublished).

Özgül, N., Bölükbaşı, S., Alkan, H., Öztaş, Y., Korucu, M. 1991. Göller bölgesinin Tekto-stratigrafik birlikleri, Ozan Sungurlu Sempozyumu Bildirileri, 213-237.

Richter, C. F. 1936. An Instrumental Earthquake Magnitude Scale, Bull Seism Soc Am 25: 1-32.

Richter, C.F. 1948. History and Applications of the Magnitude Scale, Bur. Central Seismol Int Ser A, 17: 217-224.

Seyitoğlu, G., Scott, B.C. 1996. The cause of N-S extensional tectonics in western Turkey: tectonic escape vs. back- arc spreading vs. orogenic collapse. Journal of Geodynamics, 22, 145-153

Sokos, E., Zahradník, J. 2013. Evaluating Centroid Moment Tensor Uncertainty in the New Version of ISOLA Software, Seismological Research Letters 84, 4, 656-665.

Şaroğlu, F., Emre, Ö., Boray, A. 1987. Türkiye'nin aktif fayları ve depremsellikleri, Maden Tetkik ve Arama Genel Müdürlüğü Report no. 8174, 394, Ankara (unpublished).

Şaroğlu, F., Emre, Ö., Kuşçu, İ. 1992. Türkiye diri fay haritası, Maden Tetkik ve Arama Genel Müdürlüğü, Ankara, ölçek: 1/1.000.000.

Şengör, A.M.C., Görür, N., Şaroğlu, F.1985. Strike-slip faulting and related basin formation in zones of tectonic escape: Turkey as a case study. The Society of Economic Paleontologists and Mineralogists, Special Publication, 37, 227-264.

Ulusay, R., Kasapoğlu, E., Dirik, K., Gökçeoğlu, C. 2002. 3 Şubat 2002 Sultandağı (Afyon) Depremi Saha İnceleme Raporu, Hacettepe Üniversitesi M.F. Jeoloji Müh. Bölümü, 44, Mart 2002, Ankara (in Turkish).

Uysal, Ş. 1995. Graben formation in the collisional belts: an example from SW Anatolia, Eşençay graben. In: Pişkin, D., Ergün, M., Savaşçın, M.Y. and Tarcan, G. (eds), International Earth Science Colloquium on the Aegean Region Proceedings, 273-287.

Bulletin of the Mineral Research and Exploration

http://bulletin.mta.gov.tr

The electric power production targeted Unconventional Geothermal Systems (UGS), some conceptual designs and their thermodynamics classification

Aydın ÇİÇEK[a*]

[a]*General Directorate of Mineral Research and Exploration, Energy Raw Material Research and Exploration Department, Ankara*

Invited Article

Keywords:
Geothermal Energy, EGS, UGS, Heat transfer, Hydraulic fracturing.

ABSTRACT

The geothermal energy is a renewable and relatively clean energy resource. The amount of geothermal energy stored just in the upper crust of the earth is large enough to meet the world's energy needs for thousands of years. Unfortunately, only a small portion of this potential can be utilized today by the conventional methods. The rest corresponds to the hot, fluid-poor areas which cannot be utilized by the current technology. The first concrete steps towards the utilization of such high potential areas emerged in the late 1960s and early 1970s. These studies have gradually continued in the following years, and many new terms and conceptual designs have been proposed so far. Unfortunately, no comprehensive definition has been established on this subject yet. This may bring about some difficulties such as the failure to express the intended concept in the right manner, the inability to determine the legal boundaries for the regulations required by the countries to make use of these areas which pose high risks in the commercial point of view. In this paper, some of the major terms and conceptual designs used for the projects targeting the power generation from fluid-poor hot areas are discussed. Furthermore, all of these terms have been gathered under the title of "Unconventional Geothermal Systems-UGS" and these designs are classified according to the types of thermodynamic system for the first time in this study. In addition, some new suggestions that can be used to define the definitional boundaries of these terms are put forward.

Received Date: 21.10.2019
Accepted Date: 09.12.2019

1. Introduction

The conventional geothermal exploration activities significantly increased following the legislation of the "Geothermal Resources and Natural Mineral Waters Law of Turkey (No: 5686) in 2007. The installed geothermal power capacity significantly increased from nearly 20 MWe to ~1.514,7 MWe as of September 2020. This value is foreseen to exceed 2.000 MWe in the next few years with the projects which are in planning phase, licensed phase and construction phase. According to these numbers, Turkey ranks first in Europe and 4th in the world in terms of power generation from the geothermal energy.

A conventional geothermal system consists of 5 fundamental components; the heat source, the reservoir rock, the cap rock, the recharge area and the working fluid. Particularly, the reservoir rock, the recharge area, the cap rock and the working fluid must be at desired levels for a viable conventional geothermal system. Otherwise, it will not be possible to commercially use the heat energy stored inside the earth. In fact, the conventional geothermal systems constitute less than 1% of the overall geothermal areas with high temperatures at accessible depths (0-10 km). Majority of these fields correspond to currently unexploitable fluid-poor hot areas.

Citation info: Çiçek, A. 2020. The electric power production targeted Unconventional Geothermal Systems (UGS), some conceptual designs and their thermodynamics classification. Bulletin of the Mineral Research and Exploration 163, 211-228. https://doi.org/10.19111/bulletinofmre.660706.

**Corresponding author: Aydın ÇİÇEK, aydin.cicek@mta.gov.tr*

The first concrete steps towards the utilization of fluid-poor areas began in the late 1960s and early 1970s in "The Valles Caldera" region of New Mexico, the United States. In 1972, this region was selected as a test area (https://openei.org/wiki/Fenton_Hill_HDR_Geothermal_Area). Then, the Arab-Israeli War in 1973 caused some problems in oil and gas supply in the world. This led the countries to conduct research on the fluid-poor hot areas. Thus, the Fenton Hill HDR Project accelerated. Following this, some developed countries such as Germany, Japan, France etc. took part inside similar projects due to promising primary results. Moreover, the experience gained from the project and tremendous energy potential have paved the way for the emergence of some new pilot projects in some other countries.

Extensive research carried out particularly since 2008 have unearthed the presence of 295 °C bottom hole temperatures between 0-5.000 m in Turkey. As in the world, some of these hot areas present the characteristics of conventional geothermal systems in Turkey while many others not. This shows that there are many fluid-poor hot areas in Turkey. Based on this, necessary awareness is needed to evaluate these areas in Turkey. Therefore, one of the main aims of this study is to raise awareness on this subject in Turkey.

In this context, in the first part of this study, the terms related to the fluid-poor hot areas are discussed and grouped under the title of "Unconventional Geothermal Systems-UGS". In the second part, evolution of the UGS term through time is briefly summarized. In addition, some fundamental criteria are proposed here to understand whether a geothermal system is UGS. In the third part, power production targeted significant conceptual UGS designs are classified based on thermodynamic system types. In the final part, various suggestions on UGS are put forward for Turkey.

2. Some UGS Sub-concepts

Plenty of terms have been proposed to define the studies conducted on the utilization of hot, fluid-poor areas so far. These terms and many associated concepts may vary by the system temperature, flow rate, the enhancement methods, the geological characteristics and the depth etc. Optimization processes in engineering designs are generally project-based and vary according to engineering provision (Canoğlu and Kurtuluş, 2016; 2017; Canoğlu, 2019). Today, majority of the UGS projects are only applied commercially in the areas with low temperature. The number of UGS projects producing long-term commercial energy is almost negligible. However, the dizzying potential of such projects globally attracts the attention of many countries and energy companies (Figure 1). However, no satisfying summary has been found on the fundamental principles of such systems. As a result, this study has emerged based on this motivation. Unless otherwise stated, all contents referred to as "Unconventional Geothermal Systems-UGS" during this study are valid only for power production.

In this study, the concept to be addressed as UGS was first put forward by a series of patented scientific studies. These studies constitute the base of Fenton Hill Project, known as "Hot Dry Rock (HDR)". However, the term HDR has not been able to completely represent many other project sites emerged with similar motivations. Therefore, many new terms have arisen on this subject. As a result, the first concept has undergone many changes through time. It has been used under various titles such as "Enhanced Geothermal Systems (EGS), Engineered Geothermal Systems (EGS), Hot Wet Rock (HWR), Deep Geothermal Energy (DGE), Petrothermal Systems (PS), Hot Fractured Rock (HFR), Hot Sedimentary Aquifers (HSA) and Unconventional Geothermal Systems (UGS) etc. In this study, all these terms are collectively gathered under "Unconventional Geothermal Systems (UGS)". Some important ones are summarized below.

The first high-temperature UGS concept was coined as Hot Dry Rock (HDR). In fact, this term was first suggested in the late 1960s and early 1970s by the employees of the Los Alamos National Laboratory in the Fenton Hill site, the New Mexico, the United States (Brown et al., 2012). The HDR is often used for high temperature crystalline and brittle rocks with no natural geothermal fluid production (Brown et al., 2012). Based on this, the first and only project that complies with the HDR term is the Fenton Hill project (Brown et al., 2012).

The second term that can be classified under the concept of UGS is the "Enhanced Geothermal Systems-EGS". This term was first coined by Grassiani et al. (1999). Tester et al. (2006) described this concept as

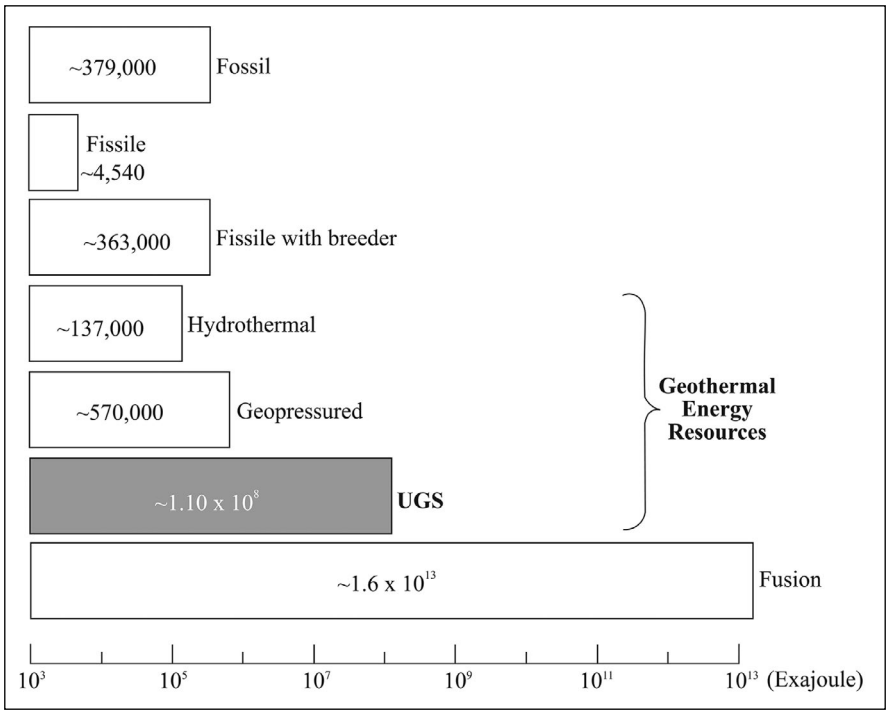

Figure 1- Some of the energy types and their potentials suggested on the global scale (After Armstead and Tester, 1987).

"the reservoirs where engineering methods have been applied for the commercial recovery of heat from low porosity/permeability geothermal resources" (Hıdıroğlu and Parlaktuna, 2019). However, Breede et al. (2013) have referred to the term as "all the geothermal systems enhanced by engineering methods". In addition, some conventional geothermal system applications (e.g. acidizing and fracturing) may also refer to as "enhancement". So, this leads to some confusions. In this study, the definition suggested by Breede et al. (2013) is adopted based on etymology. In addition, the term "Engineered Geothermal Systems-EGS is also used as an alternative to "Enhanced Geothermal Systems-EGS". It is mostly used in the same sense as "Enhanced Geothermal Systems".

Another term considered in this study is the "Hot Wet Rock-HWR". HWR was mainly used by Japanese researchers (e.g. Takahashi and Hashida, 1993). It is often used for brittle and hot rocks that do not produce commercial natural geothermal fluids despite conventional well completion work.

The next one that may be addressed under the UGS is the "Deep Geothermal Energy-DGE". DGE is mostly used by Western European researchers. Some researchers have subdivided the deep geothermal systems into two as "hydrothermal" and "petrothermal" systems (e.g. Breede et al., 2015; Hıdıroğlu and Parlaktuna, 2019). This term is still under hot debate (Breede et al., 2015). The majority uses this term as the geothermal systems for > 20 ºC and > 400 m, whereas some others use the "Medium Depth Geothermal Systems" term for 400-1.000 m depth range (Breede et al., 2015). They suggested "Deep Geothermal Systems" for the geothermal systems for > 1.000 m deep hot geological rocks (Breede et al., 2015). Indeed, this inherently covers both conventional and unconventional geothermal systems. It also causes further conceptual confusion.

Another common term is Petrothermal Systems. This was first coined by Roberts and Kruger (1982) (Breede et al., 2015). PS is typically used for the fields which do not have commercial permeability and > 150 °C (Breede et al., 2015). Today, on the other hand, power can also be generated at temperatures below 150 °C. Therefore, this term also cannot exactly cover the concept intended herein.

Another important term is the "Hot Fractured Rock-HFR". This was first proposed by Genter et al.

(2003) for hot and typically crystalline rocks with natural pre-existing fractures or artificial fractures (Breede et al., 2015). Based on etymology, HFR has a broader meaning, representing both conventional and unconventional hot rocks fractured via the artificial methods. In this context, this term may also be used for "the conventional geothermal reservoirs where the power generation is commercially possible, and the wells can be enhanced by fracturing method". Briefly, this also cannot fully cover the desired concept either.

Recently, the term "Hot Sedimentary Aquifers-HSA" has intensively appeared in the scientific studies (e.g. Breede et al., 2015). The first researcher who suggested this is unknown. The depth range, temperature, porosity, permeability, density of the reservoir rock, cap rock etc. of the system have led to serious discussions and brought the concept confusion to another level. Hence, the term HSA, like many others, is quite controversial. Yet, based on the etymology, the term HSA should be used for "all the sedimentary geothermal systems with commercial power production potential". Because, the fluid-poor hot rocks do not necessarily have to be sedimentary in origin. There are many such practical examples in the literature. Accordingly, the term HSA remains also insufficient to fully explain the concept aforementioned.

The "Unconventional Geothermal Systems-UGS" term is extensively used in recent literature (e.g., He et al., 2018). The UGS term can be defined as "*any hot rock without commercial natural geothermal fluid production after conventional well completion works*". Accordingly, the term UGS is regarded as more inclusive for the concept. Based on this, the UGS term is preferred in this study.

Apart from these, there are many other less known terms in the literature. Some are "Deep Heat Mining", "Stimulated Geothermal Systems", "Deep Geothermal Probes". These were described by Breede et al. (2015) to some extent. The interested reader can refer to Breede et al. (2015) for further detail.

3. The History and Definition of Electric Power Targeted UGS Concepts

The first definition related to the UGS concept emerged at the beginning of the 1970s in Fenton Hill rocks as "Hot Dry Rock-HDR" (Brown et al., 2012). In some subsequent projects such as Hijiori/Japan, Soultz-sous-Foréts/France, it is understood that the target reservoirs are not completely dry. Instead, they are filled with natural noncommercial geothermal fluids (Kuriyagawa, 1987; Takahashi and Hashida, 1993; Genter et al., 2010; Serpen, 2019). These showed that the term "HDR" is not enough to fully describe the desired concept. The concept formerly called as "Hot Dry Rock-HDR" has been later recalled as "Hot Wet Rock-HWR" (Takahashi and Hashida, 1993) particularly since 1993. Studies in the Soultz-Sous-Foréts Project led to the emergence of another term called as "Enhanced Geothermal Systems-EGS". This has been commonly used especially following the study of Grassiani et al. (1999). Afterwards, many well completion operations, frequently used in fluid poor hot areas, have been successfully applied in many subsequent conventional geothermal projects. Therefore, this showed that not only the fluid-poor hot rocks but also many conventional geothermal studies may be evaluated under the "Enhanced Geothermal Systems-EGS" (Breede et al., 2013). In recent studies, the concept has come to be known as "Unconventional Geothermal Systems". Because, the concept is quite different from conventional geothermal systems. Based on this, a more inclusive term, the "Unconventional Geothermal Systems-UGS", has emerged recently. This seems more inclusive than others. Thus, UGS is used in the course of this work.

Unfortunately, some target zone(s) cannot produce commercial natural geothermal fluid even all conventional well completion techniques are applied such as simple acidizing, simple nitrogen injection etc. Many geothermal projects failed due to insufficient commercial geothermal fluid production although the rock temperature is quite sufficient. If a project aims to commercialize such a geothermal system by applying unconventional engineering techniques such as sophisticated hydraulic fracturing, sophisticated acidizing, sophisticated thermal fracturing etc., this system can undoubtedly be considered as UGS.

Various types of working fluids may be used in an UGS work. If conventional geothermal fluid is used as working fluid in fluid-poor hot rocks, it must be supplied outside of the geothermal reservoir(s) that have commercial electricity generation potential. Otherwise, this should be regarded as

typical conventional reinjection operation. The use of unconventional working fluids or non-power producing conventional thermal waters originated from a low temperature reservoir as the main heat recovery agent such as CO_2, NH_3 etc., shows that this system is not a conventional geothermal system. Therefore, such a system can undoubtedly be regarded as UGS.

The hydraulic fracturing technique is widely used to enhance well productivity in both some recent geothermal and oil/gas projects. However, the artificial fractures required to increase productivity reclose due to earth stresses. To solve this problem, some special materials (i.e. proppant) are injected into the fractures. This technique is not normally preferred in a conventional geothermal system. Therefore, applying such a technique may be regarded as an unconventional geothermal operation. This shows that such a project is undoubtedly an UGS project.

Project costs are vital for a viable geothermal study. Therefore, cost management is carefully considered during the implementation of geothermal projects. However, despite the cost increase, some costly engineering practices (i.e. sophisticated hydraulic fracturing, acidizing, thermal fracturing etc.) are required to increase the productivity of hot and fluid-poor rocks. Although not used in a typical conventional geothermal project, unusually high grade well equipment is needed to avoid such problems in an unconventional geothermal project. Therefore, the widespread use of the unusual well equipment helps us to determine whether a project is UGS or not.

Commercial fluid production is crucial in a conventional geothermal project. Based on this, if any rock unit is hot and fluid-poor, some unconventional engineering designs are required to overcome these obstacles. Hence, an unusual conceptual design needs to be used to exploit the stored earth heat energy. Therefore, application of such a design shows that the project is UGS. These designs are further discussed below.

4. Substantial UGS Designs Targeting Electric Power Production

Despite the experience and know-how gained from a number of UGS projects since the early 1970s, this technology has not yet reached the desired level in the long term. On the other hand, global warming, fossil fuel depletion, energy supply security concerns, dizzying UGS potential, etc. have led to the emergence of many new conceptual designs. Apart from the most widely known design (i.e. classical UGS design), some other less known UGS conceptual designs are discussed in this paper. They are also classified here for the first time according to thermodynamic system types (Figures 2, 3, 4, 5, 6, 7, 8, 9 and 10).

Existing UGS designs can be grouped under three main headings according to thermodynamic system types. They are (1) Open-loop UGS designs, (2) Closed-loop UGS designs and (3) Hybrid UGS designs. The "Open-loop UGS designs" are the designs where there is direct contact between the working fluid and the main target zone. Hence, there is both heat and mass transfer between the working fluid and the main target zone in such systems. In the Closed-loop UGS designs, on the other hand, there is no direct mass transfer between the working fluid and the main target zone. In these, only heat transfer is expected. In the scope of this study, the Hybrid UGS designs are defined as the designs where some characteristics of both "Closed and Open-loop UGS" systems exist at the same time. They are summarized in table 1.

4.1. The Open-loop UGS Designs

There are numerous UGS designs classified under this topic in the literature. Open-loop UGS designs are quite common in practice due to huge experience and know-how gained from previous projects since 1970s. On the other hand, the major disadvantages of them are induced seismicity, scaling, healing (i.e. reclosing) of the induced fractures, loss in working fluid, limited working fluid option, displacement in the earth surface, risk of flow-channeling (i.e. short-circuit flow) in working fluid etc. (Table 1).

Many "Open-loop UGS design" sub-classes exist in the literature. Only some significant designs are briefly summarized here. They are (1) Classical UGS design, (2) Multi-stage UGS design, (3) Hot Ductile Formations UGS design, and (4) Eavor-Loop UGS design (Table 1, figure 2, 3, 4 and 5).

4.1.1. The Classical UGS Design

Among the Open-loop UGS designs, the most significant one is the "Classical UGS design"

Table 1- Some conceptual UGS designs suggested based on the thermodynamic system, their advantages, disadvantages and risks.

Explanations	Open loop UGS designs				Closed loop UGS designs		Hybrid UGS designs	
	Classical	Multi-stage	Hot ductile formations	Eavor-loop	Simple "U" or "L" shaped	Finned "U" or "L" shaped	Multiple Micro-hole Array	The Earth Energy Extraction System
Advantages, risks, obstacles and disadvantages								
Number of projects implemented	3	3	N/A	1	0	0	0	0
Flexibility in working fluid	1	1	1	3	3	3	1	1
CO_2 storage potential	2	1	1	0	0	0	1	1
Mineral extraction potential	N/A	N/A	3	0	0	0	N/A	N/A
Purification of unusable waters	N/A	N/A	3	0	0	0	N/A	N/A
Thermal stresses	0	0	N/A	1	0	0	1	1
Induced seismicity	3	2	0	0	0	0	1-2	1-2
Scaling	2	2	2	1	0	0	1-2	1-2
Back-closure risk of induced fractures	3	2	3	0	0	0	3	3
Losses in working fluid	3	1-2	N/A	0	0	0	1-2	1-2
Vertical displacement	2	1	N/A	0	0	0	1	1
Flow-channeling risk (i.e. short-circuit) in working fluid	3	1	N/A	0	0	0	0-1	0-1
Contamination of shallow aquifers	2	1	1	0	0	0	1	1
Predicted costs	2	1	N/A	2	3	2	3	3
Effective heat exchange area	2	3	3	1	1	2	3	3
Predicted internal energy consumption	3	2-3	3	0	0	0	2	2
Current feasible technical and technological infrastructure	2	3	N/A	3	3	1-2	2-3	2-3

* 0: Never or negligible, 1: Very few, 2: Moderate, 3: High and N/A: Not applicable.
** The evaluations may vary with many parameters such as the tectonic regime, temperature, depth, state of the geological structures through the main target zone, lithological features, technical and technological advancements.

(Figure 2). This has many variations based on well number and configuration such as single-well, double-well (i.e. doublet), triple-well (i.e. triplet) etc. As the detailed description is beyond the scope of this study, it will not be discussed further here.

The concept of the Classical UGS design was first suggested as HDR (Brown et al., 2012). It has been widely used as "Enhanced Geothermal Systems-EGS" particularly since early 2000s. In the late 1960s and early 1970s, this design was first proposed by the employees of the Los Alamos National Laboratory in the United States (Brown et al., 2012). The model can be described as "an artificial geothermal reservoir formed by fracking of usually fluid-poor crystalline hot rocks". On the other hand, non-crystalline rocks are also targeted in some similar practical applications.

Water-based conventional fluids are frequently preferred as the working fluid in these designs. Recently, extensive theoretical work has been done to use some alternative fluids such as "CO_2" and "N_2O". These studies have significantly increased in recent years. But no significant practical application is found in the literature. Classical UGS designs have not reached the technologically desired level yet. Due to simplicity, easy supply of working fluid, practical experience and know-how gained since the early 1970s, it is still applied in many projects. Although it has been implemented in dozens of projects, there are many obstacles to overcome in them (Table 1).

There are many practical projects on that type of Open-loop UGS. Some significant projects are as follows; (e.g. Fenton Hill, Newberry, Raft River, Coso), Germany (e.g. Bad Urach, Bruschal,

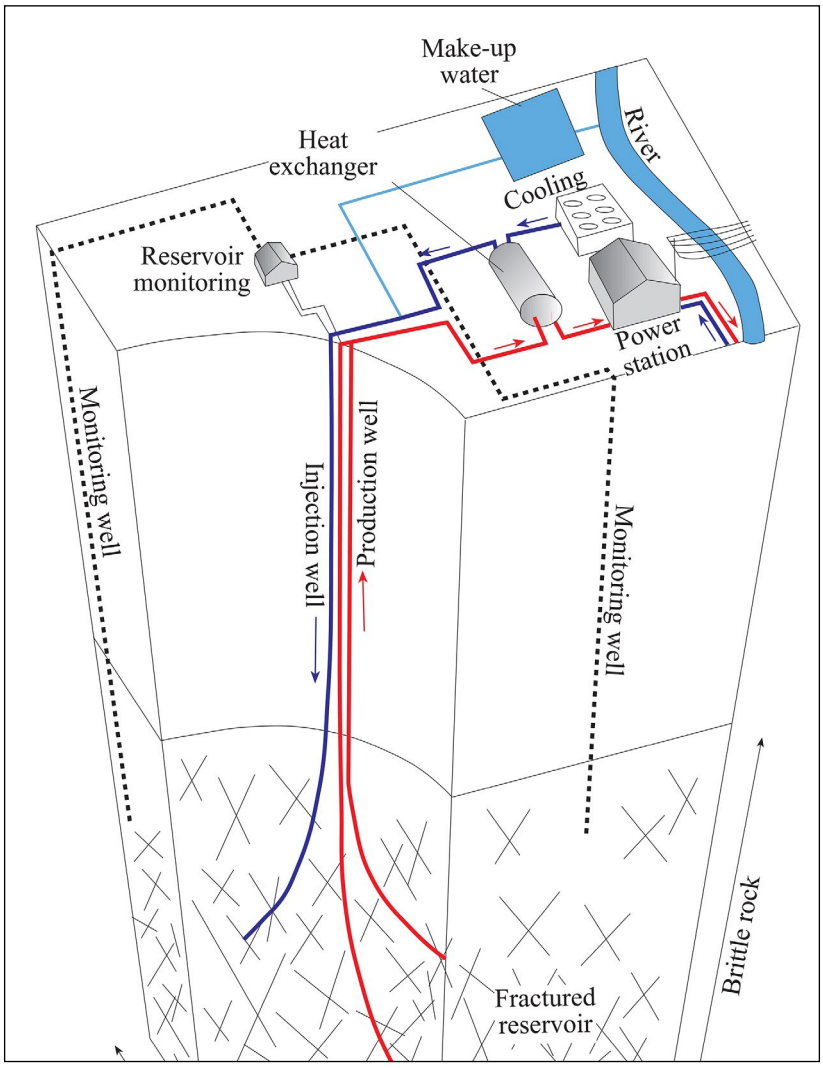

Figure 2- Schematic representation of the Classical UGS design (Re-drawn from Geothermal Explorers Ltd., 2003).

GENESYS project), France (Soultz-sous-Forêts), Japan (Hijiori and Ogachi).

Some problems terminated or paused these projects. They were briefly discussed in Çiçek, (2019). There have been done many research studies to overcome these problems. The strongest advantage of the system is the enormous amount of know-how and experience gained as a result of numerous applications. Classical UGS designs have many advantages and disadvantages compared to others (Table 1).

4.1.2. The Multi-stage UGS Design

The Multi-stage UGS design is another type of the "Open-loop UGS" design (Figure 3). The first study dealing with the multi-stage UGS conceptual design is unknown. In these, heat exploitation is provided via stage by stage hydraulic fracturing along the main target zone (Figure 10). The main purpose of the Multi-stage hydraulic fracturing is to increase the heat exchange area as in the Classical UGS.

In such studies, the Multi-stage hydraulic fracturing operation is carried out sequentially and systematically along different stages (levels) in the well (Figure 10). In addition, stage size, geometry and distance between stages require careful planning. Otherwise, unwanted consequences may develop (Li and Zhang, 2017). For example, if the distance between each fracture is chosen short, undesired fracture geometries may occur (Li and Zhang, 2017). This type of geometric fractures

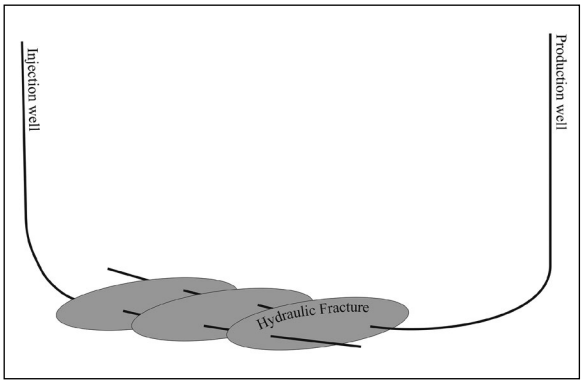

Figure 3- Schematic representation of the Multi-stage UGS design (Re-drawn from Shiozawa, 2015).

may cause interaction among themselves, which may also cause other problems (e.g. Li and Zhang, 2017). In planning phase, earth stress orientations along the main target zone, cooling-induced stresses, stress anisotropies, pore water pressure distribution, stress magnitudes, discontinuity geometries, fracture propped width or equivalent net pressure, planned fracture height, formation (rock) stiffness etc. need to be taken into account (https://dnicolasespinoza.github.io/; Li and Zhang, 2017).

There are some important differences between Multi-stage UGS designs and Classical UGS designs. These differences are mostly due to hydraulic fracture dimensions, geometry and size (Table 2).

Water-based conventional fluids will most likely be used as working fluid in future projects. It is officially reported that the hydraulic fracturing phase of the FORGE project has been successfully completed (https://openei.org/wiki/EGS_Collab_Project_Overview).

Problems encountered with conventional UGS are also quite possible in Multi-stage UGS designs (Table 1). However, the Multi-stage UGS designs have more practical hydraulic fracturing technique, solid know-how and huge experience gained from unconventional oil projects. Therefore, this is expected to be implemented in many other near-future UGS projects.

4.1.3. The Hot Ductile Formations

Another important Open-loop UGS design is known as the "Hot Ductile Formations UGS" (Figure 4). It was first introduced by a private company called "GeoSierra" (http://www.geosierra.com/geothermal.html).

In this, some vertical fracture sets with different azimuths are formed within the hot and ductile geological formation (Figure 4). The fracture sets (i.e. cells) cover an area of approximately 0,324 km^2 (80 acre). A production well in the center of each cell is surrounded by three injection wells (http://www.geosierra.com/geothermal.html) (Figure 4). According to current technology-based research studies, such a design is unlikely to be commercial on its own (http://www.geosierra.com/geothermal.html). For this reason, it is thought that projects based on this will be more commercial if more than one benefit is obtained (http://www.geosierra.com/geothermal.html). In this context, it is planned to achieve four main outputs in such a project: (1) the power production, (2) extraction of secondary elements such as Li, Si, Mn, B etc. from the mineral waters, (3) purification of mineral waters and earning extra income, and (4) CO_2 storage.

In the initial stage, CO_2 is planned as working fluid. However, conventional water-based fluids may also be used as needed (http://www.geosierra.com/geothermal.html).

It is considered that the implementation of such a project may have so many advantages as stated in

Table 2- Main differences between Multi-stage and Classical UGS designs.

	Multi-stage UGS design	**Classical UGS design**
1	The fractures are usually normal to the well axis and are penny-shaped	It varies from project to project.
2	Fracture orientations are relatively more regular.	Fracture systems are relatively irregular.
3	Fracture frequencies are quite systematic and more homogeneously distributed throughout the well.	Fractures are generally concentrated in certain zone(s).
4	It consists of dozens of stages.	Usually it does not exceed a few stages.
5	Fracture sizes are relatively smaller.	Fracture dimensions are relatively larger.

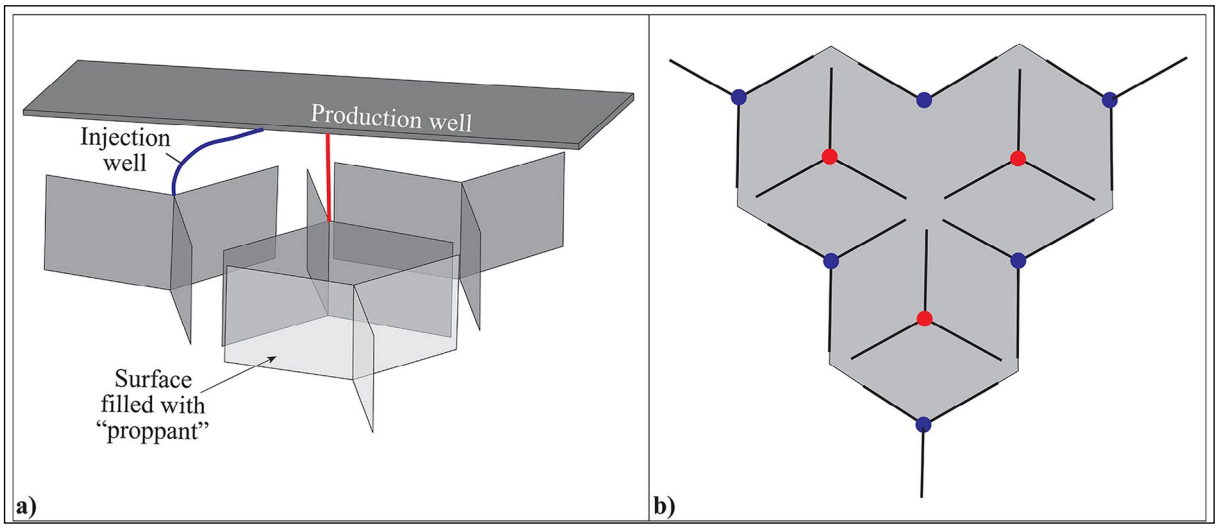

Figure 4- Schematic representation of the Hot Ductile Formations UGS design. a) 3D side view and b) top view (http://www.geosierra.com/geothermal.html).

table 1. On the other hand, main significant disadvantage of this design is the lack of any practical experience and know-how.

It has been announced that a pilot project is planned in the "Salton Sea" geothermal field in the state of California, USA in the near future (http://www.geosierra.com/geothermal.html). The significant side effects of this design are not known yet.

4.1.4. The Eavor-Loop UGS Design

Another Open-loop UGS design is the "Eavor-Loop UGS". It was first proposed and implemented as a pilot project in the Rocky Mountains near Alberta, Canada under the leadership of Eavor Technologies LLC. The other partners are Precision Drilling, Shell New Energies, Shear Fluids, Certus Oil and Gas, Rangeland Engineering Canada, the University of Alberta, Codeco-Vanoco Engineering, the University of Toronto, Rangeland Engineering Canada, Enlighten Geoscience Ltd., Petrel Robertson Consulting, Chinook Petroleum, and GL (Figure 5) (https://eavor.com/press/).

Considering the information disclosed publicly, there is no hydraulic fracturing operation along the main target zone (https://eavor.com/press/). In this, two opposing geothermal wells on the surface are linked from toe to toe by horizontal drilling technology inside the main target zone (https://eavor.com/press/). Later, additional pad(es) are drilled approximately parallel to main axis of the well (https://eavor.com/press/). Hence, it is aimed to form a commercially efficient surface area for geothermal exploitation (https://eavor.com/press/). According to the presented information, the Eavor-Loop design has been introduced as a Closed-loop design. However, in this, both mass and heat transfer are expected between the working fluid and the wellbore wall (https://eavor.com/press/). Although this may be regarded as a physically Closed-loop system, it seems more convenient to regard it as an "Open-loop UGS design" based on thermodynamic system types.

This project consists of three main phases: (1) the surface studies and drilling, (2) practical efficiency test of the physically Closed-loop system and (3) the thermodynamic production tests (https://eavor.com/press/). In the first phase of this project, the two opposing wells were tied toe to toe in the main target zone (https://eavor.com/press/). In the second phase, the target wells were successfully sealed, and a physically Closed-loop system was achieved inside 15 m thick sandstones in 2019 (Figure 5a) (https://eavor.com/press/; Robert Winsloe, official e-mail communication, 2019). In addition, third phase was successfully achieved in 2020 as well (https://eavor.com/press/). The pilot project still continues as of September 2020 (https://eavor.com/press/). Moreover, Enex Power Germany GmbH and Eavor Technologies Inc. have agreed on a letter of intent to form a

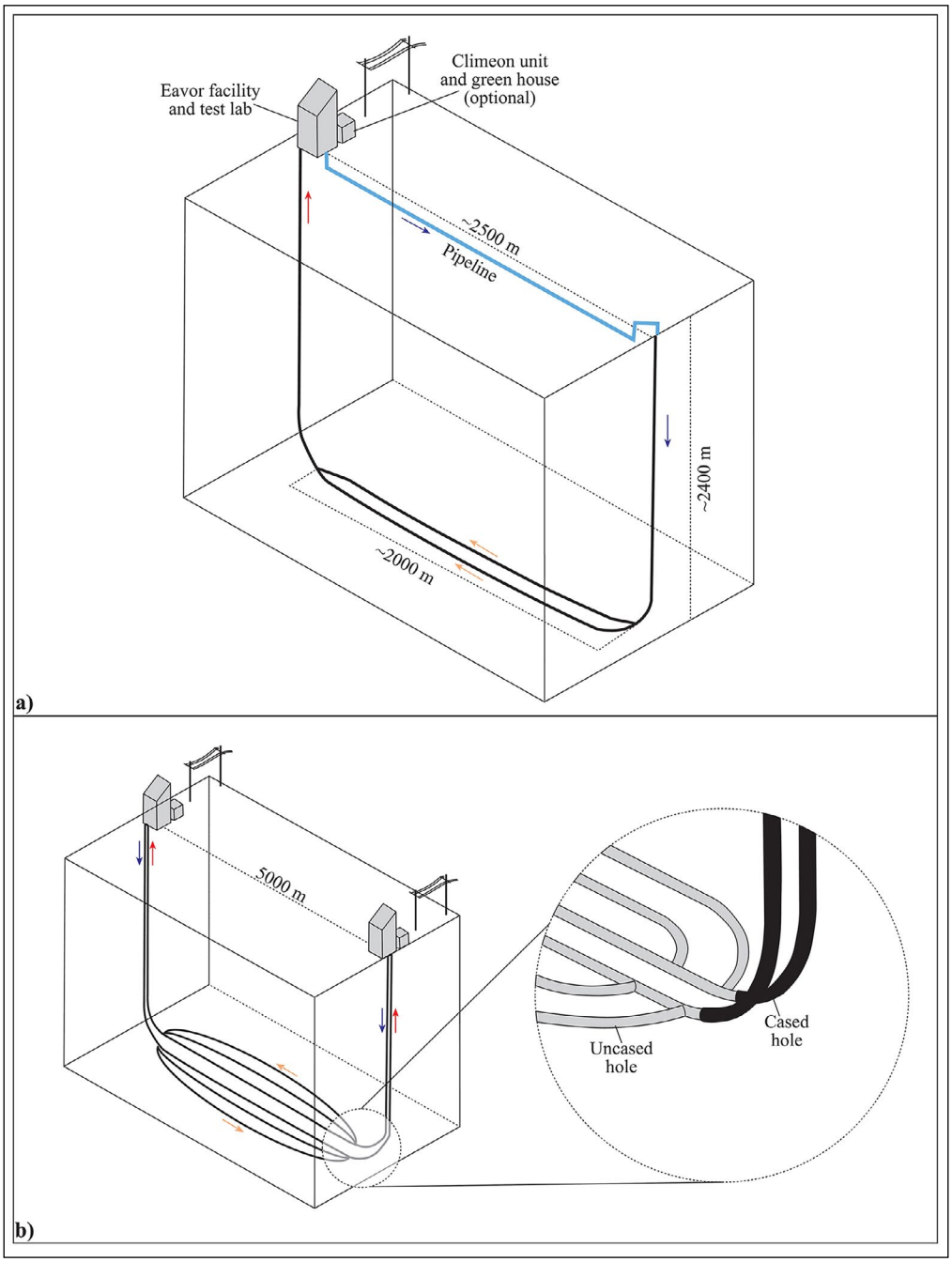

Figure 5- Schematic representation of the Eavor-loop UGS design. a) Eavor-Loop design implemented on a pilot scale, b) more comprehensive Eavor-Loop design (https://eavor.com/press/).

geothermal project development company to construct Eavor-Loop heat and power projects within Enex's existing geothermal license area in Bavaria, Germany (https://eavor.com/press-release/eavor-announces-commercial-eavor-Loop-project-be-built-geretsried-germany). Accordingly, a commercial power project is planned via "full-scale Eavor-Loop UGS design". Some of the extracted heat has the potential to be used in residential heating as secondary revenue (https://eavor.com/press-release/eavor-announces-commercial-eavor-Loop-project-be-built-geretsried-germany).

There are some questions about the conceptual design of the project. As a result of the inquiries made, two slightly different designs have been observed in

the official web page of the Eavor Technologies LLC. (Figure 5).

According to official information presented in written form by Eavor Technologies LLC officials, the water-based fluids with special additives is being used as the working fluid in order to increase the heat exchange and reduce the friction (Robert Winsloe, official E-mail communication, 2019).

This seems to eliminate many problems experienced in the "Classical UGS design" (Table 1). Furthermore, it is expected to have thermosiphon effect within the system as the density of heated working fluid decreases with respect to increase in the temperature along its path. The effect is expected to have positive consequences on the net power output of the system during operation. Nevertheless, it is inevitable that there will be some mass transfer between working fluid and the main target zone. Therefore, this may bring about some scaling and associated problems in the long term (Table 1).

4.2. The Closed-loop UGS Designs

There are various types of Closed-loop UGS designs in the literature. These studies were mostly inspired by geothermal heat pump designs. They generally emerged as a result of the perception that the problems experienced in Open-loop Classical UGS designs may not be solved in the near future. Consequently, the demand for them has increased recently.

Closed-loop UGS designs have some significant advantages over Open-loop UGS designs such as flexibility in working fluid options, reduced seismicity, scaling, vertical displacement, flow-channeling (i.e. short-circuit fluid circulation) etc. (Table 1). These designs are not widely practically implemented in power projects, especially due to expected inefficient heat exchange area. However, it has become important recently. Because, many novel alternative working fluids have emerged lately. In this study, only two crucial types are briefly discussed below: (1) Simple U and L-shaped UGS designs and (2) Finned L-shaped UGS designs (Table 1, figures 6 and 7).

4.2.1. The Simple U and L-shaped UGS Designs

The Simple U and L-shaped UGS designs are the most well-known varieties of the Closed-loop UGS designs (Figure 6). It is unknown when and by whom it was first suggested. Some used these in their theoretical studies (e.g. Riahi et al., (2017).

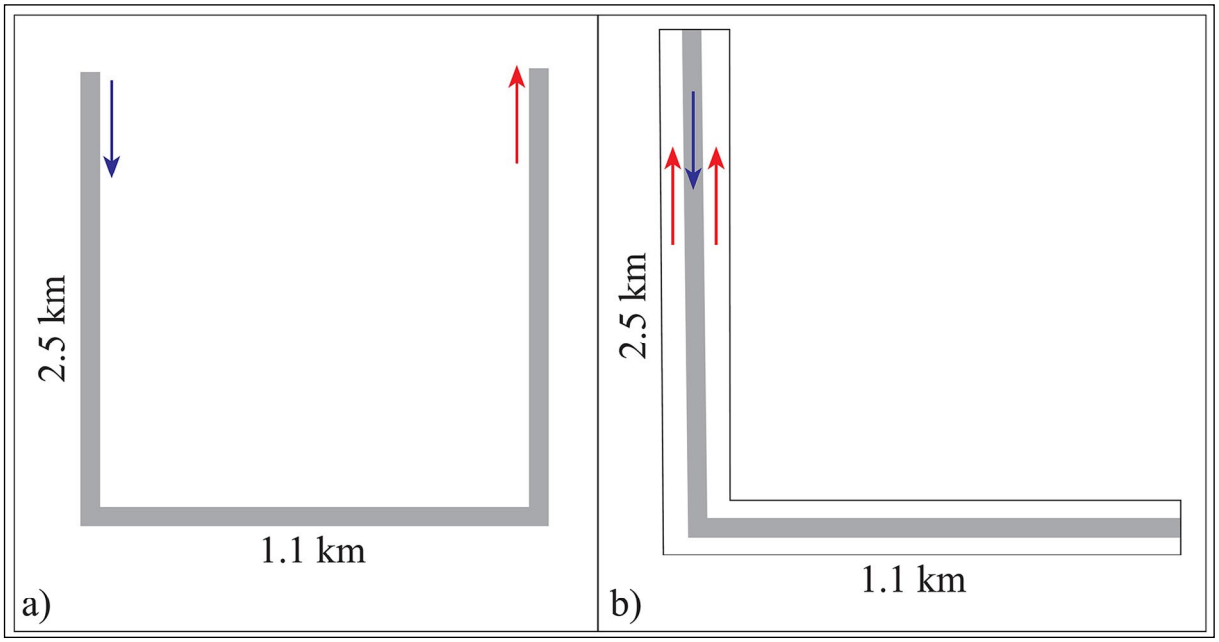

Figure 6- Schematic representation of the Simple "U" and "L"-shaped UGS designs, a) Simple "U"-shaped design and b) Simple "L"-shaped design (Re-drawn from Rihai et al., 2017).

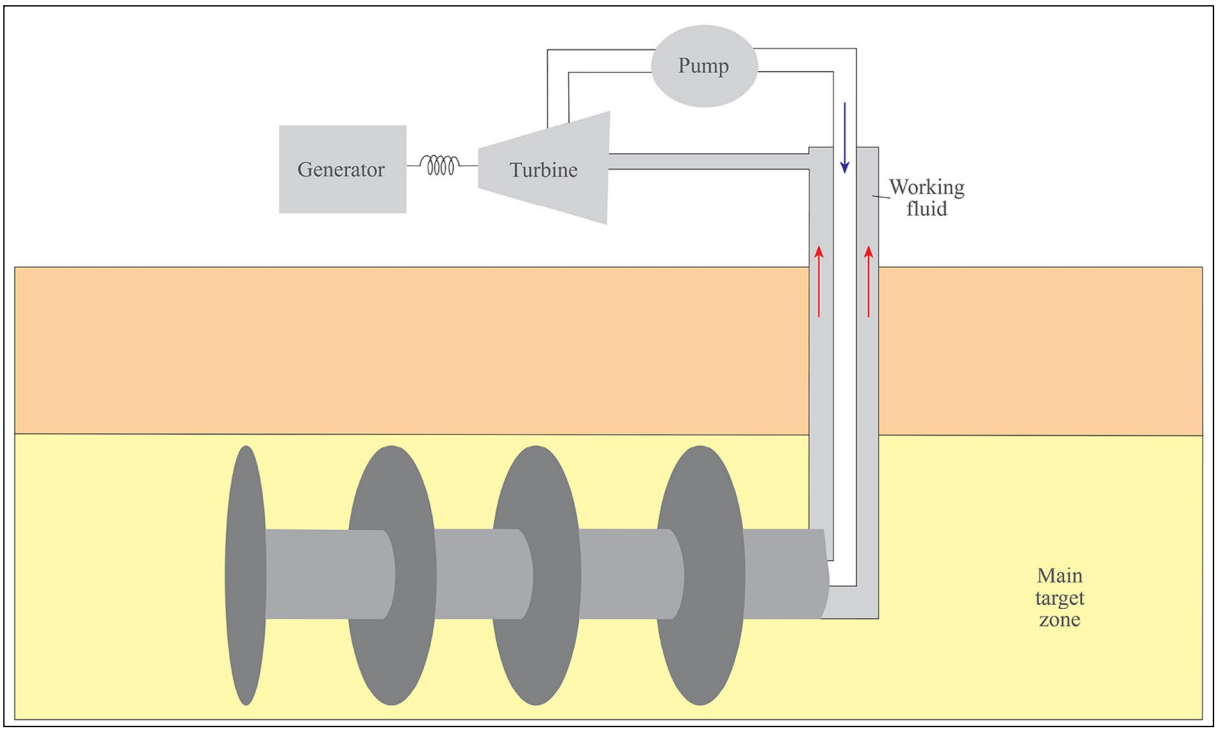

Figure 7- Schematic representation of the Finned "L"-shaped UGS design (Re-drawn from Taleghani, 2013).

Although these are simple designs, they are generally not preferred as the heat exchange surface area needed to generate power is insufficient. There are two well-known variations of them known as "U" and "L" shaped types (Figure 6). In "U" shaped designs, usually two opposing boreholes are tied toe to toe at depth via horizontal drilling technology (Figure 6a). On the other hand, a single "L"-shaped well with inner tubing is formed in the "L" shaped types (Figure 6b). The wells are first drilled vertically until the target depth, then diverted nearly or completely to horizontal along the main target zone. The drilling operations are then stopped. Later, the wellbore is cased with cemented casing. After all, the heat is exploited by using a suitable working fluid. In the U-shaped designs, the working fluid is usually directly circulated inside the casing, whereas, in the L-shaped designs, the working fluid is circulated through a secondary pipe (i.e. tubing) set inside the casing. The working fluid is retaken through the annulus in between (Figure 6b). In addition, some parts of the casing and the tubing are insulated to prevent heat loss. In some Simple U and L-shaped sub-types, it is recommended to drill a series of additional ultra-slim holes parallel to the main axis of the well, similar to the Eavor-Loop design mentioned above. Later on, the walls of these extra legs are sealed with a cemented casing. Thus, the effective heat transfer area needed for power production is achieved.

These designs require extremely high temperatures and commercially accessible geological units for commercial power generation. Many other parameters are considered in well planning and system design of "U" and "L" shaped UGS such as distance between well locations, temperature profile, target depth etc.

These have many advantages and disadvantages like any others (Table 1). The main disadvantage of them is the significant increase in project costs due to the large number of drilling expanses. Therefore, they are not widely preferred in contemporary UGS practices. However, modeling studies and new developments in working fluid technology have led to the increase in popularity of such designs in recent years (Riahi et al., 2017). Unfortunately, they have some disadvantages such as the flexibility in working fluid options, possible reduced contamination risk of the freshwater reservoirs and existing technological infrastructure as well as others (Table 1).

Although there is no well-known practical power generation project on this, some heating-targeted applications are common particularly in Germany.

4.2.2. The Finned L-Shaped Design

Another important type of the Closed-loop UGS design is the "Finned L-Shaped" design. This significantly differs from the simple "U" and "L"-shaped counterparts in a way that some fins are formed normal to the well axis along the main heat recovery zone (Figure 7). Although this is quite common in ground source heat pump applications, it was first proposed by Taleghani (2013) for power generation. The major disadvantage of such designs is the technological barriers to underground fin applications. However, it is thought that the existing technological barriers will be overcome with the future R and D studies. Therefore, such designs may become important in the near future.

In this, as with simple "U" and "L" shaped designs, geological units should be suitable for commercial projects. The most promising aspect of this is the injection of materials with suitable thermal properties to accelerate the exploitation of heat energy. Thus, it is thought that the required effective heat exchange surface area can be obtained.

Such designs are highly flexible in terms of working fluid. No project open to the public is yet known regarding this type of novel designs for high temperature systems. On the other hand, despite the technological barriers, it is expected that the number of researches will increase in the following years thanks to many potential advantages it has. The most important two advantages of these systems are (1) possibility to have an effective heat transfer area with shorter and less conventional wells, and (2) access to numerous effective alternative working fluid options (Table 1). Such a design is thought to be promising because it reduces the costs and some technical challenges in comparison to simple "U" and "L"-shaped counterparts. On the other hand, the most important disadvantage is the current technological barriers in the construction of effective underground fins (Table 1).

4.3. The Hybrid UGS Designs

There are many conceptual UGS designs under this topic in the literature. These studies mostly aim to take some of the strengths of Open and Closed-loop designs and combine them under a single design. Only two main types are considered within the scope of this study. They are (1) The Multiple Microhole Array and (2) Earth Energy Extraction System (Table 1, figure 8 and 9).

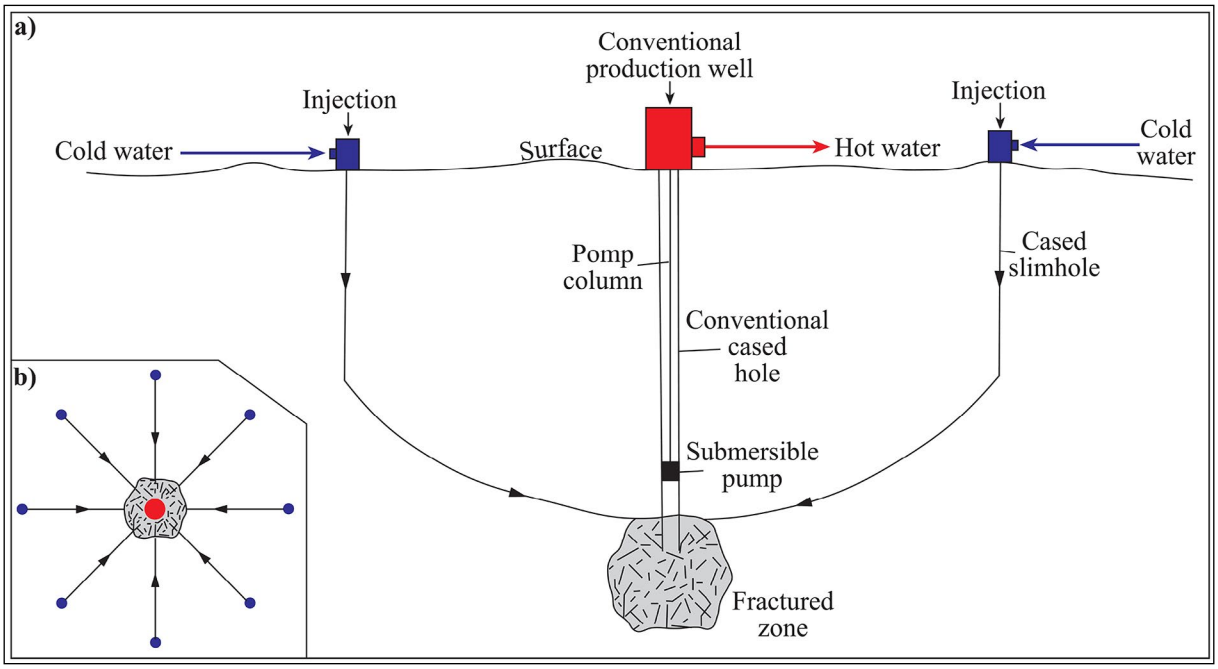

Figure 8- Schematic representation of the Earth Energy Extraction System UGS design (Re-drawn from Sanyal et al., 2005), a) side view and b) top view.

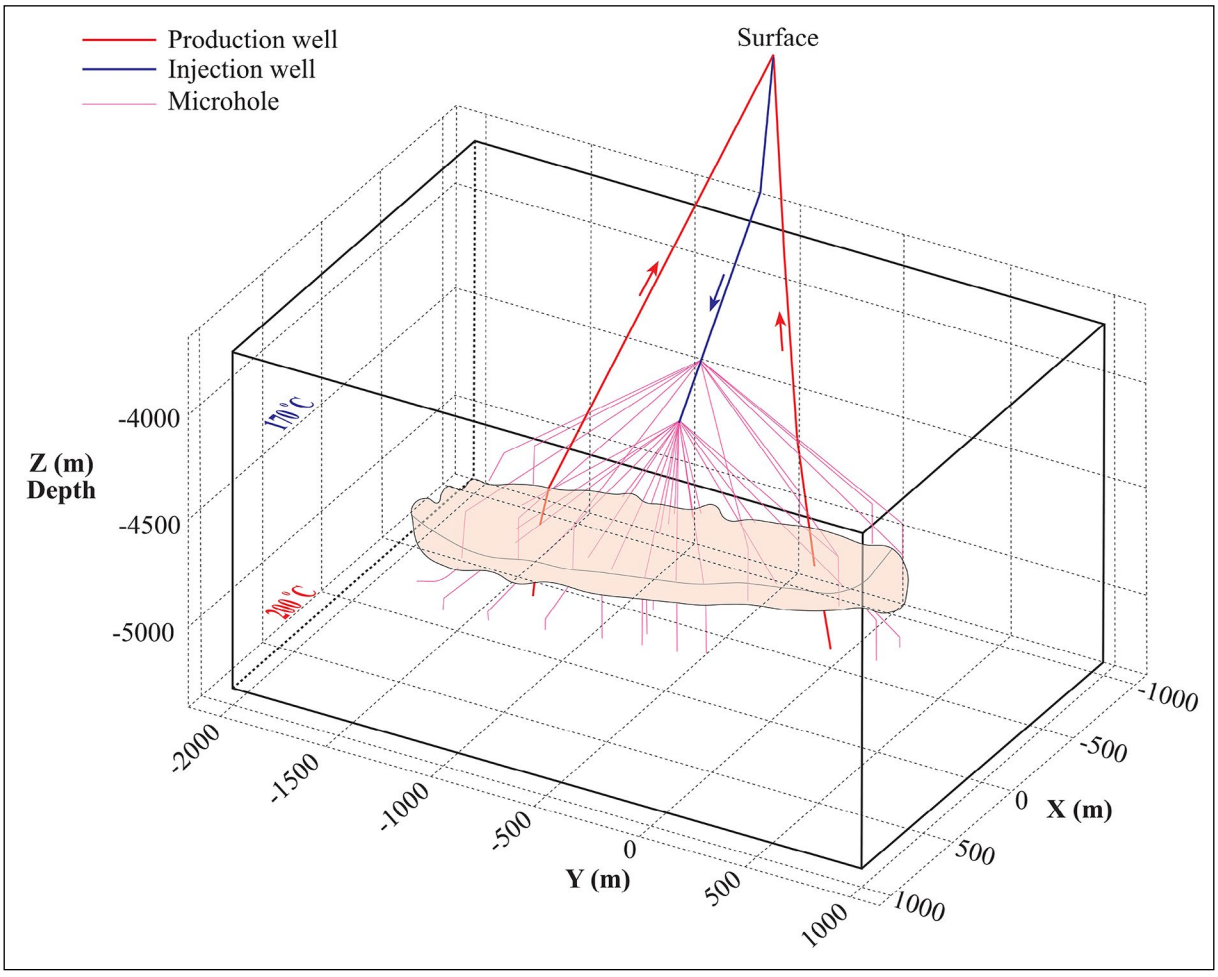

Figure 9- Schematic representation of the Multiple Micro-hole Array UGS design (adopted from Finsterle et al., 2013).

4.3.1. The Multiple Microhole Array

This is one of the most important type of the Hybrid UGS design (Figure 8). Although the first proposed design is unknown, it became popular with some patented studies after 1996 (e.g. U.S. Patent No: 5,515,679 and 6,247,313B1, Zhang et al., 2012; Finsterle et al., 2013).

The Multiple Microhole Array UGS design is possible inside any suitable geological medium. In this, large number of ultra-slim holes (mostly <10 cm) are drilled through the main target zone (Figure 8). The main purpose here is to increase the effective heat exchange area and to prevent some obstacles. These obstacles are localized reservoir associated with flow-channeling (i.e. short-circuit) in working fluids and reduced energy extraction as in many Open-loop UGS designs (Table 1).

In this type, water-based conventional fluid is proposed as the working fluid (Finsterle et al., 2013). However, some alternative fluids like CO_2 also seem possible. It has still not reached the technologically desired practical level yet. In addition, no commercial-scale practical study has been found on the Multiple Microhole Array UGS design so far. In addition, as of 2020, no practical project has been found based on this.

It aims to reduce or eliminate the problems experienced both Open and Closed-loop designs (Table 1). However, although reduced, all problems such as scaling and hydraulic fracturing are also expected (Table 1). In addition, the other significant disadvantage of this is the risk of shallow drinking reservoir contamination, especially in shallow applications (Table 1). These studies are still ongoing on this subject.

4.3.2. The Earth Energy Extraction System (Triple-E)

Another important Hybrid UGS design is the "Earth Energy Extraction System" proposed by Sanyal et al. (2005) (Figure 9). However, this UGS was inspired by another patented study (i.e. U.S. Patent no: 6,247,313B1, 19 June 2001). The Earth Energy Extraction System is similar to the Multiple Microhole Array design in many ways (Table 1). In this, suitable fluid-poor, hot and brittle rocks are utilized with relatively localized fracturing operations (Figure 9). In top view, a conventional production well is surrounded by many ultra-slim injection wells (<10 cm diameter) (Figure 9b). The main purpose of this is generally quite similar to other hybrid systems (Table 1).

In the Earth Energy Extraction System, it is anticipated that water-based fluids will be used as the working fluid. However, some other alternative working fluids seem also possible. The main advantages of it are reduced induced seismicity risk, reduced losses in working fluid, reduced vertical displacement risk, reduced risk of flow-channeling (i.e. short-circuit) in working fluid, increased effective heat exchange area etc. (Table 1). This system has not reached the technologically desired level so far. In addition, as of 2020, no commercial practical study has been found on the Earth Energy Extraction System UGS design.

It aims to reduce or eliminate the problems experienced both Open and Closed-loop UGS designs (Table 1). However, although reduced, all problems related to scaling and fracturing are expected to some extent as well (Table 1). In addition, the other significant disadvantage of this is the risk of shallow drinking reservoir contamination, especially in shallow applications (Table 1). Nowadays, studies are still ongoing to overcome these problems.

5. Conclusions and Suggestions

So far, numerous terms are collected under the "Unconventional Geothermal Systems-UGS". These terms can cause conceptual confusion. Hence, the original meaning of this concept should be expressed

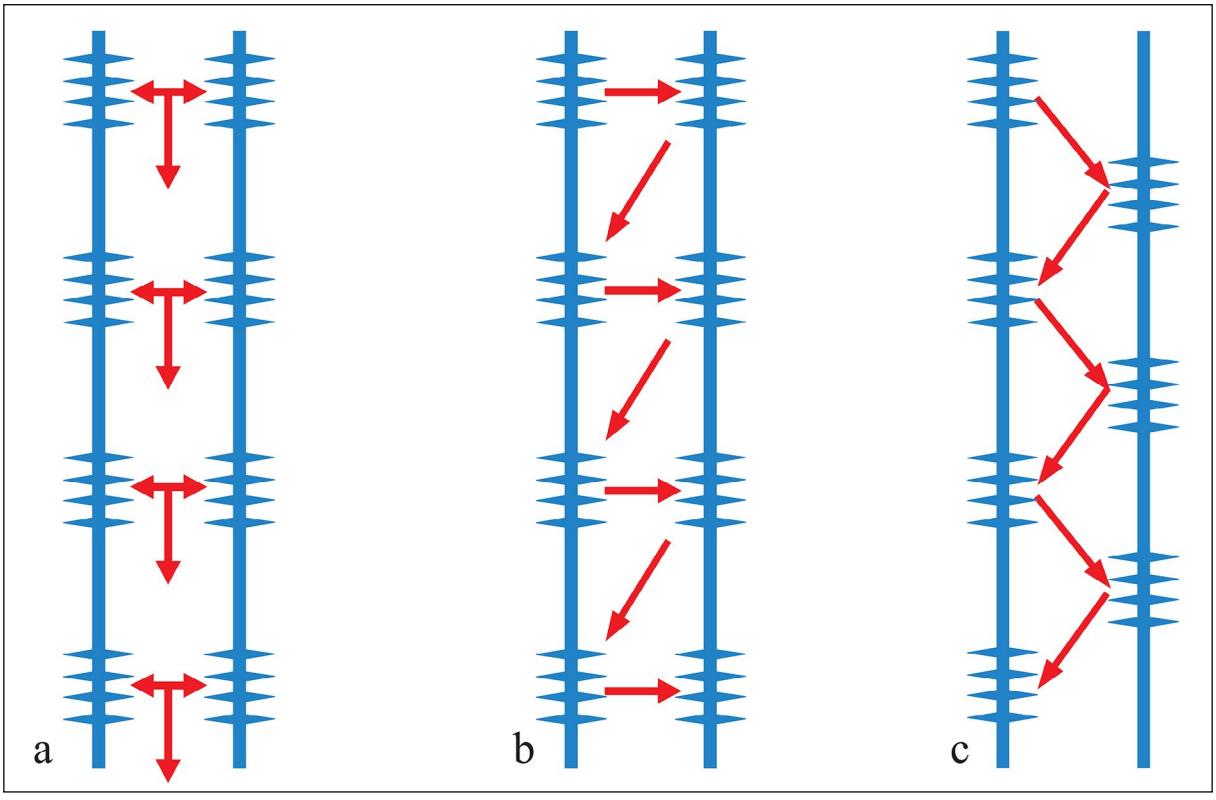

Figure 10- Main types of Multi-stage hydraulic fracturing; a) simultaneous hydraulic fracturing, b) sequential hydraulic fracturing (zipper-frac) and c) modified zipper-frac (Re-drawn from Nagel et al., 2013).

in full. In addition, these uncertainties may cause some problems in determining the limits of the legal regulations regarding some state-supported funds. In this context; some restrictive criteria are needed to determine whether a study is UGS or not. So, the most important criteria are briefly summarized as: (1) lack of commercial conventional geothermal fluid production even despite all conventional well completion techniques are applied such as simple chemical treatment, water-loss, compressor test, pumping tests etc., (2) application of sophisticated unconventional well enhancement techniques such as advanced hydraulic fracturing, acidizing, nitrogen treatment etc., (3) in case, conventional geothermal fluid(s) (i.e. typical conventional geothermal production fluid) is/are used as working fluid through the main target zone, the fluid(s) should be supplied out of conventional power producing geothermal reservoir(s), (4) use of unconventional fluids as the main working fluid such as CO_2, NH_3 etc., (5) the proppant and associated additive injection into the target zone in order to keep the fractures open, (6) extensive use of unusually high grade well equipment such as high pressure casing, wellhead elements etc. required for extreme operations, (7) use of unusual conceptual designs to exploit earth heat. If a geothermal study includes any of these criteria, it can easily be regarded as a UGS.

Based on thermodynamic system types, it is possible to group conceptual UGS designs under three topics: (1) Open-loop UGS designs, (2) Closed-loop UGS designs and (3) Hybrid UGS designs. These consist of many sub-types. Each design discussed here has its own advantages and disadvantages.

For Turkey, the following suggestions can be made with respect to UGS

1- The national geothermal energy potential should be comprehensively calculated, and an inventory should be prepared for some crucial depths such as 1, 3, 5 km in the light of the available data on UGS,

2- A comprehensive national action plan needs to be prepared with broad participation of stakeholders regarding UGS,

3- Young bright researchers need to be trained and supported for future UGS projects,

4- As in developed countries, government support and incentive should be provided to companies and/or institutions that implement or plan to implement UGS projects,

5- Awareness/knowledge of the society, investors and public need to be increased by organizing domestic workshops, conferences etc. on UGS,

6- The exploration/research stage of these projects generally requires much longer time periods compared to the conventional geothermal systems. Therefore, the specified exploration-operating license periods in the geothermal law need to be extended,

7- A team of the expert researchers needs to be established with high practical and theoretical experience in the areas of expertise that are vital for UGS projects such as structural geology, hydrogeology, water chemistry, inclined or horizontal drilling technologies, microseismic monitoring, hydraulic fracturing, reservoir geomechanics, fluid mechanics and heat transfer etc.,

8- The hydraulic fracturing technique, fluid mechanics and heat transfer studies have been extensively utilized in the conventional geothermal reservoirs, the UGS reservoirs, the petroleum reservoirs and the coal bed methane extraction studies etc. In addition, they are also crucial for not only Earth Sciences but also other areas of expertise such as Civil Engineering, Mechanical Engineering, Space and Aviation studies etc. Based on this, some high-tech national research laboratories need to be established similar to Los Alamos National Laboratory in The United States,

9- After the necessary infrastructure is prepared, it is appropriate to carry out a joint research project consisting of relevant public institutions/organizations, universities and private sector stakeholders in a pilot field.

Acknowledgements

I thank Dr. Arif Mert Eker, Dr. Oktay Çelmen, Dr. Hafize Akıllı, Hakan Özkan, Mehmet Vekli, Fatih M. Özişli, M. Hüseyin Yıldırım and the referees of this paper for their useful contribution into the development of this study with their valuable criticisms.

References

ABD Patent ve Marka Ofisi, Patent No: 5,515,679, May 14, 1996.

ABD Patent ve Marka Ofisi, Patent No: 6,247,313B1, June 19, 2001.

Armstead, H. C. H., Tester, J. W. 1987. Heat Mining. E. and F. N. Spon, London and New York, 478 p.

Breede, K., Dzebisashvili, K., Liu, X., Falcone, G. 2013. A systematic review of enhanced (or engineered) geothermal systems: past, present and future. Geothermal Energy, 1, 4.

Breede, K., Dzebisashvili, K., Falcone, G. 2015. Overcoming challenges in the classification of deep geothermal potential. Geothermal Energy Sciences, 3, 19-39.

Brown, D.W., Duchane, D.V., Heiken, G. Hriscu, V.T. 2012. Mining the Earth's Heat: Hot Dry Rock Geothermal Energy. Springer-Verlag, 657 p.

Çiçek, A. 2019. Enerji hedefli geleneksel olmayan jeotermal sistemlerin (UGS) uygulandığı sahalarda yaşanan önemli teknik sorunlar. MTA Doğal Kaynaklar ve Ekonomi Bülteni, 28, 73-77.

Canoğlu, M.C., Kurtuluş, B. 2016. Body type optimization of water structures and engineering parameters determination of natural structural materials: an example from Kışlademirli Dam (Kütahya). Karaelmas Science and Engineering Journal, 6, 2, 250-264.

Canoğlu, M. C., Kurtulus, B. 2017. Permeability of Savcıbey dam (Bilecik) axis location and design of grout curtain. Bulletin of the Mineral Research and Exploration, 154, 157-168.

Canoğlu, M. C. 2019. Selection of Suitable Dam Axis Location Considering Permeability and Grout Curtain Optimization Environmental and Engineering Geoscience, 25, 1, 15-25.

Eavor Technologies Inc. https://eavor.com/press/.September 12, 2020.

Espinoza, G. https://dnicolasespinoza.github.io/, September 12, 2020.

Finsterle, S., Zhang, Y., Pan, L., Dobson, P. Oglesby, K. 2013. Microhole arrays for improved heat mining from enhanced geothermal systems. Geothermics, 47, 104-115.

Genter, A., Guillou-Frottier, L., Feybesse, J.-L., Nicol, N., Dezayes, C., Schwartz, S. 2003. Typology of potential hot fractured rock resources in Europe, Geothermics, 32, 701-710.

Genter, A., Evans, K., Cuenot, N., Fritsch, D., Sanjuan, B. 2010. Contribution of Exploration of Deep Crystalline Fractured Reservoir of Soultz to the Knowledge of Enhanced Geothermal Systems (EGS). Comptes Rendus Geoscience, 342, 502-516.

GeoSierra LLC. http://www.geosierra.com/geothermal.html. September 12, 2020.

Geothermal Explorers Ltd., 2003. Schematic representation of the Classical UGS design

Grassiani, M., Krieger, Z., Legmann, H. 1999. Advanced power plants for use with HDR/enhanced geothermal technology. Bulletin D'Hydrogéologie, 17, 165-172.

He, Z., Zhang, Y., Feng, J., Ding, Q., Li, P. 2018. An EGS Site Evaluation Method for Geothermal Resources Based on Geology, Engineering and Economic Considerations. PROCEEDINGS, 43rd Workshop on Geothermal Reservoir Engineering, Stanford University, Stanford, California, February 12-14, 2018, SGP-TR-213.

Hıdıroğlu, İ. A., Parlaktuna, M. 2019. Dünyada Kızgın Kuru Kaya (HDR) Projeleri ve Türkiye'nin Muhtemel HDR Alanları. Jeotermal Elektrik Santral Yatırımcıları Derneği, 6-7 Şubat GT2019 Türkiye Jeotermal Kongresi Bildiriler Kitabı, Ankara, 91-103.

https://eavor.com/press-release/eavor-announcescommercial-eavor-loop-project-be-builtgeretsried-germany. September 12, 2020.

Kuriyagawa, M. 1987. Hot dry rock geothermal energy in Japan. Geothermics, 6, 4, 401-403.

Li, S., Zhang, D. 2017. A fully coupled model for hydraulic fracture growth during multi-well fracturing treatments: enhancing fracture complexity. SPE-182674-MS.

Nagel, N., Zhang, F., Sanchez-Nagel, M., Lee, B. 2013. Quantitative Evaluation of Completion Techniques on Influencing Shale Fracture 'Complexity'. In ISRM International Conference for Effective and Sustainable Hydraulic Fracturing. International Society for Rock Mechanics. May 22-23, 2013. Brisbane, Australia.

OpenEI, https://openei.org/wiki/Fenton_Hill_HDR_Geothermal_Area, September 12, 2020.

OpenEI, https://openei.org/wiki/EGS_Collab_Project_Overview, September 12, 2020

Riahi, A., Moncarz, P., Kolbe, W., Damjanac, B. 2017. Innovative Closed-Loop Geothermal Well

Designs Using Water and Super Critical Carbon Dioxide as Working Fluids. Geothermal Resources Council Bulletin, 7-10, 42nd Workshop on Geothermal Reservoir Engineering, Stanford University, Stanford, California, February 13-15, 2017, SGP-TR-212.

Roberts, V., Kruger, P. 1982. Utility Industry Estimates of Geothermal Electricity-Geothermal power production to continue rapid growth through the year 2000. Geothermal Resources Council Bulletin, 7-10.

Sanyal, S.K., Granados, E.E., Butler, S.J., Horne, R.N. 2005. An alternative and modular approach to enhanced geothermal systems. Transactions Geothermal Resources Council, 29, 139-144.

Serpen, Ü. 2019. Sıcak Kuru Kayalar'ın (EGS) Potansiyeli, Geçmişi, Geleceği ve Gerçekler, 14. Ulusal Tesisat Mühendisliği Kongresi Bildiriler Kitabı, 17-20 Nisan 2019, İzmir, 238-249.

Shiozawa, S. 2015. Designing Enhanced Geothermal and Hydraulic Fracturing Systems Based on Multiple Stages and Proppant. MSc Thesis, University of Texas at Austin, 86 p. (unpublished).

Taleghani, A. D. 2013. An Improved Closed-Loop Heat Extraction Method From Geothermal Resources. Journal of Energy Resources Technology, 135/042904-1.

Takahashi, H., Hashida, T. 1993. New Project for Hot Wet Rock Geothermal Reservoir Design Concept. Proceedings, 18th Workshop on Geothermal Reservoir Engineering Stanford University, Stanford, California, USA, 26-28 Ocak 1993, SGP-TR-145, 6 s.

Tester, J. W., Anderson, B. J., Batchelor, A. S., Blackwell, D. D., DiPippo, R., Drake, E. M., Garnish, J., Livesay, B., Moore, M. C., Nichols, K., Petty, S., Toksöz, M. N., Veatch Jr., R.W. 2006. The future of geothermal energy-impact of enhanced geothermal systems on the United States in the 21st Century. MIT (Massachusetts Institute of Technology) Cambridge MA., 372 s.

Winsloe, R. 2019. official e-mail communication.

Zhang, Y., Pan, L., Dobson, P., Oglesby, K., Finsterle, S. 2012. Microhole for Improved Heat Extraction From EGS Reservoirs: Numerical Evaluation. Proceedings, 37th Workshop on Geothermal Reservoir Engineering, Stanford University, Stanford, California, January 30- February 1, 2012, SGP-TR-194.

ACKNOWLEDGEMENT

We would like to thank to the honored reviewers whose names are written below by contributing to the Bulletin of the Mineral Research and Exploration during the article review process between 6th of December 2019 and 29th of November 2020 in the name of the Executive Publication Editorial.

Emel ABDİOĞLU YAZAR (Trabzon-Turkey)
Naveed AHSAN (Pakistan)
Mustafa AKYILDIZ (Adana-Turkey)
Nihat Hakan AKYOL (Kocaeli-Turkey)
Ercan AKSOY (Bitlis-Turkey)
Adile Melis SOMAY ALTAŞ (İzmir-Turkey)
Raşit ALTINDAĞ (Isparta-Turkey)
Şafak ALTUNKAYNAK (İstanbul-Turkey)
Mehmet ALTUNSOY (Antalya-Turkey)
Fetullah ARIK (Konya-Turkey)
Keisuke ARIYOSHI (Japan)
F. Emre ARTUN (İstanbul-Turkey)
Kürşat ASAN (Konya-Turkey)
Ümit AYDIN (Ankara-Turkey)
Can AYDAY (Eskişehir-Turkey)
Namık AYSAL (İstanbul-Turkey)
Turhan AYYILDIZ (Ankara-Turkey)
Gulam BABAYEV (Azerbaijan)
Çağlayan BALKAYA (Isparta-Turkey)
Kürşat BEKAR (Trabzon-Turkey)
Tolga BEKLER (İstanbul-Turkey)
Özcan BEKTAŞ (Sivas-Turkey)
Viviana BOLANOS BENITEZ (Ireland)
Marcelle K. BOUDAGHER-FADEL (Germany)
Ali BÜLBÜL (Denizli-Turkey)
Osman CANDAN (İzmir-Turkey)
Elizabeth CATLOS (USA)
Tolga ÇAN (Adana-Turkey)
Ömer Faruk ÇELİK (Kocaeli-Turkey)
Murat ÇINAR (İstanbul-Turkey)
Begüm ÇIVGIN (Ankara-Turkey)
Emin ÇİFTÇİ (İstanbul-Turkey)
Güldemin DARBAŞ (Kahramanmaraş-Turkey)
Cengiz DEMİR (Trabzon-Turkey)
Yılmaz DEMİR (Rize-Turkey)
İsmail DEMİRCİ (Ankara-Turkey)
Gökhan DEMİRELA (Aksaray-Turkey)
Orhan DENGİZ (Samsun-Turkey)
Mehmet Kürşat DİLMAÇ (Erzurum-Turkey)
Feyza DİNÇER (Nevşehir-Turkey)
Abdurrahman DOKUZ (Gümüşhane-Turkey)
Derman DONDURUR (İzmir-Turkey)
Muhammed DUMAN (İzmir-Turkey)
Hüseyin EKİNCİ (Çanakkale-Turkey)
Yaşar EREN (Konya-Turkey)
Mustafa ERGİN (Ankara-Turkey)
Orkun ERSOY (Ankara-Turkey)
Korhan ESAT (Ankara-Turkey)
Aynur BÜYÜKUTKU GEÇER (Ankara-Turkey)
Yurdal GENÇ (Ankara-Turkey)
Ahmet GÖKÇE (Sivas-Turkey)
Candan GÖKÇEOĞLU (Ankara-Turkey)
Ali GÖKGÖZ (Denizli-Turkey)
Tolga GÖNENÇ (İzmir-Turkey)
Muhittin GÖRMÜŞ (Ankara-Turkey)
Chris GREEN (England)
Murat GÜL (Muğla-Turkey)
Levent GÜLEN (Sakarya-Turkey)
Kurtuluş GÜNAY (Malatya-Turkey)
Ali GÜREL (Niğde-Turkey)
Ömer Feyzi GÜRER (Kocaeli-Turkey)
Zülfü GÜROCAK (Elazığ-Turkey)
Raif HALAMA (England)
Nurullah HANİLÇİ (İstanbul-Turkey)
Hakan HOŞGÖRMEZ (İstanbul-Turkey)
Hülya İNANER (İzmir-Turkey)
Selma KADIOĞLU (Ankara-Turkey)
Leyla KALENDER (Elazığ-Turkey)
Reyhan KARA GÜLBAY (Trabzon-Turkey)
Ahmet KARAKAŞ (Kocaeli-Turkey)
Zehra KARAKAŞ (Ankara-Turkey)
Hüseyin KARAKUŞ (Kütahya-Turkey)
Ali İhsan KARAYİĞİT (Ankara-Turkey)
Hakan KARSLI (Trabzon-Turkey)
Kaan Şevki KAVAK (Sivas-Turkey)
Ayberk KAYA (Rize-Turkey)
Cem KINCAL (İzmir-Turkey)
Hayati KOÇ (Mersin-Turkey)
Dimitris S. KOSTOPOULOS (Greece)
Eren KÖMÜRLÜ (Giresun-Turkey)
Halil KUMSAR (Denizli-Turkey)
Bedri KURTULUŞ (Mersin-Turkey)
Şuayip KÜPELİ (Konya-Turkey)
Akın KÜRÇER (Ankara-Turkey)
Henryk MARSZAŁEK (Poland)
Halim MUTLU (Ankara-Turkey)
Atike NAZİK (Adana-Turkey)
Faruk OCAKOĞLU (Eskişehir-Turkey)
Ayşe ORHAN (Nevşehir-Turkey)
Bülent ORUÇ (Kocaeli-Turkey)
Yashar Tavakkoli OSGOUEI (TRNC)
Kemal Mert ÖNAL (Sivas-Turkey)
Sefer ÖRÇEN (Van-Turkey)
Yüksel ÖRGÜN (İstanbul-Turkey)
Selim ÖZALP (Ankara-Turkey)
Sevda ÖZEL (Sivas-Turkey)
Çağlar ÖZER (Erzurum-Turkey)
Nazire ÖZGEN ERDEM (Sivas-Turkey)
Önder ÖZGENER (İzmir-Turkey)
Emre ÖZGÜR (Ankara-Turkey)
Erman ÖZSAYIN (Ankara-Turkey)
Serkan ÖZTÜRK (Gümüşhane-Turkey)
Oya PAMUKÇU (İzmir-Turkey)
James PUCKETTE (USA)
Enis Kemal SAGULAR (Isparta-Turkey)
Azad SAĞLAM SELÇUK (Van-Turkey)
David SANDERSON (USA)
Sönmez SAYILI (Ankara-Turkey)
Levent SELÇUK (Van-Turkey)
Fadime SERTÇELİK (Kocaeli-Turkey)
Gurdeep SINGH (India)
Şeref SÖNMEZ (İstanbul-Turkey)
Hasan SÖZBİLİR (İzmir-Turkey)
Emine SÜTÇÜ (Ankara-Turkey)
Narumi TAKAHASHI (Japan)
Onur TAN (İstanbul-Turkey)
Servet TİMUR (İstanbul-Turkey)
Savaş TOPAL (Denizli-Turkey)
Aykut TUNÇEL (İzmir-Turkey)
Ahmet TURAN (Yalova-Turkey)
Füsun TUT HAKLIDIR (İstanbul-Turkey)
Asuman TÜRKMENOĞLU (Ankara-Turkey)
Okan TÜYSÜZ (İstanbul-Turkey)
Koray ULAMIŞ (Ankara-Turkey)
M. Emin ULUGERGERLİ (Çanakkale-Turkey)
Uğur ULUSOY (Sivas-Turkey)
Murat UTKUCU (Sakarya-Turkey)
Konstantinos VOUDOURİS (Greece)
Hüseyin YALÇIN (Sivas-Turkey)
Namık YALÇIN (İstanbul-Turkey)
Doğan YAŞAR (İzmir-Turkey)
Ömer YETEMEN (İstanbul-Turkey)
İsak YILMAZ (İstanbul-Turkey)
İsmail Ömer YILMAZ (Ankara-Turkey)
Sabah YILMAZ ŞAHİN (İstanbul-Turkey)
Özcan YİĞİT (Çanakkale-Turkey)
Halil YUSUFOĞLU (Ankara-Turkey)
Yeşim YÜCEL ÖZTÜRK (İzmir-Turkey)

1. Aims of Publication

- To announce and share researches in all fields of geoscientific studies in Turkey with geoscientists worldwide.
- To announce scientific researches and practices on geoscientific surveys carried out by the General Directorate of Mineral Research and Exploration (MTA) to the public.
- To use the journal as an effective media for international publication exchange by keeping the journal in high quality, scope and format.
- To contribute to the development of Turkish language as a scientific language.

2. Scope

At least one of the following qualifications is required for publishing the papers in the Bulletin of Mineral Research and Exploration.

2.1. Research Articles

2.1.1. Original Scientific Researches

- These articles cover and contribute to the main subjects of the earth sciences, the original scientific researches and its results related to all aspects of disciplines in geoscience like exploration and evaluation of the underground sources and environmental problems, and
- The studies, which apply new aspects and methods for the solution of problems about the earth sciences and researches, which apply new aspects and methods for the solution of the problems, in the engineering sciences carried out in MTA.

2.1.2. Review Articles

These papers include comphrehensive scholarly review articles that summarize and critically assess previous geoscientific researches with a new perspective and reveal a new approach.

2.2. Discussion/Reply

- This type of article is intended for the discussion of papers that have already been published in the latest issue of the Bulletin. The discussion/reply type articles, which criticize all or a part of a recently published article, are published in the following first issue if it is submitted within six months after the publication of the Bulletin.
- The discussions are sent to the corresponding author of the original paper to get their reply before publication. The discussions abut the paper with two or more authors are sent only to the corresponding author.
- If the review article is not published within the prescribed preiod then it is published alone. Later sent replies are not published. Re-criticising of the replies is not allowed.
- The authors should obey the rules of scientific ethics and discussions in their discussion/reply papers. The papers in this category should not exceed four printed pages of the journal including figures and tables etc. The format of the papers should be compatible with the "Spelling Rules" of the Bulletin.

2.3. Short Notes

- The short notes part of the Bulletin covers short, brief and concisely written research reports for papers including the data obtained from ongoing and/or completed scientific researches and practices related to geoscience and new and/or preliminary factual findings from Turkey and worldwide.
- The short notes will follow a streamlined schedule and will normally be published in the following first or second issue shortly after submission of the paper to the Bulletin.
- This type of articles should not exceed four printed pages of the journal including figures, tables and an abstract.

3. Submission and Reviewing of Manuscripts

- Manuscript to be submitted for publishing in the Journal must be written clearly and concisely in Turkish and/or English and prepared in the Bulletin of Mineral Research and Exploration style guidelines. All submissions should be made online at the http://dergi.mta.gov.tr website.
- The manuscript submitted for reviews must not have been published partially or completely previously in another journal.
- The rejected manuscripts are not returned back to

author(s) whereas a letter of statement indicating the reason of rejection is sent to the corresponding author.

- Submitted manuscripts must follow the Bulletin style and format guidelines. Otherwise, the manuscript which does not follow the journals' style and format guidelines, is given back to corresponding author without any reviewing.
- Every manuscript which passes initial Editorial treatise is reviewed by at least two independent reviewers selected by the Editors. Reviewers' reports are carefully considered by the Editors and associated editors.
- The manuscript that need to be corrected with the advices of reviewer(s) is sent back to corresponding author(s) to assess and make the required corrections suggested by reviewer(s) and editors. The authors should prepare a letter of well-reasoned statement explaining which corrections are considered or not.
- If there are any suggestions given by editors and referees that are not accepted and corrected by the author, then it should be sent to the Editor's Office with corrected copies of the report explaining the reason for not accepting these suggestions and corrections.
- Figures and tabless should be 1/3 of the main text.
- To be published in the Bulletin of Mineral Research and Exploration, the printed lenght of the manuscript should not exceed 30 printed pages of the journal including an abstract, figures and tables. The publication of longer manuscripts will be evaluated by Editorial Board if it can be published or not.
- The authors must do the reviewer's corrections and proposals in 60 days and must upload to the system.
- At the printing stage after the last control, the first print of the manuscript are sent to the author/ authors in pdf version and asked from the author/ authors to make the press control.

4. Publication Language and Periods

- The Bulletin of Mineral Research and Exploration is published at least twice a year and each issue is published both in Turkish and English. Thus, the manuscripts are accepted in Turkish or English. The spelling and punctuation guidelines of Turkish Language Institution are preferred for the Turkish issue. However, the technical terms related to geology are used in accordance with the decision of the Editorial Board.

5. Spelling Draft

Manuscripts should be written in word format in A4 (29,7 x 21 cm) size and double-spaced with font size Times New Roman 10-point, margins of 25 mm at the sides, top and bottom of each page.

The formulas requiring the use of special characters and symbols must be submitted by the symbols part of the Microsoft Office Word Program on computer.

Initial letters of the words in sub-titles must be capital. The first degree titles in the manuscript must be numbered and left-aligned, 10 point bold Times New Roman must be used. The second degree titles must be numbered and left-aligned, they must be written with 10 point normal Times New Roman. The third degree titles must be numbered and left-aligned, they must be written with 10 point italic Times New Roman. The fourth degree titles must be left-aligned without having any number; 10 point italic Times New Roman must be used. The text must continue placing a colon after the title without paragraph returns (See: Sample article: http://bulletin.mta.gov.tr).

One line spacing must be left after paragraphs within text.

Paragraphs must begin with 0,5 mm indent.

The manuscript must include the below sections respectively;

o Title Page

o The Name and Surname of the author and * sign (Adress, e-mail adres must be given at the bottom of the page)

o Abstract

o Key Words

o Introduction

o Body

o Discussion

o Conclusion

o Acknowledgements

o References

5.1. Title Page

The title must be short, specific and informative and written with small letters font size Times New Roman 12-point bold. The title mustn't contain the subjects insufficiently processed in the article.

5.2. Author(S)'S Name, Addresses and Email Address

- The name and surname of the author/authors must be written without affiliations. Name must be written in small letters, the surname must be written in capital letters.
- At the affiliation (work adres) written after the name and the surname of the author/authors only the name of the company must be written, the author's job mustn't be written.
- Information about the adresses must be given at the next line as 10-point and italic.
- ORCID number should be taken from www.orcid.org and placed below the address.
- At the articles with two or more than two authors, the numbers must be written above the surnames of the authors, the informations about their adresses must be given at the next line by leaving one space line. Also, at this part the corresponding author must be indicated by the (*) symbol and the telephone, FAX and e-mail address of the corresponding author must be given.
- Abbreviations must not be made while writing the name of the uthor and the affiliation adres. Adresses must be given in Turkish in the Turkish version, in English in the English version.
- At the end of the article the name of the corresponding author and contact informations must be added.

5.3. Abstract

- The abstract must be understandable before having a look at the text.
- The abstract should state briefly the overall purpose of the research, the aim of the article, its contributions to the known theories, new data, principle results and major conclusions.
- Tha abstract must contain short and brief sentences.
- Addressing other sections and illustrations of the text or other writings must be avoided.
- The information, which have not been mentioned in the text, must not be in the abstract.
- The article must be written as one paragraph, preferably. Please provide an abstract which doesn't exceed 200 words.
- The abstract must be written with 10-point, normal Times New Roman in single-spaced lines.
- "Abstract" must not be given for the writings that will be located in "Short Notes" section.
- The English abstract must be under the title of "Abstract".

5.4. Key Words

Immediately after the abstract, please provide up to 5 key words and with each words seperated by comma. These key words will be used for indexing purposes.

5.5. Introduction

- The introduction section should state the objectives of the work, research methods, location of the study area and provide an adequate and brief background by avoiding a detailed literature survey.
- Non-standard or uncommon classifications or abbreviations should be avoided. But if essential, then they must be defined at their first mention and used consistently thereafter. Seperate paragraphs could be organized for each of the subjects at the introduction part. If it is necessary, the subtitle can be given for each of them (for example method, material, terminology etc.).
- When pre-information is needed for facilitating the understanding of the text, this section can also be used (for example, statistical data, bringing out the formulas, experiment or application methods, and others).

5.6. Body

- In this chapter, there must be data, findings and opinions that are intended to convey to the reader about the subject. The body section forms the main part of the article.
- The data used in other sections such as "Abstract", "Discussions", and "Results" are caused by this section.
- While processing the subject, the care must be taken not to go beyond the objective highlighted in the "Introduction" section. The knowledge, which

do not contribute to the realization of the purpose of the article or are useless for conclusion, must not be included.

- All data used and the opinions put forward in this section must prove the findings obtained from the studies or they must be based on a reference by citation.
- The guidance and methods to be followed in processing subjects vary according to the characteristics of the subjects mentioned. Various topic titles can be used in this section as many as necessary.

5.7. Discussions

- Discussion of the data and findings that are objectively transferred in the Main Text section of the article should be done in this section. This must be written as a seperate section from the results section.

5.8. Conclusions

- The main conclusion of the study provided by data and findings of the research should be stated concisely and concretely in this section.
- The subjects that are not mentioned sufficiently and/or unprocessed in the body section must not be included in this section.
- The conclusions can be given in the form of substances in order to emphasize the results of the research and to make the expression understandable.

5.9. Acknowledgements

- In this section, the significant contributions made in the realization of investigation that form the topic of the paper is specified. While specifying contributions, the attitude diverted the original purpose of this section away is not recommended. Acknowledgements must be made according to the following examples.
- This study was carried out within scope of .....project.
- I/we would like to thank to …… for contributing to the development of this article with his/her critiques.
- Academic and/or authoritorial affiliations are written for the contributions made because of requirement of ordinary task.
- For example:
- “Prof. Dr. İ. Enver Altınlı has led the studies”.
- “The opinions and warnings of Dr. Tandoğan Engin are considered in determining the chemistry of chrome minerals.”
- The contributions made out of the requirement of ordinary task:
- For example:
- “I would like to thank to Professor Dr. Melih Tokay who gives the opportunity to benefit from unpublished field notes”; “I would like to thank to the preliminary-Plan Chief Engineer Ethem Göğer, State Hydraulic Work, 5th Zone”. Academic and / or task-occupational titles are indicated for such contributions.
- The contributions, which are made because of requirement of ordinary task but do not necessitate responsibility of the contributor mustn’t be specified.
- For example:
- Sentences such as “I would like to thank to our General Manager, Head of Department or Mr. / Mrs. President ……who has provided me the opportunity to research” must not be used.

5.10. References

- All references cited in the text are to be present in the reference list.
- The authors must be sure about the accuracy of the references. Publication names must be written in full.
- Reference list must be written in Times New Roman, 9-point type face.
- The reference list must be alphabetized by the last names of the first author of each work.
- If an author’s more than one work is mentioned, ranking must be made with respect to publication year from old to new.
- In the case that an author’s more than one work in the same year is cited, lower-case alphabet letters must be used right after publication year (for example; Saklar, 2011*a, b*).
- If the same author has a publication with more than one co-author, firstly the ones having single author

are ranked in chronological order, then the ones having multiple authors are ranked in chronological order.

- In the following examples, the information related to works cited is regulated in accordance with different document/work types, considering punctuation marks as well.
- If the document (periodic) is located in a periodical publication (if an article), the information about the document must be given in the following order: surnames of the author/authors, initial letters of author's/ authors' first names. Year of publication. Name of the document. Name of the publication where the document is published, volume and/ or the issue number, numbers of the first and last pages of the document.

For example:

Gürsoy, M. 2017. Munzur Dağları Alt Miyosen çökelleri mollusk topluluğu ve paleoekolojisi (Doğu Anadolu, Türkiye). Maden Tetkik ve Arama Dergisi 155, 75-99.

Pamir, H.N. 1953. Türkiye'de kurulacak bir hidrojeoloji enstitüsü hakkında rapor. Türkiye Jeoloji Bülteni 4, 1, 63-68.

Robertson, A.H.F. 2002. Overview of the genesis and emplacement of Mesozoic ophiolites in the Eastern Mediterranean Tethyan region. Lithos 65, 1-67.

- If more than one document by the same authors is cited, firstly the ones having single name must be placed in chronological order, then the ones having two names must be listed in accordance with chronological order and second author's surname, finally the ones having multiple names must be listed in accordance with chronological order and third author's surname.
- If the document is a book, these are specified respectively: surnames of the author/authors, initial letters of author's/authors' first names. Year of publication. Name of the book (initial letters are capital). Name of the organization which has published the book, name of the publication wherethe document is published, volume and/ or the issue number, total pages of the book.

For example

Einsele, G. 1992. Sedimentary Basins. Springer-Verlag, p 628.

Meriç, E. 1983. Foraminiferler. Maden Tetkik ve Arama Genel Müdürlüğü Eğitim Serisi 23, 280p.

- If the document is published in a book containing the writings of various authors, the usual sequence is followed for the documents in a periodic publication. Then the editor's surname andinitial letters of their name /names are written. "Ed." which is an abbreviation of the editor word is written in parentheses. Name of the book containing the document (initial letters are capital). Name of the organization which has published the book. Place of publication, volume number (issue number, if any) of the publication where the document is published, numbers of the first and last page of the document.

For example:

Göncüoğlu, M.C., Turhan, N., Şentürk, K., Özcan, A., Uysal, Ş., Yalınız, K. 2000. A geotraverse across northwestern Turkey. Bozkurt, E., Winchester, J.A., Piper, J.D.A. (Ed.). Tectonics and Magmatism in Turkey and the Surrounding Area. Geological Society of London Special Publication 173, 139-162.

Anderson, L. 1967. Latest information from seismic observations. Gaskell, T.F. (Ed.). The Earth's Mantle. Academic Press. London, 335-420.

- If name of a book where various authors' writings have been collected is specified, those must be indicated respectively: book'seditor/editors' surname/surnames, and initial letters of their name/ names. "Ed." which is an abbreviation of the editor word must be written in parentheses. Year of Publication. Name of the book (initial letters are capital). Name of the organization which has published the book, total pages of the book.

For example:

Gaskel, T.F. (Ed.) 1967. The Earth's Mantle. Academic Press, 520p.

- If the document is an abstract published in a Proceedings Book of a scientific activity such as conference/symposium/workshop …etc. , information about the document must be given in the following order: surnames of the author/authors, initial letters of author's/authors' first names. Year of publication. Title of the abstract. Name, date and place of the meeting where the Proceedings Book

is published, numbers of the first and last pages of the abstract in the Proceedings Book.

For example:

Öztunalı, Ö., Yeniyol, M. 1980. Yunak (Konya) yöresi kayaçlarının petrojenezi. Türkiye Jeoloji Kurumu 34. Bilim Teknik Kurultayı, 1980, Ankara, 36

Yılmaz, Y. 2001. Some striking features of the Anatolian geology. 4. International Turkish Geology Symposiums 24-28 September 2001, London, 13-14.

- If the document is one of the unpublished documents as report, lecture notes, and so on., information about the document must be given by writing the word "unpublished" in parentheses to the end of information about the document after it is specifiedin accordance with usual order which is implemented for a document included in a periodic publication.

For example:

Akyol, E. 1978. Palinoloji ders notları. EÜ Fen Fakültesi Yerbilimleri Bölümü, 45 p., İzmir (unpublished).

Özdemir, C. Biçen, C. 1971. Erzincan ili, İliç ilçesi ve civarı demir etütleri raporu. General Directorate of Mineral Research and Exploration Report No: *4461*, 21 p. Ankara (unpublished).

- The followings must be specified for the notes of unpublished courses, seminars, and so on: name of the document and course organizer. Place of the meeting. Name of the book, corresponding page numbers.

For example:

Walker, G. R. Mutti, E. 1973.Turbidite facies and facies associations. Pacific Section Society for Sedimentary Geology Short Course. Annaheim. Turbitides and Deep Water Sedimantation, 119-157.

- If the document is a thesis, the following are written: surname of the author, initial letter of the author's first name. Year of Publication. Name of the thesis. Thesis type, the university where it is given, the total number of pages, the city and "unpublished" word in parentheses.

For example:

Seymen, İ. 1982. Kaman dolayında Kırşehir Masifi'nin jeolojisi. Doçentlik Tezi, İTÜ Maden Fakültesi, 145 s.İstanbul (unpublished).

- Anonymous works must be regulated according to publishing organization.

For example:

MTA. 1964. 1/500.000 ölçekli Türkiye Jeoloji Haritası, İstanbul Paftası. Maden Tetkik ve Arama Genel Müdürlüğü, Ankara.

- The date, after the name of the author, is not given for on-printing documents; "in press" and / or "on review" words in parenthesis must be written. The name of the article and the source of publication must be specified, volume and page number must not be given.

For example:

- Ishihara, S. The granitoid and mineralization. Economic Geology 75th Anniversary (in press).

- Organization name, web address, date of access on web address must be indicated for the information downloaded from the Internet. Turkish sources must be given directly in Turkish and they must be written with Turkish characters.

For example:

- ERD (Earthquake Research Department of Turkey). **http://www.afad.gov.tr**. March 3, 2013.

- While specifying work cited, the original language must be used; translation of the title of the article must not be done.

6. Illustrations

- All drawings, photographs, plates and tables of the article are called "illustration".

- Illustrations must be used when using of them is inevitable or they facilitate the understanding of the subject.

- While selecting and arranging the illustrations' form and dimensions, page size and layout of the *Bulletin* must be considered, unnecessary loss of space must be prevented as much as possible.

- The pictures must have high quality, high resolution suitable for printing.

- The number of illustrations must be proportional to the size of the text.

- All illustrations must be sent as separate files independent from the text.
- While describing illustrations in the text, abbreviations must be avoided and descriptions must be numbered in the order they are mentioned in the text.
- Photographs and plates must be given as computer files containing EPS, TIFF, or JPEG files in 600 dpi and higher resolutions (1200 dpi is preferred) so that all details can be seen in the stage of examination of writing.

6.1. Figures

- Drawings and photos (except for the plates in the text) will be evaluated together as "Figure" and they must be numbered in the order they are mentioned in the text.
- The figures published in the Bulletin of Mineral Research and Exploration must be prepared in computer considering the dimensions of single-column width 7.4 m or double-column width 15.8 cm. Figure area together with the writing at the bottom should not exceed 15.8x21in maximum.
- Unnecessasry details must not be given in figures or care must be taken not to use much space for information transfer.
- Figures must be arranged in such a way to be printed in black/white or colored.
- The figure explanations being justified in two margins must be as follows:

Figure 1- Sandıklı İlçesinin (Afyon); a) güneybatısının jeolojik haritası, b) İnceleme alanının genel dikme kesiti (Seymen 1981), c) Türkiye'nin önemli neotektonik yapıları (Koçyiğit 1994'den değiştirilerek).

Figure 1- a) Sandıklı ilçesinin güneybatısının jeolojik haritası, b) İnceleme alanının genel dikme kesiti (Seymen, 1981), c) Türkiye'nin önemli neotektonik yapıları (Koçyiğit 1994'den değiştirilerek).

- Drawings must be made by well-known computer programs painstakingly, neatly and cleanly.
- Using fine lines, which can disappear when figures shrinks, must be avoided. Symbols or letters used in all drawings must be in Times New Roman and not less than 2 mm in size when shrink.
- All standardized icons used in the drawings must be explained preferably in the drawing or with figure caption if they are too long.
- Linear scale must be used for all drawings. Author's name, figure description, figure number must not be included into the drawing.
- Photos must be in quality and quantity that will reflect the objectives of the subject.

6.2. Plates

- Plates must be used when needed a combination of more than one photo and the publication on a special quality paper.
- Plate sizes must be equal to the size of available magazine pagespace.
- Figure numbers and linear scale must be written under each of the shapes located on the Plate.
- The original plates must be added to the final copy which will be submitted if the article is accepted.
- Figures and plates must be independently numbered. Figures must be numbered with Latin numerals and plates with Roman numerals (e.g., Figure1, Plate I).
- There must be no description text on Figures.

6.3.Tables

- All tables must be prepared preferably in word format in Times New Roman fonts.
- Tables together with table top writing must not exceed 15x8 cm in size.
- The table explanations being justified in two margins must be as follows:

Table 1- Hydrogeochemical analysis results of geothermal waters in the study area.

7. Nomenclature and Abbreviations

- Non-standard and uncommon nomenclature abbreviations should be avoided in the text. But if essential, they must be described as below: In cases where unusual nomenclatures and unstandardized abbreviations are considered to be compulsory, the followed way and method must be described.
- Full stop must not be placed between the initials of words for standardized abbreviations (MER, SHW, etc.).
- Geographical directions must be abbreviated in English language as follows: N, S, E, W, NE …etc.

- The first time used abbreviations in the text are presented in parenthesis, the parenthesis is not used for subsequent uses.
- The metric system must be used as units of measurement.
- Figure, plate, and table names in the article must not be abbreviated. For example, "as shown in generalized stratigraphic cross-section of the region (Figure 1……..."

7.1. Stratigraphic Terminology

Description of Stratigraphic units must be done acoording to rules of International Stratigraphic Guide (https://stratigraphy.org/guide/)" and "Turkey Stratigraphy Committee" (https://www.mta.gov.tr/v3.0/sayfalar/birimler/belgeler/Stratigrafi_adlama_kurallari.pdf). In addition, should be paid to attention to the use of Chronostratigraphy (lower, middle, upper, etc) and Geochronology (early, middle, late etc.) of the units, which have been updated by the "International Stratigraphy Committee" and accepted to be used in Turkish/English (https://stratigraphy.org/chart)."Approved/officialandunapproved/unofficial" rules must be followed in naming and using all stratigraphic units.

7.2. Paleontologic Terminology

Fossil names in phrases must be stated according to the following examples:

- For the use of authentic fossil names;

e.g. Limestone with *Nummulites*

- When the authentic fossil name is not used;
- e.g. nummulitic Limestone
- Other examples of use;

e.g. The type and species of *Alveolina / Alveolina* type and species

- Taxonomic ranks must be made according to the following examples:
- The names of the fossils should be stated according to the rules given below:
- For the first use of the fossil names, the type, spieces (cf., aff. ve gr.) and the author names must be fully indicated;

Alveolina aragonensis Hottinger, 1960, not reference

Alveolina cf. *aragonensis* Hottinger, 1960, not reference

Alveolina aff. *aragonensis* Hottinger, 1960, not reference

Alveolina gr. aragonensis Hottinger, 1960 not reference

- When a species (cf., aff. ve gr.) is mentioned for the second time in the text;

A.aragonensis

*A.*cf.*aragonensis*

*A.*aff. *aragonensis*

A. gr. *aragonensis,* not reference

- It is accepted as citiation if stated as *Alveolina aragonensis* Hottinger (1960). Cited Hottinger (1960), stated in the Reference section.

Plate / Plate, In the descriptions of the figures / figures: Plate / Plate, In the descriptions of the figures / figures: Genus / Subgenus or Type / Subtype text should be written in bold and Italic, surname / surnames and year should be written normally.

Ordo: Foraminiferida Eichwald, 1830 Super family: Alveolinacea Ehrenberg, 1939	Not reference, Not stated in the Reference section
Family: Alveolinidae Ehrenberg, 1839	
Type genus: *Borelis* de Montfort, 1808	
Type species: *Borelis melenoides* de Montfort, 1808=*Nautilus melo* Fitchel and Moll, 1798	
Borelis vonderschmitti (Schweighauser, 1951) (Plate, Figure, Figure in Text)	Schweighauser, 1951 not reference
1951 *Neoalveolina vonderschmitti* Schweighauser, page 468, figure 1-4	Cited Scweighauser (1951), stated in the Reference section.
1974 *Borelis vonderschmitti* (Schweighauser), Hottinger, page, 67, plate 98, figure 1.7	Cited Hottinger (1974), stated in the Reference section.

Parahaymanella hakyemezae Acar, 2019;

Pseudohottingerina burdurensis Acar, 2019.

- The statement of plates and figures (especially for the articles of paleontology):

a for the statement of species mentioned in the body text; ***Borelis vonderschmitti*** (Schweighauser, 1951)

(Plate, Figure, Figure in the body text).

b. When cited for other articles;

1951 ***Neoalveolina vonderschmitti*** Schweighauser, page 468, figure 1-4, figure in body text.

1974 ***Borelis vonderschmitti*** (Schweighauser), Hottinger, page 67, plate 98, figure 1-7.

c. For the citation in the text

(Schweighauser, 1951, page, plate, figure, figure in the body text)

(Hottinger, 1974, page, plate 97, figure 67, plate 98, figure 1-7, figure in the body text).

8. Citations

All the citiations in the body text must be indicated by the last name of the author(s) and the year of publication, respectively. The citations in the text must be given in following formats.

- For publications written by single author:

- It is known that fold axial plain of Devonian and Carboniferious aged units around Istanbul is NS oriented (Ketin, 1953, 1956; Altınlı, 1999).

- Altınlı (1972, 1976) defined the general characteristics of Bilecik sandstone

- For publications written by two authors:

- The upper parts of the unit contain Ilerdian fossils (Sirel and Gündüz, 1976; Keskin and Turhan, 1987, 1989).

- For publications written by three or more authors:

According to Caner et al. (1975) Alıcı formation reflects the fluvial conditions.

The unit disappears wedging out in the East direction (Tokay et al., 1984).

- If reference is not directly obtained but can be found in another reference, cross-reference should be given as follows:

- It is known that Lebling has mentioned the existence of Lias around Çakraz (Lebling, 1932: from Charles, 1933).

9. Reprints

The author(s) will receive 2 two hard copies of the related issues.

10. Copyright and Conditions of Publication

- It is a condition of publication that work submitted for publication must be original, previously unpublished in whole or in part.

- It is a condition of publication that the authors who send their publications to the Bulletin of Mineral Research and Exploration hereby accept the conditions of publication of the Bulletin in advance.

- All copyright of the accepted manuscripts belong to MTA. The author or corresponding author on behalf of all authors (for papers with multiple authors) must sign and give the agreement under the terms indicated by the Regulations of Executive Publication Committee. Upon acceptance of an article, MTA can pay royalty to the authors upon their request according to the terms under the "Regulations of Executive Publication Committe" and the "Regulations of Royalty Payment of Public Office and Institutions"

All the information and forms about the Bulletin of Mineral Research and Explorations can be obtained from http://bulletin.mta.gov.tr